DISCLAIMER

This report was prepared as an account of work sponsored by an agency of the United States Government. Neither the United States Government nor any agency thereof, nor any of their employees, makes any warranty, express or implied, or assumes any legal liability or responsibility for the accuracy, completeness, or usefulness of any information, apparatus, product, or process disclosed, or represents that its use would not infringe privately owned rights. Reference herein to any specific commercial product, process, or service by trade name, trademark, manufacturer, or otherwise does not necessarily constitute or imply its endorsement, recommendation, or favoring by the United States Government or any agency thereof. The views and opinions of authors expressed herein do not necessarily state or reflect those of the United States Government or any agency thereof. Reference herein to any social initiative (including but not limited to Diversity, Equity, and Inclusion (DEI); Community Benefits Plans (CBP); Justice 40; etc.) is made by the Author independent of any current requirement by the United States Government and does not constitute or imply endorsement, recommendation, or support by the United States Government or any agency thereof.

SAND2025-02745R

RANGERS

Methodology for Design and Performance Assessment of Engineered Barrier Systems in a Salt Repository for HLW/SNF: Synthesis Report

BGE TEC 2025-07

Technical Report

RANGERS

Methodology for Design and Performance Assessment of Engineered Barrier Systems in a Salt Repository for HLW/SNF: Synthesis Report

BGE TEC 2025-07

Project Coordinators
Eric Simo (BGE TEC)
Ed Matteo (SANDIA)

Authors
Eric Simo (BGE TEC)
Ajmal Gafoor (BGE TEC)
Philipp Herold (BGE TEC)
Paola Leòn Vargas (BGE TEC)
Andree Lommerzheim (BGE TEC)
Andreas Keller (BGE TEC)
David Seidel (BGE TEC)
Kristopher L. Kuhlman (Sandia)
Edward Matteo (Sandia)
Carlos M. Lopez (Sandia)
David Fukuyama (Sandia)
Richard S. Jayne (Sandia)
Melissa M. Mills (Sandia)

How to cite: Simo, E., Gafoor, A., Herold, P., Leòn Vargas, P., Lommerzheim, A., Keller, A., Seidel, D., Kuhlman, K. L., Matteo, E., Fukuyama, D., Lopez, C. M., Jayne, R. S. and Mills, M. M. (2025). Methodology for Design and Performance Assessment of Engineered Barrier Systems in a Salt Repository for HLW/SNF - RANGERS: Synthesis Report. Technical Report. BGE TEC 2025-07. BGE TECHNOLOGY GmbH, Sandia National Laboratories, Peine, Albuquerque.

The research work that is the basis of this report was funded by the German Federal Ministry for the Environment, Nature Conservation, Nuclear Safety and Consumer Protection (BMUV) represented by the Project Management Agency Karlsruhe (Karlsruhe Institute of Technology, KIT) under contract number FKZ 02.E.11839. The authors alone, however, are responsible for the contents of this study.

The Sandia co-authors of this report were funded by the US Department of Energy Office of Nuclear Energy's (DOE-NE) Spent Fuel and Waste Science and Technology (SFWST) program. Sandia National Laboratories is a multimission laboratory managed and operated by National Technology & Engineering Solutions of Sandia, LLC, a wholly owned subsidiary of Honeywell International Inc., for the U.S. Department of Energy's National Nuclear Security Administration under contract DE-NA0003525. This report has been co-authored by employees of National Technology & Engineering Solutions of Sandia, LLC under Contract No. DE-NA0003525 with the U.S. Department of Energy. The employees own all right, title and interest in and to the report and is solely responsible for its contents. The United States Government retains and the publisher, by accepting the report for publication, acknowledges that the United States Government retains a non-exclusive, paid-up, irrevocable, world-wide license to publish or reproduce the published form of this report or allow others to do so, for United States Government purposes. The DOE will provide public access to these results of federally sponsored research in accordance with the DOE Public Access Plan `https://www.energy.gov/downloads/doe-public-access-plan`.

RANGERS

Methodology for Design and Performance Assessment of Engineered Barrier Systems in a Salt Repository for HLW/SNF: Synthesis Report

BGE TEC 2025-07

Project Coordinators	Eric Simo (BGE TEC) Ed Matteo (SANDIA)

Date	2025
Client	BMUV / US Department of Energy

Total pages: 362

Authors:	Reviewer:	QS:	Release:
E. Simo, K. Kuhlman	M. Polster, P. Herold	W. Schmidt,M. Polster	T. Berlepsch
2.11.2024	30.01.2025	30.01.2025	27.02.2025

Contents

List of Figures

List of Tables

1. Executive Summary

Salt formations have long been recognized as a highly favorable host rock for the final disposal of high-level radioactive waste (HLW) in deep geological repositories. Their unique properties, including exceptional impermeability, self-healing capabilities, and thermal conductivity, make them a reliable natural barrier for the deep disposal of radioactive waste. This report focuses on the development and application of a methodology for assessing the integrity and performance of the Engineered Barrier System (EBS) within salt-based repositories, a critical component of the multi-barrier system ensuring safe radioactive waste disposal.

The RANGERS project, a collaboration between BGE TECHNOLOGY GmbH (BGE TEC) and Sandia National Laboratories (SNL), leverages decades of expertise from Germany and the United States to establish a unified approach for the design, evaluation, and performance assessment of EBS in salt repositories. The methodology developed under this project provides a comprehensive framework for addressing the regulatory, geotechnical, and safety requirements for HLW repositories, ensuring containment and isolation over regulatory timeframes.

At the core of this methodology is the integration of Features, Events, and Processes (FEP) analysis to evaluate the loads and stresses acting on the EBS, predict its evolution, and assess its performance through rigorous numerical simulations. The approach begins with the selection of a geological site and repository design, followed by the definition of a tailored sealing concept. The repository system, comprising the geological site, infrastructure, and EBS, is subjected to FEP analysis to identify relevant processes affecting the EBS's structural and functional integrity. This analysis informs the integrity assessment, which evaluates the EBS's capacity to withstand thermomechanical, hydraulic, and chemical loads over regulatory timeframes.

The integrity of the repository system is verified through a dual-path framework, consisting of an Integrity Demonstration under a reference scenario and an Integrity Evaluation under alternative scenarios. This comprehensive approach, as outlined in regulatory guidelines, provides a deeper understanding of repository robustness and reliability. The Integrity Demonstration ensures the sealing function by analyzing hydraulic resistance and structural stability under thermal-hydraulic-mechanical-chemical (THMC) conditions. It is inspired by engineering standards such as EUROCODE, utilizing partial safety factors to address uncertainties in loads and resistance, ensuring structural integrity of the EBS. The Integrity Evaluation, meanwhile, focuses on the hydraulic evolution of the EBS under alternative scenarios, enhancing robustness and resilience by optimizing its design. While mechanical analysis dominates integrity demonstration, the hydraulic evolution assessed in alternative scenarios directly contributes to radiological performance, aligning these evaluations within the broader performance assessment framework.

Building on this approach, a robust and comprehensive modeling concept has been developed to derive systematic numerical analyses for both integrity and performance assessments. This advanced concept enables precise and rigorous safety evaluations, ensuring the long-term containment of high-level radioactive waste (HLW) and spent nuclear fuel (SNF). By leveraging recent advancements in performance assessment (PA) codes and the availability of powerful computational resources, the concept integrates a wide range of FEPs into unified numerical models. These models employ variable discretization strategies tailored to the specific focus of each investigation, allowing for optimized resolution and computational efficiency. This ap-

proach ensures that all critical aspects of repository performance are captured with sufficient accuracy, enhancing confidence in the overall safety and robustness of the repository system.

The present report consolidates two separate studies into a synthesis document: one focusing on the development of the methodology, and the other on its application to a generic repository system in salt formations through numerical analyses.

Key findings from the RANGERS project, derived from the application of this methodology, confirm that the engineered barrier system (EBS) can withstand THMC repository conditions, maintain structural integrity, and ensure effective containment under repository conditions:

- Thermal Evolution and Backfill Compaction: The crushed salt backfill, which serves as the long-term sealing component in repository drifts, achieves significant compaction within approximately 1,000 years. Elevated temperature, generated by the decay heat from HLW and SNF, facilitate rapid compaction in the early stages, ensuring effective containment within decades of emplacement. Thermal conductivity of the salt rock contributes to efficient heat dissipation, minimizing the impact on the structural stability of the repository.
- Mechanical integrity: The repository system demonstrates robust mechanical stability under thermomechanical loads. Dilatancy zones, which form locally around the drift and shaft walls, are predicted to remain spatially limited and recover naturally over time due to salt's creep and convergence properties. This recovery ensures the repository's structural integrity over extended timescales. It has been shown that the sealing components in the EBS will be subject to compressive stresses over time as a result of the creep behaviour of the salt.
- Hydraulic Sealing Performance: Hydraulic assessments reveal minimal fluid migration through the shaft seal, with calculated inflow volumes into the infrastructure remaining below significant levels for up to 50,000 years. This ensures the hydraulic sealing function of the EBS under both normal and extreme scenarios. The evolving permeability of the compacted crushed salt is shown to effectively prevent advective transport of potential contamined fluids, further contributing to the containment function.
- Gas Generation and Transport: Simulations indicate low gas pressures within the repository due to the initial migration of evaporated water into the surrounding salt rock, driven by elevated temperatures. This process reduces the potential for gas-induced hydraulic loading, ensuring that the EBS's structural integrity is maintained over time. Further analyses have shown that, at low gas pressures, the influence on the compaction of crushed salt is relatively modest, allowing the backfill to consolidate as intended. However, at elevated gas pressures, the impact becomes more pronounced, with the potential to significantly delay the compaction process by several decades, or in extreme cases, even centuries. Under conditions of extremely high gas pressure, the compaction process may not only be halted entirely but could also reverse, leading to the dilation of the backfill material.
- Integrated Performance Assessment: The methodology effectively integrates the results of numerical simulations into an overarching performance assessment framework. This includes evaluating the evolution of the EBS under the reference and alternative scenarios. These assessments have shown that gases generated within the repository will

be dissolved in the crystalline water of the salt. It is therefore unlikely that high gas pressure will develop in a salt repository. The developed numerical simulations can now be further elaborated for the consideration of radiological assessment.

The findings emphasize the suitability of salt formations and the engineered barrier system for radioactive waste disposal. The RANGERS methodology offers a structured workflow for designing, evaluating, and optimizing EBS performance in salt repositories. By focusing on the integrity and functionality of each EBS component and its evolution, the methodology reduces uncertainties in performance assessment models and ensures compliance with stringent regulatory standards.

The project RANGERS provides a solid foundation for advancing EBS integrity assessments, optimizing repository designs, and improving long-term safety for HLW disposal. The results validate the EBS's capacity to maintain its structural and functional integrity over regulatory timeframes, supporting sustainable, long-term radioactive waste management in salt repositories. Through its rigorous and adaptable framework, the RANGERS project establishes a new standard for the safe and effective disposal of radioactive waste in salt formations.

PART 1: METHODOLOGY

2. Introduction

Salt formations are one of the potential host rocks for the final disposal of high-level radioactive waste (HLW) in deep geological repositories, both in Germany and the United States. The safe isolation of radioactive waste in these repositories relies on a multi-barrier system, combining engineered and natural barriers. The natural barrier is provided by the salt rock itself, known for its self-sealing properties and long-term stability. The engineered barrier, on the other hand, comprises sealing components strategically placed within the repository to enhance its containment capabilities. In both Germany and the United States, long-term safety assessments require demonstrating the integrity of the natural barrier for a period of up to 1 million years. Concurrently, the engineered barrier system (EBS) must maintain its structural and functional integrity until the long-term seal, such as the granular salt backfill material, has re-consolidated to its final low porosity and permeability.

Based on extensive expertise and experience with engineered barriers in salt formations, BGE TECHNOLOGY GmbH and Sandia National Laboratories have partnered to develop a robust methodology for the integrity and performance assessment of EBS in HLW repositories through the RANGERS project. This collaborative effort aims to establish a unified approach to geotechnical engineering, repository design, integrity and performance evaluation of EBS in salt repositories.

This report presents a comprehensive framework for the design and evaluation of EBS in salt-based repositories, offering detailed guidance on regulatory compliance, safety concepts, design and long-term performance. The developed methodology provides a structured pathway for designing and assessing the EBS's performance, aligned with the specific geological site and repository concept. From the selected geological site and repository design, a tailored sealing concept is defined, which forms the basis of the EBS. The overall repository system, comprising the geological site, repository infrastructure, and EBS, is then subjected to a rigorous analysis of Features, Events, and Processes (FEPs). Only FEPs relevant to the EBS are considered, from which the loads and stresses acting on the system are derived. These loads form the foundation for the integrity assessment. The FEPs are also used to evaluate the evolution of the EBS over the reference period in the scope of performance assessment.

By focusing on the long-term structural integrity and containment effectiveness of the EBS, the RANGERS project sets a new standard for the future of safe radioactive waste disposal in salt formations. Through comprehensive performance assessment simulations, this project ensures that the EBS will meet the stringent safety requirements necessary to demonstrate the safety proof of HLW repositories in salt.

3. General Context

Rock salt formations are considered in Germany and in the United State as suitable host rock for the final disposal of radioactive waste. A radioactive waste repository in salt can take advantage of the extremely low connected porosity and practical impermeability of natural rock salt formations to solutions on one hand, and their self-healing ability on the other hand, to achieve long-term secure containment of the disposed waste and its isolation from the biosphere Kreienmeyer et al. (2008). In a repository in rock salt, it is generally assumed that there are no pathways in the undisturbed host rock that allow the inflow of solutions from the overburden into the disposal areas. Through appropriate exploration, it is ensured that no solution inclusions are encountered in the host rock or that they are emptied during the excavation of the mining structures (Kindlein et al., 2018). This makes rock salt a safe medium for radioactive waste disposal in deep geological formations.

The safety of a repository in a salt formation is based on a multi-barrier concept. The multiple barriers in salt repositories consist of a technical barrier, a geological barrier, the crushed salt backfill serving as long term barrier, and the geotechnical barriers. The technical barrier is provided by the disposal casks. The safety function of the casks is to ensure the safe transport and handling during the operational phase and to ensure the requirements for retrievability and recoverability up to 500 years in Germany (StandAG, 2023). The geological barrier is provided by the salt host rock. The geological barrier aims to ensure the long-term and secure containment of radioactive waste. The effectiveness of a repository in rock salt is highly dependent on the integrity of the geological barrier in the rock formation (Mönig et al., 2012).

Another important barrier for a salt repository is the backfill material, crushed salt. Due to its self-healing properties, this barrier ensures the safe containment of radioactive waste for long periods of time, even beyond the time frame required for quantitative verification (Müller-Hoeppe and Krone, 1999). During the excavation of the mine, the geological barrier is breached, temporarily creating direct pathways from the waste to the biosphere. In addition, in areas close to the excavations, the geological barrier is damaged and locally weakened. To ensure long-term stability and permanent filling of the cavities, the mined salt rock generated during excavation will be used as backfill material, filling excavations with essentially the same material as the surrounding geological barrier. Over time, the compaction of the backfill material develops a sealing effect comparable to that of the undisturbed geological barrier. The time required to reach the final states can vary from tens to thousands of years. It depends on the convergence rate, moisture content, and ambient temperature. Therefore, additional geotechnical sealing structures such as shaft seals and drift seals are planned, which will provide a specified sealing ability directly at the closure of the repository (Mönig et al., 2012).

According to AkEnd (2002), the closure of shafts holds a similar significance in terms of long-term safety as the function of the geological barrier. In AkEnd (2002), it is recommended: “A repository mine, whose safety case is primarily based on geological barriers, must be sealed with a geotechnical barrier, the shaft seal, in any case.” The shaft seal is the most crucial safety component as it restores the integrity of the containment area (Müller-Hoeppe and Krone, 1999). Its main function is to prevent water or solution ingress from the overlying rock into the repository after its closure. In the event that radionuclides are mobilized during the post-closure phase, the shaft seal ensures their retention within the repository through appropriate sealing measures. The concept of a shaft seal includes sealing components,

similar to those of a drift seal, as well as supporting and load-bearing elements (Kreienmeyer et al., 2008).

In a repository for radioactive waste, drift seals are of significant importance as a safety element at the edge of the enclosing rock area. The drift seal must seal off the anthropogenic pathways for solution ingress into the repository, thereby compensating for the temporary loss of safety caused by the construction of the repository (Orzechowski, 2018).

During the post-closure phase, these sealing structures are subject to external influences and alteration processes (e.g., thermal, mechanical, hydrological, and chemical), which may affect their effectiveness throughout the entire assessment period. Because of the presence of the long-term seal, both shaft and drift seals, must not provide their function during the complete post-closure phase. Thus, the shaft seals and drift seals must remain sufficiently tight until the hydraulic resistance of the backfill material is high enough to prevent or limit the ingress of solutions to the waste, achieving the protection level specified in the safety requirements (Mönig et al., 2012).

The design of the geotechnical barriers is a challenging task. These structures require a reliable and well-documented verification that extends their safety assessment well into the post-operational phase and includes critical situations, such as the ingress of solutions. The verification procedures from current engineering recommendations and guidelines only address above-ground structures with a lifespan of approximately 100 years and the possibility of maintenance and repair, but not to underground structures that require a post-operational lifespan of several thousand years without active intervention (Orzechowski, 2018). The shaft seal for instance in a salt repository is designed to remain functional until the occurrence of the next ice age, which is estimated to occur in 50,000 years. However, after the ice age, changes in hydrogeological and topographic conditions caused by glaciation introduce significant uncertainty in predicting the chemical composition of infiltrating waters. Consequently, designing robust seals capable of withstanding these uncertain chemical conditions becomes impossible. In later periods, after the ice age, the primary sealing function is achieved by the host rock and the compacted backfill (Rübel et al., 2016). For the drift seals, a similar or longer functional life time can be expected. The shaft seal would be expected to lose its function first, being the first geotechnical structure in contact with corrosive water. After the failure of the shaft, the drift seals would also provide resistance to flow, keeping brine away from the waste. Therefore, a methodological approach to the design of the engineered barrier system over such a long period of time is critical to the overall safety of a repository in salt.

In Germany, significant efforts have been made to design and assess the safety of engineered barrier systems for repositories in salt formations. These efforts are aimed at ensuring the long-term isolation and containment of radioactive waste. Several noteworthy projects exemplify these efforts and are outlined below.

A new approach to evaluating the effectiveness of barriers in a repository system, as proposed by Müller-Hoeppe and Krone (1999), presents a methodology for evaluation the effectiveness of an underground repository system and its geotechnical barriers in a salt host rock. The key aspect is the introduction of a method for estimating the risk posed by a repository. The fundamental assumption is that a mine specifically designed for disposal purposes is excavated in an undisturbed salt formation. After disposal, the mine is sealed using a multi-barrier system, which requires comprehensive evidence for the entire system as well as individual compo-

nents. No institutional control is planned following the closure of the repository. Referring to past experiences with flooded salt mines, it is noted that while salt itself is impermeable, there is a distinction between the pure material (halite) and the salt rock formation, which is characterized by layering and geometric features. The authors proposes the following definition of tightness as a central argument to assess the safety of the disposal in salt (Müller-Hoeppe and Krone, 1999): *A barrier is considered tight if the penetration front of the contaminated fluids does not reach the opposite end of the barrier within the designated period of exposure.*.

According to Müller-Hoeppe and Krone (1999), previous considerations assumed the premature failure of barriers as a regular load case, and then considered them as flow barriers in the verification process, assuming gradual release of contaminants. However, if barrier failure is assumed as a normal load case, it eliminates the significant advantage of the salt host rock, as the compaction of the backfill is disrupted and it does not become hydraulically resistive. This assumes the occurrence of an event that only happens in exceptional cases. Such an approach is not provided in engineering and buildings standard such as the Eurocode (DIN EN 1990, 2010) or in the regulations for the design of nuclear facilities by the Nuclear Technology Committee (Kerntechnische Ausschuss (KTA), 1988). These standards initially assume the expected behavior of the system during the design process (Müller-Hoeppe and Krone, 1999).

In this context, Müller-Hoeppe and Krone (1999) proposes a verification method using the limit state design concept with partial safety factors for model and material uncertainties, similar to the Eurocode methodology. However, this method focuses on tightness rather than structural stability. The essential steps are as follows: 1. Description of the limit state for which the actions and resistances are determined. 2. Development of models for actions (i.e. loads or impacts), material properties, and geometric values. The aim is to demonstrate that the limit states are not exceeded using the determined design values and selected models.

The authors also raise concerns about the feasibility of applying verification concepts to probabilistic approaches. Probabilistic verification with a specified confidence level requires a sample size proportional to the reciprocal of the confidence level, which significantly increases computational demands. Given the complexity of the system, this approach appears impractical due to the substantial computational resources required. Only for very improbable scenarios where a low confidence level on the order of 10^{-2} is sufficient, is this fully probabilistic method considered applicable (Müller-Hoeppe and Krone, 1999). However, it is important to note that this statement should be reconsidered in light of the advancements in computational capacities in recent years (Sanders, 2020; Kuhlman et al., 2024).

The approach put forward by Müller-Hoeppe and Krone (1999) has been further developed in the project ISIBEL. The project ISIBEL (Verification and Evaluation of the Instrumentation for the Safety Assessment of High-Level Radioactive Waste Repositories – Buhmann et al. (2008)) provides a systematic inventory of the state of research and development in the disposal of heat-generating radioactive waste. Work package 5 of this project focuses on the status of design and planning of geotechnical barriers. The follow-up project ISIBEL II, called KOMTESSA, incorporated findings from the previous project and mentioned these results in a chapter on geotechnical barriers.

In the ISIBEL project, the impacts and resistances are derived from a collection of features, events, and processes (FEP) that are generic to salt repositories and need to be specified

for a specific site. The goal of this project is not to provide specific evidence but rather to demonstrate how such evidence can be obtained and that it is theoretically feasible. As described in Müller-Hoeppe and Krone (1999), the aim is to show how the safe containment can be demonstrated through a combination of geological and geotechnical barriers, and how the maximum individual dose or maximum risk can be determined using release scenarios. The regular demonstration in this project does not involve conservative release scenarios but focuses on the safe containment of the waste. Possible developments and their probabilities are derived from a combination of scenario analysis (Buhmann et al., 2008).

The ISIBEL project considered release scenarios but did not perform a detailed analysis of their likelihood of occurrence. In the safety concept, developments outside the probable range of the repository are differentiated from less likely and unlikely developments. Release scenarios (design-based events) are considered for the less likely developments, while the unlikely developments serve to assess their impact and enhance the understanding of the system (Buhmann et al., 2008).

Following the proposed approach in Müller-Hoeppe and Krone (1999), the integrity assessment consists of two components. The requirements for hydraulic properties are derived from the long-term safety analysis (LZSA) and need to be demonstrated for geotechnical barriers. Together with the structural integrity evidence, they constitute the functional demonstration for the safety of geotechnical barriers (Buhmann et al., 2008).

The VSG Project (Preliminary Safety Analysis of the Gorleben Site) was a major scientific study undertaken to evaluate the long-term safety and feasibility of using the Gorleben salt dome as a repository for high-level radioactive waste in Germany. VSG integrated previous developments and research efforts, and provided a comprehensive overview. The methods developed in ISIBEL have been refined. Unlike the ISIBEL project, the updated safety requirements of the Federal Ministry for the Environment, Nature Conservation, and Nuclear Safety (BMU) from 2010 are available in the VSG and can be incorporated (BMU, 2010). This means that the theoretical considerations from previous projects have been transformed into directives by the responsible institution, and policy decisions have been made regarding open questions such as monitoring and the possibility of retrieval.

The VSG safety concept is based on the fundamental safety requirements:

- Integrity concept (continuity and barrier function of the engineered barrier system remain intact),
- Containment concept (rapid and tight containment of waste through salt rock and barriers), and
- Criticality exclusion.

14 objectives and 17 measures are derived to concretize these requirements. Some of them are directly linked to the EBS. From the safety concept, a verification concept is derived. The VSG verification concept demonstrates how compliance with limits and requirements can be quantitatively demonstrated under the measures mentioned in safety concept. It serves as the basis for all work within the system analysis in the project. The verification includes the following aspects:

1. Procedure for delineating the engineered barrier system.
2. Preservation of the engineered barrier system and its components during the verification period.
3. Criticality exclusion.
4. Containment of radioactive waste within the multi barrier system.
5. Radiological consequences/release scenarios.

The second point specifically addresses the verification of the engineered barrier system. The verification period continues until another barrier can demonstrably fulfill the safety function. During this period, the hydraulic resistance and structural integrity of the EBS must be maintained (Mönig et al., 2012). In this purpose, coupled analyses consider thermal, hydrological, mechanical, and chemical (THMC) processes and examine aspects such as crack limitation, stability, durability, integral permeability, and failure probability that was introduced as verification criteria in the project ISIBEL. Similar to the ISIBEL project, feasibility and robustness must be demonstrated (Mönig et al., 2012).

In the context of the VSG project, Müller-Hoeppe et al. (2012b) proposed a comprehensive design for the engineered barrier system (EBS) specifically tailored to the Gorleben site, which has been extensively studied. This design represents the first of its kind for a high-level radioactive waste repository in Germany. It has since served as a foundation for subsequent research and development, as well as a source of inspiration for EBS designs in other host rock formations. In a subsequent analysis by Müller-Hoeppe et al. (2012a), the proposed design was evaluated to ensure compliance with the safety and verification concept discussed earlier.

To achieve this, geochemical process modeling was employed to simulate dissolution and precipitation processes within the shaft sealing elements. This modeling considered the inflow of brine from the overburden and the resulting changes in solution composition throughout the entire sealing system. Geomechanical process modeling was also conducted to assess the mechanical loads on the sealing elements, including rock pressure and hydraulic pressure, to verify no damage would occur. Furthermore, hydraulic assessments were performed to determine the water flow through the sealing system and assess whether the permeability of the system met the required safety function of preventing contact between the waste and external water sources. Based on the results of the performance assessments, design modifications were implemented to finalize the layout of the sealing system.

Building on the pioneering work of Müller-Hoeppe et al. (2012b), the practical design of shaft seals was a focal point of the ELSA project. This project seeks to further advance the knowledge and implementation of shaft seals for repositories of high-level radioactive waste. The insights and findings from Müller-Hoeppe et al. (2012b) have provided valuable inspiration and guidance for the design considerations in the ELSA project. By incorporating the site-specific characteristics of different host rock formations, the project aimed to develop practical and effective designs for shaft seals that ensure the long-term safety and containment of radioactive waste. The focus was on existing and planned shaft seals in repositories located in clay and salt formations. Insights into the use of materials in geotechnical barriers were discussed, which can be applied to the shaft seals examined in this report and incorporated

into recommendations. Due to the requirements for sealing former mining shafts outlined in relevant standards, there is a greater wealth of experience in sealing shafts compared to drift seals (Kudla and al., 2020).

Within the ELSA project, a comprehensive analysis was conducted, providing a detailed description of shaft seal systems in various rock formations. This analysis encompassed an in-depth examination of rock mechanics properties, flow and transport processes, and the specific conditions present at each sealing location. It is crucial to consider that shaft seals serve as the primary geotechnical barriers, being the first point of contact for infiltrating solutions from the overlying strata or the shaft itself. As a result, the range of infiltrating solutions for which shaft seals need to be designed is relatively large compared to those encountered at drift seals. This distinction is significant as it directly influences the chemical environment experienced by the drift seals located within the repository, situated behind the shaft seal. Furthermore, it is noteworthy that the presence of geochemically unsaturated brine solutions at the barrier represents a key differentiation from the drift seals within the repository.

During the second phase of the ELSA project (ELSA II), significant advancements were made in the development and testing of functional elements for shaft seals. Extensive laboratory programs have been conducted to refine and evaluate the materials used in shaft seals. Field experiments have been carried out to assess the constructibility of shaft seals, including the backfilling of a mock-up shaft. Additionally, simulations have been performed to analyze the settlement stability of the gravel column in the shaft during seismic events. The results demonstrate that the expected settlement after a seismic event will be within the range of centimeters, indicating the effectiveness of the design in maintaining stability. These findings contribute to the overall improvement and reliability of shaft seals for repositories of high-level radioactive waste (Kudla and al., 2020).

The assessment of safety for underground closure structures in salt rock formations was also studied by Wagner (2005). Given the lack of practical experience in constructing long-term secure underground closure structures, this dissertation presents a semi-probabilistic approach to safety assessment.

For this purpose, distribution functions (deterministic value, normal or log-normal distribution) are defined for the influencing factors of different closure elements, and failure probabilities for individual elements (i.e., bentonite sealing elements, gravel columns) are calculated using these distributions. A deterministic model is established to represent the failure mechanism. Subsequently, input parameters for this model are linked to the stochastic models, and failure probabilities are calculated using the Monte Carlo method (Wagner, 2005).

Wagner also acknowledges the need for large sample sizes to determine small failure probabilities as a significant weakness of this method. However, considering the considerably improved computational power today, this statement needs to be reassessed. A maximum volume flow of Q = 10 m^3/year (Wagner, 2005) within a demonstration period of one million years is assumed as the limit state for the design. It is emphasized that the imprecise data basis and the difficulty of determining material properties for such long periods make it critical to evaluate the derived nominal values of failure probabilities (Wagner, 2005).

Wagner (2005) determines failure probabilities related to the service life for drift closure structures ranging from 10^{-4} and $6 \cdot 10^{-3}$. The failure probability can be interpreted as a mono-

tonically increasing function of time during the demonstration period, with failure occurring at a random point in time. Improving the results can be achieved through investigations of input parameters, their probabilities, and the arrangement of redundant elements. The calculated failure probabilities in the study can only describe the considered limit states, making the determination of these limit states a crucial task in the design process (Wagner, 2005).

Furthermore, Wagner (2005) notes that a rational determination of the limit value for failure probability is not straightforward. As demonstrated in the past, it is a politically made decision indirectly reflected in the safety requirements of the Federal Ministry for the Environment, Nature Conservation and Nuclear Safety (BMU) through the establishment of limit values. However, the linkage between failure probabilities and compliance with these limits or a limit risk remains the task of the safety case (Wagner, 2005).

Orzechowski (2018) presents an approach to reconcile requirements from existing standards with those related to long-term safety for a repository. The relevant standards are based on past experiences and consolidate established knowledge in a methodical and structured manner for practical application. However, the fundamentals for designing repositories significantly deviate from those of existing standards, making their direct transferability uncertain. Two crucial aspects are the extended demonstration period in a repository and the requirement for maintenance-free operation.

In the relevant standards, the demonstration period for typical structures is on the order of 100 years, during which failure can be reasonably excluded. When this period is extended without appropriately considering safety measures, the failure probability for structures increases to an unacceptable level Orzechowski (2018)[pp. 128, 131]. According to Orzechowski (2018), simply increasing the resistance values does not address this issue since it would exceed the magnitude of typical material properties. Furthermore, the problem is exacerbated by the impracticality of maintenance for the closures in the intended system, which rules out later inspections and repairs. Orzechowski (2018) concludes that the validity of the design with the principle of partial safety factors is questionable.

In Müller-Hoeppe et al. (2017), the assertion by Orzechowski (2018) is reassessed. Müller-Hoeppe et al. argue that if the potential values for the characteristics during the demonstration period are known, there is no basis for simply extrapolating the failure probability from the standards. Such extrapolation relies on a statistical distribution of values that cannot become arbitrarily large while the applicable laws of nature remain valid. This representation may be appropriate for continuous processes (e.g., corrosion) due to the varying deterministic components. However, this statement should be qualified when considering infrequent events (e.g., earthquakes) (Müller-Hoeppe et al., 2017).

Orzechowski (2018) also introduces a five-step methodology aimed at combining approaches from standards and long-term safety. In the first step, requirements from both schemes are initially considered separately. Then, conditions and specifications are derived from the FEPs relevant for the design in the chosen scenarios. In the second step, these conditions are compared and supplemented with the requirements from the standards. Subsequently, in step three, the actual planning process for the barrier is carried out. Step four involves comparing the properties with the requirements, leading to either confirmation of the construction or, through iteration, revising the structure or adjusting the basis for the requirements. The fifth step entails documenting the process.

In summary, the design of engineered barrier systems in salt geotechnical barriers has reached a mature state of development. However, designing geotechnical barriers for repositories in salt formations over a long period of time presents significant challenges and requires a reliable and well-documented demonstration of their safety.

Different approaches have been proposed to address these challenges. One approach, as suggested by Müller-Hoeppe and Krone (1999), is based on a semi-probabilistic philosophy that incorporates safety factors to account for the spatial and temporal variability of the materials used in the system.

Another approach, advocated by (Wagner, 2005), is a fully probabilistic method. While this approach provides a more comprehensive assessment of the failure probability and resilience level of the engineered barrier system, it requires a significant amount of computational effort.

The criticism raised by Orzechowski (2018) regarding the use of safety factors can be disregarded by carefully considering the underlying physical and chemical processes governing the degradation of the building materials. This consideration helps to better determine the necessary safety factors. Additionally, Orzechowski (2018) acknowledges the verification criteria proposed by Müller-Höppe in the ISIBEL project (Buhmann et al., 2008).

Overall, these different approaches and considerations contribute to the ongoing development and improvement of engineered barrier systems for repositories in salt formations. They will be further developed in the present report in a broader context of an engineered barrier system (EBS) centric view of the safety assessment of repositories in salt.

4. Overview of the methodology

Based on the international methodological standards, the evolution of HLW/SF repositories in salt formations must be analyzed in terms of a safety case, which means an assessment of the total system performance (IAEA, 2008). In the USA and Germany, site-specific concepts have been analyzed for salt domes (Gorleben site) and bedded salt formations–WIPP site and generic German sites (the KOSINA project, (Bollingerfehr et al., 2018)). Safety and safety demonstration concept for repositories in salt should take full credit of the favorable properties of salt formations. This concept is based on the safe containment of radioactive waste in a specific part of the host rock formation (the containment-providing rock zone – CRZ), which comprises the geological barrier and the EBS, including the backfill (crushed salt or run-of-mine salt). The long term safety of the mine excavations will be ensured by the crushed salt. Crushed salt acquires its sealing capacity through compaction, driven by the convergence of the host rock. Convergence rate increases with heat produced from radioactive decay and increases with higher humidity and the water content in the rock. After several thousand years, it is expected that the crushed salt will reach the same mechanical and hydraulic properties as undisturbed rock salt. Until this time, the EBS ensures the confinement of the disposed waste.

The methodology presented in this report was developed within the RANGERS project and serves as the base for the detailed integrity and performance assessment of the EBS. It summarizes the main aspects to consider during the design, the integrity assessment of the EBS, and the treatment of the EBS in the integrated total performance assessment. It comprises elements of the regulatory framework from which a safety concept is developed for a given geological site. This is the basis for the development of a repository concept and a sealing concept for the selected geological site. The evolution of the resulting repository system can be analyzed by utilizing a standardized FEP catalog that describes all features characterizing the system and all processes and events occurring during future evolution. The abstraction of the developed scenarios into modeling cases are the basis for the numerical based integrity assessment and performance assessment (Kuhlman et al., 2024).

4.1 VSG concept for integrity assessment

Maintaining the integrity of the repository system must be demonstrated for the reference scenario, the most probable evolution of the repository, as per EndlSiAnfV (2020). Less probable variant scenarios should be considered within the framework of the radiological long-term assessment, according to EndlSiAnfV (2020). Any alteration of the barrier effect must then be taken into account in the radiological consequence analysis. The proposed methodology extends this requirement to the integrity assessment of the repository system. This is because the analysis of alternative scenarios provides essential insights into the robustness of the repository system and can be used to optimize it (i.e., considering role of different safety functions). This has been already acknowledged in integrity analysis methodology adopted in the preliminary safety assessment of the Gorleben site (Beuth et al., 2012). This methodology formally comprises two parts:

- Integrity demonstration: The integrity analysis for the reference scenario.
- Integrity evaluation: The integrity analysis for less likely repository evolutions.

Figure 4.-1 illustrates a process diagram for the integrity analysis. In practice, the two parts of the integrity analysis are indistinguishable. They differ only in the consequences resulting from their analysis. The results of the integrity evaluation are further used in the analyses for the radiological long-term assessment and for determining the robustness of the repository system, while the results of the integrity demonstration analyses flow directly into the evaluation of whether the repository is meeting its ultimate objective of confining radioactive waste over the verification period. In the event that the integrity demonstration for the likely scenarios cannot be established, the safety requirements are not met. Then the repository concept and/or the site selection must be reexamined (Kock et al., 2012; Beuth et al., 2012).

The application of this approach in the proposed methodology allows a bifurcation in the process chain to assess the integrity of the EBS by examining in one branch the integrity demonstration for the reference scenario and in another branch, the integrity evaluation is carried out in closed interaction with the integrated performance and radiological assessment of the repository system. This step is carried out by means of comprehensive and specific numerical analyses of the behavior of the EBS under thermal-hydrological-mechanical and chemical (THMC) conditions. The link between the two types of assessment plays a key role in the optimization of the EBS.

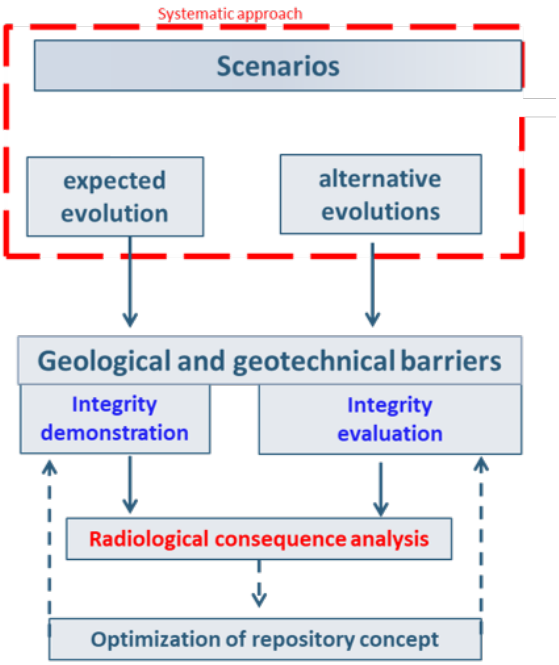

Figure 4.-1: VSG concept for integrity assessment of geological and geotechnical barriers extract from Beuth et al. (2012).

4.2 Methodology for integrity and performance assessment of the EBS

Figure 4.-2 gives an overview of the proposed methodology using the birfucation inspired by the VSG philosophy.

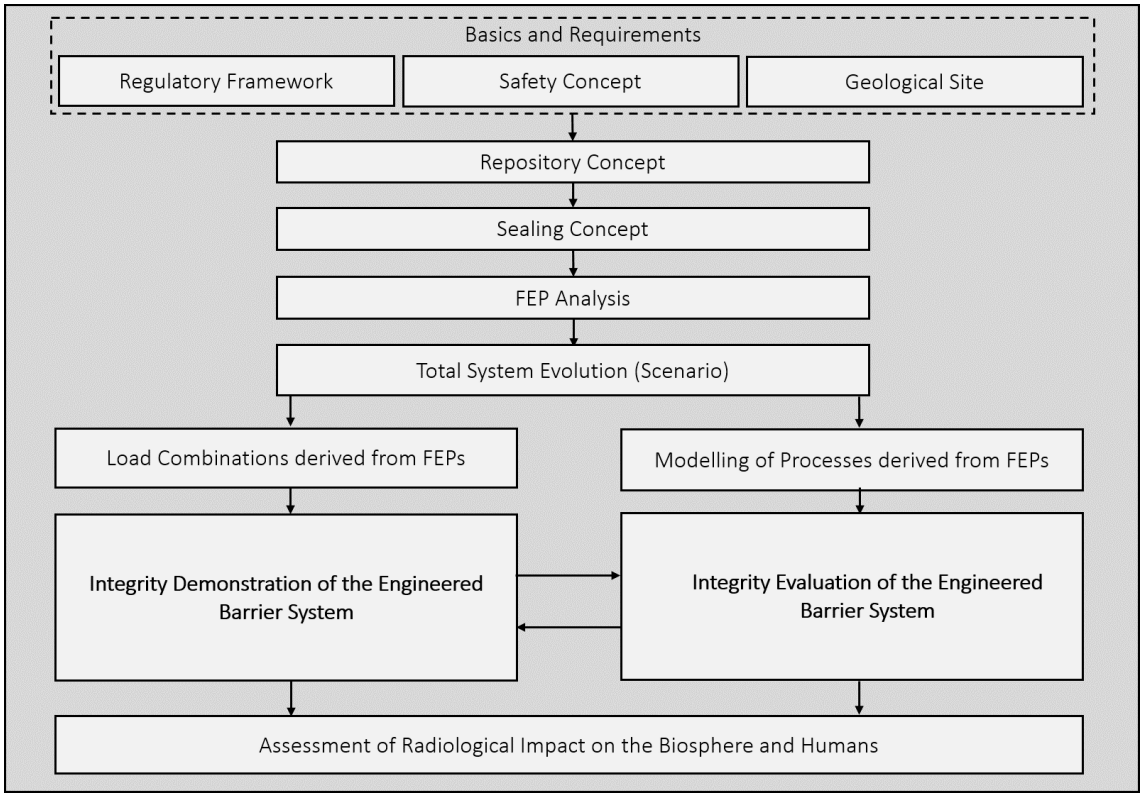

Figure 4.-2: RANGERS methodology diagram for the design, integrity and performance of the engineered barrier system (EBS) in a salt repository.

4.2.1 Basics and requirements

The methodology begins with the regulatory framework, which establishes the foundational requirements for constructing a repository. From this framework, a safety concept is developed, serving as the cornerstone for the design of the repository system, where radioactive waste will be securely confined. The safety concept articulates, through detailed explanations and structured arguments, how the interplay of natural conditions, engineered measures, and dynamic processes collectively ensures safety in the technical sense (Mönig et al., 2012). It embodies the overarching strategy to achieve the key objectives of concentration, isolation, and secure confinement of radioactive waste (BGE, 2022b).

The geological conditions at the site form critical boundary conditions for the repository and play a key role in defining the mine layout. The dimensions, thickness, and geomechanical properties of the rock formation directly influence the selection of the emplacement concept and the positioning of emplacement areas, access drifts, and other subsurface infrastructure such as utility and operational facilities.

4.2.2 Repository and sealing concept

The repository concept, as a technical component, is significantly influenced by the characteristics of the waste form and the selection of waste packages, as well as the corresponding emplacement method. Various emplacement concepts are available, including vertical or horizontal borehole disposal and drift disposal. Operational factors, such as whether shielded or unshielded waste packages are used, further impact this decision. Understanding the waste package design and the basic requirements for emplacement drifts or boreholes enables the precise selection of equipment and the design of drift geometry and lengths. A well-developed repository concept should also outline the necessary equipment and processes for excavation, emplacement, and other key operational activities.

The sealing concept encompasses the conceptual design of the geotechnical barriers or the Engineered Barrier System (EBS). It specifies the intended functions of these barriers and defines the timeframes over which these functions are required to ensure the safe containment of radioactive waste.

4.2.3 FEPs and scenario development

A comprehensive description of the repository system forms the foundation for conducting a robust long-term safety assessment. An internationally recognized tool for this purpose is the development of a Features, Events, and Processes (FEP) catalogue. The primary goal of the FEP catalogue is to characterize the initial state (features) of the repository system and to identify events and processes that may influence its future evolution. This tool not only fulfills the requirements for demonstrating long-term safety (e.g., through scenario development) but also enhances the clarity and traceability of evaluations, which are critical for gaining public acceptance.

The FEP catalogue outlines the key features that define the repository system, as well as the events and processes that are likely to occur during its future evolution. The interactions between features, events, and processes are systematically described in the form of scenarios. These scenarios are developed based on information from the FEP catalogue and are designed to account for uncertainties in predicting the repository system's future evolution.

Since future system evolution cannot be precisely predicted, a spectrum of potential future scenarios must be identified to address these uncertainties. FEPs within the catalogue are categorized according to their probability of occurrence. The combination of probable and expected FEPs forms the basis for an expected reference scenario, which represents the most likely evolution of the repository system. However, other potential evolutions cannot be excluded. For example, deviations in hydrochemistry could accelerate the corrosion of EBS components, potentially leading to the failure of one or more barriers.

Scenario development represents the next critical step in this process and will serve as the foundation for the integrated performance assessment of the repository system. By systematically identifying and categorizing FEPs and their interactions, the FEP catalogue ensures that the repository system is evaluated comprehensively, transparently, and in a manner that addresses both safety and public confidence.

To verify the performance of the Engineered Barrier System (EBS), it is crucial to identify the

processes that may impair its function during the evolution of the repository system and to evaluate its long-term integrity under expected future boundary conditions. The focus should be on identifying and assessing the most relevant processes occurring in the near-field of the barriers, where interactions are most critical. To achieve this, subsystem-specific FEP (Features, Events, and Processes) lists and scenarios must be developed and systematically evaluated. Additionally, it is essential to account for the interactions between the near-field and the far-field to fully understand the loads acting on the EBS.

Within the framework of a numerical-based safety demonstration concept, these subsystem-specific FEPs are aggregated into scenarios and translated into numerical models. These models allow for direct consideration of the specific processes and coupled phenomena associated with the FEPs. The more FEPs that are integrated into a numerical model, the closer the model will align with the realistic evolution of the repository system. However, due to the current technical limitations of numerical modeling tools, it is often necessary to use multiple models to adequately account for all FEPs and their interactions with the EBS.

This systematic approach ensures that the numerical simulations provide a robust basis for assessing the EBS's performance and verifying its ability to maintain its intended functions over the repository's operational and post-closure phases.

4.2.4 Integrity demonstration

The integrity demonstration of the EBS focuses on the sealing function and consists of several specific lines of evidence. It includes for sealing function the hydraulic resistances of the EBS, contact zone, and excavation disturbed zone (EDZ). Evaluation of the structural integrity of EBS includes the structural stability, crack limitation, deformation limitation, (if applicable) filtration stability, and chemical/ mineralogical long-term stability. Because the EBS is an engineered structure, the procedure for the design and integrity demonstration of the EBS can rely on adequate regulations or recommendations in engineering. In Germany, the EBS is seen as structures of civil engineering and their adequate design has to be verified by a technical functional proof in accordance with EUROCODE (national implementation by DIN-EN-1997-1 (DIN EN 1997, 2014), DIN-EN-1990 (DIN EN 1990, 2010)) (Müller-Hoeppe et al., 2012b,a). In the USA, the national engineering code requirements such as (ACI 318-14, 2014) for structural Concrete can be considered for the design of the EBS in compliance with other state specific regulations. The aim is to verify the required level of reliability of EBS construction.

The methodological approach bases on the concept of ultimate limit states in combination with the partial safety factor method. Therefore, the quantitative values of actions (i.e., impacts) or loads that may impair a structure's safety function are compared with the value of the structure-specific load resistances. With regard to construction integrity it is necessary that the load resistance is higher than the impacts. If the ultimate limit state is exceeded, the construction fails. For geotechnical barriers, ultimate limit states (e.g. cracking and deformation) can be described by crack limits (e.g., material specific fracture strength and dilatancy), deformation limits (e.g., volume and shear deformations) and tension limits (e.g., fluid pressure criterion).

The objective of the partial safety factor method is to cover uncertainties, for example, variations of representative values and modeling inaccuracies. For application of this method the values of the impacts or loads and the load resistances are multiplied by safety factors. The load resistances depend on construction material properties and the outline design of the

EBS. The load resistances and the ultimate limit states are specific for a selected EBS design.

The EBS will be dimensioned according to technical regulations although their functional lifetime exceeds the usual functional lifetime of conventional structures in civil engineering (50 to 100 y) significantly. In order to extend the verification far beyond the conventional time of the engineering structure, one can rely on materials with proven long-term stability that can be demonstrated by natural analogues. It is also important to take into account the corrosion and alteration of the geomaterials in the design and verification process. Therefore, the chemical/mineralogical long-term stability of the EBS in contact with corrosive infiltrating waters must also be shown.

In the same way hydraulic resistance of the EBS can be verified. For the integrity assessment, the contact zone to the surrounding rock as well as the excavation damaged zone have to be considered beside the constructed barrier itself.

4.2.5 Integrity evaluation

The integrity evaluation of the EBS focuses on the hydraulic evolution of the EBS for the alternative scenarios identified that affect the EBS. During this analysis, the EBS sealing function under altered conditions is analyzed and metrics can be derived from this analyses to optimize the EBS and to increase its robustness. For the integrity evaluation, no mechanical analyses are considered. This is the scope of the integrity demonstration. The integrity evaluation is intrinsically connected with the integrated performance assessment of the repository because the process involved in the alternative scenarios affect the radiological evolution of the repository system. Depending on the modeling approach, the integrity evaluation can be treated in the scope of the performance assessment of the repository system. These two assessments are therefore combined in the proposed methodology.

The integrity evaluation and performance assessment are intrinsically linked. While integrity demonstration focuses on meeting regulatory safety requirements, integrity evaluation provides insights into optimizing the EBS's robustness. This dual approach ensures that the repository system not only meets immediate safety standards but also remains resilient against uncertainties.

4.2.6 Summary

The methodology developed within the RANGERS project provides a framework for assessing the integrity and performance of the Engineered Barrier System, optimizing repository designs, and ensuring the long-term safety of high-level radioactive waste (HLW) disposal in salt repositories. It integrates key elements, including regulatory requirements, safety concepts, geological conditions, and repository design, into a cohesive approach for evaluating the performance of the EBS and its role in isolating radioactive waste. The components of the proposed methodology will be described in the following chapters.

5. Prerequisites

5.1 Regulatory framework

The national statutory and sub-statutory regulations establish the essential framework for the disposal of radioactive waste.

In Germany, these include, among others, the Atomic Energy Act (AtG 10), the Radiation Protection Ordinance (STV 08), and the Federal Mining Act (BBG 09) with its associated Federal Mining Ordinance (ABV 09) and especially the The StandAG, or Standortauswahlgesetz, which is the German law on the selection of repository sites for the disposal of radioactive waste (StandAG (2023)).

The StandAG (2023) empowers the Federal Ministry for the Environment, Nature Conservation and Nuclear Safety (BMUV) to establish safety requirements for final disposal (§ 26(3) StandAG) and requirements for conducting preliminary safety investigations (§ 27(6) StandAG) through regulations based on these safety principles. Based on these authorizations, the "Regulation on Safety Requirements and Preliminary Safety Investigations for the Final Disposal of High-Level Radioactive Waste" was published in October 2020. It includes the "Regulation on Safety Requirements for the Final Disposal of High-Level Radioactive Waste" (Endlagersicherheitsanforderungsverordnung – EndlSiAnfV) (EndlSiAnfV, 2020) and the regulation on requirements for conducting preliminary safety investigations in the site selection process for the final disposal of high-level radioactive waste (Regulation on Preliminary Safety Investigations for Final Disposal - EndlSiUntV)(EndlSiUntV, 2020) (BGE, 2022a).

Additionally, the relevant international recommendations from the International Commission on Radiological Protection (ICRP), the International Atomic Energy Agency (IAEA) (2011), and the OECD Nuclear Energy Agency (2004) must also be considered, especially in terms of providing supplementary or detailed guidance to the national regulations. The International Atomic Energy Agency (IAEA) (2011) has been formulated for all types of repositories, including near-surface ones. More specific requirements for a deep geological repository can be found in International Atomic Energy Agency (IAEA) (2006) (Mönig et al., 2012).

In the US, the safety standards and regulations play a crucial role in evaluating the safety of a conceptual geologic repository for high-level radioactive waste (HLW) and spent nuclear fuel (SNF) managed by the US Department of Energy (DOE). The specific regulations from the US Environmental Protection Agency (EPA) and the US Nuclear Regulatory Commission (NRC), namely 40 CFR 197 (U.S. Environmental Protection Agency, 2001) and 10 CFR 63 (U.S. Nuclear Regulatory Commission, 2001) for Yucca Mountain, are not applicable to a separate DOE HLW/SNF repository. However, the existing EPA and NRC regulations for geologic repositories still remain in effect, as outlined in 40 CFR 191 (U.S. Environmental Protection Agency, 1985) and 10 CFR 60 (U.S. Nuclear Regulatory Commission, 1983), which govern the disposal of high-level radioactive waste (MacKinnon et al., 2012).

Nevertheless, these existing regulations may be replaced for a future DOE HLW/SNF repository (they were developed almost 30 years ago), to enhance consistency with the more contemporary approach to regulating geologic repositories, which emphasizes a risk-informed, performance-based methodology in U.S. Nuclear Regulatory Commission (2004), similar to the site-specific regulations for Yucca Mountain. Despite the uncertainty surrounding specific

future safety standards, a robust safety case can still be constructed based on the existing standards (40 CFR 191 and 10 CFR 60) or on generic standards that incorporate internationally recognized dose or risk metrics important for establishing repository safety (MacKinnon et al., 2012) .

If the DOE decides to pursue the development of a deep geologic repository for DOE-managed HLW and SNF, additional requirements, such as those outlined in the National Environmental Policy Act (NEPA) (U.S. Congress, 1969) and 40 CFR 1500–1508 (Council on Environmental Quality, 1978), would need to be fulfilled. An Environmental Impact Statement (EIS) (US Department of Energy, 1980) mandated by NEPA for any future new repository in the Delaware Basin could potentially leverage the EIS prepared for the Waste Isolation Pilot Plant (WIPP) (U.S. Department of Energy (DOE), 1997) and the technical foundation established in the present study (MacKinnon et al., 2012).

Lastly, the WIPP Land Withdrawal Act, Public Law 102–579 (U.S. Congress, 1992) as amended by Public Law 104–201, Section 12 (U.S. Congress, 1996), prohibits the disposal of HLW or SNF at the WIPP site (only defense-generated transuranic waste is licensed for disposal at WIPP). However, the extensive presence of Salado bedded salts in the Delaware Basin of southeast New Mexico and western Texas suggests that much of the technical basis developed for the WIPP site could be applied to other potential salt repository sites in the same region (MacKinnon et al., 2012).

5.2 Safety concept

The safety concept describes, through verbal and argumentative means, how the combination of natural conditions, technical measures, and ongoing processes collectively contribute to achieving safety in the technical sense (Mönig et al., 2012). It reflects the fundamental strategy to achieve the goals of concentration, isolation, and secure confinement of radioactive waste (BGE, 2022b).

In Germany, the basis for the development of a safety concept within the framework of the licensing documents is anchored in the StandAG where the fundamental safety requirements are defined. It is given as:

- *The radioactive and other pollutants in the waste must be concentrated and securely contained within a confinement-providing rock zone or, in accordance with § 23 (1) in conjunction with (4), within these barriers mainly based on technical and geotechnical barriers, with the aim of keeping these substances away from the biosphere. For a period of one million years, it must be ensured, with regard to the protection of humans and, to the extent it concerns the long-term protection of human health, the environment, that exposures due to releases of radioactive substances from the repository are negligible compared to natural radiation exposure.*
- *It must be ensured that the impacts of final disposal on humans and the environment abroad are no greater than permissible in the country.*
- *It must be ensured that, during the operational phase, the possibility of retrieval of the emplaced waste exists, and that sufficient provisions are made for potential recovery of the waste for a period of 500 years after the intended closure of the repository.*

- *The repository must be designed and operated in such a way that no interventions or maintenance work are required for reliable long-term containment of the radioactive waste in the post-closure phase."*

The EndlSiAnfV elaborates on these fundamental requirements outlined in the StandAG and specifies the requirements for formulating a safety concept. Section § 10 of the EndlSiAnfV states:

- *(1) In a safety concept, it must be demonstrated how the objective of concentrating and securely containing the radioactive waste according to § 4 paragraph 1 is to be achieved. The entire repository system, including its construction, operation, decommissioning, and the assessment period, must be taken into account.*
- *(2) The expected developments of the repository system during the assessment period form the basis for the development of the safety concept. Deviating developments must be considered.*
- *(3) The safety concept must consider the results of the comprehensive preliminary safety investigation according to § 18 paragraph 1 sentence 2 of the Site Selection Act. In particular, changes compared to the preliminary safety concept based on the comprehensive preliminary safety investigation must be indicated and justified.*
- *(4) It must be demonstrated that the optimization of the safety concept according to § 12 paragraph 2 has been completed.*
- *(5) The safety concept must include a representation of all planned barriers of the repository system, in particular the essential barriers according to § 4 paragraph 3, their respective safety functions, and their interaction. The representation must also include a closure concept for sealing cavities that have been loaded with radioactive waste. It must be shown that the safety functions of the repository system and its barriers are insensitive to internal and external influences and disturbances, and that the behavior of the barriers is well predictable.*
- *(6) The safety concept must also include: 1. a schedule for the construction, operation, and decommissioning of the repository, demonstrating how the safety of the repository according to § 17 can be ensured and how the radioactive waste can be maintained in a safe condition, 2. a representation of the measures ensuring the retrievability of the emplaced radioactive waste until the start of decommissioning according to § 13, and 3. a representation of the provisions made to enable the recovery of the emplaced radioactive waste according to § 14.*
- *(7) The safety concept must take into account measures necessary until the completion of decommissioning, 1. to ensure the necessary protection of the repository from interference and other influences by third parties, and 2. for the monitoring of nuclear material.*

BGE (2022a) as the implementer in Germany summarizes the basic safety requirements for a repository system regulated in the StandAG and the EndlSiAnfV as follows:

- *The assessment period is one million years from the intended closure of the repository" (§ 3 (1) EndlSiAnfV).*
- *Future developments of the repository system and the geological situation at the repository site must be considered during the assessment period (§ 3 (2) EndlSiAnfV).*
- *The intended repository system must ensure the secure containment of radioactive waste passively and maintenance-free through a robust, tiered system of various barriers with different safety functions" (§ 4 (2) EndlSiAnfV).*
- *All underground cavities must be excavated in a geologically benign manner and subsequently closed in a way that preserves the relevant properties of the barriers necessary for the secure containment of radioactive waste (§ 9 (2) EndlSiAnfV), and they must be limited to an unavoidable extent (§ 11 (4) EndlSiAnfV).*
- *The preliminary safety investigations must comply with the state of science and technology (§ 27 (2) StandAG).*
- *The disposal casks emplaced in the repository must be retrievable until the start of decommissioning of the repository (§ 13 (1) EndlSiAnfV).*
- *Sufficient provisions must be made to enable the recovery of the emplaced repository packages during decommissioning and for a period of 500 years after the intended closure of the repository (§ 14 (1) EndlSiAnfV).*
- *Regarding operational safety, the operation must have been successfully tested in advance (§ 16 (1) EndlSiAnfV), and the relevant plant conditions for*

Furthermore, the following safety requirements exist regarding the achievement of the protection objectives of concentration and secure containment, as well as exposure. These requirements are to be examined based on criteria specified in the EndlSiAnfV and in the long-term safety analysis (BGE, 2022a):

- *Compliance with limits regarding the mass and quantity of substances released from the essential barriers of the repository system (§ 4(5) EndlSiAnfV).*
- *Demonstration of the integrity and robustness of the essential barriers, as well as the robustness of additional barriers (§§ 5 and 6 EndlSiAnfV).*
- *Estimation of radiation dose values throughout the assessment period (§ 7 EndlSiAnfV).*
- *Prevention of self-sustaining chain reactions (§ 8 EndlSiAnfV).*

In order to ensure compliance with the aforementioned safety requirements, it is necessary to formulate measures within the repository concept, sealing concept, and verification concept. Within the scope of the VSG project, various measures pertaining to the sealing concept have been developed. Although these measures were initially based on outdated safety requirements of the BMU (BMU, 2010), they remain partially valid for the new safety requirements of the EndlSiAnfV. These measures provide the framework for the development of the sealing concept and will be presented in the relevant section dedicated to the sealing concept.

5.3 Geological site

The geological conditions of the site form the primary constraints for the repository and the delineation of the mine layout. Both Germany and the United States are in the nascent phases of their site selection procedures (MacKinnon et al., 2012; BGE, 2022b), indicating that there is not a specific site or rock type under specific scrutiny that could guide the further elaboration of the repository concept. During the site selection phase, preliminary site explorations, encompassing deep drilling or mining excavation, will yield an array of technical data such as geological, hydrological, geochemical, geophysical, and thermal-mechanical data from the potential sites (MacKinnon et al., 2012; BGE, 2022b).

At this stage, one leans on prior research projects to comprehend the characteristics of the salt geological formations. From the available geological exploration data available in Germany, a representative overall geological situation with a synthesized sequence of layers was created for the generic considerations in the KOSINA project (Völkner et al., 2017a). This will serve to illustrate the proposed methodology.

5.3.1 Salt formations in USA

The main historical survey and nation-wide inventories of salt formations in the contiguous United States was conducted in the 1960s (Pierce and Rich, 1962) and 1970s (Johnson and Gonzales, 1978). These efforts started with high-level studies of the regions with bedded and domal salt formations at appropriate depths for a radioactive waste repository (Figure 5.-1). It was noted that salt deposits are "widely distributed" in 24 of the 50 states (Pierce and Rich, 1962).

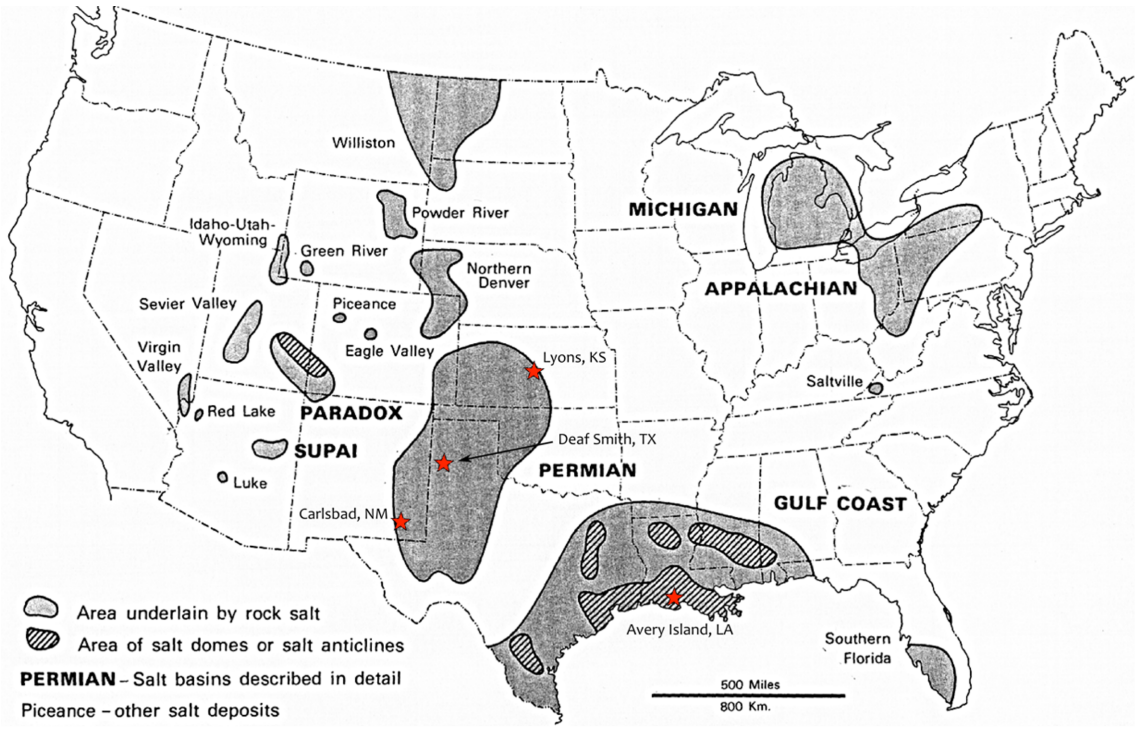

Figure 5.-1: Map of bedded and domal salt deposits in the United States. (Kuhlman et al., 2012; Johnson and Gonzales, 1978).

These studies were done in response to initial investigations by the US National Academy of Sciences into the concept of radioactive waste disposal that indicated disposal in salt formations would likely be feasible and would be worth pursuing further investigations (Hess et al., 2057; Lomenick, 1996).

There have been several more detailed historical investigations into locations for disposal in salt, including bedded and domal salt sites (see red stars in Figure 5.-1). The bedded salt of the Permian Basin underlies several states (New Mexico, Texas, Oklahoma, Colorado, and Kansas – Figure 5.-2), and has been the subject of three separate salt repository investigations (Kuhlman et al., 2012).

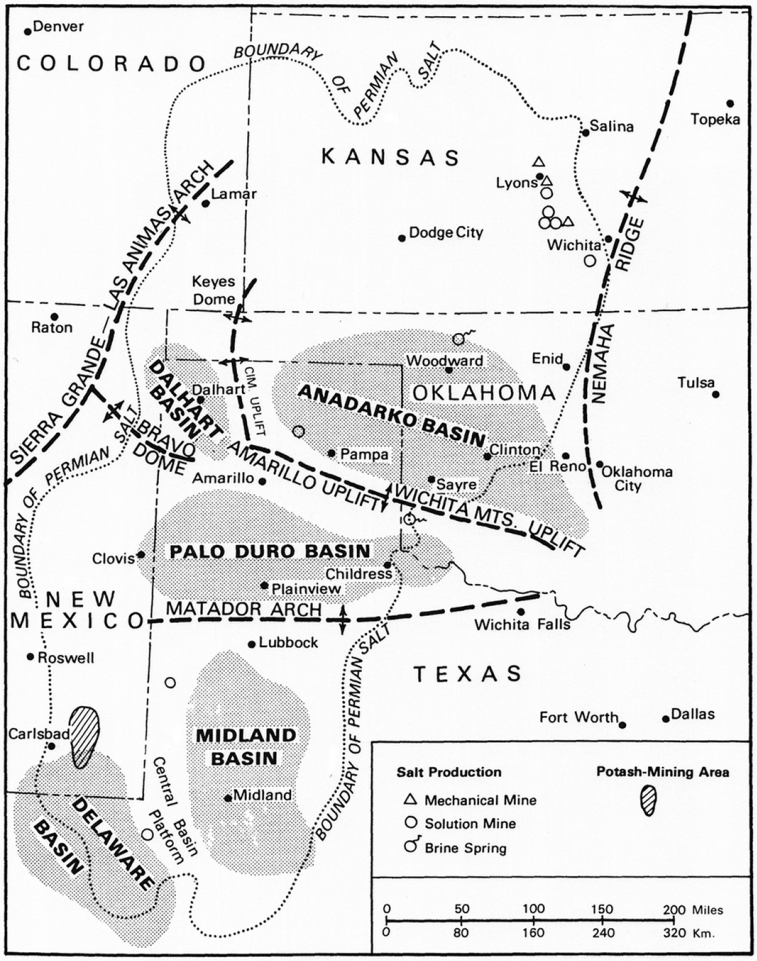

Figure 5.-2: Distribution of sub-basins within larger Permian Basin (Johnson and Gonzales, 1978).

In in the 1960s in Lyons Kansas (Figure 5.-2), Project Salt Vault (Bradshaw and McClain, 1971) utilized a bedded salt mine as an underground research laboratory, with the initial expectation that the facility could be used for disposal after the initial investigation. Due to local opposition to the project and unanswered questions about solution mining activities in the area, the investigation moved on to salt sites elsewhere (Lomenick, 1996).

By the mid-1970s, the site selection process then turned its focus to bedded salt of the Delaware basin (Figure 5.-2) in southeastern New Mexico (Kuhlman et al., 2012). After the ini-

tial site investigation into the Salado formation with boreholes in the late 1970s (Powers et al., 1978), the first excavations that would become WIPP began in the early 1980s (US Department of Energy, 1980). During construction, the licensing process was still being finalized, and the details of the exact mission for the WIPP site continued to change until the Land Withdrawal Act (U.S. Congress, 1992, 1996) (no spent fuel or high-level waste at WIPP, only defense-generated transuranic waste). After approval form the US EPA and New Mexico Environment Department (NMED), WIPP accepted its first shipment of transuranic waste in 1999.

A series of drif-scale thermal/mechanical demonstration experiments were conducted at WIPP (Matalucci, 1987) for a future salt-based site for heat-generating waste, which located in bedded salt of Palo Duro Basin (Figure 5.-2) in Deaf Smith County, Texas Office of Civilian Radioactive Waste Management (1988). This site was investigated from the surface through boreholes, but was abandoned by 1987 when Yucca Mountain was picked by law to be the final destination for high-level waste and spent fuel in the United States (Lomenick, 1996).

From the late 1970s into the 1980s, underground research laboratory experiments relevant to radioactive waste disposal were conducted in a mine at the salt dome at Avery Island, Louisiana (Van Sambeek et al., 1980; Kuhlman et al., 2012). This location was never seriously considered for disposal, but is characteristic of the numerous salt domes in the US Gulf Coast, which evolved in a manner characterized by Figure 5.-3.

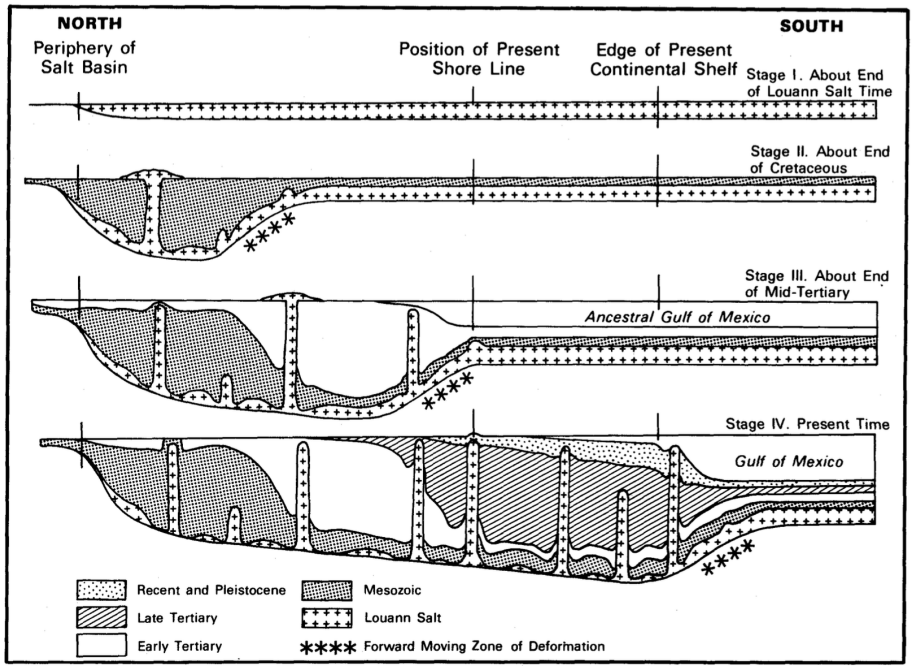

Figure 5.-3: Evolution of domal salt in the US Gulf Coast Johnson and Gonzales (1978).

Additional investigations were performed in other sedimentary basins (e.g., Michigan, Appalachian, and Williston basins – Figure 5.-1), but no significant site characterization activities were performed related to radioactive waste disposal (Lomenick, 1996). Other salt domes in the Gulf Coast and a salt anticline (i.e., Paradox Basin) were briefly investigated, but no significant site activities were conducted.

5.3.2 Salt formations in Germany

The enactment of the Site Selection Act (StandAG, 2023) in 2013 marked the restart of Germany's search for a suitable site for a high-level radioactive waste repository. In accordance with § 13 StandAG and the objectives outlined in § 1 (3) StandAG, the Federal Company for Radioactive Waste Disposal (BGE) is considering three potential host rock types: rock salt, claystone, and crystalline rock.

During the first step of Phase 1 in the site selection process, BGE identified sub-areas across Germany with favorable geological conditions for hosting a high-level waste repository within one of the three host rock types. This assessment resulted in 90 sub-areas, covering approximately 54% of Germany's land area.

In the second step of Phase 1, BGE is conducting representative preliminary safety analyses for each of these 90 sub-areas to evaluate and refine the selection of suitable regions for further exploration in Phases 2 and 3. As part of this phase, and in compliance with § 6 (4) EndlSiUntV (EndlSiUntV, 2020), a preliminary repository design is being developed. This design must define key aspects, including a description of essential barriers in accordance with § 4 (3) EndlSiAnfV (EndlSiAnfV, 2020), their fundamental characteristics, spatial extent, and other repository system components, such as potential sealing and backfill measures.

In this project, we do not consider Phase 1 of the Site Selection Act, as it is already being implemented by BGE. Instead, our focus is on providing insights that are more relevant for the later phases of the site selection process. Rather than concentrating on a specific site, we present a comprehensive overview of salt formations in Germany. From this analysis, we introduce a generic model, which serves as the basis for illustrating the proposed methodology within this project.

Salt formations are composed of sequences of sedimentary rocks that form through the repeated evaporation of water in ocean basins under arid climatic conditions. Initially, fine clastic sediments settled on the basin floor. As salinity increased, carbonates were deposited, followed by sulfates, and finally chlorides, which precipitated and accumulated at the bottom. The repetition of this cycle resulted in the formation of layered salt deposits, with combined thicknesses reaching up to several hundred meters (Figure 5.-4,a).

Due to the relatively low density of salt and its ability to deform plastically (creep), older and more mobile salt layers in some cases began migrating upward toward the surface. Concurrently, salt from surrounding areas moved laterally toward the center, resulting in thicker accumulations of salt with increased geological complexity, known as salt pillows (Figure 5.-4,b). This upward migration stretched and thinned the overlying sedimentary layers.

As uplift continued and the deposit evolved, the flanks of the salt became steeper, eventually rupturing the overlying sediment layers. This process culminated in the formation of salt domes (Figure 5.-4,c). These features often exhibit significant micro-folding within the salt layers, contributing to their complex geological structure.

In Germany, rock salt has been deposited in several sequences, forming distinct lithostratigraphic groups. From oldest to youngest, these groups are: Rotliegend, Zechstein, Röt, Muschelkalk, Keuper, Malm, and Tertiary. Among these, only the Zechstein-Salinar and, in

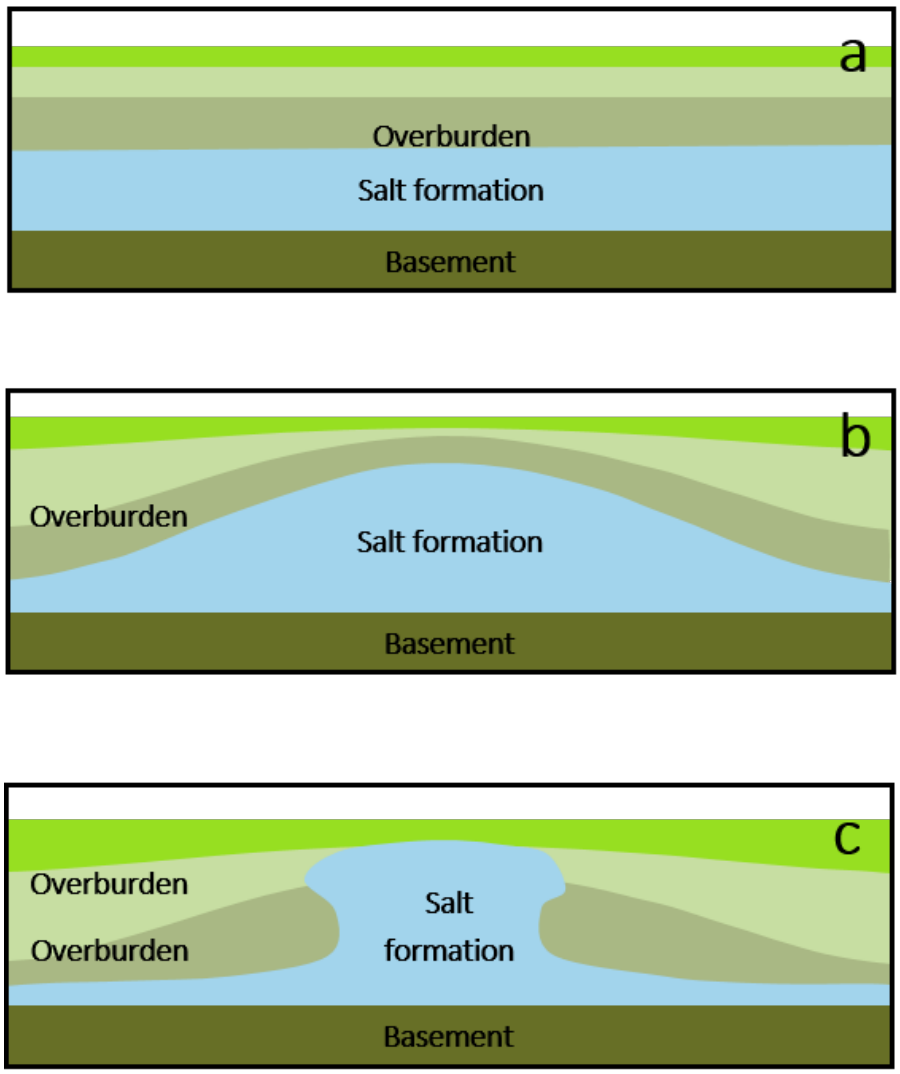

Figure 5.-4: a. Schematic diagram of a flat bedded salt after Völkner et al. (2017a), b. Schematic diagram of a salt pillow after Völkner et al. (2017a) and c. Schematic diagram of a salt dome after Klinge et al. (2007).

specific cases, the Malm-Salinar are considered potentially suitable for hosting a repository, based on regulatory requirements (Reinhold et al., 2014). The Malm-Salinar, consisting of interbedded salt, clay, and anhydrite layers, occurs in highly localized successions. This necessitates further investigation to define its boundaries before generic models can be developed (Reinhold et al., 2014).

The InSpEE project, which explored the distribution and geological properties of salt structures in Germany (von Goerne et al., 2016), highlighted that the genesis of pillow salt structures is primarily influenced by rock salt deposits from a single stratigraphic unit, such as the Zechstein. In rare cases, two evaporitic sequences of different ages may contribute to the formation of salt pillows, but in Germany, such structures typically occur at depths exceeding 2,000 meters below sea level (Gast and Riesenberg, 2016; Pollok et al., 2016). Consequently, the Zechstein-Salinar is the focus of this study and has been converted into a generic geological model.

The Zechstein-Salinar is stratified into seven formations, listed from bottom to top: Werra, Stassfurt, Leine, Aller, Ohre, Friesland, and Fulda. The Werra, Stassfurt, and Leine formations are generally the thickest, while the others accumulate only a few tens of meters in thickness. Each formation begins with basal fine clastic sedimentation, followed by carbonates and evaporites. The evaporite sequence follows the typical order of precipitation: from the bottom up, anhydrite, rock salt, potash, and magnesia salts. Local geological conditions cause significant variations in the thickness of each layer.

In the southern part of the former North German Basin, the base of the rock salt layers begins at depths of several hundred meters, reaching more than 5,000 meters at the basin's center. Favorable deposition zones for repository development are primarily located in the southern regions of the North German Basin. The most promising basins are shown in Figure 5.-5.

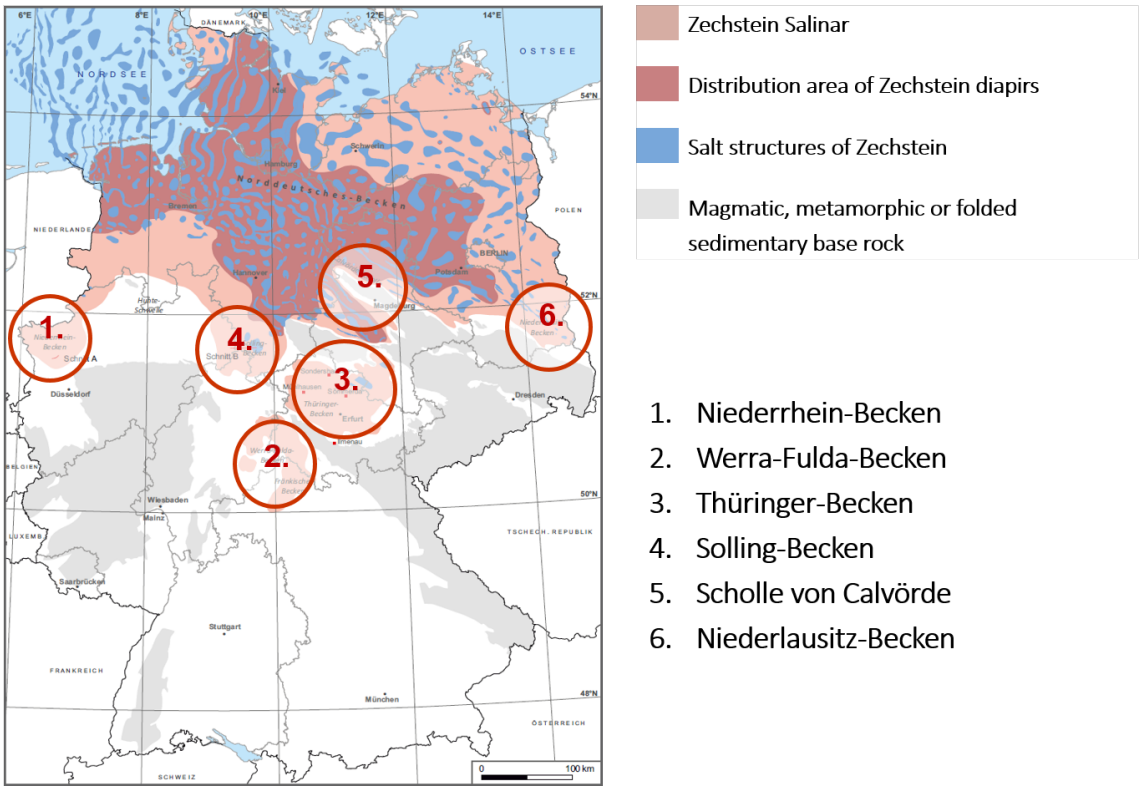

Figure 5.-5: Schematic distribution of Zechstein salt formations in Germany, modified after Reinhold et al. (2014).

5.3.3 Description of a generic salt pillow geological model

As Germany has not yet selected a specific geological site for final waste disposal, this case study uses a generalized dataset representing a salt pillow. This dataset captures the fundamental properties of the most promising basins for repository development. While the geological settings between individual sites in these regions vary, their shared deposition and formation processes enable their behavior to be described using a generic geological model. Such a model reflects the key characteristics of multiple potential sites, facilitating the application of standardized technical measures.

To create the generic geology, the real lithology of reference areas (Reinhold et al., 2014) was

used as the basis for deriving a synthetic sequence of layers for the Stassfurt (z2) and Leine (z3) formations within the Zechstein evaporites (Völkner et al., 2017a). Additional regional-geological information on the sedimentary sequence was incorporated to define the underlying rock layers and the overlying sediments above the Leine Formation (Bollingerfehr et al., 2018). Using this approach, a total of 18 regionally well-characterized lithostratigraphic units, abbreviated with lowercase letters and numbers, were defined.

To optimize computational efficiency for the generic 3D geological model, these 18 lithostratigraphic units were grouped based on similar geomechanical properties into 12 homogeneous zones, abbreviated with uppercase letters and numbers.

Figure 5.-6 illustrates the lithostratigraphic units and their corresponding homogeneous zones as derived from the KOSINA project (Bollingerfehr et al., 2018). These layers form the lithological structure of the salt pillow and serve as the foundation for the generic geological model used in this study.

Following, a literature review of homogeneous geological salt layers including appropriate constitutive models as well as thermal, mechanical and hydraulic parameters of geological homogeneous layers was conducted in KOSINA (Liu et al., 2017) to provide the model input data. Table 5.-1 summarizes material parameters used for the numerical model calculations for the bedded salt formations, the overburden and the basement rocks.

In the thermo-mechanical calculations, the lithostatic pressure gradient for all layers is set to 0.022 MN/m³ and the thermal conductivity for the salt formations excluding potash seam and main anhydrite is a parameter dependent on temperature (Bollingerfehr et al., 2018).

Table 5.-1: Model parameters of homogeneous zones after Liu et al. (2017)

Homogeneous zones	**Symbol**	ρ (kg/m^3)	λ (W/(m · K))	c_p (J/(kg · K))	α (1/K)	E (GPa)	ν (-)
Quaternary	Q	2000	2.3	950	$1.0{\cdot}10^{-5}$	0.1	0.33
Tertiary	T	2100	2.1	905	$1.0{\cdot}10^{-5}$	0.5	0.33
Bunter	S	2500	2.6	760	$1.0{\cdot}10^{-5}$	15	0.27
Aller rock salt	NA4	2235	5.2	860	$4.0{\cdot}10^{-5}$	25	0.27
Anhydritmittelsalz	AM3	2275	5.0	860	$3.5{\cdot}10^{-5}$	30	0.27
Potash seam Ronnenberg	K3	1850	1.5	903	$2.5{\cdot}10^{-5}$	16	0.26
Leine rock salt	NA3	2160	5.2	860	$4.0{\cdot}10^{-5}$	25	0.25
Main anhydrite	A3	2700	4.2	860	$1.6{\cdot}10^{-5}$	60	0.25
Potash seam Staßfurt	K2	1850	1.5	903	$2.5{\cdot}10^{-5}$	17	0.28
Staßfurt rock salt	NA2	2160	5.2	860	$4.0{\cdot}10^{-5}$	33	0.25
Anhydrite/carbonate	A2/C2	2700	4.2	860	$1.6{\cdot}10^{-5}$	30	0.27
Underlying red	R	2500	2.7	760	$1.0{\cdot}10^{-5}$	17	0.27

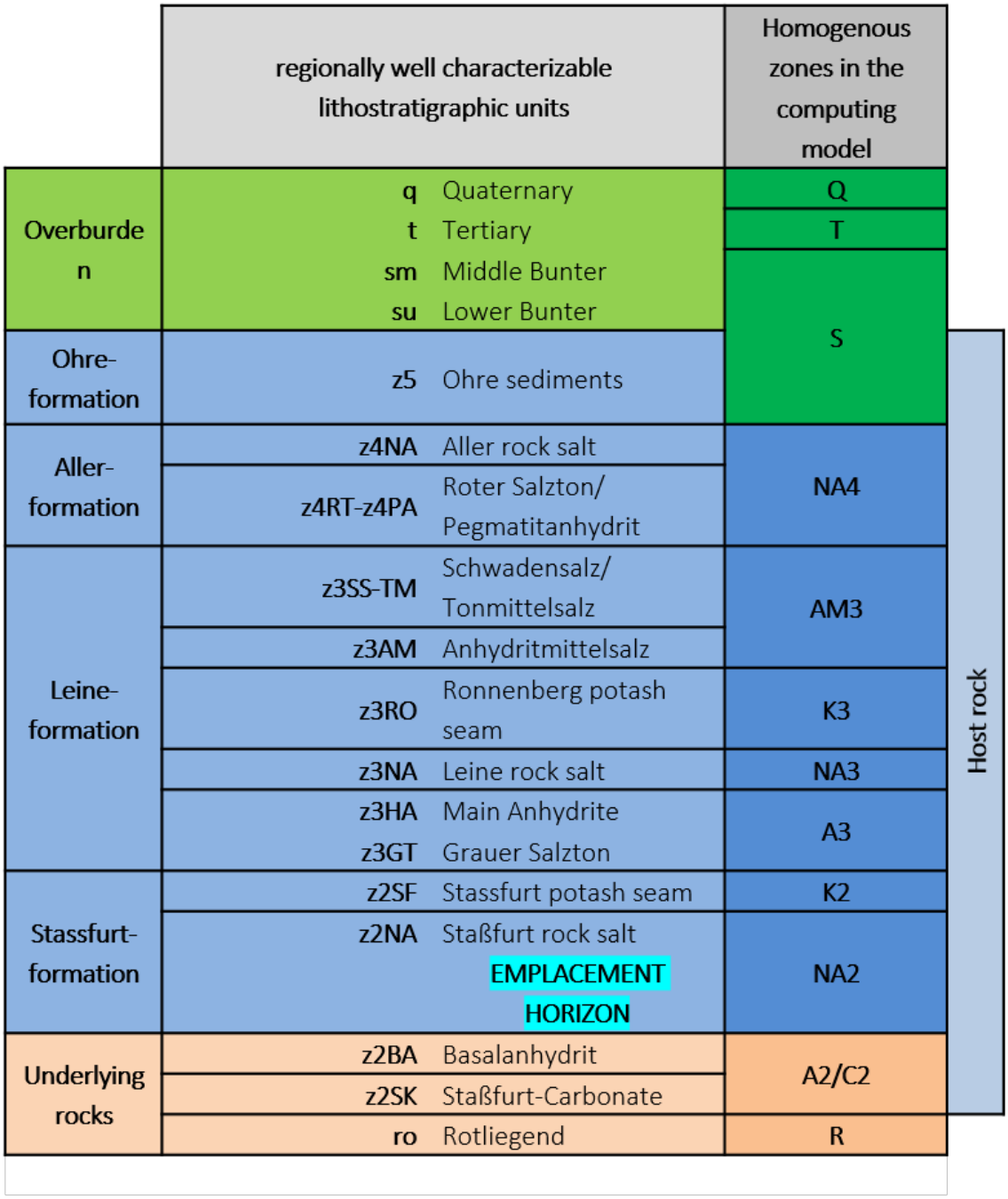

Figure 5.-6: Generalized standard profile of North German salt formation composed of well charactierizable lithostratigraphic units that are grouped to homogenous layers, after Bollingerfehr et al. (2018).

The generic geological model of the salt pillow from the KOSINA project is situated on the southern crest of the North German Basin. This region is geomorphologically shaped by ground and end moraines from the Elster and Saale glacial stages, with topography ranging between 45 and 75 meters above sea level (Völkner et al., 2017a). To represent a typical setting in this area, the previously defined 18 lithostratigraphic layers were assigned thicknesses as shown in Figure 5.-7, and the top of the Stassfurt rock salt was given a general dip of 5° to 7°. Using this information, a 12.5 km long reference profile (AA') oriented east-west, along

with three additional north-south profiles (BB', CC', and DD') approximately 10 km in length, were designed to intersect perpendicularly (Völkner et al., 2017a).

In these reference profiles, the upper boundary of the Stassfurt rock salt, identified as the potential repository host layer, lies at depths ranging from 460 to 1,045 meters below ground level (bgl). With a thickness of 150 to 600 meters, the lower boundary of the Stassfurt rock salt extends to depths of 670 to 1,220 meters bgl (see Table in Figure 5.-7). The greatest thickness of the salt pillow occurs at the intersection of profiles AA' and CC'.

Additionally, it is notable that at the crest of the pillow, the overburden layers have been eroded. Conversely, toward the ends of the profiles, the overburden thickness increases significantly (Völkner et al., 2017a). This variability highlights the geological complexity of the salt structure and its potential implications for repository design and implementation.

Lithostratigraphic units	Color in the model	Thickness in [m]	
		min	max
q		75	
t		90	
sm		0	270
su		5	300
z5		5	
z4NA		45	
z4RT-z4PA		5	
z3SS-TM		15	
z3AM		50	75
z3RO		18	
z3NA		25	165
z3HA		8	50
z3GT		5	
z2SF		17	30
z2NA		150	600
z2BA		15	
z2SK		35	
ro		100	

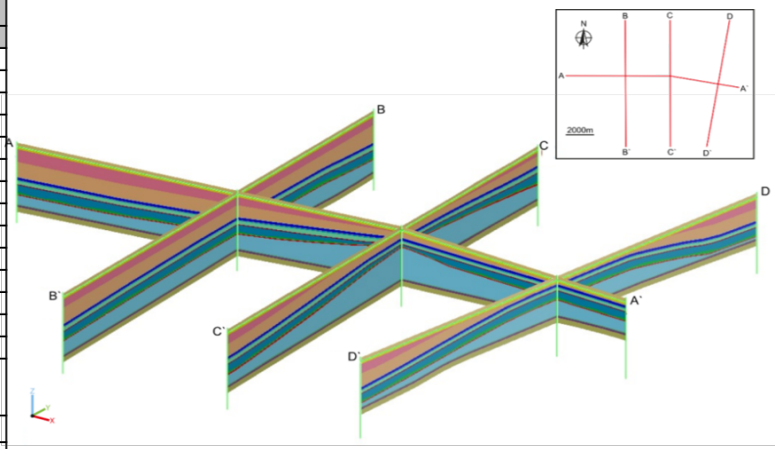

Figure 5.-7: Thickness of layers and generic geological profiles in the "salt pillow" model region.

The thickness of the cover rock, comprising the lithostratigraphic units Q, T, sm, and su, varies significantly across the model area. It ranges from approximately 800 meters in the west to around 140 meters in the east. The evaporitic host rock, consisting of the Stassfurt, Leine, Aller, and Ohre formations, reaches a thickness of over 800 meters at the center of the salt pillow.

No modeling of potentially existing cap rocks atop the salt was undertaken. Instead, the geological units overlying the z2NA layer in the center of the salt pillow are significantly thinned, with the Middle Bunter (sm) layer being nearly absent. However, away from the salt pillow, the sm unit thickens considerably, exceeding 300 meters at the western edge of the model area (Bollingerfehr et al., 2018).

Within the North German Basin, numerous fault zones are known to exist, with predominant orientations following NNE-SSW and WNW-ESE to NW-SE directions. However, the model does not incorporate fault tectonics or salinar tectonics (Baldschun et al., 2001). The characteristics of faults within the pre-saline horizons, as well as the fragmentation of the main anhydrite into blocks, are not included in the reference profile and are therefore excluded from

the 3D model derived from the profile (Bollingerfehr et al., 2018).

Table 5.-2: Vertical extension of the Staßfurt rock salt (z2NA) in the reference profile

Parameter	Min	Max
Depth of top	-390 m NN (460 m bgl.)	-975 m NN (1,045 m bgl.)
Depth of base	-600 m NN (670 m bgl.)	-1,150 m NN (1,220 m bgl.)
Thickness	150 m	600 m

The 3D-modeled area is defined by the length of profile AA' and the width determined by the intersecting profiles BB', CC', and DD'. Within this 3D model (see Figure 5.-8), the Stassfurt rock salt sequence, selected as the emplacement horizon, reaches a maximum thickness of 600 meters at its center. However, this thickness diminishes rapidly, decreasing to less than 300 meters toward the edges of the model and thinning further to below 100 meters in the northeast (NE) and southeast (SE) regions.

The base of the emplacement horizon (z2NA base) lies at a depth of approximately 600 meters below sea level (bsl) (about 670 meters below ground level (bgl)) in the east and deepens to over 1,200 meters bsl (more than 1,270 meters bgl) in the northwest (NW). Similarly, the depth of the top of the emplacement horizon (z2SF base) decreases westward, reaching over 1,000 meters bsl. In the center of the salt pillow, the top of the emplacement horizon lies at a shallower depth of less than 400 meters bsl.

In all figures, the dashed line marks areas where the thickness of the Stassfurt rock salt exceeds 300 meters, emphasizing zones with adequate thickness for potential repository emplacement.

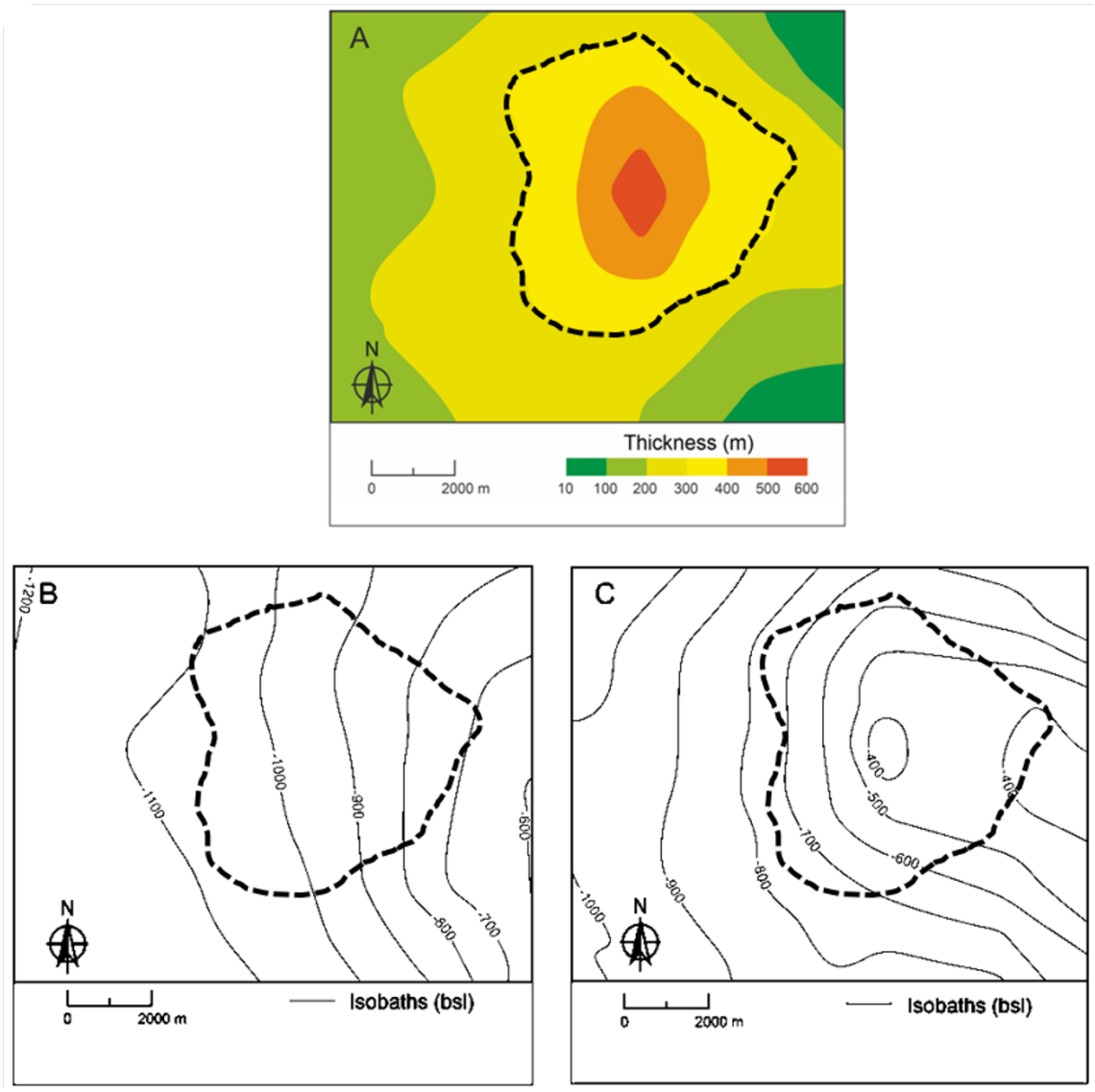

Figure 5.-8: Thickness (A) and depth maps for base (B) and top (C) of the z2NA model unit in the “salt pillow” model type (Bollingerfehr et al., 2018).

6. Repository concept

6.1 Regulatory requirements

In salt, a repository concept has to be developed in accordance with the safety concept and the safety requirements. The safety requirements to be fullfiled by the repository concept in Germany have been explicitely addressed in paragraph § 11 of the EndlSiAnfV. Those requirements are (EndlSiAnfV, 2020, p. 7–8):

- *The technical design of the final repository must be derived and optimized from the safety concept.*
- *It must be demonstrated that the optimization of the design of the final repository according to § 12 paragraph 2 of the EndlSiAnfV is complete.*
- [...] *all results from the exploration of the final repository site, particularly the geological findings from the underground exploration, including their uncertainties and their relevance for the safety and robustness of the final repository system, must be taken into account.*
- *The violation of the geological formation and the containment-providing rock zone (CRZ) with shafts, excavations or drillings, must be restricted to the unavoidable extent for the safe construction, safe operation, and safe closure of the final repository.*
- *For all intended technical components of the final repository, the conditions for safe operation must be documented, justified, and taken into account in the design of the final repository.*

§ 11 of the EndlSiAnfV also requires that the repository concept should include the definition of the essential barriers as per § 4 paragraph 3 of EndlSiAnfV. It should include the location and dimensions of the CRZ. Additionally, the definition of the further barriers of the final repository system, taking into account the final repository packages, emplacement technology, and emplacement geometry, should be defined. The positioning and technical execution of all underground cavities, particularly areas intended for the emplacement of final repository packages, as well as all surface accesses, should be clarified. The specifications of the installations and machines used for handling the final waste packages must be detailed. An emplacement concept, particularly the arrangement and handling and control of the final repository packages, should be developed. Measures to ensure the retrievability of already emplaced final repository packages and the decommissioning measures including the closure measures, should be planned and implemented.

Additionally, design requirements and technical measures have been defined that altogether will ensure compliance with the objectives of the safety concept. The following requirements are related to the site selection procedure (StandAG, 2023):

- The construction of the repository will be done in a stable geologic region with characteristics that are well predictable for the demonstration period, e.g. no active fracture zones, no relevant seismic activity, very low salt diapirism and resulting subrosion.

- The disposal fields will be located at a depth that excludes any natural impairment of the CRZ from the surface, e.g. erosion of glacial channels. So, for northern Germany, a depth between 600 m and 800 m below sea level has been pursued.
- The thickness of the CRZ has to be 100 m at minimum.
- Due to the extremely low permeability of the undisturbed salt rock there is no relevant groundwater flow. Therefore the mass transport of radionuclides by advection will be comparable to that by diffusion.

For mine construction / operation the following requirements are defined:

- The mine workings of the repository are completely surrounded by host rock.
- The construction of disposal fields will be in a well-characterized salt formation with very low humidity and high plasticity (high creeping rates).
- The void volume to be excavated for the mine will be minimized, and excavation will be done by techniques that disturb the rock as little as possible.
- Loaded disposal fields will be backfilled and abandoned (operation in retreating mode).
- The halite layers of the salt formations have favorable properties to meet the containment function.

The halite layers have a very low permeability so that slow diffusion is the dominating process of mass transport and advection is of little relevance. Salt plasticity will seal any impairment of the rock due to mechanical impacts. Humidity in halite is very low. In the host rock surrounding the disposal areas, a CRZ will be defined that will not be affected by any impacts from the surface (e.g. ice ages) or evolutions of geosphere (e.g. fracture zones).

Several of the technical measures have the safety function to seal the unavoidable perforation of the geologic barrier rapidly and effectively. The long-term goal is to restore the host rock's integrity and to avoid evolutions that result in an impairment of the CRZ. In detail, the following technical measures are included:

- Shaft seals, drift seals, borehole seals, and buffer: To comply with their safety function, these barriers have a low integral permeability, which minimizes an advective solution flow. The integrity of these barriers has to be demonstrated for 50,000 years. For this period the development of hydrochemistry can be predicted (no glacial induced changes of hydrochemistry) and the compaction of the crushed salt backfill in the mine excavations has been completed.
- Backfill: The safety functions of the backfill comprise the stabilization of the excavations and the limitation of fluid flow. Backfilling will be done with crushed salt, that reaches similar mechanical and hydraulic properties like the surrounding salt formation after completion of compaction.
- Temperature limit: Temperature limits have been defined to avoid an alteration of the spent fuel elements and the glass matrix of the vitrified reprocessing waste and – in

combination with safety distances – the degradation of carnallite layers with low thermal stability

- Disposal Canisters: The disposal canisters will be designed to be retrievable during the operation period and to be manageable for 500 years after repository closure and they will be loaded in such a way that criticality can be excluded.

A penetration of the geologic barrier is inevitable during mine construction and will result in its local impairment. In the long term, creep processes promoted by the plastic properties of the salt host rock will lead to the closure of such mine openings. Thus, in the long term, the original properties of the geologic barrier will be restored. To overcome this period, engineered high-performance shaft and drift seals will be constructed, which will provide the required sealing immediately after installation. To guarantee the long-term sealing in the excavated part of the formation, the mine workings will be backfilled with crushed salt that is stable in the long term. Over time, the properties of this backfill will become similar to the surrounding host rock.

6.2 Repository concept development

6.2.1 Considered geological site – Determination of the available space

The geology surrounding a nuclear waste repository must provide conditions that ensure both safe operation and secure long-term containment. To distinguish clearly inadequate conditions from those that are potentially suitable, the StandAG (StandAG, 2023) outlines specific preconditions for nuclear waste repositories in Germany. According to these regulations, a site is classified as geologically unsuitable and excluded if it fails to meet any of the defined exclusion criteria. Additionally, a set of minimum requirements is used to evaluate and weigh the overall suitability of a site.

The requirements define the necessary characteristics of the geological space around the repository and include qualitative criteria outlined in the preliminary safety analysis of the Gorleben site (Mönig et al., 2012), which were further quantified in the KOSINA project (Bollingerfehr et al., 2018). These criteria can be summarized as follows (see Figure 6.-1):

1. The depth of the repository has to be between 500 m (600 m according to the safety concept) and 1,000 m below ground level.

2. The minimum distance between drifts or cavities to top and bottom of the rock salt layer is 50 m. The rock salt layer therefore needs to be thicker than 100 m.

3. There has to be a 500 m lateral safety pillar around the repository.

4. A minimum distance of 300 m between disposal rooms and shafts must be observed.

In order to determine the available space for a repository within the considered geology, the safety distances are applied. Based on the boundary positions the respective criteria separate the suitable from the unsuitable areas within the rock salt formation. Only those areas are considered for a repository layout that satisfy all requirements:

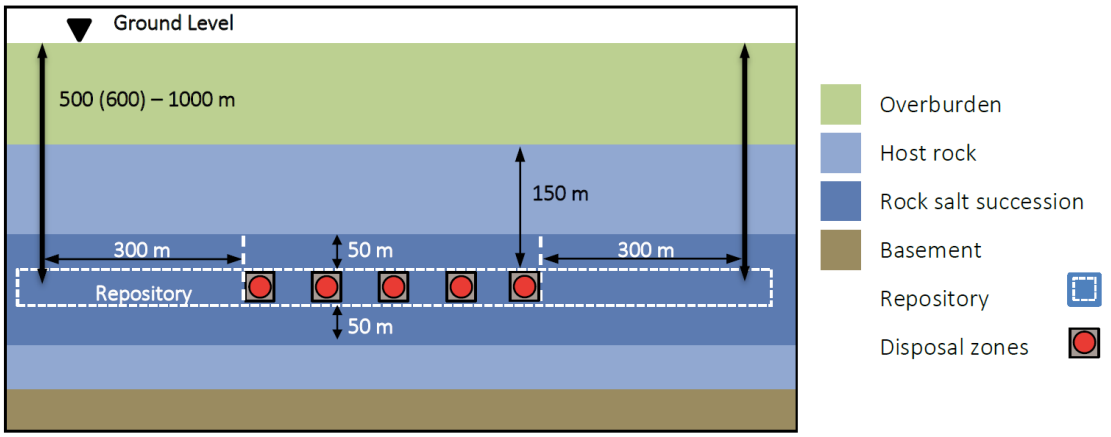

Figure 6.-1: Safety distances of the sample repository in rock salt.

1. The generic geology offers a rock salt thickness of more than 100 m over the whole map section except the far southeast and northeast corner. Therefore the layer offers enough distance for the repository towards the upper and lower boundary of the rock salt.
2. As the covering evaporites have more than 150 m thickness in total, this criterion does not affect the suitability of the rock salt layer.
3. The minimum depth of 600 m below ground limits the position of the repository in the central and eastern part to a little extent, while the maximum depth of 1,000 m affects the western part.

Figures 6.-2 and 6.-3 illustrate the simplified geological formation of the study area. The safety boundaries delineate the rock salt zone into unsuitable areas that fail to meet the defined limits (indicated in blue) and suitable areas that comply with the requirements (highlighted in yellow). The dashed line represents the intersection of the two profiles.

With a north-south and east-west extent exceeding 8 kilometers each, and a vertical range of more than 300 meters, the available space within the rock salt zone offers significant potential to host a repository. This zone can accommodate a variety of repository sizes, configurations, and depths. Consequently, this 3D body serves as the geological basis for the repository design.

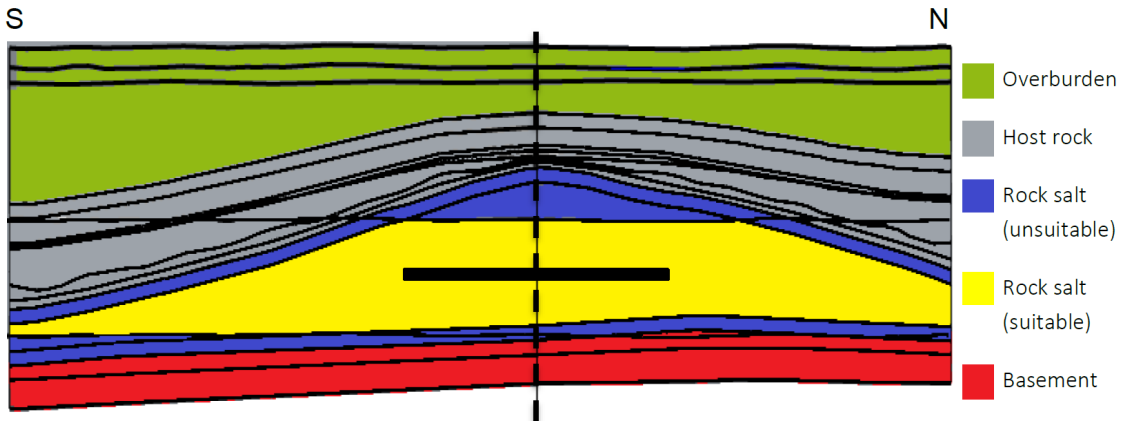

Figure 6.-2: South-north cross-section near profile C-C' with simplified geology, restricted by safety distances for a repository (3x superelevated).

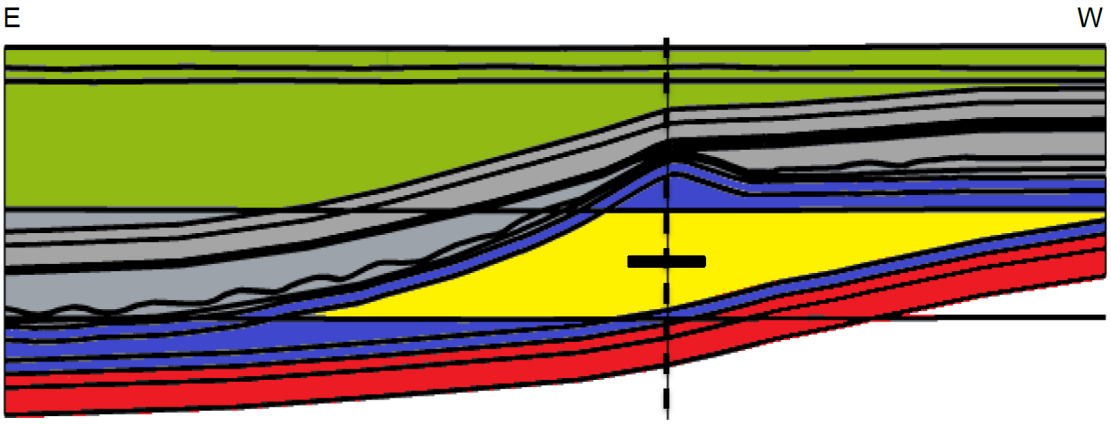

Figure 6.-3: East-west cross-section near profile A-A' with simplified geology, restricted by safety distances for a repository (3x superelevated).

6.2.2 Repository design

HLW and SNF repositories must ensure long-term safety while maintaining operational safety during their construction and use. The design of the underground structures requires a careful balance between geological conditions, technical feasibility, and regulatory requirements. To achieve an optimal design, the process involves multiple iterative design cycles, where feedback from each cycle informs subsequent refinements.

The repository design is driven by the available space within the geological setting and the defined nuclear inventory. The stepwise approach first determines the geometry of individual excavations and organizes them into patterns that are specifically tailored to the geological conditions. Initially, one or more repository concepts are developed, and casks are selected accordingly for the various types of nuclear waste. Following this, the technical tasks are outlined, beginning with the handling of individual casks (how they will be transported, emplaced, or retrieved) and extending to considerations of necessary equipment and ventilation systems. These tasks ultimately define the geometry of the drifts. The entire process is illustrated in Figure 6.-4.

To ensure the stability of drift contours and the pillars between them, geomechanical design is essential. Simultaneously, thermal design optimizes the spacing between casks, and, if needed, increases the distance between drifts to manage heat output. By allowing sufficient space around critical areas, the repository design not only enhances passive safety but also facilitates the installation of the engineered barrier system (EBS).

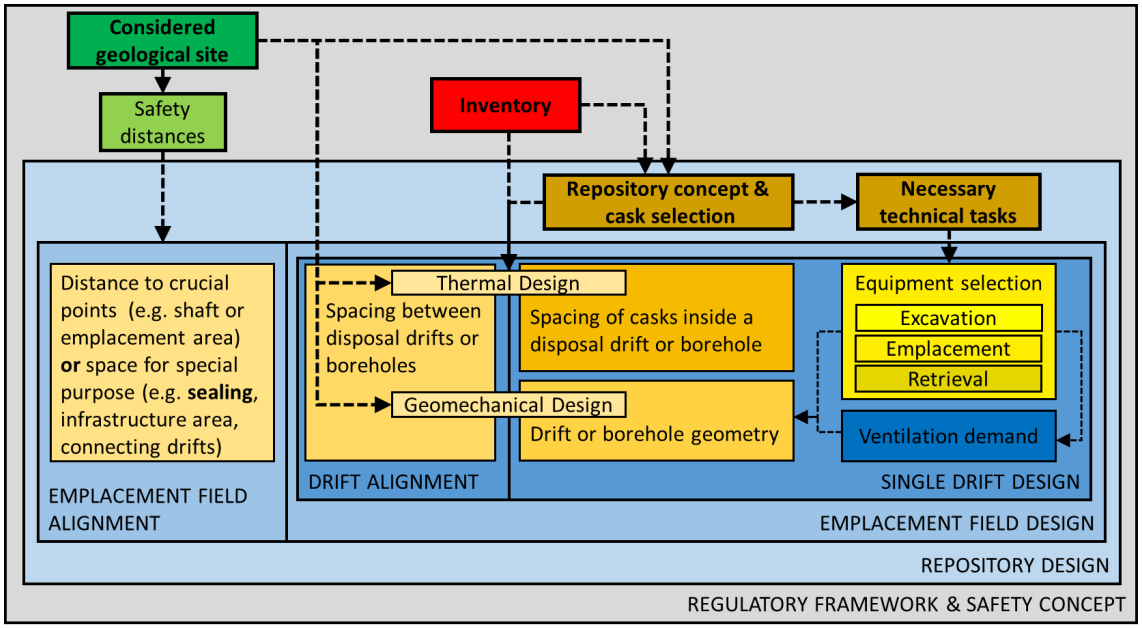

Figure 6.-4: Concept of the repository design within the legal framework.

The design is then used to plan geotechnical barriers, to verify their integrity considering different scenarios based on FEP analysis and finally to simulate radionuclide migration. If these assessments are successful, the layout can be considered as the final one.

The repository concept considers the disposal of self-shielded casks in horizontal emplacement drifts (ED) in one level only. These emplacement drifts that are later backfilled with crushed salt are allowed to reach a maximum temperature of 200 °C. To take advantage of the salt pillow's thickness the repository is vertically centered in the suitable rock salt zone at a depth of approximately 750 m bgl. The sublevel structure is composed of the northern and southern emplacement wing and a central infrastructure area that hosts two vertical shafts. Each wing represents an emplacement area with multiple emplacement fields each containing a number of emplacement drifts. The straight drifts and cross-cuts intersect at a 90° angle. Additional radii are planned for the transportation of casks via rail-based transport system.

Two shafts serve as dedicated fresh air intake and exhaust pathways, ensuring adequate ventilation while minimizing the disruption of the natural barriers. This design approach maintains the integrity of the geological layers, balancing operational needs with the preservation of the repository's natural isolation properties.

The infrastructure area and the emplacement drift are separated by at least 300 m of undisturbed rock salt. In order to minimize the quantity of access drifts only one drift leaves the infrastructure area to the west and one to the east. These split after about 100 m towards north and south. Each of these straight access drifts to the emplacement wings reserves a length of 500 m for the construction of drift seals in addition to the first 100 m. To ease the

installation of the EBS these access drifts are inclined according to the allowed parameters of the transportation system. The shafts are located at the thickest part of the salt pillow to ensure that the longest natural barrier of rock salt can be used for sealing. Finally a lateral safety pillar of 500 m is applied (Figure 6.-5).

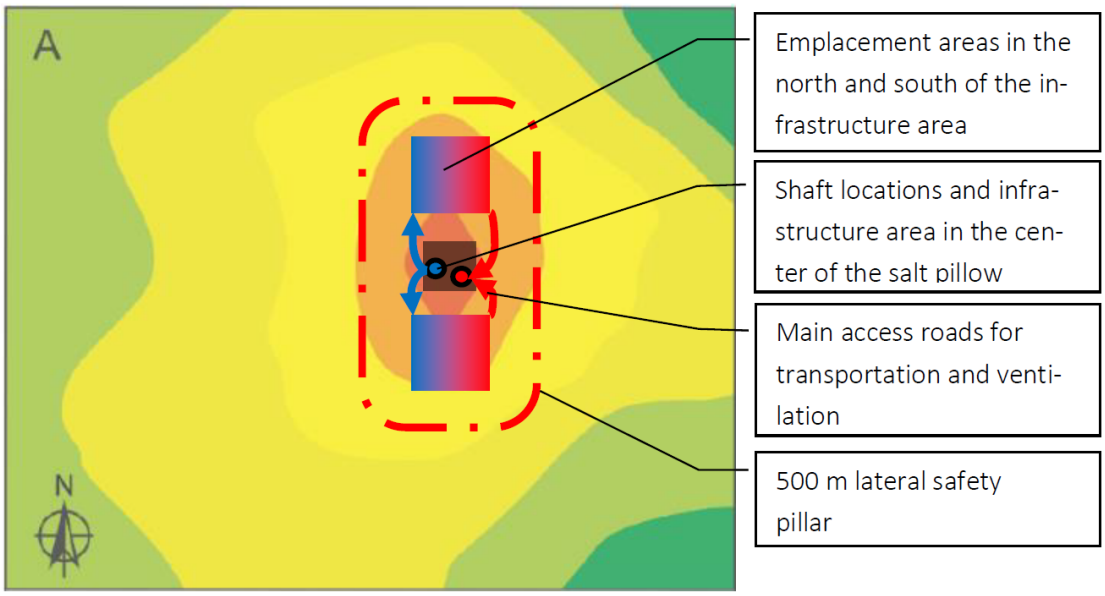

Figure 6.-5: Elements of the repository concept within the selected geological site.

The HLW/SNF inventory of Germany consists of different types and quantities of waste. There are SNF from pressurized water reactors (PWR), boiling water reactors (BWR) as well as from pressurized water reactors of the Russian type (VVER). Additionally there are three types of waste from reprocessing (CSD), structural parts from dismantling the SNF cells as well as SNF from prototype and test reactors. According to the safety and repository concept these need to be separately packed into different types of self-shielded casks. Table 6.-1 summarizes the radioactive waste inventory in Germany. The heat generating waste from SNF will be packed in a total of 2,120 POLLUX-10 casks. During packing the structural parts will be separated and loaded into 2,620 MOSAIK casks of type II. The different types of waste CSD-V, -B and -C coming from reprocessing will be loaded into a total of 887 POLLUX®-9 casks. Spent nuclear fuel from prototype and nuclear test reactors will be disposed of in different types of CASTOR casks which are specially made for each type of waste. These sum up to a total of 530 casks (Bollingerfehr et al., 2018). The selected casks provide enough shielding to handle them without additional transportation cover.

6.2.3 Thermo-mechanical design of the repository

This section describes the optimization of the repository by means of thermal-mechanical computations. The objective is to optimize the spacing between the casks in disposal drifts and between the drifts within the salt formation by maintaining a design temperature of no more than 200 °C at the cask surface.

Table 6.-1: Summarized German nuclear inventory after Bollingerfehr et al. (2018)

Type of Waste	Quantity	Type of cask	Quantity
SNF	10,445 ton heavy metal	POLLUX®-10	2120
CSD-V	3,729 coquilles	POLLUX®-9	415
CSD-B & C	4,244 coquilles	POLLUX®-9	472
Structural Parts	Depending on SNF	MOSAIK® (Type II)	2620
SNF from prototype and nuclear test reactors	905,767 ball fuel elements + 2,536 fuel elements	CASTOR® THTR/AVR/KNK	461
	1,359 fuel elements + 16 fuel rods	CASTOR® MTR2	69

Repository layout

The thermal design and optimization of space requirements are based on a schematic concept of the underground layout of the repository. This concept influences the thermal design and the calculation method for determining space requirements. The repository layout was previously described. It consists of an infrastructure area, where two shafts provide access to the surface, connects to the disposal area through two main drifts. These main drifts run parallel to each other and are interconnected at regular intervals by crosscuts. From these crosscuts, the disposal drifts branch off, which are parallel to each other and to the main drifts. The disposal drifts are blind, meaning they only have one access point from the crosscut. In the disposal drifts, the waste containers are placed on the floor.

Waste packages

The drift disposal concept for salt formations draws significantly from the comprehensive insights obtained from the preliminary safety analysis at the Gorleben site, as detailed by (Bollingerfehr et al., 2013). This analysis not only explored the feasibility of waste emplacement in drifts but also contributed to the foundational knowledge in this domain. Furthermore, the advancement in emplacement technology for the final disposal of POLLUX® casks, as documented by Engelmann et al. (1995), continues to stand as contribution to the state of the art in drift disposal methodologies and techniques.

In this concept, spent fuels and reprocessed waste are package in POLLUX® casks. The remaining waste type such as waste from prototype, research and experimental reactors are packaged in various CASTOR® casks. For the thermal design, only the heat generating waste in POLLUX® casks are considered. Minimal spacings based on mining and pillow stability requirements are considered for the disposal of the CASTOR® casks.

Figure 6.-6 illustrates the temporal evolution of the thermal output of different types of fuel elements in a loading configuration equivalent to that of PWR fuel elements. The mixed loading, comprising 89% UO2 and 11% MOX, conservatively covers the heat release from the UO_2 fuel elements used in BWR (Boiling Water Reactor) and VVER (Water-Water Energetic Reactor) reactors. The thermal output for pure MOX fuel element loadings is compared in the figure.

Additionally, Figure 6.-6 presents the thermal power of reprocessed waste. It exhibits a decay

behavior distinct from that of the fuel elements. The heat output of such wastes remains at the level of the UO_2 fuel elements initially, then declines more significantly after 50 years post-reprocessing.

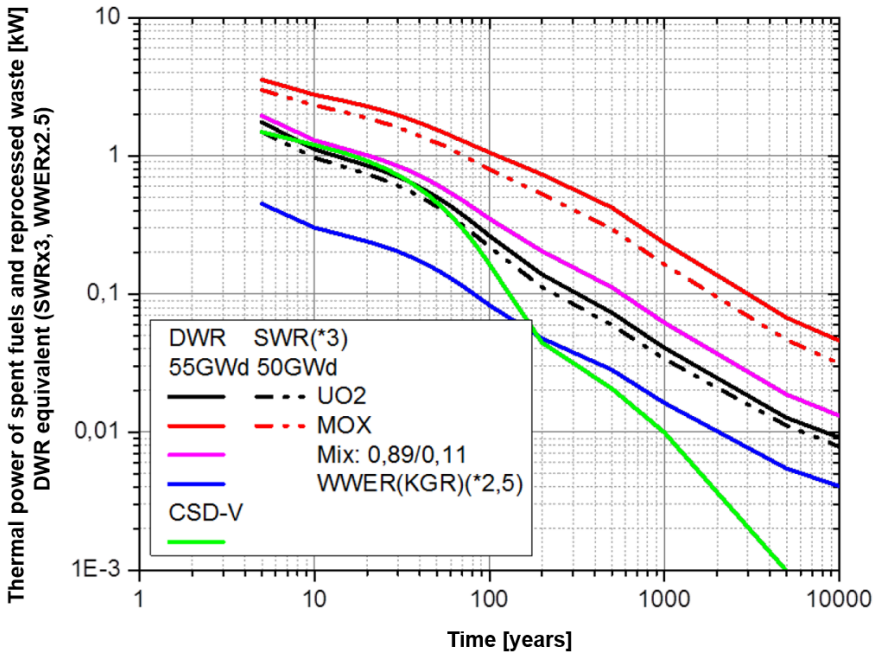

Figure 6.-6: Heat power of different heat generating radioactive waste.

The POLLUX® cask was specifically designed and engineered for final disposal in salt formations. For this study, it is assumed that POLLUX® casks can accurately approximate future final disposal containers for drift disposal in rock salt in all relevant characteristics, ensuring that using this type of container does not introduce a significant error in determining the space requirements for disposal variants.

The POLLUX® container consists of an inner and an outer container, see Figure 6.-7. The inner container is made of fine-grain structural steel (material 1.6210) and is hermetically sealed with a screwed primary lid and a welded secondary lid. The interior is divided into several chambers, each of which can accommodate a fuel rod assembly with fuel rods from two PWR assemblies or six BWR assemblies. By adjusting the interior, the storage of CSD molds is conceptually possible. Figure 6.-7 illustratively shows a POLLUX® container with withdrawn fuel rods from ten PWR assemblies (POLLUX®-10). The external shielding container, like the primary and secondary lids, is made of ductile cast iron (material 0.7040). This shielding container is not required to be leak-tight and is closed with a screwed lid. In the shell, rods of polyethylene are inserted in radially distributed bores to reduce neutron dose rates. The structural design and material selection of the container ensure the fundamental requirements for retrievability during the operational phase. Regarding the requirement of handle-ability of the container up to 500 years (retrievability), no corresponding studies have been conducted yet. The container underlying this analysis has a length of 5.517 meters and a diameter of 1.56 meters (Bollingerfehr et al., 2013).

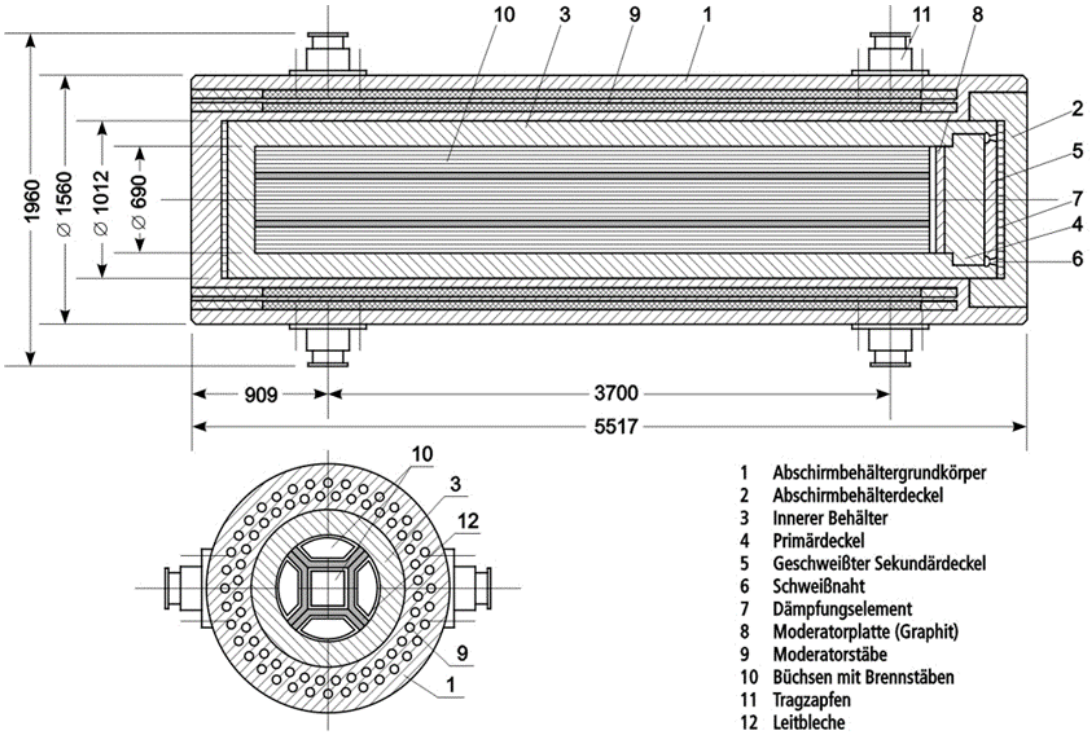

Figure 6.-7: Schematic illustration of a POLLUX® cask (Bollingerfehr et al., 2013).

Numerical modeling

The design temperature for disposal in rock salt was set at 200 °C on the outer surface of the final disposal container, aligning with the limit temperature established in previous projects Bollingerfehr et al. (2013, 2018). Thermal design calculations are conducted for this temperature, varying the casks and drift spacings within a parameterized calculation model. This model, representing the repository, needs to illustrate thermal superpositions and the resulting temperature increases. Such representation can be achieved by considering thermal symmetry boundary conditions as a quarter model of a cask embedded in a partial model of the rock formation, allowing the simulation of a horizontally extensive disposal field with a grid based on cask and drift distances. In this model, the distance from the drift axis to the model boundary in the transverse direction of the drift equals half the drift distance, and the distance from the cask's end face to the model boundary in the drift direction equals half the cask distance. The resulting thermal superpositions are conservative and only occur in storage fields with very long storage drifts and a large number of such drifts. This modeling approach has the advantage of not requiring the entire repository to be modeled, reducing time and numerical effort. The calculation model is depicted in Figure 6.-8, showing a drift filled with crushed salt in a salt formation where a final disposal cask is stored. The cask in the model comprises two components: an outer casing for shielding against radioactive radiation and a container basket holding the high-level radioactive wastes, acting as a heat source in the model.

For this analysis, models were created for disposal depth of 810 m below the ground level.

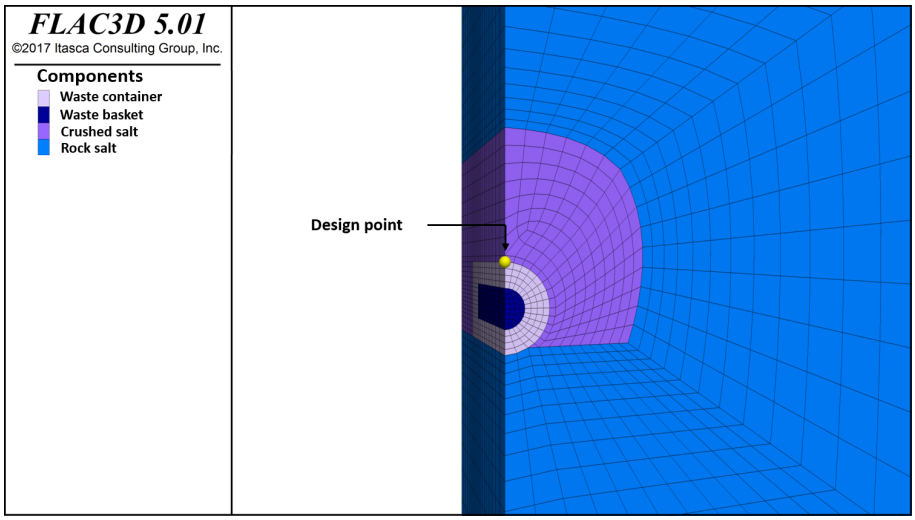

Figure 6.-8: Numerical model for the thermo-mechanical design of disposal drifts with heat generating waste.

Table 6.-2 summarizes the material areas used in the model to simulate thermal propagation in the near field - rock salt. The crushed salt considered in the calculation model is compacted over time under the influence of lithostatic stresses, changing its thermal properties, particularly its thermal conductivity. The mechanical material model of the crushed salt capturing this compaction behavior and its material parameters are detailed in Bollingerfehr et al. (2013). The compaction of the crushed salt, dictated by the material properties of the rock salt, exhibits a viscosity-dependent deformation behavior influenced by stress and temperature, hence time-dependent. The material model used for rock salt is also described in Bollingerfehr et al. (2013).

Table 6.-2: Density and thermal parameters of the components in the near field of the disposal drift (η: porosity, T: temperature)

Components	**Density (kg/m³)**	**Heat Capacity (J/kg K)**	**Thermal Conductivity (W/m K)**
Container	7000	515	15
Container basket	7000	500	20
Crushed salt	f(η) : 1430 – 2200	f(η) : 562 – 864	f(η) : 5.4 – 0.7
Rock salt	2200	864	f(T) : 5.4 – 4.2

The computations was carried out thermo-mechanically with FLAC3D in the version 5 (Itasca Consulting Group, Inc., 2021).

Modeling results

The thermal design is conducted by varying the spacing between the drifts. The spacing between the casks was set to a constant value of 3 meters allowing to dispose the maximum amount of casks in a single drift. The drift spacing was varied in increments of five meters. For the design, the loading of the casks with ten fuel elements was considered based on the experience gained from previous projects. The temperature evolution curves for different spacing at the design point are depicted in Figure 6.-9.

The temperature evolution at the design point of a cask in the central area of a disposal field, loaded with PWR mixed fuel elements based on their thermal output, is characterized by up to three peaks. The first peak is reached immediately after storage and is due to the thermal-mechanical behavior of crushed salt. Right after emplacement, the crushed salt acts as an insulator due to its initially low thermal conductivity, leading to the formation of the first temperature peak. This peak is influenced by the load and the distance between the casks. Subsequently, as the thermal conductivity of crushed salt increases due to compaction, the temperature drops. Whether a second peak, a plateau, or a mildly increasing or decreasing region forms around 50 years depends on the geometric configuration. Another temperature peak forms after about 400 years due to thermal superposition effects. Depending on the geometric setup, different peaks may be significant for the design. The temperature progression in a disposal field where VVER fuel elements are emplaced shows similar behavior as the PWR fields. The thermal outputs of PWR mixed and VVER fuel elements have approximately the same rate of change.

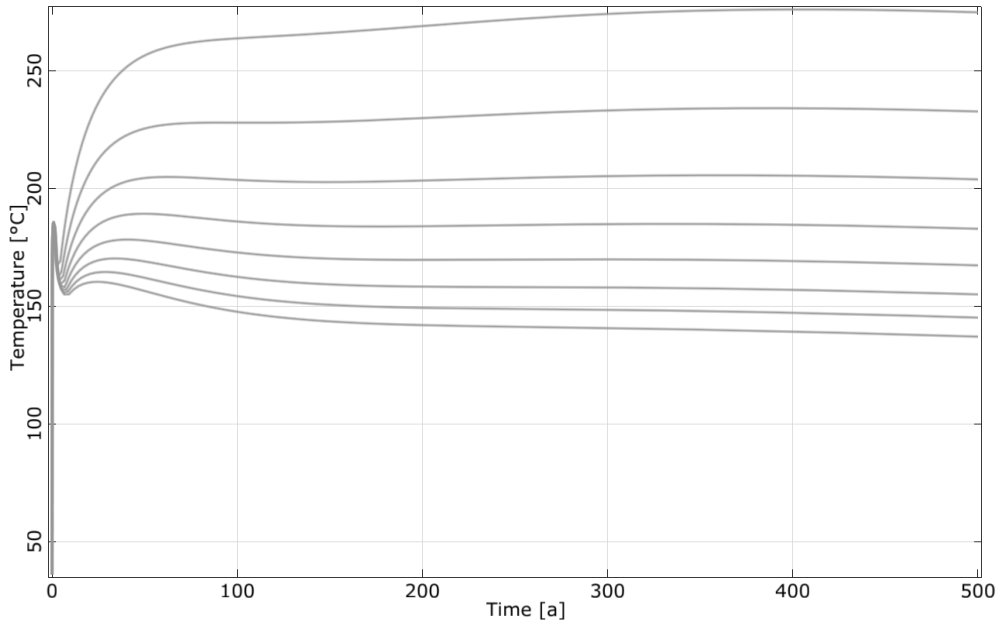

Figure 6.-9: Temperature evolution at the design point of a POLLUX® cask with PWR spent fuels.

The temperature peaks from Figure 6.-9 were plotted in Figure 6.-10 as a function of the drift spacing, identifiable by the support points. In Figure 6.-10, it results that a spacing of about 37.5 m and higher is necessary to meet the temperature limit of 200℃ at the cask surface. Thus the spacing of 37.5 m is assumed for the planning of disposal fields emplaced with PWR spent fuels. The same spacing is conservatively assumed for VVER emplacement fields as the thermal output of this waste type is similar to that of PWR but with a lower amplitude.

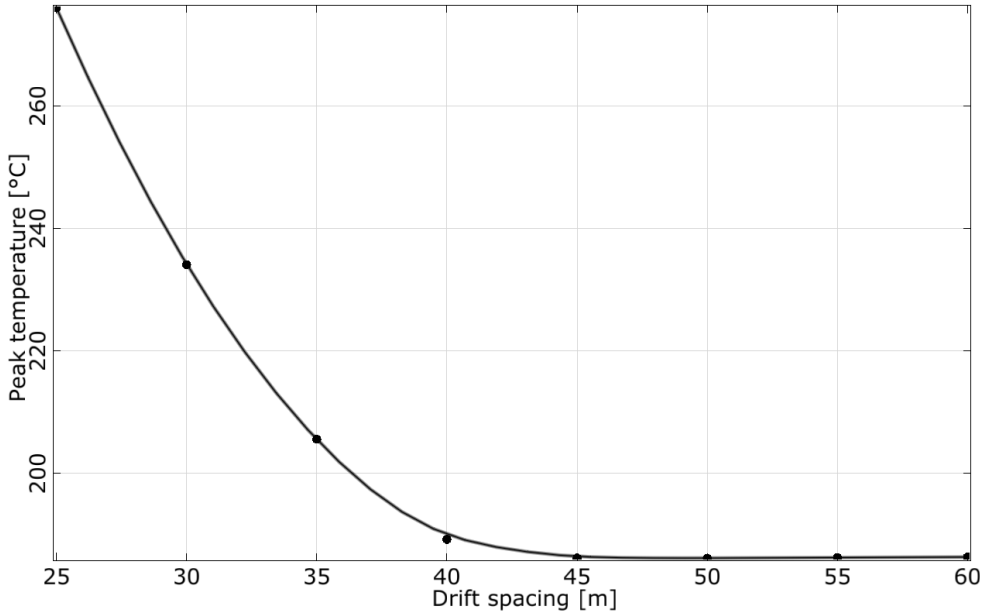

Figure 6.-10: Temperature peak as a function of the drift spacing for POLLUX® cask with PWR spent fuels.

The thermal design for the CSD-V emplacement field is carried out analogously to the spent fuel with a cask spacing of 3 meters and a cask loaded with a maximum of 9 CSD-V canisters.The temperature evolution curves for different spacings at the design point are depicted in Figure 6.-11. The design calculations for disposal areas with CSD-V are performed similarly to those for areas with fuel elements. The characteristic temperature progression for CSD-V, marked by two temperature peaks, is due to a more significant drop in its thermal power curve, as shown in Figure 6.-6. A first temperature peak forms immediately after storage due to the previously mentioned thermal-mechanical behavior of crushed salt. The second temperature peak is reached around 40 years after storage. Depending on the container load and geometric configuration, either the first or the second temperature peak may be critical. Instead of a second peak, a slightly declining temperature plateau may also form.

The thermal design for the CSD-V emplacement field is carried out analogously to the spent fuel with a cask spacing of 3 meters and a cask loaded with a maximum of 9 CSD-V canisters. Thus, only the drift spacing was optimized. The temperature peaks from Figure 6.-11 were plotted in Figure 6.-12 as a function of the drift spacing, identifiable by the support points. In Figure 6.-12, it results that a spacing of about 15 m and higher is necessary to meet the temperature limit of 200℃ at the cask surface. Thus the spacing of 15 m is assumed for the planning of disposal fields emplaced with CSD-V reprocessed waste.

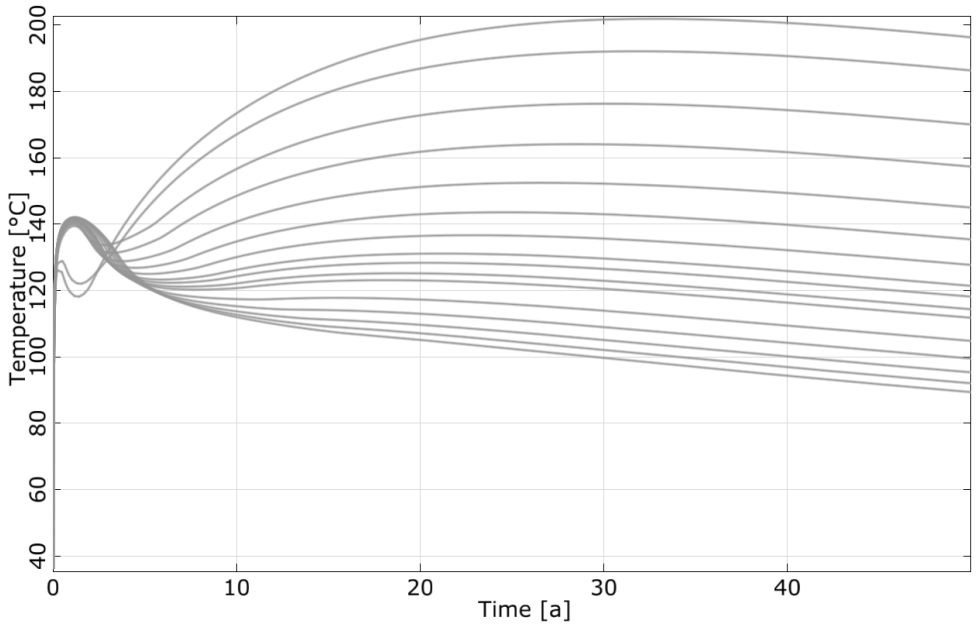

Figure 6.-11: Temperature evolution at the design point of a POLLUX® cask with CSD-V waste.

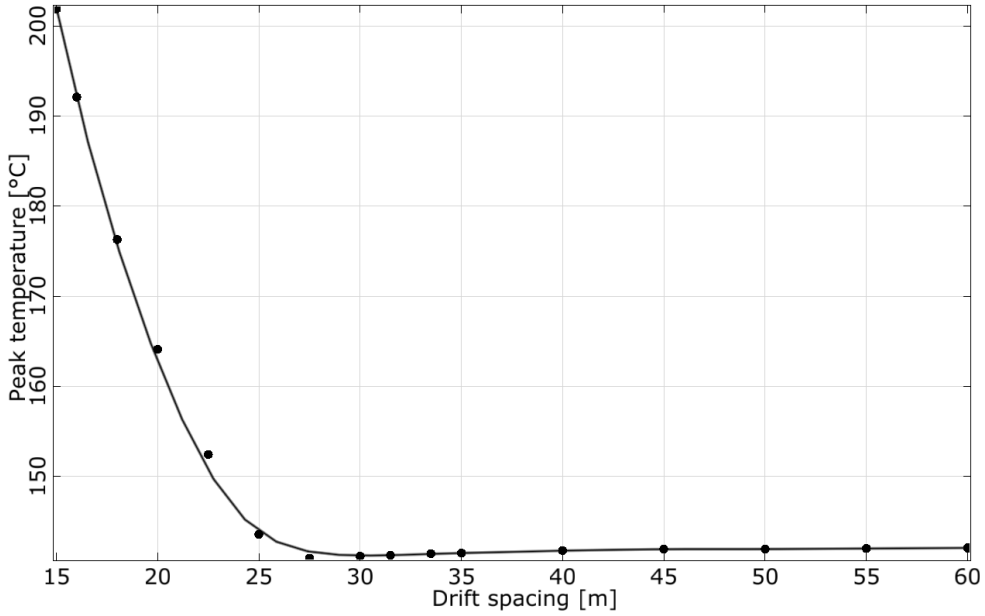

Figure 6.-12: Temperature peak as a function of the drift spacing for POLLUX® cask with CSD-V waste.

6.2.4 Layout of the repository

The rectangular drift system consists of the following types of drifts that are arranged in one level only:

- Infrastructure cross cut (east-west orientation) from the infrastructure area towards the main drifts
- Main drift for waste transport (north-south orientation)
- Main drift for excavation transport (north-south orientation)
- Cross cuts between the main drifts inside an emplacement wing (east-west orientation)
- Emplacement drifts (north-south orientation)

The sizes of the drifts are derived from the KOSINA project (Bollingerfehr et al., 2018) (see Figure 6.-13), leaving the spacing of casks as the primary design consideration at the scale of individual drifts. From the thermo-mechanical design, the following spacings are derived:

- POLLUX®-10 casks containing spent nuclear fuel (SNF) are spaced 3 meters apart (shoulder to shoulder) within a drift, with a spacing of 37.5 meters between the axis of a cask in one drift and the axis of a cask in an adjacent drift.
- POLLUX®-9 casks with CSD-V require a minimum spacing of 3 meters within a drift and 15 meters between drifts.
- For other POLLUX®-9 and CASTOR casks, a 1-meter spacing is maintained within drifts for technical reasons, with the minimum possible spacing required between emplacement drifts.

In addition to optimizing the repository thermo-mechanically, a geomechanical design is necessary to ensure the stability of the salt pillars. A general rule of thumb dictates that a rock salt pillar should be at least twice the width of the adjacent drifts. For this model, it is specified that the pillar must be twice the width of the widest adjacent drift. This approach ensures stability, even in the event of retrieval operations, by considering the largest potential size of both current and future drifts.

The size of the main drifts remains unchanged during retrieval, as these drifts do not experience obstacles or significant heat concentration. Similarly, emplacement drifts used for structural parts can be reopened without alteration. However, the retrieval process for POLLUX® casks involves modifications. Based on the ERNESTA project concept (Herold et al., 2018), retrieval is carried out by first creating smaller parallel drifts on either side of the original drift. The remaining salt between these smaller drifts is then removed in a second step, resulting in a full retrieval profile with a width of 9.7 meters.

For CASTOR® casks, the retrieval process is modified. In this case, a single adjacent drift is used to prepare for reopening the emplacement drift, rather than creating dual parallel drifts. This variation accommodates the specific requirements of CASTOR cask retrieval.

For the given inventory, the selected spacing between drifts corresponds to the largest required distance based on retrieval needs and thermal considerations. Table 6.-3 and Figure 6.-13 summarize the properties and dimensions of the drifts, including the adjustments necessary for retrieval operations.

Table 6.-3: Width of drifts and required rock salt pillars in meters

	Main Drift Control Area	Main Drift Monitoring Area	ED spent fuels Pollux®-10 SNF	ED vitrified waste Pollux®-9 CSD-V	ED cold waste CASTOR®	ED structural parts MOSAIK®
Drift width required for emplacement	7.60	6.80	5.10	5.10	5.10	5.50
Drift width required for retrieval	7.60	6.80	9.70	9.70	7.10	5.50
Optimized spacing from thermal design (axis - axis) [wall – wall]	0.00	0.00	37.50 [32.40]	15.00 [9.90]	0.00	0.00
Geomechanical rock pillar width (wall - wall)	15.20	13.60	19.40	19.40	14.20	11.00

If different types of drifts are adjacent to each other the larger required distance is used. An exception is made between emplacement drift for SNF and cold drifts e.g. the emplacement drift for structural parts or the main drifts as these will not increase the maximum temperature.

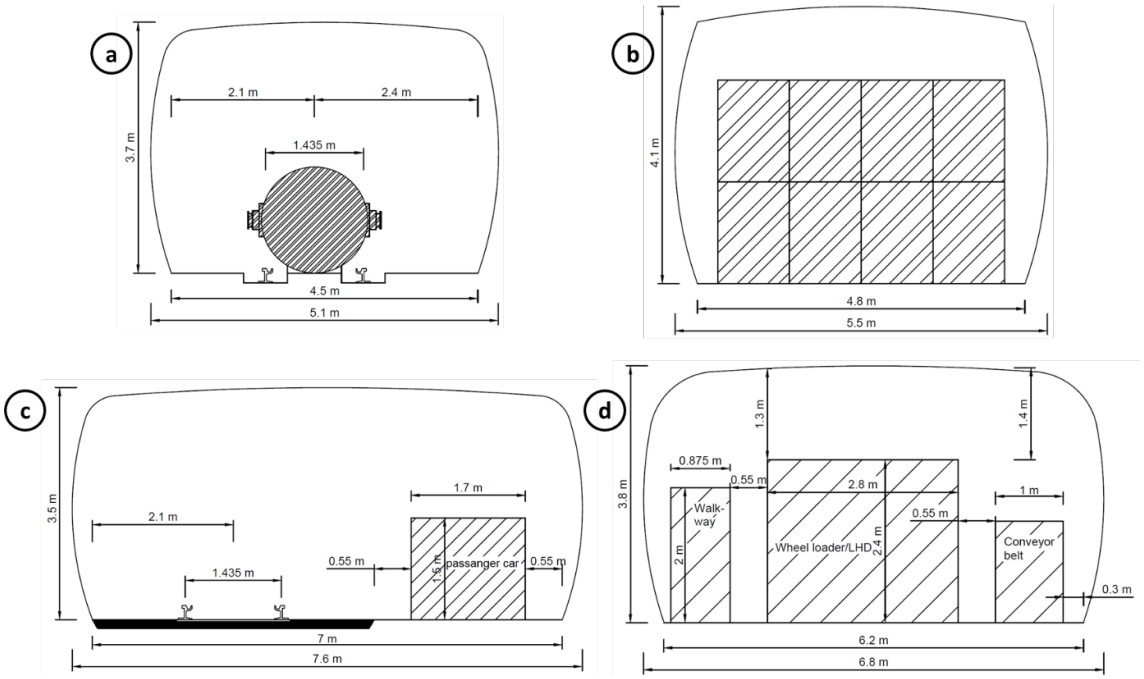

Figure 6.-13: Illustration of the drift profiles for POLLUX® emplacement drift (a), MOSAIK emplacemnet drift (b), main drift for waste package transport (c) and main drift for mining operations (d).

The emplacement drift are planned with a length of 250 m of which 225 m can be used for

disposal. Based on the spacing of casks and their length the maximum quantity per emplacement drift can be calculated. The total quantity of a cask type divided by the quantity per emplacement drift equals to the number of emplacement drifts needed. The distance between main drifts is 800 m. The crosscuts that develop the emplacement fields are planned with a maximum length of about 790 m. Based on the spacing between drifts the number of drifts per cross cut is calculated. The number of emplacement drifts divided by emplacement drift per crosscut finally gives the quantity of emplacement fields needed. In this case a total of 5.8 emplacement fields is needed, see Table 6.-4.

Table 6.-4: Number of emplacement fields required for different types of waste

	POLLUX®-10	**POLLUX®-9**	**CASTOR® var. types**	**MOSAIK® type II**
Cask quantity [m]	2,120	887	530	2,620
Cask length [m]	5.60	5.60	2.90	1/7
Cask spacing [m]	3	3	1	0
Number of casks per 225 m usable ED	26	26	57	1,800
Number of ED needed	82	35	10	2
Drift spacing (axis - axis) [m]	37.5	29.1	21.3	16.5
Number of drifts per 790 m crosscut	20	26	36	46
Number of fields required	4.1	1.3	0.3	0.04

The arrangement of the drifts uses following principles:

- One emplacement drift can only be used for one type for waste
- If one type of waste requires a multiple emplacement drifts these should be grouped together
- “Hot” waste is disposed in fields near to the infrastructure area to foster salt creep and therefore the self-sealing of drifts that have been backfilled with crushed salt
- The emplacement process starts at the far end of one wing close to the main drift of the monitoring area. It continues in a retreating operation towards the main drift control area.
- At first the already packed and comparatively “cold” waste types in CASTORS are disposed of, POLLUX®-9 and POLLUX®-10 follow in the next steps
- Waste out of structural parts is commissioned during the packing of SNF. Therefore in both fields an emplacement drift is required. As it needs to be open until the last bit of structural waste is taken from SNF it should be closer to the infrastructure area
- One emplacement drift can only be used for one type for waste
- If one type of waste requires a multiple emplacement drift these should be grouped together
- “Hot” waste is disposed in fields near to the infrastructure area to foster salt creep and therefore the self-sealing of drifts that have been backfilled with crushed salt
- The emplacement process starts at the far end of one wing close to the main drift of the monitoring area. It continues in a retreating operation towards the main drift control area.

- At first the already packed and comparatively “cold” waste types in CASTORS are disposed of, POLLUX®-9 and POLLUX®-10 follow in the next steps

Figure 6.-14 illustrates the layout of the proposed repository. The design features a symmetrical arrangement of three emplacement fields in each wing, providing sufficient space for the anticipated waste inventory. Although all six fields are not fully required, the northern wing will be the first to commence operations. This wing will host spent nuclear fuel (SNF) from test and prototype reactors, waste from reprocessing, and a smaller portion of SNF, including associated structural components.

At a later stage, the southern wing will be developed and begin operations. It will accommodate the remaining SNF inventory along with its corresponding structural parts. If additional emplacement drifts are needed during the operation of the northern wing, which is expected to utilize 100% of its capacity, the southern wing includes reserve capacity to meet this demand.

The final repository design fits well within the suitable space of the salt pillow, with a total length of less than three kilometers and a width of approximately 800 meters. The compact yet efficient layout ensures optimal utilization of the geological formation, as shown in the figure.

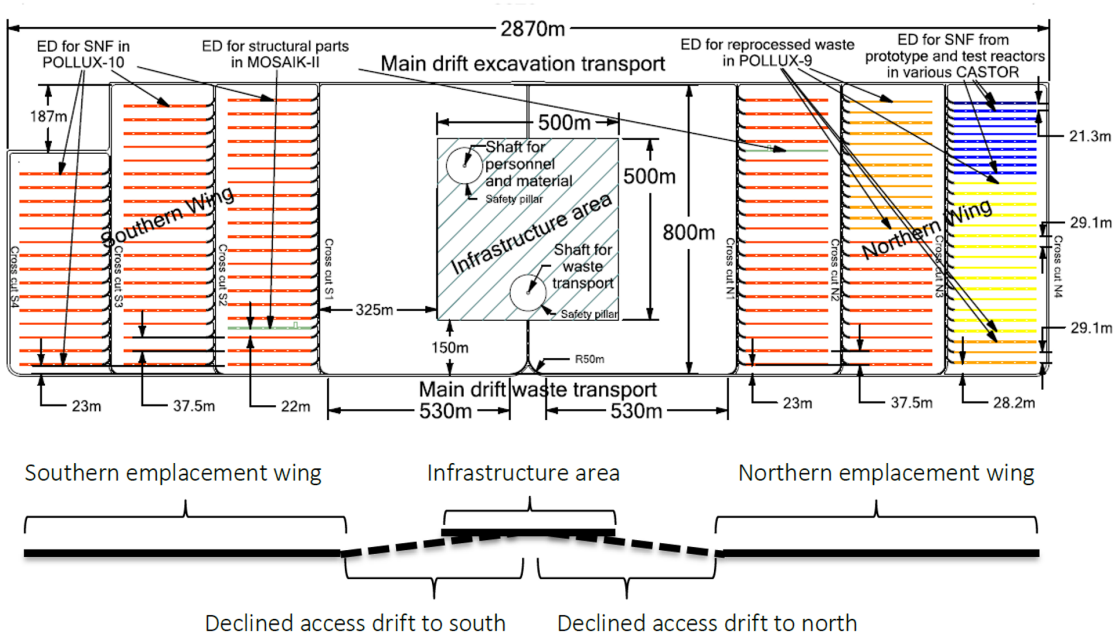

Figure 6.-14: Repository design in topview and frontview.

The emplacement fields are separated from the infrastructure area by at least 300 meters of undisturbed rock salt, ensuring robust isolation. The two shafts are strategically positioned with safety pillars far apart, ensuring they do not influence each other. The straight drifts provide multiple advantages, including the ability to install belt conveyors and maintain clear visibility during operations.

Waste transportation is envisioned to be carried out using an electric locomotive. The locomotive will move forward through the main drifts, turn into a crosscut, and pass the switch for

the active emplacement drift. It will then stop, reverse into the emplacement drift, and proceed with waste emplacement. To ensure smooth operation, a maximum inclination between 2.5% and 4.0% is deemed suitable for the locomotive on straight sections. For the access drifts connecting the infrastructure crosscut to the emplacement wings, an inclination of 4.0% will be used to facilitate the construction of seals (see Figure 6.-14).

Figure 6.-15 shows a stylistic 3D representation of the repository system where the developed repository mine is integrated into the generic geological formation. Here we can see that the shafts are located where the salt pillow thickness is maximum.

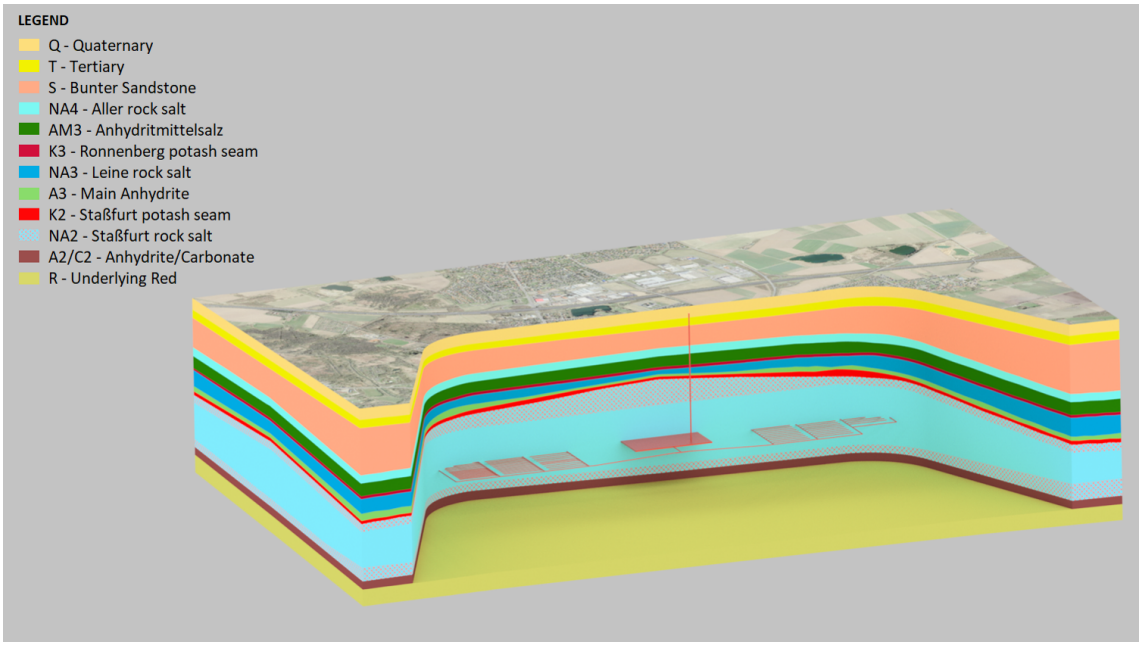

Figure 6.-15: Generic repository system for RANGERS (with courtesy of BGR (Völkner et al., 2017a)).

7. Sealing Concept

The sealing concept includes the conceptual design of the geotechnical barriers or the EBS and describes the functions and functional periods of those barriers.

7.1 Regulatory requirements

In general, when designing a deep geological repository, it is essential to ensure that the deposited radioactive waste remains reliably isolated from the biosphere over a long period of time. This is also the key statement of Section 4 of the EndlSiAnfV (EndlSiAnfV, 2020). It states:

> *(1) The radioactive waste to be deposited in the repository system must be concentrated and securely enclosed with the aim of keeping the contained radionuclides away from the biosphere for at least the assessment period.*
>
> *(2) The intended repository system must ensure the safe confinement of the radioactive waste passively and maintenance-free through a robust, layered system of various barriers with different safety functions.*

The use of the term repository system indicates that the secure confinement must be achieved through the interaction of the geological barrier (the rock of the repository site) with the technical and geotechnical barriers. Even the most suitable location can only serve as a safe repository with the repository rock if it is possible to adequately seal the necessary penetrations of the repository rock after the completion of the waste emplacement (Wunderlich et al., 2022).

The EndlSiAnfV (EndlSiAnfV, 2020) specifically requires the inclusion of a sealing concept in the development of the safety concept (Section 5, §10). Furthermore, measures to concretize the sealing concept are to be specified in the repository concept (Section 5, §11). In Section 2, §19, the EndlSiAnfV further detailed which components of the repository system has to be sealed and closed by stating that the sealing and closure of the repository includes, in particular, the as complete as possible backfilling of all underground cavities and their sealing, as well as the dismantling of technical facilities that impair long-term safety.

In the United States, the shaft sealing system developed for the Waste Isolation Pilot Plant (WIPP) and reviewed and certified by the Environmental Protection Agency (EPA) can serve as a foundation for the development of a sealing concept for a salt repository safety case. If a Department of Energy (DOE) repository for High-Level Waste (HLW) and Spent Nuclear Fuel (SNF) were to be located in the Delaware Basin bedded salt, any modifications made to the WIPP seal design would enhance its primary functions. These functions include limiting the migration of waste constituents to regulatory boundaries, restricting the flow of formation water through the seal system, preventing structural failure of system components, and mitigating subsidence and accidental entry. As a result, the DOE can have a high level of confidence that the sealing system for a repository containing DOE HLW/SNF will meet the requirements associated with the performance of the repository system (MacKinnon et al., 2012).

7.2 Reference to the safety concept

According to EndlSiAnfV (2020), the safety concept must provide an overview of all planned barriers within the repository system, particularly the essential barriers, their respective safety functions, and how they interact. The essential barriers are defined as the barriers on which the secure containment of radioactive waste primarily relies. In addition to the essential barriers, the safety concept also defines additional barriers that work together with the essential barriers to prevent or limit the release of radionuclides.Thus, the sealing elements are to be divided into essential barriers and additional barriers. To differentiate the functions of each barrier conceptually, safety functions are assigned to the essential barriers, while protective functions are assigned to the additional barriers.

In this context, the safety function is defined as a property of a component within the repository system that fulfills safety-related requirements for the secure containment of radionuclides. To enable these safety or protective functions to be performed by each component, specific performance targets must be assigned during the conception of the individual modules of each component. Performance targets are measurable or calculable quantities or characteristics by which the fulfillment of the associated safety function can be quantitatively assessed. To achieve these performance targets, it is necessary to formulate specific design requirements for the construction of the structures or their individual modules. These requirements must be adhered to in order to definitively achieve the desired performance targets of the structure. From the design requirements, design specifications are derived, which serve as the basis for the manufacturing and construction of the structure or its individual parts. Compliance with the design requirements must be verified during the construction of the structure, taking into account quality assurance measures.

Design premises of the sealing concept can be derived from the safety concept (see section 5.2) and the regulatory frame (see section 5.1). The Ordinance on Safety Requirements for the Disposal of High-Level Radioactive Waste (EndlSiAnfV 2020) states that

> *[...] the integrity of the system of essential technical and geotechnical barriers shall be demonstrated for the expected developments during the verification period and its robustness shall be justified. It shall be demonstrated that the properties of the further barriers of the repository system relevant for the safe confinement of the radioactive waste and, in particular, of the rock mass in the emplacement area are maintained at least over the period of time during which they are required according to the safety concept.*

Further it is required to demonstrate the integrity of the essential technical and geotechnical barriers. This assessment shall demonstrate the safety functions of the barriers and their resistance against chemical and physical processes resulting in corrosion or erosion, the stress state or changes in the stress state and the temperature development over time. Following this the sealing concept must be:

1. designed in a diverse redundancy
2. composed of a modular system to react on variations in the geological environment shaft and drift seals

3. separated in different modules/elements with sealing function and stability function
4. able to cover different functional periods of the modules/elements and guarantee the function over the required period

Diverse redundancy means that different components with possibly different functional principles work together. With this type of redundancy, the risk of systematic error is minimized.

Waste form and disposal waste package represent components of the EBS as well. In the considered safety concept for salt, based on the German regulatory frame, both technical components of the EBS have no explicit long-term sealing function. They provide at first operational safety function. Within the sealing concept the geotechnical barriers of shaft and drift sealing as well as the backfill are considered. The following design includes the shaft and drift sealing. The backfill inside all emplacement drifts, cross cuts and main drifts is made of crushed rock salt.

Shaft seal and drift seal are connected to specific safety functions as the sum of properties to fulfill the required safe containment of the radionuclides. This safety function can be broken down to further target properties, defining measurable or calculable characteristics of single modules/elements by which the fulfillment of the associated safety function can be quantitatively assessed. The target properties will be translated in design requirement by giving the measureable characteristics a value of a range to be fulfilled. The design requirement will defined within the design process of the EBS. The resulting preliminary design is afterwards evaluated in the EBS assessment and the PA.

As previously mentioned in the preceding section, specific measures need to be formulated to provide concrete details to develop a sealing concept outlined below. These measures are derived from the safety concept and serve as the basis for the development of the are incorporated into the repository concept. From research projects and safety assessment evaluation like the preliminary safety assessment for the Gorleben Site (Mönig et al., 2012), KOSINA (Bollingerfehr et al., 2018) and RESUS (Bertrams et al., 2020), several measures has been formulated in the safety concept concerning the sealing of a repository in salt. Although, these measures were derived from previous safety requirements (BMU, 2010), they are still valid for the requirements formulated in EndlSiAnfV (2020). Those measures are (Mönig et al., 2012):

- In the shafts and access tunnels connecting the infrastructure area to the emplacement areas, sealing structures with a specified hydraulic resistance are constructed and quality assured. These sealing structures must remain sufficiently tight until the hydraulic resistance of the compacted salt crushed salt is sufficiently high to prevent or limit the inflow of solutions to the waste. Therefore, their effectiveness must be ensured for at least the duration required for adequate backfill compaction. The design of the sealing structures is based on load cases that cover a range of possible future developments during their required service life as much as possible.
- The open cavities in the mine workings of the emplacement areas are backfilled with crushed salt. The cavity convergence due to salt creep leads to compaction of the crushed salt, reducing its porosity and permeability. Near the heat-generating waste, crushed salt compaction is accelerated by locally elevated temperatures. The cavity convergence is limited by the volume of crushed salt. The earlier onset of confining

stress compared to unfilled mine workings and the overall reduced extent of salt creep lead to accelerated healing of the rock salt in the excavation disturbed zone and a reduction in differential stresses within the rock mass. Furthermore, the introduction of backfill significantly reduces the initial cavity volume that can be filled with solution.

- In the access drifts, a sufficient sealing effect of the backfill is aimed to be achieved within a short period. Therefore, the crushed salt in the access drifts belonging to the emplacement areas is slightly moistened to reduce its resistance to compaction and achieve faster compaction
- Moisture introduced near the waste in the repository is minimized. The aim of this measure is to limit corrosion of the waste containers and thus the generation of gas and gas pressure buildup within the repository. For heat-generating waste, where only small amounts of residual moisture may be present, crushed salt backfill with very low moisture content is used in the mine workings of the emplacement fields.
- The design of the shaft sealing structures is based on the use of multiple sealing elements made of different materials, each with diverse functional properties due to their respective construction

7.3 Components of the sealing concept

The sealing concept for a repository in salt involves geotechnical barriers and the backfilling of cavities, at least in the emplacement areas, with compacted crushed salt. The geotechnical barriers encompass shaft seals and selected drift seals. Together with the containment-providing rock zone, they ensure the confinement of the radioactive waste in the early phase of the repository evolution during the period when the crushed salt has not yet fully developed its sealing effect (Mönig et al., 2012).

The shaft seal is the most important safety-related closure, as it restores the integrity of the containment-effective rock mass. Its main function is to prevent water/solution ingress from the overlying rock into the repository after its closure and, in the event that radionuclides are mobilized during the post-closure phase, to retain them within the repository through appropriate sealing. The concept of a shaft seal includes sealing components as well as supporting/structural components (Kreienmeyer et al., 2008). The shaft seals are designed to withstand the expected fluid pressures (hydrostatic pressure from the water column in the overburden and surrounding rock). The design of the shaft seals assumes a functional lifespan of 50.000 years (up to next ice age) in Germany, during which their functionality must be ensured. After this time period of about 50.000 years, increased hydraulic permeability of the shaft seals and therefore enhanced solution ingress into the infrastructure area are assumed for the reference scenario. If solutions reach the drift seals, partial dissolution of the sealing materials or precipitation of dissolved inventory in the pore space can occur. At that time, the backfilled crushed salt in the access drifts already exhibits a low permeability similar to the intact rock (Beuth et al., 2012).

At defined locations separating the emplacement areas from the infrastructure area within the repository mine, drift seals are constructed. Their purpose is to prevent solutions from reaching the emplacement fields or to delay the spread of contaminated solutions until the compacted crushed salt can assume the barrier function of sealing repository system. For the reference scenario, a functional lifespan of 50.000 years is assumed for the tunnel seals,

during which their functionality must be ensured. The required integral permeability is set at $5 \cdot 10^{-17} m^2$ (Beuth et al., 2012). The drift seals must be designed to withstand the rock pressure exerted by the surrounding rock. This pressure is determined by considering possible stress redistributions based on petrostatic considerations" (Kreienmeyer et al., 2008, p. 42). For drift seals, the separation of sealing and supporting components is recommended, as well as the design with redundant and diverse components and materials (Kreienmeyer et al., 2008).

In salt repository concepts developed in Germany (VSG (Mönig et al., 2012), KOSINA (Bollingerfehr et al., 2018)), the infrastructure area is to be backfilled with non-compactable gravel made of basalt or serpentinite. Unlike crushed salt, this non-compactable backfill undergoes only slight compaction due to the increasing convergence, quickly generating confining stress. The infrastructure area, filled with non-compactable backfill, serves as a reservoir for solutions entering through the shaft and from the host rock. It can also serve as a reservoir for gases generated within the repository due to corrosion of the disposal caks. In the preliminary safety case for the Gorleben site, the backfilled infrastructure area was planned to served as a reservoir to collect $5.100 m^3$ of fluid resulting form the inflow of solution through the shaft into the infrastructure area (Beuth et al., 2012).

Besides the geotechnical barriers, the waste packages and the waste form are also part of the EBS and the sealing concept.

7.4 EBS design guidance

The design of the EBS will be prepared in a stepwise approach with the possibility of additional iterations, if safety function or requirements cannot be fulfilled by the preliminary design. The approach considers the previously named R&D activities such as (Mönig et al., 2012; Buhmann et al., 2008; Wagner, 2005; Orzechowski, 2018; Kudla and al., 2020; Kreienmeyer et al., 2008). The necessary steps are:

1. Identification of boundary conditions and requirements, including knowledge about the actual site, the repository concept and the safety concept
2. Identify the relevant process classes and corresponding impacts to the EBS based on the FEPs
3. Identify usable construction materials, based on chemical environment and technical feasibility
4. Develop a preliminary design (draft) out of the knowledge grained in (1), (2) and (3) and name the different components
5. Identify the necessary assessments to proof integrity of the EBS
6. Determine dimensions of the barrier and its components
7. Prepare a preliminary or simplified assessment for the most relevant safety functions (commonly hydraulic resistance and mechanical stability)
8. Start a new iteration at (4) if safety function are not met

Sanders (2020) illustrated the named stepwise approach, see Figure 7.-1.

The requirements (Position 1 in Figure 7.-1) and impacts (Position 2 in 7.-1) to the single barrier are derived from the total repository system and allow a formulation of target properties. Thus, a consideration of the entire system is not necessary for the design of the sealing concept or its single elements. Thermal impacts result from the natural rock temperature, operation of the repository (e.g. ventilation) and the thermal output of the radiological decay (of the emplaced waste). With respect to the given temperature limits target properties to the EBS are given e.g. by limiting the hydration temperature of used concrete based materials. Additionally the used materials have to be stable under the given temperature conditions. Hydraulic impacts result from gas or fluid pressure. Hydraulic conductivity represents the corresponding target property. Mechanical impacts are divided in static and dynamic impacts. Static impacts result from the local stress field and potential thermo-mechanical impacts. Dynamic impacts result from earthquakes. Mechanical target properties are e.g. the stiffness of the materials. Chemical impacts are given by the geological setting at the actual sealing location and the expected gases or brines. The composition of them influence the material selection and can result in target properties for chemical composition of the usable materials.

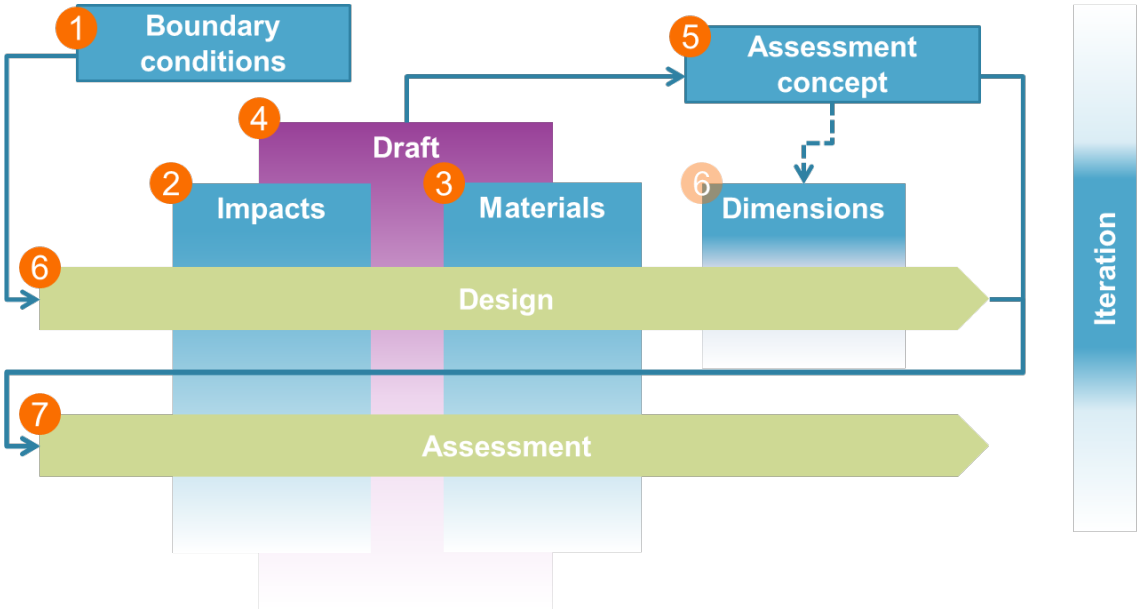

Figure 7.-1: Illustration of the design process for EBS, based on Sanders (2020).

The EBS design process for the RANGERS project considers existing preliminary designs as developed in other R&D projects, too. The transfer of those concepts represent the step (4) of the presented method, see Figure 7.-1. The considered shaft sealing concept is based on Herold et al. (2020) and a design variation deduced from this. The considered drift sealing concept is inspired by Bollingerfehr et al. (2018) with modifications of the long-term sealing element. All concepts are described in the following sub-sections. The preliminary assessment (6 in Figure 7.-1) as well as the full assessment (7 in Figure 7.-1) are prepared with the RANGERS project.

7.5 Reference shaft sealing concept for a repository in bedded salt formation

7.5.1 Reference design of the shaft seal

For shaft closure the shaft sealing concept developed within the ELSA 2 project (Herold et al., 2020) and as a second option a slightly modification is considered. Both sealing concepts follow the design principle of complete filling of the shaft column. The main sealing element consists of bentonite (preferably dry-installed binary mixture of briquettes and granulate). Equipotential segments are incorporated into the bentonite sealing element. The following combinations are possible with the bentonite sealing element:

- Bentonite - bitumen/asphalt
- Bentonite - saltclay mixture

A design with combinations of bentonite/clay with bitumen/asphalt is typically used for the closure of conventional mines with solution-filled mine workings. The transition between bitumen and the binary bentonite mixture in the dry initial state is constructed from a low-permeable intermediate layer of compacted fine-grained filler material (e.g. fine sand with limestone powder, 0.1 µm to 1 mm, with a permeability (k) ranging from $10^{-14}\,m^2$ to $10^{-15}\,m^2$). This minimizes both the sinking of the bentonite pellets and powder into the viscous bitumen and the penetration of bitumen into the pore space of the binary mixture. Combinations of the binary bentonite mixture and compacted crushed salt-clay mixture are possible. Table 7.-1 summarizes the considered sealing elements and their sealing principles.

Table 7.-1: Summary of considered sealing elements, principle of operation and design parameters

Material	**Sealing capacity of the material**	**Contact zone**	**EDZ**
Bitumen / Asphalt	Impermeable for liquids	if bitumen wets the wall and the wetting is maintained during the application of liquid pressure, the contact zone is tight.	Little effect (only if bitumen can penetrate into cracks)
Salt-clay mixtures	Gas permeability $> 10^{-16}$ m^2 Liquid permeability unknown	Influence on contact zone not yet investigated (probably good connection to rock face possible with sufficient compaction)	The installation of the mixture has (probably) no influence on the ALZ but cannot be excluded for dynamic impulse compaction
Bentonite	Liquid permeability $< 10^{-17}$m^2	Swelling pressures of 1 to 2 MPa are possible for Ca-bentonite, provided that εV = 0. For in-situ structures, the swelling pressures depend on the deformations actually occurring.	Reduction of EDZ permeability depending on contact pressure
MgO-concrete (C3, used in ELSA2)	Liquid permeability $2 \cdot 10^{-18}$ to $5 \cdot 10^{-18}$ m^2	Tight connection to rock possible. Influence of the "expansion pressures" of the MgO-concrete not yet sufficiently investigated, as these depend on the possible deformation of the MgO-concrete.	Reduction of the permeability of the ALZ depending on the contact pressure

Starting from the shaft sump, the deepest parts of the shaft as well as the subsurface landing station will be filled with MgO-concrete. In this area the MgO-concrete fulfills abutment function. Above the landing station MgO-concrete is considered as sealing element. In this case recuttig of the shaft contour is possible. In theory, thin asphalt layers or injections (e.g. sodium silicate) can be added to improve sealing function, especially at the contact area but results of the large borehole tests performed in Kudla and al. (2020) as well as experiences at the Asse II mine (Heydorn et al., 2016) show that contact gap injections are not required for sealing elements made of MgO-concrete. To guarantee chemical stability of the MgO-concrete a gravel column filled with Mg-salt (e.g. Brucite) is installed above the MgO-concrete. Water intakes from above will be saturated with Mg when it passes the gravel column. The gravel column represents also an abutment for the bentonite sealing element. Above the bentonite a column of compacted salt-clay mixture is installed. The location of the bentonite below the salt-clay mixture should ensure a saturation of intake water with Na and provide a stable chemical composition of the brine entering the bentonite. At the salt top a bitumen filled gravel column will be installed, covering surrounded anhydrite and clay layers too. Table 7.-2 summarizes the shaft sealing elements in the shaft, their position and their installation method for the reference shaft sealing concept. Inside the salt formation no shaft liner will remain. Recutting of the contour (extensions of the diameter) are possible. Outside the salt formation and at the salt top, a watertight liner is installed and will remain. In the area of the overburden a simple gravel column will be installed. The following figures 7.-2 and 7.-3 illustrates the described design. The next table summarizes the sealing properties of the different elements.

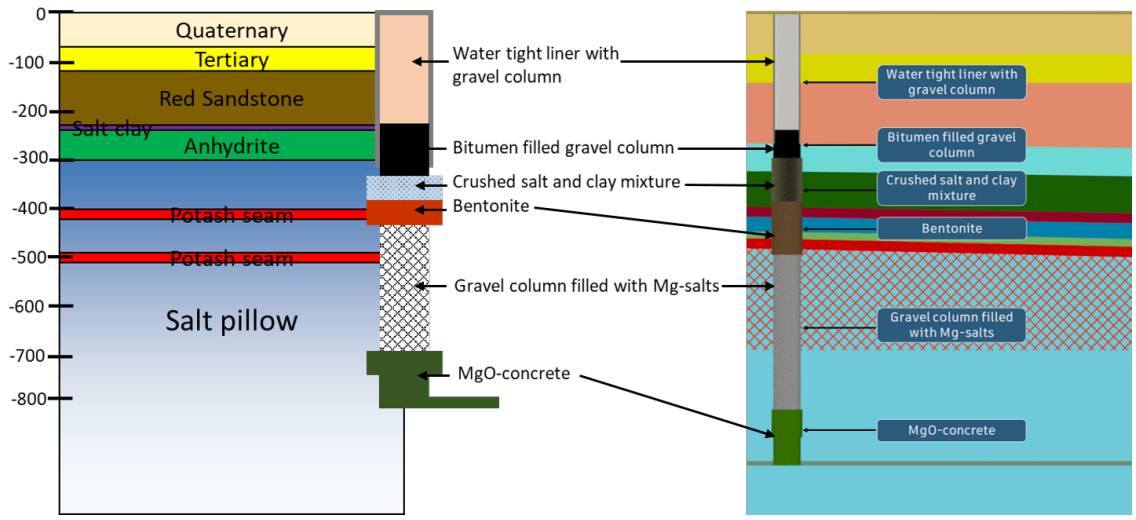

Figure 7.-2: Illustration of the shaft sealing concept developed in Herold et al. (2020) (left) and adapted to the actual geological situation at shaft 2 of the the generic reference model (right).

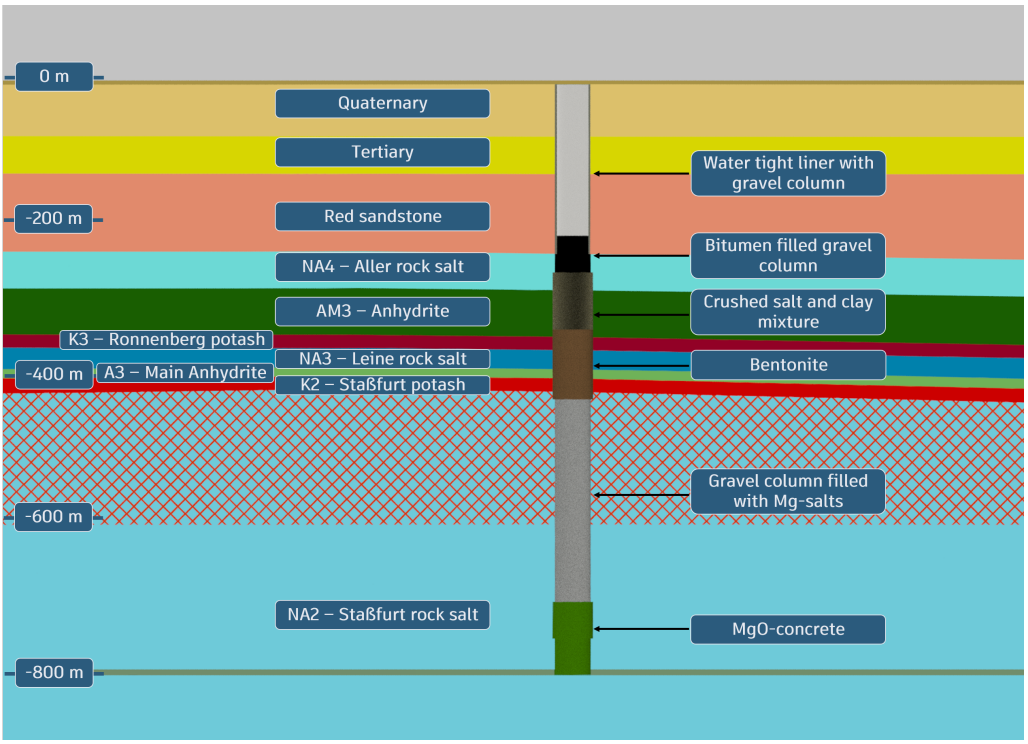

Figure 7.-3: Illustration of the shaft sealing concept.

Table 7.-2: Shaft sealing elements, position, material and installation method for the reference shaft sealing system

Component	Top (depth below surface)	Bottom (depth below surface)	Construction material and installation method
Bitumen-filled gravel column	206	256	Similar to ERAM in-situ test, material properties from ELSA
Crushed-salt-clay-mixture	256	334	Composition from ELSA 2, dynamic impulse compaction
Bentonite	334	429	Ca-Bentonite Type “Saltzdetfurth”, binary mixture with conventional compaction
Gravel column	429	705	Material like VSG, dumping by pipe
MgO-concrete (sealing element)	705	755	Material like VSG, cast in place
MgO-concrete (abutment)	755	805	Material like VSG, cast in place

7.5.2 Optimization or alternative design of the shaft seal

Bentonite produces a swelling pressure and creates an active contribution to the sealing as well as healing of the EDZ. Additionally the convergence of the host rock close EDZ over time. The convergence increases with depth. If the bentonite is located in areas with less convergence, the sealing properties could be improved because of the swelling pressure. The optimization of the closure concept include a changed position of the bentonite and crushed salt element. The bentonite will be located closer to the salt top. The crushed salt element below. Unsaturated water is not able to dissolve the bentonite. Table 7.-3 summarizes the shaft sealing elements in the shaft, their position and their installation method for the alternative shaft sealing concept. When the water crosses the bentonite over time it will saturate and is not able to solve the crushed salt, see Müller-Hoeppe et al. (2012b). The contact of unsaturated water with bentonite have to be considered during the selection of the bentonite Figure 7.-4 and Figure 7.-5.

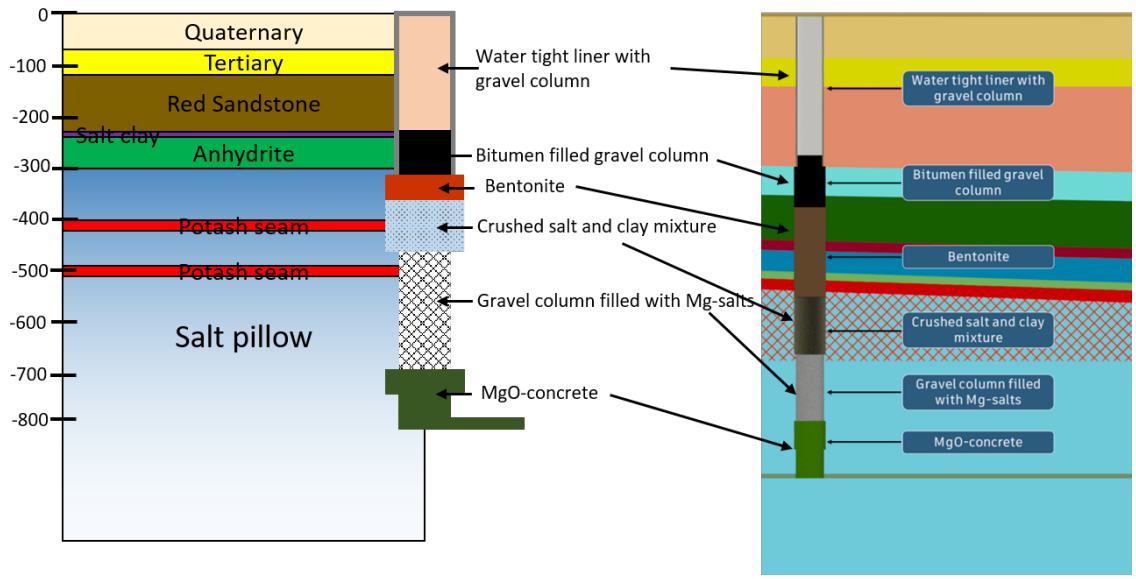

Figure 7.-4: Illustration of the alternative shaft sealing concept adapted to the geological situation at shaft 1 of the generic reference model.

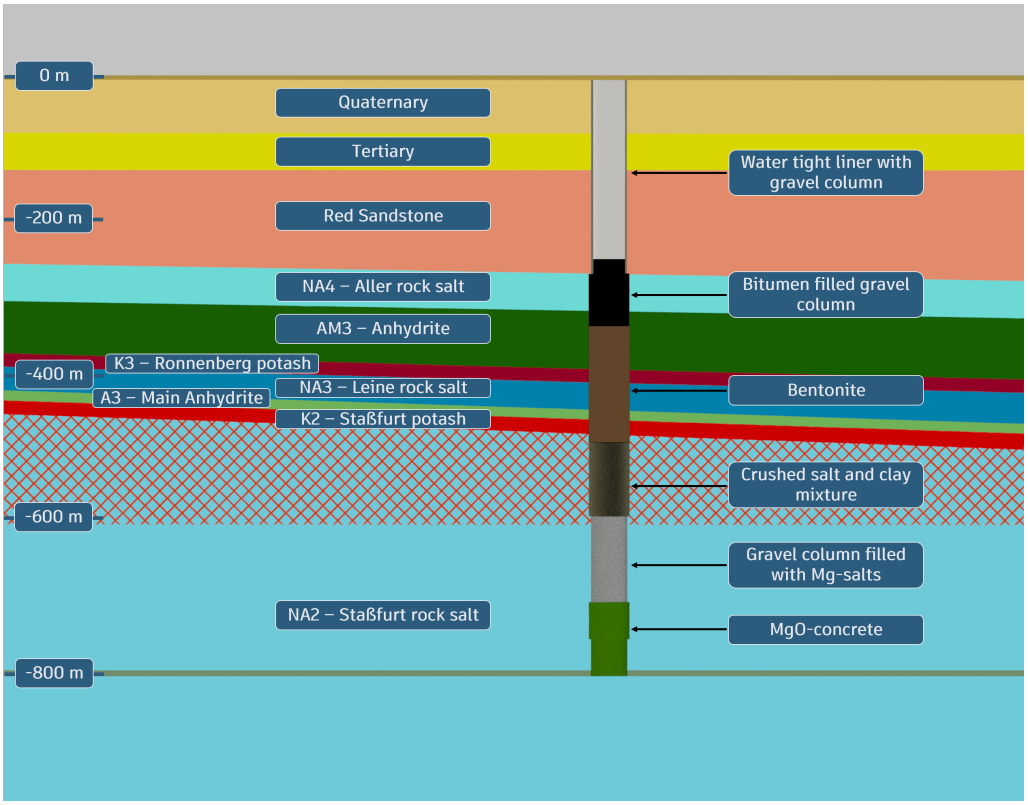

Figure 7.-5: Illustration of the alternative shaft sealing concept.

Table 7.-3: Shaft sealing elements, position, material and installation method for the alternative shaft sealing system

Component	Top (depth below surface)	Bottom (depth below surface)	Construction material and installation method
Bitumen-filled gravel column	241	331	Similar to ERAM in-situ test, material properties from ELSA
Bentonite	331	488	Ca-Bentonite Type Saltzdetfurth, binary mixture with conventional compaction
Crushed salt-clay mixture	488	588	Composition from ELSA 2, dynamic impulse compaction
Gravel column	588	705	Material like VSG, dumping by pipe
MgO-concrete (sealing element)	705	755	Material like VSG, cast in place
MgO-concrete (abutment)	755	805	Material like VSG, cast in place

The location of the two shaft sealing systems in the geological formation is illustrated in Figure 7.-6.

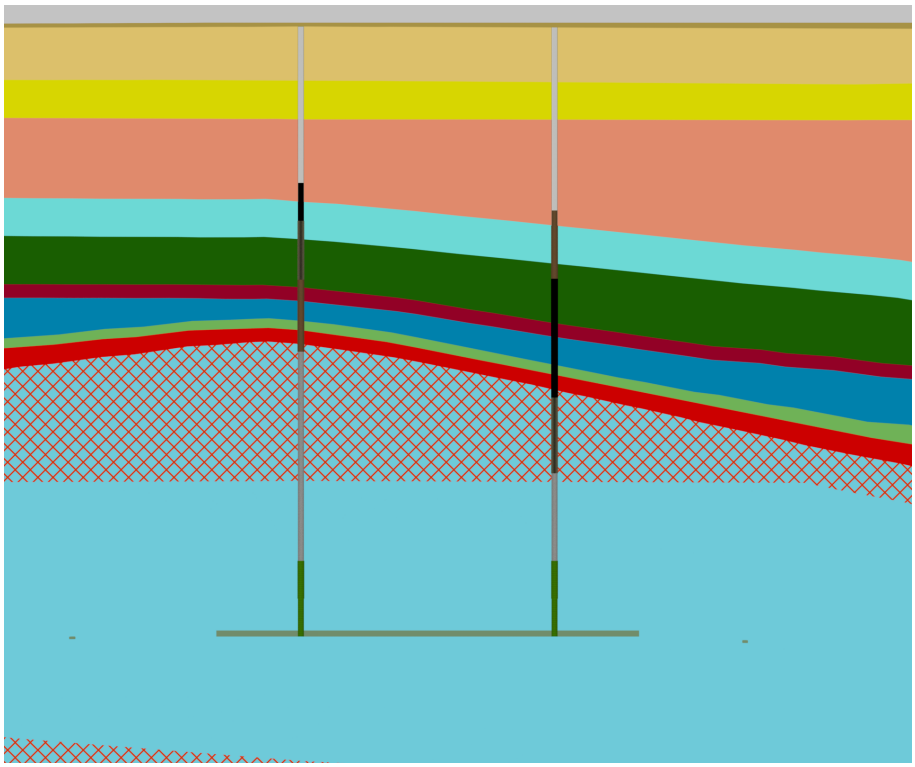

Figure 7.-6: Illustration of both shaft sealing concepts in the geological model used in RANGERS.

7.6 Conceptual designs for drift sealing in HLW/SF repositories in salt

Conceptual designs for drift sealing in HLW/SF repositories are presented in Müller-Hoeppe et al. (2012b); Bollingerfehr et al. (2018). Practical experiences in the construction of drift

seals made of concrete are known e.g. from Asse II mine, see Heydorn et al. (2016); Meyer et al. (2019); Köhler et al. (2019).

The drift seals, as designed for the Gorleben site, considers two sealing elements made of MgO-concrete. Both are covered by concrete based abutments to guarantee mechanical and local stability. All elements are placed in a row and with direct contact to the rock, Figure 7.-7. Bollingerfehr et al. (2018) consider in principle the same design, including concrete based sealing elements and abutments. In between the sequence of sealing elements and abutments, an additional long-term sealing element is considered. For a length of 300 m the drift has to be backfilled with crushed rock salt. “The compaction of the crushed salt, which is driven by salt creep, results in a very low permeability of the crushed salt over a certain period of time. Evidence must be provided that sealing by the compacted backfill material is fully developed by the time the performance of the engineered barriers can no longer be demonstrated” (Bollingerfehr et al., 2018).

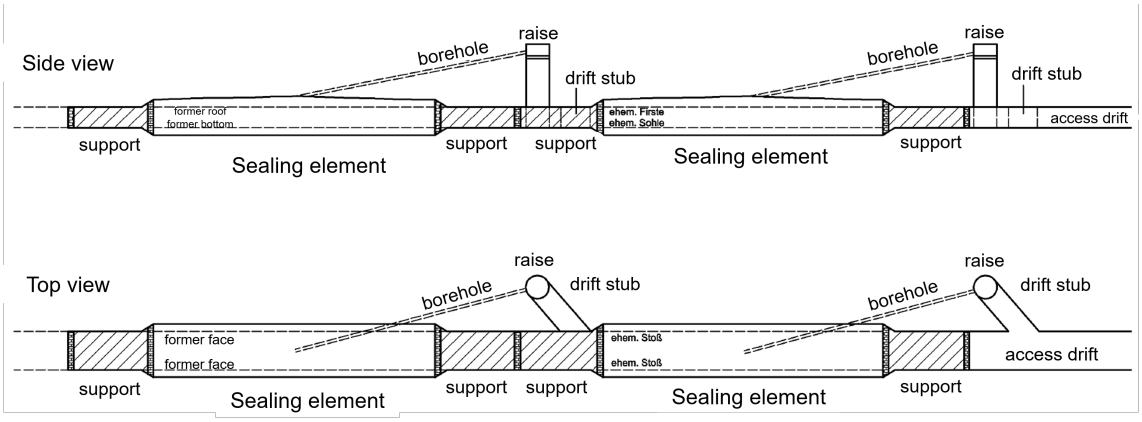

Figure 7.-7: Conceptual design of the drift seal in Müller-Hoeppe et al. (2012b).

In conventional mining practices, including the Asse II mine, the filling of concrete-based sealing elements is typically achieved by drilling from an upper mine level down into the sealing location. However, in the generic repository design, only a single mine level exists. To accommodate this constraint, an upwards-directed raise (see Figure 7.-7) has been proposed. This design provides the necessary height difference for filling the sealing elements and ensures the highest possible filling grade.

The roof of the sealing element is designed with a cone shape sloping towards the wells, which terminate at the highest point of the roof in the center of the sealing element. This configuration facilitates efficient concrete distribution. The spreading behavior of MgO-concrete during filling has already been demonstrated for distances of up to approximately 25 meters (Müller-Hoeppe et al., 2012b).

The total length of the sealing element is limited to 50 meters, allowing the concrete to flow evenly in both directions from the center. This design ensures effective filling and minimizes the risk of voids within the sealing element, optimizing its structural and sealing performance.

Using a raise and cope-shape roof represents a high additional technical effort during construction of the sealing. To simplify the construction it is proposed to implement an inclination at the sealing location, already during excavation. Highest point of the drift segment have to

be located at the shaft side. Concreting will be done from this side. The flow angle of MgO-concrete (e.g., A1-mixture form Asse II mine (Müller-Hoeppe et al., 2012b)) is approximately 1.2°. If the drift has an inclination of 1.5° concreting can be done without the raise and a cone-shape roof. The establishment of air pockets due to locally larger flow angles or roughness of the roof can be avoided by concreting under pressure.

To enhance the speed of compaction of the crushed salt in the designated area of the long-term seal, it is moistened before backfilling. The effect of accelerated creep of moistened crushed rock salt was demonstrated successfully in laboratory scale (Buhmann et al., 2008). Experience from mining industry and Asse II mine point to the fact, that in large scale or industrial scale the moisture will not stay in a homogeneous distribution. It is known that a gravity driven separation will occur and moisture accumulate at the drifts floor. A technical solution to avoid this separation represents the use of salt-clay mixtures, similar to shaft sealing (Kudla and al., 2020). A premixed blend offers a homogeneous distribution of clay and connected water in the salt and provides an additional sorption capacity by the clay. The installation of the salt-clay mixture can be done with the same methods as the pure crushed rock salt is installed. DBE (1995) successfully demonstrated the backfill installation with slinger technique. Comparable backfilling methods are also known from other repository projects. To minimize the occurrence of roof gaps, SKB tested backhoe loaders and vibro-plates to compact the backfill during installation, see Figure 7.-8. Kudla and al. (2020) tested the use of conventional vibro-plates in preparation of shaft sealing successfully, too. This method could be suitable for the installation of mixtures of crushed salt and clay. The technical feasibility of this technology was tested by Pötzsch et al. (2018), see also (Pötzsch, 2021), for the installation of crushed salt mixed with polyhalite. An evidence (experimental or large scale) for the use of vibro technique to compact salt-clay mixtures in drifts is currently missing.

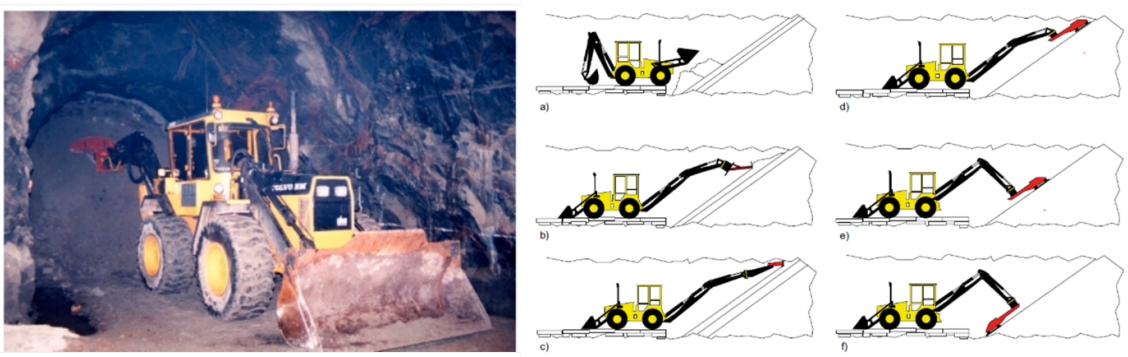

Figure 7.-8: left: In situ experiment backfill compaction (SKB IPR-01-17), right: Illustration of compaction within inclined layers of backfill material in a drift (SKB R-06-71).

7.7 Reference drift sealing concept for a HLW-repository in salt

The drift sealing system designed within the scope of the RANGERS project comprises a combination of abutments, drift seals, and a long-term crushed salt seal. In the repository concept presented here, four drift sealing systems are strategically located in the two main drifts, effectively closing all access to the emplacement wings.

Each drift seal incorporates two sealing elements made of MgO-concrete, which are securely bound by concrete-based abutments to ensure mechanical stability and maintain their positions. MgO-concrete is also chosen for the abutments due to its geochemical stability, which

complements the surrounding rock environment. All components are installed in direct contact with the host rock to enhance sealing performance.

As recommended by Kock et al. (2012), the excavation-damaged zone (EDZ) should be removed to the extent possible immediately before the installation of the drift sealing system. In the construction area, the EDZ is expected to extend between 10 and 30 cm. Any residual damage zone that remains after removal can be sealed using injections if necessary, ensuring the integrity of the sealing system.

Between the sequence of MgO-concrete sealing elements and abutments, an additional long-term sealing element made of crushed salt is included. This crushed salt is enriched with clay admixtures to partially fill the pores, reducing permeability in the early compaction stages and accelerating the process of achieving a fully compacted state. However the effectiveness of this novel crushed salt-clay material still requires further validation.

The long-term seal extends over a length of 300 meters between the drift seals. Each MgO-concrete seal, including its abutments, has a total length of 115 meters, ensuring robust containment. The overall design ensures that the sealing system provides itself a diverse and redundant multi-barrier system, leveraging both mechanical and geochemical stability for long-term repository safety.

The drift sealing system is specifically designed to function under the unique conditions of a salt repository. This comprises:

- Mechanical Stability: The concrete-based abutments provide structural support, ensuring that the MgO-concrete sealing elements remain fixed under geological and operational stresses.
- Geochemical Compatibility: The use of MgO-concrete reduces the risk of chemical interactions with the expected inflowing waters, preserving the integrity of the seals over long timescales.
- Long-Term Isolation: The crushed salt seal, with or without clay admixtures, compacts under geological pressure to provide an impermeable barrier, isolating the repository from surrounding environments.

Figure 7.-9 illustrates the proposed design of the drift sealing system as installed in the main drifts. This multi-component system ensures effective containment of radioactive waste, with redundancy provided by the combination of MgO-concrete seals and the long-term crushed salt seal.

While the proposed concept introduces the crushed salt-clay mixture as an innovative sealing material, further research is essential to validate its performance. Experimental studies are required to demonstrate its enhanced compaction capabilities, achieving sufficiently low permeability values at low porosities. Additionally, numerical investigations should focus on developing robust constitutive material models that accurately capture the mechanical and hydraulic behavior of the mixture under repository-relevant conditions.

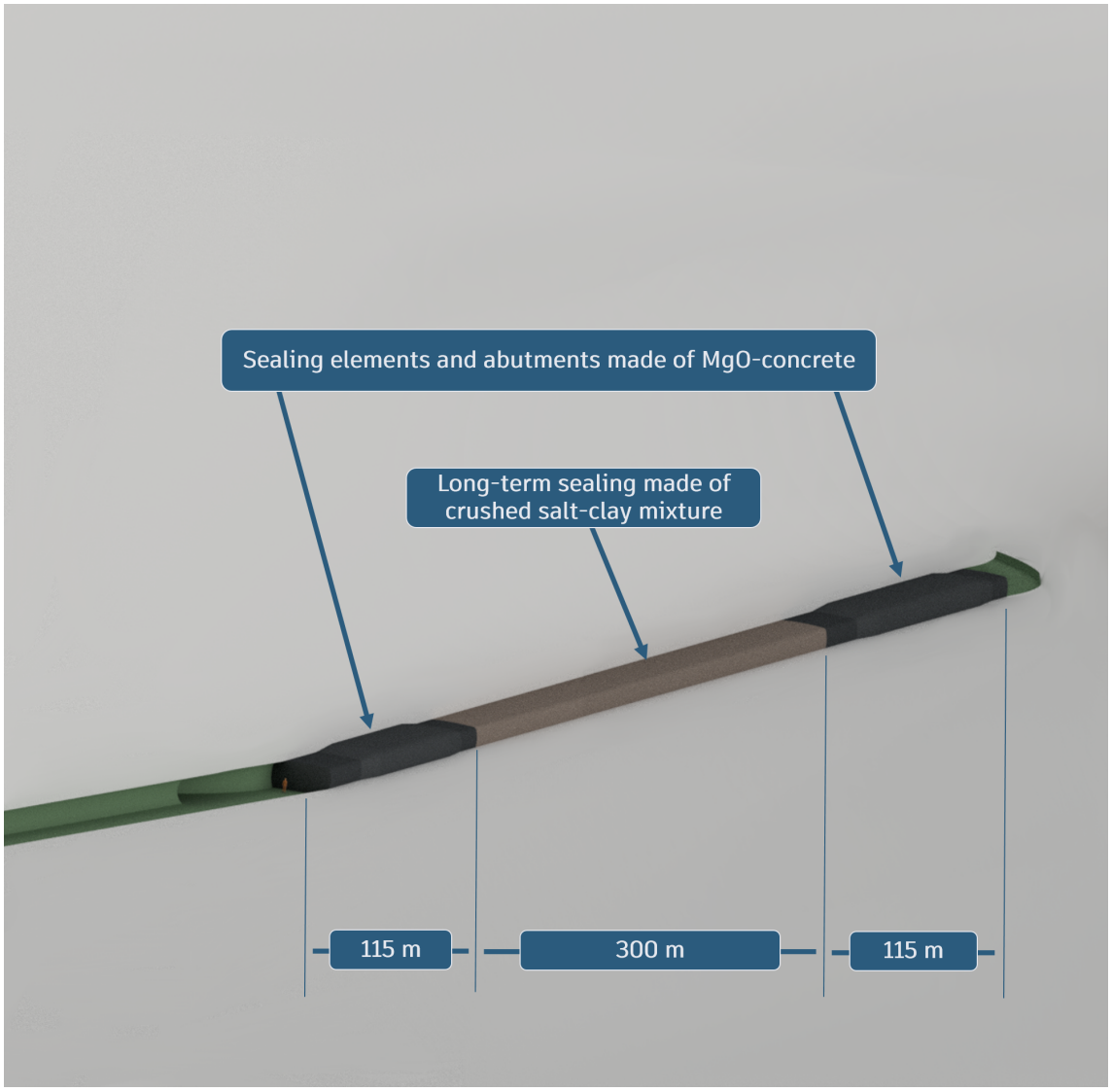

Figure 7.-9: Illustration of the drift sealing concept as designed for the RANGERS case study.

8. FEP and Scenarios for EBS

8.1 Fundamentals

8.1.1 Linkage between integrity proof of EBS and FEP / scenarios

The methodology for integrity proof of the Engineered Barrier system (EBS) is fixed in technical regulations and has to be linked with the methodology for long term safety assessment (incl. FEP and scenarios). Therefore the impacts, loads and load resistances as well as design situations of the technical functional proof have to be assigned to FEP and scenarios. Thus components of the geotechnical barriers can be dimensioned using the partial safety factors method.

In the R&D project RANGERS, two categories of FEP lists as descriptions of repository system evolution are provided:

- a more general FEP list giving a comprehensive description of repository system and
- two specific FEP lists for the nearfield of the geotechnical barriers

The compilation of a comprehensive FEP catalog for a repository system is a quite extensive task and exceeds the scope and purpose of the RANGERS project. Therefore it is obligatory to rely on the FEP catalog and the combined scenarios from a former project as an example. For Germany, the only adequate project on HLW-disposal in a salt dome structure is the Preliminary Safety Assessment for the Gorleben Salt Dome (VSG) (Wolf et al., 2012). For US only generic studies on HLW disposal in salt formations are available.

One objective of the project was to analyze an existing generic numerical model of a salt pillow that has been developed for the R&D project KOSINA (Völkner et al., 2017b). The geological structure of this model differs from the structure of the Gorleben salt dome, but the geological formations are identical and the layout of the repository mine with drift emplacement is similar. For the KOSINA project, neither a FEP catalog nor a scenario development have been prepared. But in principle, FEP catalogs for HLW repositories in salt formations are quite similar. There are only very few FEP that are site specific and not relevant for other sites. Differences only become apparent when details of specific characteristics of features or processes are analyzed. The main objective of the RANGERS project is to develop a methodology and procedure for performance assessment as well as to test their applicability and functionality. Therefore an exemplary investigation has to be done and some small discrepancies between the description of the repository system and its evolution and the numerical model are tolerable.

The descriptions of the RANGERS FEP will be done on a very general level and site-specific FEP of the Gorleben salt dome, that are not relevant for the KOSINA model, will be excluded.

The more detailed FEP lists for the nearfield of the geotechnical barriers have been adapted and specified according to the requirements of the EBS performance assessment.

8.1.2 Features, Events and Processes

A FEP list gives a summary of features characterizing the initial properties of a repository system at the end of the operational period and relevant information on events and processes which might influence the future evolution of the repository system. In the context of a safety assessment, the FEP list is highly relevant as it is the connecting link between the fundamentals (site description, geoscientific long-term prognosis and radioactive waste inventory), the repository concept, and the system analysis. Apart from the compilation of the most relevant basics, the FEP list reflects the interrelation between the site specific conditions and the modifications resulting from the disposal of radioactive waste. Therefore it is a sound basis for scenario development, for process analyses, for demonstrating the integrity of geological and geotechnical barriers and for the analysis of the radiological consequences. In the context of the RANGERS requirements, first a comprehensive FEP-list for the whole repository system has to be considered. For specific analysis of the boundary conditions in the nearfield of the geotechnical barriers it is useful to extract specific, detailed FEP lists for the corresponding subsystems.

The German state-of-the-art in FEP and Senarios has been developed in R&D projects ISIBEL / VSG (Bollingerfehr et al., 2013) and ANSICHT (Lommerzheim et al., 2019) as well as most recently in the documents for the license application for closure of the ERAM repository (not yet published). Objectives for the methodology are to reflect all relevant future evolutions as comprehensively as possible. Furthermore scenarios will be derived systematically and transparently from the FEP catalog. Measures to increase completeness of a FEP list are:

- a comparison with the NEA-FEP database which is a compilation of numerous international FEP lists from different host rocks,
- bottom-up and top-down approaches to identify relevant FEP,
- plausibility checks of the sequences and inter-dependencies of the FEP as well as
- consideration of indications from the geoscientific long-term prognosis, the scenario development and the process analyses.

Basic principle for all FEP lists (incl. the NEA-FEP-list) is their composition from two major FEP-groups:

- the “features” or “components”, that describe all elements of the repository system, and
- the “processes” (and “events”), that affect the components and describe the future evolution of the repository system.

With regard to the definition of FEP there is a broad scope of discretion: e.g. it is possible to describe one component in one FEP or to define each element or each property of the component in a separate FEP. So the NEA-FEP-list is very detailed with a high degree of itemization. In German projects, an intention was to define FEP in such a manner that the FEP are clearly separated and overlaps are avoided. Furthermore “components” including their proper-ties are completely described in one FEP. Looking at the interaction between the FEP

in causal sequences, a direct interaction between two “components” is not possible, but only via connecting “processes”. So a “process” may influence the properties of a “component”, and vice versa (e.g. the process “concrete corrosion” modifies the chemical, mechanical and hydraulic properties of the component “drift seal” and, conversely, the chemical and hydraulic properties of the "drift seal" influence the intensity of "concrete corrosion").

Two FEP-categories, that are parts of the NEA-FEP-list, were excluded from the German-FEP-lists due to regulatory reasons: “features/processes of the biosphere” and “future human actions”. A basic reason is, that neither a prognosis of the future biosphere nor of future human actions is possible and therefore corresponding FEP cannot be defined. The assessment of radionuclide release in future biosphere and the evaluation of potential human intrusion scenarios will be handled by stylized scenarios defined by the regulator.

8.2 Description of repository system by FEP

To be comparable with the US data for layered salt formations, the RANGERS project relies on data for the KOSINA project that focused on layered and pillow-like salt formations. Geology, repository concept and numerical models are described in chapters 5. and 6.. But neither for this geology nor for that repository concept a FEP catalog has been developed in the KOSINA project. Due to the limited capacity in the RANGERS project it was not possible to develop a special FEP catalog for German flat bedded salt formations. Therefore the FEP catalog relies on the VSG FEP catalog with exchange of Gorleben specific FEP by KOSINA specific FEP. Looking at the RANGERS specific tasks, the repository system description has been restricted to a FEP list with a short description of the FEP meaning. The dependencies between the FEP are not given here but can be from the VSG FEP catalog (Wolf et al., 2012). The structure of the FEP catalog has been updated to the recent state-of-art as given by the ANSICHT (Krull et al., 2004; Reinhold et al., 2008; Völkner et al., 2017a; Liu et al., 2017) and ERAM projects (not yet published), see Table 8.-1.

Table 8.-1: FEP-list of the RANGERS-specific repository system in a salt pillow

FEP No	FEP Name	Description
Processes with direct impact on EBS function (= Initial-FEP) are red marked.		
Processes with impact on radionuclides mobilization and transport are green marked		
Compartment Geosphere		
Features		
2.2.02.01	Host rock	Describes the chemical, hydraulic, mechanical and thermal properties of the host rock at the time of repository closure (Völkner et al. 2017). Salt pillar includes Staßfurt, Leine, Aller and Ohre formations. thickness of disposal formation (Hauptsalz) up to 600 m at repository level
2.2.02.02	Faults and joints in the host rock	Describes the chemical, hydraulic, mechanical and thermal properties of the faults and joints in the host rock (Völkner et al. 2017). They are relevant for carbonate, anhydrite and clay formations.
2.2.03.01	Adjacent rocks	Describes the chemical, hydraulic, mechanical and thermal properties of over (Bunter, Tertiary, Quaternary) and underlying (Red Formation) rocks at the time of repository closure (Völkner et al. 2017).

FEP No	FEP Name	Description
2.2.04.01	Faults and joints in the adjacent rocks	Describes the chemical, hydraulic, mechanical and thermal properties of the faults and joints in the adjacent rocks (Völkner et al. 2017). Important in consolidated rocks (Bunter, Red Formation)
2.2.07.01	Fluids in the host rock	describes the quantities and the chemical properties of brine and hydrocarbons in the intergranular crystall framework. Furthermore fluids are often accumulated in faults and joints of anhydrite and carbonate layers and due to permeation processes they may intrude from the top of salt formation or underlying formations (Liu et al. 2018)
2.2.07.02	Gas in the host rock	describes the quantities and the chemical properties of free gases or adsorbed gases at crystal boundaries and gaseous hydrocarbons. Furthermore gases are often accumulated in faults and joints of anhydrite and carbonate layers and due to permeation processes they may intrude from the top of salt formation or underlying formations (Liu et al. 2018)
2.2.08.01	Fluids in the adjacent rocks	describes the quantities and the chemical properties of pore water and water on faults and joints of competent formations (Liu et al. 2018).
2.2.08.02	Gas in the adjacent rocks	describes the quantities and the chemical properties of free gases or adsorbed gases in pores and gaseous hydrocarbons (Liu et al. 2018)
2.3.01.01	Geomorphology	The relief and shape of the surface environment and its potential evolution with time
2.3.04.01	Surface Water	Characteristics of rivers and lakes and their potential evolution
Events and Processes		
Geologic and climatic processes		
1.2.01.01	Neotectonic movements	Describes recent tectonic movements resulting in deformations in geosphere that characterize the recent stress field of the region.
1.2.01.03	Vertical movements of lithosphere	Describes very slow, large-scale epirogenetic movements (up or down-lift) of the lithosphere due to the underlying movement of the crustal plates.
1.2.02.01	Crustal deformation	Describes deformations of geosphere that are not caused crustal plate movements, e.g. isostatic movements
1.2.03.01	Earth quake	Release of accumulated geologic stress via rapid relative movements in the geosphere
1.2.07.01	Erosion	Include processes for disintegration of sediments and transport of erosion products.
1.2.07.02	Sedimentation	Deposition of particles from a transport medium.
1.2.08.01	Diagenesis	Transformation of sediments by compaction, cementation and crystallization.
1.2.09.01	Salt diapirism	Uplift of salt formations from deep geological levels due to high overburden pressure, fractures and tectonic movements, thick salt formations and low density of salt.
1.2.09.02	Subrosion	Salt solution at contact between unsaturated groundwater and salt formations
1.3.01.01	Global climate change	Long term evolution of climate

FEP No	FEP Name	Description
1.3.03.01	Transgression and regression	Offshore or onshore relocation of the coast line.
1.3.04.01	Permafrost	Permanent freezing of soil and near surface rock formation during glacial periods
1.3.04.02	Cryogenic fractures	Fractures in soil and near surface rock formations due to climate induced freezing and resulting thermo-mechanical stresses
1.3.05.01	Effects of glaciers and ice sheets	Includes processes like exaration (glacial erosion) and glacial loading
1.3.05.03	Periglacial channeling	Below a glacier, melting water may erode glacial channels.
1.5.03.01	Pathways in exploration drillings	Channeling in a borehole seal
Mechanical processes		
2.2.06.01	Mechanical stress changes	Describes the transition of tension resulting from an increase or decrease of tension in the rocks or a component of the repository.
Hydraulic processes		
2.1.07.02	Fluid pressure change	Describes a change of fluid pressure because of changes of tension in components / rocks or fluid flow processes.
2.2.07.03	Groundwater flow in the overburden rock	Describes the liquid flow in overburden rock because of potential gradients.
2.2.07.04	Gas flow in the overburden rock	Describes the liquid flow in overburden rock because of potential gradients.
2.2.07.05	Groundwater flow in the host rock	Describes the liquid flow in host rock because of potential gradients.
2.2.07.06	Gas flow in the host rock	Describes the liquid flow in host rock because of potential gradients.
2.2.08.01	Liquid-mediated transport of radionuclides	Summarizes all kind of transport processes of radionuclides in liquids
2.2.08.02	Gas-mediated transport of radionuclides	Summarizes all kind of transport processes of radionuclides in gases
Chemical-microbiological processes		
2.1.09.02	Dissolution and precipitation of salt minerals	Dissolution describes transition from solid phase to liquid. Precipitation is the inverse process.
2.2.09.01	Microbial processes in the host rock and the overburden formations	Summarizes all microbial processes in the host rock and in the adjacent rocks.
Thermal processes		
2.2.10.01	Thermally-induced uplift of the overburden rock	Uplift of salt formation and overburden rocks due to thermally induced volume changes
2.2.10.02	Thermal expansion or contraction	Volume change resulting from temperature change.
2.2.10.03	Heat flow	Temperatures in geosphere are influenced by geothermal, climate and heat generating waste
Compartment: Shafts, infrastructure area and connecting drifts		
Features		
2.1.04.01	Backfill	Describes the chemical, hydraulic, mechanical and thermal properties of the backfill at the time of repository closure (Bertrams et al. 2018).

FEP No	FEP Name	Description
2.1.05.01	Borehole seals	Describes the chemical, hydraulic, mechanical and thermal properties of borehole seals for exploration drillings at the time of repository.
2.1.05.02	Shaft seals	Describes the chemical, hydraulic, mechanical and thermal properties of the shaft seal at the time of repository closure. The contact zone *) has been enclosed in the FEP (chapt. 3.5.3).
2.1.05.03	Drift seals	Describes the chemical, hydraulic, mechanical and thermal properties of a drift seal at the time of repository closure (Bertrams et al. 2018). The contact zone *) has been enclosed in the FEP. (Chapt. 3.5.4)
2.1.06.01	Technical installations	Installations remaining in the repository after closure, e.g. rock bolts, cables, shaft/drift lining *), roadway etc. and summarizes their properties
2.1.08.03	Liquids in mine excavations	describes the quantities and the chemical properties of liquids from waste, from construction material and from inflow of the surrounding rocks or via the shafts/ramp
2.1.12.02	Gas in mine excavations	describes the quantities and the chemical properties of mine air and gas from metal corrosion and microbial degradation of organic matters and from inflow of the surrounding rocks
2.2.01.01	Excavation disturbed zone (EDZ)	Tension redistribution in the geosphere results in the disintegration of a rock zone close to the mine openings. This FEP also includes concrete injections *) to reduce the hydraulic conductivity of EDZ.
		**) separate FEP in subsystem description (chap. 6.3) for detailed analysis*
Processes		
Mechanical processes		
2.2.06.01	Mechanical stress changes	Describes the transition of tension resulting from an increase or decrease of tension in the rocks or a component of the repository.
2.2.06.02	Convergence	Reduction of void volume by rock creeping.
2.1.07.03	Compaction of crushed salt	Describes the slow consolidation of crushed salt. Compaction results in a solidification and a reduction of porosity. Initiating processes are gravity forces and the load from surrounding geosphere.
2.1.07.04	Swelling, shrinking and creeping of concrete	Describes not thermal induced volume or pressure changes of concrete.
2.1.08.08	Swelling and shrinking of bentonite	Means the adsorption and release of water from the crystal interim layer of clay minerals
2.1.07.07	Displacement of the shaft seals	Describes a change of seal position in comparison with construction site
Hydraulic processes		
2.1.07.02	Fluid pressure change	Describes a change of fluid pressure because of changes of tension in components / rocks or fluid flow processes.
2.1.08.06	Liquid intrusion into mine excavations	Inflow of liquid from host rock or adjacent formations
2.1.08.07	Liquid flow in mine excavations	Describes the liquid flow because of potential gradients.

FEP No	FEP Name	Description
2.1.08.08	Gas flow in mine excavations	Describes gas flow because of potential gradients
2.1.08.04	Channeling in crushed salt	Generation of flow paths by inhomogeneous compaction or swelling or erosion of backfill
2.1.08.05	Channeling in sealing components	Generation of flow paths by inhomogeneous compaction or swelling or erosion of concrete / bentonite
2.2.07.01	Liquid-mediated transport of radionuclides	Summarizes all kind of transport processes of radionuclides in liquids
2.2.07.02	Gas-mediated transport of radionuclides	Summarizes all kind of transport processes of radionuclides in gases
Chemical-microbiological processes		
2.1.09.02	Dissolution and precipitation of salt minerals	Dissolution describes transition from solid phase to liquid. Precipitation is the inverse process.
2.1.09.03	Corrosion of metal	Describes the electrochemical reaction of metals with surrounding fluids and resulting gas generation
2.1.09.06	Corrosion of cement- or sorel-based materials	Describes the chemical degradation of concrete
2.1.09.07	Solution, transformation and regeneration of clay minerals	Describes the mineralogical and chemical transformation of clay minerals (in shaft seals) due to changes in hydrochemistry
2.1.09.08	Alteration of Anhydrite and Gypsum formation	Anhydrite (water-free Ca sulfate) is alterated by water with formation of gypsum (Ca sulfate-Dihydrate). In the course of this exothermal reaction, the volume of the solid phase significantly increases.
2.1.10.02	Microbial processes in the repository	Summarizes all microbial processes in the mine excavations including the EDZ.
Events		
2.1.07.05	Early failure of integrity of a shaft seal	Failure of a shaft seal during the functional lifetime by chemical, mechanical, hydraulic or thermal impacts.
2.1.07.06	Early failure of integrity of a drift seal	Failure of a drift seal during the functional lifetime by chemical, mechanical, hydraulic or thermal impacts.
Compartment: disposal areas		
Features		
2.1.01.01	Inventory: Radionuclides	compiles the composition, activity and quantities of the radionuclides enclosed in the radioactive waste at the time of emplacement. (Bertrams et al. 2015)
2.1.01.02	Inventory: Metal compounds	compiles the chemical composition and quantities of all metal components in the repository mine (Bertrams et al. 2015)
2.1.01.03	Inventory: Organic compounds	compiles the chemical and microbial composition and quantities of all organic matter in the repository mine (Bertrams et al. 2015)
2.1.01.04	Inventory: Other compounds	compiles the chemical composition and quantities of other materials in the repository mine (e.g. graphite (for AVR/THTR spent fuel and neutron moderator of disposal casks), concrete for mine installations and geotechnical barriers) (Bertrams et al. 2015, 2018)

FEP No	FEP Name	Description
2.1.02.01	Waste matrices	Describes the chemical, hydraulic, mechanical and thermal l properties of the waste matrices (e.g. metal, borosilicate glass) at the time of emplacement (Bertrams et al. 2015).
2.1.03.01	Spent fuel containers	Describes the composition and properties of POLLUX and CASTOR casks that ensure the waste containment during the operation period and at least 500 a during the post closure phase (Bertrams et al. 2015).
2.1.03.02	Other disposal containers	Describes the composition and properties of POLLUX and CASTOR casks for reprocessing waste and MOSAIK cask for structural parts from conditioning of spent fuel elements that ensure the waste containment during the operation period and at least 500 a during the post closure phase (Bertrams et al. 2015)
2.1.08.03	Liquids in mine excavations	describes the quantities and the chemical properties of liquids from waste, from con-struction material and from inflow of the host rock (Liu et al. 2018)
2.1.12.02	Gases in mine excavations	describes the quantities and the chemical properties of mine air and gas from metal corrosion and microbial degradation of organic matters and from inflow of the host rock (Liu et al. 2018)
Mechanical processes		
2.2.06.01	Mechanical stress changes	Describes the transition of tension resulting from an increase or decrease of tension in the adjacent rock or a component of the repository.
2.1.07.01	Convergence	Reduction of void volume by rock creeping.
2.1.07.03	Compaction of crushed salt	Describes the slow consolidation of crushed salt. Compaction results in a solidification and a reduction of porosity. Initiating processes are gravity forces and the load from surrounding geosphere.
Hydraulic processes		
2.1.07.02	Fluid pressure change	Describes a change of fluid pressure because of changes of tension in components / rocks or fluid flow processes.
2.1.08.06	Liquid intrusion into mine excavations	Inflow of liquid from the host rock
2.1.08.07	Liquid flow in mine excavations	Describes the liquid flow because of potential gradients.
2.1.08.08	Gas flow in mine excavations	Describes gas flow because of potential gradients
2.1.08.04	Channeling in crushed salt	Generation of flow paths by inhomogeneous compaction or swelling or erosion of backfill
2.2.11.01	Pressure-induced fluid infiltration into the salt rock	If fluid pressure exceeds the smallest main stress in salt rock, the permeability will be locally increased by expansion of the pore structure and fluids can infiltrate the rock.
3.2.07.01	Liquid-mediated transport of radionuclides	Summarizes all kind of transport processes of radionuclides in liquids
3.2.07.02	Advection	Transport of dissolved substances by fluid flow
3.2.07.03	Dispersion	Distribution of dissolved substances by inhomogeneous flow velocities in porous media.

FEP No	FEP Name	Description
3.2.07.04	Diffusion	Stirring of different substances by BROWN molecular movements
3.2.08.01	Lifting or sinking of waste packages	Compilation of processes that may result in a displacement of waste packages from their emplacement position.
3.2.09.01	Gas-mediated transport of radionuclides	Summarizes all kind of transport processes of radionuclides in gases
Thermal processes		
2.1.11.01	Heat flow	Means the energy transport as a result of temperature differences.
2.1.11.02	Thermal expansion or contraction	Volume change resulting from temperature change.
2.1.11.03	Vaporisation of water	Describes the transition from liquid to gas depending from the composition of the liquidl, the pressure and the temperature
2.2.10.02	Thermomigration	Migration of liquid the host rock induced by the temperature field in the surroundings of the disposal areas.
2.2.10.03	Thermal degradation of carnallite	Carnallite has a high content of crystal water that will be released with increasing temperatures at several hydration steps
2.2.10.05	Thermochemical sulfate reduction	Redox reaction of organic matters or molecular hydrogen with sulfate at high temperatures generating carbonate, sulfide, water, hydrogen sulfide or carbon dioxide.
Chemical-biological processes		
2.1.09.02	Dissolution and precipitation of salt minerals	Solid material may be partly or completely dissolved. For halite it will be a congruent dissolution, for complex salt minerals or construction or waste materials it may be an incongruent dissolution. If solubility limits are exceeded, dissolved materials may precipitate.
2.1.09.03	Corrosion of metal	Describes the electrochemical reaction of metals with surrounding fluids and resulting gas generation. If contaminated metal components (e.g. waste canisters, structural part from spent fuel conditioning,) the process contributes to RN mobilization
2.1.09.04	Corrosion of spent fuel	Chemical processes resulting in a degradation of the spent fuel matrix
2.1.09.05	Corrosion of glass	Chemical alteration of the borosilicate matrix of reprocessing waste by interaction with liquids
2.1.09.06	Corrosion of cement- or sorel-based materials	Describes the chemical degradation of concrete
2.1.09.07	Corrosion of graphite waste	Chemical alteration of the graphite matrix of research reactor fuel and moderator/reflector material by interaction with liquids
2.1.09.08	Hydrogen induced embrittlement	The intrusion of hydrogen in metal structures results in a modification of the mechanical properties.
2.1.10.01	Degradation of organic compounds	Describes the alteration of man-made (waste, cables, pipes etc.) and natural organics by chemical processes

FEP No	FEP Name	Description
2.1.10.02	Microbial processes in the repository	Summarizes all microbial processes in the mine and in the surrounding rocks
3.2.03.01	Sorption and desorption	Sorption describes the physico-chemical interaction of dissolved species with a solid phase. Desorption is the opposite effect.
3.2.04.01	Colloids	Generation of colloids and their filtration during transport
3.2.05.01	Complexation	Impact of complexing agents on the radioactive waste
2.1.12.04	Deflagration and explosion of gases	Mixtures of ignitiable gases and oxygen can deflagrate or detonate if lighted
Radiological Processes		
2.1.13.01	Radiation-induced activation	Generation of radioactive isotopes due to nuclear reaction after absorption of neutrons
2.1.13.03	Radiolysis	Radiolysis of water within a waste package can produce hydrogen, oxygen and hydroxide peroxide.
2.1.14.01	Nuclear criticality	Fissile substances are arranged in such a manner that a self-preserving nuclear reaction can take place.
3.1.01.01	Radioactive decay and ionizing radiation	Spontaneous transformation of instable atomic nuclei combined with the emission of characteristically ionizing radiation
3.2.01.01	Mobilization of radionuclides	The processes that directly affect the mobilization of radionuclides from the waste form once the waste container has failed
Events		
2.1.03.03	Failure of a spent fuel container	Failure of waste container as a consequence of undetected construction failures or impact of chemical, mechanical, hydraulic or thermal processes with design exceeding intensity during the functional period.(500 a). Starting point for RN mobiliozation
2.1.03.04	Failure of another waste container	Failure of waste container as a consequence of undetected construction failures or impact of chemical, mechanical, hydraulic or thermal processes with design exceeding intensity during the functional period.(500 a). Starting point for RN mobiliozation

8.3 Description of subsystems

For detailed investigations on EBS design and integrity a precise description of the surroundings of EBS (subsystem) and of all included components as well as the identification of processes that directly impair the EBS are necessary.

For characterization of the components material properties (mineralogy, geochemistry, density, solubility, plasticity, heat conductivity, porosity, permeability, effective strength etc.), construction properties (e.g. volume, geometry (length, width and high), surface properties, fissures etc.) as well as state variables (e.g. temperature, effective strength, microbes etc.) have to be analyzed.

To evaluate the loads that are impacting the EBS, the properties and intensity of the affecting FEP (called initial FEP) have to be determined by analyzing all components and processes that influence those FEP. In this context the FEP list can identify the interacting FEP and describe them qualitatively. To specify the properties and the intensity of processes, numerical process analyses are necessary.

8.3.1 Subsystem Nearfield of Shaft Seal

The subsystem “nearfield of shaft seal” is part of the compartment “Shafts, infrastructures and connecting drifts” (see Table 8.-1). It comprises the shaft column (incl. EDZ), the construction materials (incl. corrosion materials), fluids, all shaft installations (incl. seals, backfill, lining) and the shaft landing (Herold et al., 2020) as well as adjacent parts of the geosphere and biosphere (Keller et al., 2021b), see Figure 8.-1. The components of the nearfield are influenced by numerous mechanical, hydraulic, chemical and thermal processes initiated in the farfield. So mechanical loads not only result from lithostatic pressure but from modifications of geosphere stress field by tectonic movements (e.g. subsidence, uplift), earth quake or processes like glaciation, erosion and sedimentation. Because this subsystem cuts through the whole geological sequence, not only the host rock but also the aquifers in the overburden formations and the underground facilities are linked. Therefore a broad spectrum of hydraulic impacts is possible – from the overburden, anhydrite reservoirs and brine pockets in the salt formations and fluids that are squeezed out from the underground excavation via the infrastructure area to the shafts. Therefore liquids with a broad spectrum of hydrochemical properties have to be considered and different levels of fluid pressure. Intensive gas generation due to metal corrosion may significantly increase fluid pressure. Due to the distance between the disposal areas and the shafts there will be only a limited increase of temperature but significant thermomechemical stresses may occur. A compilation and short description of all relevant FEP of the subsystem is given in Table 8.-2. For processes their potential impact on EBS as well as an itemization of affected components is given. FEP that are excluded in a screening process due to their low probability and/or intensity are not mentioned.

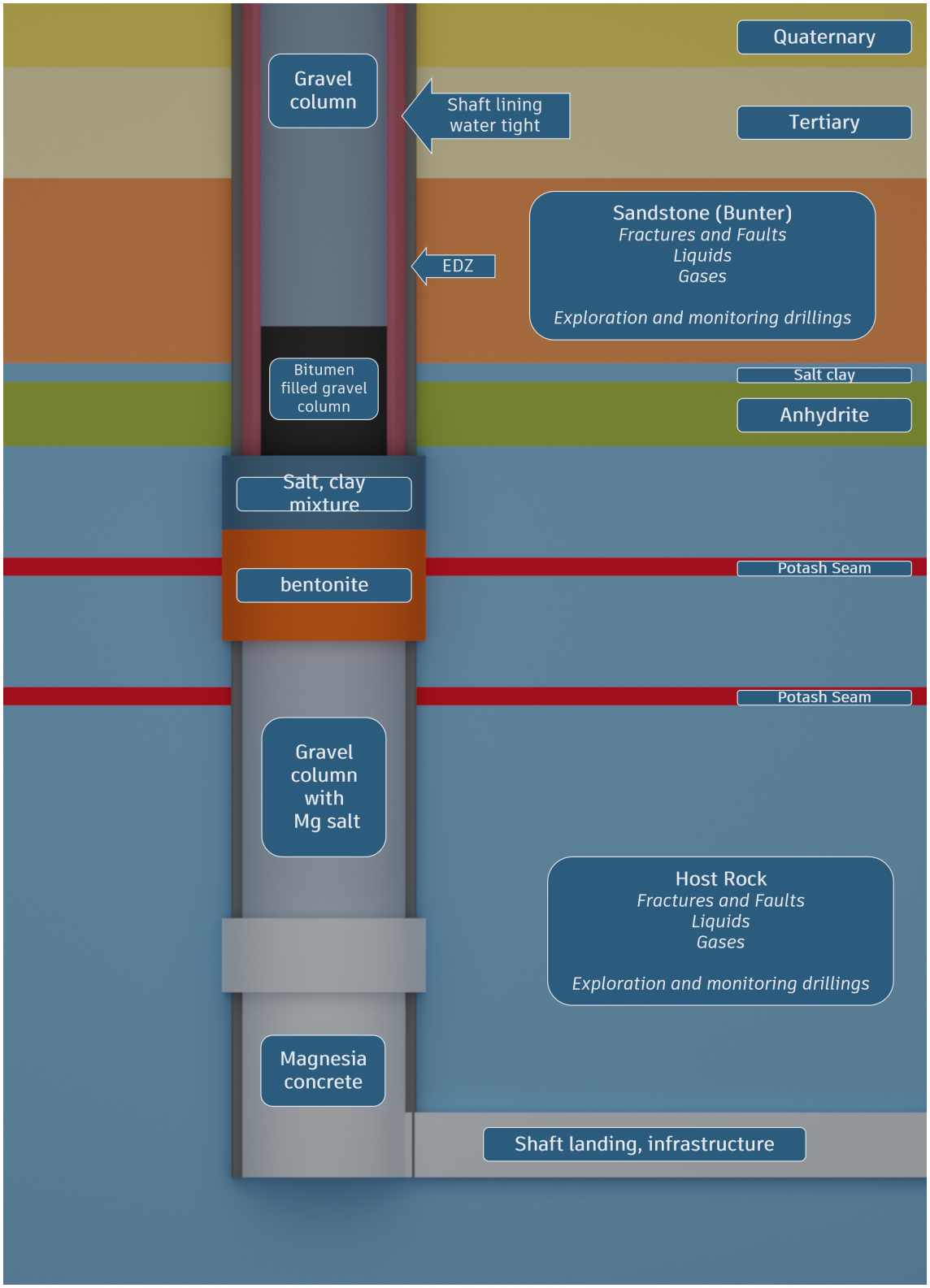

Figure 8.-1: Nearfield model for the shaft seal, FEP in italics.

Table 8.-2: FEP lists for the subsystem “Shaft seal”. Processes that may directly affect the EBS function (Initial FEP) are red marked.

					Components affected by processes																			
Subsystem Shaft	**Process Group**	**FEP (No. referring to the components mentioned in right column)**	**Description**	**Direct impact of processes on barrier function and other shaft components**	1	2	3	4	5	6	7	8	9	10	11	12	13	14	15	16	17	18	19	20
Components		1 Shaft seal	Describes the chemical, hydraulic, mechanical and thermal properties of the shaft seal at the time of repository closure. Shaft seals consist of abutments and sealing elements. The construction materials (salt concrete, magnesia concrete, bentonite, clay/salt mixture, asphalt) are adapted to the surrounding geology and the chemical impact of circulating groundwater.																					
		2 Shaft lining	Describes the chemical, hydraulic, mechanical and thermal properties of the shaft lining that is restricted to the overburden formations and to the top of the host rock. Shaft lining is designed to function during operation period. After closure shaft lining will fail after a few decades.																					
		3 Shaft backfill	Describes the chemical, hydraulic, mechanical and thermal properties of the shaft backfill (gravel column) on top of the shaft seal. The Uppermost parts the shafts have to be backfilled in compliance with mining regulations.																					
		4 Concrete corrosion products	Describes the chemical, hydraulic, mechanical and thermal properties of the concrete corrosion products of the shaft seal, concrete lining, injections and borehole seals																					
		5 Metal corrosion products	Describes the chemical, hydraulic, mechanical and thermal properties of the metal corrosion products (e.g. steel shaft lining).																					
		6 Contact Zone	Describes the geometry and the hydraulic properties of the void volume between the barrier and the drift contour. May be sealed by concrete injections or by salt creeping (convergence)																					
		7 Excavation damaged zone in the overburden formations	Describes the chemical, hydraulic, mechanical and thermal properties of the EDZ at the time of repository closure. The properties and extent of EDZ depend on the rock properties and the stabilization measures (lining). Fissures of EDZ may be closed by convergence.																					
		8 Excavation damaged zone in host rock	Describes the chemical, hydraulic, mechanical and thermal pro-perties of the EDZ at the time of repository closure. The properties and extent of EDZ depend on the rock properties and the stabi-lization measures (lining). Fissures of EDZ may be closed by convergence.																					
		9 Liquids in shaft	This FEP describes the quantities and the chemical properties of the liquids (groundwater and hydrocarbons in the shaft column incl. EDZ/contact zone,																					
		10 Gases in shaft	This FEP describes the quantities and the chemical properties of free gases and gaseous hydrocarbons in the shaft and the EDZ/contact zone.																					

					Components affected by processes																			
Subsystem Shaft	**Process Group**	**FEP (No. referring to the components mentioned in right column)**	**Description**	**Direct impact of processes on barrier function and other shaft components**	1	2	3	4	5	6	7	8	9	10	11	12	13	14	15	16	17	18	19	20
		11 Concrete injections	Describes the chemical, hydraulic and mechanical properties of the injection material. Concrete injections may be used to seal contact zone, EDZ and fractures in surrounding rocks.																					
		12 Exploration and monitoring drillings	Describes the chemical, hydraulic, mechanical and thermal pro-perties of backfilled drillings arranged at the shaft contour to explore or monitor the surrounding host rock, overburden formations. The backfilling material is adapted to the surrounding geology and the chemical impact of circulating groundwater.																					
		13 Overburden formations	Describes the chemical, hydraulic, mechanical and thermal properties of the overburden formations at the time of repository closure																					
		14 Fractures and faults in the overburden Formations	Describes the chemical, hydraulic, mechanical and thermal properties of fractures and faults and their mineralization in the overburden formations at the time of repository closure																					
		15 Liquids in the overburden formations	This FEP describes the quantities and the chemical properties of the liquids in the overburden formations. The geological formations may include several aquifers with different hydrochemistry as well as hydrocarbon reservoirs.																					
		16 Gases in the overburden formations	This FEP describes the quantities and the chemical properties of the gases in the overburden formations. Most common gases are CO2, N2 and CH4.																					
		17 Host rock	Describes the chemical, hydraulic, mechanical and thermal properties of the host rock at the time of repository closure.																					
		18 Fractures and faults in host rock	Describes the chemical, hydraulic, mechanical and thermal properties of fractures and faults and their mineralization in the hostrock at the time of repository closure																					
		19 Liquids in host rock	This FEP describes the quantities and the chemical properties of the liquids in the hostrock. Apart from very small fluid inclusions in salt and fractured anhydrite formations are potential reservoirs. Liquids in salt formations include brine (in equilibrium with surrounding salt) and hydrocarbons.																					
		20 Gases in host rock	This FEP describes the quantities and the chemical properties of the liquids in the hostrock. Apart from very small fluid inclusions in salt, fractured anhydrite formations are potential reservoirs. Common gases in salt formations include CO2, N2 and CH4.																					
Processes/Events	**Mechanical**	**Earth quake**	The release of accumulated geologic stress via rapid relative movements within the Earth's crust usually along existing faults or geological interfaces. The accompanying release of energy may result in ground movement and/or rupture.	Earth quakes may particularly affect the shaft components shortly after repository closure. Then the shaft seal is not yet fixed in the shaft column.	✓	✓	✓	✓	✓		✓	✓			✓	✓	✓	✓			✓	✓		

					Components affected by processes																			
Subsystem Shaft	**Process Group**	**FEP (No. referring to the components mentioned in right column)**	**Description**	**Direct impact of processes on barrier function and other shaft components**	1	2	3	4	5	6	7	8	9	10	11	12	13	14	15	16	17	18	19	20
		Permafrost	Soil and uppermost part of the overburden rock formations that were permanently frozen during ice age.	X) will occur after the functional lifetime of the geotechnical barriers	✓	✓	✓	✓	✓		✓	✓	✓		✓	✓	✓	✓			✓	✓	✓	
		Effects of glaciers and ice sheets	Include processes like exaration (a glacial erosion process). Glaciation will increase the mechanical load on the repository system.	X) will occur after the functional lifetime of the geotechnical barriers	✓	✓	✓	✓	✓	✓	✓	✓	✓	✓	✓	✓	✓	✓	✓	✓	✓	✓	✓	✓
		Glacial channelling	Below a glacier, melting water may erode glacial channels. May destroy uppermost parts of shaft and reduce mechanical load	X) will occur after the functional lifetime of the geotechnical barriers	✓	✓	✓	✓	✓		✓	✓	✓		✓	✓	✓	✓						
		Diapirism	Uplift of thick salt formations due to density inversion, stresses resulting from overlying rock formations and tectonic structures.	X) The uplift of the salt dome may induce stresses in the shaft seal	✓	✓	✓	✓	✓	✓	✓	✓	✓	✓	✓	✓	✓	✓	✓	✓	✓	✓	✓	✓
		Mechanical stress changes	Describes the transition of tension resulting from an increase or decrease of tension in the rocks or a component of the repository.	If stresses exceed material stability, they may result in fractures in the shaft seal and lining, the EDZ, the concrete injections, the borehole seals, the host rock and the overburden formations.	✓	✓	✓	✓	✓	✓	✓	✓	✓	✓	✓	✓	✓	✓	✓	✓	✓	✓	✓	✓
		Swelling, shrinking and creeping of concrete	Describes not thermally induced volume or pressure changes of concrete.	They will modify the properties of shaft seal, shaft lining, injection material in contact zone / EDZ and borehole sealings.	✓	✓		✓					✓		✓	✓			✓				✓	
		Swelling and shrinking of bentonite	Means the adsorption and release of water from the crystal interim layer of clay minerals	Will modify the properties of the shaft seal and close the contact zone as well as the fissures in the EDZ	✓								✓						✓				✓	
		Settlement and compaction of backfill	Settlement means the slow lowering of non cohesive materials for backfilling and closure. This leads to compaction and hardening. Driving forces for this process are gravitation and the load of the surrounding geosphere.	Will modify the properties of crushed salt and the gravel column of the shaft seal.			✓	✓					✓						✓					
		Convergence	Describes rock creeping into the mine excavations. Creeping rates depend on the mechanical properties of the rocks: high in salt formations, low in brittle hard rocks (anhydrite).	Convergence will fix the shaft seal in the shaft column and close the contact zone as well as the fissures in the EDZ						✓	✓	✓					✓	✓			✓	✓		
		Displacement of shaft sealing element	Describes the displacement of sealing elements of the shafts from their installation position by mechanical or hydraulic impacts.	The displacement of sealing elements may result in flow paths at the shaft contour	✓					✓	✓	✓			✓									
	Hydraulic	**Transgression and regression**	Offshore or onshore relocation of the coast line (flooding and landing). May be influenced by man-made climate change	A flooding of the repository site would result in an increased hydraulic pressure at the shaft seal	✓		✓	✓	✓	✓	✓	✓	✓	✓	✓	✓	✓	✓	✓	✓	✓			
		Surface water bodies	During future site evolution existing rivers, lakes etc. may be relocated and their extent/volume changed. Flooding of shafts has to be considered.	Little impact on geotechnical barriers	✓		✓	✓	✓	✓	✓	✓	✓	✓	✓	✓	✓	✓	✓	✓	✓			
		Liquid flow processes	Describes the liquid flow because of potential gradients. They may modify the hydraulic properties of the shaft seal, injection material and borehole seals.	Liquid flow processes influence fluid pressure and may result in an erosion of construction materials and increase contact zone / EDZ	✓	✓	✓	✓	✓	✓	✓	✓	✓	✓	✓	✓	✓	✓	✓	✓	✓	✓	✓	✓
		Gas flow processes	Describes the gas flow because of potential gradients. Impact of high gas pressure is described in the FEP hydraulic pressure change.	Gas flow processes influence fluid pressure and thus impair geotechnical barriers	✓	✓	✓	✓	✓	✓	✓	✓	✓	✓	✓	✓	✓	✓	✓	✓	✓	✓	✓	✓
		Channeling in a sealing element	Generation of flow paths by inhomogeneous compaction or swelling or erosion of bentonite / concrete or viscous fingering in asphalt	Impairment of the function of the shaft sealing elements	✓			✓	✓				✓	✓		✓								
		Hydraulic pressure change	Describes a change of fluid pressure because of changes of tension in rocks or fluid flow processes.	High fluid pressure may induce fissures in barrier constructions and EDZ									✓	✓					✓	✓			✓	✓

					Components affected by processes																			
Subsystem Shaft	**Process Group**	**FEP (No. referring to the components mentioned in right column)**	**Description**	**Direct impact of processes on barrier function and other shaft components**	1	2	3	4	5	6	7	8	9	10	11	12	13	14	15	16	17	18	19	20
		Diffusion	Stirring of different substances by BROWN molecular movements.	The process is relevant for mass transport but will not directly affect the barrier function.	✓	✓	✓	✓	✓	✓	✓	✓	✓	✓	✓	✓	✓	✓	✓	✓	✓	✓	✓	✓
		Dispersion	Distribution of dissolved substances by inhomogeneous flow velocities in porous media.	The process is relevant for mass transport but will not directly affect the barrier function.	✓	✓	✓	✓	✓	✓	✓	✓	✓	✓	✓	✓	✓	✓	✓	✓	✓	✓	✓	✓
		Liquid inflow	Describes the inflow of liquids from the host rock, the overburden formations via the EDZ into the mine openings.	Liquid inflow from geosphere will change hy-drochemistry and there-fore promote corrosion of construction materials	✓	✓	✓	✓	✓	✓	✓	✓	✓		✓	✓								
		Asphalt migration	Due to gravitation and/or hydraulic resp. mechanical loads asphalt can squeezed from shaft seals and migrate in the contact zone, the EDZ as well as pores, fractures and faults in the surrounding rock formations.	Asphalt migration results in a decrease of the asphalt volume in the shaft seal and thus impair the sealing function	✓	✓	✓	✓	✓	✓	✓	✓	✓	✓				✓	✓	✓				
		Phase transition	Describes the transition from solid to liquid or from liquid to gas depending from the composition of the material, the pressure and the temperature.	During the functional lifetime of the EBS no phase transitions will occur that can impair EBS function									✓	✓					✓	✓			✓	✓
		Dissolution and outgassing	Describes the transition of gas between gaseous phase and the dissolved phase.	The process is relevant for mass transport but will not directly affect the barrier function.									✓	✓					✓	✓			✓	✓
		Radionuclide transport in the liquid phase	Summarizes all kind of transport processes of radionuclides in liquids.	The process is relevant for release of radionuclides but will not directly affect the function of the barriers.	✓	✓	✓	✓	✓	✓	✓	✓	✓		✓	✓	✓	✓	✓		✓	✓	✓	
		Radionuclide transport in the gas phase	Summarizes all kind of transport processes of radionuclides in gas.	The process is relevant for release of radionuclides but will not directly affect the function of the barriers.	✓	✓	✓	✓	✓	✓	✓	✓		✓	✓	✓	✓	✓		✓	✓	✓		✓
	Thermal	Heat flow	Means the energy transport as a result of temperature differences. There are 3 sources for heat flow: climate, geothermy and radionuclide decay of the waste	Indirect impact, induces mechanical and chemical processes	✓	✓	✓	✓	✓	✓	✓	✓	✓	✓	✓	✓	✓	✓	✓	✓	✓	✓	✓	✓
		Thermal expansion or contraction	Volume changes resulting from temperature change. In the shafts,. TM stresses are predominately climate induced. They are only relevant during glacial periods and then they may impair all constructions in the shafts, the EDZ and the rock formations.	X) During glacial periods, thermomechanical stressses may induce fis-sures in the components of the shaft seals. Thus the function of the seals may be impaired. Due to the distance to the disposal areas, the shafts will not be impaired by thermomechanical stresses resulting from heat generating waste.	✓	✓	✓	✓	✓		✓	✓	✓		✓	✓	✓	✓	✓		✓	✓	✓	
	Chemical / biological	**Concrete corrosion**	Describes the chemical degradation of concrete	The corrosion processes will impair the function of all concrete components in the shafts: shaft seal, shaft lining, borehole seals and injections. For sealing constructions the mechanical stability of abutments may be be reduced and the hydraulic conductivity of seals increased.	✓	✓		✓					✓		✓	✓			✓				✓	
		Solution and precipitation of salt minerals	Solution describes the transition of a solid phase (salt minerals) into the liquid phase due to a change of hydrochemical boundary conditions. Precipitation is the reverse process. This process is considered for crushed salt backfill and for EDZ.	This process will modify the hydraulic properties of salt backfill and the EDZ	✓		✓					✓	✓								✓	✓	✓	
		Metal corrosion	Describes the electrochemical reaction of metals with surrounding fluids and resulting gas generation. This process will reduce the mechanical stability of metal components.	Stabilization measures, like steel lining and roof bolts, will be impaired by corrosion. This may mo-dify the properties of the EDZ.	✓	✓			✓				✓	✓		✓			✓	✓			✓	✓
		Hydrogen embrittlement	The intrusion of hydrogen (from metal corrosion) in metal structures results in a modification of the mechanical properties.	In comparison to metal corrosion of low relevance	✓	✓								✓		✓				✓				✓

					Components affected by processes																			
Subsystem Shaft	**Process Group**	**FEP (No. referring to the components mentioned in right column)**	**Description**	**Direct impact of processes on barrier function and other shaft components**	1	2	3	4	5	6	7	8	9	10	11	12	13	14	15	16	17	18	19	20
		Microbial processes	Summarizes all microbial processes in the mine and in the surrounding rocks. Important for degradation of organics, but may also force the corrosion of metal and concrete.	May directly impair the function of the shaft seal and lining by degradation of asphalt and indirectly by intensifying corrosion processes	✓	✓		✓		✓	✓	✓	✓		✓	✓	✓	✓	✓		✓	✓	✓	
		Chemical alteration of organica	Describes the alteration of organic matters in the shaft seal (asphalt, organic compounds in clay) and lining (asphalt filled joint) by chemical processes.	Lower relevance in comparison to microbial processes.	✓	✓							✓						✓		✓		✓	
		Alteration of bentonite	Describes the solution, transformation and regeneration of bentonite due to hydrochemical, biological and thermal environmental conditions. As a consequence the mineralogical and chemical properties of the bentonite have been changed.	Bentonite alteration may impair the sealing function of the bentonite seal.	✓								✓		✓				✓				✓	
		Sorption and desorption	Sorption describes the physico-chemical interaction of dissolved species with a solid phase. Desorption is the opposite effect.	The process is relevant for mass transport but will not directly affect the barrier function.																				
		Complexation	Describes the impact of complexing agents on the radioactive waste.	The process is relevant for mass transport but will not directly affect the barrier function.																				
		Colloid generation and filtration	Generation of colloids and their filtration during transport.	May have an impact on bentonite barriers.																				
	Radiological	Radiological decay and ionizing radiation	Spontaneous transformation of instable atomic nuclei combined with the emission of characteristic ionizing radiation.	The process is relevant for release of radionuclides but will not directly affect the function of the barriers.																				

8.3.2 Subsystem Nearfield of drift seal

The Subsystem nearfield of drift seal is part of the compartment “Shafts, infrastructures and connecting drifts”. It includes part of a connecting drift (with EDZ), the drift lining, the construction materials (incl. corrosion products), the drift seal consisting of a sealing element, abutments and contact zone, the backfill, fluids and adjacent parts of the host rock, see Figure 8.-2. The components of the near field are influenced by numerous mechanical, hydraulic, chemical and thermal processes initiated in the farfield. So mechanical loads not only result from lithostatic pressure but from modifications of geosphere stress field by tectonic movements (e.g. subsidence, uplift), earth quake or processes like glaciation, erosion and sedimentation. Hydraulic loads may results from brine inflow from anhydrite reservoirs and brine pockets in the salt formations as well as from liquids slowly percolating through the shaft seal and EDZ into the infrastructure area. Therefore a broad spectrum of hydraulic impacts is possible – so groundwater inflow the shaft as well as different brine types from salinar reservoirs with different hydrochemistry. The fluid pressure will depend on gas generation by metal corrosion on one hand and convergence of the underground excavations on the other hand. Due to the distance between the disposal areas and the drift seal sites there will be a moderate increase of temperature but significant thermal-mechanical stresses may occur. A compilation of all relevant FEP in the subsystem as well as their short description (components) resp. a characterization on the potential impact of processes on EBS and an itemization of affected components, is given in Table 8.-3. FEP that are excluded in a screening process due to their low probability and/or intensity are not mentioned.

Table 8.-3: FEP lists for the subsystem “Drift seal”. Processes that may directly affect the EBS function (Initial FEP) are red marked.

					Components affected by process													
Sub-system: Drift	**Process Group**	**FEP (No. referring to the components mentioned in right column)**	**Description**	**Direct impact of processes on barrier function and other mine components**	1	2	3	4	5	6	7	8	9	10	11	12	13	14	15
Components		1 Drift seal	Describes the chemical, hydraulic, mechanical and thermal properties of the drift seal at the time of repository closure. Drift seals consist of abutments and sealing elements. The construction materials (salt and magnesium concrete) are adapted to the surrounding salt rock and the hydrochemistry of possibly inflowing brine.																
		2 Drift lining	Describes the chemical, hydraulic, mechanical and thermal properties of the drift lining at the time of repository closure. Drift lining will be installed in mine excavations with a long operating time (e.g. infrastructure, access drifts) or salt formations with low mechanical stability (e.g. anhydrite). Drift lining is designed to function during operation period. After closure drift lining will fail after a few decades.																
		3 Drift backfill	Describes the chemical, hydraulic, mechanical and thermal properties of the drift backfill at the time of repository closure. Crushed salt and concrete are common backfill materials.																
		4 Concrete corrosion products	Describes the chemical, hydraulic, mechanical and thermal properties of the concrete corrosion products of the drift seals, concrete linings, injections and borehole seals.																
		5 Metal corrosion products	Describes the chemical, hydraulic, mechanical and thermal properties of the metal corrosion products (e.g. partition plates or reinforcement in concrete components, rock bolts).																
		6 Contact Zone	Describes the geometry and the hydraulic properties of the void volume between the barrier and the drift contour. May be sealed by concrete injections or by salt creeping (convergence)																
		7 Excavation damaged zone in host rock	Describes the chemical, hydraulic, mechanical and thermal properties of the EDZ at the time of repository closure. The properties and extent of the EDZ depend on the properties and the stabilization measures (lining). Fissures of EDZ may be closed by convergence.																
		8 Concrete Injections	Describes the chemical, hydraulic, mechanical and thermal properties of concrete injections that are provided to seal fractures and																
		8 Liquids in underground excavations	This FEP describes the quantities and the chemical properties of the liquids (brine and hydrocarbons in the drift incl. EDZ/contact zone,																
		9 Gases in underground excavations	This FEP describes the quantities and the chemical properties of free gases and gaseous hydrocarbons in the drift and the EDZ/contact zone.																
		10 Concrete injections	Describes the chemical, hydraulic and mechanical properties of the injection material. Concrete injections may be used to seal contact zone, EDZ and fractures in the surrounding rocks.																

					Components affected by process													
Sub-system: Drift	**Process Group**	**FEP (No. referring to the components mentioned in right column)**	**Description**	**Direct impact of processes on barrier function and other mine components**	1	2	3	4	5	6	7	8	9	10	11	12	13	14	15
		11 Exploration and monitoring drillings	Describes the chemical, hydraulic, mechanical and thermal properties of sealed drillings arranged at the drift contour to explore or monitor the surrounding host rock. The backfilling material is adapted to the surrounding geology and the chemical impact of circulating groundwater.																
		12 Host rock	Describes the chemical, hydraulic, mechanical and thermal properties of the host rock at the time of repository closure.																
		13 Fractures and faults in host rock	Describes the chemical, hydraulic, mechanical and thermal properties of fractures and faults and their mineralization in the host rock at the time of repository closure																
		14 Liquids in host rock	This FEP describes the quantities and the chemical properties of the liquids in the host rock. Apart from very small fluid inclusions in salt, fractured anhydrite formations may include fluid reservoirs (brine and hydrocarbons). Brines in salt formations are in equilibrium with surrounding salt.																
		15 Gases in host rock	This FEP describes the quantities and the chemical properties of the liquids in the host rock. Apart from very small fluid inclusions in salt, fractured anhydrite formations are potential reservoirs. Common gases in salt formations include CO2, N2 and CH4.																
Processes / Events	**Mechanical**	**Earth quake**	The release of accumulated geologic stress via rapid relative movements within the earth's crust will occur along existing faults or geological interfaces. The accompanying release of energy may result in ground movements and/or ruptures.	Earth quakes may particularly affect the drift components shortly after repository closure. Then the drift seal and the backfill are not yet fixed in the drift cross section. Later, seismic movements may yield in fractures in the drift seal. The drift lining may collapse.	✓	✓	✓	✓	✓	✓	✓	✓	✓	✓	✓	✓	✓	✓	✓
		Diapirism	Uplift of thick salt formations due to density inversion, stresses resulting from overlying rock formations and tectonic structures.	X) The uplift of a salt dome may induce stresses in a drift seal	✓	✓	✓	✓	✓	✓	✓	✓	✓	✓	✓	✓	✓	✓	✓
		Mechanical stress changes	Describes the transition of tension resulting from an increase or decrease of tension in the rocks or a component of the repository.	If the stresses are exceeding material stability, they may result in fractures in the drift seal and lining, the EDZ, the concrete injections, the borehole seals, and the host rock.	✓	✓	✓	✓	✓	✓	✓	✓	✓	✓	✓	✓	✓	✓	✓
		Swelling, shrinking and creeping of concrete	Describes not thermally induced volume or pressure changes of concrete in the drift seal, drift lining, backfill, injections and borehole seals.	This process will modify the properties of all concrete components and close the contact zone as well as the fissures in the EDZ.	✓	✓	✓	✓						✓	✓				
		Settlement and compaction of backfill and sealing materials	Settlement means the slow lowering of non-cohesive backfill materials (e.g. crushed salt) and to a minor extent construction materials like concrete. This leads to compaction and hardening. Driving forces for these processes are gravitation and convergence.	As a consequence, the hydraulic conductivity will decrease and the mechanical stability of the materials will increase.	✓	✓									✓				
		Convergence	Describes rock creeping into the mine excavations. Creeping rates depend on the mechanical properties of the rocks: high creeping in salt formations, low creeping in brittle hard rocks (anhydrite).	Convergence will fix the drift seal in the drift cross section and close the contact zone as well as the fissures of the EDZ	✓	✓	✓	✓	✓	✓	✓	✓	✓	✓	✓	✓	✓	✓	✓
	Hydraulic	**Liquid flow processes**	Describes the liquid flow due to potential gradients. Flow processes result in mass transport on one hand and may modify the hydraulic properties of the drift seal, injection material and borehole seals on the other hand.	Liquid flow transport is important for chemical processes and radionuclide spreading. Furthermore fluid flow may result in an erosion of construction materials and enlarge contact zone and/or EDZ								✓						✓	
		Gas flow processes	Describes the gas flow due to potential gradients. Gas flow is responsible for transport of volatile compounds. Impact of high gas pressure is described in the FEP hydraulic pressure change.	Gas flow transport is important for chemical processes and radionuclide spreading. Furthermore fluid pressure may impair geotechnical barriers									✓						✓

					Components affected by process														
Sub-system: Drift	**Process Group**	**FEP (No. referring to the components mentioned in right column)**	**Description**	**Direct impact of processes on barrier function and other mine components**	1	2	3	4	5	6	7	8	9	10	11	12	13	14	15
		Channeling in a sealing element	Generation of flow paths by varying concrete properties, inhomogeneous compaction or swelling or erosion of bentonite or viscous fingering in asphalt	Impairment of the function of the drift / borehole sealing elements	✓	✓	✓	✓	✓	✓	✓	✓	✓	✓	✓	✓	✓	✓	✓
		Backfill channeling	Generation of flow paths by varying concrete properties or settlement of crushed salt and inhomogeneous compaction. Due to compaction gradients, the flow paths occur predominately at the drift roof.	The sealing and stabilizing function of the backfill will be retarded.		✓													
		Hydraulic pressure change	Describes a change of fluid pressure because of changes of tension in rocks or fluid flow processes.	High fluid pressure may induce fissures in barrier constructions and EDZ	✓	✓	✓	✓	✓	✓	✓	✓	✓	✓	✓	✓	✓	✓	✓
		Diffusion	Stirring of different substances by BROWN molecular movements. Diffusion is only considered in liquids and gases and will reduce concentration gradients in those fluids. Therefore it will also influence hydrochemistry.	The process will indirectly (via hydrochemistry) influence corrosion processes at the drift and borehole seals.	✓	✓	✓	✓	✓	✓	✓	✓	✓	✓	✓	✓	✓	✓	✓
		Dispersion	Distribution of dissolved substances by inhomogeneous flow velocities in porous media. The process is linked to advective or convective mass transport and will influence hydrochemistry.	The process will indirectly (via hydrochemistry) influence corrosion processes at the drift and borehole seals.	✓		✓	✓		✓	✓	✓			✓		✓	✓	
		Liquid influx	Describes the influx of liquids from the host rock into the mine openings.	Liquid influx from geosphere will change hydrochemistry in mine and therefore indirectly promote corrosion of construction materials								✓						✓	
		Phase transition	Describes the transition from solid to liquid or from liquid to gas depending from the composition of the material, the pressure and the temperature. In mine openings evaporation and condensation are processes that will influence the distribution of humidity in the mine openings.	No relevant impact on the EBS								✓	✓						
		Dissolution and outgassing	Describes the transition of gas between gaseous phase and the dissolved phase.	The process is relevant for mass transport but will not directly affect the barrier or components functions.								✓	✓					✓	✓
		Fluid pressure induced permeation of gas into salt formations	If fluid pressure exceeds the minimum main stress in the host rock, the permeability of the salt formations will be increased and fluids can infiltrate the effected formations.	Gas permeation in salt formations may bypass the drift seals							✓	✓	✓			✓	✓	✓	✓
		Radionuclide transport in the liquid phase	Summarizes all kind of transport processes of radionuclides in liquids.	The process is relevant for release of radionuclides but will not directly affect the function of the barriers.	✓	✓	✓	✓	✓	✓	✓	✓	✓	✓	✓	✓	✓	✓	✓
		Radionuclide transport in the gas phase	Summarizes all kind of transport processes of radionuclides in gas.	The process is relevant for release of radionuclides but will not directly affect the function of the barriers or other mine components.	✓	✓	✓	✓	✓	✓	✓	✓	✓	✓	✓	✓	✓	✓	✓
	Thermal	Heat flow	Means the energy transport as a result of temperature differences. There are 2 main sources for heat flow in the drift: geothermic and radionuclide decay of the waste. Due to the depth of repository level climate impact is of low relevance. Temperature is a key issue of all chemical processes and temperature gradients may result in convective fluid flow.	Due to the distance between the barriers and the emplacement fields temperature limits for concrete and bentonite stability will to be met. Therefore temperature will not directly result in an impairment of the barriers.	✓	✓	✓	✓	✓		✓	✓	✓	✓	✓	✓	✓	✓	✓
		Thermal expansion or contraction	Volume change resulting from temperature change. At the emplacement level heat generating from waste disposal is of highest relevance. Depending on mine depth, cooling during future glacial periods may influence the emplacement level to a low intensity.	Thermomechanical stresses due to waste disposal may induce fissures in the components of the drifts.	✓	✓	✓	✓	✓		✓	✓	✓	✓	✓	✓	✓	✓	✓

					Components affected by process														
Sub-system: Drift	**Process Group**	**FEP (No. referring to the components mentioned in right column)**	**Description**	**Direct impact of processes on barrier function and other mine components**	1	2	3	4	5	6	7	8	9	10	11	12	13	14	15
		Thermochemical sulfate reduction	Redox reaction of organic matter or hydrogen with sulphate at high temperatures (starting temperature 80 °C) Resulting products are carbonate, sulphide, water, hydrogen sulphide, or carbon dioxide. The volume of the products is 10 % larger than the volume of the educts. Therefore mechanical stresses will occur.	At adequate boundary conditions the process may not impair EBS	✓	✓	✓	✓			✓	✓	✓	✓	✓	✓		✓	✓
		Thermal degradation of carnallite	The mineral carnalite is characterized by 40 weight % of crystal water that is released at different hydration levels with increasing temperature (starting temperature 80 °C)	The water from degradation of carnallite at the site of a drift seal may contribute to the alteration of construction material. Furthermore the alteration of carnallite may result in the generation of flow paths that are bypassing the drift seal.							✓					✓	✓		
		Evaporation and condensation of water	Evaporation describes the phase transition from liquid to gas phase. Condensation is the reverse process.	No relevant impact on EBS	✓	✓	✓	✓	✓	✓	✓	✓	✓	✓	✓	✓	✓	✓	✓
	Chemical / biological	**Concrete corrosion**	Describes the chemical degradation of concrete	The corrosion processes will impair the function of all concrete components in the drifts: drift seal, drift lining, borehole seals and injections. For sealing constructions the mechanical stability may be reduced and the hydraulic conductivity increased.	✓	✓	✓	✓				✓		✓	✓				
		Solution and precipitation of salt minerals	Solution describes the transition of a solid phase (salt minerals) into the liquid phase due to a change of hydrochemical boundary conditions. Precipitation is the reverse process. This process is considered for crushed salt backfill and for EDZ.	This process may modify the hydraulic properties of salt backfill and the EDZ			✓			✓	✓	✓				✓	✓	✓	
		Transformation of anhydrite to gypsum	Calcium sulphate reacts with water to generate gypsum. This exothermal reaction results in an increase of volume of 61 %. As a consequence swelling pressures of up to 4,5 MPa may occur.	This process may especially modify the hydraulic properties of the EDZ.							✓	✓				✓		✓	
		Metal corrosion	Describes the electrochemical reaction of metals with surrounding fluids and resulting gas generation. This process will reduce the mechanical stability of metal components. The enlargement of volume (factor 3.6) of the metal corrosion products will result in significant stresses in the concrete constructions.	Stabilization measures, like steel lining and roof bolts, will be impaired by corrosion. This may impair the EDZ. If the drift seal includes metal components (e.g. partition plates or reinforcements in concrete) the corrosion could also affect the sealing function.	✓	✓			✓						✓				
		Hydrogen embrittlement	The intrusion of hydrogen in metal structures results in a modification of the mechanical properties.	Low relevance for EBS alteration	✓	✓			✓						✓				
		Deflagration and explosion of gases	A deflagration or explosion resulting from the ignition of a flammable gas mixture in the repository	An explosion may have impact on the integrity of the drift seal									✓						✓
		Microbial processes	Summarizes all microbial processes in the mine and in the surrounding rocks. Microbial processes may force the corrosion of metal and concrete.	May impair the function of the drift seal, backfill and lining	✓	✓	✓					✓	✓						
		Sorption and desorption	Sorption describes the physico-chemical interaction of dissolved species with a solid phase. Desorption is the opposite effect.	The process is relevant for mass transport but will not directly affect the barriers or other components.						✓		✓	✓					✓	✓
		Colloid generation and filtration	Generation of colloids and their filtration during transport.	The process is relevant for mass transport but will not directly affect the barriers or other components.						✓		✓	✓					✓	✓
	Radiological	Radiological decay and ionizing radiation	Spontaneous transformation of instable atomic nuclei combined with the emission of characteristic ionizing radiation. After the release of radionuclides in the emplacement areas, they will be spread in the mine excavations and radiological decay will occur during transport.	The heat generation from radiological decay is a relevant thermal input in the repository system. It will result in thermomechanical stresses and influence the chemical processes. Thus all components are affected.	✓	✓	✓	✓	✓	✓	✓	✓	✓	✓	✓	✓	✓	✓	✓

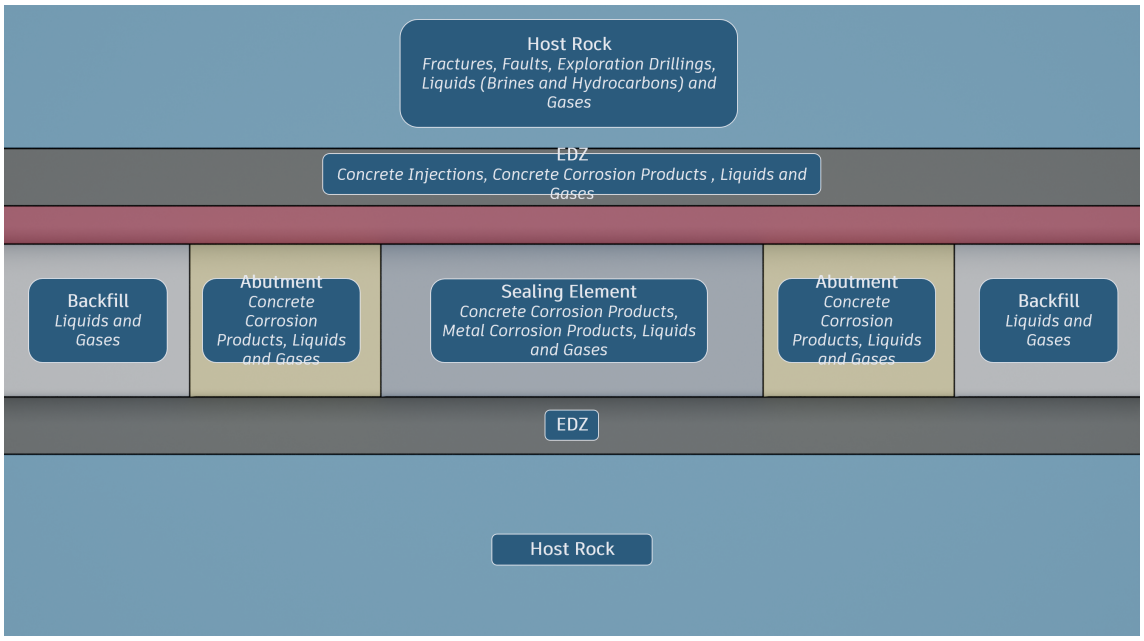

Figure 8.-2: Nearfield model for the drift seal, FEP in italics.

FEP of the farfield that have a direct impact on the subsystem drift seal are compiled in the FEP list of compartment "shafts, infrastructure and connecting drifts" in Table 8.-1.

8.4 Methodology of Scenario Development

The fundamentals of scenario development were comprehensively described in Beuth et al. (2012) and Lommerzheim et al. (2019). Therefore, only a short summary will be given here.

8.4.1 Fundamentals

The site and the repository system will undergo a specific evolution, which will be controlled both by climatic and geologic processes at the site and processes induced by the repository construction and the emplacement of heat-generating waste. Although the various influencing factors are widely understood, this real evolution cannot be predicted unequivocally in all detail.

Developing and investigating several scenarios is an internationally recognized and accepted approach to address this uncertainty (NEA, 2016). In accordance with the Safety Requirements (BMU, 2010), different kinds of scenarios have to be considered as a basis for the safety assessment of a repository system. Expected, alternative, hypothetical and human intrusion scenarios reflect the variations of possible future site evolutions (Figure 8.-4).

“Expected scenario” refers to a normal evolution forecast for the site, and evolutions normally observed at comparable locations or similar geologic situations (= Reference scenario).

“Alternative scenarios” refer to evolutions that are not expected for the site, but which may occur with regard to geological or climatic boundary conditions, the technical and geotechnical barriers and the radioactive inventory.

Expected and alternative scenarios will be systematically derived from the FEP catalog.

Other groups of scenarios include “hypothetical scenarios” and “human intrusion scenarios”. Those scenarios will be analyzed with regard to an optimization of the repository system and to assess the robustness of the system.

“Hypothetical scenarios” include evolutions that can be excluded even for most unfavorable assumptions basing on expert judgment. These scenarios include “what-if-cases”.

“Human intrusion scenarios” reflect consequences resulting from future human actions, esp. unintended human intrusion in the repository, that are relevant for the safety of the repository system. Reference scenarios for those evolutions can be derived from common recent human activities (Figure 8.-4). The basic conditions for consideration of those impacts are also defined in BMU (2010) and EndlSiAnfV (2020).

Hypothetical and human intrusion scenarios are not included in the RANGERS project.

Conceptions concerning the future evolution of a repository system are prerequisites for numerical long-term safety assessments. Therefore, the scenario development methodology aims at systematically deriving expected reference scenarios and a number of alternative scenarios that are to comprehensively represent the reasonable range of repository system evolutions (Beuth et al., 2012; Lommerzheim et al., 2019). The scenarios are characterized by FEP that will influence the future evolution of the final repository system at the reference site and their associated characteristics. An overview of the scenario development methodology is given in Figure 8.-3.

In the scenarios, possible future evolutions of the repository system during the safety demonstration period are described comprehensively. The methodology applied relies on several fundamentals, i.e. the regulatory framework, the safety concept, basic assumptions, the geologic data, the waste data and the repository concept, and integrates all data relevant to scenario development into the FEP catalog.

There are three key issues that rely directly on the guiding principles of the safety concept to start scenario development:

- “Initial barriers” are important components of the safety concept and are characterized by the safety functions “restriction of advective and diffusive mass transport” as well as “retardation of radionuclides”. They have defined properties just after repository closure and will be modified in different time frames.
- “Initial FEP” are expected processes that could impair the safety functions of the initial barriers. They provide the first starting points for scenario development.
- In addition, all possible system evolutions that involve a release of radionuclides from the waste form need to be considered. Those FEP, that are related to the mobilization of radionuclides and their transport, are additional starting points for scenario development.

A plausibility check has shown that the initial FEP consider all relevant impacts on the geological and geotechnical barriers. Therefore they are adequate starting points for scenario

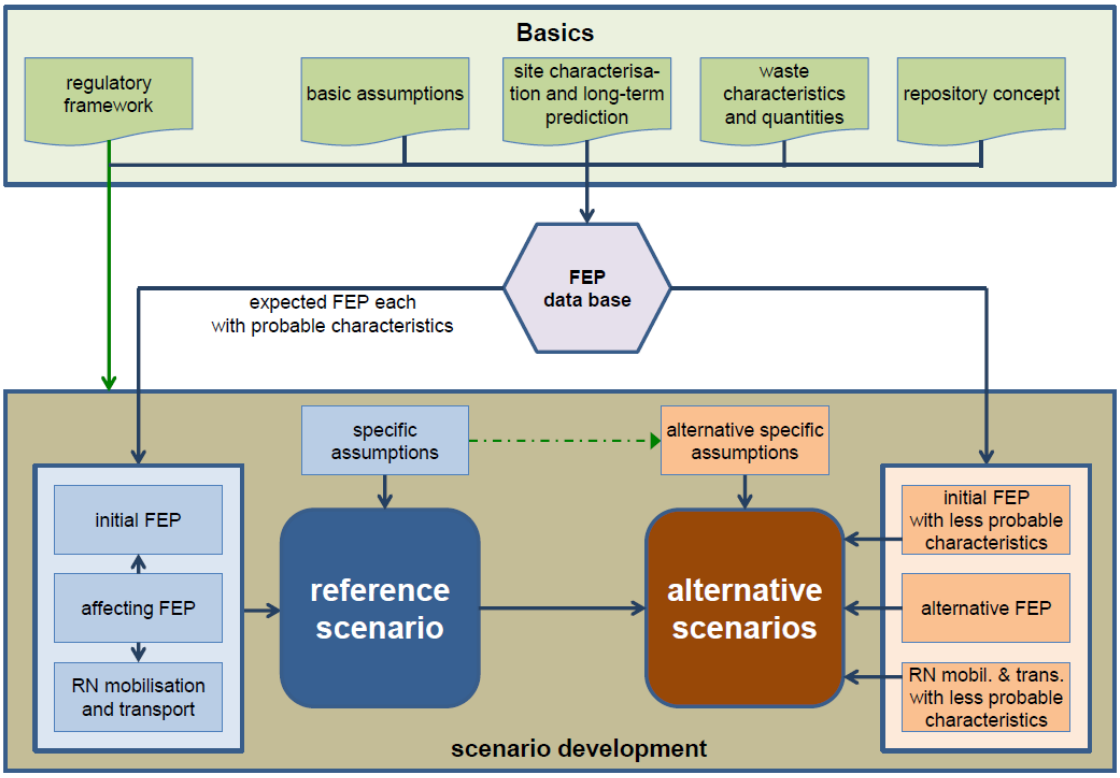

Figure 8.-3: Scenario development methodology (modified after Mönig et al. 2013).

development.

The description of FEP interaction by component-process-causal chains results in long, but clear causal chains to address important aspects of system evolution. To facilitate the generation of adequate dependence trees, a tool with break-off criteria can be applied.

8.4.2 Reference scenario

A (expected) reference scenario does not include one specific evolution but describes as broadly as possible the spectrum of probable future evolutions of a repository system.

The “initial barriers” considered in salt formations include the host rock, the shaft, borehole and drift seals as well as the backfill.

The processes that may directly affect the safety functions of the initial barriers are called initial FEP. They are marked in the FEP-Lists of Table 8.-1, Table 8.-2 and Table 8.-3.

The starting points for developing reference scenarios are:

1. specific assumptions: provide a means to deal in a transparent and traceable way with particular uncertainties, some of which may be minimized in the future while others may never be reduced at all. They especially address three aspects with high uncertainty and assume for the reference scenario:

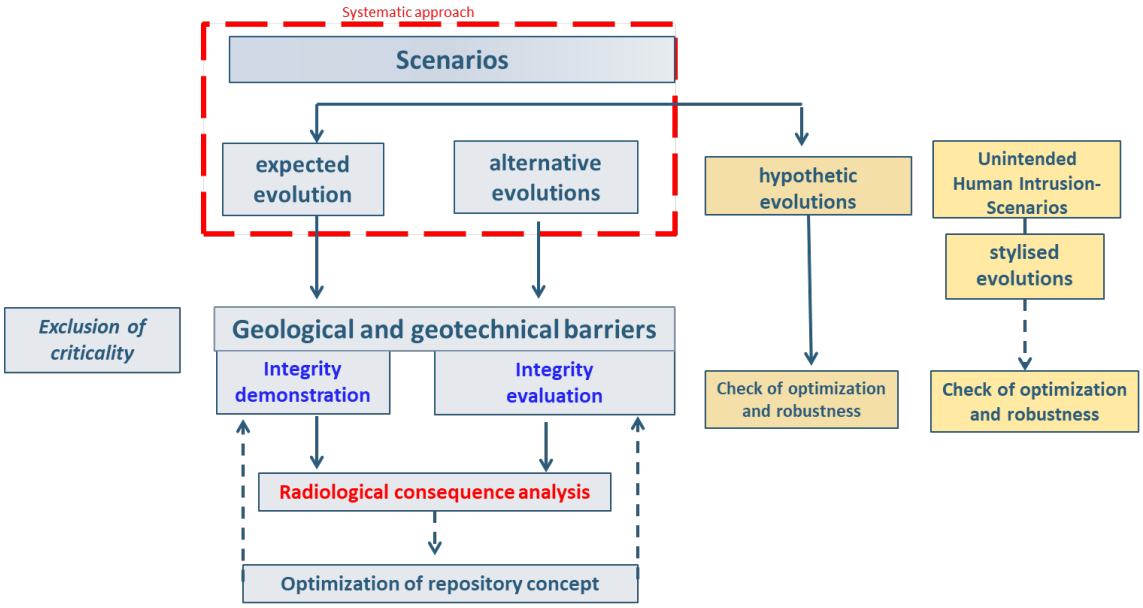

Figure 8.-4: Classification of scenarios and safety demonstration methodology (Beuth et al., 2012).

- Geology: the available geological data are representative and there are no undetected geological characteristics. The uncertainty in this point can only be reduced by future exploration .
- Safety function of technical/geotechnical barriers: All technical/geotechnical barriers work as designed. The functionality of the engineered barriers has to be verified by an integrity proof.
- Future climate evolution: Because of the persisting uncertainties in this issue all reasonable climatic evolutions have to be considered as “expected”. The evolution with the highest plausibility will be attributed to the reference scenario. Other probable climate evolutions will be analyzed as probable alternative scenarios.

2. The expected initial FEP with their probable characteristics: If appropriate information is available in the FEP catalog, the representative characteristics of those initial FEP have been taken for scenario description. Otherwise, the characteristics of the initial FEP have to be derived from their interaction with other FEP (causal chains) in combination with orienting process modeling.

3. Expected FEP characterizing the mobilization and transport of radionuclides with probable characteristics: The characteristics will be derived as described above.

Because the reference scenario results from the interaction between expected FEP, it will be expected as well.

The relevant process FEP may have different characteristics at different times and at different locations of the repository system. Therefore, it is useful to subdivide the description of the reference scenario into subsystems like near field, remaining mine excavations, host rock, and overburden to optimize the clarity and traceability of the description and to consider the interrelation between the subsystems and possible chronological limits of the initial FEP.

Due to the numerous starting points of scenarios development, the methodological approach is a “bottom-up”-type: The description starts on a broad basis and then comes to a comprehensive description of the repository system.

8.4.3 Alternative Scenarios

Alternative scenarios are evolutions that differ in exactly one aspect from the reference scenario (top down approach). The consequences on repository system evolution can be identified by an analysis of the differences to the reference scenario. Alternative scenarios can be developed from the following starting points (Figure 8.-4):

- deviations concerning the specific assumptions: This approach may yield alternative scenarios and expected scenarios – not yet covered by the reference scenario. Examples for deviations from specific assumptions, that may result in alternative scenarios, are:
  - Undetected geological properties (e.g. fracture zones or fluid reservoirs),
  - Early failure of shaft seal (or drift seal, borehole seal, etc.),
  - Modifications of the future climate evolutions, e.g. changed characteristics of glacial periods (thickness of glaciers, depth of permafrost, dimensions of glacial channels, modified duration of glacial cycles)
- Less probable characteristics of the initial FEP: for the initial FEP (see Figure 8.-4), less probable characteristics have to be defined, and the consequences on repository system analysis have to be evaluated. If a significant impact would be expected and the consequences are not yet covered by any other alternative scenario, a new alternative scenario has to be proposed. For example, for the process FEP “metal corrosion”, a corrosion rate twice as high as for normal evolution would be a less probable characteristic. Metal corrosion is a key issue for gas generation and radionuclide mobilization. Therefore this process is not only relevant with regard to the function of the disposal canisters. The consequences of a high corrosion rate are not covered by the “early failure of a disposal canister” but an additional alternative scenario with a high gas pressure is necessary.
- Less probable characteristics of the process FEP mobilization and transport of radionuclides: for the procedure to identify less probable characteristics of these processes see above. For example, for the less probable characteristics of radionuclide transport, flow processes and the hydraulic properties of the materials in the repository system and the host rock have to be considered. So, for the less probable radionuclide transport by diffusion, less probable diffusion coefficients for the materials and the host rock have to be evaluated. An adequate alternative scenario has to be defined.
- alternative FEP: process FEP describing modifications of technical features (e.g. Channeling in sealing elements and Flow paths in exploration drillings) may have a lower probability due to the comprehensive quality assurance measures for the preparation of construction materials and the performance of construction work. Therefore those FEP may be starting points for alternative scenarios.

It is possible that similar alternative evolutions result from different starting points. In this case,

various evolutions may be abstracted into one representative alternative scenario that covers the characteristics of the various evolutions.

8.5 Characterization of reference scenario

As mentioned above, the German reference scenario, that has been developed for the Preliminary safety assessment of the Gorleben site (VSG) (Beuth et al., 2012) , has been taken as an example and slightly modified to be compatible with the German concept for a salt pillow (KOSINA project). The reference scenario is characterized by the following properties and evolutions:

Specific assumptions for the reference scenario include:

- The reference climate development with a 100.000 a-cycle of glacial and warm periods is representative. During future occurence of Elster like glaciations the formation of a deep glacial channel is considered.
- Shaft and drift seals will be constructed and function as required.
- There are no misinterpreted exploration results or unknown geological properties, that result in a decrease of the safety distance between mine excavations and brine bearing formations/drillings.

The objective of the geoscientific long term prognosis is to give a forecast of future evolution of geosphere resp. of processes that may have an impact on geosphere evolution (without repository impact). Many potential future evolutions can be excluded for a repository site because the site selection has to consider the site selection criteria defined in German Site Selection Act (StandAG, 2023). The geoscientific long term prognosis is based on the actualism principle. Most evolutions of geosphere and climate are very slow and long ranging processes that started millions of years in past and will therefore also persist in future. Hence the regional evolution in past was analyzed and basing on those results the future evolutions will be predicted. As a result, for the German regions with flat-bedded salt formations, slow tectonic movements (subsidence of 0.01 mm/a), no formation of new deep fracture zones, seismicity with a design earth quake of 7.0 MSK scale and only minimal salt diapirism (0.02 mm/a) have to be expected.

For Germany, a prognosis for future climate development during the demonstration period of 1 million years (ten cycles each with 100,000 years) has been given in Beuth et al. (2012). The German flat lying salt formations occur in regions which were covered by glaciers and ice sheets with a thickness of up to 400 m in the past. Therefore the resulting mechanical load on the emplacement level will be limited. Permafrost will reach a depth of up to 300 m, periglacial channels will cut into geosphere up a depth of 200 m. Therefore those climate induced impacts will not impair the function of the CRZ.

Climate development will result in complex consequences on geosphere evolution, e.g. by modifications of hydrochemistry and geosphere stresses. Intensity of erosion will depend on topography, geological properties, vegetation and climate (precipitation) and will have a higher intensity during ice ages and a lower intensity during warmer climates (average: 0.01 to 0.02 mm/a). Subrosion rate will be low as well (<0.1 mm/a). Summarizing the impacts

from surface, none of those impacts will result in a significant impairment of the CRZ or the geotechnical barriers at the emplacement level.

As mentioned above, changes of the hydrochemistry are expected for the glacial period, but the precise hydrochemical characteristics are not predictable. Therefore an adequate design of the barriers (EBS) can not be defined. Hence for the glacial periods no integrity proof can be given. As a consequence the functional life time of the EBS is restricted to the period before the next glacial period (with well defined boundary conditions) – which means in Germany a period of 50,000 years. Therefore the main focus of scenario description for the RANGERS project is set on the pre-glacial period.

Important boundary conditions (geology, repository concept and sealing concept) for the reference scenario are described in chapters 5., 6. and 7.. For the reference scenario the expected future evolution of the repository system will be described taking the initial FEP as well as process FEP describing radionuclide mobilization and transport as starting points. They are red and green marked in the FEP Table 8.-2 and Table 8.-3. For detailed description of the scenario and a comprehensive analysis of the FEP interactions see Beuth et al. (2012). In the following text, a short compilation of the most important characteristics of the repository system evolution in the different compartments is given:

8.5.1 Geosphere

The reference geosphere of the repository system is characterized by a salt pillow consisting of Zechstein formations with a maximum thickness of 800 m. In the geological model the overburden formations (Triassic, Tertiary and Quaternary rocks) have a thickness of 140 – 800 m. The most important Zechstein formation (and the Containment Providing Rock Zone = CRZ) is the Staßfurt main halite, which is the host rock for the disposal areas and has a maximum thickness of 600 m. The halite may have a humidity of up to 5 vol %. The minimum thickness of overlying rock formations is 400 m. The competent layers of the Main Anhydrite with fluid reservoirs are fragmented by salt movements and arching. Due to a salt barrier of 350 m on average between the emplacement level and the anhydrite, a possible linkage between the reservoirs and the underground excavations is only given in the shafts. The disposal of heat generating waste results in thermal-mechanical stresses and an uplift at the top of the structure for some meters. Furthermore fractures in the host rock will be induced.

The moderate design earth quake (Intensity 7) may reactivate fractures and faults especially at the boundary between different types of rock, but large scale fractures are not expected. It has to been analyzed whether new fractures in the host rock may become flow path between fluid reservoirs and the underground excavations.

During the glacial periods the overburden formations may be partly eroded especially by glacial channels. But the CRZ will not be impaired. Permafrost may significantly modify the hydrology and hydrogeology in the overburden. Furthermore, the glacial cooling will induce thermal-mechanical stresses in the top of the salt pillow.

8.5.2 Disposal areas

The disposal areas will be situated in the Main Halite Formation. For the halite a brine content of 1 to 5 vol. % has been assumed. A safety distance between disposal fields and the car-

nallitite formations will avoid thermal degradation of carnallite and crystal water release. The repository design is adapted to comply with thermal and thermal-mechanical requirements as well as to keep safety distances to the potash seam. The disposal drifts are backfilled with crushed salt.

The temperature maximum of the waste packages will be ca. 200℃ after 80 to 100 years. After disposal, temperature will rapidly decline. After few thousand of years, the temperature maximum will decline to the original geothermal level. The heat generation will significantly increase convergence rates in the nearfield and therefore force compaction of the crushed salt. This process is important for the enclosure of the waste packages.The heating will result in thermal-mechanical stresses in the containers, the backfill, the EDZ and the surrounding host rock. The disposal casks will be designed to resist all thermal, mechanical, hydraulic and chemical impacts during a period of 500 years after closure (which is the period of recovery as defined in the regulations).

Brine inflow in the disposal drifts will be intensified by thermomigration and thus intensify metal corrosion and resulting gas generation. As a consequence fluid pressure will be enlarged. A high pore pressure will retard the compaction of the backfill. Thermochemical sulfate reduction will modify hydrochemistry in the nearfield and will also intensify container corrosion. With regard to the containment function of the technical barriers a small amount of containers with undetected failures are considered. For those containers radionuclides mobilization and transport will start shortly after closure of the repository.

8.5.3 Shafts and drifts

This compartment includes all underground excavations except the disposal areas – namely the shafts, the infrastructure area and the drifts. Also the two subsystems “nearfield of shaft seal” and “nearfield of drift seal” are located in this compartment. The closure concept for those parts of the repository comprises shaft and drift seals and a backfill of the drifts with crushed salt as well as borehole seals for the exploration drillings. The drift seals separate the access drifts to the disposal areas from the infrastructure area. After EBS construction their tight fixation in the shaft/drift contour and thereby their functionality will be accomplished by the swelling of the construction material as well as by the convergence of the surrounding rocks. The EDZ will be recut before installation of the engineered barriers. Remaining fractures will be sealed by concrete injections. The fissures in the EDZ will be closed by convergence in several 100 years.

Due to the uncertainties for the prognosis of the boundary conditions during future glacial periods, the functional period of shaft and drift seals is restricted to 50,000 years. The subsequent long term sealing of the underground excavations will be ensured by the compacted backfill (crushed salt).

The infrastructure area will be backfilled with basalt gravel and will function as a fluid reservoir. The corresponding fluids will comprise groundwater flowing in via the shaft seals/EDZ, on one hand, and limited brine volumes from reservoirs in the anhydrite as well as from brine pockets in the rock salt, on the other hand. Additionally, mine air and gas from metal corrosion or microbial processes may significantly contribute to the fluid pressure in the mine excavations. The objective of the fluid reservoir is to avoid high hydraulic loads on the shaft and drift seals prior to their fixation in the excavations contour.

All excavations are backfilled with crushed salt. The initial roof cleavage will be closed by convergence in some decades of years. Subsequently the crushed salt will be compacted in a few thousand years by convergence. Then the backfill has similar mechanical and hydraulic properties than the surrounding rock and act as a long-term barrier.

8.5.4 Nearfield of Shaft Seal

The nearfield of the shaft seal comprises the shaft installations and the shaft seal incl. the EDZ from the surface up to the shaft landing as well as adjacent parts of the host rock and the overburden formations. Those components are influenced by broad spectrum of mechanical, hydraulic, chemical and thermal processes initiated in the farfield.

So mechanical loads not only result from lithostatic pressure but from modifications of geosphere stress field by geological processes (e.g. diapirism, tectonic movements), earth quake or processes like glaciation, erosion and sedimentation. Most relevant impacts are the earth quake (may induce fissures in concrete and settle and compact the gravel abutment) as well as the diapirism (induces stresses in the barrier). The estimated intensities of those processes/events have to be considered in the design of the construction. Other processes resulting in mechanical stress changes were initiated by volume changes of construction materials (e.g. swelling, shrinking and creeping of concrete and bentonite as well as settlement and compaction of backfill). Those processes may result in small displacements of the components of the shaft seal. Convergence is a very important mechanical process ensuring the fixation and functionality of the shaft seal. Reference values for convergence will be taken from experience in other salt mines.

Because this subsystem cuts through the whole geological sequence, not only the host rock but also the aquifers in the overburden formations and the underground facilities have to be considered. Therefore a broad spectrum of hydraulic impacts is possible – from the overburden, from anhydrite reservoirs and from brine pockets in the salt formations as well as (at late times) from fluids that are squeezed out from the underground excavation via the infrastructure area to the shafts. In the repository system a two phase flow of liquid and gas is often expected. The most important hydraulic process is the fluid pressure change that is mostly linked to fluid flow processes. Those processes may impair the EBS function by channeling in the bentonite or concrete seals or by “viscous fingering” resp. asphalt migration from the asphalt seals. Fluid squeezing by convergence and gas generation are the most important processes to initiate fluid flow and to change fluid pressure. Advection, dispersion and diffusion are important processes for radionuclide transport.

At the shaft seal, a broad spectrum of liquids with different hydrochemical properties have to be considered, e.g. unsaturated groundwater from the surface and the overburden formations and different kinds of brine (Na, K, Mg / Cl, SO_4 concentrations) from divers salt formations. Although different reference liquids are considered in barrier design by adequate construction materials, corrosion and alteration processes (e.g., concrete corrosion, alteration of bentonite, microbial processes) can not be excluded during the future site evolution. This is caused by uncertainties in the prognosis of the hydrological-chemical evolution.

At early times, the corrosion of the shaft liner determines the time of water inflow from adjacent aquifers and for the corresponding hydraulic loads at the shaft seal.

The thermal boundary conditions in the shafts are dominated by the (constant) geothermal heat flow as well as by climate induced heat flow (most relevant during glacial periods). The heat flow from the disposal of high level radioactive waste is of lower relevance due to the large distance between the disposal areas and the shafts. Nevertheless, the high heat input in the disposal fields will induce significant thermal-mechanical stresses (compressive strength) at the shafts. The climate induced cooling may result in tensile stresses and the generation of fractures at the top of the salt structure. With regard to the performance assessment of the geotechnical barriers that is of lower relevance because the functional time of the barriers is restricted to the pre-glacial period.

8.5.5 Nearfield of drift seal

The repository layout provides two disposal areas each connected with the infrastructure area and the shafts by four access drifts. Each drift has to be sealed by a drift seal to avoid a water inflow from the infrastructure area to the disposal areas or a release of possibly contaminated fluids from the disposal areas. The nearfield of the drift seal comprises the drift lining, the drift seal incl. the EDZ as well as adjacent parts of the host rock (see Figure 8.-2). Those components are influenced by a broad spectrum of mechanical, hydraulic, chemical and thermal processes initiated in the farfield.

Modifications of the host rock stress field by geological processes (e.g. diapirism, tectonic movements), earth quake or processes like glaciation, erosion and sedimentation are also relevant at the emplacement level. Mining experience shows that the impact of seismic waves on the restrained geosphere decreases with increasing depth. But open parts of the mine excavations (e.g. top clefts above the backfill), the rigid concrete as well as the EDZ may be affected. If diapirism proceeds irregularly, stresses may be induced in the large drift seals. Other processes resulting in mechanical stress changes were initiated by volume changes of construction materials (e.g. swelling, shrinking and creeping of concrete). Convergence is a very important mechanical process ensuring the fixation and functionality of the drift seal. The reference convergence rate will be estimated from the experience in other salt mines.

Hydraulic conditions in the nearfield of the drift seal will be influenced by liquids in the infrastructure area. They will arise from surface or overburden formations by percolating through the shaft seal and the EDZ or from fluid reservoirs in the salt formations. Therefore the hydrochemistry of the liquids in infrastructure area may be quite inhomogeneous.

At the disposal area side of the drift seals only small amounts of brine solution from the host rock (brine pockets) will occur. But there are large amounts of metals (waste packages) in the disposals areas and their corrosion will result in an intensive gas generation, that will significantly increase fluid pressure at this side. If the leakage rate of drift seal is smaller than the gas generation rate, the fluid pressure will exceed the minimum stress in the host rock and fluid percolation in salt formations will start.

An asymmetrical fluid pressure is expected at the both sides of the drift seal, what is a special challenge for the design. At later periods, fluid pressure will be increased by convergence. In the repository system a two phase flow of liquids and gases is expected. The fluid pressure changes will be often linked to fluid flow processes. Those processes will impair the EBS function by channeling the backfill and the concrete seals. Advection, dispersion and diffusion are important processes for radionuclide transport.

Especially in the infrastructure area a broad spectrum of fluids with different hydrochemical properties have to be considered, e.g. a mixture of unsaturated groundwater from the surface and the overburden formations and different kinds of brine (Na, K, Mg / Cl, SO_4 concentrations) from the salt formations. Although different reference liquids are considered in barrier design by adequate construction materials, corrosion and alteration processes (e.g. concrete corrosion, microbial processes) can not be excluded during the future site evolution. This is caused by uncertainties in the prognosis of the hydrological-chemical evolution.

In contrast to the shaft seal subsystem, in the drift seal subsystem the heat flow from the disposal of high level radioactive waste is of highest relevance. This is explained by the smaller distance to the disposal fields. Geothermal heat flow (which is constant) as well as climate induced heat flow (only a temperature impact of 3-4 °C is expected) are of low relevance. The disposal of the heat generating radioactive waste will result in significant thermal-mechanical stresses (compressive strength) in the nearfield of the drift seal during the thermal phase, and tensile stresses after temperature decrease. Those stresses may result in fissures in the concrete constructions as well as loosening of the EDZ.

8.5.6 Radionuclide mobilization and transport

The second approach for developing the reference scenario addresses processes that are linked to radionuclide mobilization and radionuclide transport.

Radionuclide mobilization will take place in the disposal areas and will be the consequence of several casual chains of processes/events that will result in the failure of the waste package and the degradation of the different waste matrices.

Due to the specific assumption for the reference scenario that all barriers meet their design specific requirements there is only one reason for the failure of a waste package during the functional period: the existence of containers with undetected failures.

During construction as well as during quality tests mistakes will rarely occur. Those containers will fail as a consequence of lower impacts that are covered by properly designed containers.

After the functional period the failure of containers is expected resulting from mechanic, hydraulic and chemical impacts. Water can intrude a damaged container and then corrosion of the waste matrices (spent fuel, glass, metal, organics) and the mobilization of radionuclides will start. The chemical processes will also provide gas as another medium for radionuclide transport. The fluid-induced radionuclide transport by advection, dispersion and diffusion is influenced by the hydraulic properties of the mine excavations (including closure measures) and the host rock as well as on chemical processes like sorption, desorption, complexation, and colloid generation

8.6 Characterization of alternative scenarios

As described in above, there are three starting points for development of alternative scenarios. They are discussed in detail in Beuth et al. (2012). An important follow-up step in handling of alternative scenarios is the definition of comprehensive representative scenarios. Several alternative scenarios derived from different starting points may have similar consequences on repository system evolutions. For the procedure of performance assessment calculations it is

necessary to define representative scenarios bundling and covering those similar alternative scenarios.

8.6.1 Deviations concerning the climate development assumptions

The reference climate development includes assumptions for climate cycles (approx. 100,000 years basing on astronomic Milankovic cycles)) as well as for intensity of glacials (Elster, Saale and Weichsel glacials) and warm interglacial periods. Those assumptions base on an analysis of the climate development in past and corresponding interpolations to future developments (actualism principle), Those prognoses have a high inherent uncertainty.

So the 100,000 years climate cycles were characteristic for the last 800,000 years, but in former times there were also cycles of 19,000-23,000 years and 42,000 years. Short climate cycles would result in in a new glaciation in the next 20,000 to 40,000 years. But investigations have shown, that shorter climate cycle durations correspond to lower temperature amplitudes between glacials and interglacials. Therefore glacier thicknesses are reduced, permafrost will only penetrate to smaller depths and glacial channels will only cut in the uppermost part of the overburden formations. Any significant impact on the host rock from those short glacials is not expected.

Other prognostic uncertainties rely on the characteristics on the glacial periods. So the site specific maximum thickness of the glaciers or the depth penetration of permafrost can not be predicted. Therefore conservative assumptions have to be taken as a basis for characterizing the progress and the characteristics of the glacial periods.

As the RANGERS study focuses on the performance assessment of geotechnical barriers whose functional periods are restricted to the time before the next glacial period (50,000 years), possible alternative scenarios for far future climate evolutions can be neglected here.

8.6.2 Deviations concerning the functionality of geotechnical barriers

A basic assumption for the reference scenario is that all technical barriers will work as required. Therefore in the alternative scenarios, the failure of a geotechnical barrier has to be assumed. A short overview of the corresponding scenarios for the different kinds of geotechnical barriers and their consequences on repository system evolution is given below.

Those scenarios do not analyze the reasons for the barrier failure (they can be analyzed by the impact of initial FEP (compare Table 8.-1, Table 8.-2, Table 8.-3) (apart from human mistakes or construction failures)) and – in a conservative manner – take no credit from the redundancy of the different elements of the geotechnical barriers consisting of several abutments and sealing elements. As a top down approach they describe the consequences on the repository system evolution.

The barrier failure scenarios suppose a higher hydraulic conductivity for the entire barrier construction. This may result from construction failures and/or a higher hydraulic conductivity of the contact zone and/or the EDZ. Beuth et al. (2012) proposed to take the permeability of the EDZ, fissures or porous media with high porosity as reference scales for the increased hydraulic conductivity of the failed barriers. This would correspond to a hydraulic conductivity 3 or 4 times larger than for the intact barrier. Synchronous, not casually linked failures of several

barriers can be excluded (a combination of two events with a low probability is improbable).

To evaluate the most severe consequences for repository system evolution, an early point in time is assumed for the barrier failure scenarios. A relevant boundary condition at this time is that the compaction of the backfill is not yet finished.

Failure of a shaft seal: A broad spectrum of processes as well as human mistakes or construction failures may affect the functionality of the shaft seals (see initial FEP in Table 8.-2). As a consequence a groundwater flow from surface, overburden formations and/or reservoirs in the salt formations via the shafts can be initiated towards the underground infrastructure area. Therefore all processes in the repository mine that are influenced by water and hydrochemistry will be triggered and intensified. The most relevant consequences on repository system evolution would be:

The unsaturated groundwater entering via the shaft will start leaching the surrounding salt formations. This process will continue up to the saturation of the groundwater. As a consequence, void volumes at the shaft and the infrastructure chamber contour will be generated and fractures and fissures in the adjacent host rock may be elutriated. This may impair the stability of the host rock in this area. As a consequence, flow paths to brine reservoirs in the host rock may be generated and the drift seal may be bypassed in parts. On the other hand, the high humidity would increase the creeping rate of the salt (convergence) and so contribute to the closure of void volumes.

Furthermore hydrochemistry will be modified and different alteration processes at the host rock and construction materials of EBS (e.g. concrete corrosion) may be initiated.

Due to the groundwater inflow the fluid pressure will be significantly increased. This brine will percolate through the drift seal and flood the disposal areas. Here, metal corrosion of the disposal canisters will be initiated. That's also relevant for radionuclide mobilization. Fluid inflow as well as gas generation due to metal corrosion, are important for flow processes in the mine excavations and therefore for radionuclide transport.

Failure of a drift seal: Due to the drift seal failure (and the not yet compacted backfill with a higher hydraulic conductivity). There is a flow path from infrastructure area to the disposal fields and vice versa. Relevant consequences of this scenario on repository system evolution would be:

The fluids in the infrastructure area have a diverse hydrochemistry. Therefore leaching of the salt formations and concrete corrosion at the barriers will be induced. Both processes may result in bypassing / malfunctioning of the drift seal. The fluids at the side of the disposal fields are saturated with the salts in the surroundings. The disposal areas are sited in rock salt formations with a low humidity. Brine pockets in the salt formations with a fluid volume of several hundred cubic meters are rare. Therefore the hydraulic loads at both sides of the drift seal will be different what is a challenge for the drift seal design.

The brine passing the drift seal will initiate intensive metal corrosion at the waste containers in the disposal fields and intensive gas generation will be initiated. This causes an additional

fluid pressure at the drift seal. Due to the gas generation, a fluid flow back to the infrastructure area will be initiated. The high gas induced fluid pressure in the infrastructure area may impair the shaft seal. If the gas flow rate through the drift seal is lower than the gas generation rate, the gas pressure will exceed the minimum principle stress in the host rock and permeation into geosphere will start. Waste packages will fail due to corrosion. Radionuclides will be mobilized and transported through the underground excavations via the shaft.

Failure of a borehole seals: For surface exploration drillings there is a safety pillar between the boreholes and the underground mine excavations. That means, even after the failure of the borehole seal, there is no connection to the underground excavations and therefore no impact on the mine has to be considered.

That is different for underground exploration boreholes that are drilled from the mine excavations. A failure of the borehole seals of those drillings would have different consequences depending on their locations and geological boundary conditions. The most relevant types are:

Underground drillings connecting reservoirs in the host rock: Depending on the fluid volume and the hydrochemistry of the fluids, different chemical, hydraulic and mechanical processes can be initiated in the mine openings in the case of drift seal failure.

Underground drillings connecting different mine openings: Those drillings may form new flow paths in the mine excavations and even bypass the drift seals. Thus a fluid flow from the infrastructure area to the disposal areas may be facilitated and intensified or a release of possibly contaminated fluids from the disposal fields towards the infrastructure area and the shafts will be enabled.

The consequences of both system evolutions can be included in the alternative scenario “Failure of a Drift Seal”, that is described above.

Unknown geological characteristics: Due to limitations of measuring precision, malfunctions or human errors in analysis or interpretation of measuring results, some geological properties that will impair the rocks barrier function, may not be recognized. Due to mechanical, thermal-mechanical and chemical (leaching) processes, flow paths can be generated between the unknown reservoirs and the mine openings. So, for the corresponding alternative scenarios, the occurrence of brine pockets in salts, fracture reservoirs in anhydrite and fractures and faults with a high hydraulic conductivity are important. If they are not correctly identified, safety distances may not be kept and connections to the mine openings may be generated during repository system evolution. Furthermore the humidity of the salt rock due to fluid inclusions may be higher than expected. With regard to the consequences, the position and volume of the reservoirs and fractures/faults in the repository mine is crucial. Fluid inclusions are of special relevance for the disposal areas.

The consequences of unknown geological characteristics are similar to the failure of the geotechnical barriers. Therefore such evolutions are also subsumed in the corresponding scenarios.

8.6.3 Alternative characteristics of the initial FEP

As summarized in section 8.2 processes were identified that may directly affect the function of the geological and geotechnical barriers. For the reference scenario it has been assumed that the CRZ will not be impaired by those processes in expected intensity (earthquake, subrosion, permafrost, permeation of fluids in salt formations). The geotechnical barriers will be designed to resist the loads from the initial FEP in expected intensity.

Even if alternative characteristics are assumed for the geological processes, the safety function of the CRZ will not be impaired.

That is different for initial FEP affecting the geotechnical barriers:

- Migration of bitumina: if the bitumina will leak from the sealing element and migrate via fractures and faults in the surrounding rock, the sealing function of the shaft seal will be significantly reduced.
- Metal corrosion: the shaft lining includes a steel shell. The corrosion of the steel would modify hydrochemistry, what may affect the swelling capacity of the bentonite. Thus the sealing function of the shaft seal is compromised.
- Swelling and shrinking of bentonite: to assure the sealing function of the shaft seal an adequate water saturation and swelling of the bentonite is necessary. The bentonite swelling forces the fixation of the shaft seal in the shaft column and reduces the hydraulic conductivity. If swelling is reduced or if shrinking occurs, the sealing function of the shaft seal is reduced.
- Swelling, shrinking and creeping of concrete: concrete swelling closes the contact zone and initiates the closure of the fissures in the EDZ. Additionally the barrier is fixed in the cross section of the shaft or drift. Shrinking and creeping of concrete may influence the barriers properties unfavorably.
- Convergence: the salt creeping is an important process for fixation of a barrier in the cross section of a mine opening as well as for closure of the contact zone and the EDZ. If convergence rate is lower than expected, the required fixation of the EBS will only be reached with delay.
- Mechanical stress changes: the EBS is designed for expected mechanical loads (e.g. litho- and hydrostatic pressures, earth quake, thermal-mechanical stresses, swelling pressure of concrete or bentonite). If higher mechanical stresses occur, fractures may be induced in barrier components and thus the mechanical stability and the sealing function is impaired.
- Hydraulic stress changes: the EBS is designed for expected hydraulic loads (e.g. hydrostatic pressure, predicted gas generation). If higher hydraulic stresses occur, fractures may be induced in barrier components, which impair the function of the barrier
- Displacement of sealing elements: The swelling of the construction materials (e.g. bentonite, concrete) , will result in a displacement of a sealing element in the shaft. If those movements are more intensive as expected, marginal flow paths may be generated at the shaft contour.

- Setting and compacting of backfill and sealing materials: In the shaft seals, gravel columns are used as abutment. By gravel properties the compaction is limited to very small values and then does not affect the barriers function. But if compaction is significantly higher than expected, the shaft seal is not fixed in its installation location and therefore may be impaired in its function.
- Corrosion of concrete and material with Sorel phases: Different kinds of concrete are provided as sealing elements and abutments in shaft seals and drift seals. The functionality of those barrier components will be significantly reduced by corrosion.
- Dissolution and precipitation of salt minerals: crushed salt is used as long term sealing in shaft seals and drift seals. If MgCl-brine or only partly saturated liquids from the overburden intrude the crushed salt layers they may be partly dissolved and thus their function affected. The same process may also occur in the EDZ.
- Microbial processes: microbial sulfate reduction may contribute to concrete corrosion and additionally occur in the EDZ. This alteration process will modify the hydraulic properties of the material.

If considered with unfavorable characteristics all processes mentioned above may result in an impairment or failure of a EBS. Therefore the detrimental impact of those processes and the consequences of repository system development can be analyzed in the two alternative scenarios described in the previous section :

- failure of a shaft seal, and
- failure of a drift seal

8.6.4 Alternative characteristics of the initial FEP mobilization and transport of radionuclides

For the evaluation of the radiological consequences of repository system evolution, the FEP RN mobilization as well as radionuclide transport in the liquid phase and RN transport in the gas phase are of highest relevance.

With regard to radionuclide inventory, uncertainties may occur in terms of their chemical form (e.g. gaseous or easily mobilized). Considering radionuclide mobilization, hydrochemistry is very important, first for corrosion of the waste container, and second for the alteration of the waste matrix. For hydrochemistry a band width has been defined resulting from uncertainties with regard to concentrations, composition and distribution of the constituents. Therefore, if hydrochemistry deviates significantly from the boundary conditions assumed for design and closure planning, an early failure of the waste container may occur and corrosion of the waste matrices (metal, glass, organics) may also be enhanced. Corrosion of waste matrices is combined with radionuclide mobilization. The hydrochemistry and the amount of free water also influences the intensity of gas generation induced by the corrosion process. Gas is an important transport medium for volatile radionuclides.

Radionuclide transport relies on fluid flow and transport (advection, dispersion, diffusion) processes. The intensity of those processes depends on the hydraulic (porosity, permeability)

and chemical (sorption, desorption, complexation, colloid generation, filtration) properties of the media flowed through (barriers, backfill, EDZ, host rock).

Therefore the alternative scenario on radionuclide mobilization and transport is closely linked to the alternative scenarios on the failure of barriers.

8.7 Summary

Out of the presented FEP and scenario analysis, a reference scenario and two alternative scenarios can be derived to analyze the design and the performance of the EBS. The reference scenario assumes an evolution of the repository as described in section 8.5. In this scenario, all technical barriers will work as expected. This scenario is described by the initial FEP as well as the process FEP describing radionuclide mobilization and transport. Only for this (reference) scenario, the integrity of the EBS has to demonstrated according to EndlSiAnfV (2020).

The alternative scenarios assume a failure of the components of the EBS. This is the case for the shaft and the drift seal. As has been shown in section 8.6.2, a failure of the shaft seal will cause an higher inflow of fluids from the overburden to the repository mine. A higher geochemically induced degradation of the sealing materials will be also intensified. A failure of the drift seal is combined with a higher water migration through the drift sealing elements toward the emplacement fields where a higher metal corrosion of the waste packages and consequently a higher gas transport and gas pressure build-up can be expected. For these two alternative scenarios, the integrity of the EBS has to be evaluated. EndlSiAnfV (2020) states in §4 (6) that , it shall be verified and demonstrated that the repository system retains its function during the assessment period for the alternative scenarios. EndlSiAnfV (2020) further requires in §12 (3) that It shall be ensured that measures for optimizing the repository system derived from alternative scenarios do not significantly impair the safety of the repository for the expected developments.

It follows from the requirements of the EndlSiAnfV (2020) that the integrity of the repository as whole, and of the EBS in particular, has to be *demonstrated* for the reference scenario. For the alternative scenarios, the integrity has to be *evaluated* with the aim at showing the robustness the system. These two approaches are the core principles underlying the safety and performance assessment of the EBS and they are well illustrated in Figure 8.-3.

9. Abstraction of scenarios into model computation cases

Given the complexity and non-linear evolution the repository system, with numerous influencing factors, the safety assessment of the repository system can only be achieved based on numerical simulations. Scenarios form the foundation for quantitative safety assessment simulations, utilized for purposes such as integrity analysis or radiological consequence analysis. The conversion of the scenarios into numerical assessment cases is a non trivial task that demands careful thoughts because the described scenarios cannot be directly depicted and evaluated using a single numerical code.

To carry out the model computations, computation cases are defined, each of which represents model abstractions of the scenarios with defined parameter values, parameter ranges, or characteristics pertaining to the statistical distributions of the parameter values (Beuth et al., 2012). Each computation case takes into account the numerical code and the FEP assignable to that program. Therefore, a computation case can be understood as a numerical model of a sub-aspect of a scenario (Kock et al., 2012).

For the numerical analysis of the individual scenarios, multiple computation cases are typically defined. This is partially attributable to the fact that the multitude of processes to be considered in a scenario often cannot be completely depicted or dealt with using just one calculation program. Furthermore, depending on the safety-related issue to be assessed for a scenario (e.g., integrity analysis, long-term radiological analyses), it determines which calculation programs should be employed. Conversely, it is conceivable that a comprehensively defined computation case is suitable for evaluating the effects of two or more scenarios. In any case, it is crucial to demonstrate the applicability of the computation cases for the respective scenarios, and ensure that the computation cases defined for a scenario collectively allow for a comprehensive assessment of all safety-related issues (Beuth et al., 2012). Figure 9.-1 schematically illustrates the stages and elements, starting from the development of scenarios, their abstraction into computation cases, as well as the modeling and analytical evaluation. The overall appraisal of all results from the model computations is then performed in the synthesis report.

Some limitations arise however when the described scenarios cannot be directly depicted and evaluated using a calculation program. This may be due to certain processes not being depictable or only limitedly depictable in terms of modeling, perhaps because the process is extremely complex and the necessary calculation programs, tools, or data for modeling to the required degree of detail are not available. Alternatively, it could be because understanding of the process is less well-developed, resulting in uncertainties in the process description (Beuth et al., 2012). In such cases, further research and developments work is necessary to increase the understanding of such processes and to qualify numerical tools to take into consideration (Kock et al., 2012).

Another challenge is to demonstrate that the numerical analyses are comprehensive in terms of the processes considered and in terms of the completeness of the processes to represent a given scenario. Also, the interaction between the processes in the scope of numerical analyses should be considered. Kock et al. (2012) recommend to focus on the smallest possible number of representative cases, thus systematically generating comprehensive computation cases from scenarios. However, no general methodology for this process currently exists. This is especially due to the fact that all model computations incorporate simplifications (e.g.,

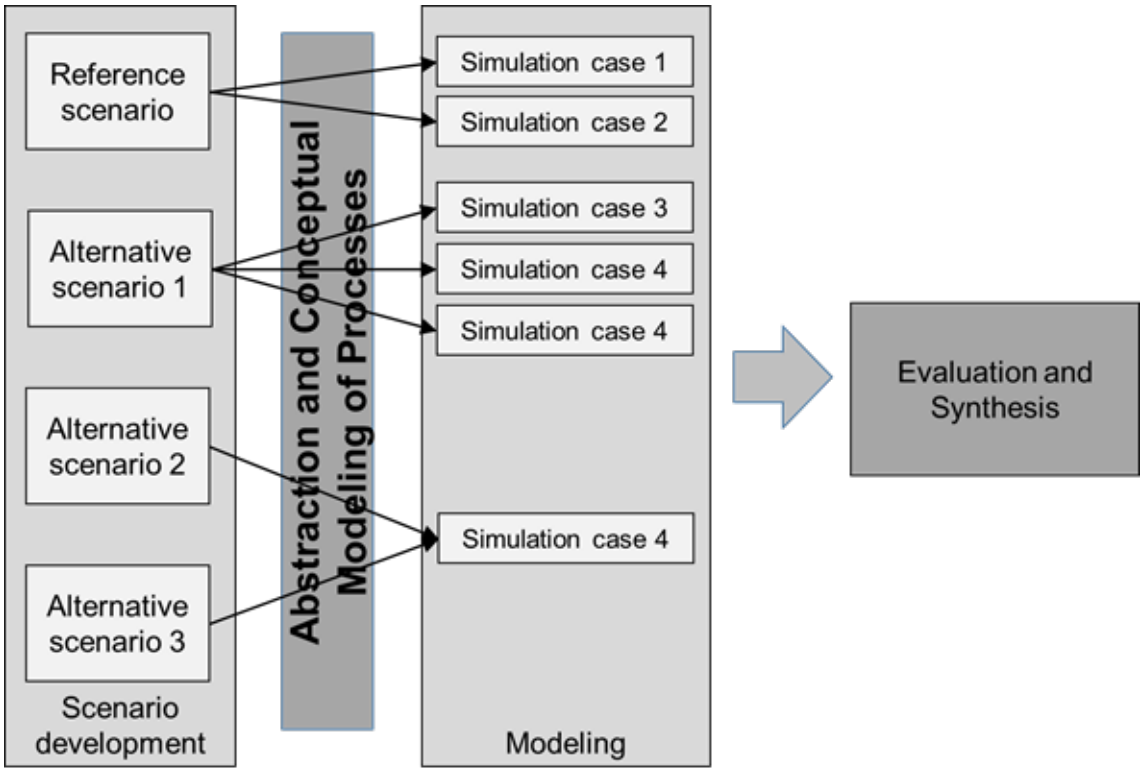

Figure 9.-1: Schematic workflow describing the modeling of processes as intermediary step between the development of scenarios and PA simulations and Assessment after Beuth et al. (2012).

concerning the level of detail of repository systems). As already mentioned, not all processes are well understood and can be proceeded through computations.

In the scope of the Preliminary safety assessment of the Gorleben site (VSG), the strategy of abstracting scenarios into computation cases consisted on determining in a first step whether a FEP used in the scenario is relevant in terms of integrity analysis or radiological consequence analysis. Then, computation cases for integrity assessment were considered for modeling using different calculation programs, with which the scales and processes relevant to the integrity analysis can be considered. In an additional second step, it was examined which calculation program each FEP could be assigned to. The aim was to account for as many processes as possible occurring within the scenarios in the quantitative integrity analysis. This step also reveals which processes might require further research or development, especially concerning their implementation in numerical codes, primarily due to possible missing connections. Following that approach, it was possible to consider the majority of the processes and the scales relevant to the integrity analysis in different and carefully selected numerical codes so that computation cases comprehensively covered the considered scenarios (Kock et al., 2012). Figure 9.-2 illustrates how the initial FEP have been assigned to the different numerical codes guided by the premise of examining as many coupled processes as possible and covering the processes of the reference scenario with as few computation cases as possible.

As for the alternative scenarios that affect the EBS, they have to be considered during the radiological consequence analyses according to EndlSiAnfV (2020) in §4 (6). This does not

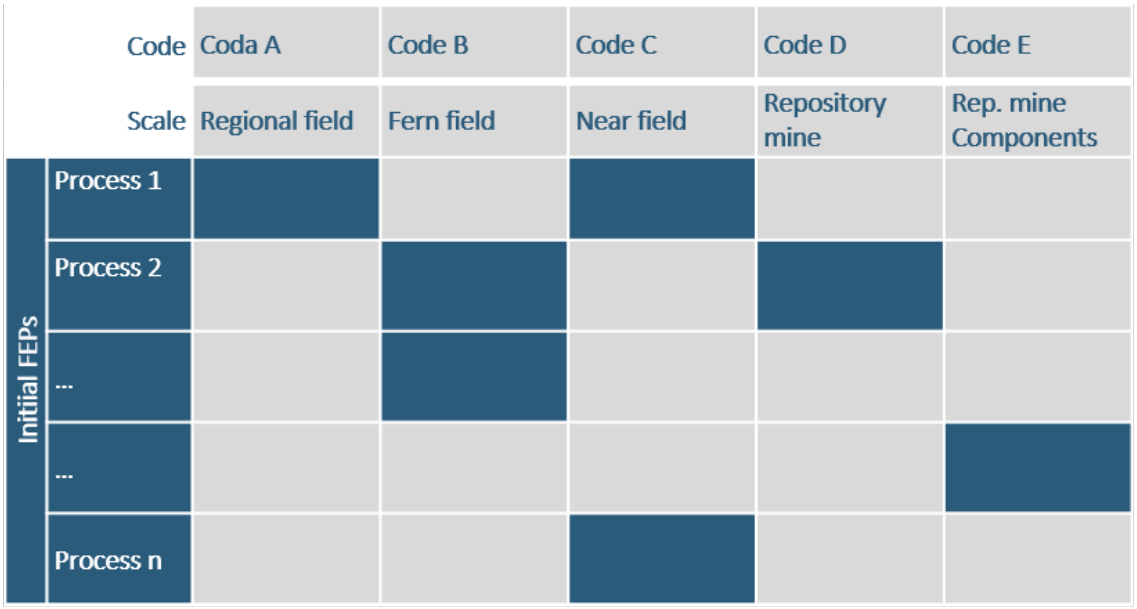

Figure 9.-2: Assignment of initial FEP to numerical codes following Kock et al. (2012).

imply that alternative scenarios play no role in the integrity analysis. It is conceivable that even a less probable development could influence the barrier effect of the final nuclear waste repository. Therefore, those scenarios have to be considered in the scope of the integrity evaluation of the EBS. The analysis of the alternative scenarios also plays a key role in the optimization and the evaluation of the repository system in general and of the EBS in particular following the requirement formulated in EndlSiAnfV (2020) (§12 (3)). In the VSG studies, the hydraulic evolution of the shaft seal has been analyzed for the reference scenario and for the alternative scenario evolving a failure of the shaft seal. The objective was to verify whether the sealing system is fundamentally capable of preventing the access of surface, overburden, and formation waters to the radioactive waste, even in the event of a shaft seal failure. Additional objectives were to examine whether a sufficient temporal delay of the salt solution's occurrence in front of the drift seals is ensured, even in case of a shaft seal failure, so that the compaction of the salt backfill has progressed sufficiently. From this evaluation, it was possible to determine the pressure or pressure build-up rates as inner boundary conditions on individual sealing elements, which are examined in detail in the context of the in-depth integrity verification (Müller-Hoeppe et al., 2012a).

Based on the experiences gained from previous projects discussed above, one can derive the following rules in the abstraction of scenarios into simulations:

- The reference scenario is described by the identified initial FEP. Thus the abstraction of these initial FEP into simulations allows the numerical representation of the reference scenario. The more initial FEP are considered the more complete will be the modeling of the reference scenario.
- The premise guiding the abstraction is to consider as many coupled processes as possible and to cover as many processes of the reference scenario as possible with as few computation cases as possible.
- The abstraction of scenarios into simulation is carried out based on the available com-

putational capabilities. Each computation case takes into account the numerical code and the FEP assignable to that program.

- Depending of the computer code at hand several computation cases are necessary to represent a scenario.
- Alternative scenarios that consider the EBS should be treated in the scope of the integrity evaluation and of the radiological consequence analyses. The abstraction of this scenario are not carried out by the initial FEP but by representing the expected events that occurs when those scenarios arise.
- Initial FEP and other processes that cannot be analyzed through modeling should be treated verbal argumentatively based on the actual state of knowledge covering these processes.

To follow these rules, the proposed methodology recommends the use of more realistic integrated models where most of the components of the subsystems to be analysed are explicitly considered in the numerical model. Those components are described in tables 8.-2 and 8.-3 for the subsystems shaft seal and drift seal. By applying this strategy, the interactions between the components are automatically considered. Initial FEP affecting each of these components are to be considered during the numerical analyses by means for example of adequate constitutive models (e.g. use of a qualified constitutive swelling model to represent the swelling of bentonite) or by taking assumptions in the modeling to represent the effect of an initial FEP in a specific component (e.g. representing the effects of swelling of bentonite by initializing the stresses resulting from the swelling effect in the bentonite component of the model). Components and processes that cannot be included in such an integrative numerical model can be treated in dedicated numerical analyses at the component level. The possibility to use surrogate models in the future represent a promising way to include the effects of complex processes into the integrated model. Implementing this strategy necessitates the use of extensive numerical models that range from the component level to the broad fern field level and requires high performance computing capabilities to cary out the simulation cased. This strategy has been tested in the modeling work package of the project RANGERS.

10. Integrity Assessment

The goal of the Integrity Analysis is to determine whether the assumed developments of the repository system lead to loads that could compromise the integrity of the CRZ over the verification period (Kock et al., 2012). Taking into account the CRZ concept, the integrity analysis has to be carried out for the geological barrier and for the EBS. In each case, a verification concept is needed to evaluate the state of the barriers over the course of the repository evolution. The verification concept is derived from the safety concept which itself has to comply with the regulatory requirements. Based on the EndlSiAnfV (2020), a methodology for the verification of integrity of EBS in salt repositories is derived in this chapter.

10.1 Regulatory requirements

The secure containment of radioactive waste in salt repositories is ensured through the combined effort of the geological barrier and the engineered barrier system. The EBS is specifically designed to seal the rock mass that has been penetrated in order to install the repository. From the primary objective of protecting humans and the biosphere from the harmful effects of the disposed radioactive waste, fundamental object-specific requirements for the EBS arise. Those requirements are anchored in the regulations in force.

The safety philosophy underpinning the EndlSiAnfV (2020) highlights the critical importance of the containment-providing rock zone (CRZ) within the host rock formation as a key geological feature ensuring the long-term containment and isolation of radioactive materials. The legislation distinguishes between two types of barriers within this system:

- Essential Barriers (wesentliche Barrieren): These barriers are fundamental to the secure containment of radioactive waste within the CRZ.
- Additional Barriers (weitere Barrieren): These barriers complement the essential barriers, providing an additional layer of defense to further prevent the migration of radionuclides.

In repositories located in salt formations, the salt host rock serves as the essential barrier due to its unique properties, such as low permeability, plasticity, and self-healing capabilities. The geotechnical barriers, such as those within the Engineered Barrier System (EBS), function as additional barriers, complementing the host rock's containment capabilities by sealing the repository and mitigating fluid migration.

While the EndlSiAnfV provides detailed guidelines for the integrity assessment of essential barriers, it offers limited regulatory specifications for additional barriers. Given the supporting role of these barriers in the overall safety concept, more detailed and comprehensive regulatory requirements may be necessary to ensure their performance is rigorously assessed and optimized.

This need is particularly significant for the EBS in salt repositories, as the EBS plays a crucial role in sealing the repository and preventing fluid migration into or out of the system. Unlike the salt host rock, which forms a natural barrier, the EBS must rely on engineered solutions, such as drift and shaft seals, to achieve the same impermeability. In the context of salt formations, where the EBS represents the only potential pathways for fluid migration, we recommend

extending the requirements formulated for essential barriers (e.g., the salt host rock) to include the EBS up to the end of the planned life time of the EBS. This extension would ensure that the EBS meets the same rigorous standards for long-term integrity and containment as the host rock itself.

By applying equivalent regulatory requirements to the EBS, the overall robustness and safety of repositories in salt formations can be significantly enhanced, ensuring compliance with long-term safety objectives.

In this regard, EndlSiAnfV (2020) requires that the properties of the technical and geotechnical barriers, which are relevant for the secure containment of radioactive waste, are maintained for at least the period during which these barriers are required according to the safety concept (§ 5 (1)). For the EBS, the primary properties referenced by the regulation is the sealing properties of the shaft and the drift sealing system as well as the sealing properties of the long term seal made of crushed salt in the repository mine.

Further requirements concerning the integrity of the EBS as part of the CRZ are formulated in § 5 (2) of the same regulation where it is stated that the integrity of the CRZ should not be significantly impaired by the development of temperature, and by possible changes in the chemical conditions in the repository.

Specific requirements for the geological barriers in § 5 (2) also apply for the EBS because the contact zone between the EBS elements and the geological barriers are a critical path that need to be verified in order to secure the safe containment of the CRZ. Therefore the dilatancy strength at the contact zone between the EBS and the rock formations in the CRZ should not be exceeded due to expected stresses (dilatancy criterion), and the expected fluid pressures should not exceed the fluid pressure capacities at the interface EBS/rock formations in a manner that leads to a significant increase in fluid pathways in the CRZ (fluid pressure criterion). The dilatancy criterion is used to assess the impact of mechanical damage to the rock mass caused by deviatoric stress, whereas the fluid pressure criterion takes into account the formation of flow paths driven by fluid pressure (Kock et al., 2012).

One can summarize from these regulative requirements that the THMC evolution of the repository system should not endanger the sealing properties of the EBS embedded in the CRZ. From this premise, a specific integrity assessment concept for the EBS can be developed.

10.2 Basis for the design of EBS

Geotechnical engineered barrier structures are typically characterized by their layered construction. Within these structures, individual components fulfill various functions. Common components include sealing elements and abutments, complemented by backfill columns and filter layers. Depending on the specified requirements and system properties, these subsystems can be arranged in a diverse and redundant manner. For each of these components, specific safety functions are assigned. These safety functions dictate the different individual assessments to be carried out for each component.

Viewing geotechnical engineer barriers as geotechnical structures facilitates the direct application of engineering standards in their design and assessment. This approach is in line with the internationally recognized state of the art and is realized using the method of partial safety

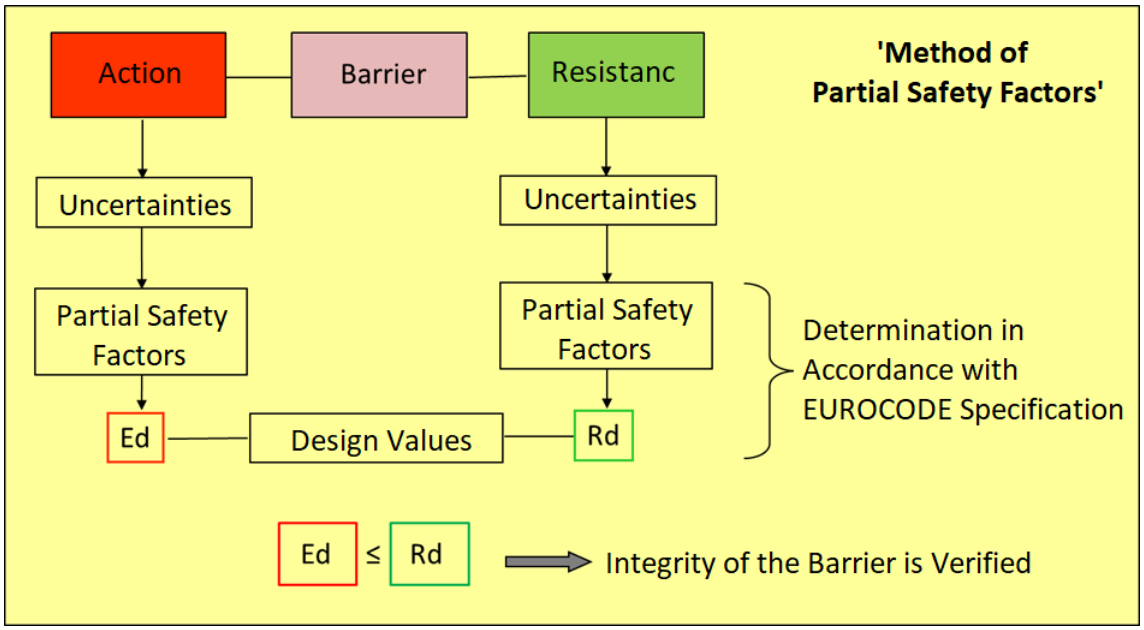

Figure 10.-1: Basic principle of the method of partial safety factors (Jobmann et al. 2017b).

factors. The semi-probabilistic, reliability-oriented safety proof concept of partial safety factors is based on the Eurocode standards (DIN EN 1990, 2010) and is recognized in the construction industry for assessing load-bearing capacity. This method has been exemplarily applied to an element of a generic shaft closure in a previous research project (Eberth and Müller-Hoeppe, 2009), and within the preliminary safety analysis for the Gorleben site (VSG) for the design and assessment of the closure concept for shafts in rock salt (Müller-Hoeppe et al., 2012b,a). Another application example is contained in Kudla et al. (2013), demonstrating the assessment procedure using a sealing and a supporting element in rock salt.

The transfer of the practical construction approach to the assessment concept for geotechnical barriers allows the description of the structure and its properties in respective design situations by equilibrium states. The actual assessment is conducted through a limit state consideration, where the effects on the structure are compared with the resistances of the construction. Calculation cases arise according to the design-determining combinations of effects and system properties (similar to the load cases in the Eurocode) with which the limit state consideration can be carried out.

Referring to a limit state is sensible since both loads and resistances arise from typical distribution functions. The resulting scatter of both sizes leads to a range of possible states. The limit state describes the condition in the structure where the construction just meets the requirements and beyond which compliance with the design requirements is no longer given. Formally, to meet the requirement condition, it must apply that the resistances are greater or equal to the effects. The design values are determined from the characteristic values of the loads and the properties of the barrier in combination with the partial safety factors. This approach is illustrated in Figure 10.-1. This procedure is applied to all loads and resistances.

Design values for individual assessments are derived from the characteristic values of loads and properties of the barrier, combined with the respective partial safety factors. By applying the method of partial safety factors, both the loads and resistances, or the included parame-

ters of the target relationship, are assigned partial safety factors. Loads (E_d) are multiplied by the partial safety factors, thus increasing them. In contrast, resistances (R_d) are divided by the partial safety factors, thereby reducing them. This approach and the application of partial safety factors generally cover uncertainties in the representative values of influences and uncertainties in the construction properties.

Model uncertainties in loads and resistances are captured as necessary depending on the model formation via model factors. In cases of high accuracy of the models, model factors are typically not considered (Eberth and Müller-Hoeppe, 2009).

The basic requirement is

$$E_d \leq R_d$$

thus breaking down into concrete calculations for both terms. On the influence side, for E_d,

$$E_d = \gamma_{Ed} \cdot E(F_{di}; a_{di}; X_{di})$$

with F_{di} = Design values of various influences (i), a_{di} = Design values of the respective geometric sizes, X_{di} = Design values of the respective material properties.

The design values of the influence F_d are determined by multiplying the characteristic individual value (F_k) with the partial safety factor of the influence (γ_f).

$$F_d = \gamma_f \cdot F_k$$

For the design values of the material properties X_d, according to previous explanations,

$$X_d = (\eta \cdot X_k)/\gamma_m$$

with η = Conversion factor for load duration, humidity, etc., X_k = Characteristic value of the material properties, γ_m = Partial safety factor of the material property.

On the resistance side, the design resistance is derived from

$$R_d = 1/\gamma_{Rd} \cdot R(a_{di}; X_{di})$$

with: γ_{Rd} = Partial safety factor for model uncertainty in the resistance model.

The individual verifications of the considered limit states are to be conducted “in the range of load-bearing capacity proofs”, meaning that the reliability level of a load-bearing capacity proof is achieved. This safety concept is necessary to ensure a design that meets the requirements. For the considered structures, the proof of impermeability is seen within the range of a load-bearing capacity proof, as the loss of impermeability can pose a “danger to life and limb” (DAfStb, 2011). Unlike the definitions of the Eurocode, the term load-bearing capacity is not solely understood as mechanical stability. It serves as a synonym for preventing a danger to

life and limb and can also be applied to hydraulic resistance. Adherence to the reliability level for load-bearing capacity in the respective proof ensures the functionality of the construction.

The application of an appropriate reliability level is necessary for a requirement-compliant design, as otherwise, a failure of the impermeability or structural integrity could pose a “danger to life and limb”. This particularly affects the confidence level of the reliability proof. The probability of failure pf is sufficiently described for a load-bearing capacity proof with 10^{-4} over the intended use or functional duration (DAfStb, 2011). Thus, the functional proof includes that the barrier, over its lifespan, does not fail prematurely with a probability of failure pf $\leq 10^{-4}$, or the survival probability ps of the barrier is ps = 1 − pf (Müller-Hoeppe and Krone, 1999).

The various influencing factors can be determined both through deterministic and probabilistic methods. For instance, the geometry of the construction results from the design, and loads can be identified based on statistical data and limit value estimations. Material properties can also be derived from a statistical basis (Müller-Hoeppe and Krone, 1999). If the current regulatory framework does not describe suitable partial safety factors, these can be determined through probabilistic methods or calibration (Kreienmeyer et al., 2008). Figure 10.-2 schematically illustrates the methods for determining partial safety factors.

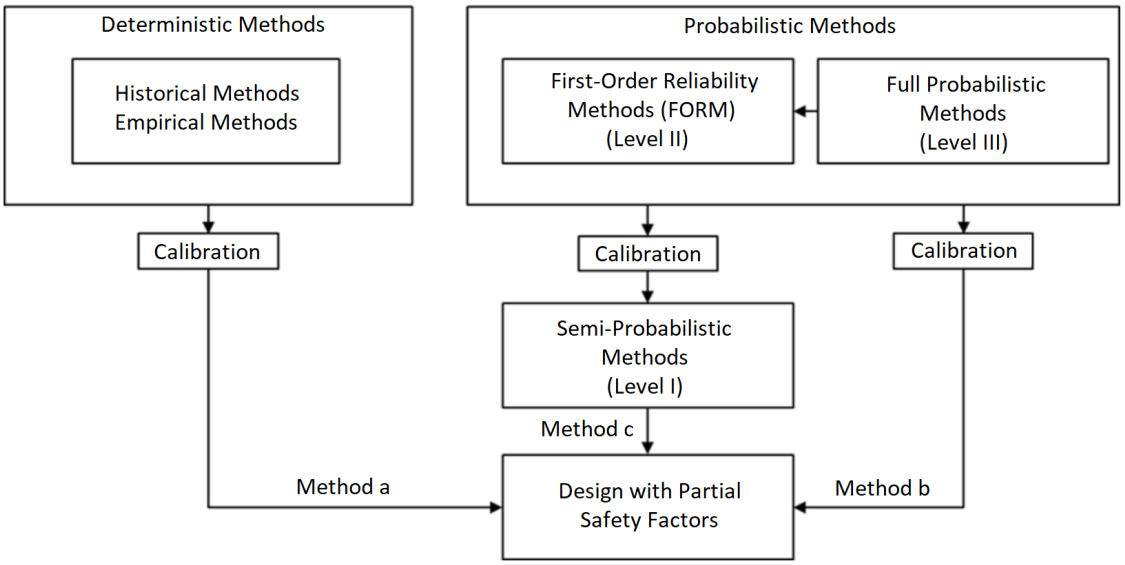

Figure 10.-2: Reliability methods for determining partial safety factors (DIN EN 1990).

The technical regulations that can be used for assessment primarily include:

- Eurocode 0, Basis of structural design (DIN EN 1990, 2010)
- Eurocode 1, Actions on structures – Part 4: Actions on silos and liquid retaining tanks (DIN EN 1991, 2010)
- Eurocode 7: Geotechnical design – Part 1: General rules (DIN EN 1997, 2014)
- GDA Recommendations Geotechnics of landfills and contaminated sites (DGGT, 1997)
- DAfStb Guideline Concrete construction when dealing with substances hazardous to water (DAfStb, 2011)

10.3 Integrity assessment and verification concept of the EBS

As prescribed in the regulatory requirements, The EBS must exhibit sufficient hydraulic resistance during a defined functional period to prevent fluid transport into or out of the repository. To ensure the preservation of these properties over the functional period, the structural integrity of the construction must be demonstrated. If the barrier's resistances in a specific design case are sufficient against the impacts or combination of impacts, and if the feasibility of the construction is proven, then the functional verification is considered established. The basic structure of this proof is shown in Figure 10.-3.

The basis for this proof is the conceptual design of the individual barriers, described in the sealing concept. The subsequent verification is essentially divided into two steps.

In the first step, structural integrity verification must be provided for each individual barrier. To demonstrate structural integrity, the impacts or loads acting on each barrier after its construction must first be specified. This can be determined using the site-specific FEP catalog. From this catalog, those FEPs that describe an impact on the specific barrier can be identified. Once the FEPs and thus the impacting processes are identified, the impacts on each barrier can be specified.

In the second step, it must be proven that using all geotechnical barriers, including the backfill in the repository mine, the advection criterion can be maintained. For this purpose, the hydraulic resistances of all barriers and backfills are considered in conjunction, and it is examined whether the total hydraulic resistance is sufficient. In this context, and with a focus on the required redundancy and diversity of the barrier system, it is necessary to examine to what extent the failure of individual barrier components might affect the integrity verification. For this purpose, the hydraulic conditions must be specified. This involves the hydraulic resistances of all barriers and backfills, as well as the hydraulic gradients that will eventually establish themselves in the mine, as these drive the flow through the barrier system. If it can be demonstrated that the advection criterion is also met, then the verification of the integrity of the EBS is considered established.

Furthermore, (EndlSiAnfV, 2020) requires in §6 (4) that, It is to examine and demonstrate that the manufacturing and construction of the barriers, according to these specifications, can be quality-assured in the required quantity. The planned quality assurance must correspond to the current state of science and technology. The manufacturing and construction of the barriers must have been successfully tested under realistic conditions. Their function under these conditions needs to be examined and demonstrated. Consequently, a new criterion of constructability must be established.

The regulations in (EndlSiAnfV, 2020) mandate not only the demonstration of integrity but also the robustness of the Containment Rock Zone (CRZ), a requirement that extends to the Engineered Barrier System (EBS). The methodology presented herein offers insights into how the robustness of the EBS can be effectively demonstrated.

The following sections explain the individual proofs and the methodology used for verification.

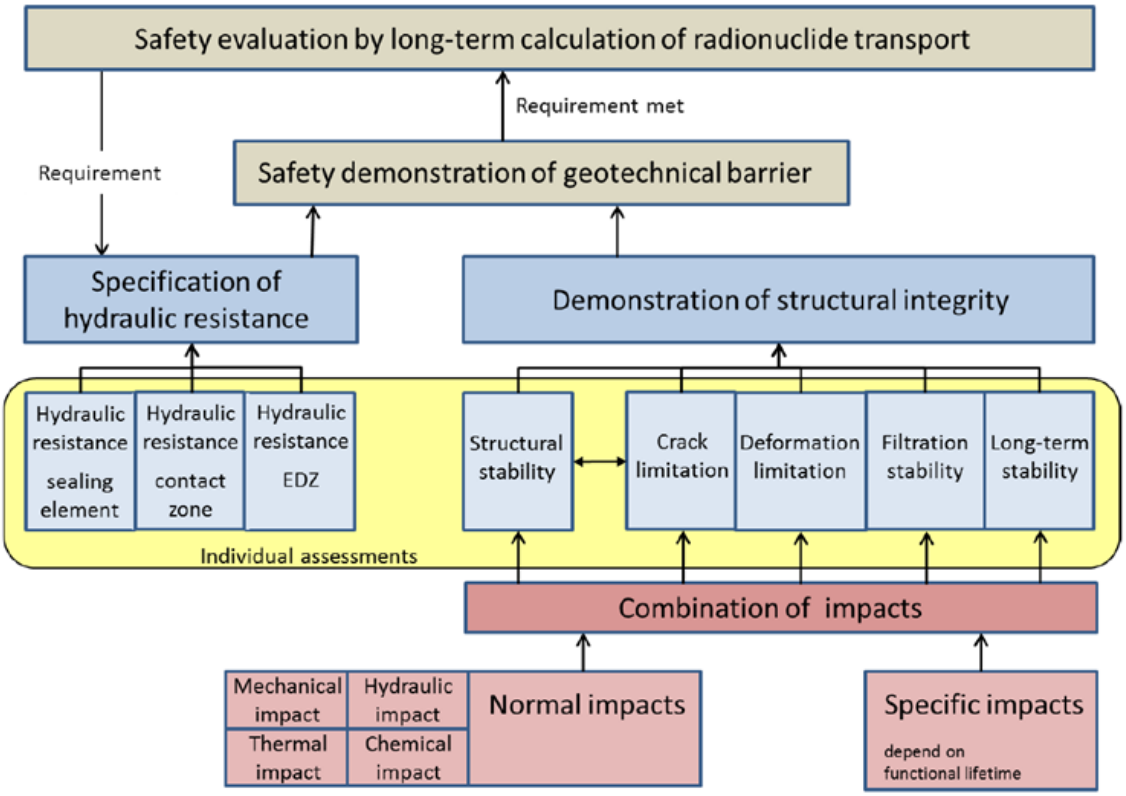

Figure 10.-3: Integrity assessment diagram (Müller-Hoeppe et al., 2012b).

10.4 Demonstration of the structural integrity

The demonstration or verification of structural integrity comprises the following five individual verification criteria (Müller-Hoeppe et al., 2012b):

- Structural Stability (commonly referred to as “Load-bearing Capacity”)
- Crack Limitation
- Deformation Restriction
- Filter Stability
- Long-term Stability (also known as “Durability”)

Should any of these five individual proofs fail, the conceptual design of the respective barrier must be revised until all can be successfully demonstrated.

10.4.1 Structural Stability

Sealing effectiveness and load distribution are the two main functions of a geotechnical barriers. Within a barrier, these functions are assumed by different elements, typically assigning only one of these functions to each element. Load distribution and mechanical load-bearing capacity are functions of abutments, which can be cohesive or non-cohesive.

The load-bearing capacity of non-cohesive abutments, such as gravel columns in shaft closures, is primarily defined by settlement stability.

Cohesive building materials, like concrete abutments that develop adhesion within the material and with adjacent rock due to binders, are covered by the crack limitation proof for mechanical load-bearing capacity. For cohesive materials, any mechanical damage is always preceded by crack formations. If crack limitation can be proven for these materials, mechanical damage is ruled out, and the proof of mechanical load-bearing capacity is established. If crack limitation proof is unsuccessful, mechanical load-bearing capacity must be separately demonstrated.

The proof of crack limitation is established if no cracks occur in the structure. If it can be shown that no damage occurs to a cohesive abutment during the analysis of loads acting on the concrete element, then the proof of crack limitation is considered fulfilled. If complete crack freedom cannot be demonstrated, then the limitation of cracks must be shown as part of the usability proof. For concrete, fracture criterion by Ottosen (1977) can be used for assessment. Accordingly, the criterion is defined as follows: It must be demonstrated that no significant damage occurs during the functional period within the verification period.

10.4.2 Crack Limitation

Crack limitation proof is relevant for both sealing elements and abutments. Crack formations are encouraged by mechanical overloading of individual subsystems (see above section) or thermal-mechanical-chemical processes during installation and over repository evolution.

An example of crack formation due to volume or temperature changes is the cooling process of hot-installed bitumen or asphalt seals, where the sealing material undergoes cooling-induced volume shrinkage. As observed in practice, this shrinkage can reduce the effective sealing length of the seal by contracting and detaching from the contour in the upper part of the seal (Herold et al., 2020).

The formation of cracks in sealing materials is influenced by the mechanical and hydraulic conditions imposed on the seal and its contact area. Specifically, crack formation can occur when the fluid pressure criterion is violated, meaning the fluid pressure exceeds the smallest principal stress within the seal or at its interface with the surrounding rock (Müller-Hoeppe and Krone, 1999). A notable example of this phenomenon was observed in a large-scale shaft closure experiment conducted in Salzdetfurth, where excessively rapid loading of a bentonite seal element resulted in seal damage (Teichmann et al., 2002).

More generally, cracks are expected to form when the material's strength limits are exceeded under mechanical loading. This can occur due to stresses caused by external loads, thermal expansion, or differential settlement. Proper design and gradual loading are therefore essential to ensure the integrity of the sealing material and to avoid crack formation during both the construction and operational phases of the repository.

10.4.3 Deformation Restriction

Engineered barriers are typically characterized by one or more sealing elements being held in position by abutments. This is especially necessary for swelling material seals. The swelling process of the sealing material only leads to sealing if the planned swell pressure within the

seal is achieved. If the seal undergoes unplanned large volume expansion due to swelling, the planned swell pressure is not achieved. The abutments, especially in drift sealing systems, must therefore be deformation-stable and firmly anchored in the rock to ensure positional stability.

Especially for shaft closures, to ensure the positional stability of the seals, proof of sufficiently small settlements in the abutments and filter layers, which act as support for the respective seals, is required.

The proof of deformation stability involves demonstrating that the abutment itself is positionally stable and allows only minor expansion or deformation of adjacent sealing elements. In this context, (Wagner, 2005) noted that limited displacement of an abutment, for example, due to the swelling pressure of the bentonite, can be tolerated without causing a bentonite sealing element to become so loosened that its sealing effect is impaired. The criterion can be defined and quantified as follows: It must be proven that potential displacements of the abutment away from the bentonite sealing element are less than 3% of the length of the adjacent bentonite sealing element.

It should be noted that the investigations leading to the aforementioned 3% limit for displacement were conducted exclusively with Ca-bentonite (reference material). It is currently not ruled out that using a different type of bentonite, for example, sodium-dominated, might slightly alter this limit. This needs to be verified in the given case.

For crushed salt, the deformation of the host rock could, under certain conditions, displace the abutment, potentially increasing the initial volume of the space where the long-term seal is installed. This expansion of the initial volume may result in an extended compaction period before the seal reaches its intended functionality. To evaluate this effect and its implications on the sealing performance, a numerical analysis is required to simulate the interactions between the host rock deformation, abutment displacement, and crushed salt compaction behavior.

10.4.4 Filter Stability

The subsystems of individual closures, especially sealing elements made of granular materials, must be tested for their filter stability. This stability can be characterized by preventing erosion and suffusion processes in the considered subsystem. High hydraulic gradients due to fluid ingress from possibly existing aquifers can pose an increased risk of erosion and suffusion during the saturation phase. This must be countered by constructive measures. A lack of filter stability can, for example, lead to a reduction in the tightness of sealing elements.

When assessing the risk of material transport, a distinction is generally made between cohesive and non-cohesive materials based on the classification according to DIN 18196 (2011). Medium-plastic fine and mixed-grain mineral mixtures that possess effective cohesion are classified as cohesive materials. Coarse-grained and slightly plastic fine-grained mineral mixtures are considered non-cohesive materials.

Cohesive materials are significantly less sensitive to all forms of material transport compared to non-cohesive materials. Due to their internal binding forces, cohesive materials consist of interlocked and thus less mobile particles than non-cohesive materials. Under certain flow conditions, larger material parts, known as aggregates, can be dislodged from the composite.

The risk of material transport decreases with increasing cohesion. Cohesive materials can absorb so much water at stress-free interfaces (e.g., at crack surfaces and cavities due to manufacturing defects or natural influences) that they almost completely lose their internal binding forces and thus their strength. In combination with flowing water, the risk of material transport increases (BAW, 2013b).

Clays or bentonites, from which sealing elements are made, are categorized as cohesive materials. In cohesive materials, individual particles are bound to each other by chemical and/or physical binding forces to the extent that individual particles are not freely movable. However, movable aggregates (group of interconnected particles) can form along weak zones in cohesive materials. The vulnerability of cohesive materials to material transport is significantly lower than that of non-cohesive materials due to the typically present aggregate size.

In the evaluation of filter stability, a fundamental distinction is made between two types of material transport: suffusion and erosion.

Suffusion refers to the rearrangement and transport of fine fractions of a material within the pore space of the coarse fraction's grain framework (BAW, 2013b,a). Here, the supporting grain framework remains unchanged, and no destruction of the material structure occurs. As a result of suffusion, the pore volume and permeability of the material increase, while its density decreases. With the increased permeability of the material, groundwater flow increases at a constant hydraulic gradient. Progressive suffusion can facilitate erosion processes if the stability of the supporting grain framework is reduced by the removal of fine material.

In order to prevent suffusion, the installation of filter layers has to be taken into account in the design process. The filter should not be designed to retain the entire fine and re-arrangeable grain spectrum. Otherwise, fine particles can deposit in front of the filter layer, reducing the hydraulic permeability. This increases the fluid pressure in front of the filter. The design of a grain filter for suffusive materials can follow the procedure by Lafleur et al. (1993). For the grain size distribution of the designed filter itself, proof against suffusion is also required to ensure the filter remains functional.

Erosion is defined as the relocation and transport of almost all grain fractions of a soil caused by water flow (BAW, 2013b,a), resulting in a change in the supporting structure. Erosion processes can pose an acute threat to the stability of an earth or massive construction. For the assessment of filter stability in sealing structures made of cohesive or binding materials, contact erosion and joint erosion are relevant. Internal erosion is covered by suffusion safety, and the proof against external erosion on the surface of a body is based on hydraulic calculations in the case of layer-parallel flow. This is not relevant for seals in underground drift and shaft seals, as layer-normal flow must be assumed in these cases.

10.4.5 Durability

According to the safety requirements (EndlSiAnfV, 2020), the integrity of the CRZ must be proven for the stipulated period of 1 million years. For the geotechnical barriers, a functional period must be defined in line with developments, during which their functionality must be ensured.

The definition of the functional period of the geotechnical barriers depends on the long-term

development of the final repository system. In salt repositories, significant uncertainties exist regarding the compaction rate of the crushed salt and its permeability in compacted state relative to the degree of compaction. This is especially the case at advanced stages of crushed salt compaction, i.e., at very small porosities. Depending on the prevailing temperature and the presence of moisture, the compaction of the crushed salt until the required properties are achieved can take several decades to several thousand years. Due to these uncertainties, the design of the EBS is based on a target value for the functional duration of 50,000 years.

The integrity and verification concept is based on the EUROCODE, which was designed for structures with a service life of less than 100 years. This raises the question of whether the concept is viable for the defined service life of the EBS of 50,000 years. The only difference between a material used in standard technical constructions and one applied in a final repository lies in the required duration of the material's durability and its properties. While in typical technical applications, material durability needs to be proven for up to 100 years, in the context of a final repository, the durability and the material properties must be demonstrated for a significantly longer period up to 50,000 years. The key point to tackle this problem resides in the evaluation of the long-term stability of the materials used in the construction of the EBS. The design of a structure based on the EUROCODE concept is valid for higher functional time periods if one can show that the expected degradation of the material from which the structure is made is either limited or non existent under the loading, environmental and geological conditions to be expected.

In this regard, the long-term durability must be demonstrated for the entire respective EBS. In practice and according to regulatory standards, "durability" is defined as sufficient resistance of the material to environmental influences. The criterion is defined as follows: It must be proven that the properties of the elements of a closure structure are preserved over the defined functional period.

The durability or long-term behavior of the used materials can be evidenced by natural analogs. This is especially the case for clay and salt sealing materials used in the shaft and drift closure structures. These materials have a proven long term stability as the clay and salt geological formations have been formed several hundred millions years ago. In this regards, the dimensions of the sealing elements made of materials with proven natural analogs should be as large as possible to act as the natural analogs. An initial conclusion that can be drawn is that the thickness of the sealing element is a crucial factor. It has already been substantiated through historical analogs that particularly massive constructions tend to endure over long periods. A significant advantage in this context is the underground location of the sealing element. Historical structures located underground and made from durable materials often exhibit a high degree of preservation (Müller-Hoeppe and Krone, 1999).

For building materials where property-altering alteration processes are expected, such as cement-based concrete materials, geochemical analyses are necessary to evaluate or optimize the stability of the cement structures in contact with the groundwater solution to be expected in the repository over the functional period. For instance, it has been proven that Sorel concrete are geochemically stable in MgO-rich waters. Thus, it is therefore possible to design the EBS in such a way that MgO-rich waters can be expected in the repository. Materials like bitumen or asphalt, considered impermeable to liquids and gases, are also seen as long-term stable materials (Herold et al., 2020), but over a proof period of 1 million years, changes–for example microbial activities– cannot be ruled out, so functional periods must be

defined for these materials.

10.5 Demonstration of hydraulic resistance

The hydraulic resistance or sealing or tightness criterion is applied in engineering and describes, in terms of the method of partial safety factors, the limit state of sealing (Müller-Hoeppe and Eberth, 2009): A barrier is considered tight if, during the functional period, the front of the infiltrating medium contaminated with pollutants does not reach the opposite front of the barrier. This definition provides a sufficient criterion for tightness. However, applying this criterion requires defining a verification period, as without it, the criterion remains indeterminate.

For geotechnical barriers, in accordance with the safety concept, a verification period of 50,000 years is established. Therefore, it seems appropriate to select an exposure period of 50,000 years for the quantitative demonstration of sealing. The position of the penetration front then provides a design criterion for proving sealing.

The required thicknesses of the sealing elements in the geotechnical barriers to ensure sealing are then determined only by the physical properties of the penetrating medium, such as viscosity, pressure, etc., and of the barrier, like permeability, porosity, saturation, etc. This reduces the task to determining the properties of the penetrating medium and ensuring the required barrier properties over the verification period (Müller-Hoeppe and Eberth, 2009).

In terms of the limit state of sealing, impacts on and resistances of the sealing structure must be determined. The impacts are characterized by the penetrating fluid and other FEPs that can affect the hydraulic transport through the sealing structures in the planned sealing site. The possibility of unfavorable deviations of impacts from their representative values is captured by a partial safety factor. The same applies to the possibility of unfavorable deviations of resistances from their representative values, where resistances are typically characterized by the representative values of material properties and the geometric data of the construction.

Partial safety factors generally represent factors by which the numerical expression of unfavorable impacts is increased or the numerical expression of resistances is decreased. The partial safety factor for material properties is introduced to consider the possibilities of unfavorable deviations of material properties from their characteristic values and a partial safety factor to capture unfavorable deviations of the geometric data from characteristic (set) values (of the construction) governed by tolerance specifications. Furthermore, a partial safety factor is conceivable to account for uncertainties in the design and assessment.

10.6 Demonstration of constructability

All components of a closure structure must be manufacturable or constructible under the local conditions of the planned sealing site. In this regard, the EndlSiAnfV (2020) requires in §6(4) that: The properties required for long-term safety of technical or geotechnical barriers must be specified in the safety concept. It must be examined and demonstrated that the production and construction of the barriers according to these specifications are possible with the required quality assurance. The intended quality assurance must correspond to the state of the art in science and technology. The production, construction, and function of the barriers must have been successfully tested, insofar as their robustness cannot be otherwise demonstrated and

there are no safety reserves to an extent that would allow forgoing testing.

This leads to the following criterion: It must be proven that the closure structures can be constructed under the local conditions of the planned sealing site in such a way that their assigned performance objectives are met.

Fundamentally, the assessment can be conducted by comparing with similar structures that have been erected nationally or internationally and have been successfully tested. If comparable structures have not yet been constructed, the proof of manufacturability can also be provided through the execution of a large-scale in-situ experiment, which encompasses both the construction and the functional test. In this regard, the factors listed in DGGT (1997) should be appropriately applied to the assessment of underground closure structures and detailed. These factors include:

- Manufacturing prerequisites
- Handle-ability and sensitivity to errors of the manufacturing process
- Sensitivity of sealing materials to installation stresses
- Testability
- Possibilities for improvement and repair

In addition, a quality assurance program must be provided, which includes test plans describing the quality-assuring procedural steps and quality agreements describing the quality-assuring properties. The Eurocode (DIN EN 1990, 2010) notes that, if applicable, EN ISO 9001:1994-08 (1994) can also be used for quality management measures. In the case of barriers in a final repository, a comparison with the IAEA recommendations on quality management should also be made (IAEA, 2008). Only after the presentation of a feasible quality assurance program for the function-defining properties can the functionality of the individual barrier component be proven.

10.7 Demonstration of robustness

In EndlSiAnfV (2020) robustness is defined as the insensitivity of the safety functions of the final repository system and its barriers to internal and external influences and disturbances. Because, the proposed verification concept is based on the semi-probabilistic, reliability-oriented safety concept, the robustness of the EBS in the scope of integrity assessment can be analyzed by means of partial safety factors that affect the loads acting on the EBS and the properties of the materials (resistances) used in the EBS. In this regard, the safety factors account for the uncertainties of the EBS in the repository system.

The safety factors used in the design correspond to a specific probability of survival of the structure which is inversely correlated with a probability of failure. By decreasing, the probability of failure for the verification period, i.e 50000, one can increase the robustness of the system. For that, the safety factors need to be calibrated for the defined probability of failure. One refers to Figure 10.-1 for calibration method of safety factors.

A different approach may consist in progressively increase the safety factors to determine the limit under which the system will collapse. This state corresponds to the lowest probability of

failure of the structure. Such an approach is usually used in the design of tunnel constructions and it is called as phi-c-reduction (Itasca Consulting Group, Inc., 2021). In the context of the EBS with different materials involved in contact which different geological layers, this approach is more difficult to implement and requires a considerable computational effort.

Another method to explore the robustness of the system is through extreme state analyses. In this approach, parameters are chosen to be extreme – even 'unrealistically' so – in an attempt to push the system to the limits of its robustness (so-called what-if scenarios). This approach was pursued in the scope of VSG in several integrity assessment analyses. For example, in the thermal-mechanical calculations involving the mine structure, the heat input into the final repository was altered to very unrealistic values to test the behavior of the final repository system under extreme conditions. Similarly, unrealistically high values were used in the hydraulic calculations within the mine structure, for instance, for the fluid saturation of the backfill (Kock et al., 2012).

The limit state approach can also be combined with the semi-probabilistic, reliability-oriented safety concept. Such a combination is useful for the cases where the safety factors for specific impacts cannot be easily estimated. In this case, one can consider unrealistic manifestation of such impacts to assess the robustness of the system.

Another approach consists of determining the probability of failure the system through a fully probabilistic methodology. In this approach, the factors influencing the resistance and the impacts on the structure are described by the probability functions. The limit state analysis of the system are performed with Monte Carlo simulations to determine the robustness of the system. This approach has been employed by Wagner (2005) for the design of a shaft sealing structure in a salt repository. Although this approach represents the most complete one, it remains the most challenging due to the urge amount of simulation cases to be realized. It remains non practicable even regarding the rapid advancement in the development of numerical tools. Model simplifications are therefore necessary. On the other hand, this approach can be useful in the determination of safety factors that can be used in other methods discussed above.

In conclusion, the assessment of the robustness can be considered as part of the integrity evaluation as the system is pushed way above the safety criteria to be met in the scope of the integrity assessment. Different methods can be used to assess different specific cases. Those cases depend on the local situation at the planned sealing site. A combination of all the discussed approaches is also possible. The robustness evaluation requires a significant computational effort. Further work is necessary to determine how complete a robustness analysis can be performed with the available numerical tools of today.

11. Integrity evaluation

Integrity evaluation encompasses the integrity analysis for less likely repository evolutions. According to EndlSiAnfV (2020), the integrity of the CRZ (therefore of the EBS) is not to be demonstrated for the alternative scenarios. But those scenarios have to be considered in the optimization of the repository system as required in §12 of EndlSiAnfV:

> *The safety concept and technical design of the final repository must be optimized considering all circumstances with attention to the balance of measures to achieve the following goals:*
>
> 1. *The long-term safety of the final repository, particularly the quality of the safe enclosure of radioactive waste and the robustness of the final repository system, and*
> 2. *The optimization is complete when further improvement of safety can only be achieved with disproportionately high effort.*
> 3. *In the optimization of the final repository, in addition to the expected and alternative developments according to § 3 paragraphs 3 and 4, the hypothetical developments and developments based on future human activities according to § 3 paragraphs 6 and 7 must also be considered. It must be ensured that measures to optimize the final repository system, which are derived from alternative developments, do not significantly impair the safety of the final repository for the expected developments.*

Based on these requirements, the integrity evaluation is considered in the proposed methodology by providing essential insights about the robustness and the optimization of the EBS. In our understanding, only the alternative scenarios are relevant for the integrity evaluation of the EBS. Less likely scenario such as human intrusion or other hypothetical scenarios occur independently of the EBS.

By focusing on the alternative scenario, one already assumed that the integrity of the EBS is partly not verified. In this case the integrity evaluation does not considered the structural integrity of the EBS but focused only on the hydraulic resistance of the EBS under harsher conditions, i.e. when only a part of the EBS is still functional. From the FEP, the main alternative scenarios affecting the EBS are the failure of a shaft seal, and the failure of a drift seal. The evolution of the repository for such conditions is the main objective of the integrity evaluation.

In the past, the integrity evaluation was considered in the radiological long-term assessment. According to BMU (2010), the maintenance of the integrity of the CRZ must be demonstrated for probable developments. Less likely developments, as per BMU (2010), should be considered within the framework of the radiological long-term assessment. It is conceivable that even a less likely development could influence the barrier effect of the CRZ. Any change in the barrier effect must then be taken into account in the radiological consequence analysis (Kock et al., 2012).

In the propose methodology for the EBS, we propose to separately evaluate the EBS within the repository system independently of the radiological evolution. Although the methodology

for performance assessment is also applicable for the integrity evaluation. This is especially the case because the advancements in the development of numerical tools for performance assessment allow the simulations of complex models at repository scale. In this regards, the modeling of the EBS can be integrated in a model dedicated for the performance assessment of the repository system.

11.1 Methodology for performance assessment

Performance assessment plays a critical role in the safety case for a waste repository, as emphasized by the US NWTRB (Nuclear Waste Technical Review Board). It is primarily aimed at a quantitative evaluation of post-closure safety, through a thorough analysis of repository performance and a comparison of this performance with quantitative design requirements and safety standards. Additionally, it estimates how quantifiable uncertainties may influence repository performance (MacKinnon et al., 2012).

This type of assessment necessitates both conceptual and computational models that encompass the pertinent features, events, and processes (FEP) that are or could be significant to safety. These models need to accurately capture the physical, chemical, and biological processes that might occur within the repository system over its lifetime and beyond. This requires a deep understanding of the repository design, the waste being stored, the geological environment in which the repository is located, and the potential interactions between these components.

Essentially, performance assessment seeks to understand and quantify the behavior of a waste repository under various scenarios, including both expected and less probable evolutions of the repository system. By comparing these findings against safety standards and design requirements, it is possible to determine whether the repository is safe for long-term storage of waste and to identify any areas where further investigation or design changes may be needed.

Following MacKinnon et al. (2012), a thorough performance assessment includes quantification of the long-term, post-closure performance of the repository, the evaluation of uncertainties and the comparison with safety requirements. Figure 11.-1 illustrates the performance assessment methodology that has been used in the certification of different radioactive waste repositories in the US like the WIPP defense TRU waste repository (U.S. Department of Energy, 1996) and the Yucca Mountain License Application (U.S. Department of Energy, 2008). This proven methodology is now the starting point for further development in the safety assessment of future repositories especially in salt.

The PA approach depicted in Figure 11.-1 brings together different sets of data to provide confidence in the safety of the system after closure. This encompasses: (1) the fundamental technical groundwork for the safety evaluation models, akin to some safety case concepts like the assessment basis (see, for instance, (Nuclear Energy Agency, 2004); (2) an exhaustive analysis of scenarios and FEP, ensuring a robust evaluation of post-closure performance; (3) a quantitative and qualitative description of the sealing functions of the barriers; and (4) analyses of uncertainties and sensitivities, pinpointing areas needing more data for the subsequent phase of repository advancement (MacKinnon et al., 2012).

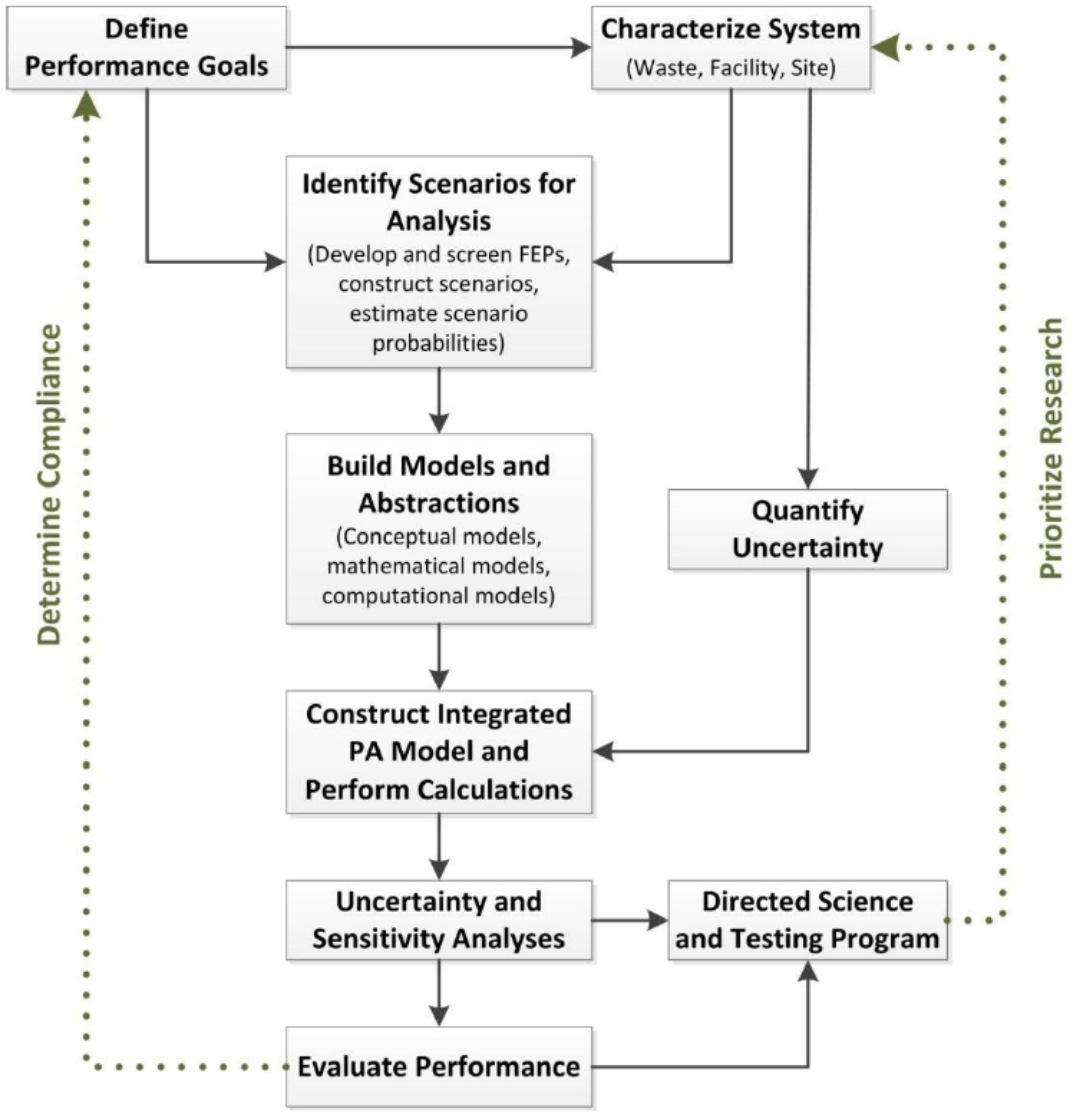

Figure 11.-1: Performance assessment methodology (MacKinnon et al., 2012).

A conceptual model framework requires a coherent representation of all pertinent FEP. The features of a conceptual model are the physical components of the engineered barrier system (EBS) and the surrounding natural barrier system (NBS). Primary features include radionuclide inventories, waste forms, waste packages, buffer materials, seals, drifts, shafts, host rock, surrounding stratigraphy, groundwater, fractures, aquifers, wells, springs, soil, etc. For implementation in a PA model, the conceptual model framework provides information regarding repository layout, e.g., the sizes and locations of waste packages, drifts, buffer/backfill, shafts, and seals. In addition, the conceptual model provides information beyond the repository to describe the dimensions, properties, and locations of important features in the surrounding geosphere and accessible biosphere.

Important processes and events in the conceptual model are those that could significantly affect the movement of radionuclides in the EBS and NBS. Such processes and events include waste package corrosion, waste form dissolution, radionuclide release, radioactive decay, heat

transfer, aqueous transport, advection, diffusion, sorption, aqueous chemical reactions, precipitation, buffer chemical reactions, gas generation, colloidal transport, earthquakes, inadvertent human intrusion of the repository, etc. A FEP database can be used to help identify a full set of potentially important FEP for a specific conceptual repository model. Many of the FEP in a FEP database may be included in the PA model. In a comprehensive PA, excluded FEP (i.e., FEP not included in the PA model) must be addressed in separate analyses and arguments (Mariner et al., 2015).

11.2 The role of EBS in performance assessment in salt repository

The release of radionuclides from the host rock acting as an effective barrier (CRZ) can occur via diffusive transport due to concentration gradients or advective transport due to potential differences along two distinguishable transport pathways. This can either be the transport through the host rock unaffected by the mine workings or along the drifts and shafts excavated for the construction of the repository. In salt, a transport through the host rock is only possible in the EDZ and in cases where the integrity of the geological barrier is not met. In this case, advective transport can take place through the fractured rock or in region where the salt dilantancy criterion is not met. In the case of an intact geological barrier which is to be shown in the scope of the safety integrity assessment of any specific site, only the second mode of transport through the backfilled drift network and shafts is possible. In these conditions, the confinement of the radioactive waste relies largely on the EBS. Essentially, the radiological evaluation of the repository can be limited to the region that has been excavated and later backfilled. Interaction with the geological layers takes place only in the EDZ surrounding the excavated volume. In this context, it becomes obvious to study with high accuracy how the fluid transport will occur during the evolution of the repository system in the repository mine and in the shafts as realistic as possible. Increasing the understanding of this process will help to better assess the potential of optimization of the EBS. This is exactly for this reason why the proposed methodology emphasizes an EBS centric PA assessment of salt repositories.

11.3 Performance Assessment modeling approach for the RANGERS project

Due the advancements in the numerical development of PA codes in recent years and the computational capabilities actually available, a modeling approach that is based on a direct coupling with process model codes used for the integrity analyses of the EBS is put forward. The core of this approach relies on a single highly detailed conceptual and numerical model of the repository system that resolves all components of the system going from the components of the shaft and drift sealing structures to the geological layers. The simultaneous use of this performance and integrity assessment allows an implicit coupling of the two kind of assessments. Specifically, an implicit coupling can be established by transferring data from between the code. Thus, one can derive from the thermal-mechanical process codes in which the compaction of the crushed salt backfill in the drift system is computed, the porosity evolution in the repository that can be used to compute the permeability in the PA code for the fluid transport modeling at repository scale in PFLOTRAN. Conversely, the pressure build up of gases computed in the PA codes can be used to assess as an influencing boundary conditions in the compaction analyses. The pressures of fluid computed in the PA codes can also be used as structural loads for the design and integrity of the shaft and drift seals.

12. Concluding Remarks

Rock salt is considered a highly suitable host material for the disposal of radioactive waste due to its unique combination of favorable properties. Its exceptional impermeability and low porosity effectively prevent the migration of radionuclides, ensuring long-term containment and isolation from the biosphere. The self-healing capability of rock salt, due to its creep deformation under pressure, seals any microfractures that may occur, further enhancing the integrity of the repository system. Additionally, rock salt's thermal conductivity aids in the dissipation of heat generated by high-level waste, reducing the impact on the repository's structural stability. These characteristics, combined with the geological stability and widespread availability of salt formations, make rock salt an ideal choice for the safe and secure disposal of radioactive waste, providing a reliable barrier against environmental contamination for millennia.

The safe isolation of radioactive waste in rock salt formations depends on a multi-barrier system, with the engineered barrier system (EBS) playing a critical role. Since rock salt formations are naturally impermeable, any potential advective transport of fluids into or out of the repository can only occur through the EBS. Therefore, the EBS must be meticulously designed, utilizing sealing components strategically placed throughout the repository to ensure containment until the long-term sealing element, the crushed salt backfill, fully assume its safety function.

Within the framework of the project RANGERS, a methodology for the generic design and performance assessment of EBS in repository in salt has been developed. The methodology aims at describing a workflow on how to assess the integrity of EBS of generic repositories in salt and how to handle them in the scope of integrated performance assessments. It is based on the experience gained in Germany and in the USA in the design, construction, and evaluation of seals from several research projects.

The methodology developed aims at providing the necessary route to follow when designing and assessing the performance of the EBS in a salt repository. Based on the selected geologic site and the proposed repository concept, a sealing concept is defined from which the EBS results. The resulting repository system, which consists of the geologic site, the repository mine, and the EBS, is subsequently subjected to a FEP analysis. In this context, only the FEP related to the EBS are taken into account. From the FEP, the loads acting on the EBS are derived, which then serve as the basis for an integrity assessment of the EBS. Based on these FEP, the evolution of the EBS in the repository over the reference period is assessed. This is used to assess the performance of the EBS within the scope of integrated performance assessment simulations.

The methodology focuses also on the link between EBS integrity and performance assessment and helps to reduce the uncertainties concerning the treatment of EBS in PA modeling. It also brings an EBS-centric view on PA by focusing on the processes occurring at each component of the EBS and their evolution over the lifetime of the repository. The improved understanding of the repository system that can be gained from this approach will help to optimize the sealing concept for repositories in salt.

PART 2: MODELING APPLICATIONS

13. Introduction

The Engineered Barrier System (EBS) plays an important role in ensuring the long-term safety and containment of high-level waste (HLW) and spent nuclear fuel (SNF) in deep geological repositories in salt formation. As part of a multi-barrier system, the EBS works alongside the natural barrier, which is the salt formation itself and the technical barrier comprising the disposal casks. The primary function of the EBS is to maintain containment during a defined period until the backfill used in the repository made of crushed salt, develops its sealing capacity through compaction. Over the time, the backfill eventually compacts to a state of low porosity and permeability, acting as a long-term seal. However, until this process is complete, the EBS must retain its structural and functional integrity. Regulatory guidelines in Germany currently require the EBS to remain effective for up to next ice age, that is expected in 50,000 years (Müller-Hoeppe et al., 2012b). The significant hydro-geological and topographic changes expected during an ice age could make it impossible to accurately predict the hydro-chemical conditions within the EBS in the repository system at that time.

In response to these challenges, BGE TECHNOLOGY GmbH (BGE TEC) and Sandia National Laboratories (SNL) have jointly developed a comprehensive methodology for the design and safety assessment of engineered barrier systems within the scope of the RANGERS project. This methodology is tailored for repositories in salt formations. The developed methodology provides a structured approach for designing and assessing the performance of the EBS in salt-based repositories. Follow up the development of a repository concept at a specific site, a sealing concept based on the geological characteristics of the selected site and the overall repository design is developed. The entire repository system, comprising the geological site, repository infrastructure, and EBS, is then subjected to a Features, Events, and Processes (FEP) analysis, focusing solely on those FEPs that affect the EBS. The derived FEPs help identify the loads and stresses acting on the EBS, which serve as the foundation for conducting an integrity assessment. This analysis helps predict the EBS's evolution and performance over the regulatory time frame, feeding into integrated performance assessment simulations.

Based on this approach, a robust modeling concept has been developed, allowing for systematic numerical analyses required for both integrity and performance assessments. This concept enables precise and stringent safety assessments, ensuring the long-term containment of HLW and SNF. The present report focuses on the application of this methodology to a generic repository system in salt formations, detailing the processes and outcomes of the developed approach.

14. Modeling Concept

The modeling concept is derived from the methodology for design and performance assessment of EBS developed in RANGERS. The key objective of this methodological approach is the performance assessment of geotechnical barriers within the safety assessment of a salt repository system. The methodological approach was developed in accordance with the German specifications of the EndlSiAnfV (Final Repository Safety Requirements Ordinance). It is summarized in Figure 14.-1. According to EndlSiAnfV §5 (1), the integrity of the EBS must be examined, demonstrated, and justified for the expected evolution over the planned functional time. Based on this, a distinction is made between the integrity demonstration and the integrity evaluation. The integrity demonstration conducts the integrity assessment for the reference scenario (or expected evolution). In the integrity evaluation, alternative scenarios relevant to the EBS are addressed. This step is not explicitly required in the EndlSiAnfV but creates the basis for a better evaluation of the robustness proof and for illustrating the optimization potential of the EBS. This is particularly important since the alternative scenarios represent states of the EBS that deviate from the reference case beside representing evolutions with a lower probability of occurrence. The analysis of the repository system for such unfavorable cases lays the fundamentals for a better assessment of the robustness proof and for illustrating the optimization potential of the EBS as prescribed in EndlSiAnfV §6 (1).

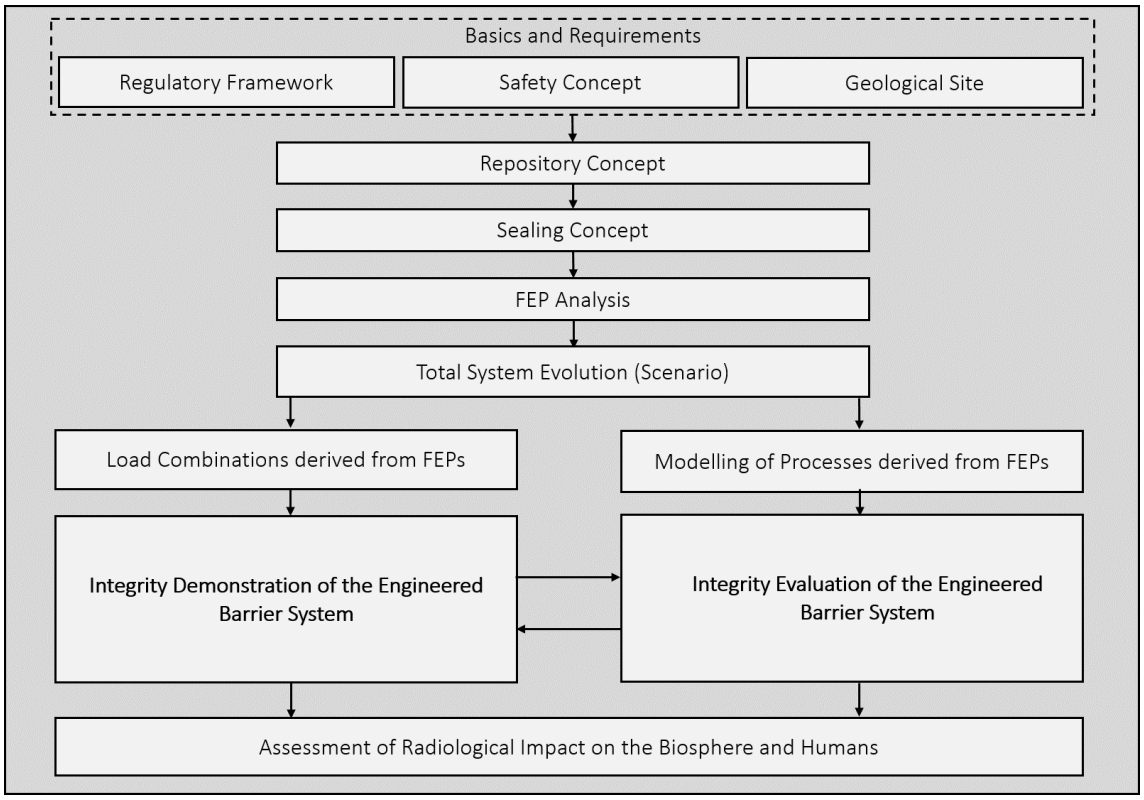

Figure 14.-1: RANGERS methodology diagram for the design, integrity and performance of engineered barrier system in salt repositories.

14.1 Integrity demonstration

The integrity demonstration primarily provides evidence of the preservation of mechanical integrity and hydraulic resistance. Partial safety proofs based on the verification concept developed by Müller-Hoeppe et al. (2012b) are used for this purpose, taking into account the concept of partial safety factors. The partial proofs must be provided for hydraulic permeability, mechanical stability, and long-term stability over the envisaged functional period. The proof of manufacturability is discussed in the SOTA (State of the Art) report of the RANGERS project (Keller et al., 2021a).

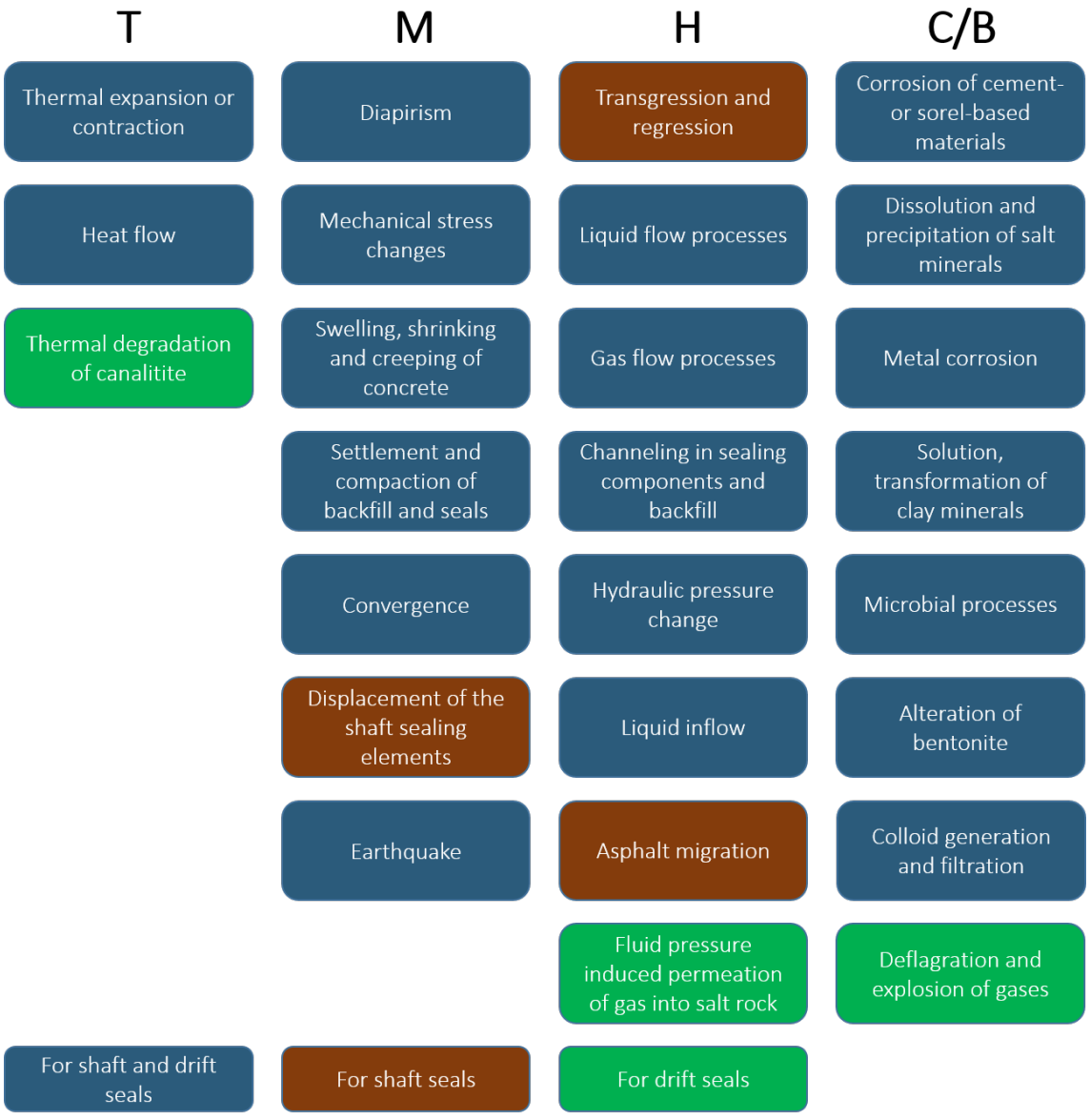

Figure 14.-2: Summary of all initial FEP impacting the EBS established in Table 7.2 and 7.3 of the methodology report (Simo et al., 2024): blue color represents FEP relevant for the shaft and drift sealing system, brown color shows FEP relevant only for shaft sealing system and green color: FEP relevant for drift sealing system.

The integrity demonstration is to be performed for the reference scenario. The reference

scenario is described by the so-called initial barriers, initial Features, Events and Processes (FEP) and FEP that are linked to radionuclide mobilization and transport. The initial barriers are the key components of the EBS. The initial FEP are processes that may directly affect the functionality of the EBS and are therefore relevant for EBS performance assessment. They were described in greater detail in the methodology report (Simo et al., 2024). Figure 14.-2 summarizes all initial FEP that are relevant for the design and performance assessment of the EBS. They are based on expert judgment and therefore not exhaustive.

In the next step, the initial FEP are further evaluated based on their relevance for the partial verification proof that needs to be fulfilled in the course of the integrity demonstration. This assessment can be carry out specifically for each component of the EBS such as the shaft or the drift sealing system. The FEP are combined to check the verification criteria according to the conceptual model presented in Figure 14.-3

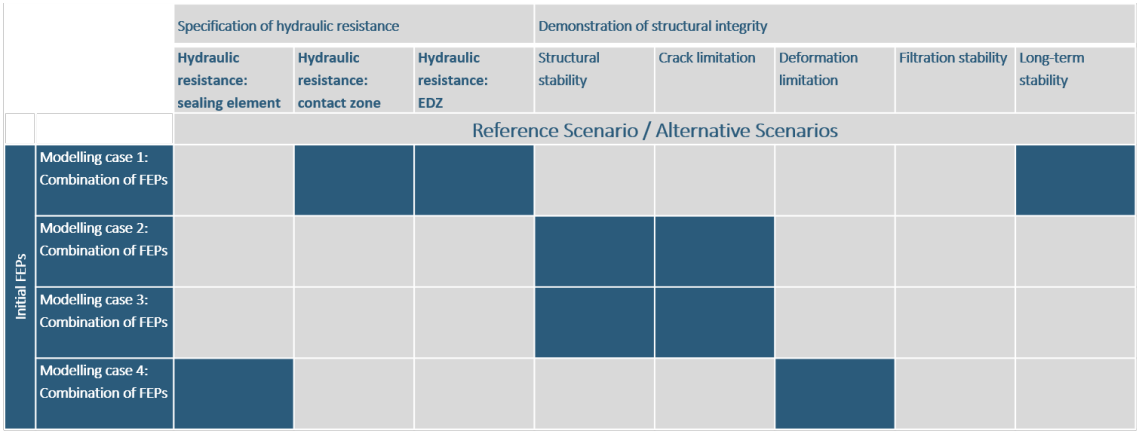

Figure 14.-3: Conceptual definition of modeling cases to check the verification criteria.

For the long-term stability of the EBS, the geochemical conditions in the repository system play an important role in the potential degradation of the construction materials from which the EBS is made. Geochemical changes can be further driven by temperature or temperature may affect the properties of geomaterials and endanger their sealing properties over time. From this, one derives that FEP from the chemical and thermal process classes are relevant for the assessment of the long-term stability proof. Therefore, thermal and geochemical analyses are needed to carry out the proof. The FEP used for this analyses are highlighted in Figure 14.-4

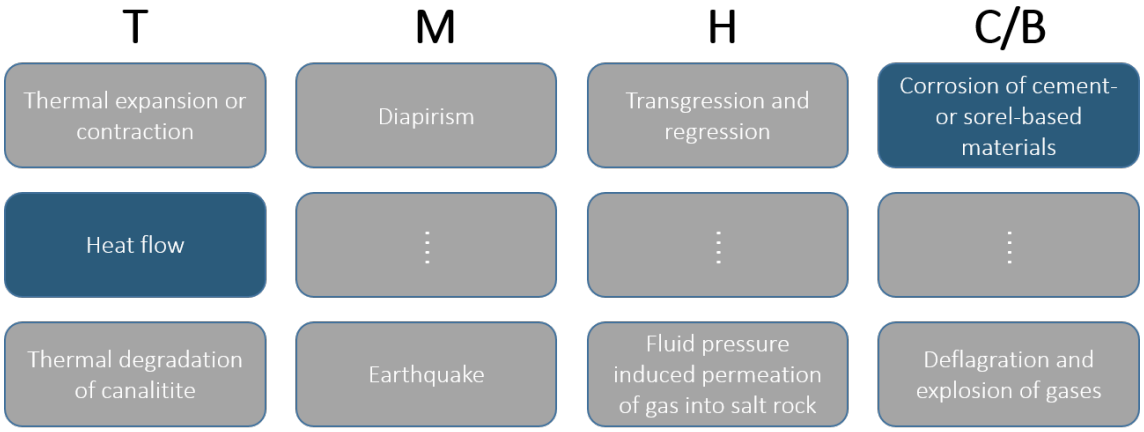

Figure 14.-4: Initial FEP of relevance for the long-term stability proof. FEPs deemed irrelevant are excluded from this figure.

As for the mechanical integrity proof, a differentiation is to be made between the components of the EBS as different loads can be relevant for some components but can be neglected for other components. In general, all FEP leading to mechanical impacts should be considered in this step. The FEP identified for the verification proof are highlighted in Figure 14.-5. Those FEP cover the thermal, mechanical, and hydraulic processes.

The chemical FEP can be excluded from the integrity proof because those FEP lead typically to a degradation of the materials. These chemical degradation processes are already considered in the long-term stability proof. For the case where the effect of the chemical FEP cannot be quantitatively predicted, as it is the case in ice age conditions, the assessment of the EBS performance resulting from the chemical damage is investigated in the integrity evaluation.

Although the processes of swelling, shrinking or creeping might be driven by chemical processes at a microscale, their impact on the barrier are mechanical and thus does not technically belong to the chemical process.

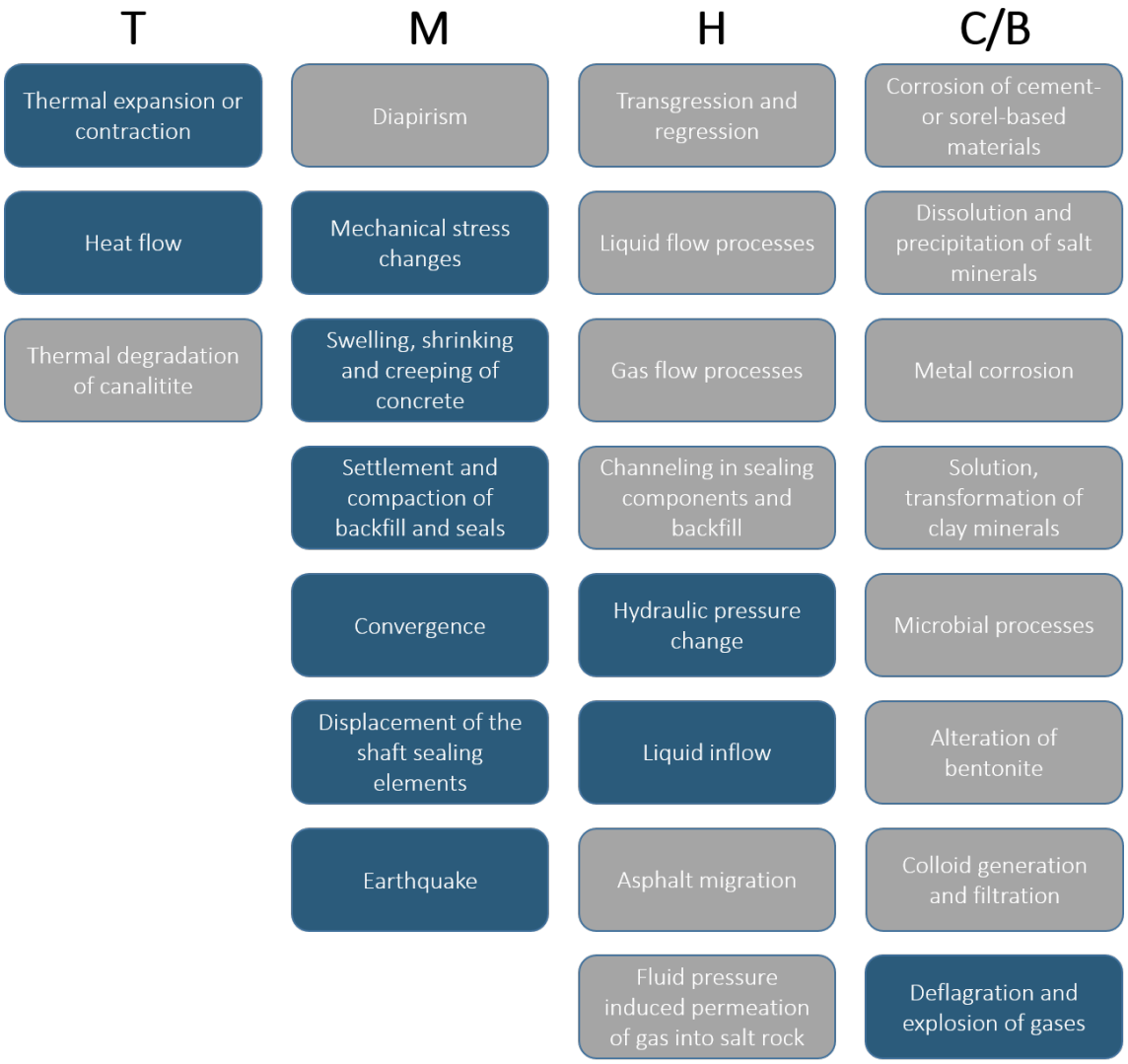

Figure 14.-5: Initial FEP of relevance for the mechanical integrity proof.

The hydraulic resistance will be analyzed by FEP of the hydraulic process class. Those FEP are important to describe the hydraulic evolution of the repository system and thus the performance of the EBS upon hydraulic flow. They are highlighted in Figure 14.-6

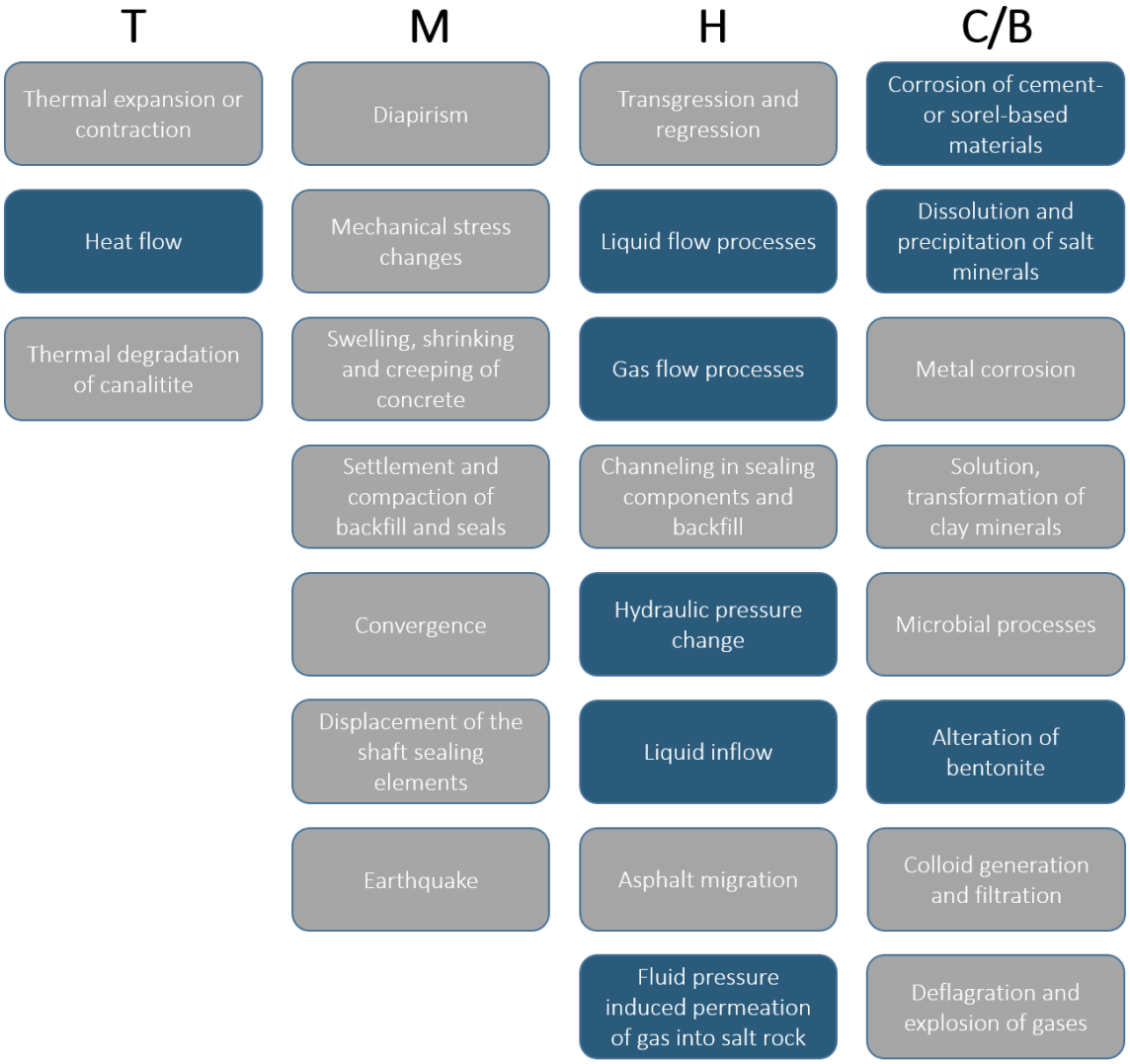

Figure 14.-6: Initial FEP of relevance for the hydraulic resistance proof.

From the initial FEP, some FEP remained unused or are not considered in the different partial verification proofs elaborated above. This is because those FEP cannot be assessed numerically or are not yet well understood to be conceptualized in numerical applications (for instance: microbial processes, alteration of bentonite or colloidal generation and filtration, asphalt migration). They could also be not relevant for the specific assessment of the EBS (e.g., thermal degradation of carnallite if there is no potash layer at geological site or transgression and regression if the repository system is not located in coastal region). For such FEP, a verbal argumentative approach is adequate based on experimental evidence. They require further research effort for a quantitative assessment and can be added later in the numerically based assessment as soon as new scientific findings are available.

14.2 Integrity evaluation

The integrity evaluation assesses the state on the system for alternative scenarios. The alternative scenarios relevant for the EBS have been identified and characterized in the methodology report. Those scenarios consider unfavorable characteristics of initial FEP resulting in an impairment or failure of an EBS. Therefore the detrimental impact of those processes and the consequences on the repository system development will be analyzed in two alternative scenarios which are the failure of a shaft seal, and the failure of a drift seal. This means from the modeling point of view that the conceptual models used in the assessment of the integrity demonstration need to be modified by considering a shaft or a drift seal failure. For the integrity evaluation, hydraulic analyses are predominantly required. This is because the alternative scenarios assume that mechanical integrity is no longer present. The assessment of the overall system in such situations is the objective of the integrity evaluation. Mechanical modeling case can also derive from the alternative scenarios. The most prominent of them is the additional hydraulic load acting on the drift seal when a failure of the shaft seal is assumed. This has to be evaluated numerically.

In this report, we present some exemplary analyses for integrity evaluation in chapter 21. and chapter 22..

14.3 Summary

In summary, starting with the repository system and the description of the near-field of the EBS, a specific FEP list for the EBS was developed in the methodology part of RANGERS. From this study, the initial FEP have been identified. The relevant alternative scenarios for the EBS have been also developed. By this procedure, a stringent derivation strategy of modeling cases from this FEP and scenarios was finally achieved. The abstraction of FEP into modeling scenarios requires the formulation of mathematical models that accurately capture the underlying mechanisms of these FEP. In the context of numerical assessments, these mathematical representations are further refined into computational models. Subsequently, these models are solved within a numerical framework that embodies either the entire repository system or a subsection of it. Adhering to the guidelines proposed in the methodology report, it is imperative to employ a comprehensive and realistic integrated model that encompasses the majority of the EBS components. This approach is crucial for accounting for the interaction between the FEP in the analysis. Fortunately, advancements in computational methods over the past decades have significantly enhanced the capabilities of numerical simulators. These programs can now simulate increasingly intricate processes and manage larger domains, thereby transforming the recommendations into feasible practices.

To illustrate the methodology and the modeling concept, Various modeling assessments were carried out in the scope of RANGERS. These modeling activities covers a great majority of FEP and aim at fulfilling all the criteria included in the verification concept. The modeling work is divided between the partners Sandia and BGE TECHNOLOGY using their expertise in a synergistic manner to deepen the feasibility of performance assessment in salt repositories. The numerical activities are summarized for the integrity demonstration and the integrity evaluation in Figure 14.-7 and Figure 14.-8

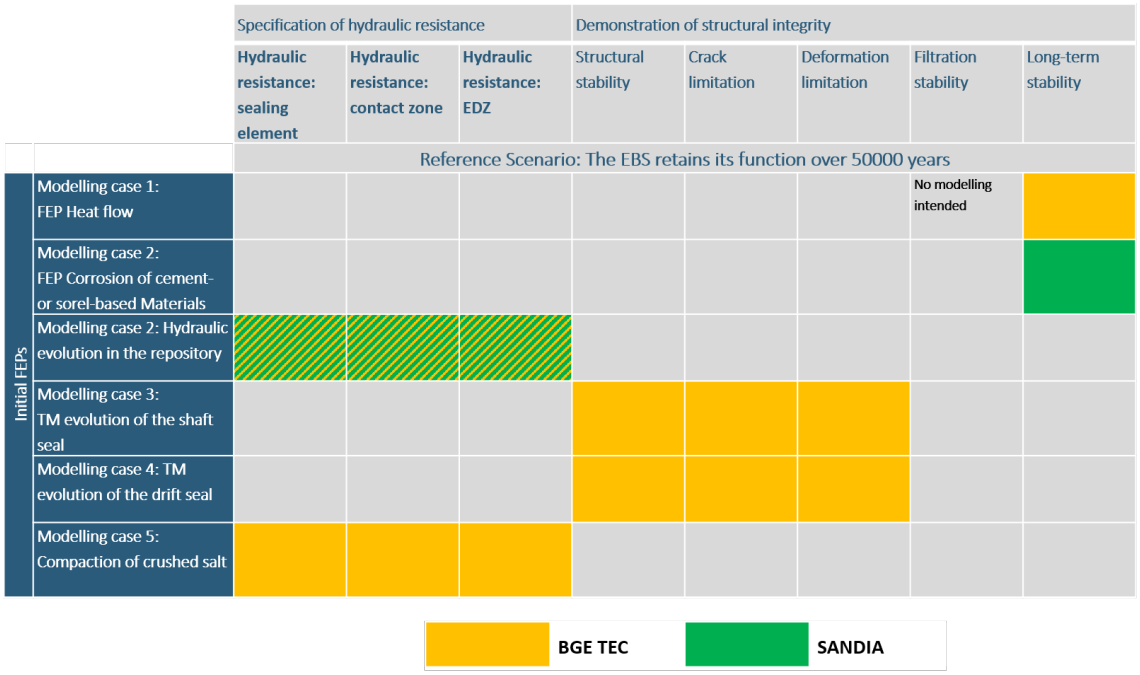

Figure 14.-7: Numerical modeling to assess the integrity demonstration.

Figure 14.-8: Numerical modeling to assess the integrity evaluation.

15. Model and Workflow Development

15.1 Developments in PFLOTRAN for performance assessment of salt repositories

Motivated by application to the RANGERS project, Sandia has undertaken a series of significant initiatives aimed at enhancing the modeling capabilities for salt repositories using PFLOTRAN – an open-source massively parallel reactive flow and transport simulator, the project homepage is given at `https://pflotran.org/`. These advancements improve the applicability of high-performance parallel flow and transport simulations, with a particular focus on incorporating Thermal, two-phase Hydrological, and Chemical (TH^2C) processes in a salt repository. Using these enhancements, we are now beginning to be equipped to simulate the majority of the FEPs linked to radionuclide mobilization and transport in a salt repository in an integrated manner, increasing reliability in our models and removing many practical simplifications previously needed to simulate these conditions. This integrated approach not only enhances the accuracy of our simulations but also provides a better understanding of the complex interactions within salt repositories, thereby contributing significantly to our ability to predict and manage their behavior over time. The different developments will be described in this section. A benchmark exercise that was carried out to verify the developments will be also described in this section. Modeling applications are shown using these new developments.

15.1.1 Salinity-dependent PFLOTRAN equations of state

The dissolution of salt (halite or sodium chloride) can significantly change the solution density, enthalpy, viscosity, and saturation pressure. In a multi-phase system, these changes become particularly important in reaching an accurate solution that includes boiling and condensation of water. Of primary importance is the solubility of salt in water. PFLOTRAN now has implemented several equations of state, including the formulation described by Sparrow (2003) to find the temperature-dependent solubility (Nole et al., 2022).

The solubility, X_{sat} in terms of mass fraction, is expressed as a function of temperature, T(℃):

$$X_{\text{sat}} = 0.2628 + 6.275 \times 10^{-6} T + 1.084 \times 10^{-6} T^2 \tag{1}$$

The mass fraction used in the Sparrow equations of state can be related to molality by:

$$X = \frac{mM_{\text{NaCl}}}{1000 + mM_{\text{NaCl}}} \tag{2}$$

where X is the mass fraction of salt, m is the molality of the solution (mol NaCl/kg H_2O) and M_{NaCl} is the molar mass of NaCl (58.443 g/mol).

The density of brine is a function of temperature, pressure, and salt concentration. Two options for density computation are available: Sparrow (2003), and Batzle and Wang (1992).

The Sparrow equation for brine density, ρ_b^{SP} (kg/m^3), is a function of salt concentration, X (mass fraction) and temperature, T (℃):

$$\rho_b^{SP} = A + BT + CT^2 + DT^3 + ET^4 \tag{3}$$

where:

$$A = (1.001 + 0.7666X - 0.0149X^2 + 0.2663X^3 + 0.8845X^4) \times 10^3$$
$$B = 0.0214 - 3.496X + 10.02X^2 - 6.563X^3 - 31.37X^4$$
$$C = (-5.263 + 39.87X - 176.22X^2 + 363.53X^3 - 7.784X^4) \times 10^{-3}$$
$$D = (15.42 - 167X + 980.7X^2 - 2573X^3 + 876.6X^4) \times 10^{-6}$$
$$E = (-0.0276 + 0.2978X - 0.2017X^2 + 6.3453X^3 - 3.914X^4) \times 10^{-6}$$

The Batzle and Wang formulation first calculates pure water density ρ_w (g/cm^3) as a function of pressure P (MPa), and temperature T (°C):

$$\rho_w = 1 + 1 \times 10^{-6}(-80T - 3.37T^2 + 0.00175T^3 + 489P - 2TP + 0.016T^2P - 1.3 \times 10^{-5}T^3P - 0.333P^2 - 0.002T^2)$$

The Batzle and Wang formulation then uses the pure water density to calculate a brine density ρ_b^{BW} (g/cm^3) as a function of pressure, temperature, and salt concentration, S (ppm / 10^6):

$$\rho_b^{BW} = \rho_w + S(0.668 + 0.44S + 1 \times 10^{-6}(300P - 2400PS + T(80 + 37S - 3300S - 13P + 47SP))) \quad (4)$$

A correction was made to the original Batzle and Wang density subroutine, which incorrectly computed the molar density of water from the mass density, ρ_b^{BW}, without removing the salt component. Molar density is now calculated as follows:

$$\rho_{w,\text{molar}} = \frac{\rho_b^{BW}(1 - S)}{M_{H_2O}} \quad (5)$$

where $\rho_{w,\text{molar}}$ is the molar density of water (kmol/m^3), ρ_b^{BW} is the Batzle and Wang brine density (kg/m^3), S is the salt mass fraction (ppm/$1 \cdot 10^6$), and M_{H_2O} is the molar mass of water (kg/kmol).

Vapor pressure lowering with increased solute concentration is an important consideration of multi-phase flow near the boiling point. Increased concentrations of salt in brine lowers the vapor pressure, increasing the boiling point of the water. PFLOTRAN now has implemented two options for vapor pressure calculation: Sparrow (2003) and Haas Jr. (1976).

The Sparrow formulation calculates vapor pressure, P_{vap}^{SP} (MPa) as a function of temperature, T (°C) and dissolved salt concentration, X (mass frac.):

$$P_{vap}^{SP} = A + BT + CT^2 + DT^3 + ET^4 \quad (6)$$

where:

$$A = (0.9083 - 0.569X + 0.1945X^2 - 3.736X^3 + 2.82X^4) \times 10^{-3}$$
$$B = (-0.0669 + 0.0582X - 0.1668X^2 + 0.6761X^3 - 2.091X^4) \times 10^{-3}$$
$$C = (-7.541 - 5.143X + 6.482X^2 - 52.62X^3 + 115.7X^4) \times 10^{-6}$$
$$D = (-0.0922 + 0.0649X - 0.1313X^2 + 0.8024X^3 - 1.986X^4) \times 10^{-6}$$
$$E = (1.237 - 0.753X + 0.1448X^2 - 6.964X^3 + 14.61X^4) \times 10^{-9}$$

The Haas formulation first relates the temperature of the brine, T_b (°C), to the temperature of H_2O liquid, T_0 (°C), at the same pressure, where x is the molality (mol salt/kg solution):

$$\ln(T_0) = m\ln(T_b) + c \tag{7}$$

where:

$$\begin{aligned} m &= (a + bT_b)^{-1} \\ a &= 1.0 + a_1x + a_2x^2 + a_3x^3 \\ b &= b_1x + b_2x^2 + b_3x^3 + b_4x^4 + b_5x^5 \\ c &= 0 \end{aligned}$$

The Haas formulation for vapor pressure, P^{HA} (bar), is then calculated as a function of the H_2O liquid temperature, T_0 (°C):

$$\ln(P^{HA}) = \frac{e_0}{t} + e_1 + \frac{e_2}{w}(10^{w^2} - 1.0) + e_3 10^{y^{1.25}} \tag{8}$$

where:

$$\begin{aligned} w &= z^2 - e_6 \\ y &= 647.27 - T_0 \\ z &= T_0 + 0.01 \end{aligned}$$

The constants used in the Haas vapor pressure equations are presented in Table 15.-1.

Table 15.-1: Constants for vapor pressure calculation by Haas Jr. (1976).

Constant	Value
a_1	5.93582×10^{-6}
a_2	-5.19386×10^{-5}
a_3	1.23516×10^{-5}
b_1	1.15420×10^{-6}
b_2	1.41254×10^{-7}
b_3	-1.92476×10^{-8}
b_4	-1.70717×10^{-9}
b_5	1.05390×10^{-10}
e_0	12.50849
e_1	-4.616913×10^{3}
e_2	3.193455×10^{-4}
e_3	1.1965×10^{-11}
e_4	-1.013137×10^{-2}
e_5	-5.7148×10^{-3}
e_6	2.9370×10^{5}

Liquid enthalpy is also a function of salt concentration. Here, we use the formulation of Sparrow (2003), where h is specific enthalpy (kJ/kg), T is temperature (°C), and X is mass fraction of dissolved salt in water (kg salt/kg solution),

$$h = A + BT + CT^2 + DT^3 + ET^4 \tag{9}$$

where:

$$\begin{aligned}
\mathrm{A} &= (0.0005 + 0.0378\mathrm{X} - 0.3682\mathrm{X}^2 - 0.6529\mathrm{X}^3 + 2.89\mathrm{X}^4) \times 10^3 \\
\mathrm{B} &= 4.145 - 4.973\mathrm{X} + 4.482\mathrm{X}^2 + 18.31\mathrm{X}^3 - 46.41\mathrm{X}^4 \\
\mathrm{C} &= 0.0007 - 0.0059\mathrm{X} + 0.0854\mathrm{X}^2 - 0.4951\mathrm{X}^3 + 0.8255\mathrm{X}^4 \\
\mathrm{D} &= (-0.0048 + 0.0639\mathrm{X} - 0.714\mathrm{X}^2 + 3.273\mathrm{X}^3 - 4.85\mathrm{X}^4) \times 10^{-3} \\
\mathrm{E} &= (0.0202 - 0.2432\mathrm{X} + 2.054\mathrm{X}^2 - 8.211\mathrm{X}^3 + 11.43\mathrm{X}^4) \times 10^{-6}.
\end{aligned}$$

15.1.2 Fully-coupled solute mass balance in PFLOTRAN

For flow of fresh water in aquifers, aqueous chemical species are typically dilute enough (i.e., low enough concentrations) to not significantly affect the properties of the water solvent, including its density and viscosity. This simplification forms the basis for decoupling fluid flow and reactive transport, as is typically done in PFLOTRAN or most other environmental flow and transport simulators. When the solute transport primary solution variables do not significantly impact the flow primary solution variables, then sequentially solving the flow and transport solutions can oftentimes be more efficient and sufficiently accurate.

An exception to this is the case of a brine flow system through a halite porous or fractured medium. If the pore water contains salt (as exemplified by pore water contained in a salt host rock where the rock itself can dissolve into the water), salt dissolves rapidly in high enough concentrations to meaningfully affect the density, viscosity, and saturation pressure of the pore water. It is therefore very important to consider this feedback between the solute and the liquid flow properties. Until now, modeling salinity effects on flow properties required modeling salinity development and migration as part of the transport equations and then handing off updated density and viscosity to the flow solution under the standard sequential flow and transport coupling scheme. This approach uses the brine properties from the previous timestep in each flow time step. Since these two systems are much more tightly coupled when salt comprises the porous medium and is a solute, sequential coupling in this manner requires taking very small time steps in order to avoid numerical artifacts. The developments described in this section for fully coupling a solute in PFLOTRAN's general mode (i.e., two-phase flow with energy), and are new capabilities to PFLOTRAN (Nole et al., 2022, 2023).

These additions are made to PFLOTRAN's general (two-component, multi-phase air/water flow) mode to accommodate solute transport as a third component either dissolved in the liquid phase or as a solid precipitate. GENERAL mode, in its prior formulation, implicitly solves two component mass balance equations for gas and liquid:

$$\frac{\partial}{\partial t}(\phi s_l \rho_l X^l + \phi s_g \rho_g X^g) + \nabla \cdot (\phi \alpha_l \rho_l q X^l + \phi \alpha_g \rho_g q X^g) - \phi s_l D_l \nabla X^l - \phi s_g D_g \nabla X^g = Q_l \tag{10}$$

and an energy balance equation:

$$\sum_{\alpha=l,g}\left(\frac{\partial}{\partial t}(\phi s_\alpha u_\alpha) + \nabla\cdot(q_\alpha H_\alpha)\right) + \frac{\partial}{\partial t}((1-\phi)\rho_r c_r T) - \nabla\cdot(k\nabla T) = Q \tag{11}$$

for components i = water, air and phases α = liquid, gas. See the PFLOTRAN documentation (`https://www.pflotran.org/documentation/`) for more detailed description of the variables and constitutive laws.

The newly implemented, fully implicit solute transport mode includes an additional solute component mass balance equation:

$$\frac{\partial}{\partial t}(\phi s_l \rho_l X^{l,s} + \phi s_p \rho_s X^s) + \nabla\cdot(\phi\alpha_l\rho_l q X^{l,s} - \phi s_l D_l \nabla X^{l,s}) = Q_{solute} \tag{12}$$

In this new formulation, the vapor pressure of the solute is assumed negligible, and therefore it is only present in the liquid phase. The solute can also form a solid precipitate phase (α = s), which is immobile in the pore space. Diffusion through the solid phase is considered negligible on the timescales used in our simulations and is therefore not present in this mass balance equation.

Primary variable switching is used to track phase transitions. The phase states used depend on whether the rock matrix is comprised of a soluble or insoluble material. For example, a quartz sandstone rock matrix is largely insoluble in water, therefore the possible phase states are any combination of liquid, gas, and solid precipitate. In halite rock matrix, on the other hand, readily dissolves in water, which changes the porosity of the rock matrix (Table 15.-2). The concentration of salt in the pore water is held at solubility and as salt comes out of solution, or the rock matrix dissolves, the porosity changes.

Table 15.-2: Phase states and primary variables for soluble rock matrix.

State	Primary variables
Liquid	P, X_{air}, X_S, T
Gas	P_g, P_{air}, T
Liquid/Gas	P_g, X_{air}, X_S, T
Liquid/Precipitate	P, X_{air}, X_S, T
Gas/Precipitate	P_g, P_{air}, X_S, T
Liquid/Gas/Precipitate	P_g, S_S, S_S, T
Precipitate	P_g, T^*

15.1.3 Thermal Characteristic Curves

Recent developments in PFLOTRAN have focused on implementing temperature-dependent thermal conductivity by way of thermal characteristic curves (TCCs), (Mariner et al., 2020). TCCs express thermal conductivity as a function of temperature for a given material. In the input files, this description resembles the way “characteristic curves” are implemented. A prototype of this capability was created to allow more physically realistic heat conduction modeling in salt, affiliated with the RANGERS Project and the Brine Availability Test in Salt (BATS) heater test at the Waste Isolation Pilot Plant (Kuhlman et al., 2020).

Salt is well known to have thermal conductivity that decreases with increasing temperature (e.g., see lab test data in Kuhlman et al. (2020)). The prototype capability developed for Salt R&D was expanded in scope and is now widely used in PFLOTRAN for other applications. Thermal conductivity of a salt host rock, for instance, is understood to be heavily influenced by temperature in the relevant thermal regime for repository applications (Gilliam and Morgan 1987; Vosen and Schellschmidt 2003).

The previous implementation of thermal conductivity (k_r) for use with PFLOTRAN non-isothermal flow models involved using wet (k_{wet}) and dry (k_{dry}) thermal conductivity values in a function with saturation (S) from Somerton et al. (1974). In the context of the current version, this equation is still used as the default (D) for effective thermal conductivity.

$$k_T(S) = k_{\text{dry}} + \sqrt{S}(k_{\text{wet}} - k_{\text{dry}}) \tag{13}$$

A linear resistivity thermal conductivity model, where thermal conductivity is also a function of temperature. This model assumes that the reciprocal of thermal conductivity can be modeled as a linear function with temperature. This form was suggested by Birch and Clark (1940) and fitted empirically by Blesch et al. (1983) for granite, basalt, shale, and salt. The latter study was a far-field thermal analysis of a repository that intended to evaluate environmental impact based on temperature changes in various regions. In the linear resistivity function, a is the resistivity shift parameter and a_2 is the scaling factor with the change in temperature. The temperature change is defined with respect to a reference temperature (T_{ref}), such that when $T = T_{ref}$, k_{dry} and k_{wet} are assumed to be evaluated at 0 °C as well.

The linear resistivity model is

$$k_T(S, T) = k_T(S)/[a_1 + a_2(T - T_{ref})] \tag{14}$$

where $k_T(S)$ is given by (13) and a_1, a_2 are coefficients, and T_{ref} is a reference temperature.

To model the change in thermal conductivity of the granular salt during compaction, a special form of the linear resistivity TCC was implemented. The expression was developed for reconsolidation of granular salt with air-filled porosity (see Table B.4, see “Saltgrus” of Bollingerfehr et al. (2012)),

$$k_T(S, T, \phi) = k_T(S, T)\left(1 - \frac{\phi}{\phi_{\text{ref}}}\right)^{\xi} + \left(\frac{\phi}{\phi_{\text{ref}}}\right) \cdot (b_1 + b_2 T) \tag{15}$$

where ϕ is porosity, ξ is a porosity exponent, ϕ_{ref} is a reference porosity, b_1 and b_2 are coefficients and $k_T(S, T)$ is given by (14). At $\phi = 0$ this function gives the intact thermal conductivity associated with the linear resistivity model (specified by a_1 and a_2, and proportional to $1/T$). At $\phi = \phi_{ref}$ this function gives the porosity associated with a linear conductivity model (specified by b_1 and b_2 and proportional to T). At porosity values between these two end members, the function linearly interpolates between the two thermal conductivity values.

15.1.4 Implementation of Non-Darcy flow into PFLOTRAN

In low-permeability materials, a threshold gradient can become important (Liu, 2017). This is a permeability-dependent gradient, which must be overcome before any flow can occur. Standard Darcy flow is given by

$$q = K\mathrm{i} \tag{16}$$

where q is the water flux (m/s), K is the hydraulic conductivity (m/s), and $\mathrm{i} = \frac{\mathrm{dh}}{\mathrm{dx}}$ is the hydraulic head (h) gradient (m/m; m of hydraulic head per m of distance). Liu (2014) presented a closed-form non-Darcy expression for water flux in very tight rocks in terms of a threshold gradient, $\mathfrak{I}$ (m/m), as

$$q = K\left[\mathrm{i} - \mathfrak{I}\left(1 - e^{-\mathrm{i}/\mathfrak{I}}\right)\right]. \tag{17}$$

Through a regression, Liu (2014) found the threshold gradient could be expressed in terms of the intrinsic permeability

$$\mathfrak{I} = Ak^B \tag{18}$$

where A = 4.0×10^{-12} and B = -0.78 are based on a fit to data from Liu et al. (2012).

15.2 Code Verification for performance assessment

15.2.1 Motivation

The presence of the gas phase in the repository under consideration of small amount of humidity in the host rock requires the consideration of two-phase-flow in the performance assessment of the salt repository system. Until now, the numerical investigations of two-phase flow in the repository in salt have been carried out at Sandia within a special flow mode especially developed for WIPP. Historically, WIPP was licensed with a two-phase flow simulator (BRAGFLO) for the repository that utilized a simplified flared 2D-mesh representation of the repository (DOE, 2019). WIPP uses two-phase immiscible flow under isothermal conditions. Because a 3D representation of the repository and the consideration of the heat propagation from waste (non-isothermal) are required for state of the art and performance assessments for heat-generating waste, PFLOTRAN was further developed in order to perform the assessment of a salt repository under two-phase flow assumption with energy transport.

To ensure the advancements made within PFLOTRAN are robust and to establish its capability for conducting non-isothermal multiphase simulations, it is imperative to conduct a comprehensive testing phase before advancing to performance assessment. For this purpose, one of the modeling test scenarios designed in the BenVaSim project was selected for evaluation in the RANGERS program. The BenVaSim project's objective (Lux et al., 2021) was to provide a benchmark for various THM coupled simulators using well-defined, simplified modeling tasks that target fundamental processes, particularly flow phenomena in porous media. The upcoming study is driven by the need to compare PFLOTRAN's performance with that of other simulators, especially since PFLOTRAN was not included in the original array of codes validated by BenVaSim.

15.2.2 Methodology

The test under consideration involves assessing the hydraulic response within an EBS seal under two-phase flow conditions with specific boundary constraints. The addition of a gas fluid phase introduces more realistic conditions, considering the interplay between gas and liquid phases within the repository. The disposal drifts are air filled at the time of repository closure. Following the disposal of radioactive waste, chemical reactions may occur within the repository environment, such as interactions between the metal of the waste container and the humidity of the host rock, potentially leading to gas generation. The emergence of additional gas can create pressure build-up, influencing the system's behavior and potentially inducing fracturing in the host rock.

The benchmark problem is depicted in Figure 15.-1, showcasing a model geometry of 10 m in length and 1 m in height, focusing exclusively on horizontal process dynamics. Boundary conditions are indicated by arrows, with dark blue representing liquid and light blue indicating gas boundary conditions, while black denotes mechanical effects (Czaikowski and Friedenberg, 2020).

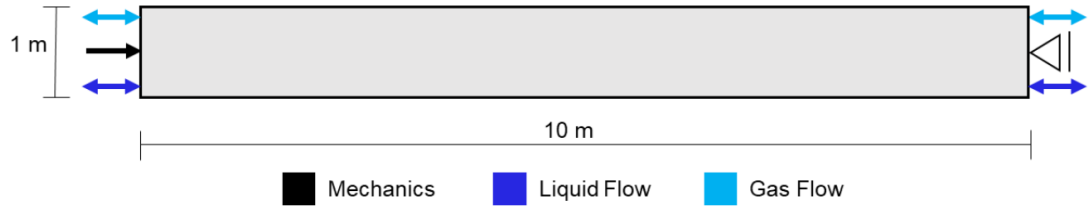

Figure 15.-1: Model geometry and considered processes (Czaikowski and Friedenberg, 2020).

The original BenVaSim problem also incorporated mechanical effects that cannot be computed in PFLOTRAN. In the selected benchmark, the mechanical process class is decoupled from the hydraulic processes. Thus, the base scenario as specified in BenVaSim was carried out in PFLOTRAN without mechanical effect and the results were compared with simulation results with OpenGeoSys (OGS) and against those obtained by GRS in the BenVaSim project, both considering mechanical effects.

15.2.3 Benchmark results

The benchmark scenario selected in this study shows a two-phase flow within a model representing partial saturation and with boundaries that allow fluid transfer. Coupling the hydraulic scenario with mechanical stress, the latter is exerted at the model's right edge, as illustrated in Figure 15.-2. Details about material properties, along with initial and boundary conditions, are summarized in Table 15.-3. Throughout the projected simulation duration of 100,000 years, these boundary conditions remain constant. The models do not include the effects of diffusion of dissolved gas in the liquid phase or diffusion of humidity in the gas phase. Initial model conditions are set with a 63% liquid saturation corresponding to a suction pressure of -13.63 MPa, alongside a gas pressure of 0.2 MPa and mechanical stress of 4 MPa. At the model's left boundary, a 50% saturation level is stipulated (resulting in a suction pressure of -16.58 MPa), with a gas pressure of 3 MPa and identical mechanical stress. The model's right

boundary is mechanically fixed, with a constant gas pressure of 0.5 MPa and an anticipated saturation level of 90% (equating to a suction pressure of -4.89 MPa).

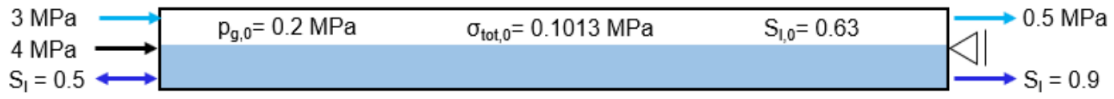

Figure 15.-2: Initial and boundary conditions for the immiscible two-phase flow benchmark Czaikowski and Friedenberg (2020).

Table 15.-3: Material parameters for the base scenario (Czaikowski and Friedenberg, 2020).

Parameter	Value	Unit
Young's modulus	650	[MPa]
Poisson's ratio	0	[-]
Porosity	0.33	[-]
Intrinsic permeability	2.5E-21	[m^2]
Biot coefficient	1	[-]
Liquid viscosity	1.0E-9	[MPa·s]
Liquid bulk modulus	2200	[MPa]
Residual liquid saturation	0.02	[-]
Residual gas saturation	0	[-]
Van Genuchten parameter	0.5	[-]
Van Genuchten pre-factor	11	[MPa]
Pore connectivity parameters	0.5	[-]

Figure 15.-3 shows the results for the gas pressure and saturation evolution problem. The figure shows the comparison of results obtained with OpenGeoSys and PFLOTRAN and those computed with CODE_BRIGHT by GRS taken from Czaikowski and Friedenberg (2020) for different locations along the seal model. A good agreement in the results obtained using the three codes is evidenced in the figure. Results with OpenGeoSys and PFLOTRAN are identical. A small discrepancy to the GRS results for the saturation evolution might be related to a different spatial and time discretization as well as in the difference in the implementation in Code_Bright. Nevertheless, all the results are similar enough to consider this benchmark conclusive.

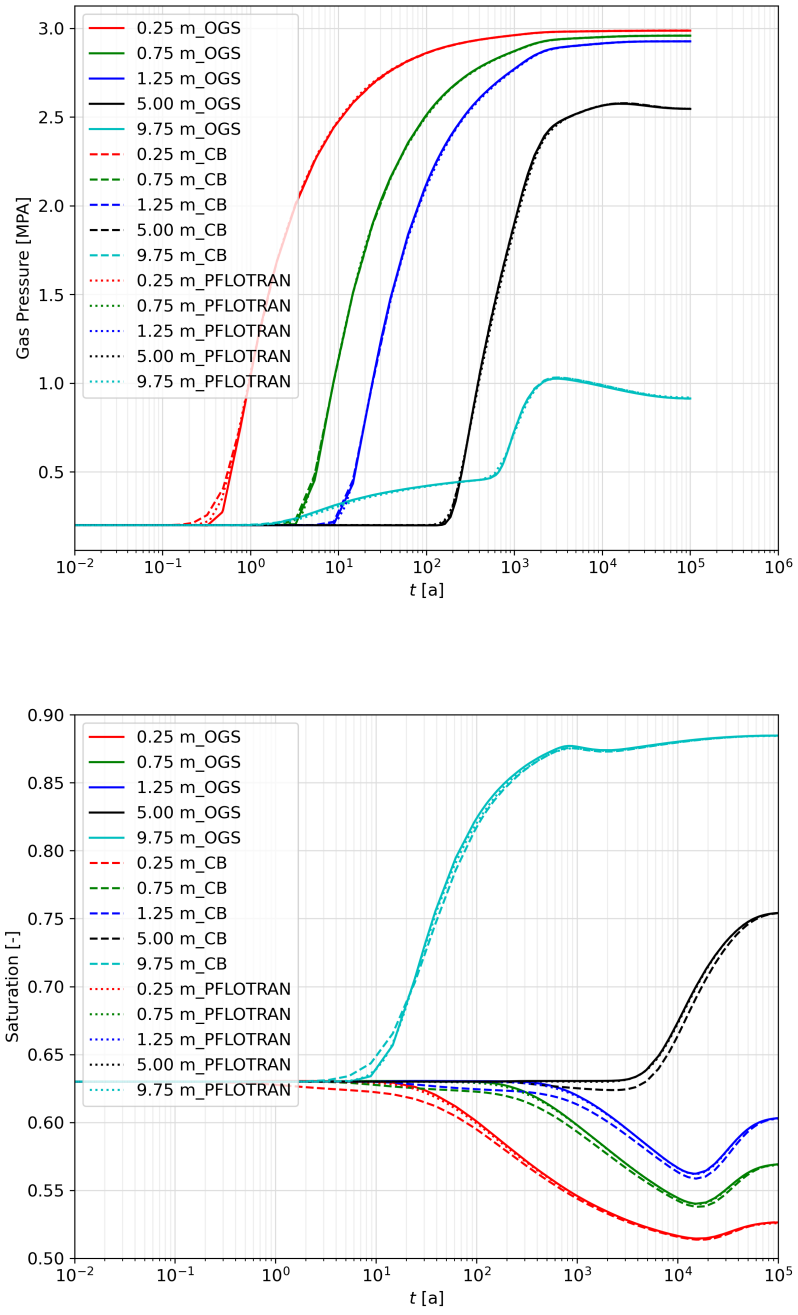

Figure 15.-3: Comparison between OpenGeoSys and PFLOTRAN results (this study) and CODE_BRIGHT results from Czaikowski and Friedenberg (2020).

16. Temperature Evolution in the EBS

High temperature can affect the long-term performance of the EBS materials. As part of the assessment of the long-term stability of the geomaterials used in the EBS, the temperature evolution in the repository is evaluated. The aim of the simulation is to estimate the temperature increase in the EBS over the course of the repository. Based on this, the effect of temperature increase on the materials from which the EBS are made can be evaluated. The present analysis serves also as input for further simulations aiming at verifying other aspect of the design and performance assessment of the EBS. This is for instance the case for the thermomechanical integrity analyses for the shaft and drift seals and the TH²C performance assessment. The results of the analysis also serve as input in the geochemical assessment as it is well known that temperature increases the rate of chemical reactions.

16.1 Repository system

The generic repository system developed in the context of the RANGERS project is based on the generic geological model developed in the KOSINA project (Bollingerfehr et al., 2018) prior to RANGERS. The generic geological model of the salt pillow from the KOSINA project is located on the southern crest of the North German Basin. This geological model consists of twelve homogenized geological layers. Homogenized because those layers were combined from smaller layers with similar properties. The thicknesses of the cover rock consisting of lithostratigraphic units Quaternary (Q), Tertiary (T), and Bunter Sandstone (S) vary in thickness across the model area from approximately 800 m to 140 m. The evaporitic host rock consists of Stassfurt (K2), Leine (NA3), Aller (NA4), and Ohre formations and reach a thickness of more than 800 m in the center of the salt pillow. No modeling was undertaken of possible cap rocks at the top of the salt. The model does not incorporate fault tectonics or salinar tectonics. The fault characteristics of the below-salt horizons, as well as the fragmentation of the main anhydrite into blocks, are not part of the reference profile and thus not included in the 3D model based on the profile.

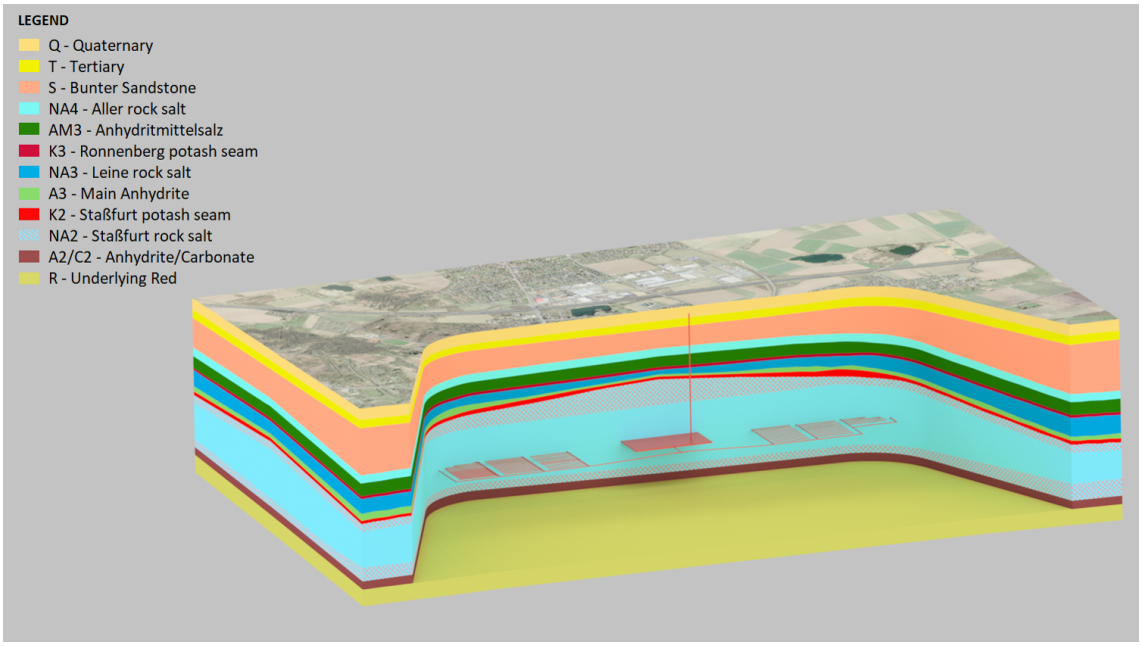

Figure 16.-1: Generic repository system for RANGERS (with courtesy of BGR (Völkner et al., 2017a)).

The repository mine is strategically situated at the core of the salt pillow, where the salt layer attains its maximum thickness, ensuring optimal geological stability and integrity. A minimum safety distance of 200 m to the overburden or at least 750 m to the surface were respected. Figure 16.-1 shows a stylized 3D representation of the repository system comprising the generic salt pillow and the repository.

The repository design considers the disposal of self-shielded casks in horizontal emplacement drifts which are later backfilled with crushed rock salt. The repository mine is composed of two main emplacement wings that have a width of 800 m and a central infrastructure area that hosts two shafts. Each wing hosts three emplacement fields. The infrastructure area and the emplacement fields are separated by at least 300 m of undisturbed rock salt. Each access drift to the emplacement wings includes 500 m interval for the construction of drift seals. The shafts can be sealed within the thickest part of the salt pillow.

In the southern section, the three emplacement fields are occupied by POLLUX®-10 containers, each housing spent fuel elements from pressurized water reactors (PWR). A similar setup is replicated in half of the northern section. A big part of the northern wing is dedicated to containing reprocessed waste in POLLUX®-9 containers. Additionally, one-third of the final disposal zone is allocated for the disposal of CASTOR® containers, which safely encase waste from prototype and experimental reactors. Complementing these arrangements, two separate drifts have been allocated for the storage of structural components from spent fuel assemblies, encapsulated within MOSAIK-II containers. These are strategically positioned in two disposal fields adjacent to the infrastructure area, see Figure 16.-2. The disposal operational time was assumed to be 30 years in the planning of the repository.

The repository planning assumes a maximum temperature of 200 °C at the surface of the waste casks. To meet this temperature requirement, the repository was first thermally de-

signed to optimize the spacings between the drifts and between the disposal casks within the drifts. The engineered barrier systems of this repository consists of four horizontal closure systems installed in the main drifts near sealing the two emplacement wings and of two shaft closure systems installed in both shafts. Each of these horizontal closures is 600 m long and is divided into two abutments made of magnesia (i.e., Sorel) concrete with a length of 50 m. Between the abutments, the 500 m long backfill seal is made of a mixture of crushed salt and clay, which itself seals after reconsolidation and compaction, taking over the long-term sealing function of the repository. For up to 50,000 years, the Sorel concrete abutments should limit any potential fluid migration within the repository mine and should protect the crushed salt seal against hydromechanical loads. The shaft closure system is made of several materials following the concept of diversity and redundancy. The shaft closure is redundant to the drift closure. The sealing elements made of Sorel concrete, salt clay, and bentonite ensure the diversity and the redundancy of the closure system. If one seal loses its function, other seals made of different material will significantly reduce the chance that the same deficiency occurs in multiple elements.

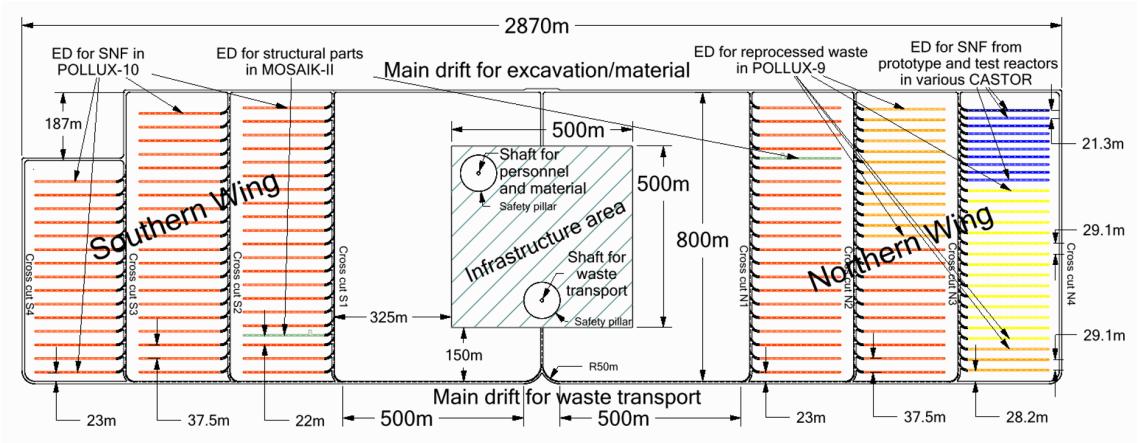

Figure 16.-2: Repository layout and waste stream distribution.

16.2 Waste inventory and thermal power

The POLLUX®-10 containers can be optionally loaded with fuel rods from 10 fuel assemblies of Western design pressurized water reactors (PWR), 30 fuel assemblies of Western design boiling water reactors (BWR) or 25 fuel assemblies from Russian design pressurized water reactors (WWER). The different container loadings are because the fuel rods from BWR fuel assemblies are two-thirds shorter than those from PWRs, allowing for triple loading in a container. The WWER fuel rods are thinner than their Western counterparts, which allows for a two-and-a-half times loading capacity.

In Western-designed PWR and BWR reactors, uranium oxide (UO_2) and mixed oxide (MOX) fuel elements included both Uranium-235 and Plutonium. Only UO_2 fuels were used in Russian-designed reactors. The decay heat of these fuels was adopted according to the burn-up calculations described in Bollingerfehr et al. (2013). These burn-up calculations apply to each characteristic decay heat per waste type without considering the burn-up and enrichment of the fuel elements.

For the storage of MOX fuel elements, which have a high heat production compared to UO_2 fuel elements, a container loading was developed that predominantly consists of fuel rods

from PWR fuel assemblies and to a lesser extent from MOX fuel assemblies (Amelung et al., 2005). The ratio used in Bollingerfehr et al. (2013) in the container loading of 89% UO_2 content and 11% MOX content corresponds to the mixing ratio that results from the ratio of the total quantities of PWR-UO_2 fuel assemblies and PWR-MOX fuel assemblies. Figure 16.-3 shows the thermal power of the individual fuel element types in a loading equivalent to loading with PWR fuel elements. The mixed loading with 89% UO_2 and 11% MOX conservatively covers the heat release of the UO_2 fuel elements from BWR and WWER reactors. The thermal power for pure loadings from MOX fuel elements can also be seen in the figure. Containers with such loading are difficult to implement while maintaining the temperature criterion of 200 °C.

The reprocessed wastes are stored in POLLUX®-9 containers. Such a container can be loaded with nine high-level waste (HLW) casks. The thermal power of a reprocessed cask is also shown in Figure 16.-3. It displays a different burn-up behavior compared to the fuel elements. The thermal power of such wastes initially remains at the level of the UO_2 fuel elements and then declines more significantly after 50 years post-reprocessing.

In the thermal calculations, the temporal development of the heat output for the various waste categories shown in Figure 16.-3 is simplified via a reduced thermal nuclide spectrum. This spectrum includes four key nuclides, with parameter values provided in Table 16.-1.

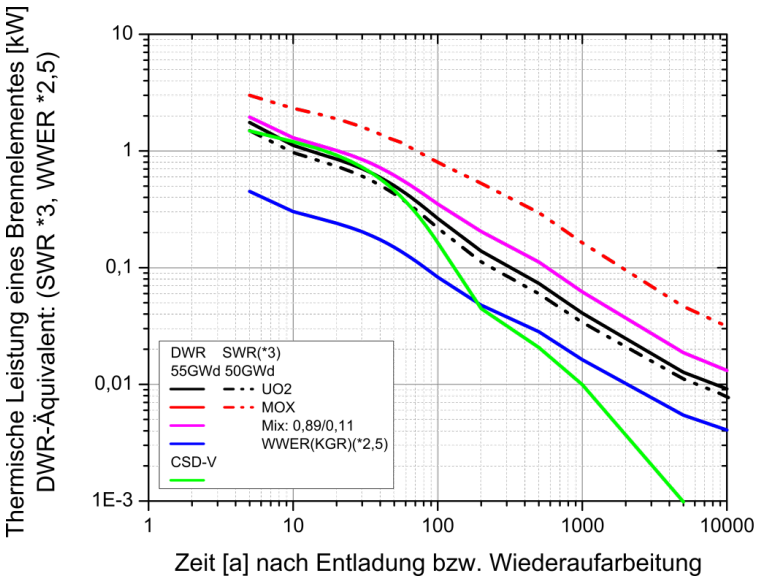

Figure 16.-3: Thermal output of a fuel element over time, loading equivalent to a PWR fuel element, as well as the thermal output of a CSD-V (Bollingerfehr et al., 2013).

Table 16.-1: Key nuclides of spent fuel elements and reprocessed radioactive waste.

	PWR-Mix 89/11	**CSD-V**	**VVER**
Nuclide 1:			
Power p [kW]	1.156	1.480	$1.126 \cdot 10^{1}$
Half-life $t_{1/2}$ [y]	$3.220 \cdot 10^{1}$	$2.799 \cdot 10^{1}$	$3.242 \cdot 10^{1}$
Nuclide 2:			
Power p [kW]	$2.267 \cdot 10^{1}$	$4.468 \cdot 10^{2}$	$2.034 \cdot 10^{2}$
Half-life $t_{1/2}$ [y]	$3.968 \cdot 10^{2}$	$4.172 \cdot 10^{2}$	$4.306 \cdot 10^{2}$
Nuclide 3:			
Power p [kW]	$2.151 \cdot 10^{2}$	$9.507 \cdot 10^{4}$	$2.402 \cdot 10^{3}$
Half-life $t_{1/2}$ [y]	$1.367 \cdot 10^{4}$	$9.649 \cdot 10^{3}$	$1.701 \cdot 10^{4}$
Nuclide 4:			
Power p [kW]	$9.466 \cdot 10^{4}$	$1.289 \cdot 10^{4}$	$8.243 \cdot 10^{5}$
Half-life $t_{1/2}$ [y]	$7.593 \cdot 10^{5}$	$2.952 \cdot 10^{4}$	$1.090 \cdot 10^{6}$

According to the final report of the German Commission for the Storage of High-Level Radioactive Waste Materials, the earliest start of storage is assumed to be the year 2050 (Endlagerkommission, 2016). At this point, the interim storage time of the wastes is up to 60 years, depending on the type of waste and the date of origin. With an assumed storage duration of 30 years, the shortest interim storage time for the fuel elements of Western design can be calculated as 57 years. For reprocessed wastes, a conservative interim storage time of 53 years is assumed.

16.3 Numerical model

The temperature evolution within a final repository is primarily determined by the existing geothermal gradient and the heat input from high-level radioactive wastes. The geothermal gradient dictates the naturally prevailing temperature at the storage horizon as a function of depth.

In the disposal drift, the thermal conductivity of the selected backfill material plays a significant role in the peak temperature. In contrast, the thermal conductivity of the host rock is crucial for heat distribution in the far field. The thermal conductivities of the overlying geological layers can also affect the temperature distribution in the far field, especially if they are significantly lower than that of the host rock. In this case, there is a delay in heat transfer to the overlying layers, resulting in a corresponding increase in temperature within the host rock layer.

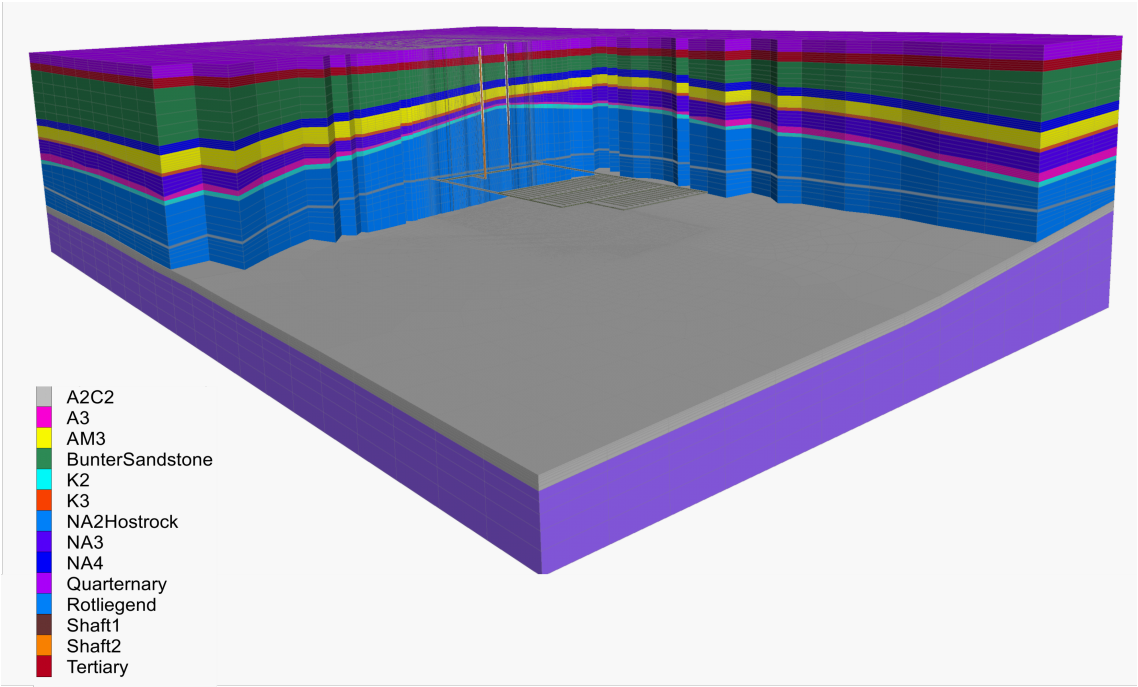

Figure 16.-4: Numerical model for the heat propagation in the entire repository system.

The numerical model developed for the present analysis is aimed at assessing the temperature evolution in the far field. Thus near field effects can be simplified. These effects were already considered in the thermal design of the repository as part of the optimization of the spacings between the drifts and between the casks, see Simo et al. (2024). Therefore, it is not necessary to resolve individual casks in the drifts (i.e. they are not explicitly modeled). Taking into account this simplification, a numerical model with a high fidelity of the drifts and seals in the repository system is realized and depicted in Figure 16.-4. In this model, all drifts were resolved and the geometrical form of each geological layers were respected. The model was parameterized in such a way that the mesh size can be easily change in the three dimensions for mesh convergence studies. The model adopted for the present analysis is about 4000 m wide, 5900 m long and extends up to 3000 m in the depth. It consists of 3.5 million elements.

At the upper boundary of the model, a constant air temperature of 9 °C is assumed. The temperature at the lower model boundary is calculated using the geothermal gradient of 30.0 K per kilometer to be approximately 100.0 °C and is consistently applied along the entire lower boundary of the model. At the lateral model boundaries, adiabatic conditions are assumed. Within the model along the depth, the mentioned geothermal gradient is assumed. Thermally, the disposal of waste is represented by a transient heat source. In the model each disposal drift acts as a heat source. The thermal load has been homogenized in each drift based on the heat power of the radioactive waste disposed in each drift. One refers to the methodology report for more details about the repository planning (Simo et al., 2024).

The thermal parameters used are compiled in Table 16.-2, sourced from Liu et al. (2017).

Table 16.-2: Thermal Properties of Geological Layers (Liu et al., 2017).

Homogeneous zones	**Symbol**	**Thermal conductivity** λ ($W/(m \cdot K)$)	**Specific heat capacity** c_p ($J/(kg \cdot K)$)	**Thermal expansion coefficient** α ($1/K$)
Quaternary	Q	2.3	950	$1.0 \cdot 10^{-5}$
Tertiary	T	2.1	905	$1.0 \cdot 10^{-5}$
Bunter	S	2.6	760	$1.0 \cdot 10^{-5}$
Aller rock salt	NA4	5.2	860	$4.0 \cdot 10^{-5}$
Anhydritmittelsalz	AM3	5.0	860	$3.5 \cdot 10^{-5}$
Potash seam Ronnenberg	K3	1.5	903	$2.5 \cdot 10^{-5}$
Leine rock salt	NA3	5.2	860	$4.0 \cdot 10^{-5}$
Main anhydrite	A3	4.2	860	$1.6 \cdot 10^{-5}$
Potash seam Staßfurt	K2	1.5	903	$2.5 \cdot 10^{-5}$
Staßfurt rock salt	NA2	5.2	860	$4.0 \cdot 10^{-5}$
Anhydrite/carbonate	A2/C2	4.2	860	$1.6 \cdot 10^{-5}$
Underlying red	R	2.7	760	$1.0 \cdot 10^{-5}$

The calculations were carried out using numerical codes FLAC3D (Itasca Consulting Group, Inc., 2021) based on the finite difference method and OpenGeoSys based on the finite element method (Bilke et al., 2025). A benchmark was carried out between the two codes showing nearly identical results for the problem at hand.

16.4 Numerical results

The numerical model for this assessment includes a detailed representation of the whole repository system with a bounding model domain box that has an extent of several km on each side. Due to the homogenization of the thermal load in each drift and reduction in the ability to represent steep temperature gradients between the cask and surrounding material, the maximum temperature in the homogenized drift is about 130 °C compared to 200 °C at the surface of the cask when individual disposal casks are represented in the numerical model. Nevertheless, this discrepancy only occurs in the near field and the developed numerical model is believed to be precise enough for the temperature evolution in the far field.

Figure 16.-5 shows the thermal evolution of the system at 500 years, by which time the repository is reaching its maximum temperature. In the figure, one can see how the heat propagates through the geological formation. This propagation is asymmetric between the two emplacement wings due to the different heat power of the different families of radioactive waste emplaced in the repository at different times.

The subsequent analysis for periods of time over 500 years was performed with OpenGeoSys. Based on the repository concept, it is assumed that an emplacement field is filled every five years starting with the fields in the northern wing (see Figure 16.-2) of the repository mine. The effect of this activation sequence can be seen in figure 16.-6. Figure 16.-6 shows a map view of the temperature evolution at a slice taken through the disposal horizon in the model. The first emplacement field in the northern wing is mostly filled with cold wastes from the prototype and test reactors (subplot at t = 9.1 a). In this field, only three drifts filled with reprocessed waste in POLLUX-9 are heat producing. In the next activated field (subplot at t = 9.1 a) where 13 drifts are filled with reprocessed waste followed by two drifts with PWR spent fuel and the

rest with VVER spent fuels (from top to bottom in subplot at t = 9.1 a), the heat generation in this field follows the thermal power characteristics of the waste as displayed in Figure 16.-3 with higher temperature to be observed in the drifts with PWR spent fuel. Drifts with VVER fuels produce less heat in this field.

The last field in the northern wing as well as all fields in the southern wing are filled with PWR spent fuels. The thermal propagation follows the activation sequence of 5 years between the fields (subplot at t 13.1, 17.1, 21.1 and 25.1 a in Figure 16.-6) with the two drifts that are reserved for the disposal of the structural elements that remains thermally inactive and only are heated from the waste in neighboring drifts.

In the post closure phase, the temperature in the repository increases significantly (Figure 16.-7) reaching a maximum value of about 130 °C in the third field of the northern wing (subplot t = 115.1 a). Almost 500 years after the start of the waste disposal, the repository is now cooling down especially in the northern wing. In the southern wing, where a higher concentration of high heat generating waste packages are disposed, the temperature remain stable at values over 120 °C in the center of the emplacement wing. At 755 years, the temperature decrease in the repository is now remarkable at all point in the repository. The cooling process is more evident at 955 years. At this time the temperature is already below 100 °C. 2055 years after the begin of disposal, the repository system is trending back towards the initial conditions dictated by the geothermal gradient.

Line plots of the temperature evolution along the length of the engineered barriers are shown in Figure 16.-8 and Figure 16.-9. The figures show the temperature profiles along the drifts and the shafts at different times. The results for the seals installed in the material drift and in the waste transport drift are similar Figure 16.-8. This is also the case for the two shaft seals temperature profile Figure 16.-9. In the drift seals, the temperature increase from the sides that are located near the emplacement fields and propagates along the length of the seals. Higher temperature increases are observed in the southern wing compared to the northern wing. There, the maximum temperature increase at the edge of the seal emplacement side is about 20 °C (about 3 to 5 K less in the northern side drift seal). The maximum temperature occurs at approximately 500 years and remains almost stable at the edges (emplacement side) of the seals up to 1000 years later. Near the shafts, the temperature in the seal increases only by 5 K with a maximum observed around 5000 years. At 5000 years the temperature in the drifts is almost homogenised at a value of 5 K higher than the initial conditions. 8000 years later the drift seal further cool down to about 1 to 2 K above initial conditions.

During the simulation, a new steady state is computed based on the different material properties of the different geological layers. This is noticeable by a deviation from the otherwise smooth gradient of temperature with depth. The temperature profiles show an increase of temperature along the shaft over the time up to about 5000 years. The maximum of temperature increase is less than 5 K after 5000 years. At 8000 years, one can observe that the cooling process has begun within the shafts (Figure 16.-9).

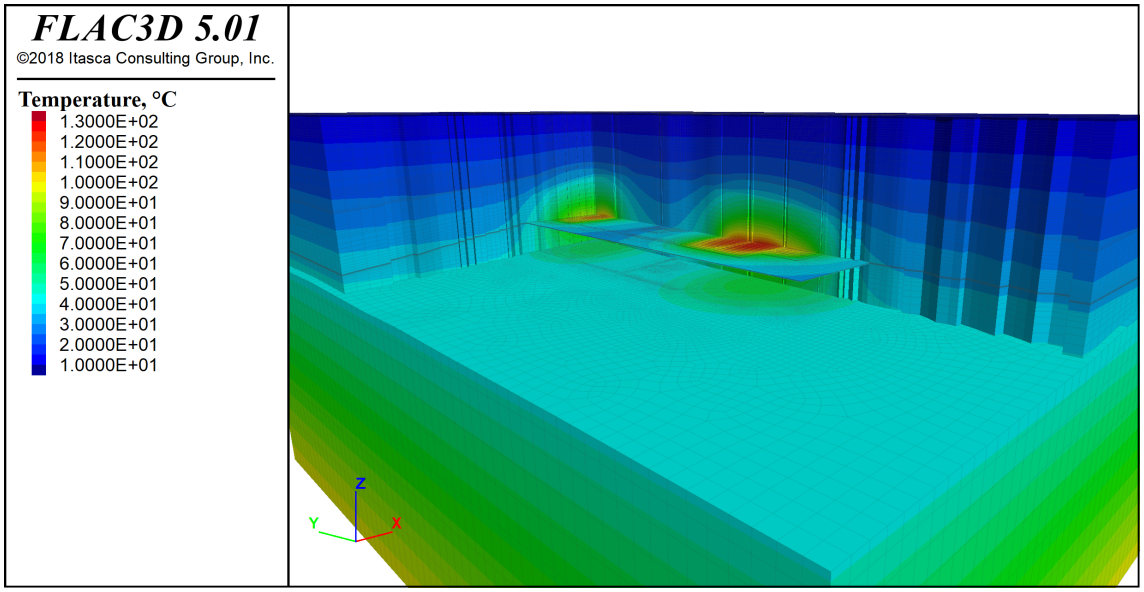

Figure 16.-5: Temperature field in the repository system at 500 years.

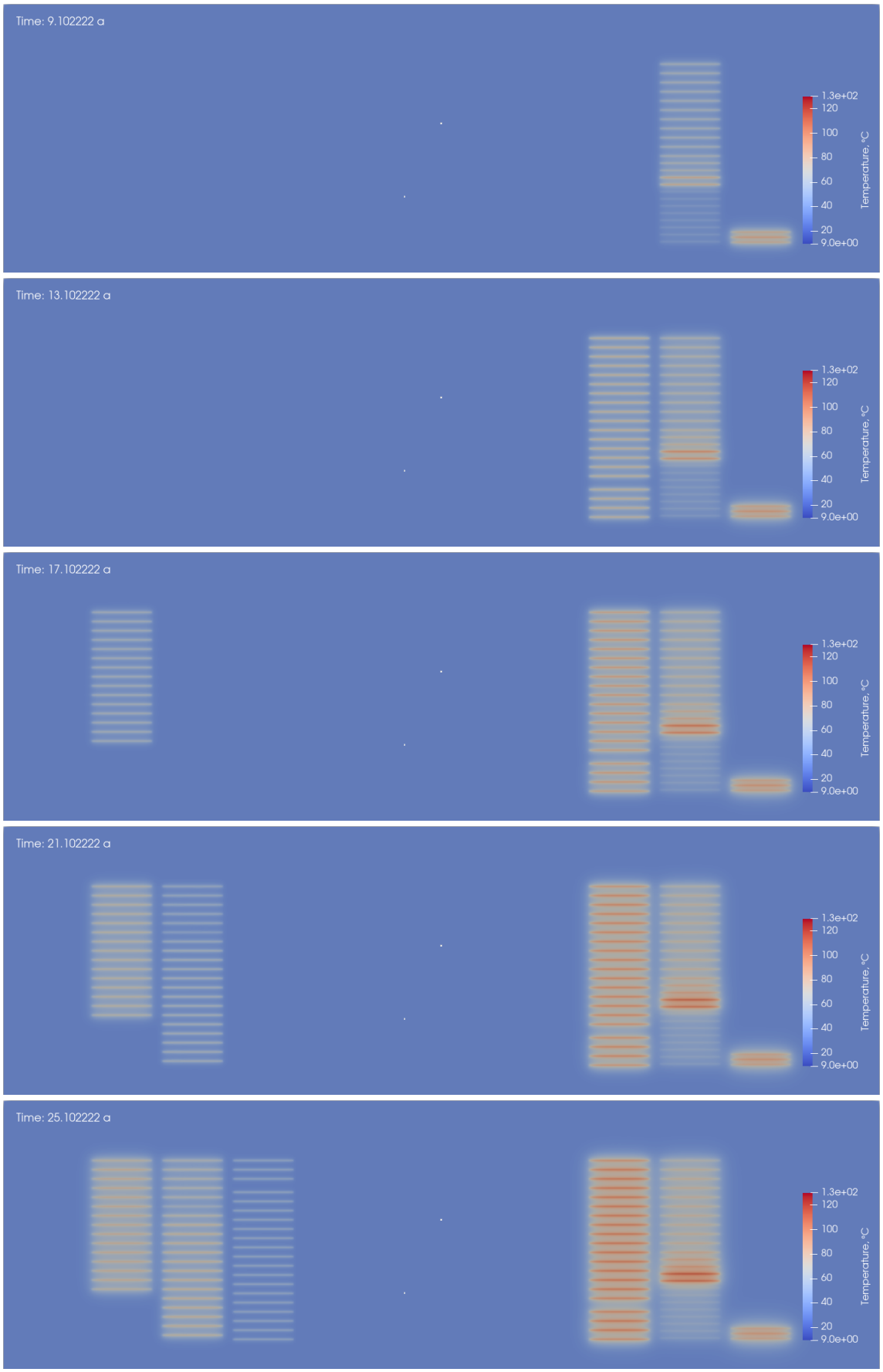

Figure 16.-6: Temperature evolution during the disposal phase, first 30 years.

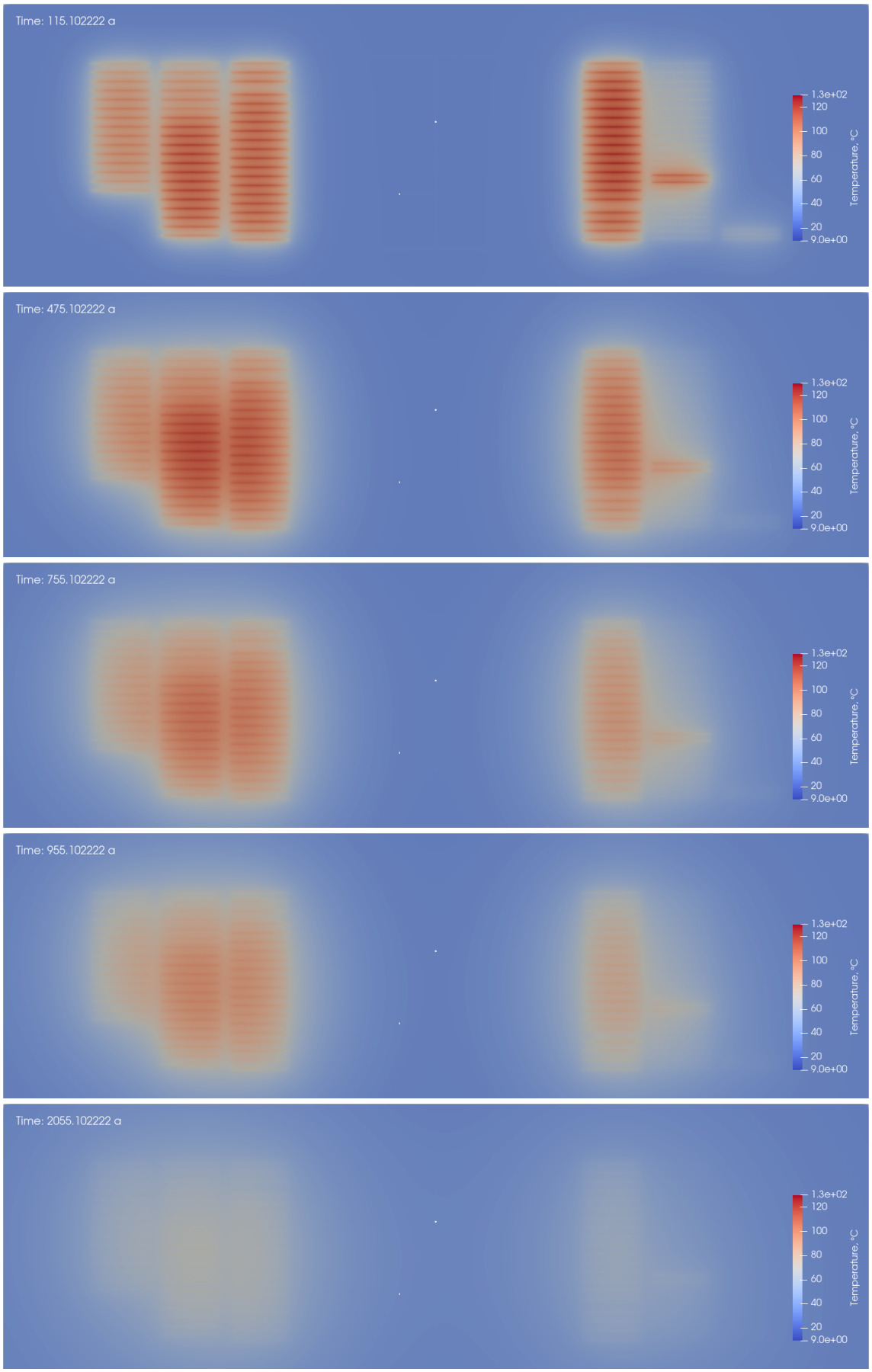

Figure 16.-7: Temperature evolution in the post closure phase up to 2,000 years.

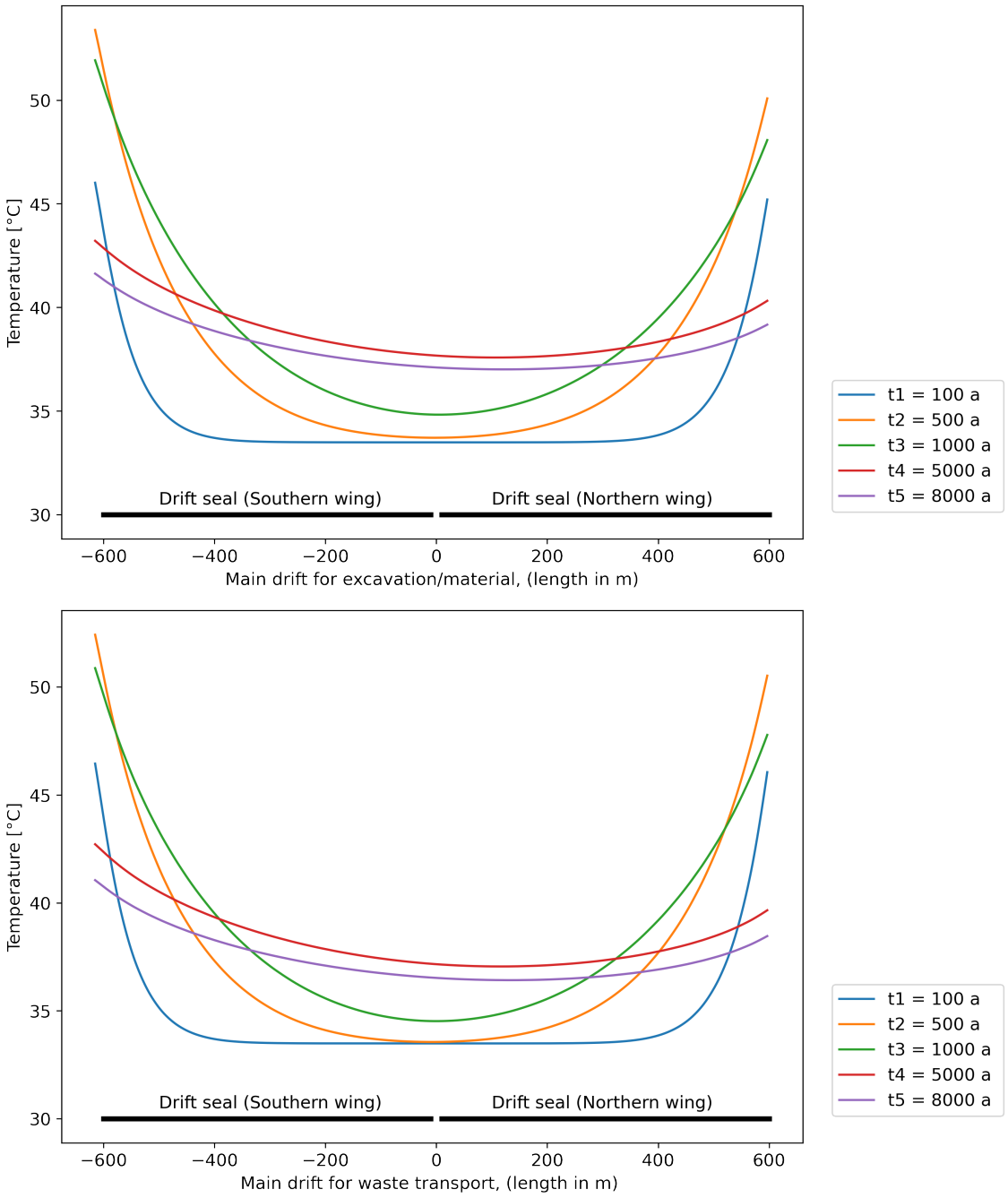

Figure 16.-8: Temperature evolution in the drift seals (top is material drift, bottom is waste handling drift). See Figure 16.-2 for the location of the seals in the repository.

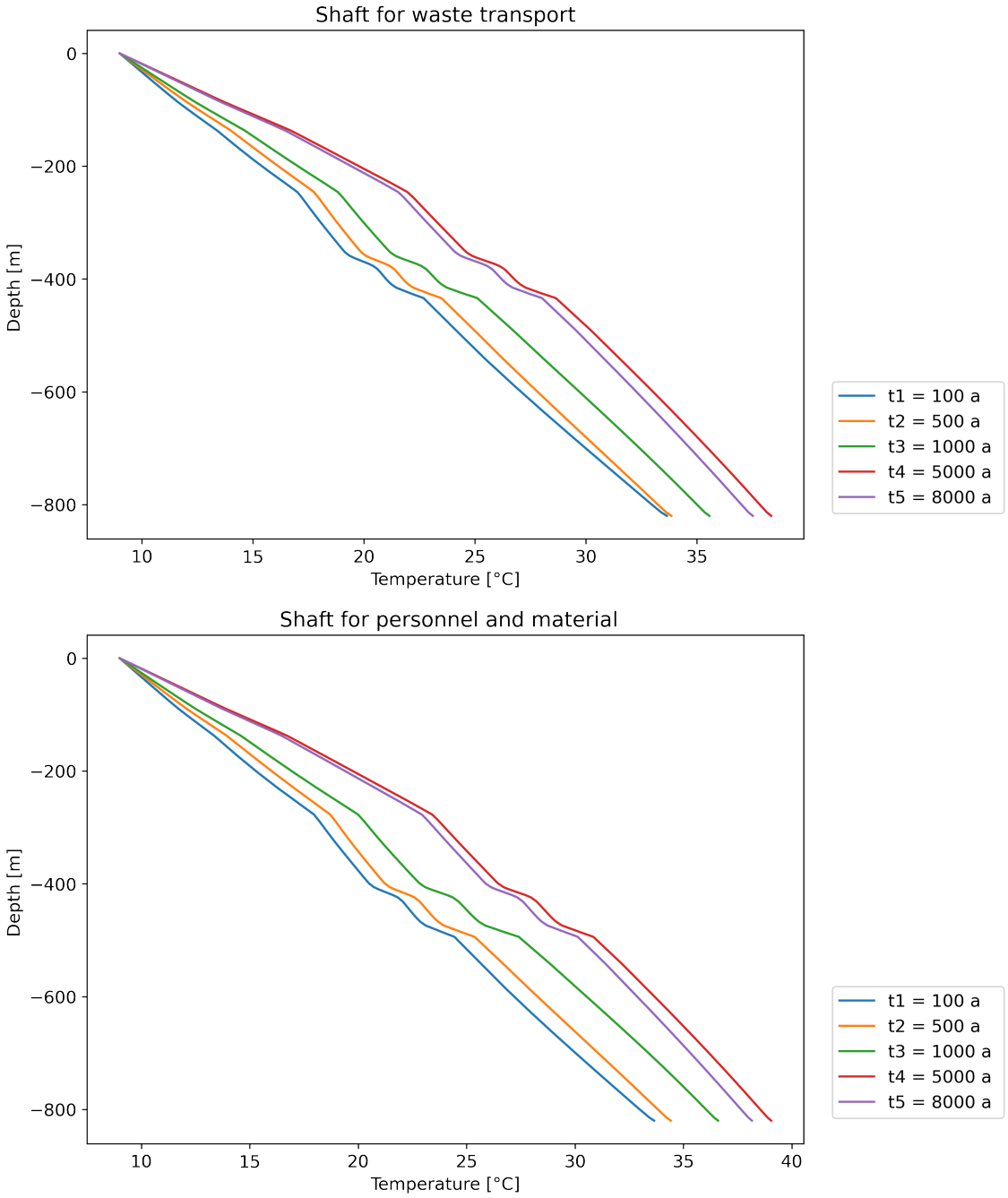

Figure 16.-9: Temperature evolution in the shafts. See Figure 16.-2 for the location of the shafts in the repository.

16.5 Discussion

The thermal analyses indicate that the temperature increase remains limited within the drift and shaft seals. A maximum temperature rise of 20 K was computed for these seals. With regard to the long-term stability of the EBS components, it can be concluded that the thermal load during repository evolution is unlikely to compromise the long-term stability of the geomaterials used in the EBS. For instance, the sealing properties of clays and bentonite do not deteriorate when exposed to temperature up to 100 °C (Villar et al., 2023). Rock salt from bedded salt formation in Germany with a water content of 0.02 up to 2% - only shows disintegration ("decrepitation") linked to the formation of microcracks above approx. 250 °C, (Bräuer et al., 2016). Sorel and salt concretes are stable up to 90 °C. This temperature limit increases with the in situ confining pressure that is to be expected in repository conditions. Higher confining stress will reduce the development of fractures.

17. Long-Term Geochemical Stability of the EBS

17.1 Scenarios

Two shaft seal leakage scenarios were investigated:

1. brine leaks down the shaft seal from a penetrated overlying formation to the repository, and

2. brine enters the repository at depth and is driven up the shaft seal due to convergence and gas generation in the repository.

The overlying formation can either be a fresh water aquifer, or water from a fractured anhydrite caprock.

The geochemical materials considered are either shaft seal materials (e.g., MgO) or the geological materials surrounding the shaft seal and making up the excavation damaged zone (EDZ) around the emplaced seal (e.g., Halite - NaCl and Sylvite - KCl). It is assumed that the salt layers that surround the shaft seal materials are much more soluble and reactive than the shaft seal materials like clay, asphalt, and gravel (Figure 17.-1).

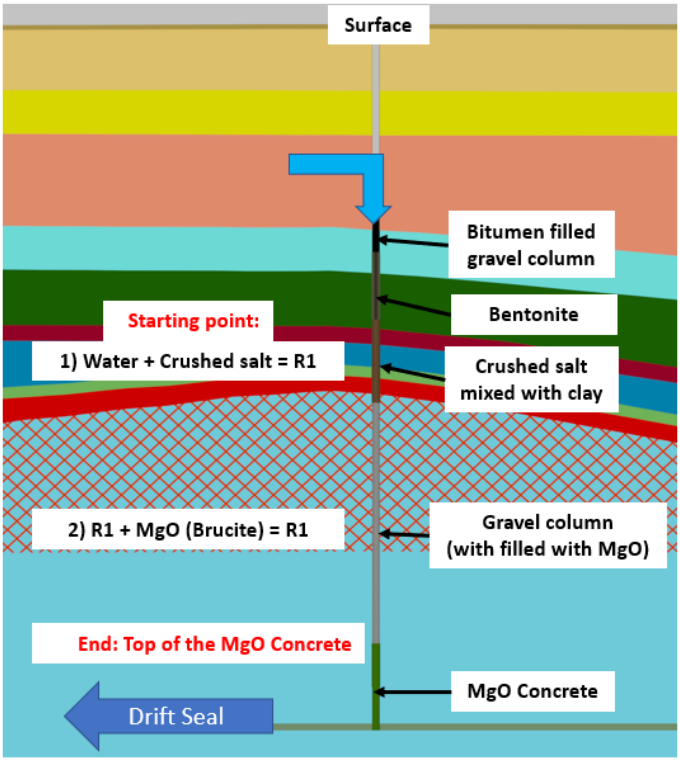

Figure 17.-1: Schematic of the shaft seal system and surrounding geology.

We used geochemical modeling to determine the stability of the solid phases with the brine as it progresses down (scenario 1) or up (scenario 2) the shaft seal/natural barrier system.

17.2 Methods

EQ3/6 version 8.0a was used to perform geochemical modeling (`https://github.com/lln l/eq3_6`). It is a reaction path simulator for isothermal batch reactions (Wolery, 2010). EQ3/6 is split into two functions that work in series: EQ3 and EQ6. EQ3 equilibrates a starting solution and computes the charge balance, accounting for formation of complexes. It can also force a charge balance by adjusting the concentration of an ion of the modeler's choice (in these models, Cl^-). Starting from the EQ3 output, EQ6 then computes the desired reaction on the equilibrated solution, dissolving and precipitating solids when necessary.

The approach for the implementation of EQ3/6 was to run an EQ3 equilibration and EQ6 reaction path simulation for the fluid as it reacts with each layer of the salt barrier. That is, the output from the reaction path calculation for a single layer, was used as the input for the equilibration and subsequent reaction path reaction for the next layer, and so on. This simulates slow flow of the fluid through the shaft seal and EDZ, assuming there is adequate time for the reactions to occur at each stage. Arbitrary kinetics have been assumed, such that the fluid reacts completely with each layer and reaches equilibrium.

EQ3/6 requires a reference thermodynamic database for its calculations. The database used for the modeling presented here (titled YMP) is included with the v8.0a release of EQ3/6 and was used previously in the Yucca Mountain Project, is currently used in the WIPP project, and has been used in generic spent fuel disposal research (Kuhlman et al., 2018). This database includes formation reactions for a wide variety of minerals and complexes, Pitzer interaction parameters, and reaction log equilibrium constants as a function of temperature.

Initial fluid compositions have been constrained as shown in 17.-1. Three representative waters have been chosen: A low-salinity surface water, a saline cap rock water, and halite-saturated Gorleben brine (Müller-Hoeppe et al., 2012b).

Table 17.-1: Initial compositions of reacted fluids.

Species	**Concentration (mol/kg H_2O)**		
	Surface Water	**Cap Rock Water**	**Gorleben Brine**
Na^+	8.07E-05	4.96E+00	5.98E+00
K^+	1.90E-06	3.61E-02	-
Ca^{2+}	1.98E-04	3.52E-02	2.00E-02
Mg^{2+}	-	5.64E-02	2.00E-02
Cl^-	8.07E-05	5.07E+00	5.98E+00
SO_4^{2-}	1.98E-04	5.15E-02	4.00E-02
SiO_2(aq)	-	5.49E-04	-
Al^{3+}	-	1.19E-05	-
HCO_3^-	3.19E-06	2.10E-03	-
pH	5.81	6.3	5.9

The shaft seal penetrates through five geologic layers. Each layer is a mixture of either two or three different salts. Below the final salt layer the shaft seal is comprised of MgO; in the

model, MgO has been represented as periclase in the thermodynamic database. In the first scenario, for both the cap rock and surface waters, reactions occur sequentially down. In the second scenario, the layers are reacted in the reverse order; Gorleben brine starts in the MgO layer and moves up. Figure 17.-2 shows the constituents of each layer and the order of reactions. Each set of reactions was simulated at 25 °C and 40 °C (isothermal), to span the range of expected geologic disposal conditions in the shaft seal.

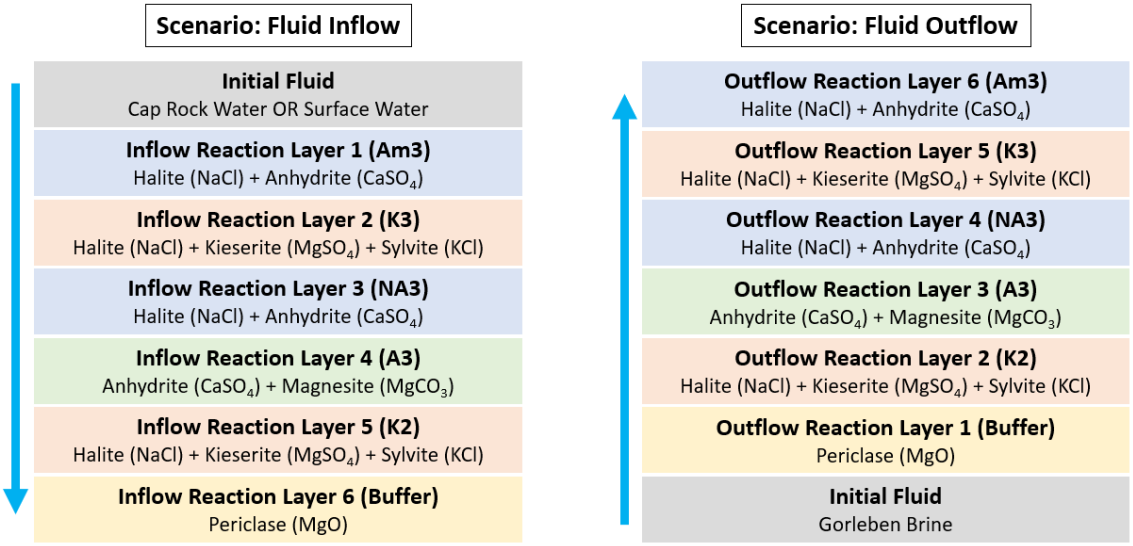

Figure 17.-2: Layers of the simulated shaft seal and salt EDZ.

EQ6 requires the mass of reacting solids to be specified and the solid phase is titrated into the liquid phase; an excess mass was specified for each salt reacted. 15 moles of each salt in each layer is titrated into 1 kg of fluid. This arrangement is like a titration into a beaker in the lab, where the liquid and solid phase salts that precipitate are all kept in equilibrium with one another. This was done to ensure the reactions progressed to completion (i.e., there was always more than enough salt available). This is similar to the approach used during brine evaporation calculations (Kuhlman et al., 2018) and by other common geochemical codes, like PHREEQC (Parkhurst and Appelo, 2013).

Additionally, EQ6 has an input option that establishes the reaction in a “fluid-centered flow-through open system.” With this, solids that precipitate as the reaction proceeds are removed; that is, they do not participate in the reaction any further. This can be likened to solids being left behind as the fluid flows through the salt mass. In this flow-through approach, the added solid phases dominate the system chemistry, rather than the precipitated solid phase (which tend to dominate in the titration mode). It was believed that this flow-through behavior is more similar to what would be expected in the field.

17.3 Results and discussion

The inlet and outlet compositions of each water type at each model temperature are shown in Figure 17.-3. Composition changes over the course of reaction steps are discussed in further detail hereafter. Notably, the composition of the surface water sees the most marked change by the end of reaction with the seal.

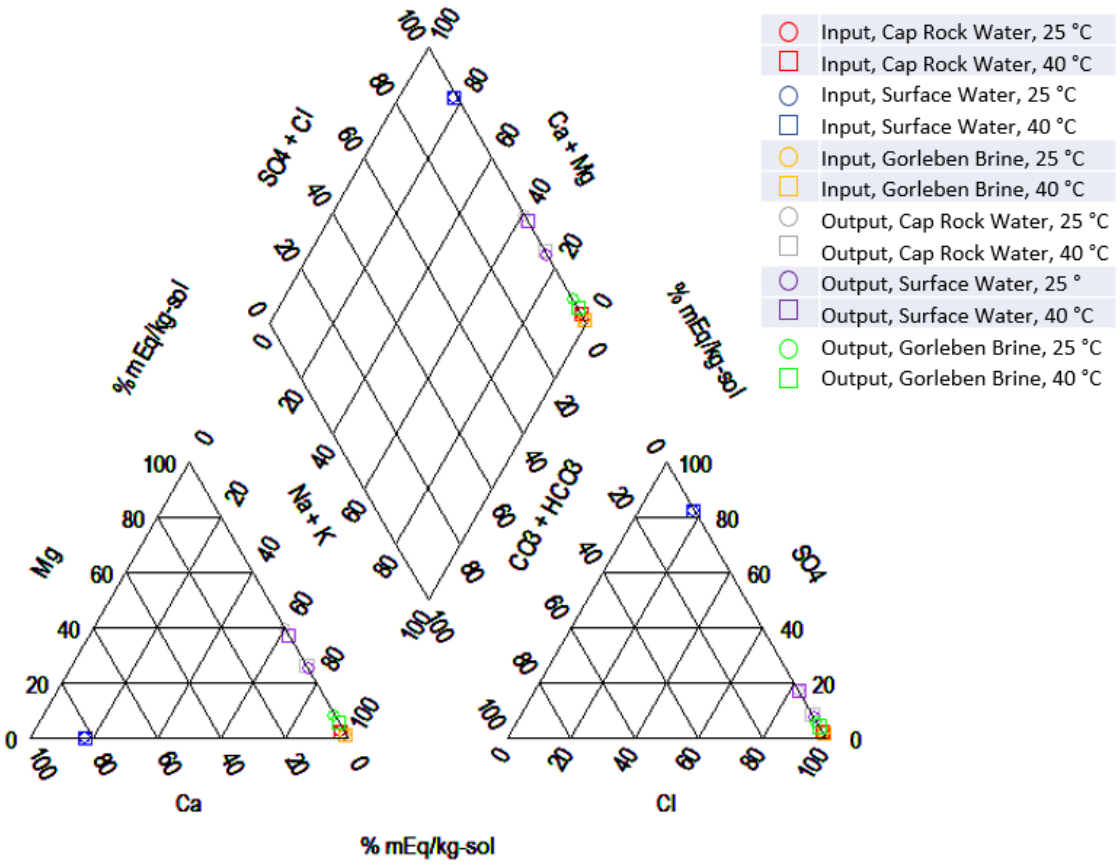

Figure 17.-3: Piper plot showing distribution of inlet and outlet waters to seal system in model.

17.3.1 Scenario: Downward flow starting with cap rock water

Reaction of the salt barrier with cap rock water at 25 °C results in the solute profiles shown in Figure 17.-4. After the first reaction step, the dissolved concentrations of Na^+ and Cl^- increase. As additional cations are introduced in subsequent layers, the concentration of Na^+ decreases; however, this change is not as notable in the concentration of Cl^- as more anions are added. By the final reaction step, the most prominent cations in the solution are Na^+, K^+, and Mg^{++}. Solution pH decreases at most steps, though it increases at step 2 (layer K3) and step 6 (MgO buffer) for a final pH in the alkaline range. Ionic strength trends upwards, increasing from an initial value below 6 molal to a final value of ~10 molal.

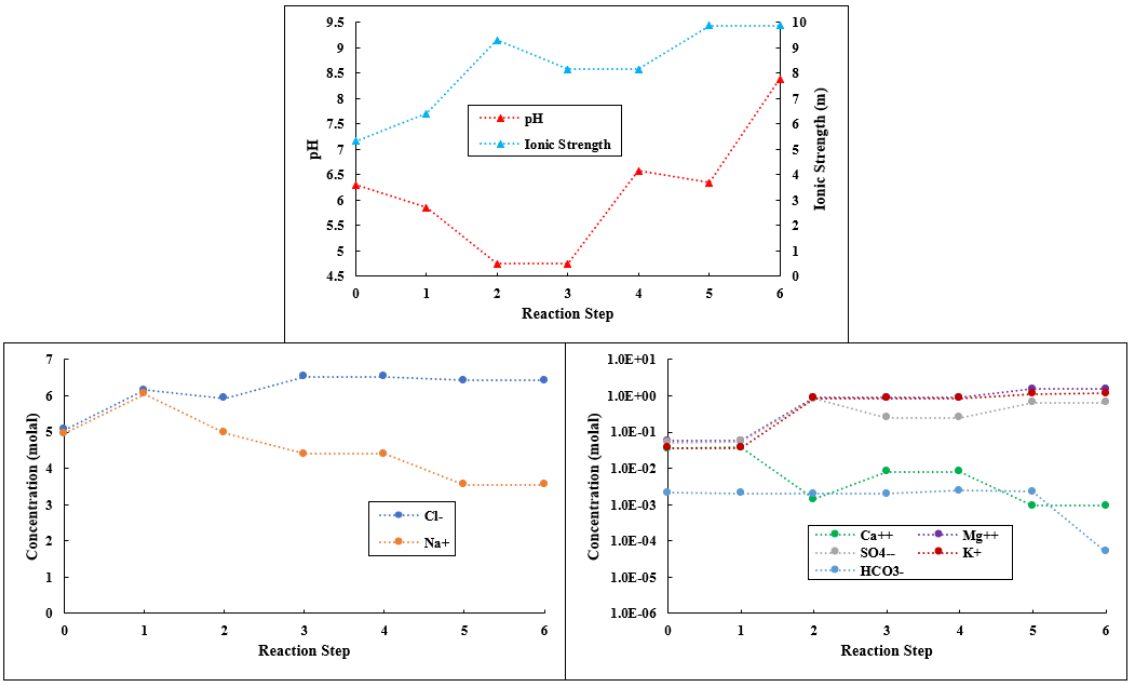

Figure 17.-4: EQ3/6 simulation results for caprock water inflow down the shaft seal system at 25 °C.

In the case where reactions are computed at 40 °C, previous observations hold (Figure 17.-5). No major differences in solute profiles are seen at elevated temperature; the same general trends persist, and the orders of magnitude of results stay the same. Some absolute values are slightly different, and there are minor differences in the later time behavior.

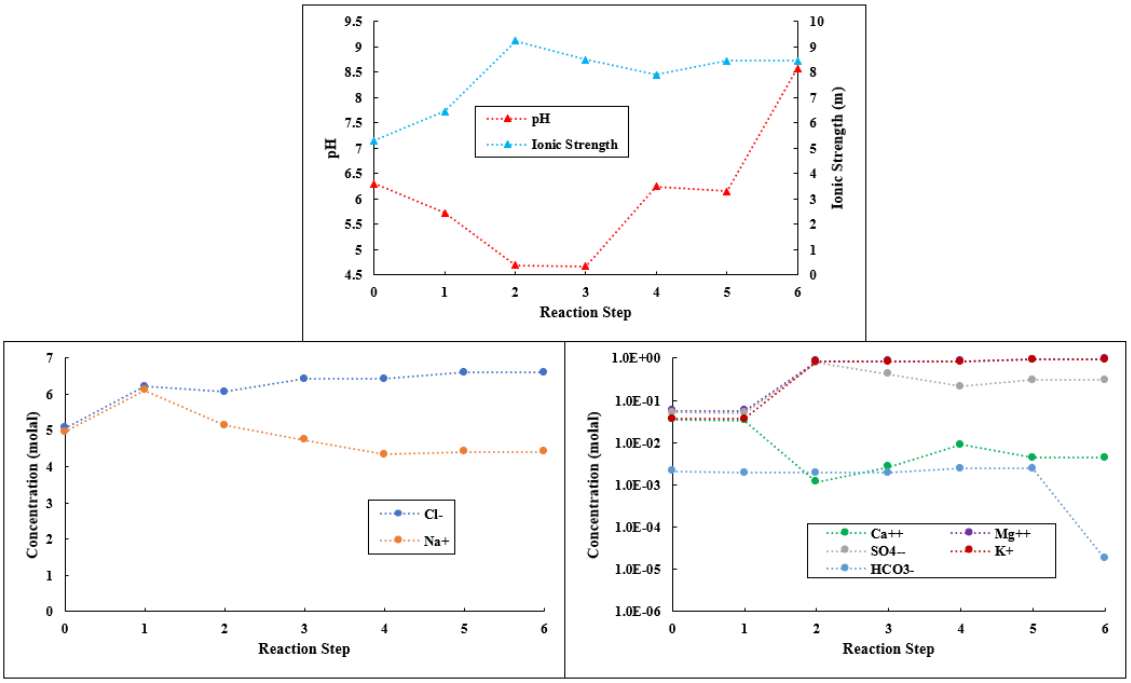

Figure 17.-5: EQ3/6 simulation results for caprock water inflow down the shaft seal system at 40 ℃.

17.3.2 Scenario: Downward flow starting with surface water

Trends for the reaction of surface water with the salt barrier follow those observed in the case of the cap rock water (Figure 17.-6). There is a notable uptick in Na^+ and Cl^- concentrations. It is worth observing that the final K^+ and Mg^{++} concentrations are higher in this case than in final cap rock water step, despite starting with a lower concentration in the initial fluid. As before, increasing reaction temperature from 25 ℃ to 40 ℃ results only in minor changes in trend shapes and absolute values (Figure 17.-7).

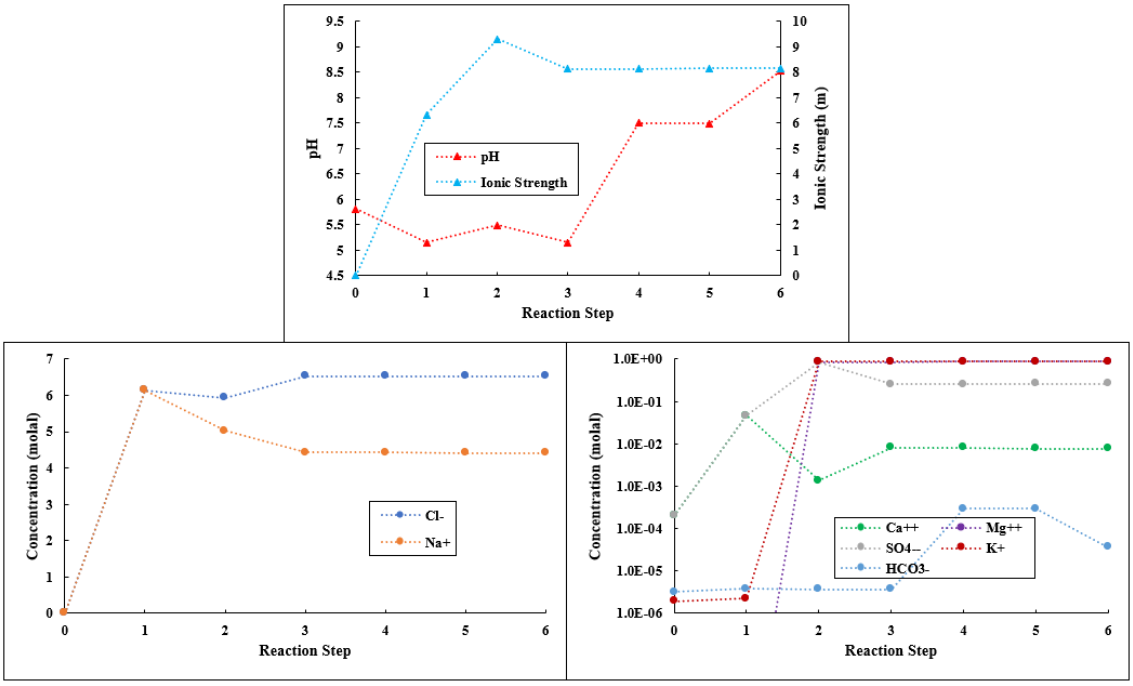

Figure 17.-6: EQ3/6 simulation results for surface water inflow down the shaft seal system at 25 °C.

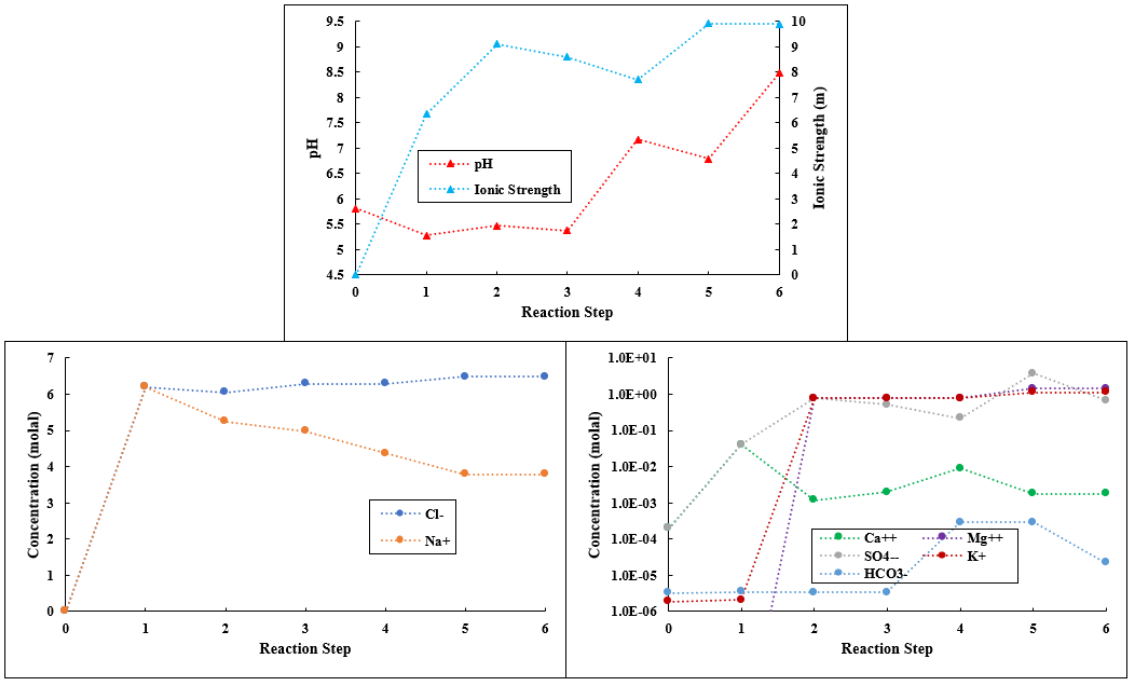

Figure 17.-7: EQ3/6 simulation results for surface water inflow down the shaft seal system at 40 °C.

17.3.3 Scenario: Upward flow of Gorleben brine

Trends observed in the reaction of Gorleben brine with the salt barrier in reverse order are shown in Figure 17.-8. Solution pH spikes due to contact with the MgO layer in the first reaction, but then stabilize at slightly alkaline pH (~8.5). The concentrations of Na^+ and Cl^- initially present in the solution remain mostly unchanged – thus, the final brine remains primarily a halite-saturated brine. The ionic strength increases, but not to the degree observed in the inflow cases. At elevated temperature, (Figure 17.-9), very minor differences are seen; trends and final values are approximately the same.

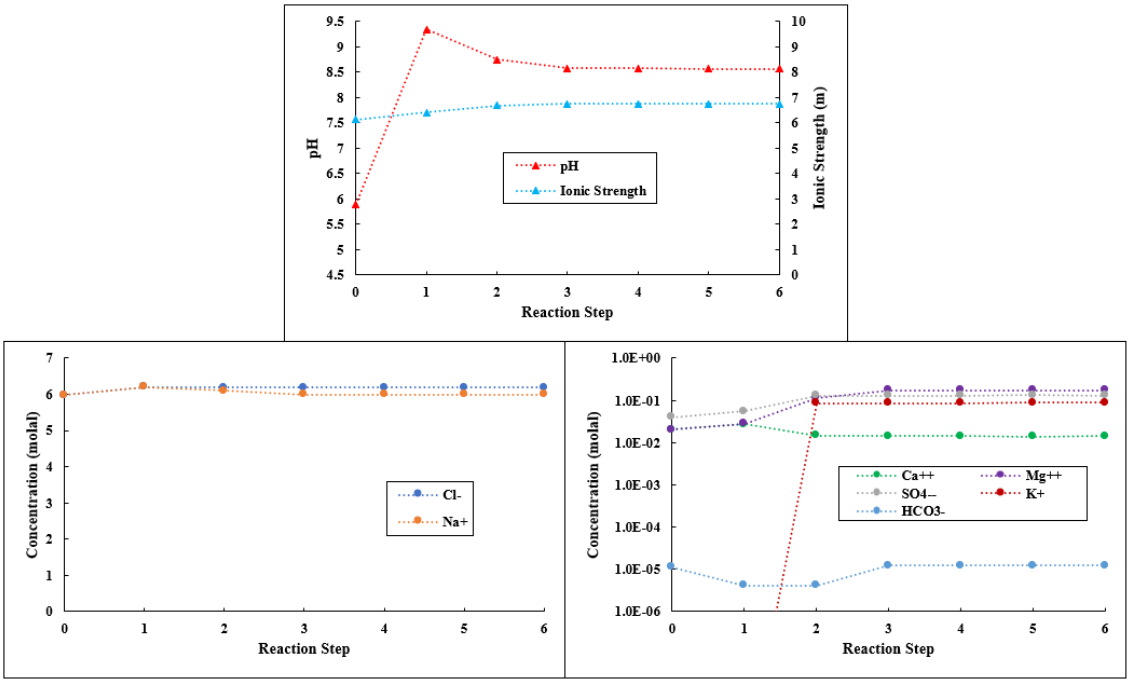

Figure 17.-8: EQ3/6 simulation results for Gorleben brine outflow up the shaft seal system at 25 °C.

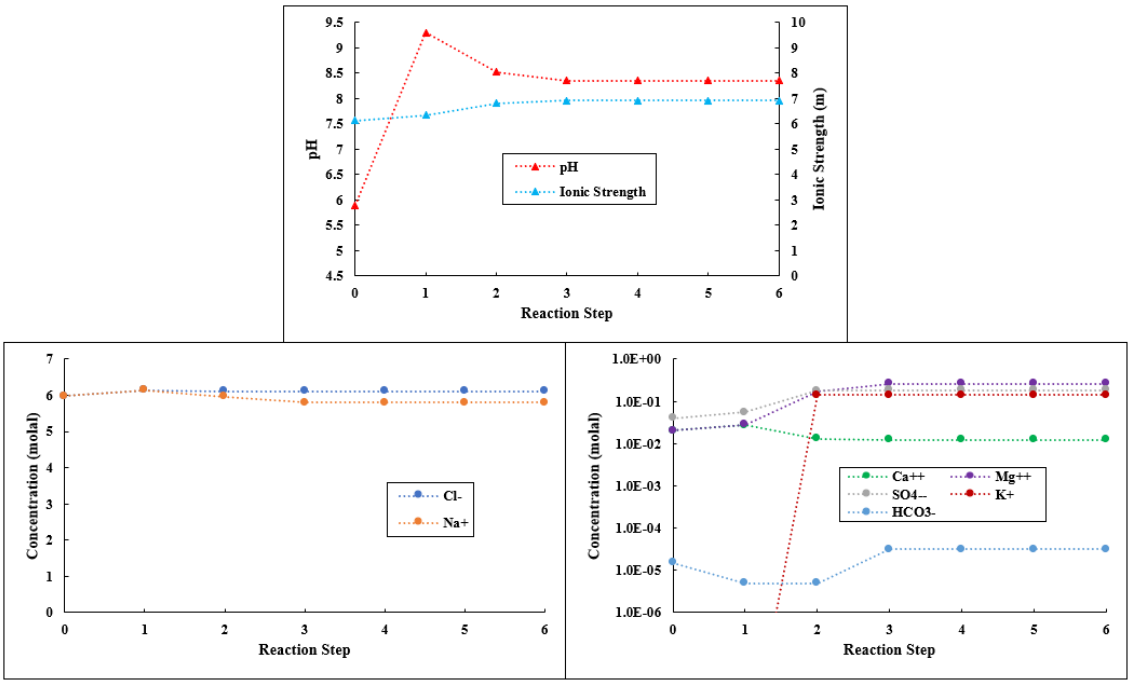

Figure 17.-9: EQ3/6 simulation results for Gorleben brine outflow up the shaft seal system at 40 ℃.

17.4 Conclusions

The reaction of each of three geologic fluids with the anticipated salt barrier produces solutions with high ionic strength and moderately alkaline pH, that consist primarily of halite. This is irrespective of the direction by which the fluid travels through the barrier. This was the anticipated behavior and function of the barrier as designed. Thus, the salt barrier could reasonably be expected to mitigate a canister breach. Further developments on this work could assess the time-dependence of this behavior, alternate configurations for the salt barrier, or minor interactions with the largely inert sealing materials.

18. Evolution of Crushed Salt Compaction in a Repository Mine

In addition to the initial barriers (drift and shaft sealing systems), further barriers contribute to the long-term containment of radionuclides in the effective confinement geological area. They do this by either delaying the access of solutions to the waste packages (e.g., crushed salt backfill) or by preventing or hindering the release of radionuclides from the effective confinement geological area (e.g., crushed salt backfill and waste matrix). The initial barriers must remain sufficiently impermeable until the hydraulic resistance of the compacting crushed salt is high enough to prevent or significantly limit the inflow of solutions to the wastes (Kock et al., 2012). In the safety assessment of salt repositories, it is crucial to determine the time when the crushed salt will gain its function as long term seal.

The understanding of the compaction behavior of crushed salt has been the scope of several research projects in the past and is still the subject of ongoing research. The projects KOMPASS (Czaikowski et al., 2023), KOMPASS-II (Friedenberg et al., 2024) and MEASURES funded by PTKA collectively focus on advancing the understanding and predictive capabilities related to the compaction and sealing behavior of crushed salt. The KOMPASS project primarily aimed at addressing prediction deficits in crushed salt compaction by improving the prognosis quality of its barrier function. This included the development of experimental methods for determining crushed salt properties at low porosities, enhancing process understanding, and advancing existing numerical models. Building on this foundation, the KOMPASS-II project further explored the thermal-hydraulic-mechanical (THM) coupled processes in crushed salt compaction, with a focus on characterizing the compaction process and its key influencing parameters. The project aimed to enhance scientific competence for using crushed salt as a barrier material by developing validated constitutive models capable of providing robust and reliable long-term prognoses. Complementing these efforts, the ongoing MEASURES project investigates THM processes in crushed salt backfill through a multi-scale approach, incorporating laboratory compaction and permeability studies, microstructural investigations, and advanced numerical modeling. The project's goal is to refine our understanding of these processes, reduce uncertainties, and improve the predictive accuracy of numerical models, enabling reliable assessments of the long-term compaction and sealing behavior of crushed salt in repository environments.

Although not yet fully refined, the constitutive models developed in these projects provide a foundation for numerically predicting the compaction behavior of crushed salt. In this study, we aim to analyze how crushed salt compacts over time during the repository's evolution, taking into account the thermal-mechanical conditions specific to the repository environment.

Modeling the compaction of crushed salt requires consideration of several key factors, including the development of stresses, the creep behavior of the surrounding rock salt, and the thermal evolution within the emplacement fields. To address these complexities, different modeling approaches were employed to predict compaction with greater accuracy across various locations in the repository mine. These approaches and their applications will be discussed in detail in this chapter.

18.1 Material parameters

In the following simulations several materials are present that need to be described thermal-mechanically. Table 18.-1 summarizes the thermal material properties used in the model to

simulate thermal propagation in the near field - rock salt. The crushed salt considered in the calculation model is compacted over time under the influence of lithostatic stresses, changing its thermal properties, particularly its thermal conductivity.

Table 18.-1: Density and thermal parameters of the components in the near field of the disposal zone (Bollingerfehr et al., 2013).

Components	**Heat Capacity [J/(kg K)]**	**Thermal Conductivity [W/(m K)]**
Container	515	15
Container basket	500	20
Crushed salt	$c_{p,CS} = c_{p,RS}(1-\eta)$ (1) where: $c_{p,CS}$: Specific heat capacity of crushed salt $c_{p,RS}$: Specific heat capacity of rock salt η : Current porosity	$\lambda_{CS} = \left(1-\frac{\eta}{\eta_0}\right)^{m} \cdot \lambda_{RS} + \frac{\eta}{\eta_0} \cdot \lambda_G$ where: m : exponent m = 1.14 η : Current porosity η_0 : Initial porosity η_0 = 0.35 λ_G : Initial thermal conductivity $\lambda_G = \lambda_{0,CS} + c_{T,CS} \cdot \theta$ $\lambda_{0,CS} = 0.42 \frac{W}{m \cdot K}$ $c_{T,CS} = 0.0027 \frac{W}{m \cdot K^2}$
Rock salt	864	$\lambda_{RS} = \frac{\lambda_{0,RS}}{1 + c_{T,RS} \cdot \theta}$ where: $c_{T,RS}$: Temperature parameter $c_{T,RS} = 0.0045 \frac{1}{K}$ $\lambda_{0,RS}$: Thermal conductivity $\lambda_{0,RS} = 5.2 \frac{W}{m \cdot K}$ θ : Temperature in °C

In Table 18.-2 the elastic material parameters as well as the densities of the components are given. The density and elastic properties of crushed salt depend on the compaction behavior of the material and necessitates advance constitutive model for accurate estimation.

Table 18.-2: Densities and elastic material parameters of the components in the near field of the disposal zone (Bollingerfehr et al., 2013).

Material	**Density (kg/m^3)**	**Young's modulus (GPa)**	**Poisson's ratio**
Salt rock	2,200	25	0.27
Crushed salt	f(η)	f(η)	0.27
POLLUX®	7,000	150	0.25

The compaction of the crushed salt, dictated by the material properties of the rock salt, exhibits a viscosity-dependent deformation behavior influenced by stress and temperature, and therefore is time-dependent. The viscoplastic behavior can be expressed by a volumetric strain component and its deviatoric counterpart. For the mechanical material model of the crushed salt considered in this study, the "CWIPP" model by (Itasca Consulting Group, Inc., 2021)

that has been modified by BGE TEC is considered. In this flavor of the model, the volumetric and deviatoric strain are given in Table 18.-3 and the material parameters are taken from Bollingerfehr et al. (2013). The model does not take into account the influence of moisture.

Table 18.-3: Viscoplastic material model for crushed salt based on CWIPP (Bollingerfehr et al., 2013).

viscoplastic total strain rate:

$$\dot{\varepsilon}^{vp}_{CS} = \dot{\varepsilon}^{vp}_{v,CS} + \dot{\varepsilon}^{vp}_{d,CS}$$

volumetric part:

$$\dot{\varepsilon}^{vp}_{v,CS,ij} = \frac{1}{3}\dot{\varepsilon}_{v,CS}\delta_{ij}$$

$$\dot{\varepsilon}^{vp}_{v,CS} = A_0 e^{-\frac{Q}{RT}} e^{B_2\rho}\left(1 - e^{-\left(B_1\frac{(\sigma_0-\sigma_v)}{B_3}\right)^{B_4}}\right)$$

deviatoric part:

$$\dot{\varepsilon}^{vp}_{d,CS,ij} = \frac{3}{2}\left(\frac{\dot{\varepsilon}^{vp}_{d,CS}}{\sigma'}\right)\sigma'_{ij}$$

$$\dot{\varepsilon}^{vp}_{d,CS} = A\left(\frac{\sigma'}{\sigma(1-\eta)}\right)^{n} e^{-\frac{Q}{RT}}$$

δ_{ij} : Kronecker delta
A_0 : Structure factor
$A_0 = 1.909 \cdot 10^{13}$ kg/d/m^3
$B_{1..4}$: Material parameters
$B_1 = 0.789$ 1/MPa
$B_2 = -19.5 \cdot 10^3$ m^3/kg
$B_3 = -26.0$ MPa
$B_4 = 1.8$
Q : Activation energy
$Q = 36.4$ kJ/mol
σ'_{ij} : Deviatoric stress
A : Structure factor
$A = 0.18$ 1/d

The corresponding porosity dependent Young's modulus assumed in the mechanical law is given in Table 18.-4

Table 18.-4: Porosity dependent elasticity Young's modulus for crushed salt (Bollingerfehr et al., 2013).

$$E_{CS} = E_{CS,f} \cdot e^{\frac{-c_E(1-\eta_0)}{\eta}}$$

$E_{CS,f}$: Young's modulus at full compaction
$E_{CS,f} = E_{RS}$
c_E : Material parameter

$$c_E = \frac{\eta_0 - 1}{\eta} \cdot \ln\left(\frac{E_{CS,0}}{E_{CS,f}}\right)$$

$E_{CS,0}$: Initial Young's modulus
$E_{CS,0} = 1$ GPa
η : Current porosity
η_0 : Initial porosity
$\eta_0 = 0.28$
$\nu_{CS} = 0.27$ (Poisson's ratio)

Over the years, several approaches have been developed to describe the thermomechanical creep behavior of rock salt, particularly within the framework of three major constitutive research projects (CODEVERGLEICH I–III), funded by the German Federal Ministry for Education and Research and the German Federal Ministry for Economic Affairs and Energy between 2004 and 2016. The first two projects focused on investigating fundamental deformation phenomena under various conditions, including transient and steady-state creep, damage-induced creep and dilatancy evolution, short-term strength and creep failure, as well as post-failure behavior (Schulze et al., 2007; Hou et al., 2007; Hampel et al., 2010).

The third project, CODEVERGLEICH III, was a US-German collaboration that involved per-

forming benchmark calculations to evaluate and compare the modeling approaches used by the partners. Key topics included the influence of temperature on deformation, as well as initial efforts to model the damage reduction and healing behavior of rock salt (Hampel et al., 2015; Salzer et al., 2015; Herchen et al., 2016).

Building on the insights gained from these collaborative efforts, the WEIMOS project commenced in 2016 to further advance and refine rock mechanical modeling approaches and numerical simulation tools for analyzing salt structures. Key topics investigated in the WEIMOS project include the deformation behavior at small deviatoric stresses, the influence of temperature and stress state on damage reduction behavior, deformation behavior resulting from tensile stresses, the impact of rock inhomogeneities on deformation behavior (Hampel et al., 2022; Wolters et al., 2022).

These projects collectively represent significant advancements in understanding and modeling the complex thermomechanical behavior of rock salt, particularly under the unique conditions relevant to repository environments. However, the models developed through these efforts are not publicly accessible. In this study, the BGR-EB model is utilized as the constitutive material model. This model incorporates two independently effective deformation mechanisms to better represent creep behavior at elevated temperatures. It is capable of capturing stationary creep and elasticity. However, it lacks features to model primary creep, secondary creep, as well as damage and healing mechanisms, limiting its ability to represent the full spectrum of rock salt behavior.

This model is summarized in Table 18.-5. Figure 18.-1 illustrates the temperature-dependent component of the stationary creep rate for the different material models for salt. In comparison to BGRa and BGRb, the BGR-EB model exhibits a higher creep deformation rate, beginning at 110 °C compared to BGRa and at 165 °C compared to BGRb.

Table 18.-5: BGR-EB creep mechanical law for rock salt (Bollingerfehr et al., 2013).

$\dot{\varepsilon}^{vp}_{RS} = V_k A_0 \left(A_{1e} \exp\left(-\frac{Q_1}{RT}\right) + A_{2e} \exp\left(-\frac{Q_2}{RT}\right) \left(\frac{\hat{\sigma}}{\bar{\sigma}}\right)^n \right)$	V_K : Creep class factor = 5.872 A_0 : Multiplier = 5.872 $A_{1,2}$: Structure factors $A_1 = 2.3 \cdot 10^{-4} \cdot \frac{1}{d}$ $A_2 = 2.1 \cdot 10^{-6} \cdot \frac{1}{d}$ $Q_{1,2}$: Activation energies $Q_1 = 42 \frac{kJ}{mol}$ $Q_2 = 113.4 \frac{kJ}{mol}$ R : Universal gas constant $R = 8.314 \frac{J}{mol \cdot K}$ T : Absolute temperature m : Stress exponent = 5 $\hat{\sigma}$: von Mises equivalent stress $\bar{\sigma}$: Reference stress = 1MPa

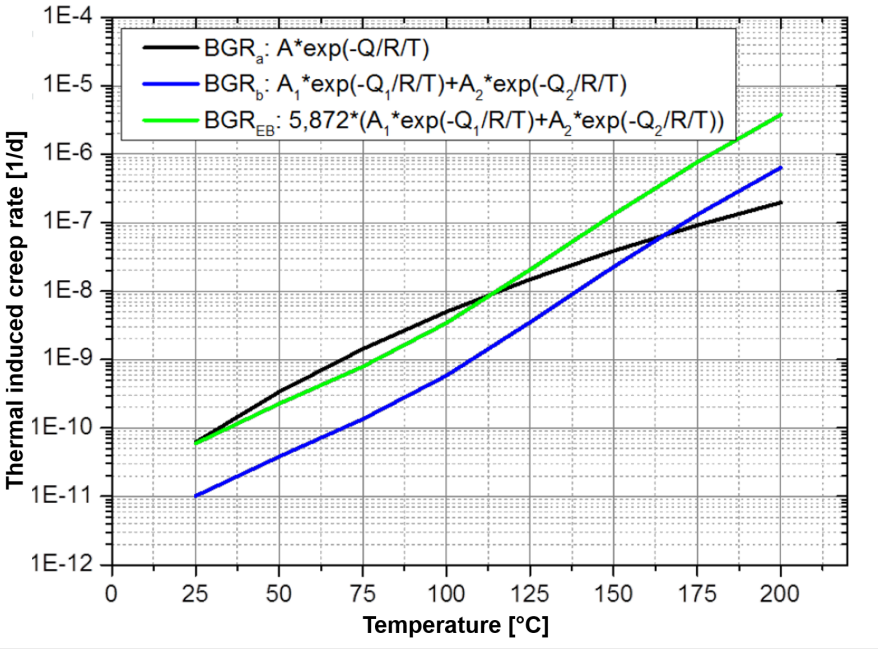

Figure 18.-1: Temperature-dependent component of the stationary creep rate for the material models BGRa, BGRb, and BGR-EB (Bollingerfehr et al., 2013).

18.2 Crushed salt compaction in the near field of the emplacement fields

The first simulation analyzes the compaction behavior in a single drift located in the middle of an emplacement field where the thermal output is maximum reaching the temperature limit of 200℃. The numerical model developed for this purpose takes into account the thermal superposition and the resulting temperature increases coming from the neighboring drifts. Such representation can be achieved by considering thermal symmetry boundary conditions as a quarter model of a cask embedded in a partial model of the rock formation, allowing the simulation of a large disposal field. This is achieved by assuming adiabatic conditions at the lateral model boundary faces. In this model, the distance from the drift axis to the model boundary in the transverse direction of the drift equals half the drift spacing, and the distance from the cask's end face to the model boundary in the drift direction equals half the cask spacing. The resulting thermal superpositions are conservative and only occur in disposal fields with very long drifts and a large number of such drifts. The model is mechanical constrained in the normal direction of the lateral and bottom boundary surfaces.

This modeling approach has the advantage of not requiring the entire repository to be modeled, reducing time and numerical effort. The calculation model is depicted in Figure 18.-2, showing a drift filled with crushed salt in a salt formation where a final disposal cask is stored. The cask in the model comprises two components: an outer casing for shielding against radioactive radiation and a container basket holding the high-level radioactive wastes, acting as a heat source in the model. The computations was carried out thermal-mechanically with FLAC3D Version 9 (Itasca Consulting Group, Inc., 2021).

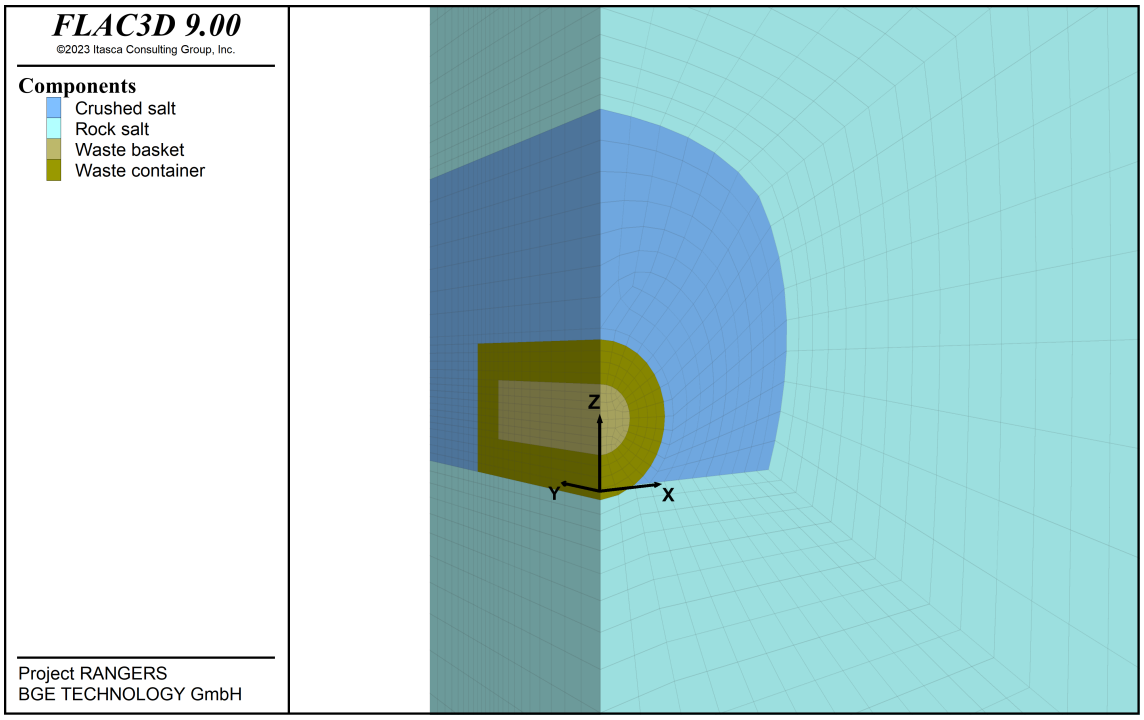

Figure 18.-2: Numerical model for the thermal-mechanical compaction in disposal drifts with heat generating waste.

The results of this simulation are depicted in Table 18.-6. The sub-figures in this table show the evolution of the temperature, displacements and porosity in the first 10 years after the disposal of the waste and the backfilling around the waste with crushed salt. Over this period of time, the temperature rises quickly to almost 200 ℃ in the cask and near the waste package. At five years, a slight decrease is observed that is due to the increase of thermal conductivity in crushed salt due to compaction. Because of the higher heat power in waste package, the temperature rises again at t = 10 years. The displacement presented here as the magnitude value, which is the square root of the sum of the displacement components, shows that high displacement occur around the cask. A region above the cask with almost no displacement can be observed. In that region, the porosity decrease is the highest, whereas region with high displacement show high porosity value, see porosity at t = 1 year. As a result, The analysis of the displacement in the model gives an idea about the compaction kinetics in the drift. Less displacement is found where compaction occurs first and vice-versa. At t = 5 years, the compaction process is completed as the porosity in the drift reaches zero in all finite zones. This rapid compaction is the result of the high temperature of up to 200 ℃ occurring in the drift. This high temperature environment helps the crushed salt to gain its sealing function faster and the disposed waste to be already confined even though the repository is still in operation.

Table 18.-6: Temperature, displacement (magnitude), and porosity evolution in a hot disposal drift.

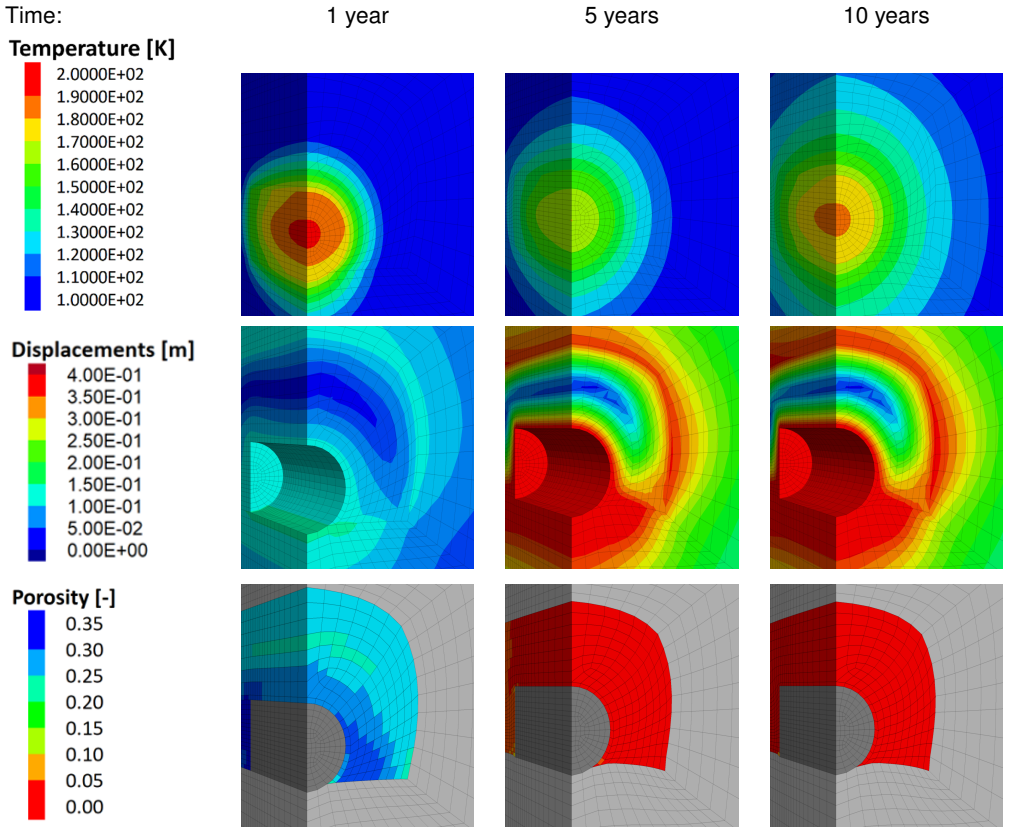

18.3 Crushed salt compaction in a cross-section of an emplacement field

The previous analysis already gives an idea how the compaction of crushed salt in the hot drifts with heat generating waste in the repository will take place. In order to analyze the compaction in the relatively colder drifts of the repository, such as the main drifts which are the pathways for a potential inflow of fluids into the repository mine, a modeling approach consisting of plain strain analysis on representative cross-sections of the repository mine was considered. This model allows to consider the thermal-mechanical effect due to the heat generation coming from the adjacent disposal drifts with PWR spent fuel.

The numerical model of the representative model region is depicted in Figure 18.-3. It consists of a cross section along the middle of the first emplacement drift in the Northern wing of the repository mine. This field has 22 disposal drifts filled with PWR spent fuel waste in POLLUX casks. One additional disposal drift is also present in this field where structural parts in MOSAIK-II casks are emplaced. The two main drifts for excavation and waste transport are also considered in the model. The geological layers at the location of the cross section were extracted from the 3D geological model. The K2 layer was merged into the salt pillow because of its negligible thickness. The disposal casks in the 22 disposal drift with POLLUX are resolved in the model. Those casks are surrounded with crushed salt backfill. The remaining drifts are fully backfilled with crushed salt. Because of the plain strain assumptions, The model represents an infinitely long repository in the longitudinal direction. The heat source in the casks are adjusted accordingly. For that, the heat source of all the casks in each disposal

drift was homogenized along the drift effective length. The right and left model boundaries are placed far enough away from the disposal area to minimize any boundary effects. Similar mechanical boundary conditions are assumed for this simulation with all lateral and bottom model boundaries being fixed in the normal direction. The minor heat dissipation in the longitudinal direction of the repository is taken into account using adiabatic boundary conditions at the front and back model boundaries. The computation is performed with FLAC3D in the version 7.

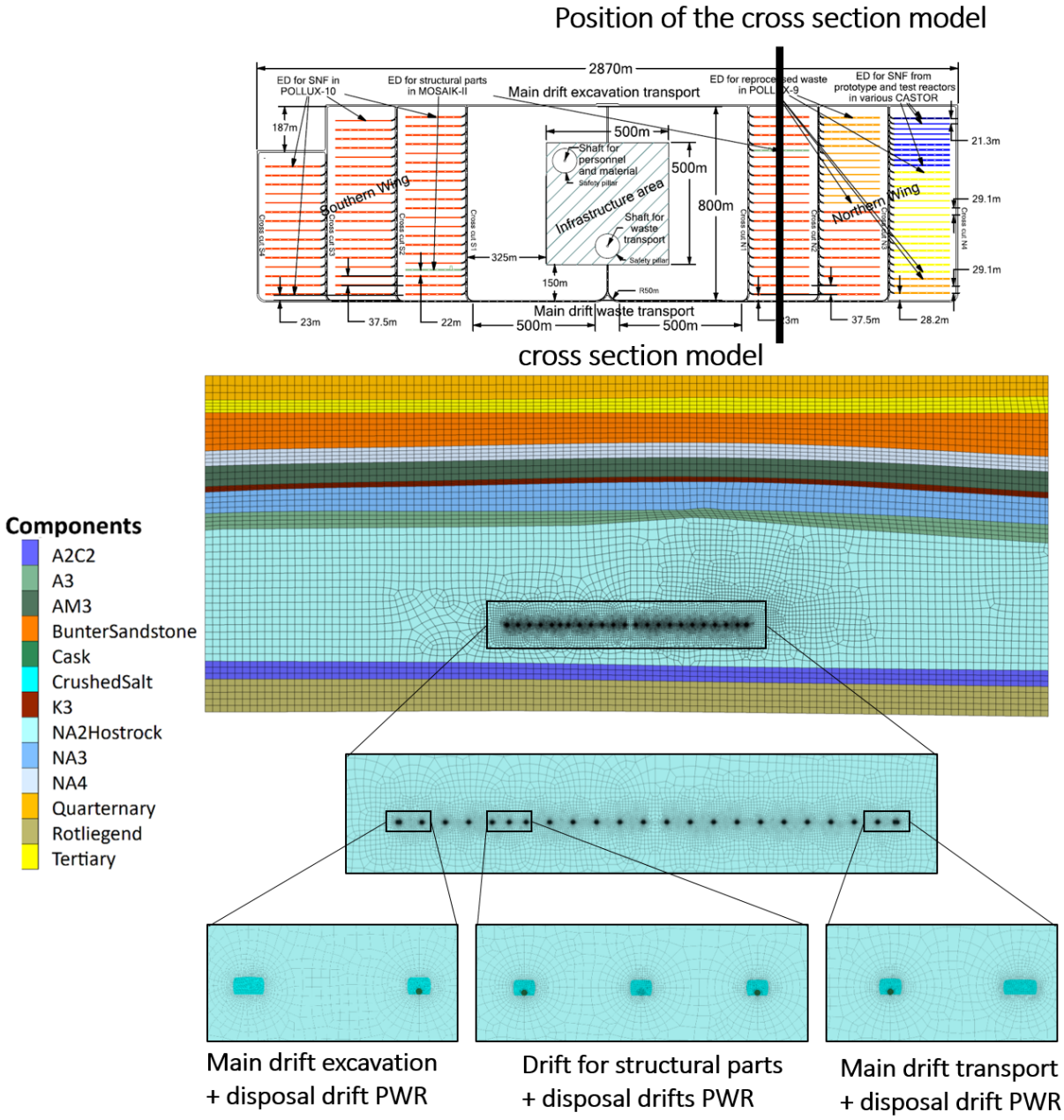

Figure 18.-3: Numerical model for the thermal-mechanical design of disposal drifts with heat generating waste.

Because of the homogenization of the heat source, the temperature evolution in the model reaches a maximum of around 100 °C in the middle of the cross section, see Figure 18.-4. An increase of approximately 15 K is observed in the main drift.

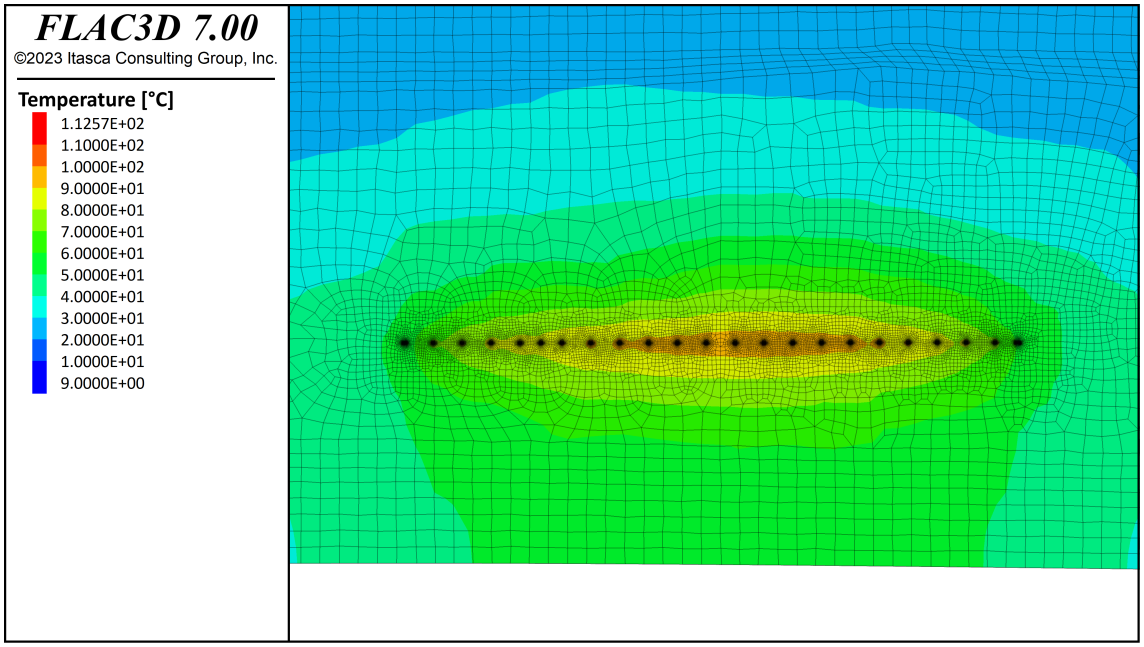

Figure 18.-4: Temperature distribution in the cross section at t = 200 years.

Table 18.-7 illustrates the porosity evolution in the crushed salt in four selected drifts along the cross-section. In the disposal drift with POLLUX cask and PWR spent fuel, the porosity decrease from 0.35 to approximately 0.2 in the first ten years of heating. Within the next 10 years, the porosity decrease reaches less than 0.05. At 30 years, the crushed salt is fully compacted with computed porosity of 0. A similar evolution can be seen in the disposal drift for structural parts with a time delay. There, the porosity at 10 years is about 0.2 and decreases to 0.1 at 20 years. 30 years after heating, is the crushed salt in that drift also fully compacted. This means that the heat coming from the adjacent drift is sufficient to help the crushed salt in this thermally inactive drift to compact as almost fast as the disposal drift with heat generating waste.

The porosity distribution in the two main drifts is similar five years after heating. The compaction does not occur uniformly across the entire cross-section. In the subsequent time, the compaction in the main drift for waste transport is faster as in the main drift for excavation. The bigger dimensions of the main drift for waste transport leads to comparatively higher convergences as in the main drift for excavation. As it can be seen in Figure 18.-4, the main drift for waste transport is also comparatively warmer as the drift for structural part limits the heat propagation towards the main drift for excavation. It results from this different compaction evolution that 30 years after the disposal, the porosity reaches 0.1 in the main drift for waste compared to 0.15 in the main drift for excavation. Nevertheless, the compaction is completed in the two main drifts at time=50 years.

Table 18.-7: Computed porosity in different drifts in the cross section.

PWR drift	Main drift excavation	Drift for structural parts	Main drift transport
Time: 1 year			
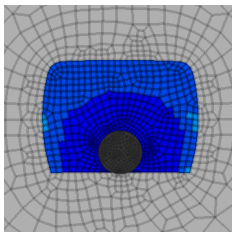	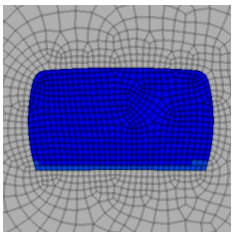	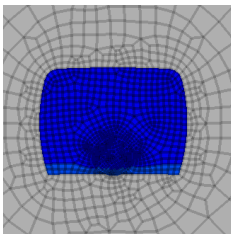	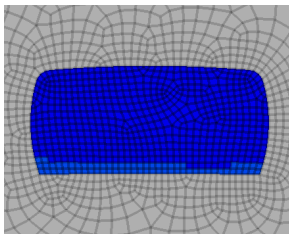
Time: 5 years			
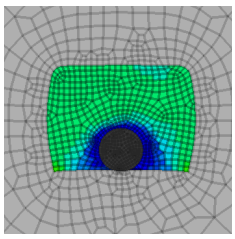	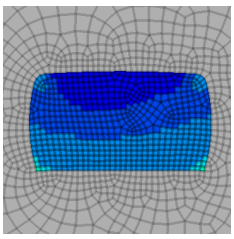	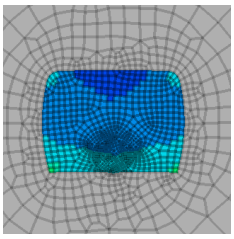	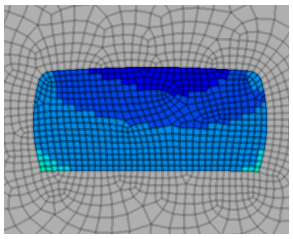
Time: 10 years			
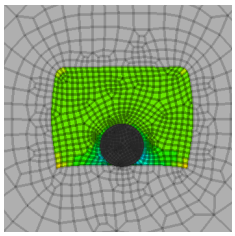	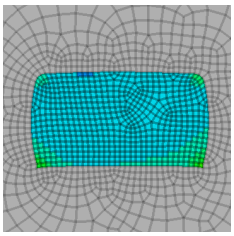	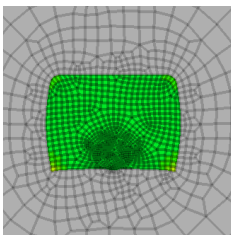	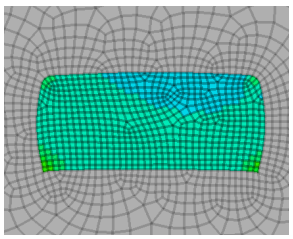
time: 20 years			
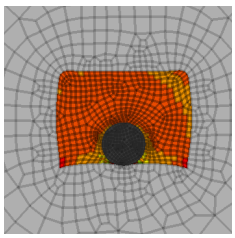	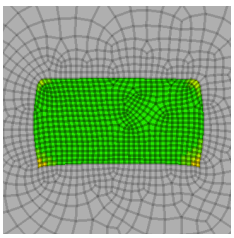	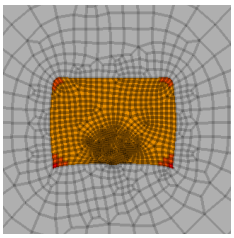	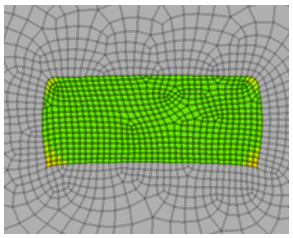
Time: 30 years			
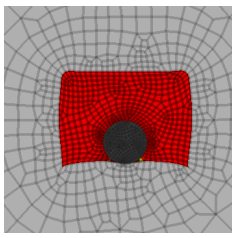	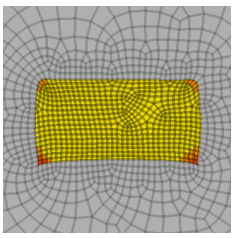	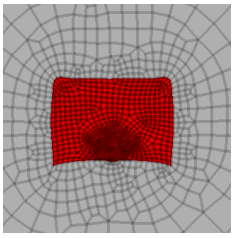	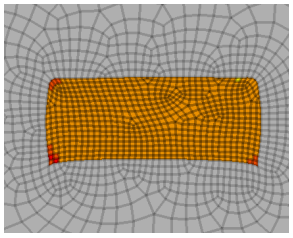
Time: 50 years			
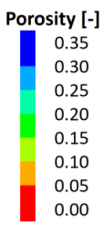	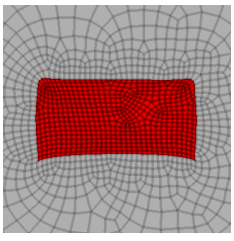	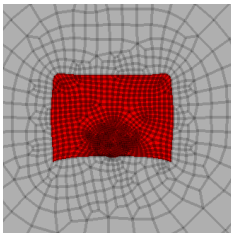	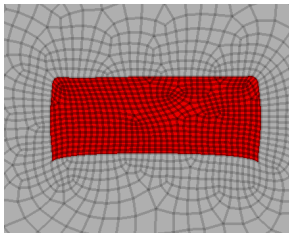

Figure 18.-5 shows the quantitative evolution of the porosity evolution over the time in all the drifts in the considered cross section. For comparison, the porosity results of the analysis of a PWR disposal drift (previous section, 3D near field simulation) is also plotted in the figure. The figure shows that faster compaction for PWR drifts are obtained using single drift model as using the cross section. The reason for this discrepancy lies in the homogenization of the heat power required for this 2D plain strain analysis leading to a temperature maximum of around 100 °C compared to 200 °C in the more precise single drift modelling. All disposal drifts with PWR in the cross section compact similarly as can be seen in the narrow band under which all porosity curves fall. Only the two disposal drifts located at the edges of the emplacement field next to the main drift take comparatively longer to compact. This clearly shows the effect of temperature as the main reason of this time delay in the compaction of these two drifts is due to the fact that these two drifts remain relatively colder due to their location. The figure also shows that the crushed salt in the drift for structural parts will take longer to compact compared to the PWR drifts. Some decades are necessary to complete the compaction in the main excavation drift and the transport drift. These results show that in the repository concept considered in this study a fast compaction is to be expected due to the the high temperature in the repository. It should be mentioned that the results from this 2D-simulation are conservative in respect to the compaction behaviour compared to a more precise 3D modeling as the comparison with the PWR single disposal drift modeling shows. Nevertheless, considering the repository lifetime of one million years, it can be derived from this simulation that the compaction process will be accomplished in the very early phase of the repository evolution. This means that the repository will be sealed and the radioactive waste will be confined quite early.

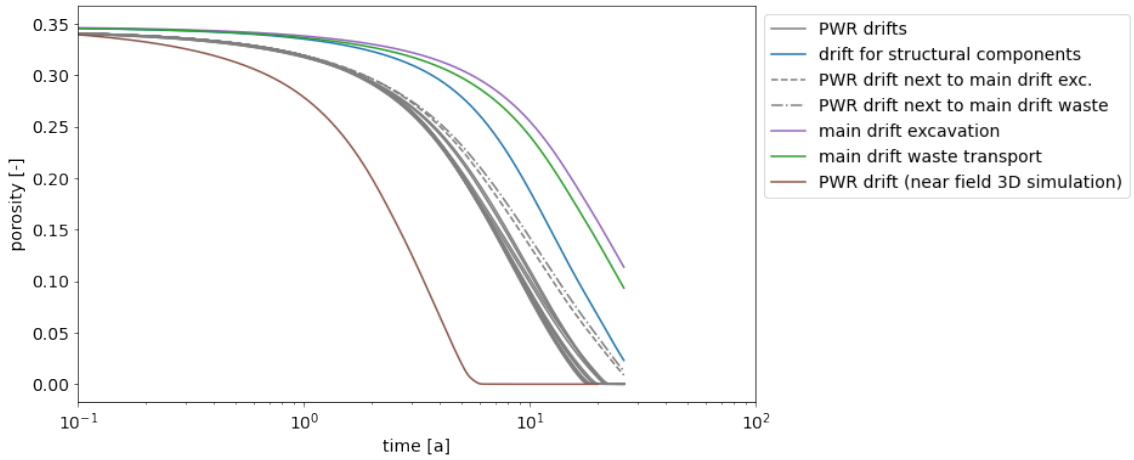

Figure 18.-5: Porosity evolution in all drift present in the considered cross section and in the single PWR disposal drift (previous section).

18.4 Crushed salt compaction in a whole repository mine

With the previous 2D approach, it is not possible to determine the compaction evolution in the drifts located away from the disposal fields. This is especially the case for the cross cuts, the main drifts or the long term seal in the drift sealing system. The compaction at this location are of importance to characterize when the repository will be ultimately sealed. To better estimate of the spatial evolution of the compaction in the repository, a 3D modeling approach was considered.

The model uses a domain representing one-quarter of the repository system. This domain includes the half of the three emplacement fields located in the Southern wing of the repository, where PWR spent fuel waste packages are disposed. The model domain also includes one of the four drift sealing systems allowing estimation of when this seal will take on its sealing function. The model domain is limited to one-quarter because of the huge computational effort associated with this simulation. In fact, the numerical model to be developed should accurately capture both the stress development and thermal expansion in the near field of the drifts backfilled with crushed salt. At the same time, it is also necessary to model the geological layers surrounding the salt pillow. The interaction between the geological layers capable of creep and those that behave rigidly, especially taking into account the complexity of the geological formation under consideration, is important to better account for the convergence of the rock. This requires a model that spans several square kilometers yet consists of centimeter-sized finite elements in relevant areas. To handle this complexity, several simplifications were made.

The containers themselves are not modeled discretely. Instead, the total heat output from all containers within a disposal drifts is summed and applied as a thermal volume load. The assumed volume is equivalent to the volume of the drift. All drifts are modeled with a rectangular cross-section. The geological units above and below the shallow rock salt formation are discretized as coarsely as possible while still allowing the different stiffnesses of the layers to be taken into account. A uniform density of 2200 kg/m³ is considered in the model, while symmetrical boundary conditions are applied, modeling only a quarter of the repository. Standard displacement and adiabatic boundary conditions were applied at the model boundaries. The lateral boundaries are 1.5 to 2 km away from the repository to avoid boundary effects. The numerical model contains 3 million elements. The finite element sizes range from 20 cm near the drifts to 100 m in the overburden. In Figure 18.-6, the numerical model is shown.

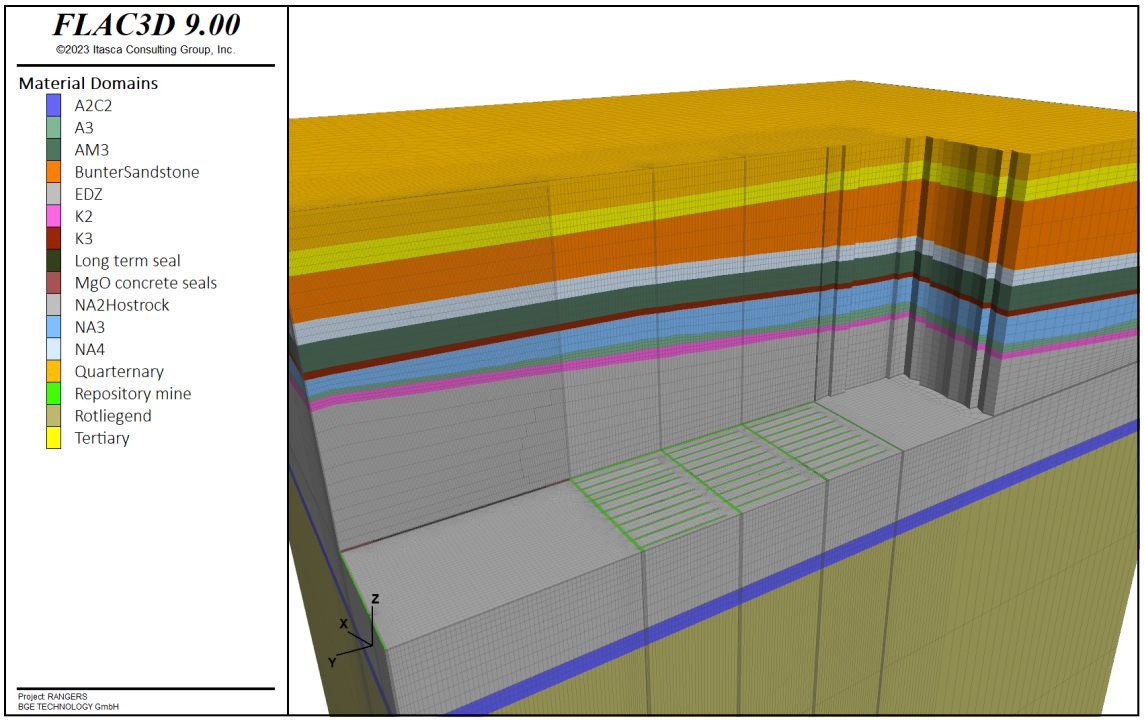

Figure 18.-6: Isometric view of the numerical model with ≈ 3 million elements for the analysis of the compaction of the crushed salt backfilled in the repository.

The material behavior of rock salt and crushed salt was implemented according to the material models presented in section 18.1. The other model units were modeled elastically or elasto-plastically, with their stiffnesses considered accordingly. The mechanical material parameters of those layers will be described in more detailed in Chapter 19. The thermal parameters of the geological units were already reported in Table 16.-2.

The simulation begins by initializing the primary state, followed by the instantaneous excavation of the drifts in the mine. Sequential backfilling continues until the mine is completely closed. The backfilling starts 20 years after excavation for the Southern emplacement wing, as prescribed in the repository concept. Every five years, one emplacement field is backfilled and thermally activated. After the backfilling of the disposal drifts, the cross drifts and the section of the main drift are closed 30 years after the beginning of the excavation.

An isotropic primary stress state is presumed, with a consistent density of 2200 kg/m³ for the overlying layers. This results in an estimated depth pressure of about 18.5 MPa at the disposal level. For undisturbed rock temperature, a temperature gradient of 3 K per 100 m is used, leading to a disposal depth temperature of 33.3 °C. A constant air temperature of 9 °C is maintained at the upper boundary of the model. At the lower model boundary, adiabatic conditions are assumed. This boundary is positioned at a significant distance from the zone of interest in the simulation, ensuring that no boundary effects are anticipated.

The results of this simulation are presented in Figure 18.-7 and Figure 18.-8.

In Figure 18.-7, the distribution of porosity across the repository mine is depicted. At 30 years, the emplacement fields have been backfilled with crushed salt. Initially, the porosity in the

drifts after backfilling is approximately 35%. The effect of sequential backfilling is particularly evident in the first emplacement drift on the right-hand side, where porosity begins to decrease, showing values below 30% in the center of the field where the temperature is highest. This drift was the first in the wing to be backfilled, 20 years after the start of the backfilling operations. The middle emplacement field, backfilled at year 25, does not yet show significant compaction, and similarly, the most recent field, just backfilled at year 30, exhibits no notable compaction.

Ten years later, the compaction in all fields has significantly progressed. In all fields, porosity has reduced to at least 20%. The lowest porosity values, ranging from 5% to 10%, are observed in the center of the fields where heat generation is most intense. Similarly, in the main and cross drifts, which were backfilled right after the emplacement fields were closed, porosity evolution mirrors that of the emplacement drifts. In the cross drifts, the porosity follows a pattern similar to that at the edges of the emplacement drifts, while in the main drift, the lowest porosity values are observed along the center of each field.

By year 69, compaction has largely completed in most of the drifts, with porosity reaching near-zero values, except for the drifts at the edges of the emplacement fields and the drift containing non-heat-generating structural components. After 100 years from the start of backfilling, compaction across the emplacement zone is nearly complete. Only in the main drift and its intersections with cross drifts does porosity continue to evolve, showing values between 5% and 10%.

In Figure 18.-7, it is evident that the porosity in the long-term seal at the edge of the emplacement zone is progressively decreasing, reaching values between 15% and 25%, 100 years after backfilling. A detailed view of the porosity evolution in the long-term seal is provided in Figure 18.-8 shows the reconsolidation of the crushed salt seal between the MgO seals (in magenta) from 100 to 750 years after backfilling. The figure illustrates the compaction progression from the emplacement side (right) toward the shaft side (left). This is clearly noticeable in the porosity distribution at 200 and 300 years. This compaction progression reflects the heat propagation from the emplacement fields. By year 400, porosity in the seal has nearly reached zero. After 700 to 750 years, compaction of the long-term seal is effectively complete, with only small pockets near the MgO seals showing porosity above zero, likely due to the assumed rigid contact between the MgO concrete and the crushed salt/clay mixture. A more accurate representation of this interface would require the use of interface elements in the model.

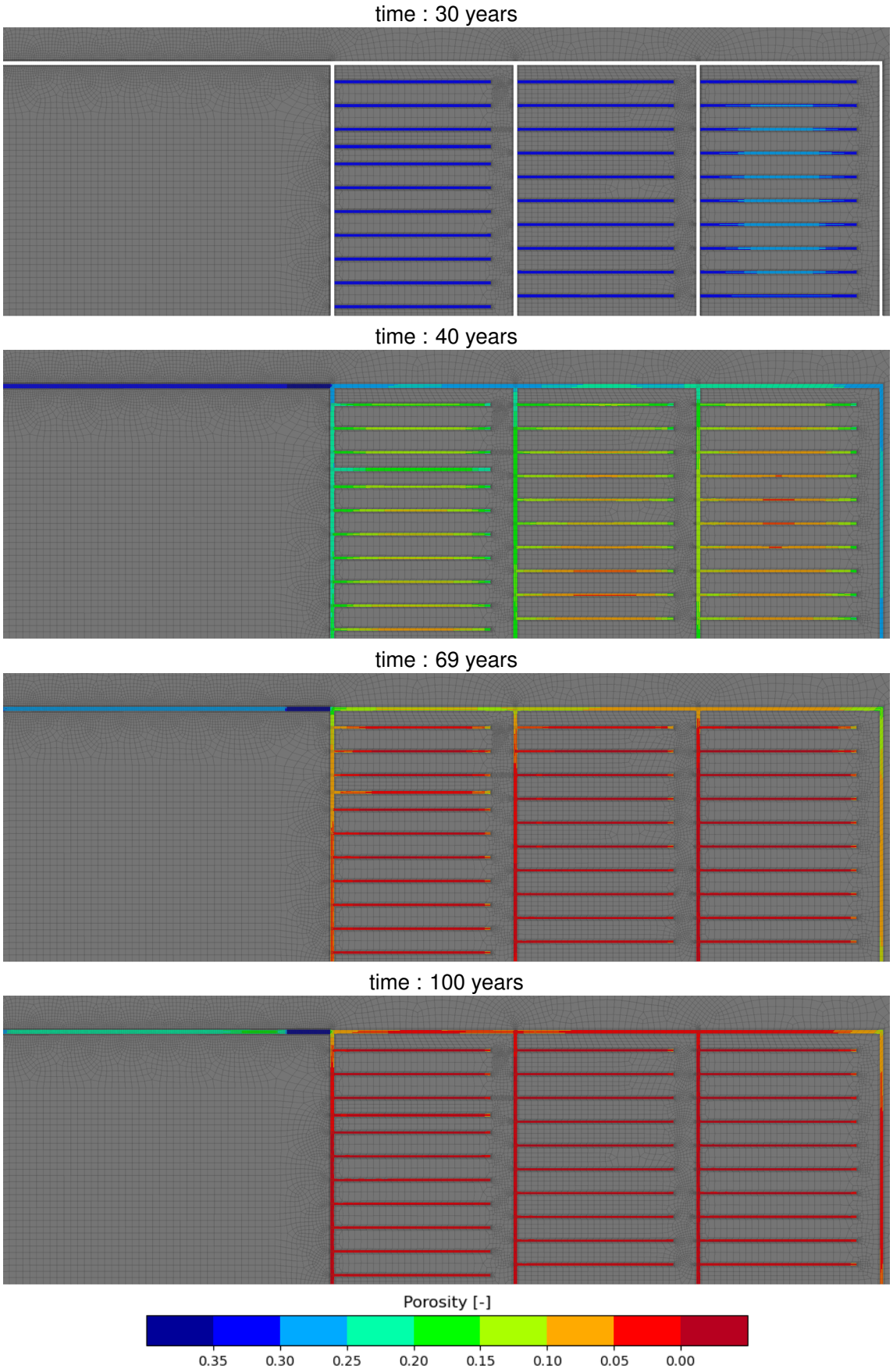

Figure 18.-7: Compaction evolution in the repository after 100 years.

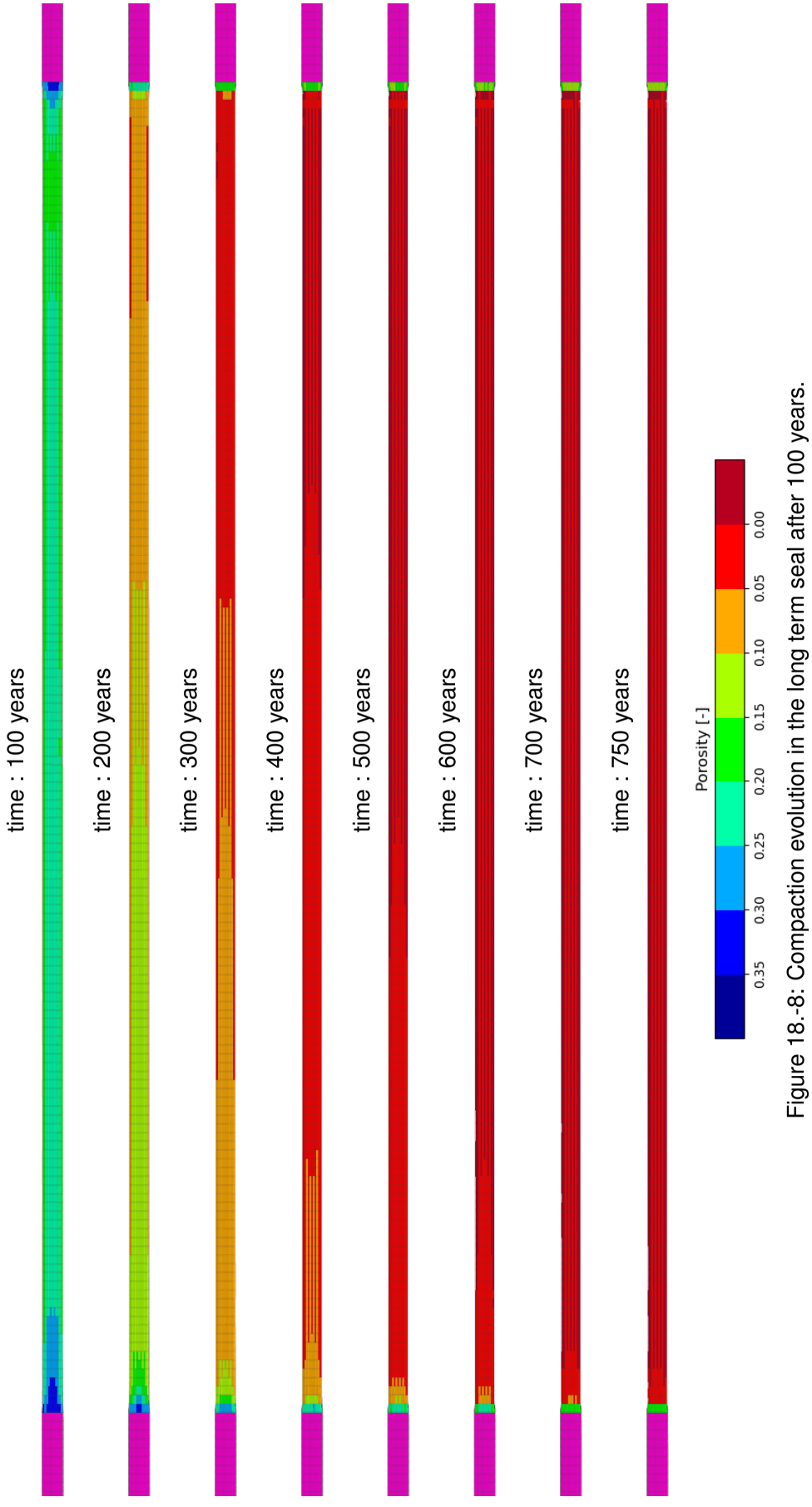

Figure 18.-8: Compaction evolution in the long term seal after 100 years.

18.5 Summary: Evolution of crushed salt compaction in a repository mine

The long-term containment of radionuclides in a salt repository relies heavily on the effectiveness of multiple barriers, including the reconsolidating crushed salt backfill, which serves as a long-term sealing element. The crushed salt gradually compacts due to lithostatic pressure, eventually reducing its porosity and permeability to levels that prevent the inflow of solutions to the waste packages. Understanding the compaction behavior of crushed salt is crucial for safety assessments.

This study analyzed the compaction behavior of crushed salt under the thermal-mechanical conditions of a repository. Various modeling approaches were employed to predict how crushed salt compacts over time in different areas of the repository mine. The compaction was assessed for both hot and cold repository zones, including disposal drifts and main drifts.

Key findings include:

- Early compaction: In drifts containing heat-generating waste (e.g., POLLUX casks), compaction occurs rapidly due to high temperatures (up to 200℃). In these areas, porosity can decrease from 35% to near zero within 5 to 30 years depending on the modeling approach, completing the compaction process relatively quickly.
- Gradual compaction in colder drifts: In drifts with structural components and main access drifts, where heat is less intense, compaction occurs more slowly. These areas may take several decades to reach full compaction, but the process still occurs well within the repository's operational timeline.
- Long-term seal: After 100 years, the long-term seal at the edges of the repository also shows substantial compaction, with porosity nearing zero after 700 to 750 years. This compaction ensures the repository's effective sealing over the long term, aiding in the isolation of radioactive waste.

The results from these simulations highlight that the compaction process in salt repositories is predictable. The use of crushed salt as a backfill material provides an effective long-term sealing mechanism, significantly contributing to the repository's overall safety and containment performance. Moreover, the rapid compaction of the crushed salt in thermally active zones suggests that sealing functions are achieved early in the repository's life cycle, providing confidence in the long-term isolation of radioactive waste.

This study confirms that the compaction process, although influenced by varying thermal and mechanical conditions, is completed early in the repository's operational phase, thereby ensuring the long-term safety and containment of radioactive waste in salt-based repositories.

The primary result of this analysis is that the confinement of radioactive waste in salt repositories is achieved relatively early in the repository's life cycle. This has several important implications:

- Since the long-term seal is projected to achieve its full functionality within less than 1,000 years, based on the simulation results, the required functional lifetime of the EBS

could potentially be reduced to just a few thousand years, rather than the previously assumed 50,000 years.

- To better define the required lifetime of the EBS, it is essential to use advanced and highly accurate constitutive material models for crushed salt and crushed salt clay mixtures. Only with precise modeling can the uncertainties regarding the longevity of the EBS be minimized.
- To further reduce uncertainty, it is advisable to use a high temperature limit in the repository design. The current limit of 200 °C has proven effective and is therefore recommended for future salt repositories.
- Given that a substantial portion of the repository reaches an advanced state of compaction during the operational phase, it is feasible to implement a monitoring system to ensure that the repository behaves as expected over time.
- Additionally, the early compaction behavior suggests that it can be tested under real conditions through field experiments in salt mines, spanning several decades. Similar long-term field experiments, such as those on bentonite seals, are already underway in various underground research laboratories around the world.

19. Mechanical Integrity Assessment of the Drift Seal

In the following section, the design and integrity of the drift sealing system in salt repositories are assessed based on the methodology developed within the RANGERS project. This exercise is an example performed for the specific drift sealing system designed in generic repository system developed in RANGERS, see (Simo et al., 2024).

19.1 Safety function

According to Kock et al. (2012), the drift seal as part of the EBS should prevent or limit the inflow of solutions until the crushed salt has compacted to the extent that it can take over the sealing function. Conservative estimates of the required period for salt compaction are up to a few thousand years. To cover this period, a significantly longer duration of functionality for the sealing structures is assumed. in actual considerations, the drift seals can remain their function up to the point where significant changes in the hydrogeological and hydrochemical conditions are taking place. Such significant changes in the boundary conditions can be expected in the next ice age (Müller-Hoeppe et al., 2012b). Statements about the function of the shaft seals are therefore only possible for a period of about 50,000 years, and this period is assumed for the functional duration in the proof.

19.2 Design of the drift sealing system

The drift sealing system as designed in the scope of RANGERS consists of an assembly of abutments, drift seals, and the long-term crushed salt seal. In the repository presented here, four drift sealing systems are designed and are located in the two main drifts closing all access to the emplacement wings, see Figure 19.-1. The drift seals consider two sealing elements made of MgO-concrete. Both are bounded with concrete-based abutments to guarantee mechanical stability and fix their positions. Here also, for reason of geochemical stability, MgO-concrete is considered for the abutments. All elements are placed in a row, with direct contact to the rock. Kock et al. (2012) recommends the EDZ is removed to the extent possible immediately before the installation drift sealing system. In the construction location, the extent of the EDZ is expected to be between 10 and 30 cm. The possibly remaining residual damage zone can also be sealed by injections if necessary. In between the sequence of sealing elements and abutments, an additional long-term sealing element is considered. This sealing element is made of crushed salt that has been enriched with some clay admixtures. This clay partially fills the pores in the crushed salt, reduces its permeability at the early stages of compaction, and help the mixture to reach a fully compacted state much faster. The effectiveness of this novel material made of crushed salt and clay still need to be shown. For this study, the behavior of pure crushed salt is assumed for the long term seal. The long term seal is installed over a length of 300 m between the drift seals. The MgO concrete seals themselves have a length of 115 m including the abutments. Figure 19.-2 illustrate the design of the proposed drift sealing system install in the main drifts.

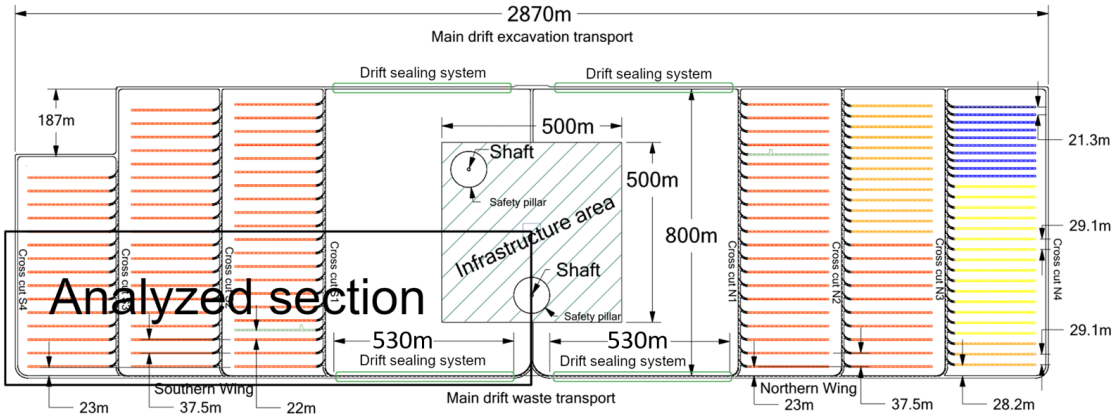

Figure 19.-1: Location of the drift sealing system in the repository mine.

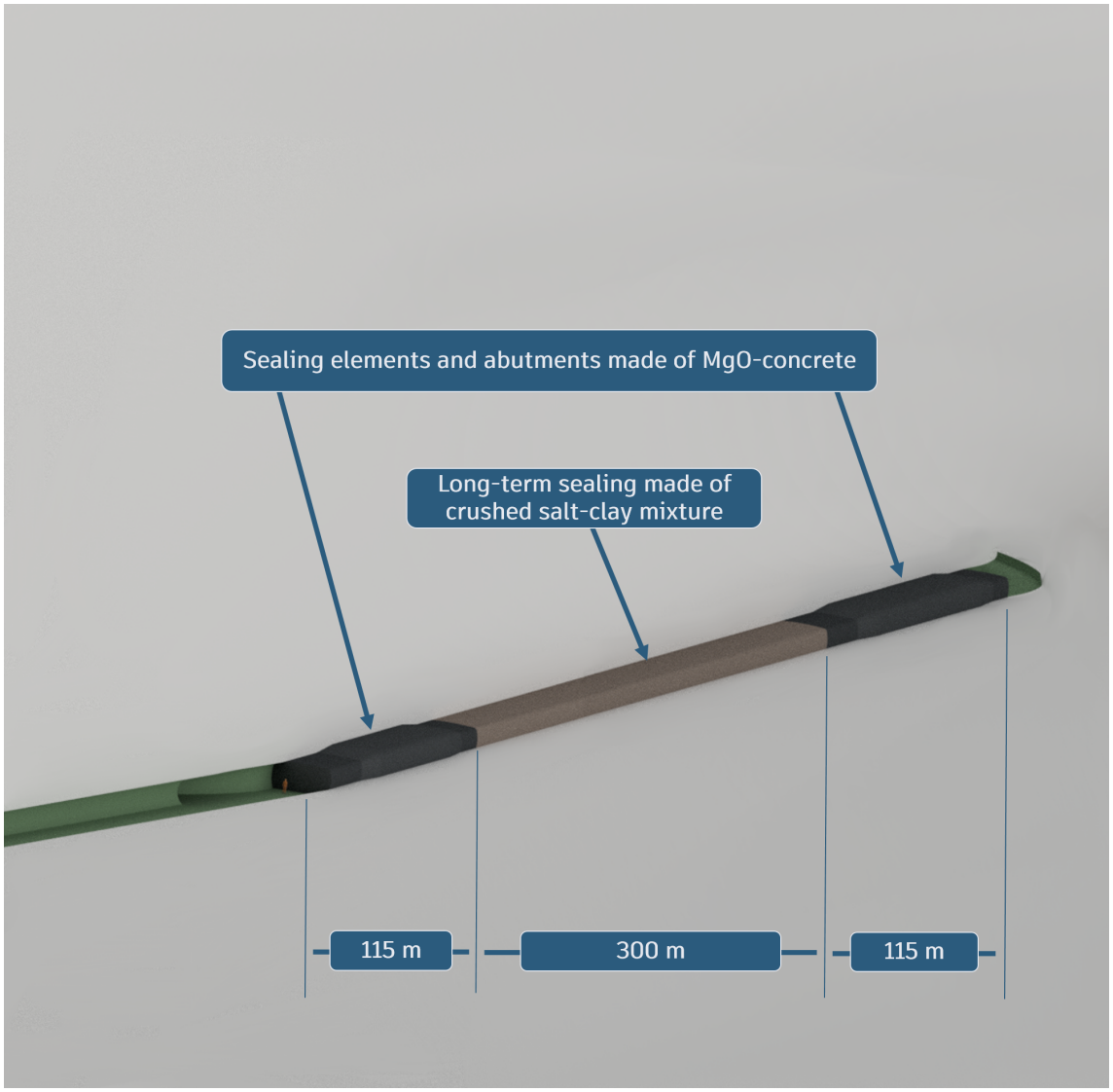

Figure 19.-2: Illustration of the drift sealing concept as designed for the RANGERS case study.

19.3 Modeling cases

The integrity assessment is based on the loads derived from the scenario and Features, Events, and Processes (FEP) development. The FEPs relevant for the mechanical integrity of the EBS were already discussed in Section 14.. These FEPs are summarized again for the drift sealing system composed of the long term seal and the MgO seals in Figure 19.-3.

Thermal expansion and contraction, resulting from heat propagation within the repository, are among the primary loading conditions on the drift sealing system, aside from lithostatic load. The combination of heat flow and the convergence of the surrounding rock leads to mechanical stress changes throughout the repository, creating significant load scenarios that must be accounted for in the integrity assessment. Additionally, time-dependent processes such as swelling, shrinking, and creeping of the MgO-concrete used in the seals affect their resistance and must also be considered.

Over the course of the repository's evolution, hydraulic changes may arise due to gas pressure build-up caused by the compression of enclosed mine air and gas generation (in the reference scenario). Alternatively, a failure of the shaft seal and subsequent water inflow through the shaft or host rock (in an alternative scenario) could also lead to significant hydraulic pressure changes. These hydraulic changes are mainly driven by liquid and gas flow processes and liquid inflow into the repository. Seismic events, such as earthquakes, must also be considered, especially given the long functional lifetime of the EBS (50,000 years), during which even rare events are eventually likely to happen. In the case of gas explosions or deflagrations, the dynamic forces generated would propagate through the rock in a manner similar to that of a seismic event, exerting comparable mechanical stresses on the repository and therefore on the drift sealing system.

The FEPs in gray in Figure 19.-3 are considered not relevant for the integrity proof of the drift sealing system for the following reasons:

- Thermal degradation of carnallite: This process is specific to certain minerals that are not present in the drift seals and in the host rock at the disposal depth, and therefore it does not directly affect the integrity of the sealing system.
- Liquid flow processes: While hydraulic pressure changes are relevant, liquid flow through pathways that do not directly intersect the seals is not a primary concern for the mechanical integrity of the drift sealing system.
- Gas flow processes: Although gas pressure build-up is considered, the actual gas flow mechanisms through other parts of the repository do not significantly impact the integrity of seals.
- Metal corrosion: This is relevant for metallic components within the repository, but not for the drift seals themselves, which are made of MgO-concrete and other non-metallic materials.
- Solution, transformation of clay minerals: This process concerns the alteration of clay minerals, which are not a component of the MgO-concrete used in the drift seals.
- Microbial processes: Microbial activity is unlikely to have any meaningful impact on the structural integrity of the drift seals, as it primarily affects organic materials or metals,

not concrete-based sealing systems.

- Alteration of bentonite: Bentonite, commonly relied upon in other repository designs, is not part of the drift sealing system in this context, making its alteration irrelevant for the seals. The potential alteration of the clay admixture in the long-term seal, although requiring scientific investigation, can be considered negligible given the natural analogues of salt-clay formation deposits that have remained stable over millions of years.
- Colloid generation and filtration: This concerns the behavior of colloidal particles in solution, which does not directly affect the mechanical integrity of the drift seals.
- Dissolution and precipitation of salt minerals: These processes primarily affect the surrounding rock salt and do not directly influence the integrity of the concrete drift seals.
- Asphalt migration: Asphalt is not a material used in the drift seals, and thus, its migration does not affect the integrity of these barriers.

By excluding these gray FEPs, we focus on the processes and scenarios that are expected to have a direct impact on the mechanical integrity of the drift seals and are most critical for the long-term safety of the repository.

From the discussions of the FEPs relevant for the drift seal, one can derive the following modeling cases to be considered in the design and integrity assessment of the drift sealing system:

- Modeling case 1: Thermal-mechanical loading on the drift seals: consideration of the FEPs heat flow, thermal expansion/contraction, mechanical stress changes, and convergence
- Modeling case 2: Thermal-mechanical loading of the drift seals with alteration of concrete: in addition to the already enumerated FEPs, the FEP swelling, shrinking and creeping of MgO-concrete are considered
- Modeling case 3: Thermal-mechanical loading with gas pressure built up: consideration of gas effects acting on the drift seal (FEPs: hydraulic pressure change)
- Modeling case 4: Thermal-mechanical loading combined with an earthquake event
- Modeling case 5: Thermal-mechanical loading with hydrostatic loading following the failure of the shaft seal (alternative scenario)

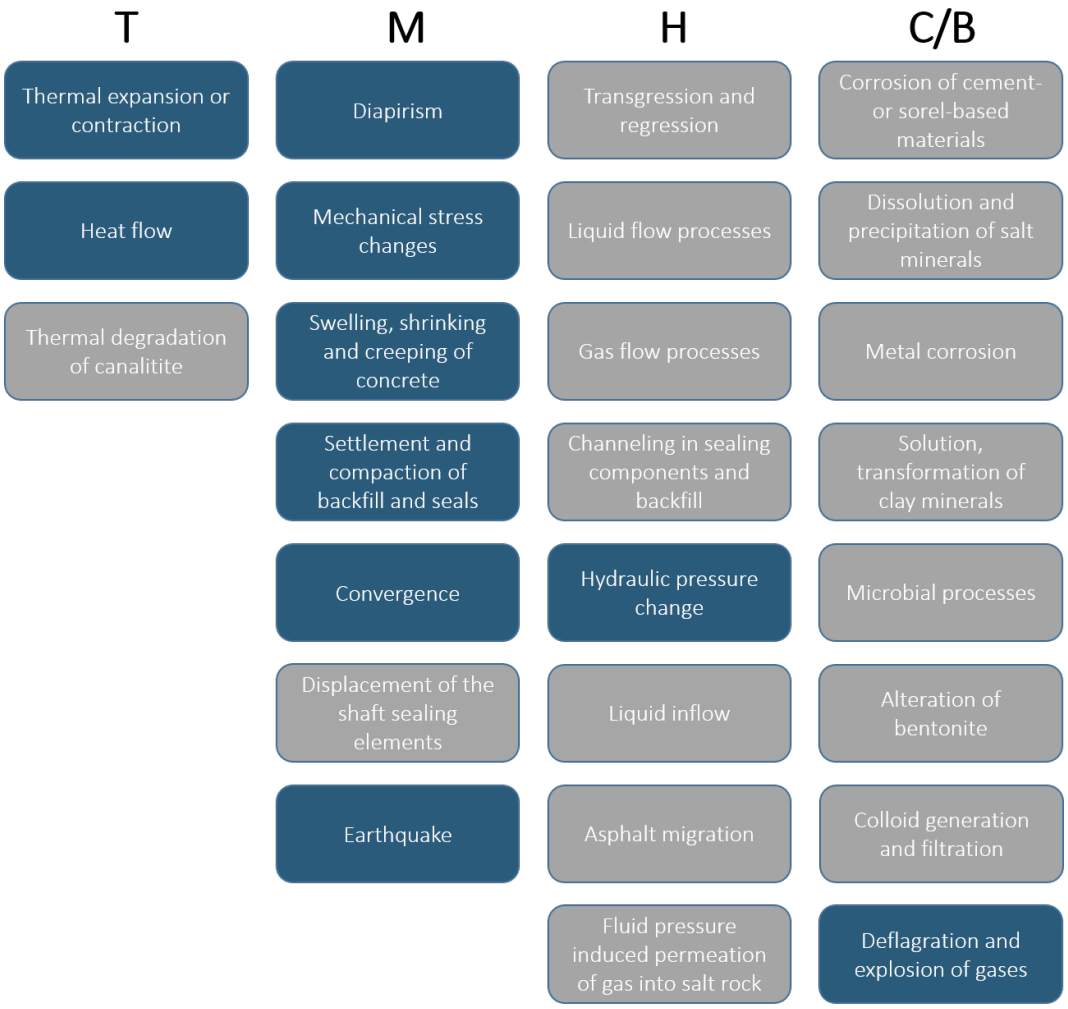

Figure 19.-3: Initial FEPs of relevance for the mechanical integrity proof of the drift seals.

Other modeling cases can be derived as the combination of the selected ones above. The thermal-mechanical evolution, which is the integral effects resulting from gravitational forces, convergence and creep of the host rock as well as the heat propagation, can be considered as the permanent design situation and serves as the basis for combination with other FEPs or modeling cases. The interaction between the drift sealing system and the surrounding rock belongs also to the permanent design situation. Especially, stresses and strains resulting from temperature increases at the contact zone need to be addressed.

In the presence of the adequate constitutive models, the time dependent behavior of the concrete materials can be also added to the permanent design situation. Autogenous swelling of the Sorel concrete is attributed to the construction phases and is therefore not considered. Solution-induced swelling does not occur, as there is only a negligible amount of solution present. (Müller-Hoeppe et al., 2012a).

The (hydraulic) load cases are occurring gradually over the time for the case of gas pressure build up. As the shaft seal is assumed to retain its function over the verification period, an inflow of water followed by a rise of fluid pressure at the edge of the drift seal can only be

considered in the scope of the alternative scenario analysis. The occurrence of earthquakes should also be considered in integrity assessment as such events will probably occur over the considered verification period of time.

In this study, the design and safety assessment will be exemplary demonstrated for the modeling case 1. Additional hydraulic analyses are required before modeling cases 3 and 5 can be analyzed. Adequate constitutive modeling is needed for the modeling of case 2. Dynamic analyses beyond the scope of RANGERS are needed for the seismic simulations in case 4.

19.4 Integrity safety concept and criteria

Five individual verification criteria have been formulated for the demonstration or verification of structural integrity. There are (Müller-Hoeppe et al., 2012b):

- Structural Stability (commonly referred to as “Load-bearing Capacity”)
- Crack Limitation
- Deformation Restriction
- Filter Stability
- Long-term Stability (also known as “Durability”)

As already stated, the drift sealing system is composed of MgO seals with their MgO abutments and the long term seal made of crushed salt-clay mixture. The first two criteria apply for the MgO components and can be combined by using adequate constitutive model for Sorel concrete. This will be described in more detail later on. These two criteria apply also for the contact zone and the EDZ.

The criterion of deformation restriction may be indirectly related to the long term seal if the displacement of the MgO seals serving as abutments for the long term seal, potentially increases the initial volume of the space where the long-term seal is installed. Instead of specifying a displacement limit, the criterion can be checked in an analysis taking into account the interactions between the MgO seals and the long term seal during the compaction process.

The absence of granular material also eliminates the need to verify the filter stability criterion. It should be mentioned that the long term seal made of crushed salt is installed in a granular state. This seal gains its function when it reaches a fully compacted solid state. No need to check the filter stability.

The long-term stability is covered in Chapter 17.

Specific requirements for the geological barriers in § 5 (2) of EndlSiAnfV (2020) applies for the contact zone between the elements of the drift sealing system and the host rock. The contact zone represents a critical path that need to be verified in order to secure the safe containment of the CRZ. Therefore the dilatancy criterion should be verified for the contact zone along the drift sealing system.

19.5 Numerical model

19.5.1 Modeling concept

The numerical model necessary to investigate the evolution of the drift seals accurately represent both the stress development and thermal propagation in the near field of the drift sealing system. Because the thermal sources are located in the emplacement field from which the heat starts to propagate within the repository, it's necessary to have a model that explicitly consider the emplacement fields. Thus, the model must cover an area of several square kilometers while consisting of finite elements that are only centimeters in size in key areas. To handle this complexity, the following simplifications were made.

First, all the drifts in the model are simplified with a rectangular cross-section. The drift seals are instantaneously backfilled. This means that the pouring of the Sorel concrete made seals and the transient effects due to concrete hydration are not considered. The geological units above and below the rock salt formation are coarsely discretized which is sufficient to account for their weight and stiffness. Symmetrical boundary conditions were used, and only a quarter of the repository was modeled. The size of the finite elements varies in the model, ranging from 20 cm in the drift seals and gradually increases in the emplacement fields and in the overburden. The lateral boundaries are 1.5 to 2 km away from the repository, ensuring that minimal boundary effects are expected. The standard displacement and adiabatic boundary conditions were applied to the model boundaries.

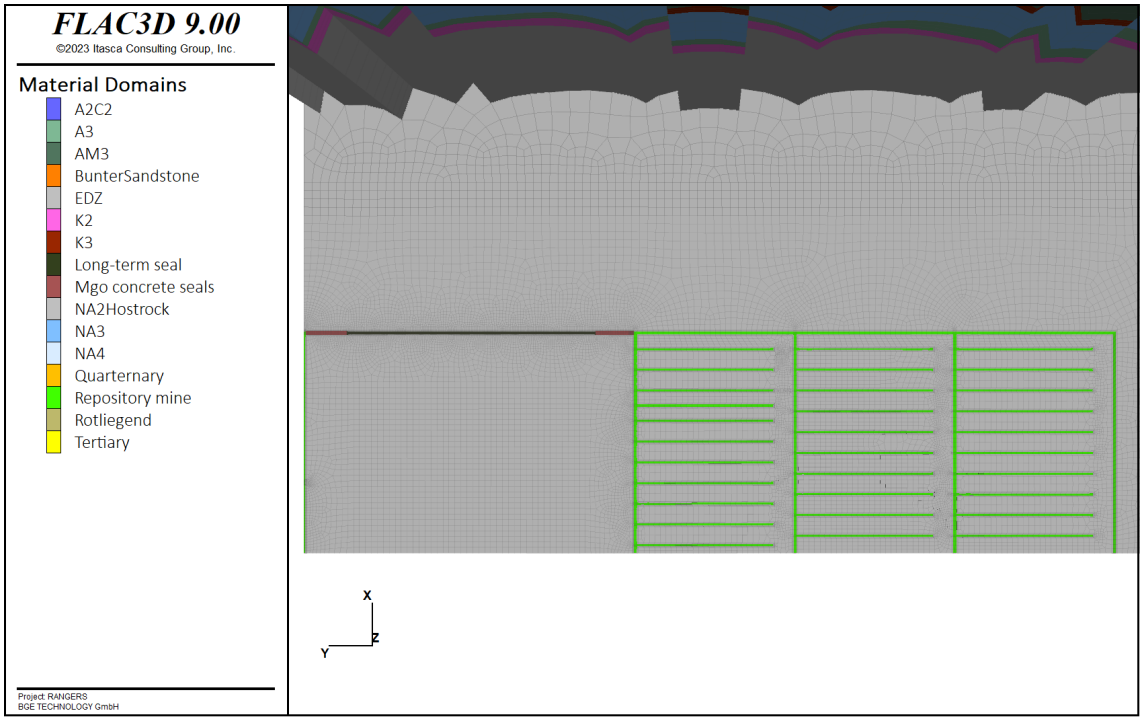

Figure 19.-4: Top view of the numerical model for the analysis of the mechanical integrity of the drift sealing system for the section depicted in Figure 19.-1.

The numerical model considered in this analysis is the one already used for the compaction analysis which also contains the drift sealing system. The cross section of the drift seal in this model consists of 11 by 5 subdivisions. In this model, all the drifts are resolved and are

used as heat sources with the corresponding thermal power of all waste packages disposed in each drift. The model has been already presented in Figure 18.-6. A top view of this model at the level of disposal depth is shown in Figure 19.-4 with an emphasis on the drift sealing system.

The modeling stages account in the simulation starts with the initialization of the primary state. It follows the excavation of the drifts in the mine, which is carried out instantaneously. A sequential backfilling is realized up to the complete closure of the mine. Thus, the main drift remains open over 30 years before the construction of the drift sealing system. Over the time, the convergence of the rock due to creep will compact all materials in the mine. This convergence process is further enhanced by the thermal propagation also considered in the model.

To limit the computational effort, the simulation was carried out thermal-mechanically over 1,200 years. This corresponds approximately to the end of the thermal phase of the repository evolution. Subsequently, the thermal phase is deactivated and the simulation continue in the mechanical process class. This allowed us to speed up the simulation by a factor of 10. The residual heat still present in the model at 1,200 years will enhanced the creeping behavior of the rock leading to more deformations and stresses on the drift sealing structure. This assumption is therefore conservative for the design of the drift seals.

19.5.2 Initial conditions

The drift sealing system is planned at the disposal level at a depth of 810 m in the Staßfurt sequence. An isotropic primary stress state is assumed, with an integral density of the overlying layers assumed to be 2.200 kg/m³. This results in a calculated depth pressure of approximately 18.5 MPa at the level of the disposal level. For the undisturbed rock temperature, the temperature gradient of 3 K/100 m is assumed resulting in a temperature of 33.3 °C at the disposal depth. Similar boundary conditions as used for the previous simulations are also assumed here.

19.5.3 Constitutive models

Different constitutive models are essential to accurately represent the complex behavior of the repository system, with a specific focus on the drift sealing system. Figure 19.-5 illustrates a cross-sectional view of a geological repository, where various geological layers and materials are assigned distinct constitutive models based on their mechanical properties.

The overburden, composed of Quaternary, Tertiary, and Bunter sandstone layers, is modeled using the Mohr-Coulomb failure criterion, appropriate for geomaterials. For the salt formations, different creep laws derived from the WIPP creep law are applied to capture the viscoplastic behavior of the salt under long-term loading conditions. FLAC3D is used for this analysis, the WIPP creep law is implemented in it already.

The main anhydrite layer, which is typically found in a fractured or broken state due to stresses caused by salt diapirism, is modeled using a reduced stiffness to reflect its fractured nature. Its plastic behavior is also simulated using the Mohr-Coulomb model, which is suitable for materials that undergo shear failure under stress.

The underburden below the salt is treated with an elastic constitutive model. Since this region is located far from the point of interest — the drift sealing system — modeling it elastically is a sufficient and efficient approximation for the purposes of this analysis.

Table 19.-1 summarizes the different constitutive models for the geological layers with their elastic material properties. The recommended creep classes for the different salt layers are given in Table 19.-2. The parameters for the creep laws BRGa and BGRb are summarize in Table 19.-3 and in 19.-4. The Mohr-Coulomb parameters of the overburden layers and main anhydrite can be found in Table 19.-5.

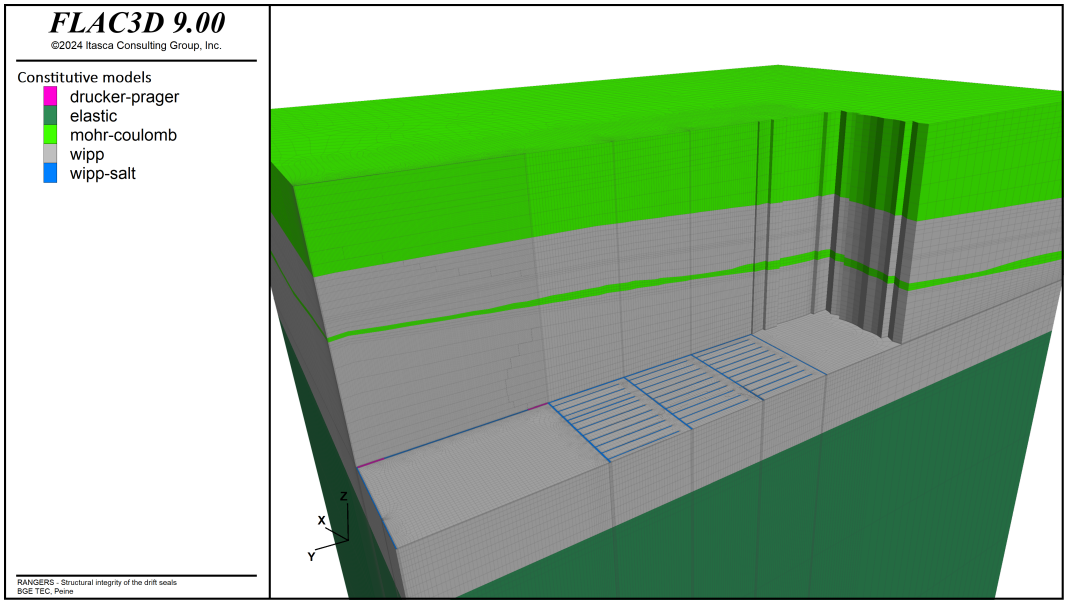

Figure 19.-5: Distribution of constitutive models used in the numerical model for the integrity assessment of the drift seals.

Table 19.-1: Mechanical properties and density of geological layers (Liu et al., 2017).

Model zones	**Symbol**	**Constitutive Model**	**Density** ρ (kg/m^3)	**Young's modulus** E (GPa)	**Poisson ratio** ν
Quaternary	Q	Mohr-Coulomb	2000	0.1	0.33
Tertiary	T	Mohr-Coulomb	2100	0.5	0.33
Bunter	S	Mohr-Coulomb	2500	15	0.27
Aller rock salt	NA4	wipp, BGR[a]	2235	25	0.27
Anhydritmittelsalz	AM3	wipp, BGR[a]	2275	30	0.27
Potash seam Ronnenberg	K3	wipp, BGR-SF	1850	16	0.26
Leine rock salt	NA3	wipp, BGR[a]	2160	25	0.25
Main anhydrite	A3	Mohr-Coulomb	2700	60	0.25
Potash seam Staßfurt	K2	wipp, BGR-SF	1850	17	0.28
Staßfurt rock salt	NA2	wipp, BGR[b]	2160	33	0.25
Anhydrite/carbonate	A2/C2	elastic	2700	30	0.27
Underlying red	R	elastic	2500	17	0.27

Table 19.-2: Recommended formula for geological zones (Liu et al., 2017).

Homogeneous zones	**Symbol**	**Recommended formula (with Prefix Factor)**
Aller rock salt	NA4	$\frac{1}{8} \cdot$ BGR[a]
Anhydritmittelsalz	AM3	$\frac{1}{16} \cdot$ BGR[a]
Potash seam Ronnenberg	K3	BGR[a]
Leine rock salt	NA3	$\frac{1}{4} \cdot$ BGR[a]
Potash seam Staßfurt	K2	BGR-SF
Staßfurt rock salt	NA2	$2 \cdot$ BGR[b]

Table 19.-3: BGR[a] parameters for rock salt (Liu et al., 2017).

Material parameter	**Symbol**	**Value**	**Unit**
Gas constant	R	8.31441	[J/mol*K]
Activation Energy	Q	5.40E+04	[J/mol]
WIPP_Model constant	A	0	[-]
WIPP_Model constant	B	0	[-]
Critical steady-state creep rate	-	-0.01	[1/s]
Structural factor WIPP_Model constant	D	0.18	[MPa^{-n} d^{-1}]
WIPP_Model exponent	n	5	[-]

Table 19.-4: BGR[b] parameters for rock salt (Liu et al., 2017).

Material parameter	**Symbol**	**Value**	**Unit**
Creep rate	crfac	$2 * 5.872$	[-]
Activation Energy	Q1	4.20E+04	[J/mol]
Activation Energy	Q2	1.13E+05	[J/mol]
WIPP_Model constant	A	0	[-]
WIPP_Model constant	B	0	[-]
Critical steady-state creep rate	ε_{dot}	-0.01	[1/s]
Structural factor D	dwipp	0.18	[-]
WIPP_Model constant	d1wipp	2.30E-04	[MPa^{-n} d^{-1}]
WIPP_Model constant	d2wipp	2.10E+06	[MPa^{-n} d^{-1}]
WIPP_Model exponent	nwipp	5	[-]

Table 19.-5: Mohr-Coulomb parameters of the overburden layers and main anhydrite (Liu et al., 2017) (Bollingerfehr et al., 2018).

Homogeneous zones	**Symbol**	**Cohesion, c** [MPa]	**Friction angle,** ϕ [°]	**Tension limit,** σ_t [MPa]
Quaternary	Q	2	27.5	0.1
Tertiary	T	5	30	0.1
Bunter	S	4	15	0.1
Main anhydrite	A3	20	35	0.1

The repository mine will be backfilled with crushed salt. It is also planned to use a mixture of crushed salt and clay for the main sealing element in between the Sorel concrete seals. In the absence of experimental data and model available to describe this novel material, we assume for the time being that the behavior of this material is similar to crushed salt (but it will likely have lower permeability at early times). In this regard, the crushed salt model presented in Table 18.-3.

An advanced constitutive model for Sorel concrete has been developed at BGE and BGE TECHNOLOGY for the license application of the Morsleben mine. This model assumes a Drucker-Prager yield surface for plasticity. The viscoelastic part of the model is described rheologically by the Burgers model. The Burgers model consists of a Maxwell element and a Kelvin element. The Maxwell element is a series connection of spring and damper elements and describes the instantaneous elasticity along with the basic creep, while the Kelvin element is a parallel connection of spring and damper elements and describes the transient creep. The deformation processes taken into account in the model is presented in Figure 19.-6. An associated thermal part is described in (Itasca Consulting Group, Inc., 2021). The solution of thermal and mechanical process classes is based on a weak coupling, meaning there is not a single system of equations to be solved, but rather two separate systems of equations, each solved independently. The model has been validated against experimental data, see Figure 19.-7.

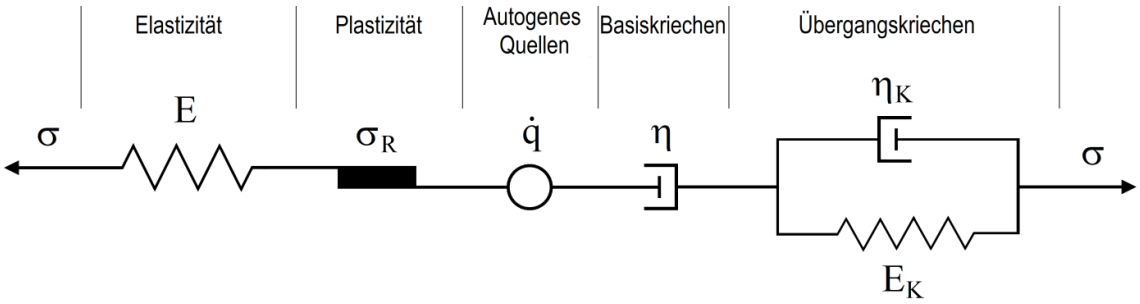

Figure 19.-6: Rheology of the constitutive model M2 for Sorel concrete.

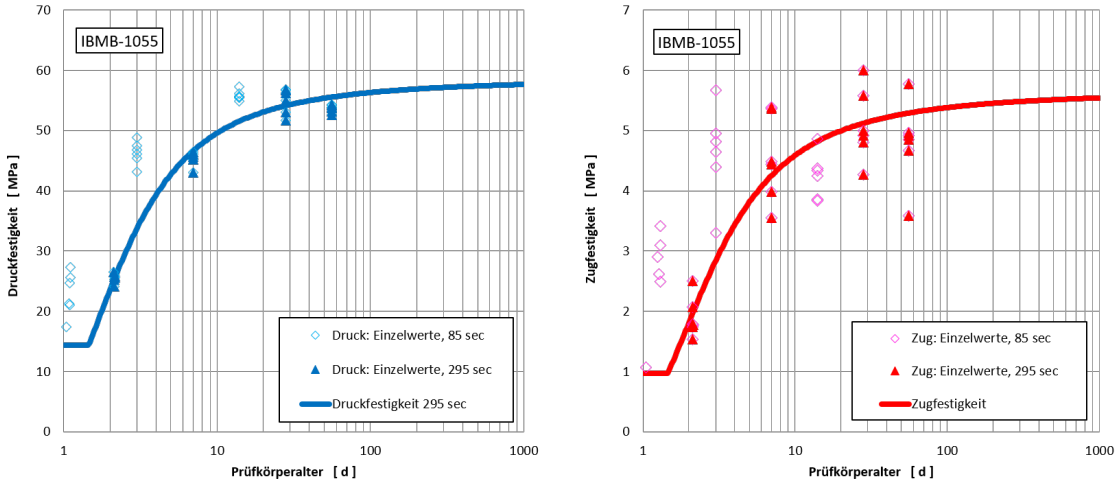

Figure 19.-7: Comparison between the model computation of compressive and tensile strength against experimental data for Sorel concrete.

The present analysis does not consider the transient effects occurring in the Sorel concrete

from the pouring of the seal to its hardened state. We focus only on the long-term evolution which is relevant for the safety case. In this case, the Drucker-Prager model from which the model is based can be used for this analysis. We therefore extracted from the initial model the Drucker-Prager parameters representing a concrete strength after 56 days which represent the long term strength of the Sorel concrete, see Table 19.-6. Further increase of concrete strength as it can be seen in Figure 19.-7 are conservatively neglected.

Table 19.-6: Drucker-Prager mechanical properties for Sorel concrete.

Property	**Value**
Density, ρ [kg/m^3]	1,900
Young's modulus, E [MPa]	20,333
Poisson's ratio, ν, [-]	0.372
Bulk modulus, K [MPa]	26,475.26
Shear modulus, G [MPa]	7,409.985
Friction-drucker, φ_φ	1.43
Cohesion-drucker, k_φ	5.6
Dilation-drucker, d_ψ	0
Tension limit, σ_t [MPa]	1.76

19.6 Numerical results

The loads acting on the drift sealing structures are the results of the thermal-mechanial evolution of the repository system. In order to understand how does load evolve, we will describe how each variable is evolving over the time.

19.6.1 Global displacements

The impacts of heat generated by the radioactive waste is one of the primary processes, alongside excavation-induced stress redistribution, that significantly affects the repository system. This was discussed in detail in chapter 16.. The impact of heat propagation on the displacement evolution at the disposal level is illustrated in Figures 19.-8, 19.-9, and 19.-10.

Figure 19.-8 presents the y-displacement in space at three times. Due to the heat generated in the disposal drifts, thermal expansion causes the surrounding rock to expand, which is evident from the displacement patterns in the first and third emplacement fields. The first emplacement field, located on the right side of the image, shows a clear expansion of the rock mass away from the emplacement. This results in displacement opposite to the y-axis for the first emplacement field, while for the third emplacement field, the displacement occurs along the positive y-axis.

In contrast, the second emplacement field shows minimal expansion. This is because the expansion of the adjacent first and third emplacement fields constrains the second field, effectively canceling out any significant deformation.

Over the time period from 100 to 1,400 years, the expansion of the rock mass becomes more pronounced, reaching its peak when the temperature is at its highest, as shown in Figure 16.-7. As the temperature starts to decrease, the expansion subsides, and the displacement gradually reduces.

The displacement along z-direction in Figure 19.-9 shows that the thermal expansion will cause an uplifting of the rock mass towards the surface. This uplifting process is concentrated over the emplacement fields and does not significantly affect the location where the drift sealing system is installed. Although the uplifting is still ongoing in the middle of the formation at 1,400 years, a recovery (i.e., decrease of displacement) can be observed at the disposal level at the emplacement fields between the time points of 700 and 1,400 years. Along the main drift, negative values of displacement (subsidience) are observed. They indicate the convergence of the rock compacting the crushed salt and long term seal in the drift.

The displacement along the x-direction, as shown in Figure 19.-10, highlights the effect of thermal expansion in that axis. Similar to the y-displacement, the rock mass expands at the disposal level, with the largest displacements occurring at the boundaries of the emplacement fields along the x-axis. This expansion extends towards the region where the drift sealing structures are installed, though moderate displacement values are observed there, gradually decreasing as the distance from the emplacement fields increases.

Notably, no displacement is seen at the center of the emplacement field located at the front of the model, which serves as a symmetrical boundary. At the top of the formation, significant displacements in the x-direction are observed, which result from the uplift process occurring in the z-direction. The presence of the anhydrite layer—a non-creeping material with high stiffness—appears to decouple the mechanical processes in the repository mine from those at the top of the formation.

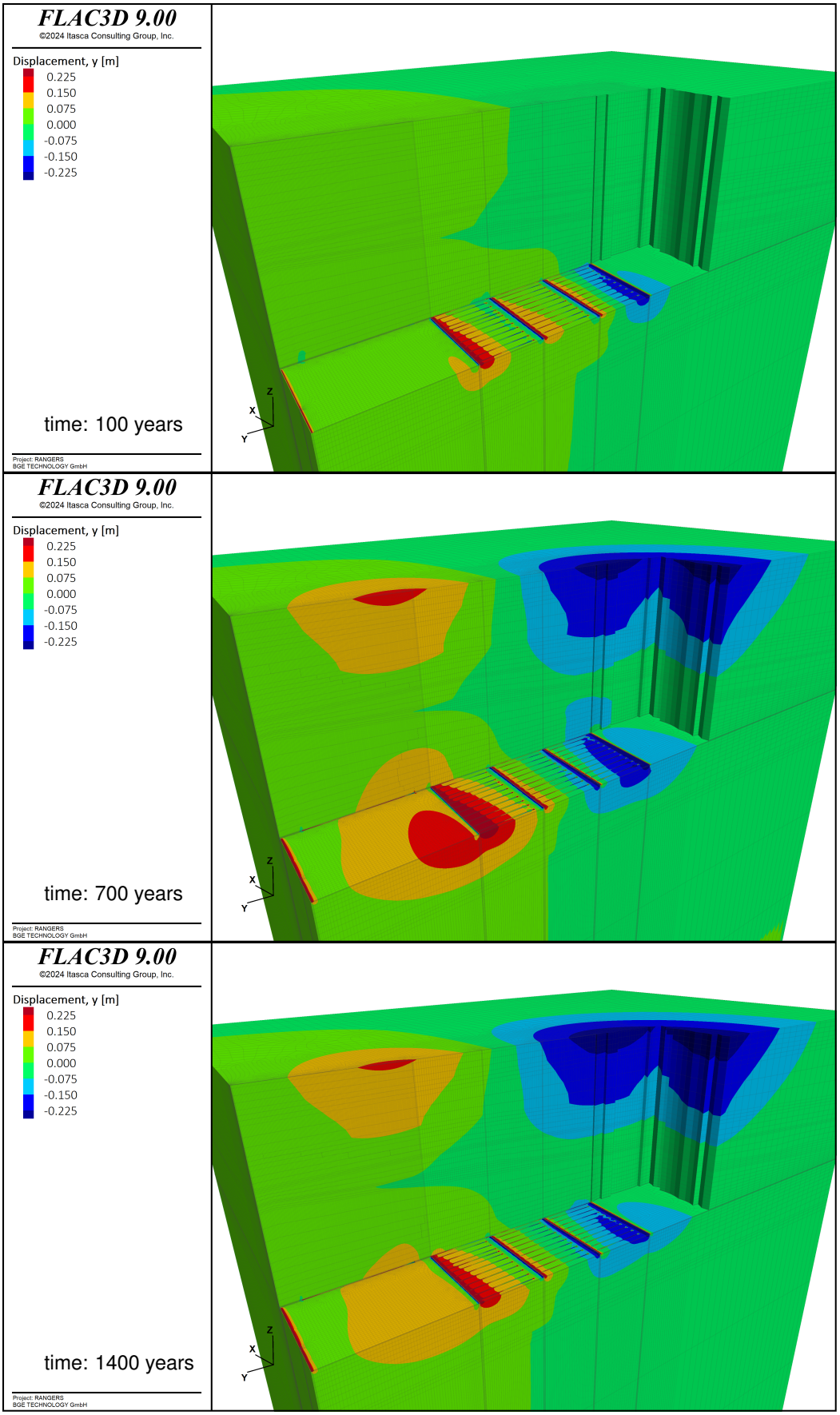

Figure 19.-8: Displacement distribution along the y-axis over time.

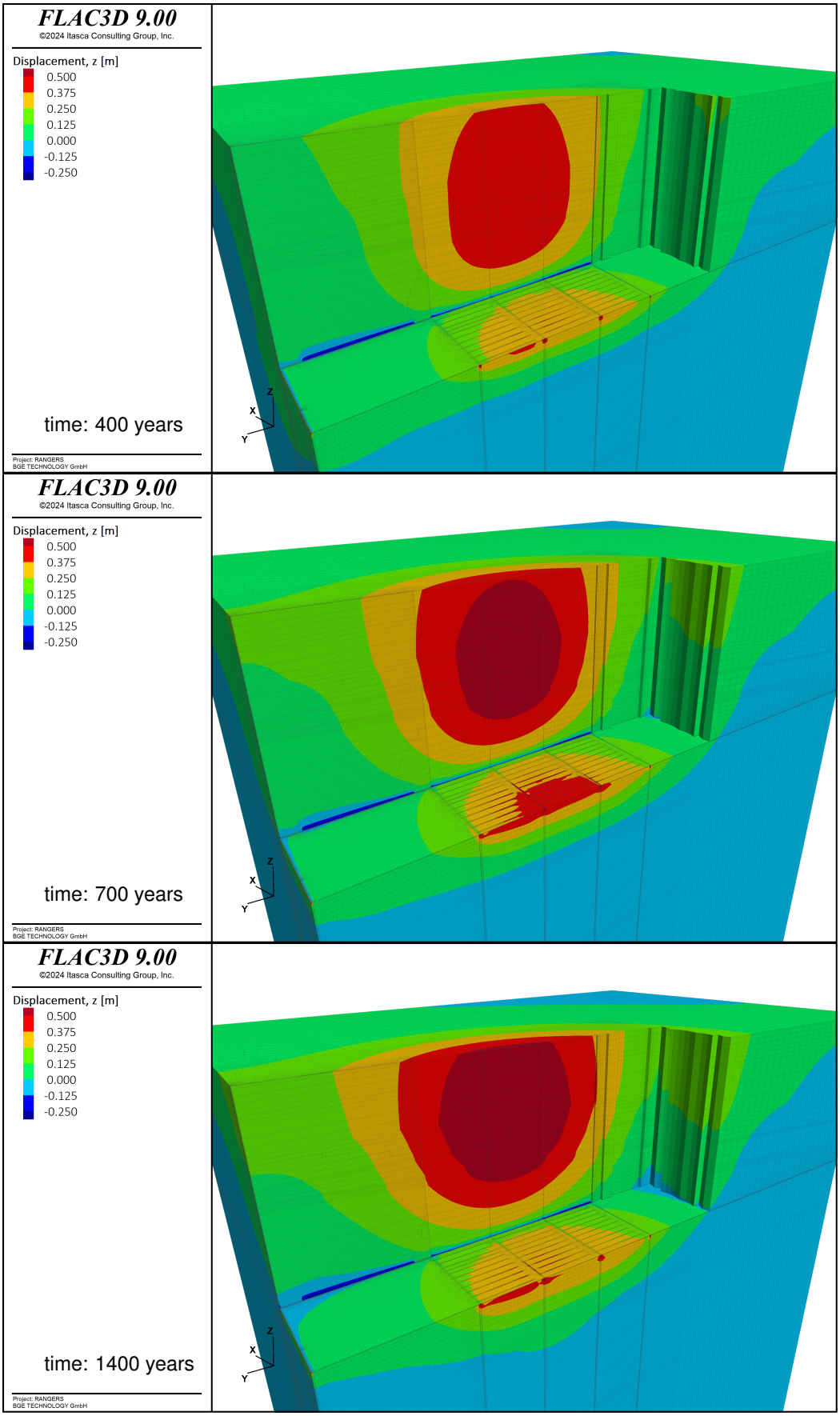

Figure 19.-9: Displacement distribution along the z-axis over time.

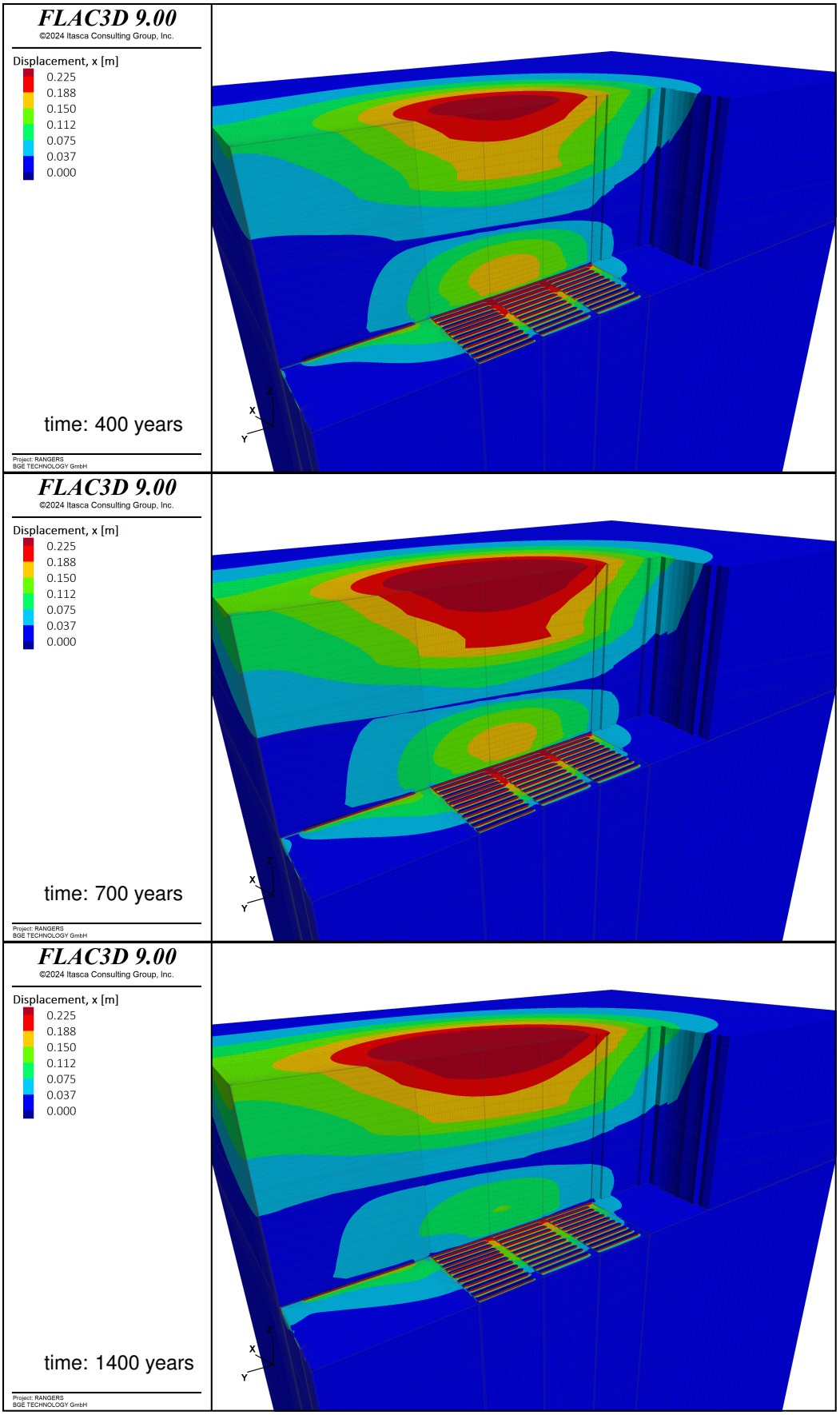

Figure 19.-10: Displacement distribution along the x-axis over time.

19.6.2 Displacements and strains in the seals

Figure 19.-11 illustrates the displacement vectors around the first Sorel concrete seal near the emplacement fields at the disposal level. The vectors represent the projected displacements on the x-y plane, with the z-component excluded. As shown in the figure, the rock mass predominantly moves in the y-direction at the level of the seal. This movement becomes most pronounced at around 700 years, coinciding with the peak temperature in the repository. At 100 years, there is minimal rock mass movement near the seal, as indicated by the small size of the vectors. By 1,600 years, the rock mass continues to move in a similar direction as at 700 years, but the smaller vector size suggests that the velocity of this movement is gradually decreasing. Due to the viscous and creeping nature of salt, which causes it to deform more rapidly than the stiffer concrete seal, it can be anticipated that rock mass movement will generate lateral skin forces along the surface of the seals. These skin forces, in turn, induce tensile loading in the seals.

This phenomenon is also observed in geotechnical applications to pile foundation. The so called negative skin friction (negative Mantelreibung in German) is a phenomenon that occurs in pile foundations when the surrounding soil settles and exerts a downward frictional force on the surface of the pile. Normally, the skin friction between the pile and the soil acts upwards and helps support the load carried by the pile. However, in certain conditions, this friction reverses, becoming negative, and adds an additional load on the pile rather than providing support. The settling of the surrounding soil generates a downward force along the pile's surface. This downward force acts against the pile, essentially pulling it down by applying a tensile force.

To test this hypothesis, we closely examine the displacement experienced by the seals over the course of the simulation. Table 19.-7 and Table 19.-8 display the displacement along the y- and x-directions, respectively, for the two drift seals — one located near the shaft and the other near the disposal side. In Table 19.-7, it is evident that the seal near the emplacement fields experiences greater displacement compared to the seal near the shaft. For both seals, displacement increases from the disposal to the shaft side, creating a heterogeneous distribution. This uneven displacement leads to an elongation or extension of the seals. For the seals to experience this extension, they must be subjected to tensile stresses, thereby validating the hypothesis.

The seal near the disposal side exhibits a maximum elongation ranging from 12 to 15 cm, occurring between 500 and 600 years after the disposal of radioactive waste. This period coincides with the thermal peak in the repository, as previously mentioned. Meanwhile, the extension of the seal near the shaft is more moderate, with the maximum displacement not yet reached even after 1,400 years.

In Table 19.-8, where the displacements of the seal along the x direction is displayed, a more homogeneous displacement distribution is observed. Here also the seal at the disposal side experiences higher displacement compare to the seal at the shaft side. The observed displacements may result also into an extension along the width of the seal. This is however limited to less than 2.5 cm for both seals. This also confirm the observations gained from the displacement vectors in Figure 19.-11 where it has been shown that the seals are mostly stressed along the y direction.

The extension of the seals discussed above can also be observed in the strain distribution within the seals, as shown in Table 19.-9, which presents the maximum principal strain in both seals over time. Only positive strain values are computed, indicating extension. Higher strain levels are reported in the center of the seal compared to the boundary regions, likely due to the tight contact with the surrounding rock. The maximum strain in the main part of both seals is less than 7.5×10^{-3}. This value remains constant over the time up to 1,400 years indicating that the rock mass movements around the seals are still active.

However, the highest strain values are observed at the edges of the seal, which is a numerical artifact. This occurs because, in the model, the seal is rigidly connected to the crushed salt. As the crushed salt compacts due to convergence, tensile forces develop at the interface with the seal, as the seal cannot accommodate the deformation of the compacting salt. This results in elevated strain at the ends of the seal.

To address this effect, interface elements or similar numerical techniques should be used to prevent such artifacts. Nonetheless, these high strain values remain localized at the seal edges and do not propagate further into the seal over time.

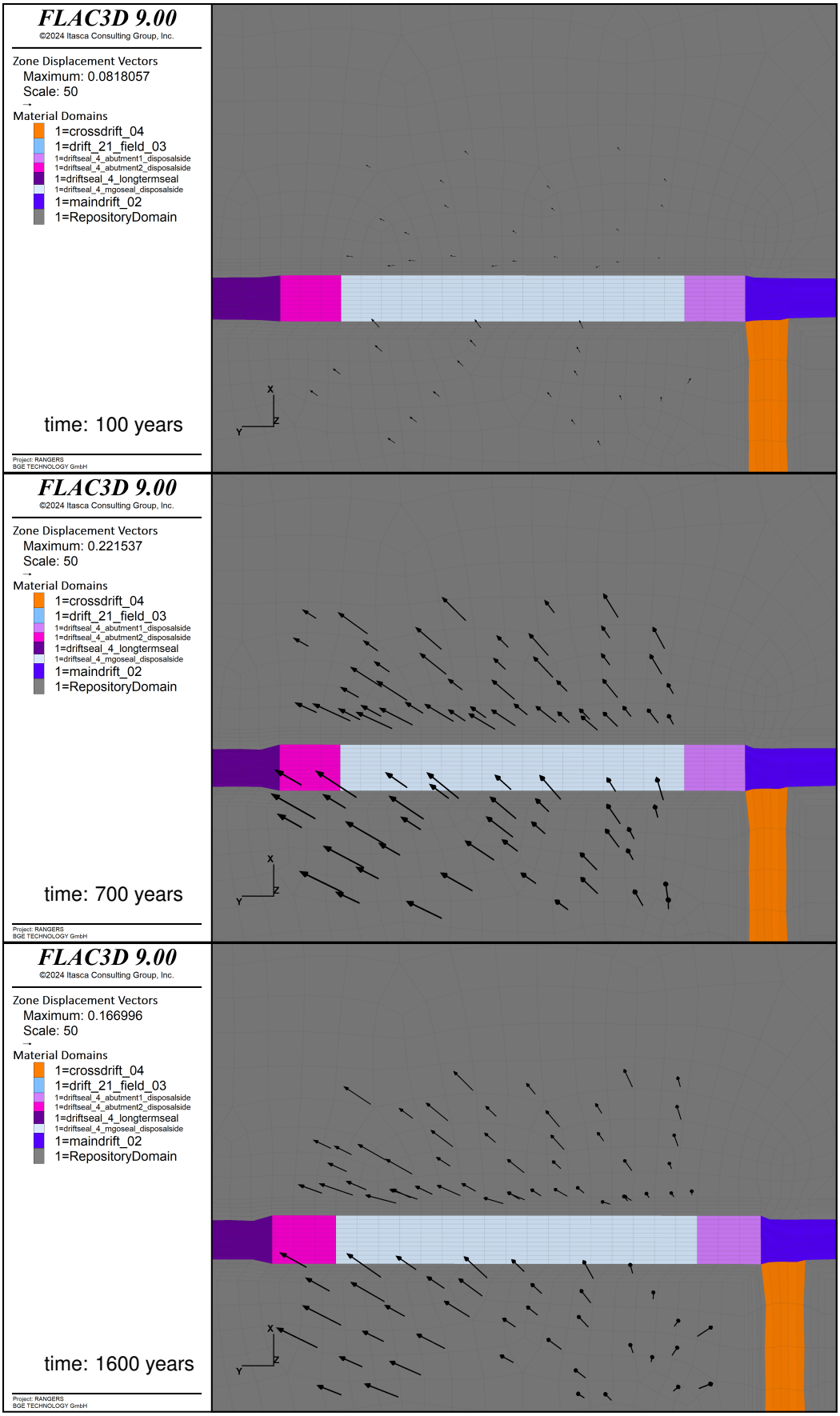

Figure 19.-11: Displacement vectors around the seal over time. Refer to Figure 19.-4 for the seal's position within the repository.

Table 19.-7: Displacement distribution in the drift seals along the y-axis over time. y-axis is along the

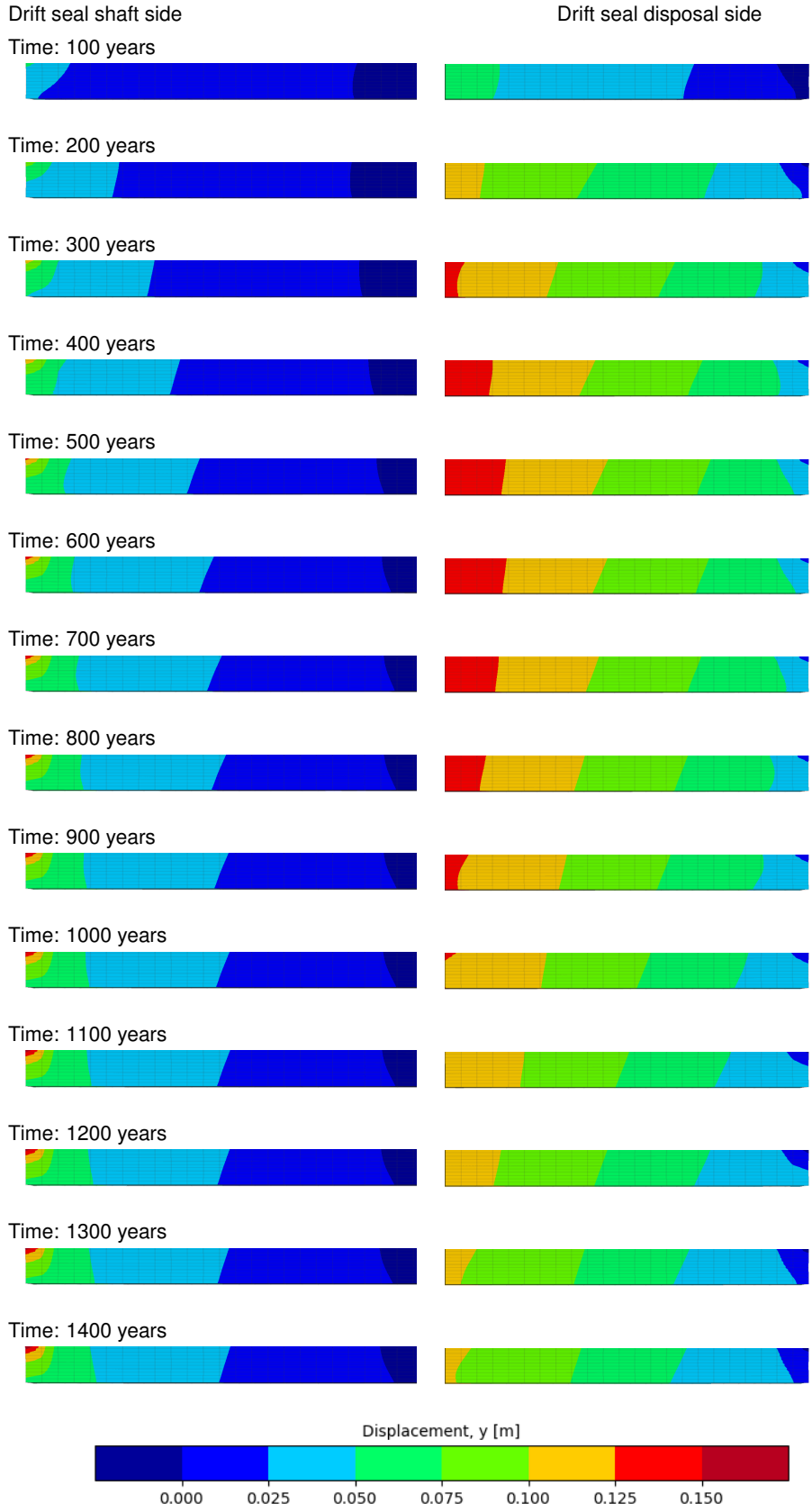

Table 19.-8: Displacement distribution in the drift seals the x-axis over time.

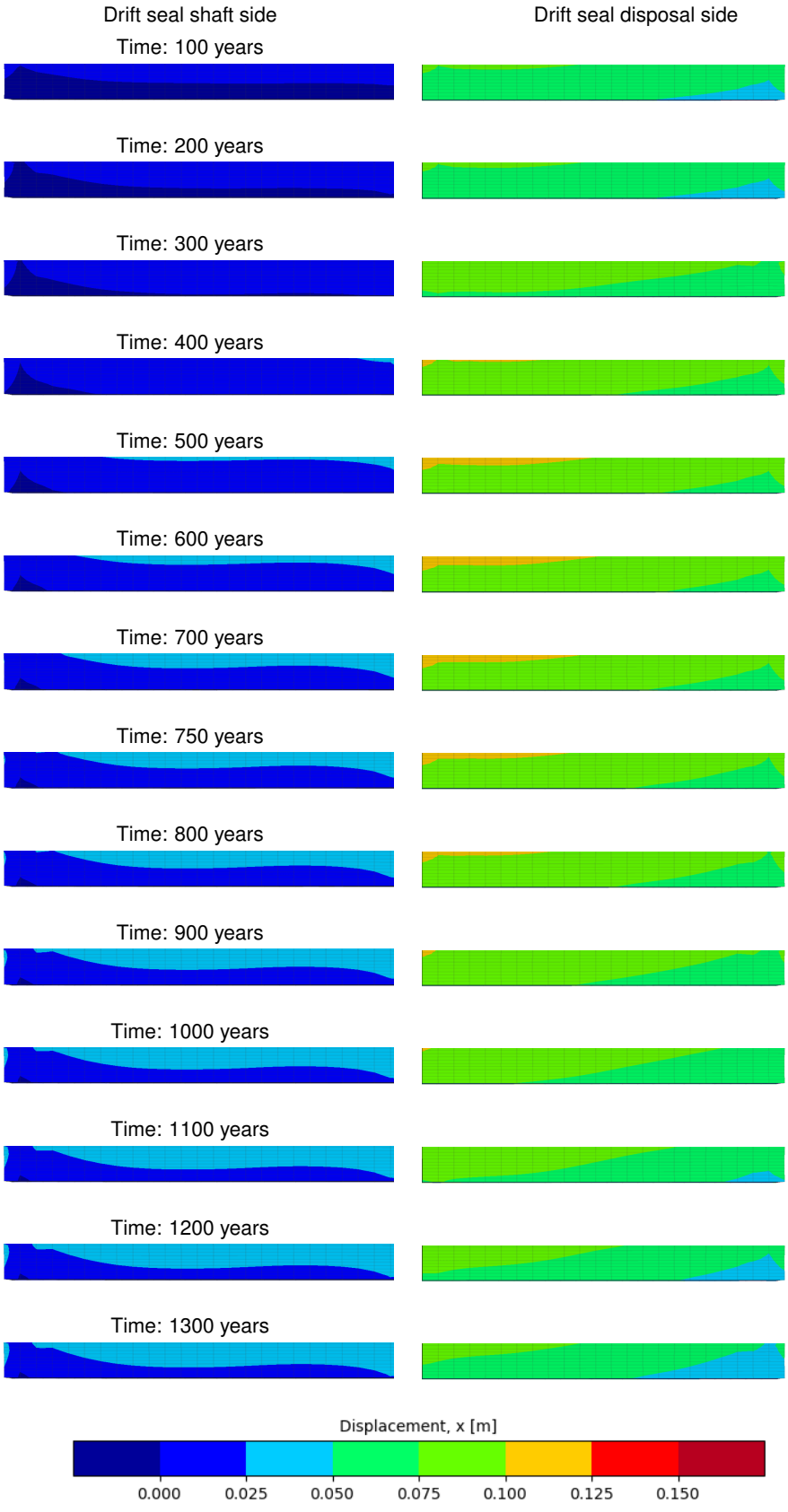

Table 19.-9: Strain distribution in the drift seals over time.

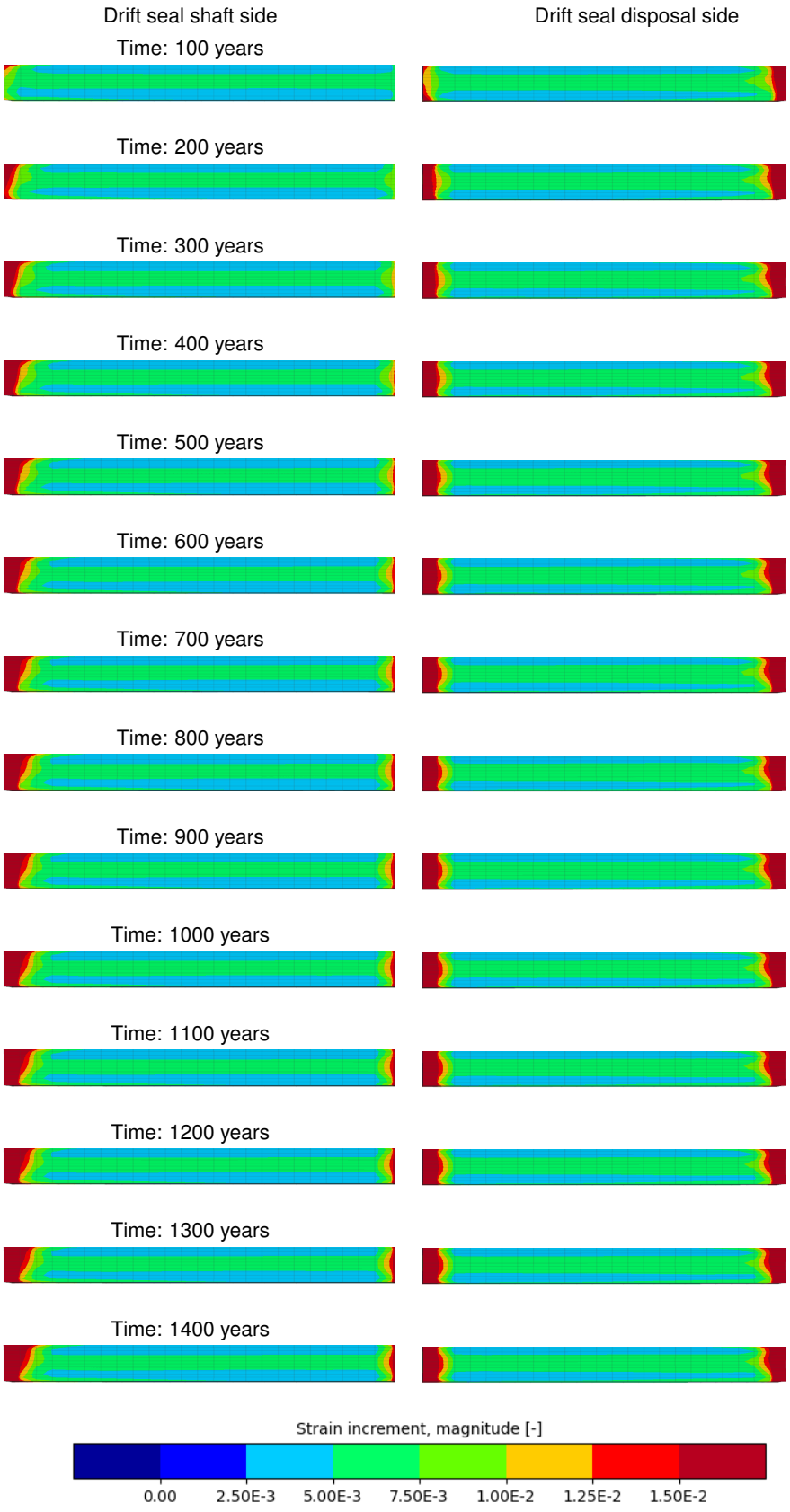

19.6.3 Stresses in the seals

The stresses responsible for the observed extension of the seals are exemplified in Figure 19.-12, which shows the distribution of the maximum principal stresses in the seal, along with the vectors indicating the direction of these stresses. It is clearly noticeable from the figure that the maximum principal stresses are primarily in the tensile region at the evaluated time, and their direction aligns with the y-axis — the same direction in which the extension of the seal has been observed. These findings further support the hypothesis that thermal expansion of the rock mass induces skin forces at the seal boundaries, leading to the development of tensile stresses and, consequently, the extension of the seals.

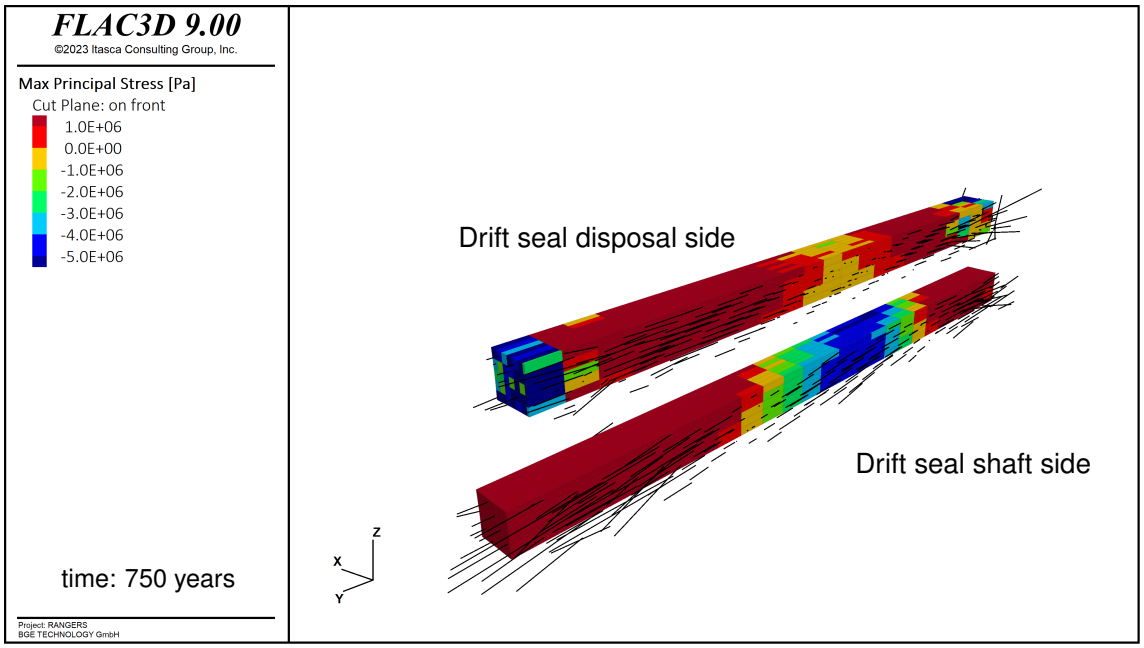

Figure 19.-12: Maximum principal stress distribution and vectors in the drift seals at 750 years.

The stresses in the seals resulting from the rock mass expansion are shown in Table 19.-10, which illustrates the evolution of maximum principal stresses in both seals at several time points. As can be expected, tensile stresses develop in the seals. The seal located near the disposal side experiences higher stress compared to the one near the shaft, due to its proximity to the heat source, where thermal expansion is more pronounced.

In the early stages of the simulation, tensile stresses begin to form at both ends of each seal. Over time, these stresses propagate toward the center of the seals. By around 800 years, the entire seal at the disposal side is subjected to tensile stresses, with this condition intensifying until around 1,400 years, when stresses exceed 1 MPa in the center. A recovery begins at the seal ends around 500 years, where the seal gradually returns to a state of compression.

The behavior of the seal near the shaft is similar to that of the seal near the disposal side, with tensile stress accumulation observed at the edges. However, unlike the disposal-side seal, there is no propagation of tensile stresses toward the center. This indicates that the thermal expansion of the rock mass near the shaft is insufficient to significantly impact the seal further. The stress state remains largely unchanged from 500 years onward, except for a stress recovery observed at the right end of the seal.

Table 19.-10: Maximum principal stress distribution in the drift seals over time.

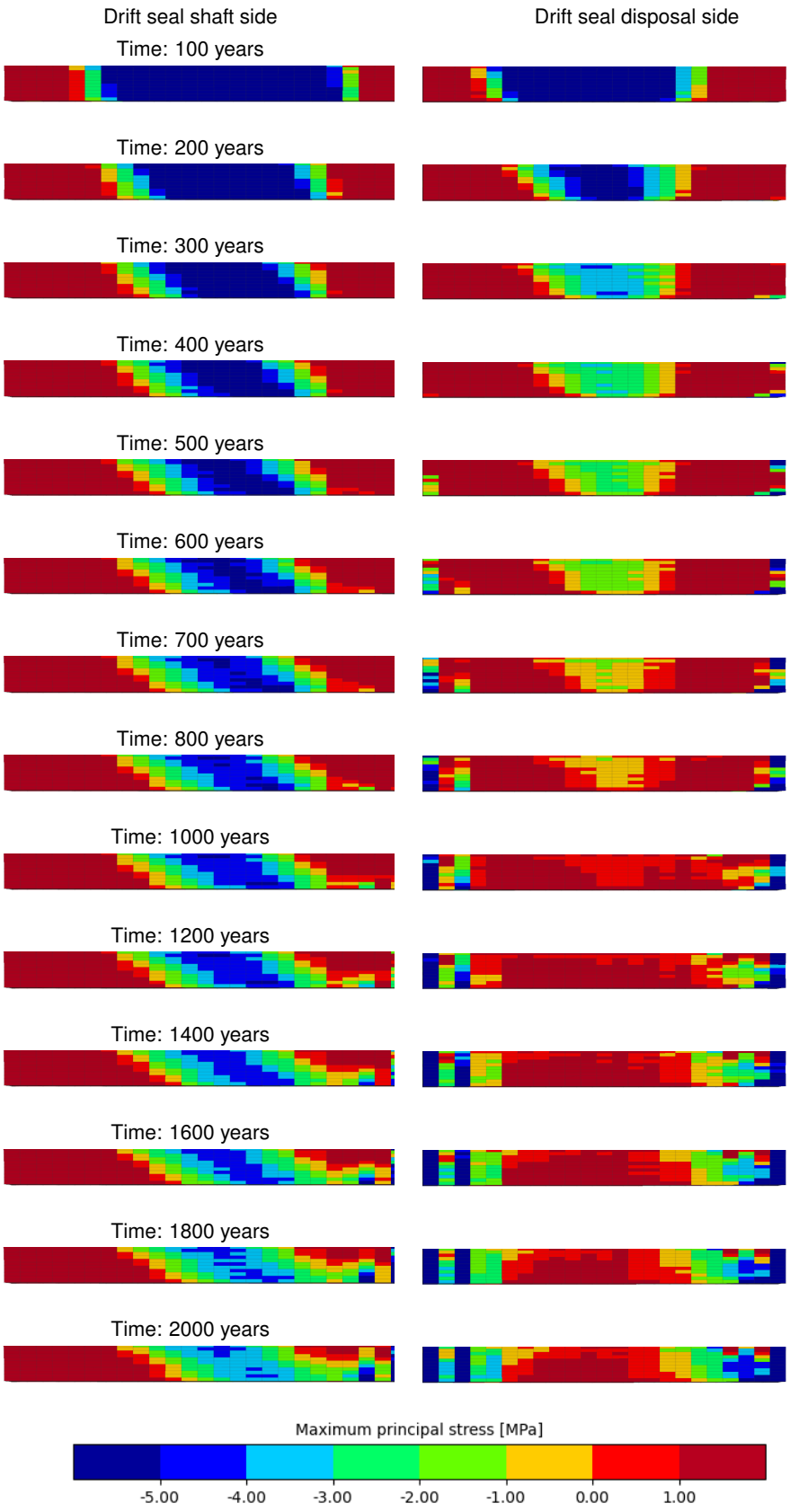

19.7 Verification of integrity

To assess the integrity of the drift sealing structure, the verification criteria discussed in section 19.4 need to be evaluated. Those criteria are Structural Stability, Crack Limitation, Deformation Restriction, Filter Stability and Long-term Stability. Additionally, the dilatancy criterion is considered to verify that the contact zone remain tight along the drift sealing system over time.

The performance of the long term seal was already discussed in section 18.4. There has been already shown that the long term seal will gain its function quite early in the repository lifetime. From the criteria mentioned above, the deformation of the seals that constrain the long term seal may affect its performance. This is fortunately not the case as the compaction of the long term seal as presented in section 18.4 already account for the deformation of the seals discussed in section 19.6.2. Both analyses were combined in a single simulation. This means the the deformation experienced by the seals did not have a negative effect on the compaction evolution of the long term seal

For the seals, we use a qualified constitutive material model that has been validated and calibrated against experimental data. The evaluation of the damage state of the sorel concrete based on this model allows us to quantify the criteria of structural stability and crack limitation.

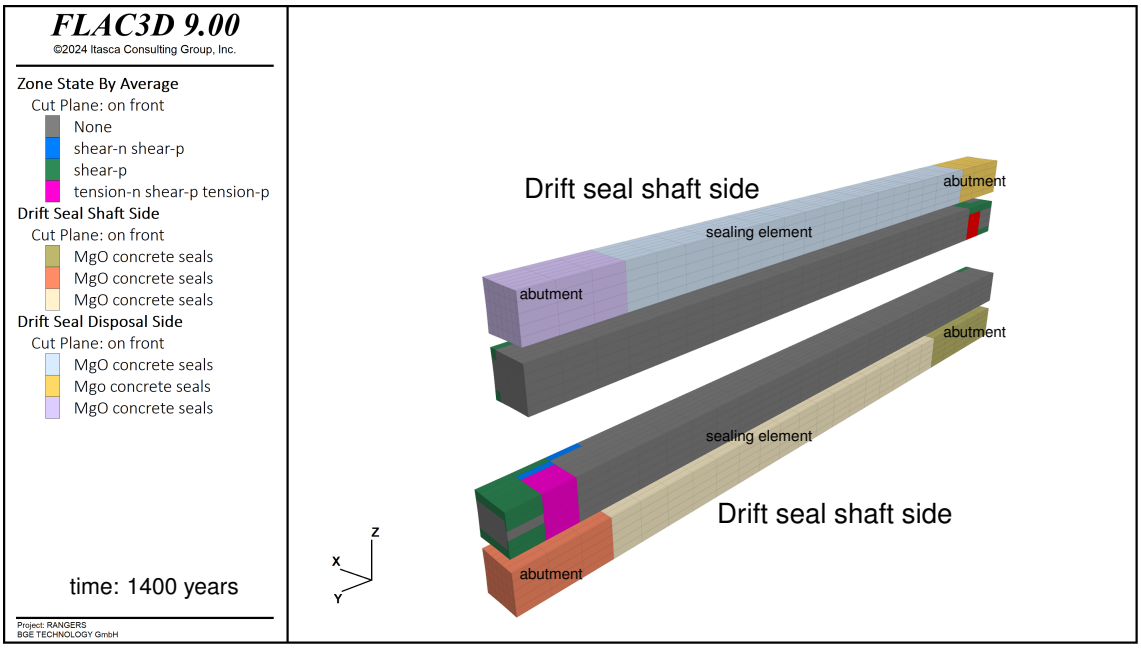

Figure 19.-13: Plasticity state in the drift seals at the end of the simulation.

Figure 19.-13 illustrates the damage in the seals due to the thermal-mechanical behavior of the surrounding rock mass, shown along a vertical cut through the middle of the seal. As observed, the damage is confined to the ends of the seals. This damage results from the numerical artifact previously identified in the strain distribution, caused by the rigid (elastic fixed) contact assumption between the seal and the crushed salt. As the crushed salt compacts, it exerts traction on the seal that would not occur in reality. As previously discussed, using interface elements or introducing thin layers with weak thickness would better model the interaction between the seal and crushed salt.

It is also important to note that the damage is located in the abutment sections of the seal, which do not serve a sealing function but instead protect the sealing section, which remains undamaged. The amount of damage in the abutments is particularly related to the coarse mesh used for this analyses. This was necessary to limit the computational effort for the analysis. Using a finer mesh will to reduce the amount of damage in the abutments. This damage must be concentrated at the interface to the crushed salt. As already mentioned. By employing an adequate numerical technique to realistically modeled the interface crushed salt/Sorel concrete, one should not expect any damage at all.

Although the seals are subjected to tensile stresses (up to 1 MPa), these stresses are not sufficient to cause any damage. As stress recovery progresses toward the compressive regime and the repository continues to cool, no further damage is expected in the long-term evolution of the repository. On the contrary, due to the compressive stresses that the seals will experience in the long term, the triaxial strength of the Sorel concrete is likely to increase, making the seals mechanically stronger than they were in the early phase after disposal.

In practice, the construction of MgO seals is typically carried out in multiple segments with separating joints between them, rather than as a single continuous structure. This approach differs significantly from the assumption underlying this study, where the seal is modeled as a single, monolithic structure constructed over a length of 100 meters in one continuous phase. For instance, at ERAM and Asse mines, no single segment is planned or built with a length exceeding 30 meters. Additionally, the incorporation of plastic joints significantly reduces the stress caused by movements in the surrounding salt. This method draws inspiration from natural analogues, such as fragmented anhydrite, where similar mechanisms are observed to mitigate stress. By adopting segmented designs with appropriate joints, the structural integrity and functionality of Sorel concrete dams in salt environments can be greatly enhanced.

The dilatancy criterion is a crucial parameter for assessing the mechanical behavior of rock salt under varying stress conditions. When the stress in the salt exceeds a certain threshold, the material begins to dilate, forming microfractures and increasing its permeability. This increase in permeability can create potential pathways for fluid ingress into the repository, particularly along the drift sealing system.

Figure 19.-14 presents the evaluation of the dilatancy criterion over time. At the end of the backfilling operation (at 30 years), the rock mass surrounding the drifts experienced significant dilatancy. However, 70 years later, the model shows signs of recovery due to the creep behavior of the salt, although areas around the long-term seal were still undergoing dilatancy. By 400 years, the affected areas had largely recovered, and by 1,000 years, no dilatancy was observed in the model.

The infrastructure drift connecting the shafts also exhibited dilatancy but recovered at a similar rate to the long-term seals. Notably, no dilatancy was observed along the MgO seals, indicating that the sealing function was effective immediately after the installation of the seals. By 500 years, it is expected that the long-term seal had fully gained its intended function. From this point onward, the drift sealing system operates as designed, following the principle of diversity and redundancy to ensure long-term containment.

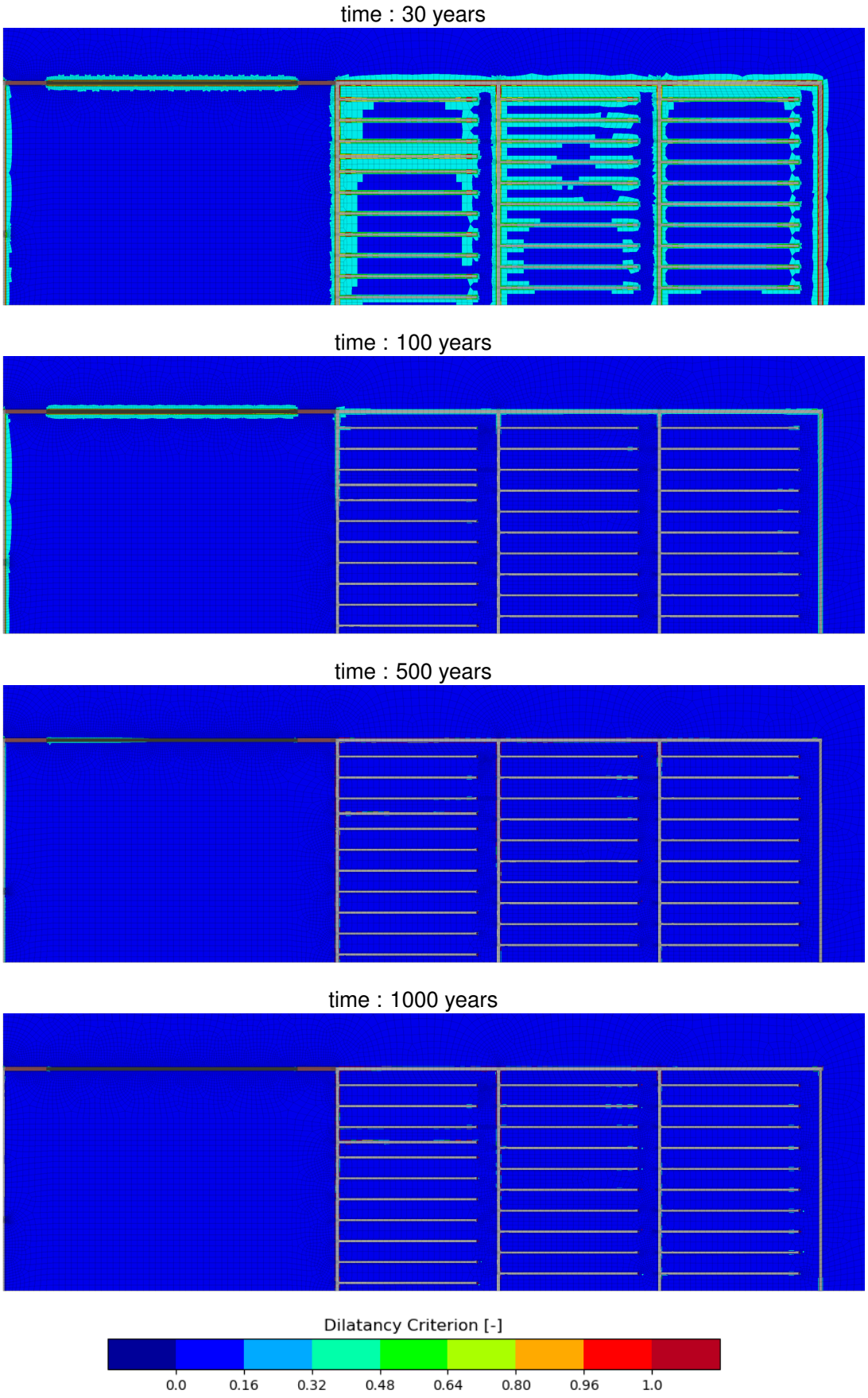

Figure 19.-14: Evaluation of the dilatancy criterion in the repository over time.

20. Mechanical Integrity Assessment of the Shaft Sealing System

In the following section, the design and integrity of the shaft sealing system in salt repositories are assessed based on the methodology developed within the RANGERS project. This exercise is exemplary performed for the two shaft sealing systems designed in generic repository system developed in RANGERS.

20.1 Safety function

According to Beuth et al. (2012), the function of the shaft sealing system is to limit the inflow of solutions from the overburden and adjacent rock formations to such an extent that only small amounts of solutions can penetrate the repository mine. The shaft seals are designed to withstand the expected fluid pressures (hydrostatic pressure of the water column in the overburden and adjacent rock formations and a potential gas pressure built up within the repository). The design of the shaft seals assumes a functional duration of 50,000 years, during which their effectiveness must be maintained. After more than 50,000 years, for the reference scenario, increased hydraulic permeabilities of the shaft seals are assumed, resulting in enhanced solution inflow into the infrastructure area. If solutions reach the drift sealing system, partial dissolution of the seal materials or precipitation of dissolved material in the pore space may occur. At this time, the crushed salt backfilled between the MgO seals as well as in the repository mine will take the function of the long term seal of the repository.

20.2 Design of the shaft sealing system

Shaft sealing systems are engineered barriers that are designed based on the diversity principle. The diversity principle is fulfilled by several seals installed in the shaft made of different materials. The shaft sealing system is redundant to the drift sealing system. Both together in addition to the technical barrier represented by the waste packages form a multi-barrier system. In RANGERS, two different designs has been elaborated inspired by prior research and development projects and have been tailored to the generic repository system used in this project.

In both designs, a first MgO concrete element is installed in the shaft sump, the deepest parts of the shaft as well as the subsurface landing station. At this depth, the MgO-concrete fulfills an abutment function. Above, a second MgO-concrete element is considered serving this time as sealing element. It follows in both designs a gravel column up to the top of the rock salt formation. To guarantee chemical stability of the MgO-concrete, the gravel column is enriched with Mg-salt (e.g. Brucite). Water intakes from above will be saturated with Mg when it passes the gravel column. The gravel column represents also an abutment for the seal that comes next. The two designs diverge by the adjustment of the seals. In the first design, a bentonite seal is emplaced at the top of the gravel column followed by a column of compacted salt-clay mixture. The location of the bentonite below the crushed salt/clay mixture should ensure a saturation of intake water with Na and provide a stable chemical composition of the brine entering the bentonite. At the salt top a bitumen filled gravel column will be installed, covering surrounded anhydrite and clay layers too. In the area of the overburden a simple gravel column will be installed.

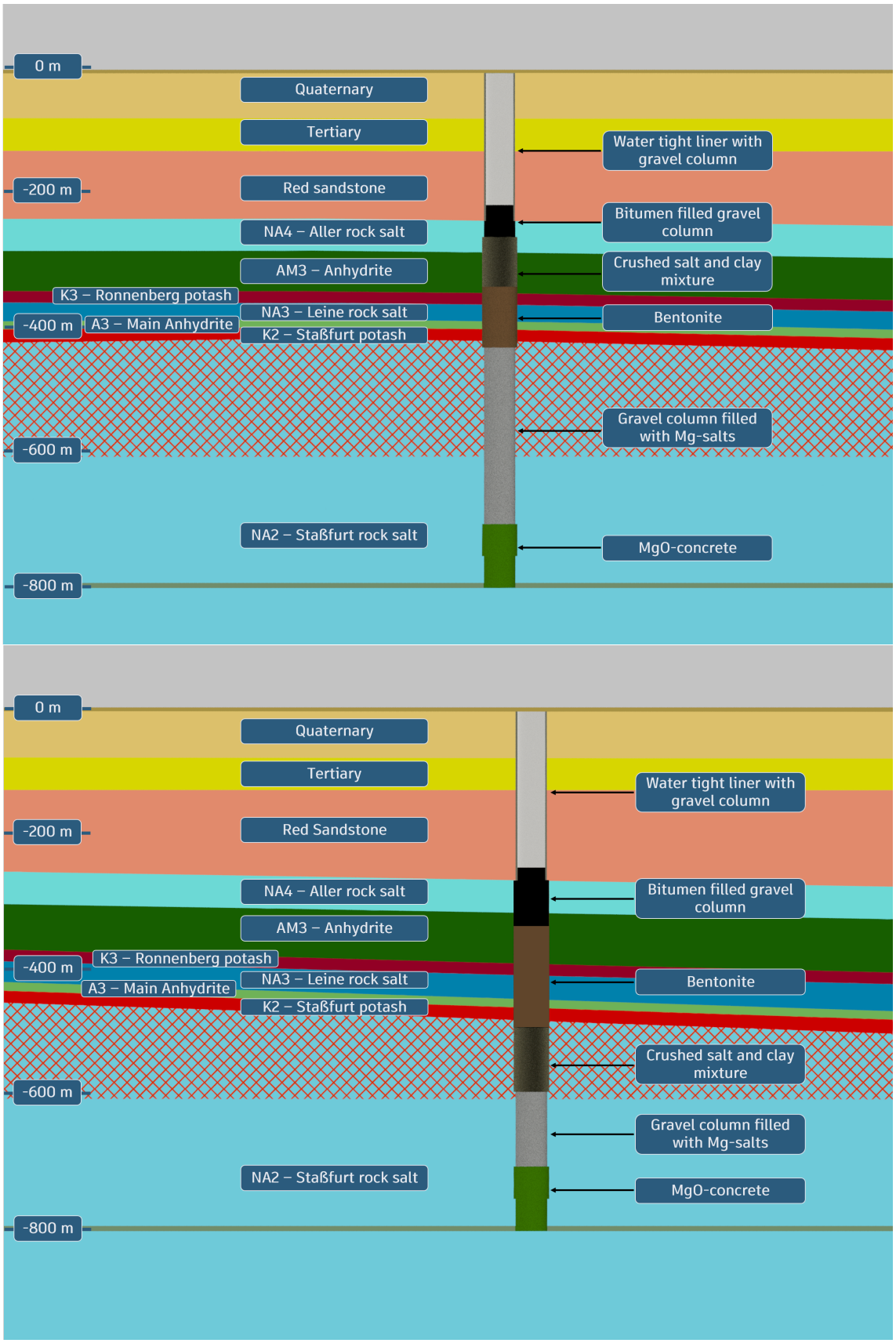

Figure 20.-1: Illustration of both shaft sealing concepts in the geological model used in RANGERS.

In the alternative design, the bentonite and salt-clay seals are permuted. This is motivated by the fact that the convergence of the rock helps to reseal the EDZ. The convergence rate increases with depth. Because bentonite due to its swelling capacity is able to close the EDZ itself, it is adequate to install the bentonite higher in the shaft and the salt/clay mixture deeper to let the convergence increase the sealing capacity of this latter seal. Above the bentonite seal, the third seal made of bitumen gravel is installed followed by the gravel column up to the ground surface as it is the case for the reference design. The location of the two shaft sealing systems in the geological formation is illustrated in Figure 20.-1. Figure 20.-2 shows the position of the shafts in the repository layout.

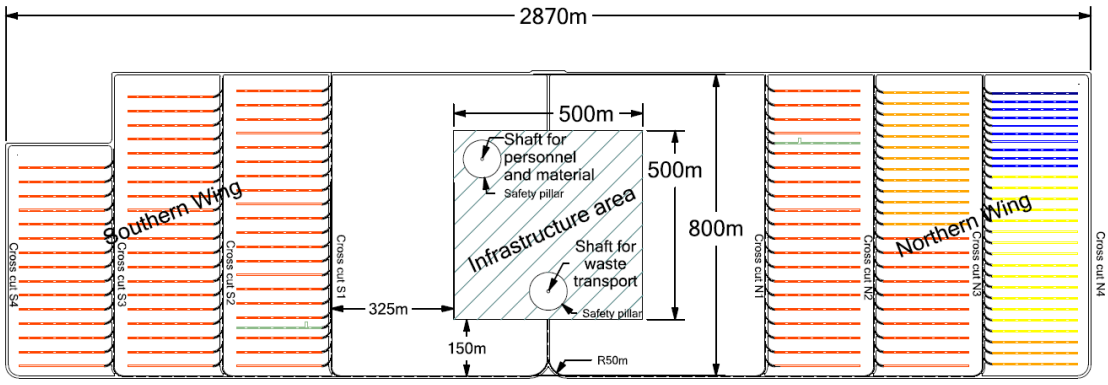

Figure 20.-2: Position of the shafts in the repository layout.

20.3 Modeling cases

The integrity assessment for the shaft seal design is based on the loads derived from scenario development and Features, Events, and Processes (FEP) analysis. The FEPs relevant for the mechanical integrity of the engineered barrier system (EBS) are discussed here in the context of the shaft seal design, as shown in Figure 20.-3.

Thermal expansion and contraction resulting from heat propagation in the repository are among the key loading conditions affecting the shaft sealing system. Heat flow, coupled with the convergence of the surrounding rock enhanced by creep together with thermal expansion of the rock, induces mechanical stress changes within the repository, creating significant loads that must be considered for the long-term safety and integrity of the shaft seal.

Time-dependent processes, such as the swelling, shrinking, and creeping of the sealing materials (e.g., bentonite and salt-clay mixtures), also play a critical role in the system's resistance over time and must be factored into the design. The swelling of bentonite may also induce some damage in the rock contour leading to potential pathways for water migration. The compaction of the seals that is expected to occur due to converge helps to compensate the deformation to be expected due to shrinkage and creep of the seals.

Furthermore, hydraulic pressure change results from the liquid inflow in the shaft starting with the saturation of the upper gravel column and the subsequent infiltration through the sealing components. The resulting hydrostatic loads need to be considered in the integrity of the shaft sealing system.

Due to its granular nature, the gravel columns in the shaft are prone to settling. This settlement can lead to subsidence within the shaft, potentially affecting the performance of the sealing materials and creating new pathways for water inflow. This issue becomes more pronounced in the event of seismic activity. To address these concerns, dedicated analyses were conducted as part of the ELSA project (Herold et al., 2018), utilizing various numerical approaches to quantify the settlement both immediately after backfilling the gravel material and following seismic events.

The settlement quantification from the ELSA project demonstrated that the applied seismic impulse was insufficient to cause significant particle rearrangement or settlement. The maximum vertical displacements recorded were approximately 2 cm, while horizontal displacements reached up to 4 cm under the specific assumed loading conditions representative for a geological site in Germany. Following the seismic loading, subsidence of around 1 cm was observed. A second identical seismic event, delayed in time, resulted in similar settlements of less than 2 cm.

However, the earthquake did influence the stress distribution within the gravel column, leading to the observation of a silo effect, which caused an increase in both horizontal and vertical stresses. The effect of the seismic event on the porosity of the gravel was minimal, indicating no significant compaction or particle rearrangement occurred.

Based on these findings, the current shaft sealing design can be considered robust and largely unaffected by the FEP “Settlement and compaction of backfill”.

The results obtained in ELSA also cover the FEP “displacement of the shaft sealing elements”. A displacement of the sealing element can occur only if the settlement of the gravel columns serving as abutment for these elements is large enough. This is fortunately not the case.

Seismic events, such as earthquakes, must also be incorporated into the design considerations, especially given the expected long functional lifetime of the shaft seals (50,000 years and beyond). They are of relevance especially in the contact zone between sealing material and rock. This should be adressed in the scope of dedicated numerical investigations.

The gray FEPs in Figure 20.-3 represent processes that are not relevant to the integrity proof of the shaft sealing system for the following reasons:

- Thermal degradation of carnallite: This process pertains to certain minerals like canallite, which are not present in the shaft seals or the surrounding rock formations. Therefore, it does not directly affect the mechanical integrity of the sealing system.
- Diapirism: This geological process involves the upward movement of material through overlying rock, typically salt, due to buoyancy. While diapirism can occur in some salt formations, the mechanical integrity of the shaft sealing system would not be influenced by this process, as diapirism primarily affects large geological timescales and is not relevant to the short- to medium-term behavior of the shaft seals.
- Transgression and regression: These are large-scale geological processes related to changes in sea level. Since the repository is designed in a stable geological setting and such processes would occur far above the repository level, they do not pose a risk to the mechanical integrity of the shaft seals.

- Corrosion of cement- or Sorel-based materials: $MgCl_2$-rich solutions are expected in small quantities, as the shaft profiles come into contact with potash salts, which are naturally present in limited amounts within the host rock. To further enhance $MgCl_2$ concentration, bischoffite deposits will be intentionally introduced into the gravel column. This approach ensures the presence of $MgCl_2$-rich solutions in the shaft, effectively creating a chemical environment that prevents the corrosion of MgO-concrete.
- Dissolution and precipitation of salt minerals: While this process affects the surrounding rock salt, it does not directly impact the concrete or clay-based shaft seals. If there is a potential for such processes, they would be monitored and controlled in the salt formation itself, with little to no effect on the seal materials.
- Gas flow processes: No gas is expected in the salt formation. Any potential gas inclusions would be detected and mitigated during shaft excavation. In the shafts, the degradation of the bitumen due to microbial processes will release gases that will flow out of the shafts through the gravel columns located above the bitumen gravel seals. Thus those gas-related processes do not pose a threat to the mechanical integrity of the shaft seal.
- Metal corrosion: Metal corrosion could affect metallic components within the repository, but this FEP is not relevant for the shaft seals themselves, which are constructed from non-metallic materials such as concrete and clay.
- Solution, transformation of clay minerals: This FEP concerns the alteration of clay minerals, which may influence the long-term sealing performance of the shaft but not its mechanical integrity. The degradation of clay-based seals could lead to increased permeability, which should be addressed in hydraulic assessments rather than in mechanical integrity assessments.
- Microbial processes: Microbial activity typically affects organic materials or metals. this process will affect predominantly the bitumen based seals in the shafts. This sealing element was for this reason purposefully located at the edge of the formation to allow the gases being generated by the microbial degradation of the bitumen to be evacuated out the shafts. Therefore no gas pressure built-up is to be expected in the shaft and no relevance to the the mechanical integrity of the shaft sealing system is foreseen. The impact of this process can be taken into account in a lost of sealing function of this material in the hydraulic assessment.
- Alteration of bentonite: This FEP is similar to the “Solution, transformation of clay minerals.” Bentonite, if used, may experience some transformation over time, which could affect its sealing performance but not the mechanical integrity of the shaft seal. Any permeability changes due to this FEP should be considered in the hydraulic assessments.
- Colloid generation and filtration: This process refers to the behavior of colloidal particles in solution, which is not relevant to the mechanical integrity of the shaft seals. While it might affect the movement of contaminants, it has no direct impact on the structural stability of the sealing system.
- Asphalt migration: Asphalt migration is expected to occur in the bitumen gravel seal. Despite its occurrence, this process is unlikely to affect the mechanical integrity in the shaft. Its relevance can be investigated as part of the hydraulic assessment by assuming an earlier failure of this sealing element. It is therefore not considered in this mechanical integrity assessment of the shaft sealing system.

- Deflagration and explosion of gases: While gas explosions could have dynamic impacts similar to seismic events, no significant gas presence is expected in the shaft area. Any gas inclusions would be identified and removed during excavation, ensuring that this FEP does not affect the mechanical integrity of the shaft seals.

By focusing on the relevant FEPs, we can address the processes that directly impact the shaft seal's mechanical integrity and ensure its long-term functionality.

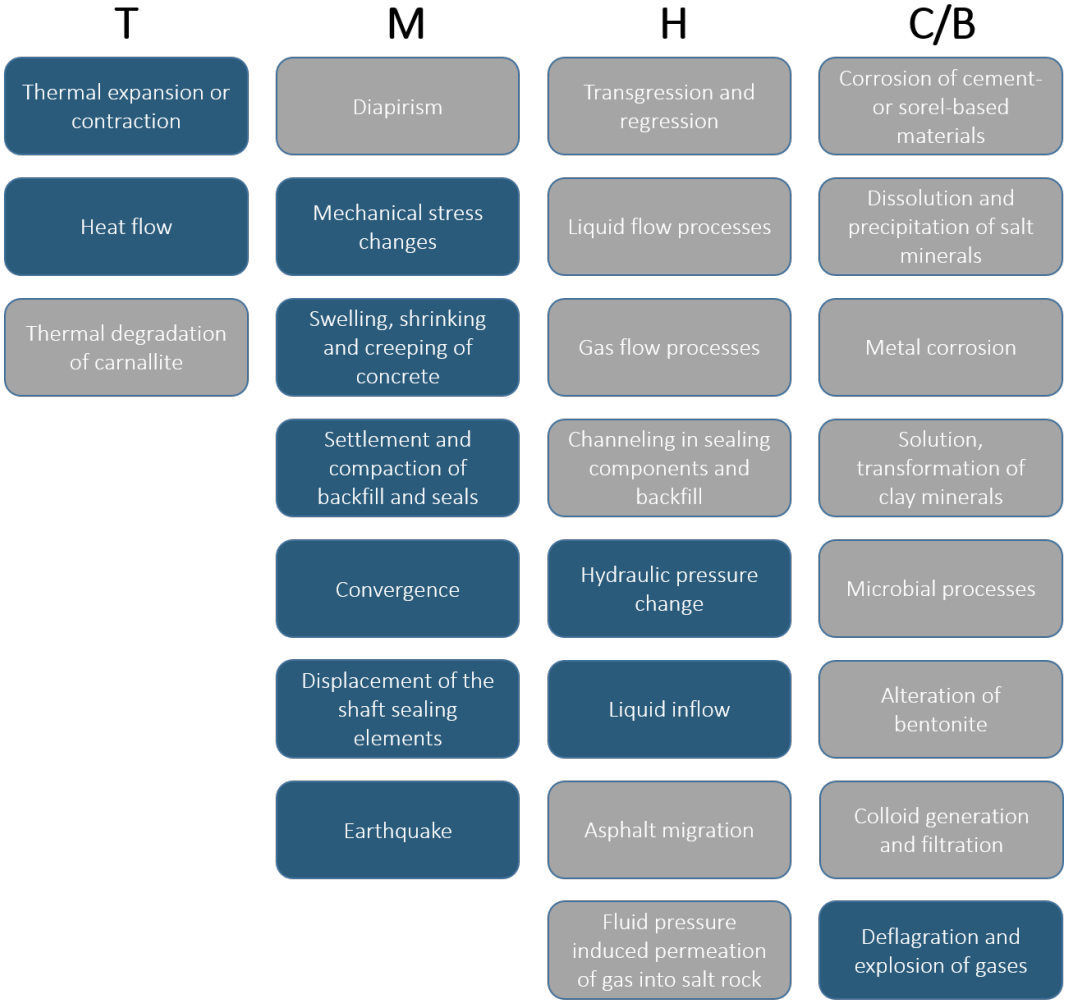

Figure 20.-3: Initial FEPs of relevance for the mechanical integrity proof.

From these discussions, we derive the following modeling cases for the shaft sealing system:

- modeling case 1: Thermal-mechanical loading: This scenario considers the combined effects of heat flow, thermal expansion/contraction, mechanical stress changes, and rock convergence.
- modeling case 2: hydrostatic pressure build-up in the shaft: This case analyzes the effects of water pressure on the shaft seal (FEP: hydraulic pressure change).
- modeling case 3: Earthquake events: Seismic activity is combined with thermo-mechanical loading to assess the impact of seismic loading at the contact zone seal/rock. system.

The interaction between the shaft seal system and the surrounding rock is part of the permanent design situation, where processes like gravitational forces, convergence, and creep of the host rock are always considered. In combination with other FEPs or modeling cases, the long-term thermal-mechanical evolution can be modeled to predict the system's performance.

Hydraulic load cases from water inflow, occur gradually over time and can be considered in the scope of the thermal-mechanical simulation as a static volumetric load acting in the shaft.

In previous projects (Müller-Hoeppe et al., 2012b), the impact of a hydraulic load from gas buildup, resulting from metal corrosion in the repository, was considered as an additional assessment case. This load could potentially affect the integrity of the shaft sealing structure from the bottom. Given the Engineered Barrier System (EBS) design implemented in this project, it is anticipated that the drift seal will significantly retard the advective transport of gases. This retardation will subject the drift seal to gas pressure loading, thereby assisting in protecting the shaft sealing from similar pressures.

It is crucial to evaluate through gas transport simulations whether the gases, after being retarded by the drift sealing system, might eventually impact the shaft sealing system at a later stage. This aspect needs further clarification to ensure the long-term stability and effectiveness of the entire sealing strategy.

In this study, the design and safety assessment will be demonstrated using modeling case 1. THM simulations are essential for evaluating modeling case 2. However, these simulations demand significant computational resources that were not available in this project. Additional dynamic seismic analyses will be required to evaluate the effects of modeling case 3.

20.4 Numerical model

20.4.1 Modeling concept

The numerical model necessary to investigate the evolution of the shaft sealing systems is designed to accurately compute both the stress development in the near field of the shaft sealing systems and the heat propagation from the emplacement fields up to the shafts. A comprehensive model that considers both the shaft sealing components, the emplacement fields, and the surrounding geological layers is required for the integrity assessment. Thus, the model must cover several square kilometers, yet consist of finite elements that are only centimeters in size in key areas like the shaft and surrounding zones of interest.

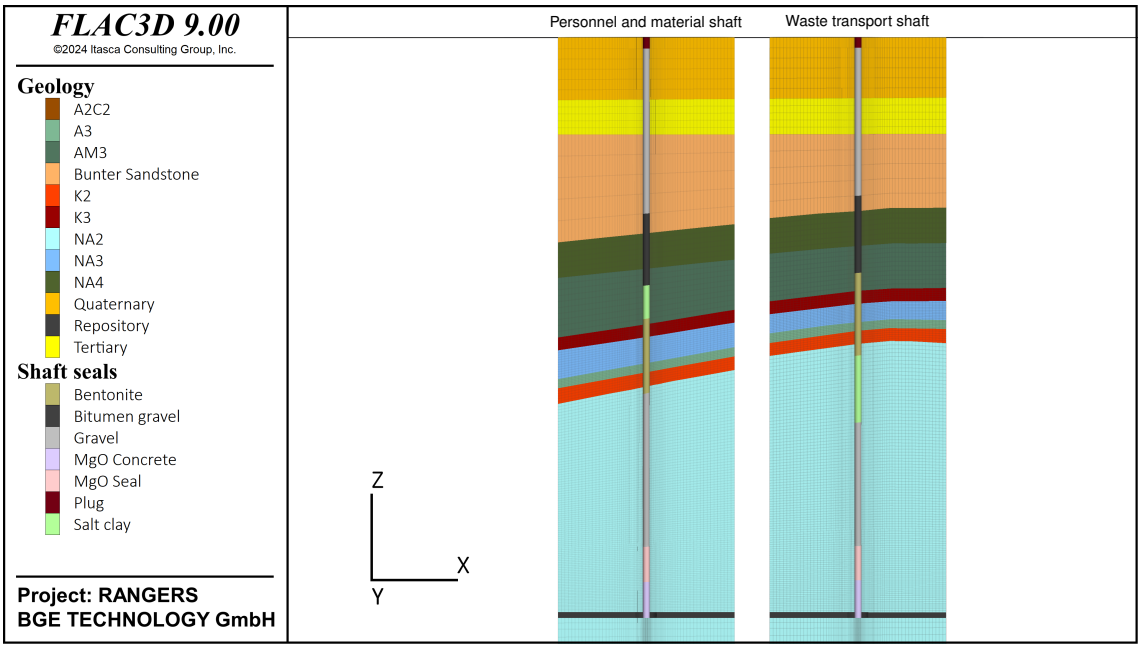

Figure 20.-4: Numerical model for the analysis of the mechanical integrity of the shaft sealing structures - near field.

To handle the complexity of the model, all disposal drifts are homogenized into disposal fields which act as heat sources. The thermal heat power of all disposal drifts is summed up and applied to these heat sources. This approach allows for the reduction of the computational burden while maintaining accurate heat propagation results in the model.

Figure 20.-4 shows the components of the two shaft sealing systems embedded in the geological layers. In this model, layers between the components were introduced to help mechanically decouple certain parts. In Figure 20.-5, the shafts and emplacement fields are shown within the context of the geology.

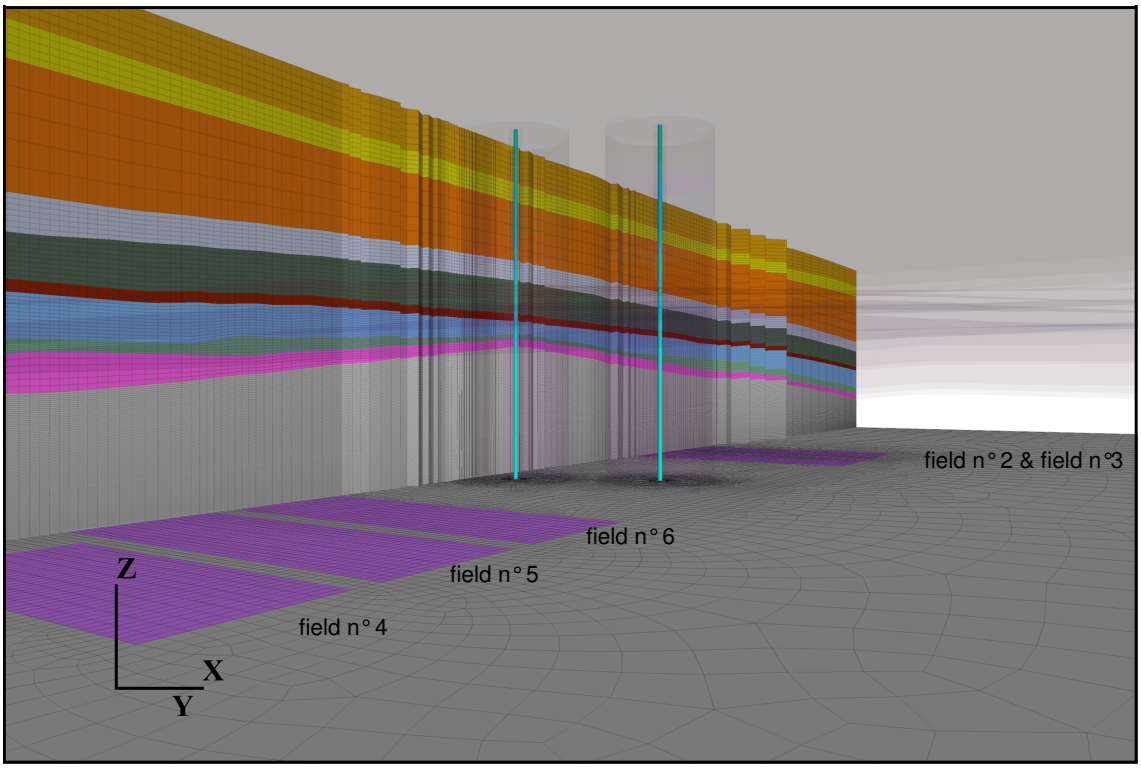

Figure 20.-5: Numerical model for the analysis of the mechanical integrity of the shaft sealing structures - far field.

The simulation stages begin with the initialization of the primary state, followed by the instantaneous excavation of the shafts and installation of a liner up to the upper boundary of the salt layers. Subsequently, sequential activation of the heat sources over 30 years is performed, simulating waste emplacement while keeping the shaft open. At year 32, the shafts are backfilled according to the sealing concept.

Due to the thermal-mechanical evolution of the repository system, the sealing components are subjected to external forces that need to be evaluated. The simulation runs first for 1,600 years thermo-mechanically. After this point, the thermal processes are deactivated to allow the simulation to continue mechanically, speeding up the computational process and extending it to 25,000 years. Running the simulation thermo-mechanically over this long period of time was not possible in the time span of the project. This approach is however not conservative since we know from the thermal analyses that the shaft is expected to experience a temperature increase till 5,000 years before the cooling process takes place. Running the simulation mechanically allows us at least to consider the higher mobility of the salt due to thermally induced creep up to 25,000 years.

Besides the base case scenario described above, an alternative simulation was performed with interface elements introduced at the contact between the sealing components and the surrounding rock. In the base case scenario, this contact was assumed to be "tight-forced," meaning direct transfer of forces between the two materials. In reality, the strength at the contact interface is limited and can fail under specific conditions. Using interface elements allows for the modeling of this potential behavior.

It is expected that a silo effect will occur in the gravel columns. Therefore, a tight-force contact can be assumed there. The contact zone between the MgO concrete and the salt is well studied, with evidence showing that in most cases the contact zone remains intact after shearing, with cracks typically occurring in the Excavation Disturbed Zone (EDZ). Therefore, a rigid contact assumption is made between MgO concrete and rock salt. Bentonite, due to its swelling pressure over time, is also assumed to develop a tight-force contact with the rock, resulting in a rigid contact assumption for the bentonite/rock salt interface.

In contrast, the contact between bitumen and rock, and the contact between the crushed salt/clay mixture and rock, are expected to be more loosely connected. Due to the viscous nature of bitumen and the plasticity of the crushed salt/clay mixture, slip at the contact interface is more likely. In these cases, a frictional (slip) contact condition is applied.

In geotechnical modeling, the interaction between different materials at their interfaces plays a crucial role in defining the system's overall behavior. In the case of the shaft sealing system, various contact conditions exist between materials such as bentonite, MgO concrete, bitumen, and the surrounding rock salt. FLAC3D, being a robust numerical tool for simulating the mechanical behavior of geotechnical systems, allows the user to define both rigid and slip contact conditions between materials.

In the present analysis, the slip contact condition for interface were used.

The slip contact in FLAC3D is governed by Coulomb's friction law:

$$\tau = \mu \cdot \sigma_n + c$$

Where τ is the shear stress at the contact interface, μ = tan(φ) is the coefficient of friction at the interface and σ_n is the normal stress acting perpendicular to the interface. c is the cohesion at the interface.

If the shear stress τ exceeds the critical value defined by the normal stress σ_n and the friction coefficient μ, relative slip occurs between the materials.

In this case, the relative displacement in the tangential direction u_t is proportional to the shear stress as long as it remains below the yield condition:

$$\tau \leq \mu \cdot \sigma_n + c$$

$$u_t \neq 0 \quad \text{if} \quad \tau = \mu \cdot \sigma_n + c$$

The coefficient of friction μ can vary depending on the materials in contact. For instance, in the case of bitumen, crushed salt/clay mixture and salt, a relatively low coefficient of friction might be assumed due to the viscous nature of bitumen. On the other hand, the friction coefficient at the contact between gravel or concrete and rock salt can be higher.

The normal and tangential stiffness at the contact surface can be defined as:

$$K_n = \frac{E\,E_r}{s\,(E_r - E)}, \quad K_s = \frac{G\,G_r}{s\,(G_r - G)}$$

where E = rock mass Young's modulus, E_r = intact rock Young's modulus, k_n = joint normal stiffness, s = joint spacing, G = rock mass shear modulus, G_r = intact rock shear modulus; and k_s = joint shear stiffness.

The result of this contact formulation is a realistic simulation of the interaction between the various sealing components and the surrounding geological materials, accounting for both tightly bonded and frictionally slipping interfaces, depending on the material properties and stress conditions.

The mechanical properties of interface at the contact between the materials in the shaft and the different geological layers are presented in Table 20.-1

Table 20.-1: Mechanical Properties of Interface Materials.

Interface Material	**Normal Stiffness,** K_n [Pa]	**Shear Stiffness,** K_s [Pa]	**Friction Angle,** φ [°]	**Cohesion,** c [Pa]
Gravel/Q	8.00×10^{10}	2.99×10^{10}	31	0
Gravel/T	1.33×10^{11}	5.08×10^{10}	31	0
Gravel/BunterS	8.11×10^{10}	3.07×10^{10}	31	0
Bitumen Gravel/BunterS	8.11×10^{10}	2.79×10^{10}	27	0
Bitumen Gravel/NA4	8.06×10^{10}	2.78×10^{10}	27	0
Bitumen Gravel/AM3	8.05×10^{10}	2.77×10^{10}	27	0
Bentonite/K3	1.98×10^{9}	7.99×10^{8}	6	50.0×10^{3}
Bentonite/AM3	1.98×10^{9}	7.99×10^{8}	6	50.0×10^{3}
Bentonite/NA3	1.98×10^{9}	7.99×10^{8}	6	50.0×10^{3}
Bentonite/A3	1.98×10^{9}	7.99×10^{8}	20	50.0×10^{3}
Bentonite/K2	1.98×10^{9}	7.99×10^{8}	6	50.0×10^{3}
Bentonite/NA2	1.98×10^{9}	7.99×10^{8}	6	50.0×10^{3}
Gravel/NA2	8.06×10^{10}	3.05×10^{10}	31	0
Salt Clay Mix/AM3	3.29×10^{11}	1.29×10^{11}	20	0
Salt Clay Mix/NA2	3.31×10^{11}	1.30×10^{11}	20	0
MgO Concrete/NA2	4.36×10^{13}	1.20×10^{13}	19	0

20.4.2 Initial conditions

An isotropic primary stress state is assumed, with an average integral density of the overlying geological layers of 2,200 kg/m³. This results in a calculated depth pressure of approximately 18.5 MPa at the repository level, which corresponds to the disposal depth. For the undisturbed rock temperature, a temperature gradient of 3 K per 100 m is assumed, leading to an estimated temperature of 33.3 °C at the disposal depth. The model is constrained in the normal direction at the lateral and bottom boundaries. The lateral boundaries are placed 1.5 to 2 km away from the repository, ensuring no edge effects are present. Same initial and boundary conditions are assumed here as in the previous simulations.

The thermal evolution of the repository is primarily driven by the heat generated from the disposal of waste. In the model, this is represented by a transient heat source, where all the disposal drifts are homogenized into broader disposal fields, acting as the heat sources. The cumulative thermal output of all disposal drifts is summed and applied to these heat sources, capturing the thermal effects of waste disposal on the surrounding rock.

During the backfilling of the shaft, gravitational forces due to the weight of the material act as the primary driving forces. A lateral earth pressure coefficient of 1 is applied to account for horizontal stresses within the backfilled materials along the shaft because of their high plastic behaviour. This does not apply to gravel, where horizontal stresses are estimated differently. This coefficient represents the ratio of horizontal to vertical stresses and is crucial for understanding the stress distribution along the shaft.

A silo effect is anticipated within the gravel column. The silo effect refers to the behavior of granular materials within a confined space, such as a column, where the material at the center of the column experiences less vertical pressure due to frictional forces at the walls, causing uneven stress distribution. This effect influences the way vertical loads are transferred down the shaft and contributes to the horizontal and vertical stress profiles along the column.

The silo effect is characterized by a reduction in vertical pressure due to the friction between the column walls and the backfill material, which supports part of the load. The vertical stress at any point in the gravel column can be calculated using Janssen's equation for silo pressures:

$$\sigma_v(z) = \frac{\rho g D}{2\mu(1-K)} \left[1 - \exp\left(-\frac{2\mu(1-K)z}{D}\right)\right]$$

Where:

- σ_v(z) is the vertical stress at depth z,
- ρ is the density of the backfill material (in kg/m³),
- g is the gravitational acceleration (9.81 m/s²),
- D is the diameter of the shaft,
- μ is the coefficient of wall friction,
- K is the lateral earth pressure coefficient, and
- z is the depth below the surface.

The results of this calculation provide a vertical stress profile showing a gradual reduction in stress with depth due to the silo effect. This stress distribution helps to explain the behavior of the gravel column in terms of load-bearing and settlement.

20.4.3 Constitutive models

The constitutive models applied to simulate the geological formations surrounding the repository have been described previously in Section 19.5.3. For the shaft sealing system, however,

different constitutive models were used, each selected based on the specific mechanical and hydraulic behavior of the materials involved. Figure 20.-6 provides an overview of all constitutive models employed in the numerical model.

For the simplest material at the top of the shaft — the plug concrete — a linear elastic model was used. This is suitable for the plug concrete, given its limited deformation and the relatively low demands on its mechanical behavior compared to other components.

Gravel column, bitumen gravel, and salt-clay mixture: These materials are assumed to exhibit linear elastic behavior. This assumption is based on the fact that no damage is expected to occur within these materials. Gravel can freely adjust under mechanical loading at the contact points between individual grains, accommodating stresses without fracturing. Bitumen gravel and salt-clay mixtures, on the other hand, are highly plastic materials capable of compensating for loading stresses through deformation. For simulation purposes, their stiffness characteristics are the primary focus, as these properties dictate their response under mechanical loads.

MgO (Sorel) Concrete: For the Sorel concrete (MgO concrete) at the bottom of the shaft, a more advanced constitutive model based on the Drucker-Prager criterion was used. This model was specifically adapted for MgO concrete using experimental results. The Drucker-Prager model provides a smooth conical yield surface, making it more suitable for materials like MgO concrete that exhibit more complex plastic flow under triaxial stress conditions. The mechanical behavior of MgO concrete is crucial for the long-term performance of the sealing system, as it must resist deformation while maintaining its sealing function. This model, including its parameters, was described in Section 19.5.3.

Bentonite: The constitutive model for bentonite was selected based on its hydrological and mechanical properties. Bentonite, known for its swelling capacity when hydrated, was modeled using the Cam Clay constitutive model. The parameters for this model were derived based on a more advanced hydrological-mechanical model for bentonite, developed by Mašín (2013), which accurately captures the material's behavior under different saturation and stress conditions. This model is particularly effective in representing the swelling and plastic deformation of bentonite during the hydration phase. After saturation, the state which is assumed in this analysis, the behavior of bentonite resembles that of other clays, making the Cam Clay model an appropriate choice for simulating its plasticity under mechanical loading.

The Cam Clay model accounts for the nonlinear elastic behavior of bentonite under low stresses and its transition to plastic flow under higher stresses. It includes a yield surface that evolves with plastic strain and takes into consideration the consolidation behavior of bentonite as it absorbs water and increases its volume. This model allows for a realistic simulation of the stress-strain relationship of bentonite under both saturated and unsaturated conditions, capturing the essential hydrological-mechanical coupling that affects the sealing performance of bentonite over time.

Table 20.-2 and Table 20.-3 provides an overview of the material properties and parameters used for each component in the shaft sealing system. These parameters are critical for ensuring that the numerical model accurately captures the behavior of each material under the expected loading and environmental conditions over the long-term evolution of the repository.

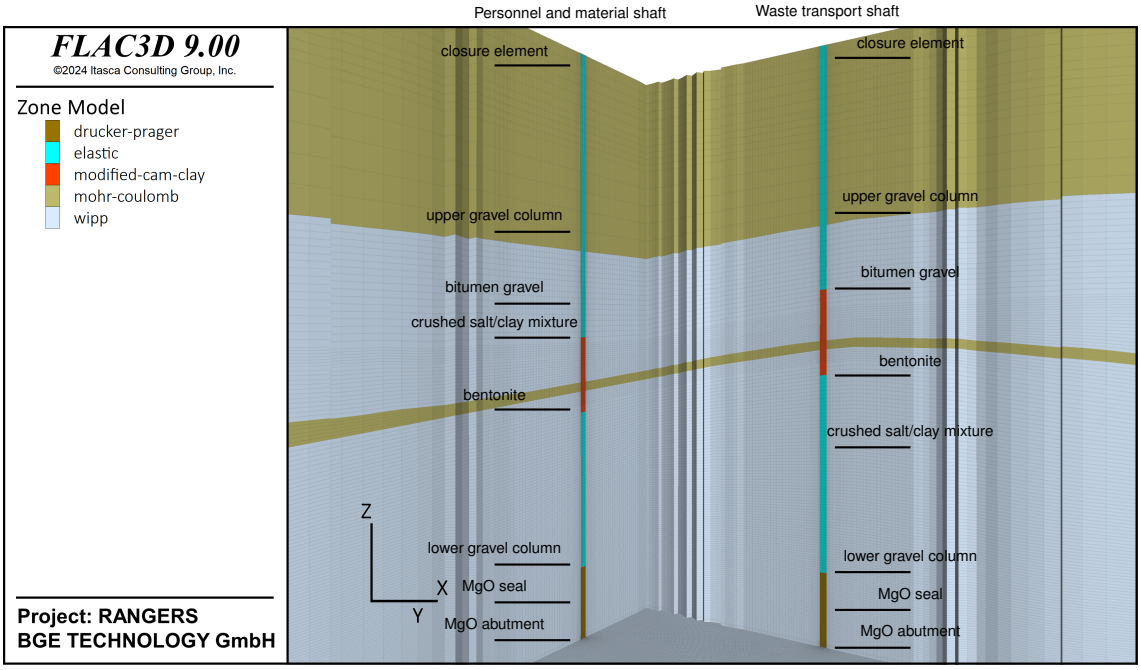

Figure 20.-6: Constitutive material models used in the numerical model.

Table 20.-2: Mechanical Properties of Backfill Materials.

Backfill	**Const. Model**	**Density,** ρ [kg/m^3]	**Young's modulus,** E [MPa]	**Poisson's ratio,** ν
Gravel	Elastic	1700	200	0.32
Bitumen Gravel	Elastic	2238	200	0.45
Salt clay	Elastic	2300	800	0.27
Concrete	Elastic	3490	31.8	0.372

Table 20.-3: Cam-Clay Mechanical Properties for bentonite.

Backfill	**Preconsolidation pressure [MPa]**	**Density,** ρ [kg/m^3]	**Young's modulus,** E [MPa]	**Poisson's ratio,** ν	**Slope of normal consolidation line,** λ	**Slope of elastic swelling line,** κ	**Stress ratio at critical state**
Bentonite	2.4	1450	20	0.24	0.25	0.05	0.98

20.5 Numerical results

20.5.1 Reference modeling case

To illustrate the numerical results that highlight the thermal-mechanical impacts on the shaft sealing system, we begin by examining the overall thermal-mechanical evolution of the repository system. This foundational analysis provides insight into how thermal and mechanical processes interact within the repository, setting the stage for understanding their specific effects on the integrity and performance of the shaft sealing components.

Figure 20.-7 illustrates the temperature evolution along a longitudinal cross-section through the shaft 1 of the repository system over time, with time increments at 150, 500, 1,000, and 1,600 years. In the figure, we see the gradual propagation and dissipation of heat from the waste emplacement fields into the surrounding salt formation.

At a time of 150 years, the heat is concentrated around the waste emplacement fields where the temperatures reach 400 K (127 °C). This temperature is lower than the temperature criterion of 200 °C due to the homogenization of the heat source all drifts in the emplacement field into a heat panel. The surrounding areas to the emplacement fields show temperatures in the range of 360 to 380 K near the waste. Beyond this zone, the region in green with temperature in the range of 320 to 340 K shows a temperature domain resulting from the thermal superposition of the heat coming from the different emplacement fields in each wing. Beyond this zone, the temperature decreases quickly, with blue areas indicating regions close to the baseline temperature of 282 K.

At a time of 500 years, the thermal impact has spread further from the waste emplacement areas, with a larger region affected by elevated temperatures. The red zones near the emplacement fields have started to reduce slightly in intensity, while surrounding areas in green and yellow show an expansion, now reaching temperatures between 320 and 360 K. The heat propagation shows a more extended impact in the salt formation.

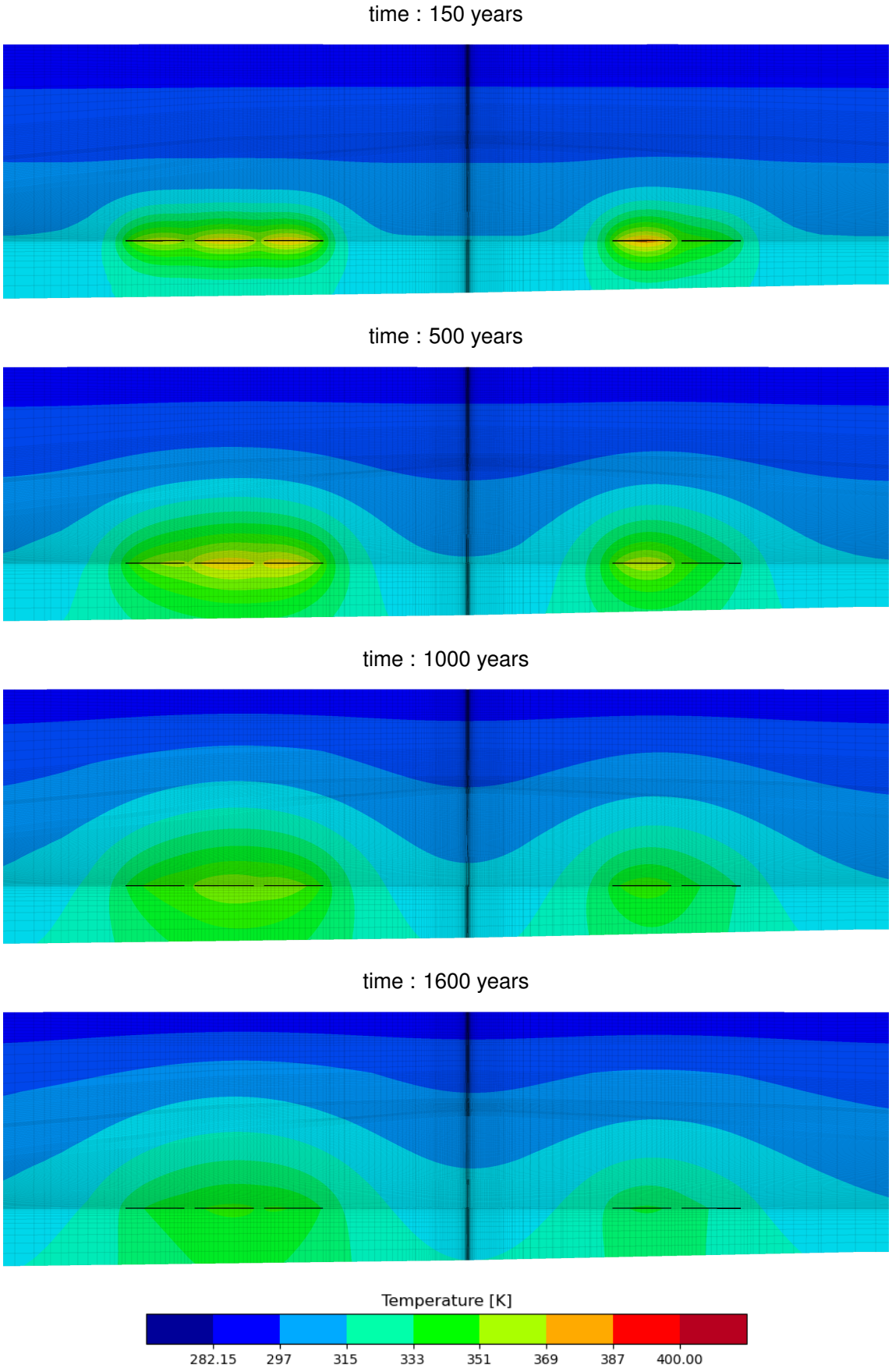

Figure 20.-7: Temperature distribution over time in the repository system.

At a time of 1,000 years, the peak temperatures in the emplacement areas have decreased further, with fewer red regions, and the dominant colors are now yellow and light green, indicating temperatures around 320 to 360 K. The surrounding salt formation is increasingly impacted by thermal diffusion, with a broader area experiencing elevated temperatures compared to earlier stages.

At a time of 1,600 years: The repository's heat impact has largely dissipated by this point. Temperatures throughout the cross-section are now predominantly in the green and blue range, indicating a decrease to the range 300 to 320 K near the waste and close to ambient temperatures further out. The temperature throughout the repository system continues to decrease, with no yellow regions remaining visible. At this stage, the thermal process was deactivated, effectively "freezing" the remaining heat within the formation. This approach was implemented to reduce computational efforts, allowing the simulation to proceed with a focus solely on mechanical processes. By doing so, the simulation was able to extend over a much longer period, reaching up to 25,000 years, while maintaining computational efficiency.

Overall, this temperature evolution illustrates the gradual cooling and dissipation of heat from the repository over time. Peak temperatures in the waste emplacement areas decline while the thermal impact expands outward initially, then diminishes as heat continues to diffuse into the salt formation. By 1600 years, the system is nearing thermal stabilization, with only a slight temperature increase observed at the bottom of the shaft. However, as detailed in the thermal analysis in Chapter 16., a further temperature rise around the shafts is anticipated up to 5000 years before the cooling process begins. This additional temperature impact could not be incorporated into this analysis, as achieving this state would have required significantly more computational time. Consequently, further computational effort is necessary to achieve more accurate and comprehensive modeling of the system behavior.

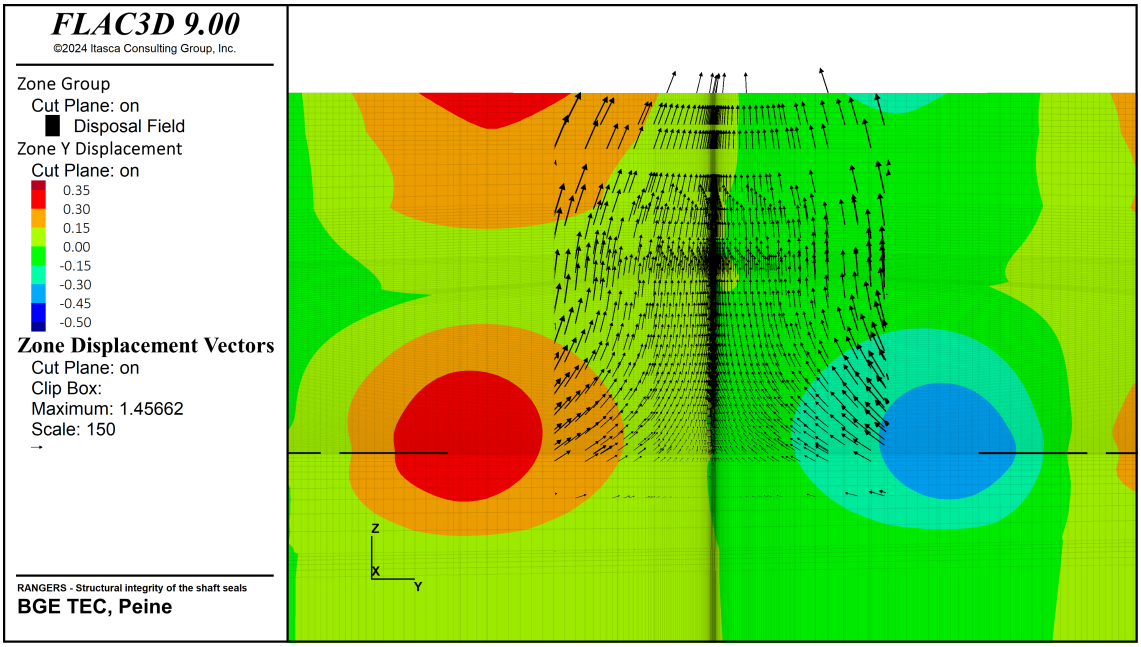

Figure 20.-8: Y-displacement distribution and displacement vectors near the shaft at 500 years.

The influence of temperature on the mechanical behavior of the rock is clearly illustrated by

examining the displacement vectors in the cross-sectional view of the repository. This is shown in Figure 20.-8, which displays both the distribution of displacements along the y-direction and the displacement vectors within the rock formation surrounding the shaft.

In the disposal fields on either side of the central shaft, zones of significant displacement are observed in red and orange, indicating areas of intensified movement near the heat sources. This displacement is primarily due to thermal expansion resulting from the heat generated by the waste. The displacement vectors further illustrate the movement of the rock mass, showing a parabolic trajectory as the rock on both sides of the shaft is pushed outward due to thermal effects and then moves inward toward the shaft.

As the rock approaches the shaft, the displacement vectors shift direction, showing a nearly vertical movement near the shaft walls. This vertical trajectory suggests that the shaft itself is being lifted by the surrounding rock mass, indicating an upward displacement due to thermal expansion in the disposal fields. Additionally, this pattern implies a compaction in the horizontal direction, as the rock mass is forced inward toward the shaft.

This analysis reveals that the shaft is likely to experience vertical elongation, accompanied by horizontal compaction. These displacement patterns provide insight into the thermal-mechanical behavior of the rock formation and the resulting stress conditions within the shaft sealing system.

Figure 20.-9 illustrates the evolution of vertical displacement (z-direction) in a longitudinal cross-section of the repository system over several time periods. The figures reveal that thermal expansion of the rock mass causes significant uplift within the formation, with the effect most pronounced in the central region, particularly above the left emplacement wing. In this area, displacement values exceed 1.5 meters. This uplift is less prominent above the right emplacement wing, where predominantly lower heat-generating waste has been disposed, as indicated in the previous temperature evolution analysis.

At 500 years, the central part of the formation exhibits noticeable vertical displacement, forming a concentrated circular zone of high displacement values (shown in red and adjacent colors) that reaches up to 1.5 m. This red zone indicates a region of maximum displacement and suggests that the central area undergoes the most substantial vertical adjustment due to sustained thermal loading from the disposal fields. The displacement primarily results from thermal expansion of the rock mass, driven by heat generated by the waste. As the simulation progresses to 1,000 years, the displacement in the central region intensifies, and the area with high displacement values expands, reflecting the continuing thermal and mechanical impact on the surrounding rock. The distribution of high displacement values suggests that the heat continues to exert a strong influence on the formation's mechanical response.

By 10,000 years, a shift is observed: the size of the high displacement zone begins to decrease in the vertical direction, while horizontally, the zone experiencing significant displacement (represented in green) expands. This suggests a redistribution of displacement as the thermal impact on the rock formation stabilizes. At 25,000 years, this pattern persists because the thermal process in the model was deactivated at 1,600 years, freezing the heat distribution within the formation. Consequently, the remaining thermal energy maintains constant conditions, causing the displacement to stabilize while still exhibiting the lasting effects of the initial thermal expansion. Although the thermal effects remain constant, the mechanical evolution

still evolves due to creep of the rock.

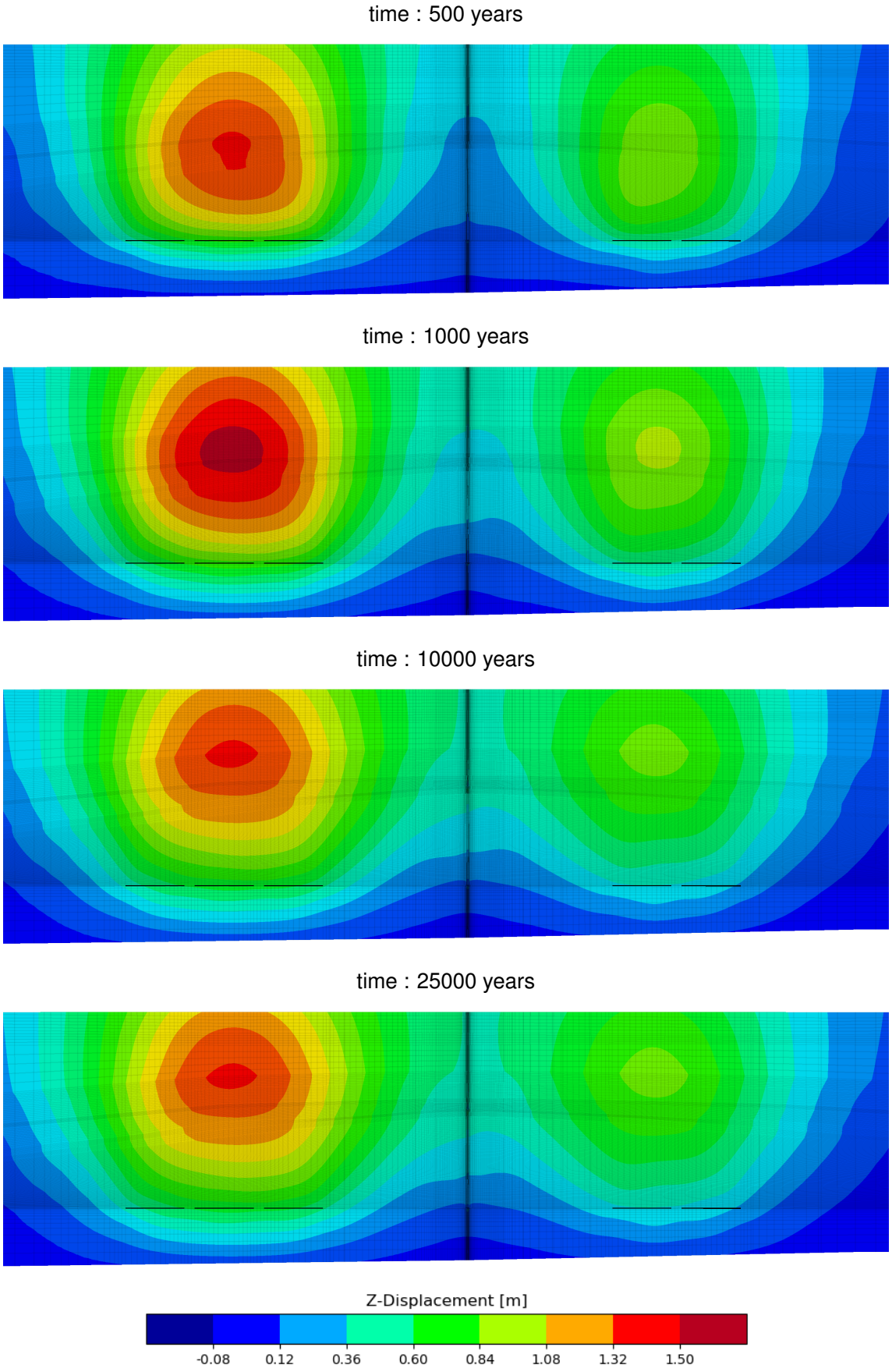

Figure 20.-9: Z-displacement distribution over time in the repository system.

Figure 20.-10 illustrates the evolution of octahedral stress along a longitudinal cross-section of the repository system over the simulation time periods. This stress distribution provides valuable insights into the mechanical response of the surrounding rock to thermal and structural loads over time, with the thermal impacts from the waste disposal fields causing significant stress variations in the salt formation.

At 500 years, regions of high stress, represented by red and orange tones (above 1 MPa), appear in the central part of the salt formation, forming a distinct shear stress band that extends diagonally from the region above the emplacement wing down towards the shaft. This shear stress band effect is more pronounced on the left side due to the higher thermal load generated by more heat-producing waste in that section. The observed stress concentration is primarily due to thermal expansion within the central rock mass. As the rock expands under thermal influence, its expansion is constrained by the stiffer anhydrite layer, leading to significant shear stresses at the contacts with or near this layer.

At 1,000 years, the stress distribution shows a notable reduction in intensity, with the diagonal oriented shear loading of the rock mass diminishing in the central region of the formation. This stress relaxation is a direct result of salt's natural creep behavior, which is highly accelerated by the elevated temperatures in the formation. The creep allows stress to dissipate more rapidly, reducing the overall stress concentrations. As the thermal expansion still evolves, new further deviatoric loaded areas are formed at the upper younger salt layer at the boundary to the overburden layers. The expansion of the rock salt is hindered at the contact to the non creeping overburden layer of Bunter Sandstone leading to the formation of new shear stress concentration.

By 10,000 years, the stress distribution has continued to spread out and decrease in intensity. The previously deviatoric loaded areas have completely vanished in exception of the anhydrite that remains highly stressed as this material does not exhibit creep to help it dissipate the stresses. The transition into green and yellow zones, corresponding to stress values between 5.0×10^5 and 8.0×10^5 Pa reflects the ongoing creep-driven dissipation of shear stresses and suggests that the surrounding rock is gradually approaching mechanical equilibrium.

At 25,000 years, most of the cross-section is represented in blue and green (below 5.0×10^5 Pa), signifying a return to lower stress values across the rock formation. Any remaining stress concentrations are minimal, highlighting the long-term relaxation of the system. By this stage, the repository environment has largely stabilized, with the salt rock nearing a mechanical state similar to its original condition. The area surrounding the shaft still shows some moderate shear stresses due to the interaction between the rock mass and the components installed in the shaft.

In summary, the octahedral stress evolution in the repository system demonstrates the initial dominance of thermal impacts from the waste disposal areas, which lead to significant shear stress, especially near stiffer geological layers like the anhydrite. However, these stresses dissipate progressively over time due to the natural creep behavior of salt, particularly under elevated temperatures. This evolution indicates that thermal loads are impactful in the short term but lessen substantially over the long timescales considered, allowing the repository to achieve a stable, low-stress state that supports the long-term integrity of the containment system.

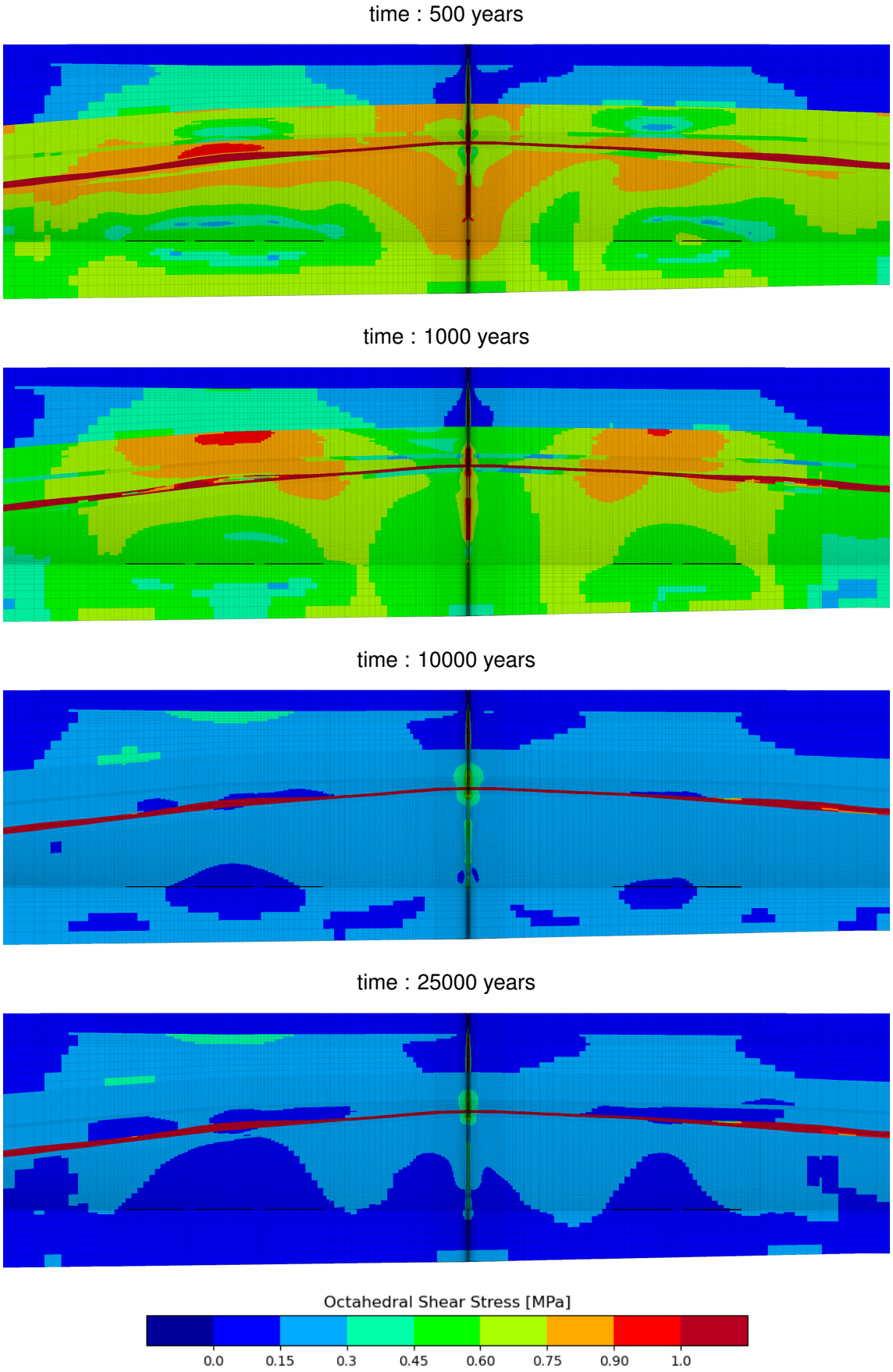

Figure 20.-10: Z-octahedral shear stress distribution over time in the repository system.

The modeling approach developed in the RANGERS project although intended for the integrity assessment of the engineered barrier system includes already all the necessary ingredients for evaluating the integrity of the geological barrier within the same model. This integrated approach enables simultaneous analyses of both the geotechnical and geological barriers, providing a more holistic view of repository stability over extended time periods.

To evaluate the geological barrier's integrity, we analyzed the dilatancy criterion across a longitudinal cross-section of the repository at various time increments: 500, 1,000, 10,000, and 25,000 years, see Figure 20.-11. The dilatancy criterion serves as a key indicator of rock stability; it shows where the stress within the rock exceeds its threshold, potentially leading to dilation, microfracturing, increased permeability, and, potentially, reduced confinement capability. A dilatancy criterion value of one or above signifies the onset of significant dilation, which could compromise the geological barrier's integrity. The dilatancy criterion used in this study, based on the microcrack limit, is formulated as follows (Cristescu and Hunsche, 1998):

$$\frac{\tau}{\sigma_s} \leq -0.01697 \cdot \left(\frac{\sigma}{\sigma_s}\right)^2 + 0.8996 \cdot \frac{\sigma}{\sigma_s}$$

where:

- τ = Octahedral shear stress, defined as:

$$\tau = \frac{1}{3}\sqrt{(\sigma_1 - \sigma_2)^2 + (\sigma_2 - \sigma_3)^2 + (\sigma_3 - \sigma_1)^2}$$

- σ = Mean stress, given by:

$$\sigma = \frac{1}{3}(\sigma_1 + \sigma_2 + \sigma_3)$$

- σ_s = Normalizing stress, set to 1 MPa.

In the early stages, at 500 and 1,000 years, minor dilatancy values of approximately 0.2 to 0.3 are observed in the upper layers of the salt formation. These zones correspond to areas of previously identified shear stress concentration, which likely results from thermal expansion effects generated by the repository's heat output. However, these dilatancy values remain well below the critical threshold of one, insufficient to create significant pathways for fluid migration or compromise the barrier's function.

Below these upper layers, the majority of the salt formation remains unaffected, as indicated by the blue color in the figure, representing a dilatancy criterion value close to zero. This suggests that most of the salt mass in the geological barrier remains its initial tightness and unlikely to experience dilation or increased permeability under the stress conditions modeled.

As the simulation progresses to 10,000 and 25,000 years, the entire rock mass shows a recovery in stress conditions, with no areas exceeding the dilatancy threshold. The absence of zones with elevated dilatancy values at these later stages demonstrates the potential of the salt formation to dissipate stress concentrations through creep. By 25,000 years, the rock structure has stabilized, with no signs of dilatancy, confirming the long-term integrity of the geological barrier.

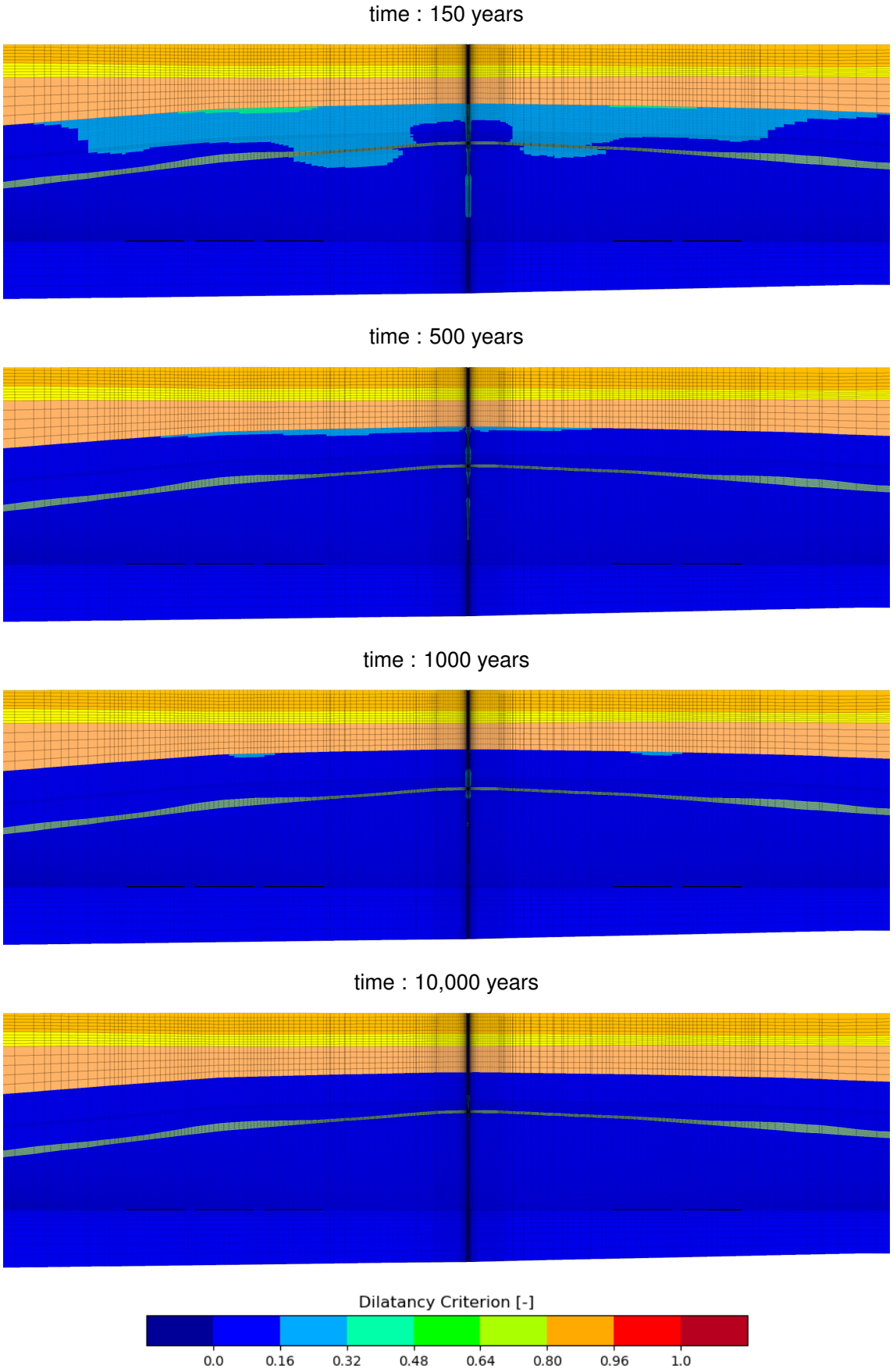

Figure 20.-11: Evaluation of the dilatancy criterion along a longitudinal cross-section of the repository system over different time periods.

This finding supports the robustness of the geological barrier in maintaining containment of the waste. The ability of the model to simulate both the engineered and geological barrier systems within a unified framework provides a powerful tool for comprehensive safety assessments. The results underscore the load bearing capacity and integrity properties of the salt formation, reinforcing its suitability as a host medium for radioactive waste disposal. This approach also highlights the potential for further refinement and extension to other repository designs, where simultaneous modeling of engineered and geological barriers may enhance understanding of long-term containment performance.

In Figure 20.-12, the plasticity state in the non-creeping layers of the geological formation, specifically the overburden and anhydrite layers, is shown to evaluate the potential impact of thermal effects and salt thermal expansion. The analysis aims to determine if these non-creeping geological layers might experience structural damage due to the stresses induced by the repository's heat.

The figure reveals that the anhydrite layer, located above the emplacement fields, does indeed show localized plasticity, indicated by pink areas. This damage is confined to regions directly above the disposal areas, where thermal expansion of the salt leads to increased stress in the overlying anhydrite. Importantly, however, the damage remains limited in spatial extent, without extending across the full width of the formation. This localized damage suggests that while the anhydrite layer is affected by the thermal expansion, it does not create continuous fracture paths or secondary migration pathways for fluid movement through the anhydrite.

In conclusion, while thermal expansion generates sufficient stress to cause minor plasticity in specific zones of the anhydrite layer, this effect is spatially restricted and does not compromise the integrity of the geological barrier as a whole. The confinement of plasticity within localized areas minimizes the potential for fluid migration, indicating that the geological barrier remains effective in isolating the repository over the assessed period.

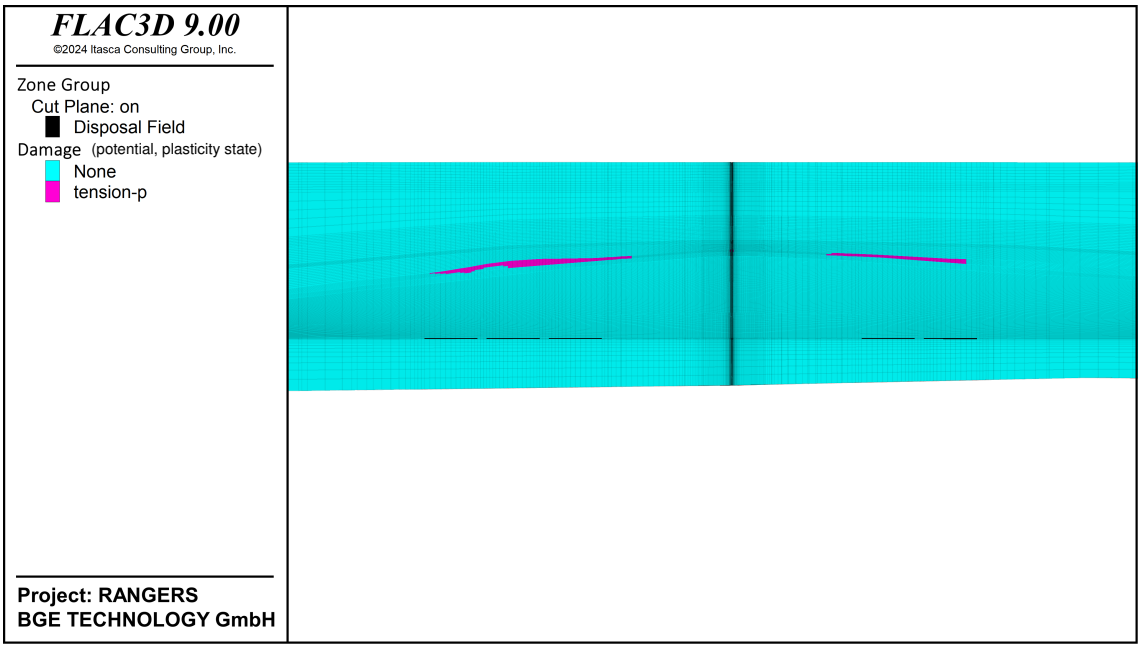

Figure 20.-12: Potential damage in the anhydrite layer at 25,000 years.

We now turn our focus to the thermal-mechanical evolution in the near field of the shaft to assess its impacts on the shaft sealing structure.

Figure 20.-13 illustrates the distribution of displacement in the x-direction within the near field around the shaft. In the upper part of the shaft, the x-displacement is primarily driven by the lateral expansion of the entire geological formation due to thermal effects. This thermal expansion of the rock mass induces outward displacement, which is evident in the shaft's surrounding regions. In contrast, the lower part of the shaft shows displacement patterns dominated by the lateral expansion of the salt rock itself, creating additional lateral pressures on the shaft structure.

In this lower region, the displacement field around the shaft exhibits a symmetrical pattern, suggesting that the shaft sealing structure is subject to compaction forces from both sides. This compaction effect is critical as it influences the stability and integrity of the shaft sealing structure over time. Notably, along the length of the MgO seal, there is an absence of lateral displacement, attributed to the high stiffness of the MgO concrete, which effectively resists deformation and maintains stability in response to lateral pressures.

Overall, this displacement pattern indicates that the shaft and its immediate surroundings experience significant lateral stresses. These stresses, arising from thermal and mechanical expansion, have to be taken into account in the integrity and design of the sealing components in the shaft.

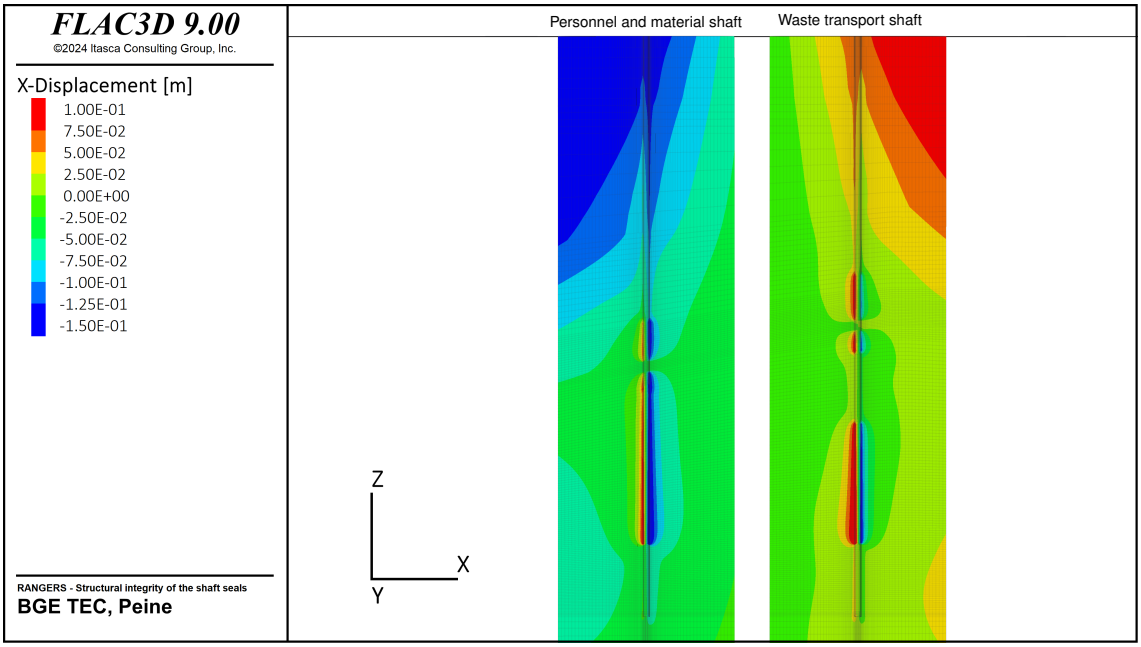

Figure 20.-13: X-displacement distribution in the near field of the shafts at 25,000 years.

Figure 20.-14 illustrates the distribution of displacement in the z-direction (vertical) within the near field around the shafts at the end of the simulation at 25,000 years.

In the upper part of the formation near the shaft, the displacement reaches substantial values exceeding 50 cm, with a near-symmetrical distribution along the shaft's length. The displacement is particularly high near personnel and material shaft, which is closer to the emplacement

fields. This pronounced vertical displacement primarily results from the thermal expansion of the rock mass, which exerts upward pressure as it heats up over time. The upward movement is most intense near the surface, gradually diminishing with depth. This trend is illustrated by the transition from red and orange in the upper regions to yellow and green tones further down the shaft, indicating a reduction in displacement.

In contrast, the lower part of the shaft exhibits relatively minimal displacement, marked by blue and green areas with values up to 20 cm. This reduced displacement reflects the cumulative nature of rock expansion. Near the thermal source, where heat initially concentrates, expansion is minimal, but it increases with distance from this focal point, leading to more significant displacement further along the shaft.

Similar pattern can be observed in Figure 20.-15 and Figure 20.-16 where the evolution of the Z-displacement over time are presented for the near field of the personnel and material shaft and the waste transport shaft. Over time an increase of the displacement increments are from top to bottom is noticeable.

These observations indicate a generally uniform response to thermal expansion forces. This displacement pattern suggests that the sealing components are primarily influenced by heave.

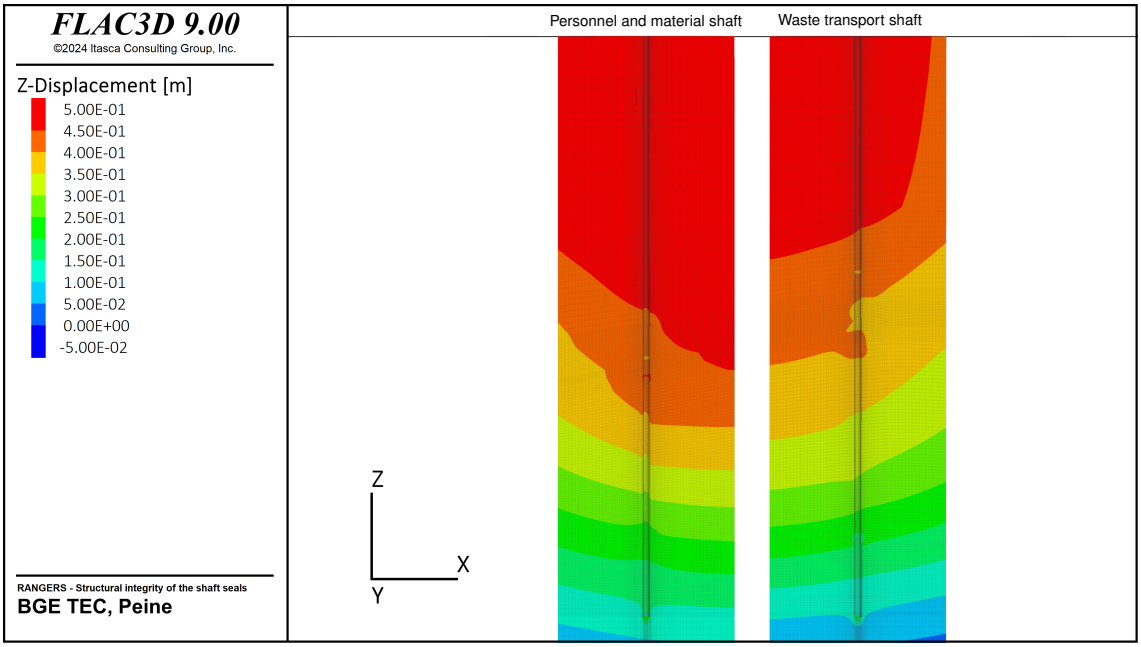

Figure 20.-14: Z-displacement distribution in the near field of the shafts at 25,000 years.

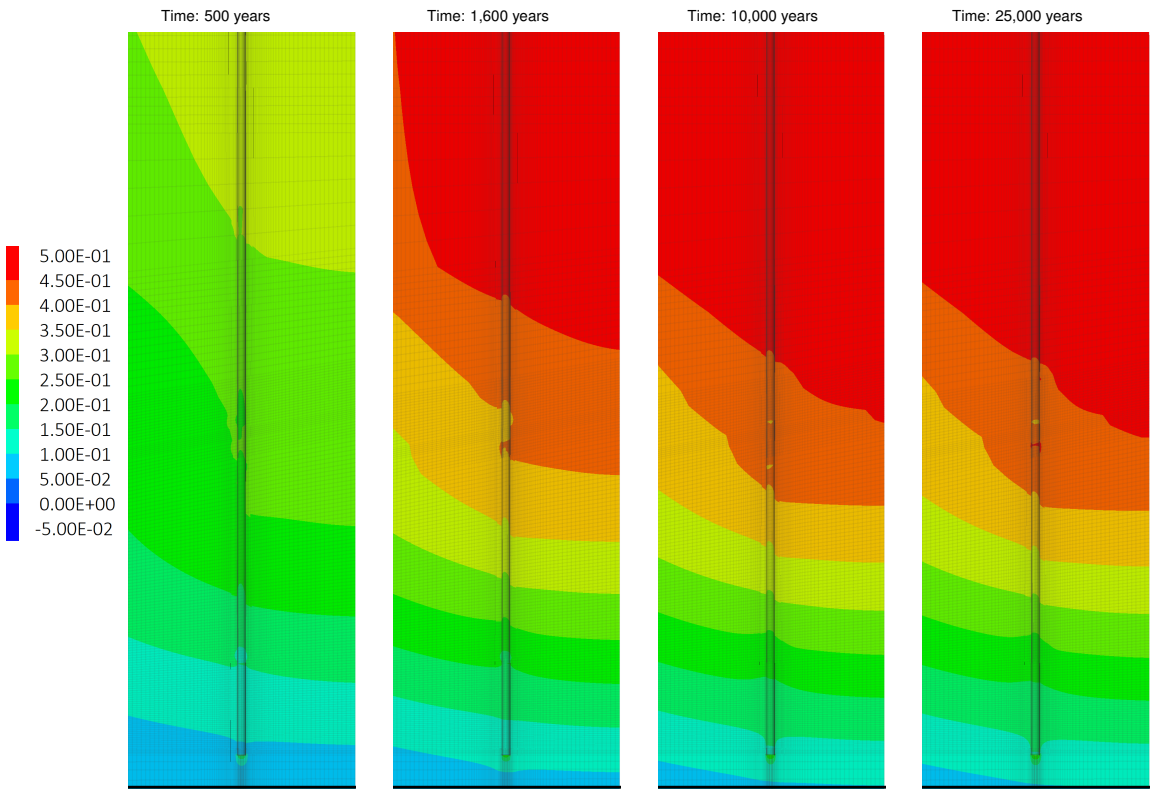

Figure 20.-15: Z-displacement distribution over time near personnel shaft.

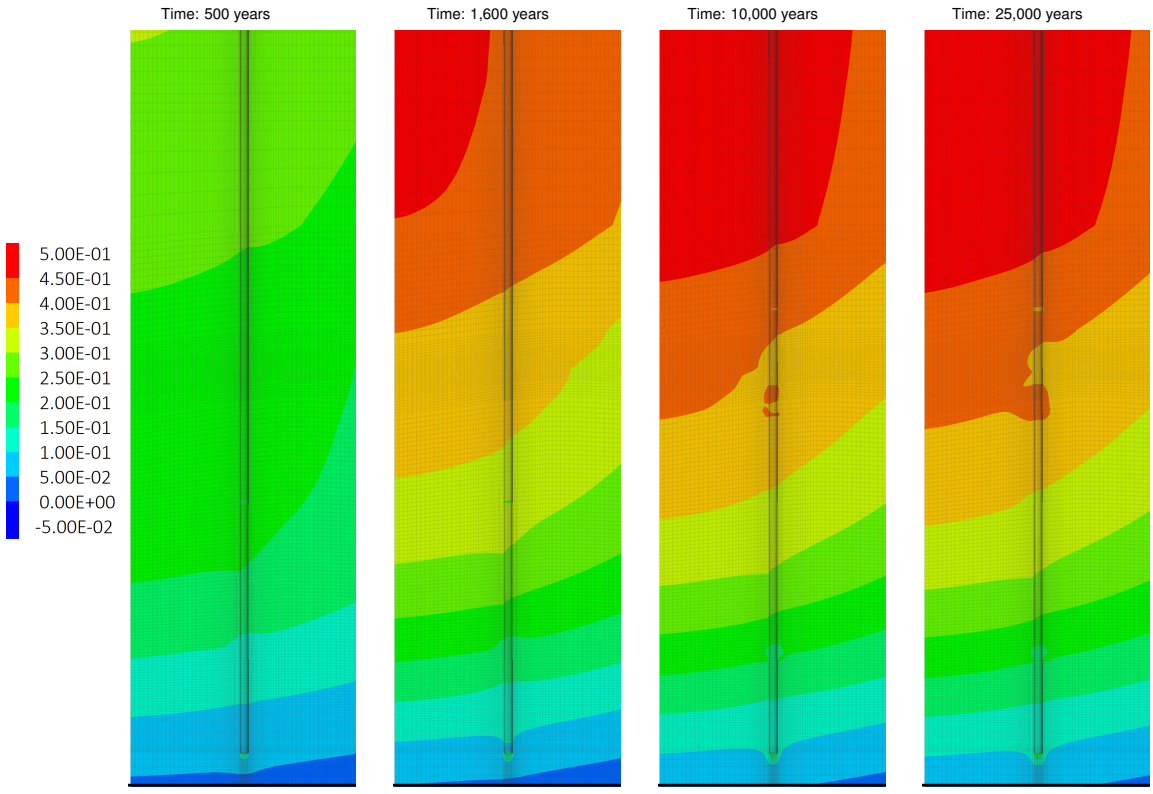

Figure 20.-16: Z-displacement distribution over time near waste transport shaft.

Figure 20.-17 illustrates the distribution of octahedral stress (Pa) within the shaft and surrounding rock, as observed in a cross-sectional view along the shaft's length. This distribution provides insights into how the shaft and its surrounding formations respond to thermal and mechanical loading.

In the upper part of the shaft within the overburden, there is a notable concentration of stress along the shaft contour, characteristic of an Excavation Damaged Zone (EDZ) typically induced by excavation processes. Moving into the upper portion of the salt formation, we observe a significant concentration of shear stress surrounding the bentonite sealing elements. This stress concentration is likely due to the bentonite being modeled as a highly plastic material, which lacks the structural rigidity to counteract the surrounding rock's deformations caused by the compression of salt as it undergoes thermal expansion. Consequently, the bentonite allows the rock's compressive movements, leading to elevated shear stress zones in its vicinity.

In contrast, the lower part of the shaft, where the sealing materials are primarily composed of gravel and MgO concrete, shows significantly reduced stress concentrations. The high stiffness of these materials effectively limits deformation, confining shear stress primarily to the immediate shaft contour and minimizing its spread into the surrounding rock. This rigidity allows the lower shaft components to better sustain the compressive forces exerted by the expanding salt, helping to preserve the shaft's structural integrity.

Materials with low stiffness, such as bentonite, may contribute to increased shear stress zones due to their inability to fully resist the compressive forces of the surrounding rock. Conversely, high-stiffness materials like MgO concrete and gravel effectively reduce stress propagation, confining shear stress to a smaller area near the shaft contour.

Figures 20.-18 and 20.-19 depict the temporal evolution of octahedral shear stress in the near field of both shafts. A similar interaction pattern between the host rock and the shaft components is observed throughout the simulation.

At t = 500 years, high stress concentrations are evident along components with lower stiffness. The MgO seals exhibit shear stresses comparable to those in the surrounding rock formation, indicating a relatively balanced stress distribution in these regions. However, at t = 1600 years, a stress recovery is apparent in the near field. Despite this, elevated stress levels persist around the bentonite seal.

By t = $10,000$ years, the stress distribution stabilizes, resembling the conditions observed at t = $25,000$ years. At this later stage, the zones of shear stress redistribution have expanded significantly around the shafts. These stress concentrations are particularly pronounced around components with lower stiffness, underscoring their impact on the mechanical interaction between the shaft components and the surrounding host rock. The progression highlights how the stiffness of the material in the shaft may affect the long-term integrity of the shaft system. A preference for high stiffness materials becomes evident.

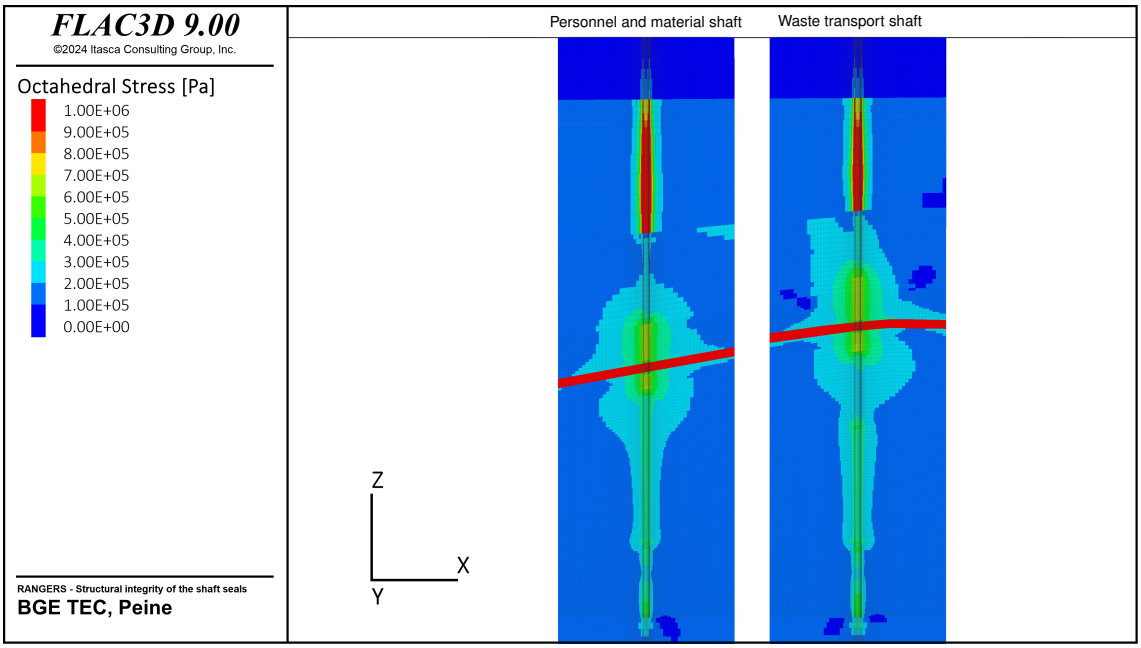

Figure 20.-17: Octahedral shear stress distribution in the near field of the shafts at 25,000 years.

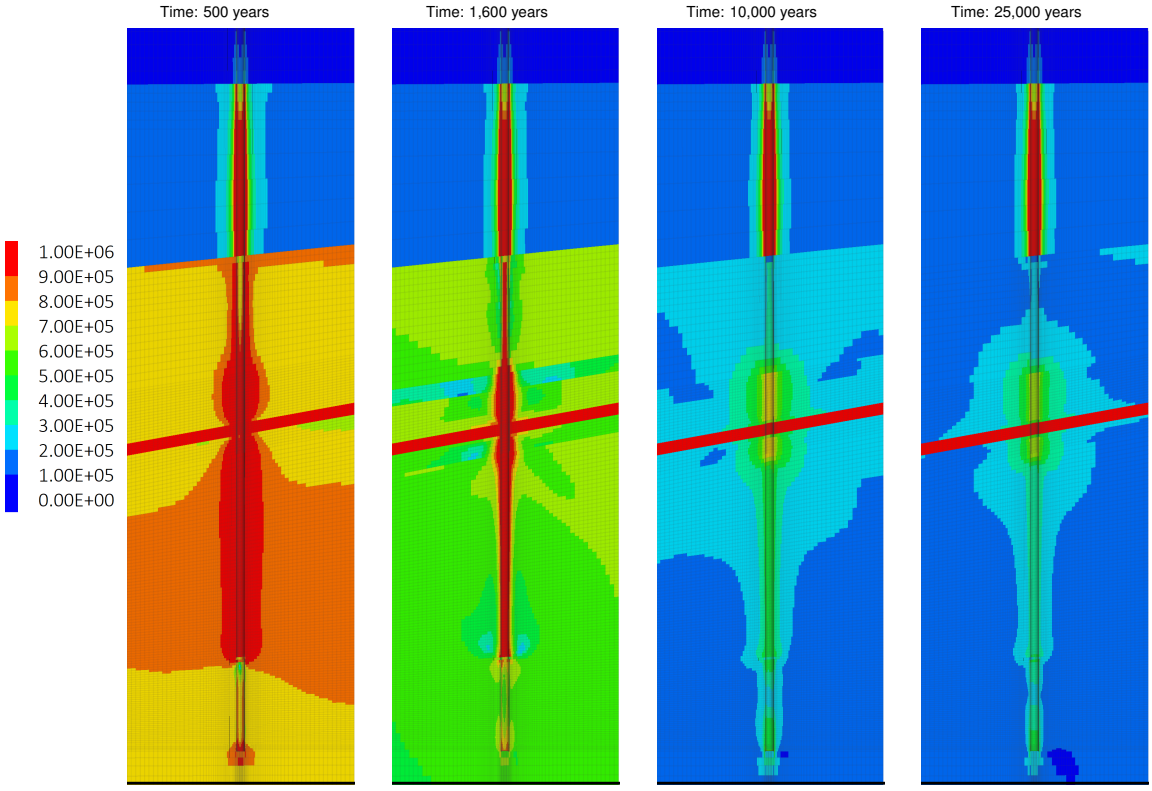

Figure 20.-18: Octahedral shear stress distribution over time near personnel shaft.

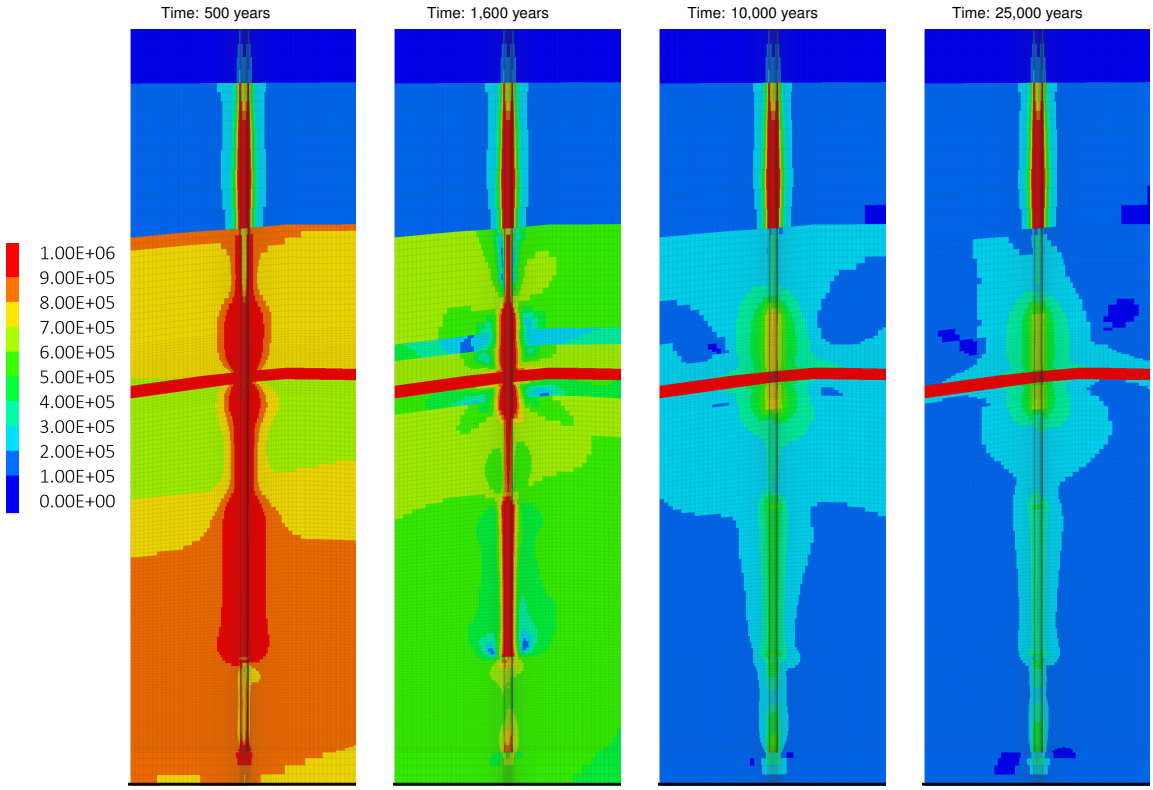

Figure 20.-19: Octahedral shear stress distribution over time near waste transport shaft.

Figure 20.-20 presents the evalutation of the dilatancy criterion along the shaft and surrounding geological formations with a zoom at the location of the bentonite. This criterion indicates the regions where the rock has reached or surpassed its dilatancy threshold, signifying areas where micro-fracturing may begin, thus potentially increasing permeability and affecting stability.

The figure primarily highlights the salt formation itself, where dilatancy is a critical factor. In the vicinity of the shaft, particularly around the contact areas with the bentonite seals, the evaluation of the dilatancy criterion shows values in the range of 0 to 0.3. These values correspond to the high shear concentration observed at this location. Outside of the bentonite length, no dilatancy is observed along the shaft. As previously discussed, this is due to the low stiffness of bentonite allowing movement of the rock. Nevertheless, these values indicate that the salt formation remains below the critical dilatancy threshold of 1, meaning it does not exhibit significant dilation or micro-cracking.

As time progresses, the salt rock around the shafts maintains its structural integrity with minimal changes in dilatancy criterion values that is expected to vanish with time. This further demonstrating the stability of the salt formation under the applied thermal and mechanical loads. This stable condition in the salt formation indicates that the geological barrier remains intact, effectively preventing any secondary migration paths or zones of increased permeability along the shafts that could compromise the repository's containment function.

In conclusion, the results demonstrate that the salt formation can withstand the stress conditions surrounding the shaft without significant dilation, confirming its effectiveness as a long-

term containment barrier.

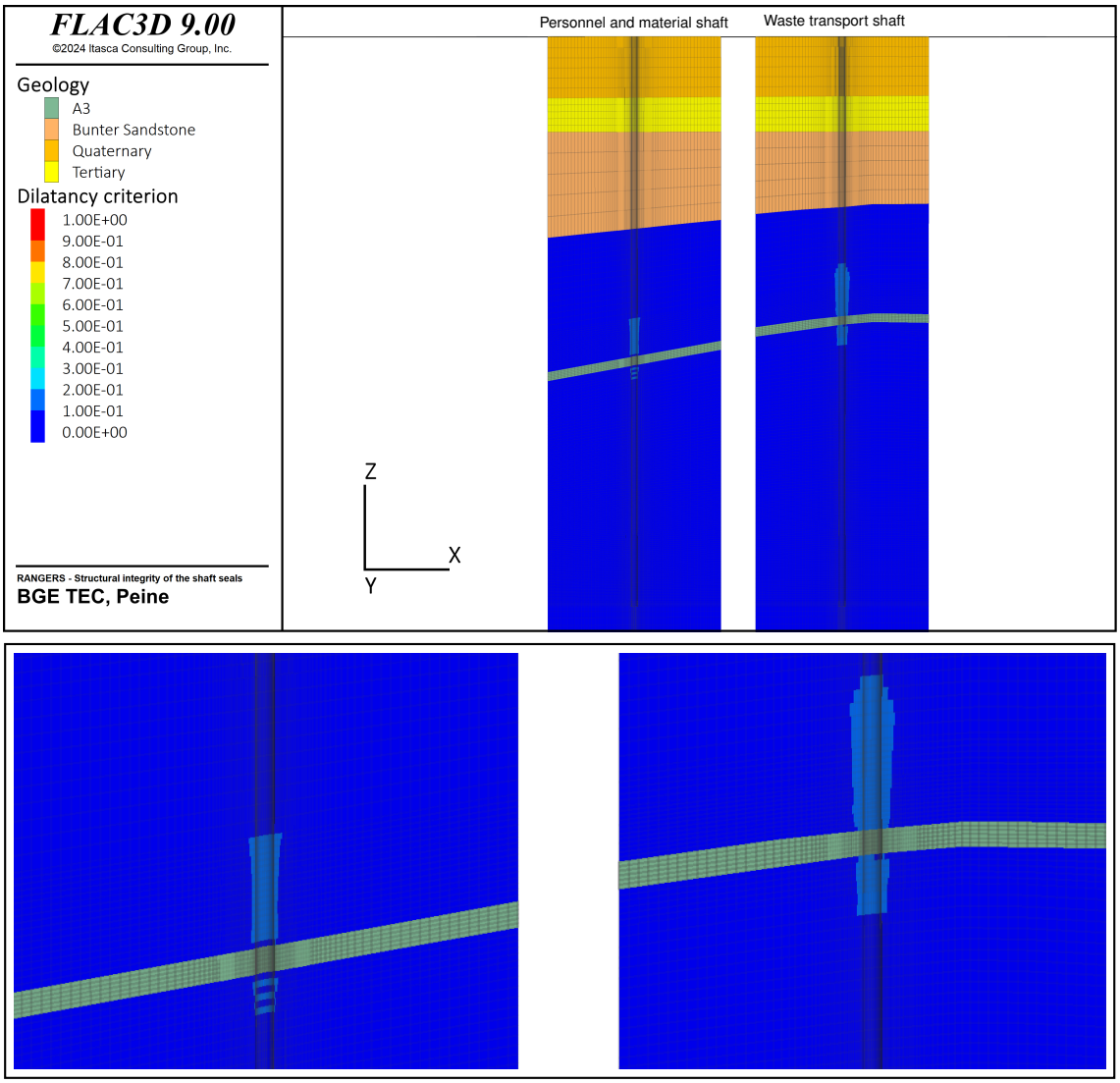

Figure 20.-20: Dilatancy criterion evaluation in the near field of the shafts at 25,000 years. Bottom figure shows a zoom a the location of the bentonite seals.

We now turn to analyzing the mechanical behavior of the shaft sealing system and its individual components in response to the thermal-mechanical evolution of the surrounding geological formation.

We have previously observed that the thermal expansion of the salt will cause a general upward displacement of the salt formation, extending up to the surface. This upward movement also affects the near-field area surrounding the shaft, as indicated in Figure 20.-14. Also it has been shown in Figure 20.-8 that the displacement vectors around the shaft are oriented upwards. Consequently, it is reasonable to conclude that the shaft sealing structure installed in both shafts will also undergo some degree of uplift.

Figure 20.-21 shows the vertical (z-direction) displacement distribution within the shaft sealing structure for both shafts. A displacement gradient is observed along the depth of each shaft,

with the largest displacement occurring near the surface — up to 0.5 m — and decreasing to about 10 cm at the bottom of the shaft. In contrast, the deeper sections of the shafts experience substantially less displacement. Similar patterns were noted for the near-field displacement around the shafts, as shown in Figure 20.-14.

The non-uniform displacement along the shaft implies that the shaft sealing structure is subject to a stretching effect. As the salt formation undergoes thermal uplift, it effectively stretches the sealing structures within the shafts, leading to tensile forces along the shaft's length. This stretching indicates that tensile stresses are likely to develop within the shaft sealing system due to the differential displacement. This observation is crucial for the integrity assessment of the sealing system, as tensile stresses can potentially impact the sealing performance if not properly accounted for in the design.

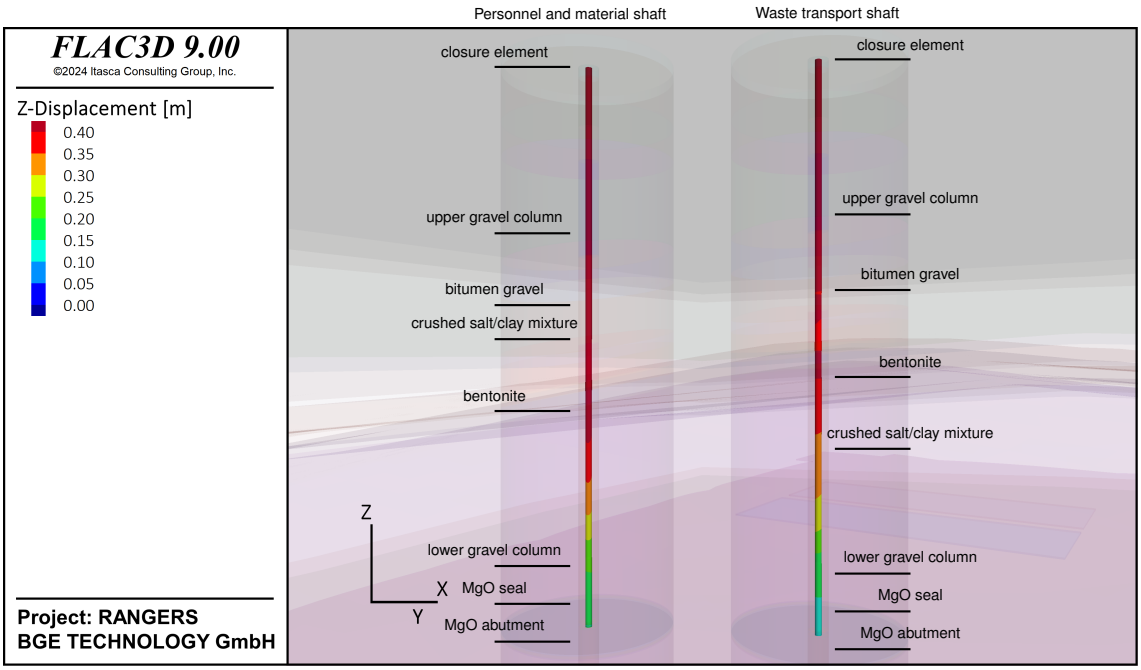

Figure 20.-21: Z-displacement distribution along the shaft sealing systems at 25,000 years.

To assess the impact of the stretching effect on the shaft sealing structures, we analyze the distribution of maximum principal stresses within the components installed in the shaft.

Figure 20.-22 presents the distribution of maximum principal stress (in Pa) along the shaft sealing structure in both shafts at the end of the simulation, at 25,000 years. This visualization provides insights into how stresses are distributed across the shaft sealing components, under the influence of thermal and mechanical effects from the surrounding rock formation.

In the upper sections of each shaft, where the gravel column is installed, the maximum principal stress are still negative reaching moderate values near zero, indicating that no tensile stresses is occurring in these sections of the shafts.

Moving deeper into the shafts, in the middle sections, the maximum principal stress generally decreases, falling within the range of -4×10^6 Pa to -6×10^6 Pa, indicating an increase of compressive forces. This increase is attributed to the low stiffness and probably the high

confining pressure exerted by the surrounding salt formation.

At the lower end of the shafts, we observe a decrease of compressive stresses reaching low value of less than 2 MPa in the MgO concrete seals. This effect is due to the high stiffness of MgO concrete, which cannot accommodate the uplifting forces generated at the shaft's boundaries. Moderate development of tensile stresses at the interface of the MgO concrete to the gravel columns can be also observed due do the rigid contact at this interface. If the uplifting process was higher, which is to be expected if we were able to run the simulation thermomechanically over the 25,000 years one could expect a buildup of tensile stresses in the MgO seals. If these stresses exceed the material's tensile strength, they could lead to tensile failure, compromising the integrity of the sealing elements if cracks were to form.

Overall, the stress distribution reveals the potential for tensile stresses to develop within the shaft sealing structure as a consequence of the uplift of the surrounding rock due to thermal expansion. This mechanism poses a critical consideration for the design of shaft sealing systems, as it may necessitate material and structural adaptations to mitigate tensile stress and prevent potential failure within the shaft seals. This analysis underscores the importance of accounting for uplift-induced tensile forces in ensuring the long-term effectiveness and resilience of the shaft sealing system.

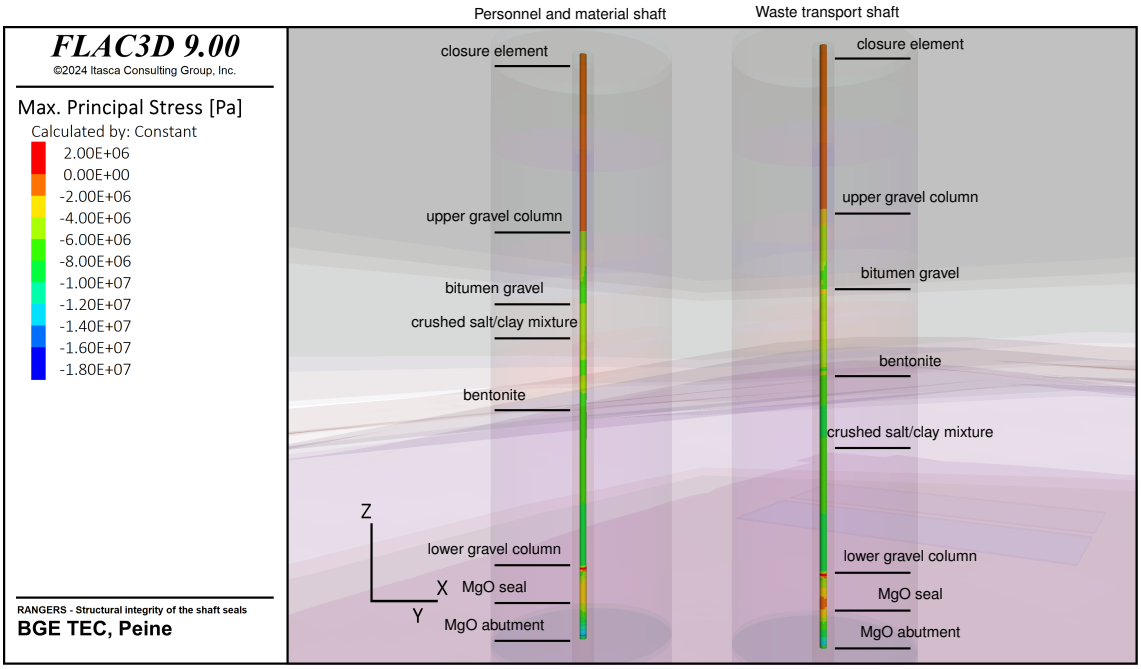

Figure 20.-22: Max principal stress distribution along the shaft sealing systems at 25,000 years.

Figure 20.-23 provides a view of the two shafts and their sealing structures, displaying the distribution of mean stress (in Pa) along the shaft length 25,000 years after the repository closure. The shafts are illustrated as vertical structures embedded within a semi-transparent representation of the geological model, allowing us to see the stress conditions within the context of the surrounding rock.

As we will observe later, the deviatoric stresses within the shaft are relatively small compared

to the mean stress. Under these conditions, the mean stress can be considered a reasonable approximation of the confining pressure in the shafts.

The figure reveals a clear distinction in confining pressure between the overburden and salt formation. In the overburden, consisting of sandy layers, the shaft sealing system experiences relatively low confining stresses. This is due to the non-creeping behavior of the sandy layers, which lack time-dependent deformation properties. However, in the salt formation, significantly higher confining pressures are observed, increasing with depth. This gradient reflects the combined effects of the surrounding rock's confinement and the thermal and mechanical loads exerted on the shaft, as previously discussed.

The results in the figure indicate that the main sealing elements — composed of bitumen gravel, a crushed salt/clay mixture, and bentonite — are subjected to confining pressures in the range of 4 to 10 MPa. Meanwhile, the MgO concrete seal and its abutment experience pressures between 12 and 18 MPa. These high confining stresses bring several advantages to the overall integrity and performance of the shaft sealing system.

Firstly, high confining stresses enhance the strength of the sealing materials, as it is well-known that the strength of materials increases under triaxial compressive loading conditions. This effect reduces the likelihood of failure in the sealing components, making them more resilient to various loading conditions. Secondly, the high confining pressures ensure that any potential micro-cracks or fractures within the sealing elements are likely to be closed or minimized. This includes closing of any voids that might have formed during installation or minor installation-related imperfections.

Furthermore, high confining stresses contribute to the long-term stability and robustness of the sealing system by compensating for potential human errors during installation. The pressure exerted on the materials aids in self-sealing processes, as it promotes compaction and densification of materials. This self-sealing effect, combined with the high confining pressure, creates an additional safety buffer that strengthens the barrier function of the shaft sealing system over time.

In summary, the presence of high confining pressures in the salt formation enhances the overall performance and reliability of the shaft sealing system. It increases material strength, promotes self-sealing of micro-cracks, and mitigates installation imperfections, thus reinforcing the shaft's role as a long-term containment solution for radioactive waste. It also emphasizes the quality of salt not as a host rock for radioactive waste but as a excellent medium for the installation of the EBS.

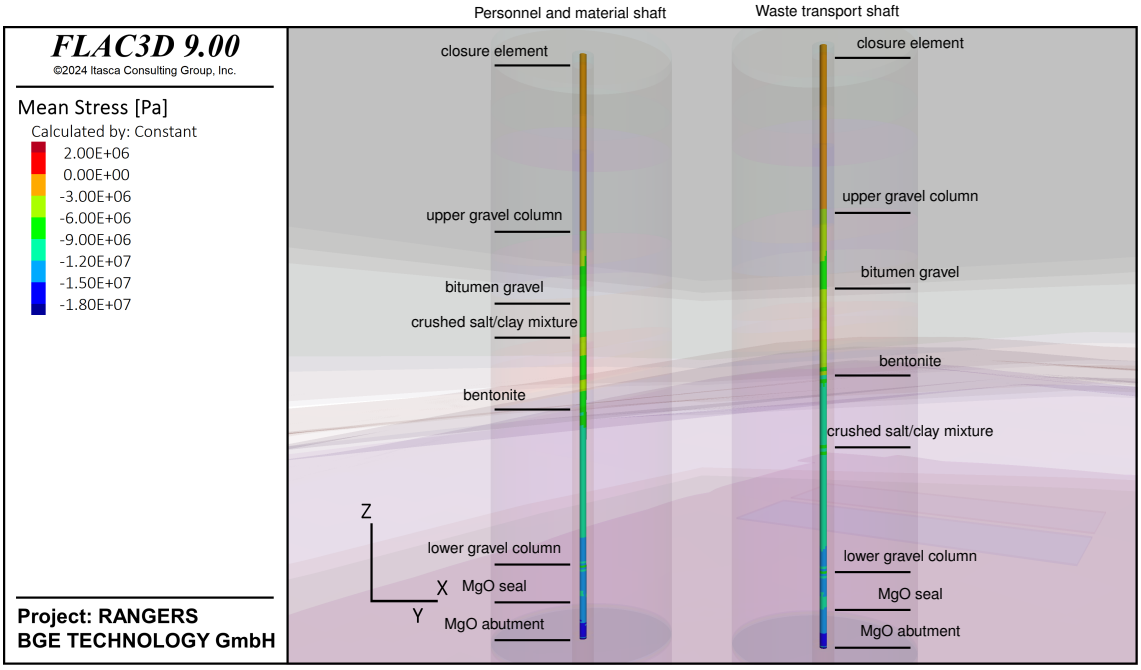

Figure 20.-23: Mean stress distribution along the shaft sealing systems at 25,000 years.

Figure 20.-24 also highlights two distinct patterns concerning the development of shear stresses along the shaft, which arise from similar factors as those discussed in the mean stress analysis. In the overburden, low shear stresses are observed due to the non-creeping, sandy nature of the upper layers. However, in the salt formation where the shaft sealing system is embedded, significantly higher shear stresses are present, distributed relatively uniformly along the depth of the shaft.

One notable exception is the bentonite element, which remains nearly stress-free. This is because bentonite, with its high plasticity, has been modeled to dissipate shear stresses through plastic yielding, effectively preventing the buildup of shear stress. The material's capacity to yield plastically allows it to absorb and redistribute mechanical loads, preventing stress concentration within this element.

Overall, the distribution of shear stress highlights the role of different materials within the shaft sealing system. For stiffer materials in the salt formation, substantial shear forces are expected. They need to be designed to sustain those shear forces. For low stiff materials such as bentonite, their plastic behavior serves as a buffer, reducing stress transfer to other sealing components. This property enhances the system's overall resilience, as it helps prevent stress localization and potential damage to other elements within the shaft sealing structure. This balanced distribution of stresses contributes to the robustness and longevity of the sealing system under thermal-mechanical loads.

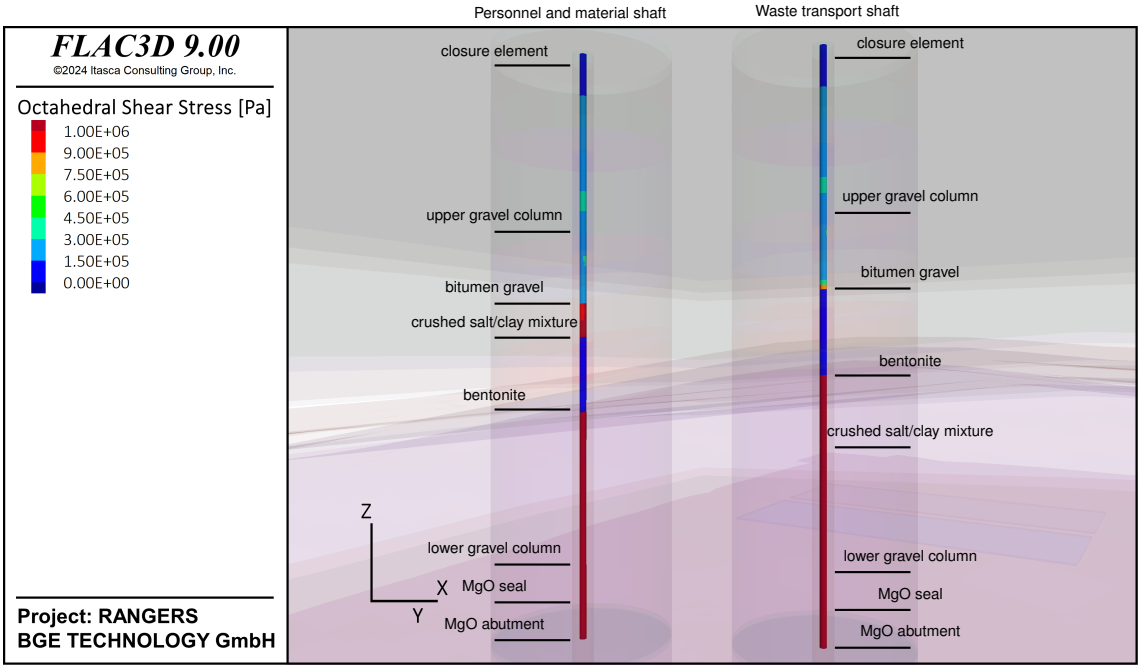

Figure 20.-24: Octahedral shear stress distribution along the shaft sealing systems at 25,000 years.

The effects of the stresses acting on the components installed in the shaft are reflected in the state of plasticity of these components, which is evaluated using constitutive models that describe their mechanical behavior. From the stress analysis discussed previously, two primary failure mechanisms emerge: tensile failure in the MgO seals, due to the tensile stresses arising from the extension of the shaft sealing structure, and shear failure in components experiencing high shear stresses. These potential failures are, however, mitigated by the high confining stresses acting on the materials, which help to counterbalance and contain these stresses.

Figure 20.-25 illustrates the state of plasticity within the shaft sealing structure after 25,000 years. The results show that only the bentonite element undergoes plastic deformation, consistent with its design as a highly plastic material intended to yield and dissipate stress. All other sealing components remain structurally intact throughout the simulation period, indicating that the integrity of the system is preserved over the verification period. This outcome underscores the positive role of high confining stress, which enhances the triaxial strength of materials, thereby improving their resistance to both tensile and shear failures.

Overall, the results demonstrate that the engineered shaft sealing structure, under the given stress conditions, is capable of maintaining integrity over extended timescales.

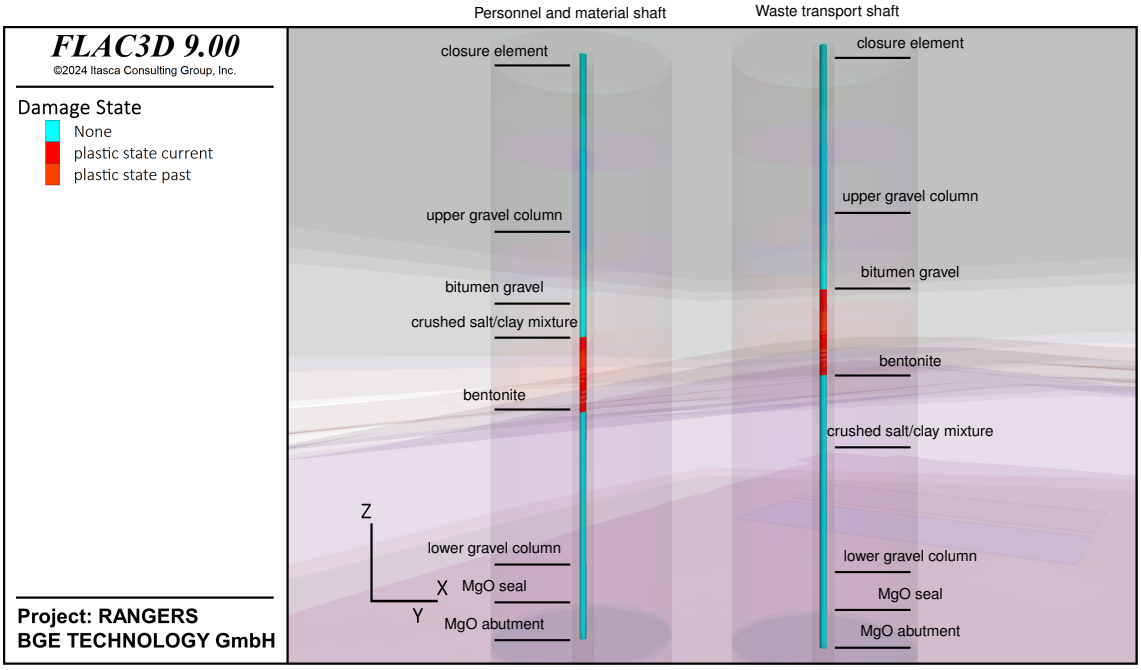

Figure 20.-25: Damage state in the shaft sealing systems at 25,000 years.

20.5.2 Modeling with Interfaces

A modeling case by using interfaces elements instead of rigid contact between the rock and the components in the shaft were carried out. This approach has the merit to be more realistic as the contact zone properties can be estimated through laboratory experiments.

Unfortunately using interfaces also bring another layer of numerical complexity and often fails when large deformation accumulate in the model. For this reason, we were able to run the simulation only for 150 years.

Fortunately, this period of time is good enough for benchmarking the reference approach using rigid contact and to understand what is going on at the contact zone.

For the benchmark, we compare the invariants of the stress tensor: mean stress of octahedral stresses. As it can be seen in figure 20.-26, only minor differences are remarkable between the mean stress distribution of the case with rigid contact and the case with interface. The same can be concluded for the octahedral shear stress in Figure 20.-27. From this analysis on can conclude that the use of rigid contact which are numerically efficient are accurate enough to model the soil structure interaction at the interface between the shaft sealing structure and the salt.

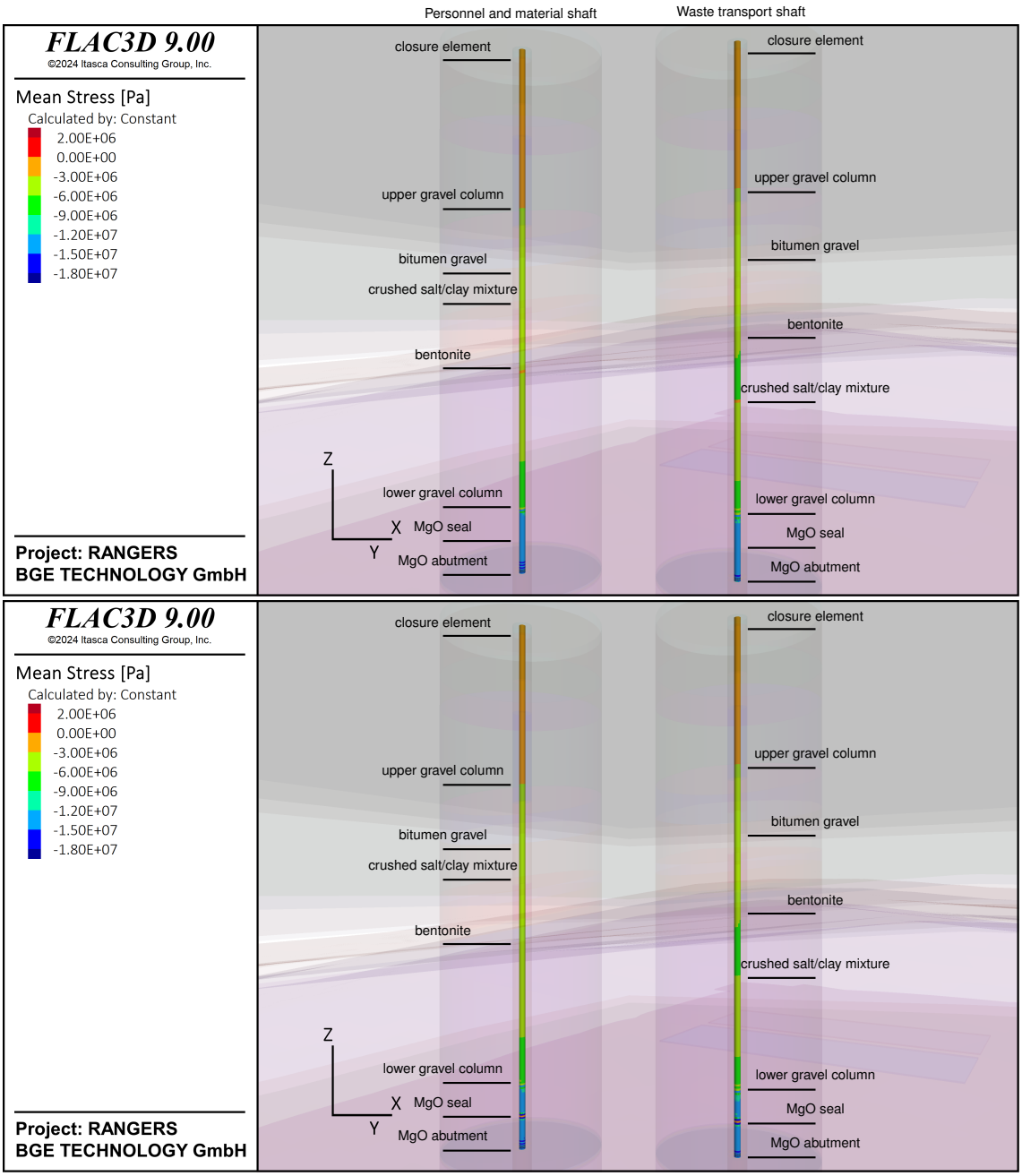

Figure 20.-26: Mean stress distribution along the shaft sealing systems at 150 years: simulation without interface (above), simulation with interface (below).

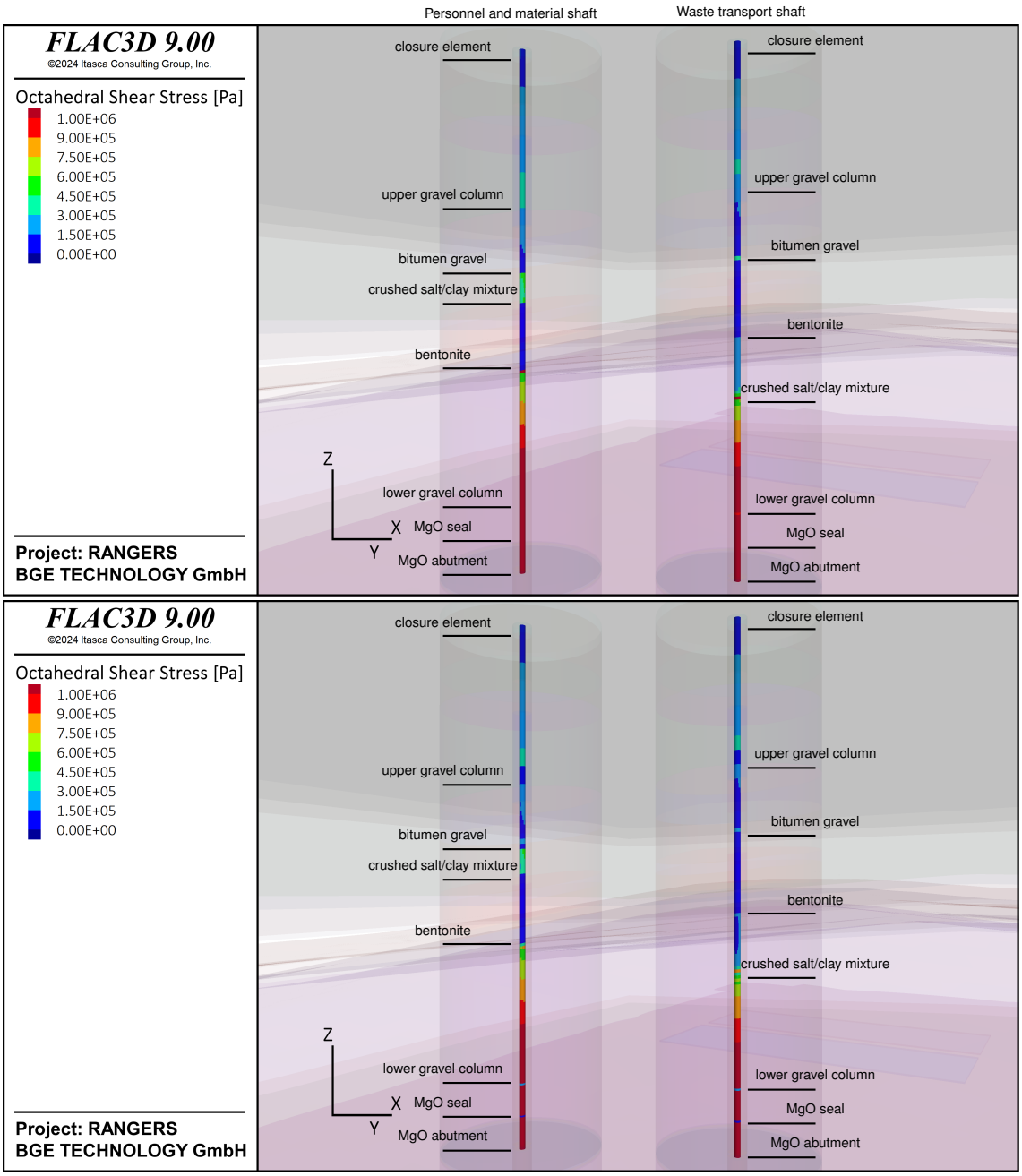

Figure 20.-27: Octahedral shear stress distribution along the shaft sealing systems at 150 years: simulation without interface (above), simulation with interface (below).

The modeling case with interface elements provides valuable insights into the behavior at the contact between the shaft sealing structure and the surrounding salt rock. In Figure 20.-28, which displays the distribution of shear stress at the interface, one can observe shear stresses in the range of 1 to 1.5 MPa occurring specifically at the interface between the MgO concrete and the salt. In contrast, the shear stresses along the rest of the shaft interface are significantly lower, generally less than 0.5 MPa. The pronounced shear stress concentration at the MgO concrete contact is likely due to the high stiffness of this material, which restricts deformation and thus generates additional resistance against the surrounding rock's thermal expansion and mechanical movement.

In Figure 20.-29, the interface normal displacement along the shaft is presented. The results show a noticeable normal displacement, amounting to several millimeters, along the length of the bentonite seal. In contrast, the normal displacements along the other segments of the shaft are negligible. This observation is consistent with the high plasticity and low stiffness of the bentonite, which allows the surrounding rock to exert additional compressive force onto the shaft, further compacting the bentonite.

These displacement and stress distributions highlight the balancing act between compaction of the bentonite and convergence in the rock. While the plastic behavior of bentonite facilitates this balance by yielding under stress and accommodating the rock's movement, it also provoke some dilation in the rock retarding the recovery of the dilatancy criterion as it has been discussed earlier. Also, In the case of MgO concrete, its high stiffness helps to limit deformation, maintaining a robust barrier but also concentrating shear stress at its interface. This dynamic indicates that the interface behavior is crucial in managing the interactions between the sealing materials and the salt. The evolution at the interface needs therefore thorough investigations in the scope of future safety and integrity assessments.

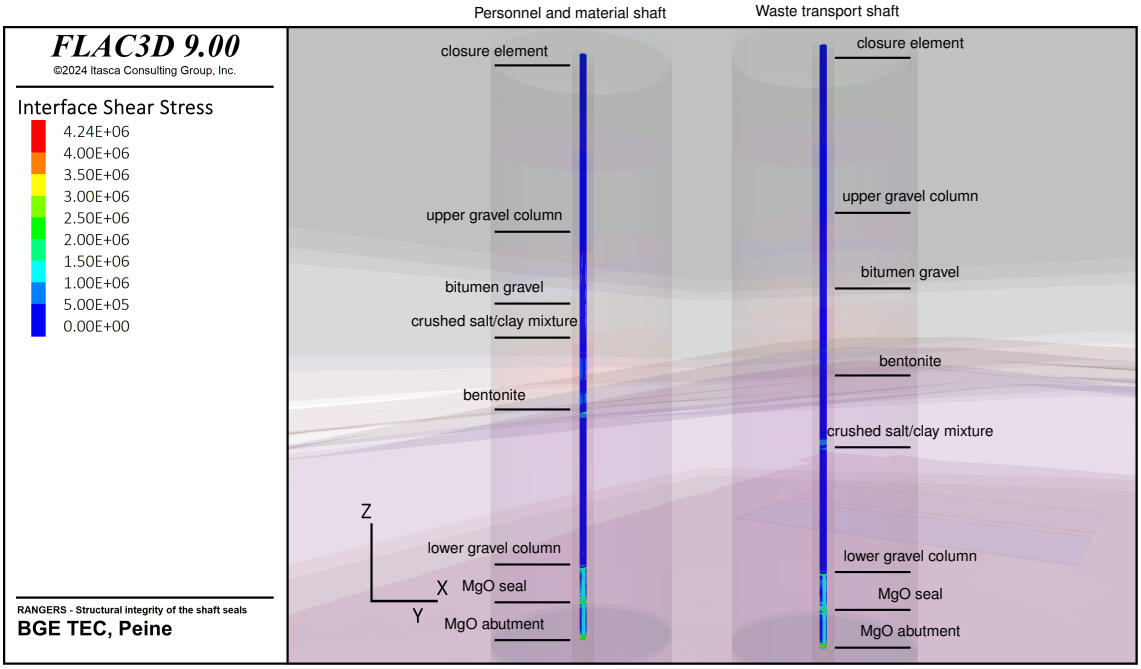

Figure 20.-28: Shear stress distribution in the interfaces at the shaft contours at 150 years.

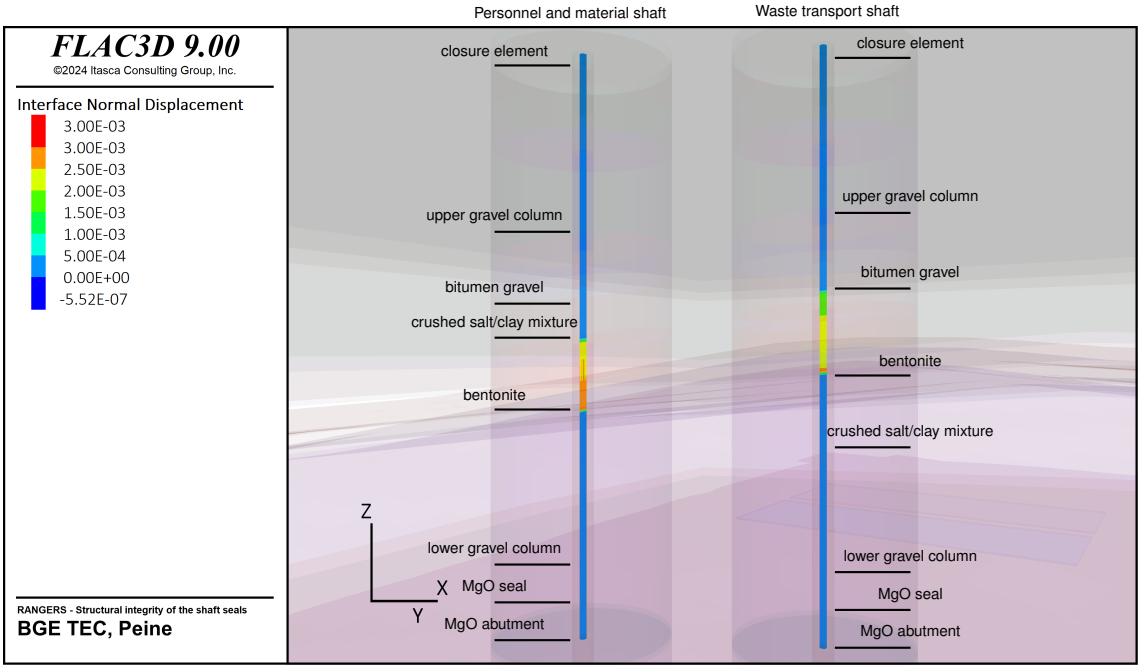

Figure 20.-29: Normal displacement distribution in the interfaces at the shaft contours at 150 years.

20.5.3 Conclusion and Barrier Integrity Assessment

The mechanical integrity assessment of the shaft sealing system demonstrates its capability to withstand thermal-mechanical loads over extended periods, ensuring effective containment within salt repositories. By examining the system's response to thermal expansion and creep behavior, we have validated that the sealing system's design and material choices are suitable for maintaining structural stability under the anticipated repository conditions. Importantly, the results confirm that the shaft sealing structure remains damage-free throughout the simulation period.

The integrity of the shaft sealing system is reinforced by several key findings:

- High confining pressure advantage: In the salt formation, the high confining pressure significantly enhances the strength of sealing materials, leading to greater resistance against tensile and shear stresses. This pressure also helps to close micro-cracks and voids, maintaining the continuity and robustness of the seal, even under variable loading conditions. The high confining pressure plays a crucial role in ensuring that the system remains damage-free over time.
- Material behavior under thermal expansion: Thermal expansion of the salt creates an upward displacement, generating tensile stresses in the shaft sealing structure. Materials with high stiffness, such as MgO concrete, may eventually experience localized tensile stresses that could lead to cracking if not managed appropriately. However, the high confining pressure helps mitigate these stresses, contributing to the damage-free status of the shaft. It also possible to build the MgO seal in different segments to limit of the tensile stresses. These findings emphasize the importance of selecting materials

and techniques that can tolerate such stresses or adapting the design to accommodate them.

- Interface and contact zone stability: The simulation of interfaces between sealing components and surrounding rock highlights the importance of realistic contact modeling. While rigid contact assumptions are efficient and adequate in many cases, certain materials with a definite contact shear strength such at the interface salt/MgO concrete require careful consideration of shear and normal stress distribution. Although, in the conditions under the high confinement of the shafts together with a possible cohesion at the contact surface, the two modeling approaches appear to be similar.
- Long-term stability and self-healing properties of salt: The salt formation, with its natural creep behavior, demonstrates an ability to dissipate stress over time, contributing to the overall containment function. The salt's self-healing properties further enhance barrier integrity by closing any minor fractures that may occur over time, thereby supporting the damage-free status of the sealing structure. Although the analyses do not account explicitly for damage of the rock and for the self-healing mechanism, the damage in the rock salt is expected to be healed due to the self-healing property of the rock salt.

In summary, the shaft sealing system in salt repositories, as evaluated in this chapter, exhibits sufficient resilience and durability to meet the stringent containment requirements of radioactive waste repositories. The high confining pressures, combined with strategic material selection and design configurations, provide a robust barrier that maintains its integrity and remains damage-free even under prolonged stress conditions. This analysis confirms that salt formations not only serve as an excellent geological barrier but also create an ideal environment for engineered sealing systems, ensuring long-term containment and isolation of radioactive waste.

21. Hydraulic Integrity Assessment of the EBS

Following the verification concept, the hydraulic resistance against inflowing fluids has to be verified for the EBS. According to Müller-Hoeppe et al. (2012b), the hydraulic assessment should focus on two main aspects. Initially, it examines whether the EBS meets the design objectives under the likely conditions of the reference scenario. Subsequently, it assesses if the EBS can still effectively prevent the inflow of liquids from the overburden to the radioactive wastes even in the event of shaft seal failure of the less probable conditions of the alternative scenario. In this case, it crucial to determine whether, there is sufficient temporal delay when the inflowing brine will reach the drift sealing system, ensuring that the compaction of the crushed salt has advanced sufficiently to take its long term sealing function in the repository (Müller-Hoeppe et al., 2012b). The subsequent effect of the brine at the edge of the drift sealing system need to be investigated to ensure that the drift sealing system provides a sufficient hydraulic resistance against the brine.

The shaft sealing system is so designed that the fluids that will ingress through the shafts will accumulated at the bottom of the shaft. For that it is planned to backfill the infrastructure area with non-compactable gravel made of basalt or serpentinite. In contrast to the crushed salt, this non-compactable backfill is only slightly compacted by the convergence and support pressure builds up quickly. By backfilling with non-compactable backfill, the infrastructure area forms a reservoir for the solutions entering via the shaft and from the host rock. This reservoir has the positive effect to retard the hydrostatic pressure build up at the edge of the drift seal. A hydrostatic pressure associated with the repository depth will only be reached after the reservoir is full and all shaft components are saturated. Therefore, depending on the amount of fluid to be expected over the lifetime of the EBS and the repository, one can design the volume of the reservoir to retard any pressure build-up in the repository.

The present study aims to provide an example hydraulic assessment for the generic repository system considered in RANGERS. For that, The fluid dynamics through the EBS will be analyzed for the reference and the alternative scenario.

21.1 Numerical model

The model considered for the analysis of the hydraulic evolution through the shaft sealing system was extracted from the numerical model used in the mechanical integrity assessment of the shaft sealing system, see Figure 21.-1. It consists of a column surrounding a shaft with a diameter of 250 m. This column contains all the geological layers around the shaft with their natural curvature as in the generic geological model. The materials in the shaft are considered in the model in accordance with the sealing concept. Their geometrical representations were carefully respected.

The EDZ and the contact zone around the shaft are not explicitly considered. Instead the analyses are carried out by taking into account the resulting system permeability made of sealing components, their contact zone to the host rock, and the surrounding EDZ in the host rocks.

Bitumen is not a Darcy medium; therefore, the bitumen seal will not be penetrated by fluid flow under normal conditions. Instead, the hydraulic load of the fluid is expected to create hydrostatic compression on all sides. Consequently, the bitumen seal can only be bypassed

through the contact zone. However, since we assume an integral permeability for the seal, the contact zone, and the Excavation Damaged Zone (EDZ), a Darcy approach is justified in this context.

Since the infrastructure area was not yet designed, the area at the disposal level around the shaft was homogenized in the model column to mimic the volume of the infrastructure area. The volume was assumed to be higher than necessary to avoid that the pressure build up in the infrastructure area influence the fluid pressure evolution in the shaft. Depending on the amount of brine that would eventually reach the infrastructure area, its volume can be adequately designed.

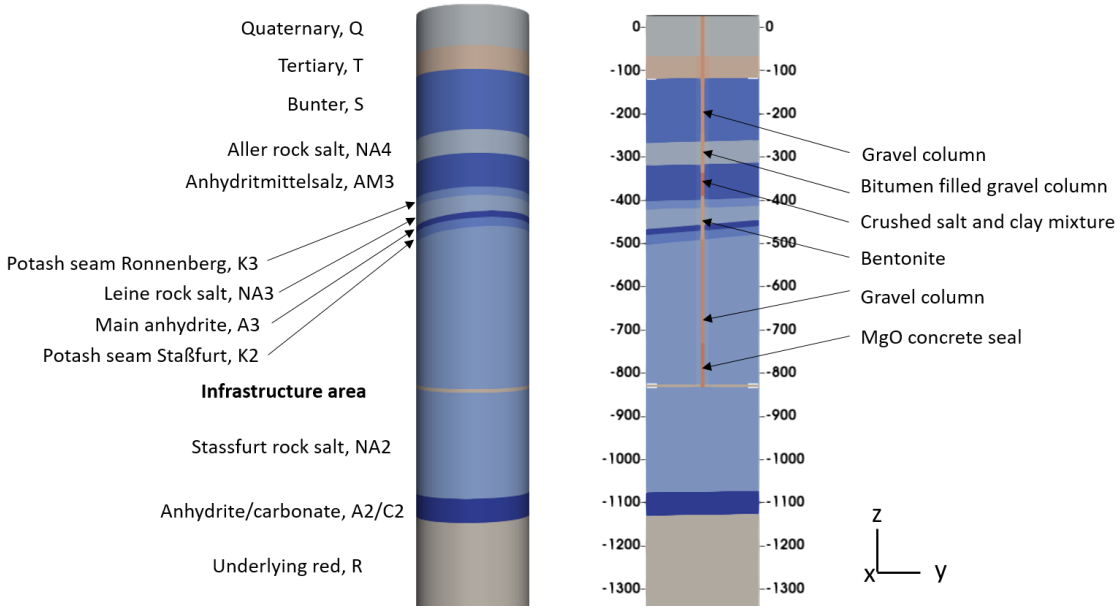

Figure 21.-1: Numerical model for the analysis of the hydraulic evolution in the shaft closure.

The materials in the shaft are partially saturated. Their initial saturation values was taken into account according to the details provided in Müller-Hoeppe et al. (2012b). For each material, a water retention curves needs to be defined that controls the saturation process. The necessary (van Genuchten, 1980) model parameters are summarized in Table 21.-1. The gravel mixture to be used for the shaft is not yet defined. Assumptions were made regarding its water retention curve. For gravel, which is generally coarse-textured with large pore spaces and rapid drainage, the residual water content close to 0.05 or lower is assumed, as gravel has low residual moisture due to large pore sizes. The saturated water content typically ranges from 0.25 to 0.35, associated with the high porosity of the gravel. A low value for the air entry suction, reflecting the high air entry value of coarse materials is assumed. This indicates gravel is likely the first material to be drained, and the last to fill. the pore-size distribution parameter is $\geq$ 2.0, indicating a less steep retention curve appropriate for materials with larger pores.

The assumptions made for gravel imply that suction (negative pressure) will develop in the material during unsaturated conditions, differentiating it from the saturated state, where positive pore pressures are observed. This means that gravel, with its large pores and high drainage capacity, will transition rapidly between wet and dry states depending on the surrounding hy-

draulic conditions. Suction in gravel is generally low due to its large pore sizes, but it still plays a critical role in governing water movement, particularly during infiltration or desaturation processes.

Table 21.-1 also lists the hydraulic parameters of the materials in the shaft according to the design requirements specified in the methodology report.

Table 21.-1: Hydraulic properties of shaft sealing components (Kock et al., 2012).

Material	**Permeability** [m^2]	**Porosity** [-]	**Gas Entry Pressure** [Pa]	**van Genuchten Parameter** n	S_{ini} [%]
Gravel Column (bottom)	10^{-9}	0.326	1.0×10^4	2	0.4
Bitumen-Gravel	1.3×10^{-18}	0.1	8.85×10^5	1.492	85
Salt Clay Mix	10^{-14}	0.1	1.0×10^5	2	21
Bentonite	7.8×10^{-18}	0.3	1.0×10^6	1.82	45
MgO-concrete	5.0×10^{-17}	0.2	2.2×10^5	1.492	80
Infrastructure (Gravel)	10^{-9}	0.38	1.0×10^4	2	0.2

The permeability as well as the porosity of each of the geological layers are given in Table 21.-2.

Table 21.-2: Hydraulic properties of the geological layers (Kock et al., 2012).

Materials	**Permeability** [m^2]	**Porosity** [-]	**Gas Entry Pressure** [Pa]	**van Genuchten Parameter** n	S_{ini} [%]
Quaternary	10^{-14}	0.25	1.0×10^6	2	100
Tertiary	10^{-14}	0.25	1.0×10^6	2	100
Sandstone (Bunter)	10^{-14}	0.15	1.0×10^6	2	100
Anhydrite	10^{-20}	0.01	1.0×10^4	2	0.2

Because intact salt is impermeable (i.e., no Darcy flow) compared to the other formations intersecting the shaft, no hydraulic transport was assumed in the salt layers for this analysis. A hydrostatic pressure is assumed in the water bearing layers of the overburden up to the end of the Bunter Sandstone. The anhydrite located between the intermediary salt layers and the salt pillow is assumed to be dry. Those salt layer prevent any water flow to reach the anhydrite layer. The same assumption is being made for the layers below the salt pillow, that are considered to be dry.

The temporal starting point of the calculations is the end of closure of the shaft. Figure 21.-2 shows the initial saturation and liquid pressure in the model. The saturation distribution in the shaft results from the pore pressure distribution based on the assumed water retention parameters.

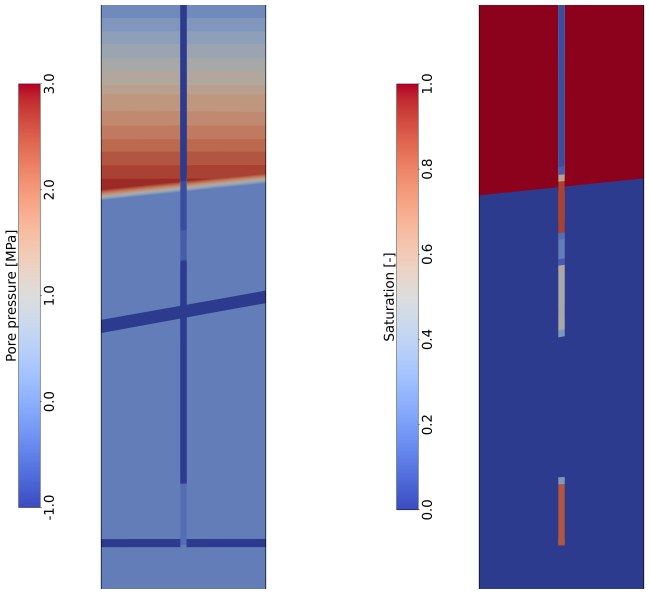

Figure 21.-2: Initial pore pressure and saturation distribution in the shaft and near field.

The simulations was carried out with OpenGeoSys (Bilke et al., 2025) using the Richards flow process class put forward by Buchwald et al. (2021).

21.2 Modeling cases

For the assessment of the hydraulic integrity of the shaft sealing system, different modeling cases need to be defined covering the reference and and the alternative scenario. All modeling cases take a different assumption about how the sealing elements in the shaft will behave over the repository lifetime. For the design of the EBS, a functional lifetime of the EBS of about 50,000 years (Müller-Hoeppe et al., 2012b) was assumed. However, to better estimate the hydraulic resistance of the shaft sealing system, we start by considering the case where the shaft seals remain intact over the verification period of one million years (modeling case 1). In the second step, we assume that the shaft sealing system is functional over 50,000 years and a damage is expected afterwards (modeling case 2). Finally, we define a more severe case that can happen if the shaft closure does not meet the design requirements necessary for the shaft to be functional over the functional time of 50,000 years. For this modeling case 3, an exemplary analysis with a sudden damage at 5,000 years is performed. These latter modeling cases covers the expectation of the alternative scenario.

21.3 Numerical results for modeling case 1

21.3.1 Hydraulic flow evolution

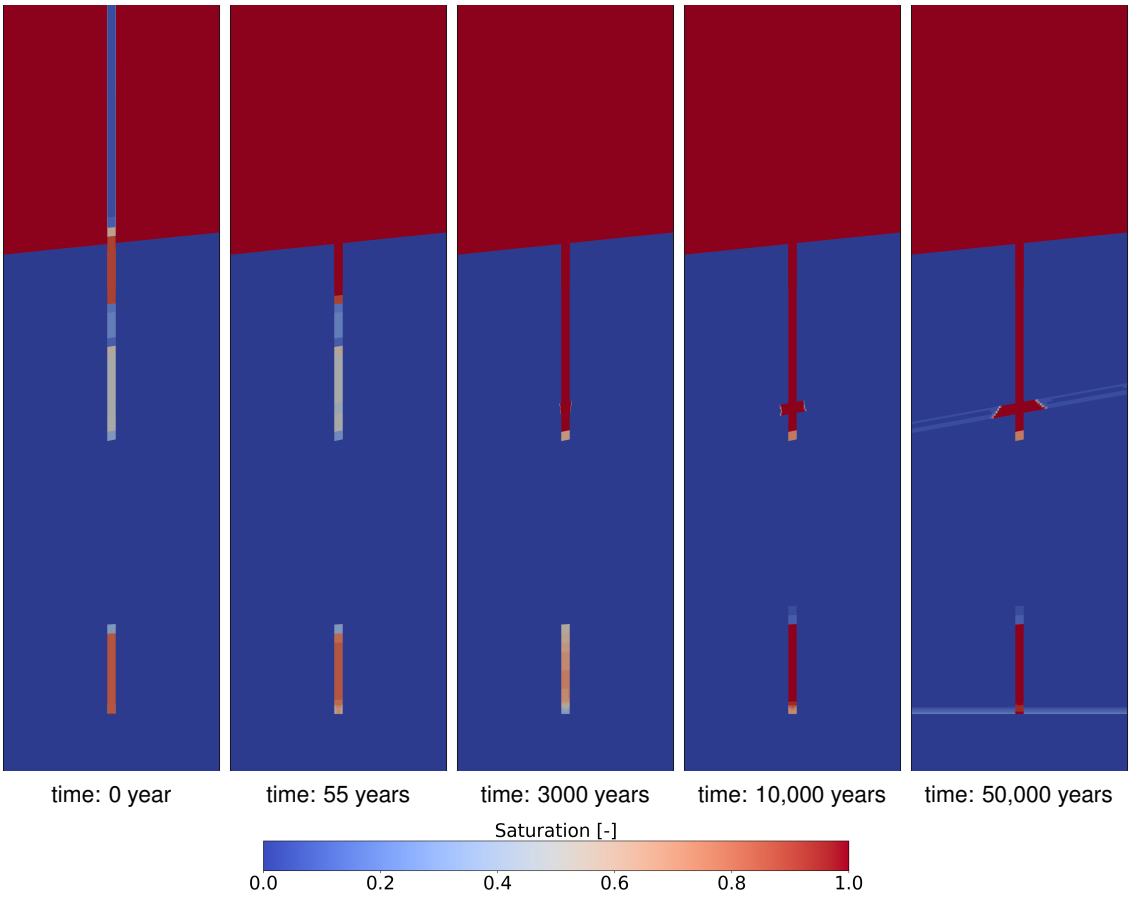

Figure 21.-3: Saturation distribution in the shaft and near field over time (first 50,000 years).

In Figure 21.-3, the saturation distribution in the shaft and its near field over time is presented up to the end of the 50,000-year verification period. At the beginning of the simulation (0 years), the materials in the shaft are partially saturated, with the gravel columns completely dry. The overburden, acting as a water-bearing layer, is fully saturated, while the salt, functioning as an impermeable non-Darcy medium, remains dry and does not participate in the hydraulic processes.

By 55 years, the upper gravel column becomes fully saturated. This occurs without accounting for the tightness of the liner in this section of the shaft. At the same time, saturation begins to increase in the bitumen-filled gravel column seal, marking the onset of fluid infiltration into the shaft seals. By 3,000 years, saturation is nearly complete in the three seals installed at the top of the salt pillow. This phase signifies the transition from localized saturation within the seals to a broader distribution, driven by the hydraulic gradient and the permeability of the materials. Interestingly, the MgO seal becomes drier over time due to the prevailing dry conditions in the repository environment, while the lower gravel column remains unsaturated.

At 10,000 years, the MgO seal shows substantial saturation across most of its length. Infiltration into the surrounding anhydrite layer is also observed, particularly around the bentonite seal. In this region, Darcy flow becomes evident, with the bentonite seal's permeability controlling the rate of water migration into the anhydrite layer. Despite this infiltration, the gravel column remains dry, as water flowing out of the bentonite seal quickly traverses the high-

permeability gravel column and infiltrates the MgO seal instead.

By 50,000 years, the saturation distribution within the shaft appears similar to the conditions observed at 10,000 years, with a more pronounced increase in saturation within the anhydrite layer. Additionally, there is a slight rise in saturation within the infrastructure area, although the lower gravel column remains unsaturated. At the end of the verification period, the saturation distribution indicates that minimal water has infiltrated the infrastructure area, suggesting limited flow into this region.

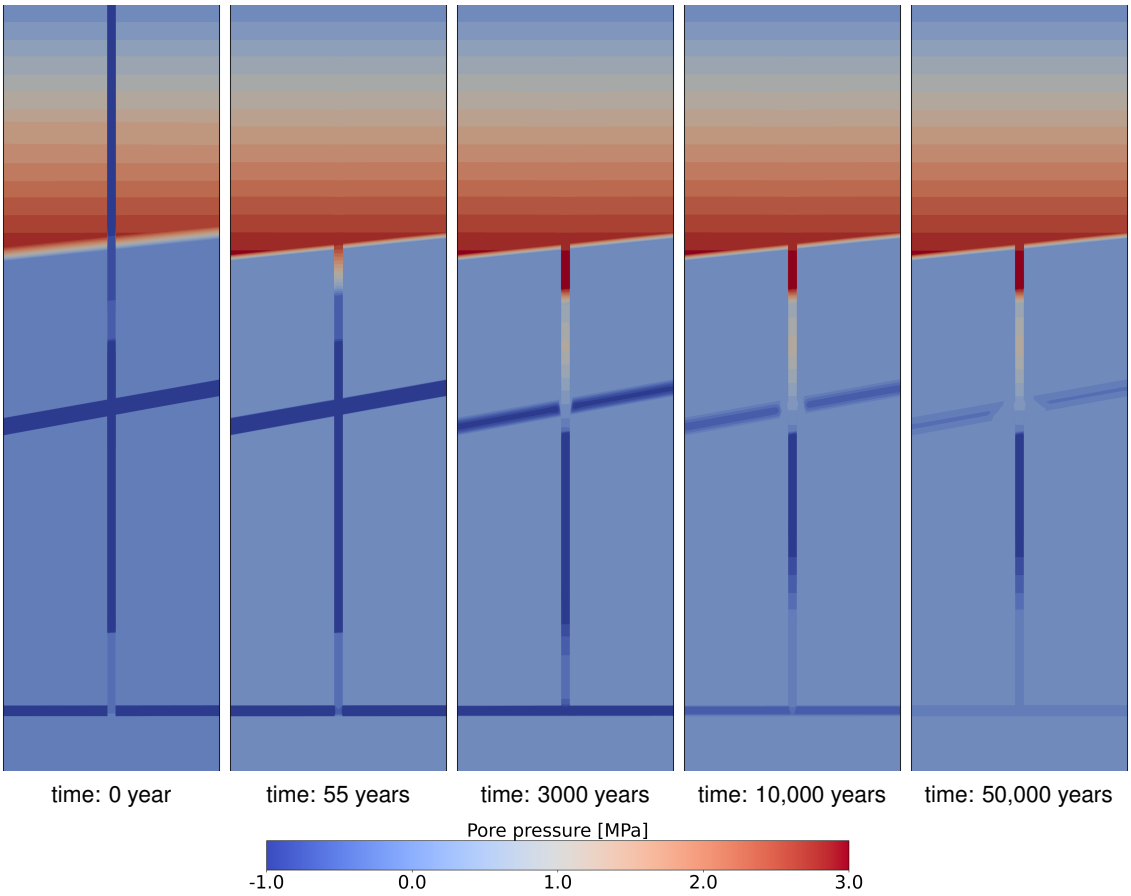

Figure 21.-4: Pore pressure distribution in the shaft and near field over time (first 50,000 years).

The progression of pore pressure over time, as shown in Figure 21.-4, highlights the evolution of hydraulic conditions within the shaft and its surrounding environment throughout the 50,000-year verification period.

At the start of the simulation (0 years), the pore pressure distribution shows a stark contrast between the water-bearing overburden and the surrounding salt and shaft components. The overburden exhibits positive pore pressure, indicative of its saturated state, while the shaft components and the surrounding salt layers exhibit minimal or negative pore pressure, i.e. suction, due to their unsaturated or impermeable nature.

After 55 years, a hydrostatic pressure is acting in the upper gravel column as a result of its saturation. There is a noticeable increase in pore pressure in the bitumen gravel seal at the

onset of the salt pillow. This corresponds to the saturation observed earlier, as the infiltration of water into this seal (in reality along the contact zone) leads to a rise in hydraulic pressure. The salt layers and surrounding infrastructure remain unaffected, maintaining their low or negative pore pressure values, reflecting their impermeable and unsaturated characteristics.

By 3,000 years, the pore pressure increases significantly in the upper seals at the edge of the salt formation. The hydraulic gradient drives fluid migration, causing increases in pore pressure in these elements. The MgO seal, under the dry conditions of the repository environment, maintains lower pore pressure compared to the other seals.

At 10,000 years, the pore pressure distribution is similar to the situation observed at 3,000 years. We observe a pore pressure increase in the anhydrite layers as a result of the localized saturation that was observed earlier. There is also a decrease of suction in the infrastructure area. The MgO seal shows a moderate increase in pore pressure along its length, while the lower gravel column remains largely unaffected, reflecting its high permeability and the quick dissipation of infiltrated brine.

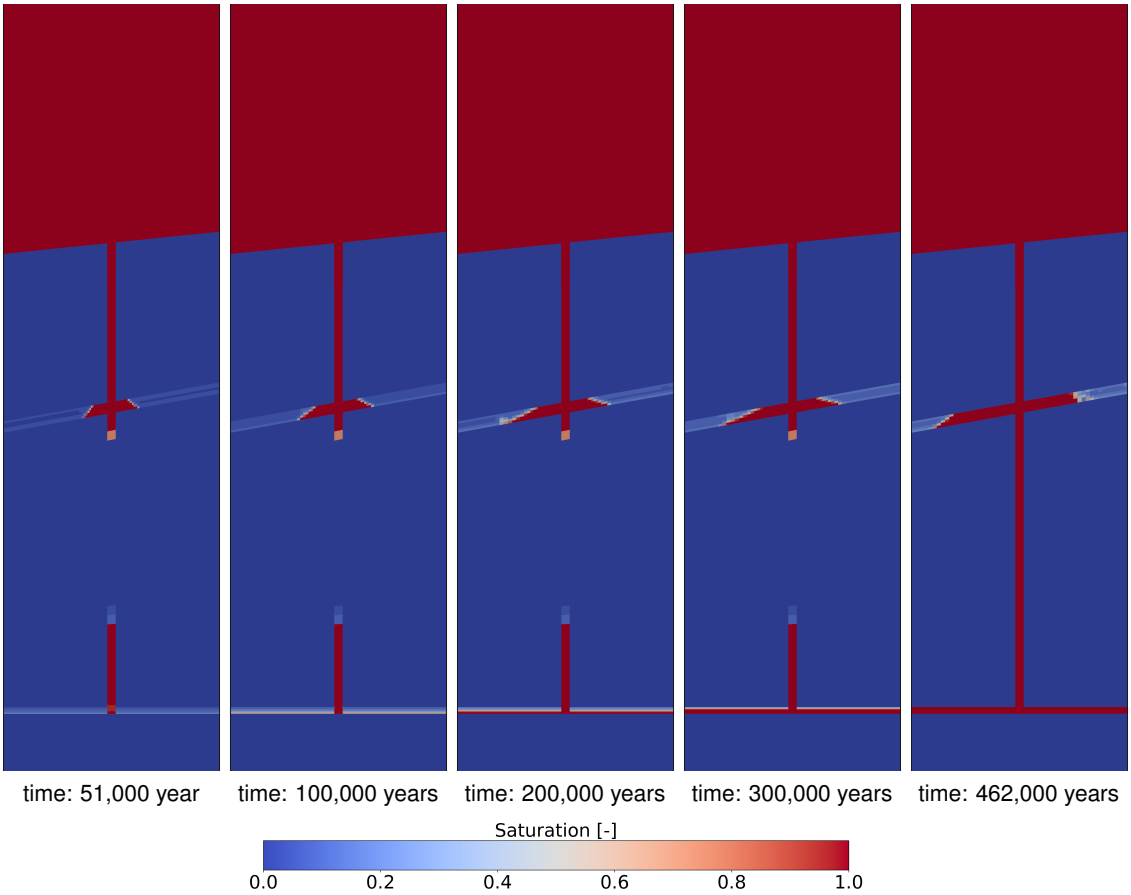

Figure 21.-5: Saturation distribution in the shaft and near field: Long-term evolution beyond 50,000 years (modeling case 1).

By 50,000 years, the pore pressure distribution reaches a near steady-state condition. The anhydrite layer exhibits more pronounced pore pressure, likely due to long-term infiltration from the shaft seals. The bentonite and bitumen-filled gravel seals maintain high pore pressure, indicative of their saturated states and roles in controlling fluid movement. The infrastruc-

ture area shows a slight increase in pore pressure over time, while the lower gravel column continues to exhibit negligible pore pressure due to its permeability and role in dissipating water flows. Overall, the evolution of pore pressure demonstrates the interplay of material permeability, hydraulic gradients, and long-term fluid migration processes in the shaft and its surrounding environment.

In this modeling case, it is assumed that the seals remain intact beyond their planned service lifetime. The hydraulic behavior of the system is analyzed over a prolonged period, extending to nearly half a million years under these conditions.

The saturation distribution shown in Figure 21.-5 highlights the continued evolution of fluid movement within the shaft and its near field, extending the timeline previously studied.

Between the end of the verification period of the engineered barrier system (EBS) at 50,000 years and 300,000 years, there is a progressive increase in saturation within the infrastructure area. This clearly indicates that the pore volume in the gravel installed within the infrastructure region is gradually being filled by water inflowing through the shaft. During this period, the surrounding anhydrite layer also exhibits increasing saturation, reflecting prolonged interaction with fluids migrating from the shaft. Despite this, the lower gravel column remains unsaturated, as water continues to flow through it without being retained.

By 462,000 years, the shaft becomes completely saturated. Saturation of the lower gravel column occurs only after the infrastructure region is fully saturated. At this stage, the system appears to have reached a near-equilibrium condition. The saturation in the anhydrite layer remains the only transient phenomenon. The saturated domain of the anhydrite layer shows a gradual but restricted evolution, extending no more than 200 m in diameter around the shaft.

Overall, the results indicate a gradual yet controlled spread of saturation over hundreds of thousands of years. The engineered shaft components effectively regulate water flow, while the surrounding geological layers demonstrate long-term adjustments to fluid migration. Quasi steady-state conditions emerge in the later stages of the simulation, confirming the stability of the system over extended timescales.

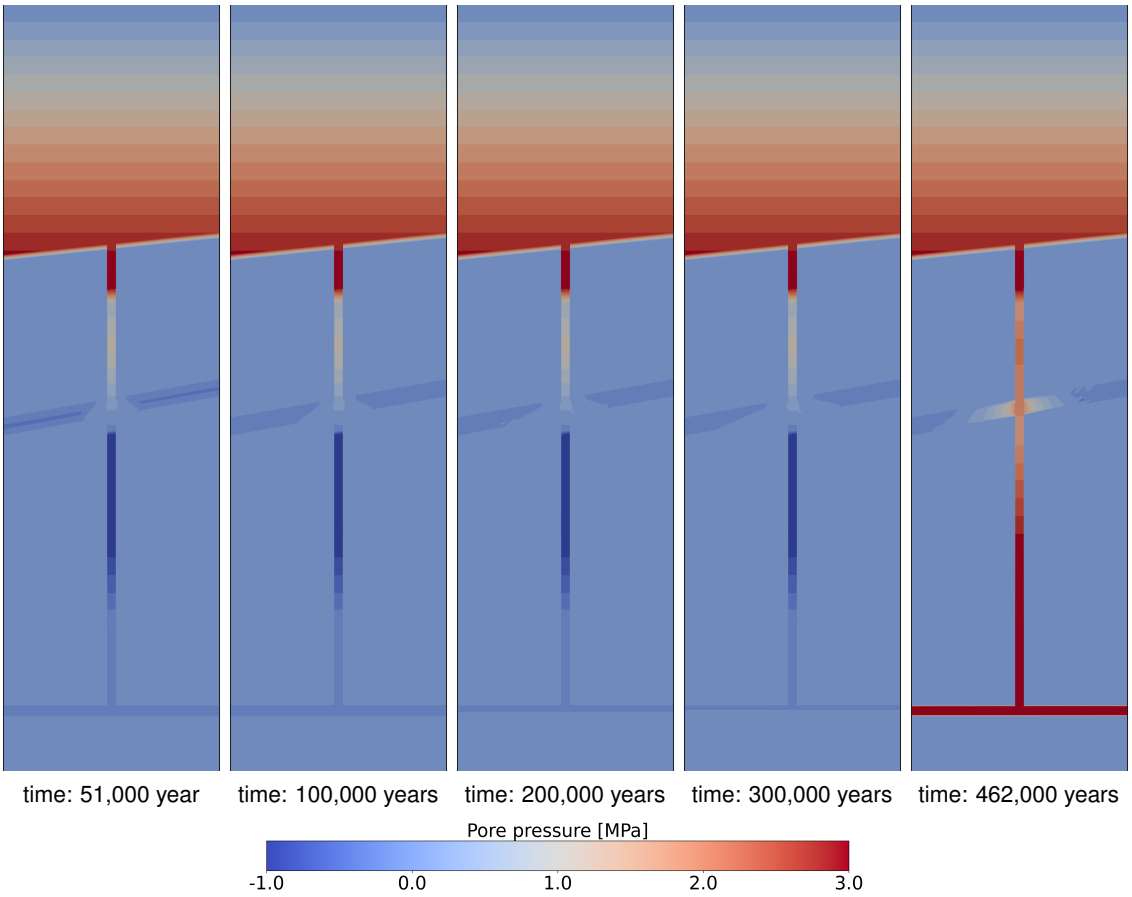

Figure 21.-6: Pore pressure distribution in the shaft and near field over time: Long-term evolution beyond 50,000 years (modeling case 1).

The corresponding pore pressure evolution in the shaft and near field is shown in Figure 21.-6. Up to 300,000 years, the pore pressure distribution appears to be in a near-equilibrium state. This state is characterized by a hydrostatic pressure in the bitumen-filled gravel, followed by an elevated pore pressure in the salt clay and bentonite seal. However, the pore pressure in these seals has not yet reached hydrostatic pressure at their respective depths. The only noticeable changes during this period occur in the infrastructure area and the anhydrite layer, where a gradual increase in pore pressure can be observed, indicating ongoing fluid migration into these regions.

At the end of the simulation (462,000 years), the system behavior changes abruptly due to the gravel column becoming fully saturated. This saturation results in a significant increase in pore pressure in the lower part of the shaft and the infrastructure area. Consequently, the pore pressure in the middle part of the shaft, particularly above the lower gravel column where the seals are located, also rises. This marks a critical transition in the hydraulic conditions, reflecting the interconnected effects of saturation and pore pressure evolution within the shaft and its surrounding environment.

21.3.2 Pressure and saturation evolution in the shaft

A quantitative evaluation of the pressure and saturation evolution within the shaft is presented in Figure 21.-7. the figure shows the profile of saturation and pore pressure over time along the shaft.

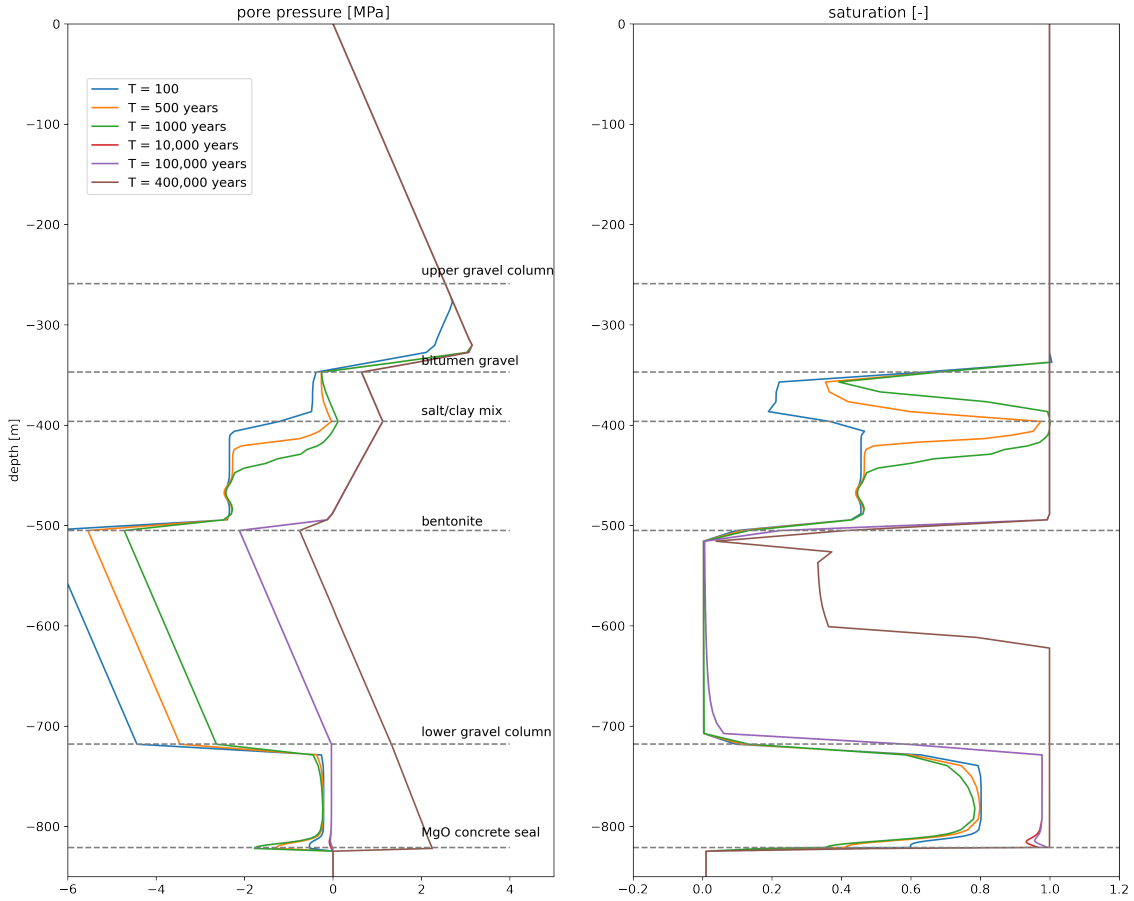

Figure 21.-7: Pore pressure and saturation profiles with depth over various time periods.

The saturation of the first sealing element, composed of bitumen gravel, occurs relatively quickly, with full saturation achieved before 100 years. By 500 years, hydrostatic pressure is already established within this element, highlighting its rapid response to inflowing water. In contrast, the salt/clay mixture seal exhibits a much slower saturation process due to its particular water retention properties. This element remains unsaturated for an extended period, achieving saturation only after 1,000 years. Despite this, the pore pressure within the salt/clay mixture remains low throughout the simulation, underscoring its limited hydraulic connectivity.

Water flowing through the salt/clay mixture infiltrates the bentonite seal, initiating its saturation. Due to the high suction capacity of bentonite, its saturation progresses slowly, with full saturation of the upper portion occurring only after 1,000 years. By 10,000 years, the bentonite seal is fully saturated across its depth.

The lower gravel column experiences suction effects over the first 100,000 years of the simulation, delaying its saturation. Positive pore pressure values, indicating saturation, are observed only in the bottom portion of the gravel column at 400,000 years, while the upper section

remains dry, reflecting the limited upward water flow in the gravel column.

The MgO concrete seal exhibits an initial drying phase, with decreasing saturation observed up to 1,000 years. Following this period, a gradual saturation process begins. By 100,000 years, saturation in the MgO seal reaches high levels near full saturation, with complete saturation achieved at 400,000 years.

The results demonstrate that full saturation of the infrastructure area occurs before the MgO seal is fully saturated. Once the infrastructure area is saturated, the lower gravel column begins its saturation process. This sequential behavior highlights the interconnected hydraulic evolution of the system and the critical role of the water retention and permeability properties of the individual sealing elements in controlling long-term water flow and pressure development within the shaft.

21.3.3 Water accumulation in the infrastructure area

Figure 21.-8 shows the volume of water that is being accumulated in the porous space of the infrastructure area that is backfilled with non-compacting basalt gravel. At the beginning of the simulation a volume of about 100 m^3 is computed in the infrastructure area. This value is mainly due to the non linearity of the water retention curve. Very high capillary values are necessary to assign a saturation of near zero. Such values lead to computational issues so that the simulation was carried out with compressible parametrization of the van Genuchten function.

Over time, the volume of water accumulated grows first steadily in a double logarithmic representation. Then at around 5,000 years an inflection point is reached where the volume increase is more important. This inflection point marks the time when the capillary forces are vanishing in the basalt gravel and therefore, there is less resistance for the saturation of the porous space.

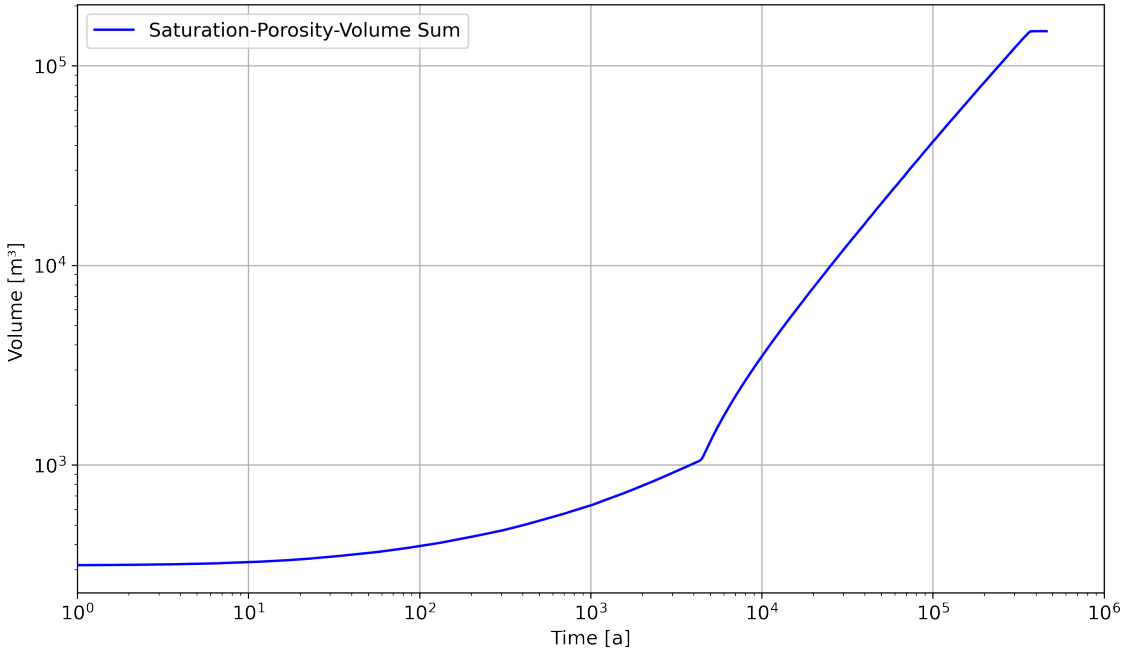

Figure 21.-8: Volume of water accumulating in infrastructure area through time for modeling case 1.

After nearly four hundreds thousand years, a plateau is reached marking the full saturation of the infrastructure area. At this time, Over less than 150,000 m³ of water has been accumulated in the infrastructure area. At the end of the verification period of the EBS, at 50,000 years, less than 20,000 m³ of water have reached the infrastructure area. Although the present modeling case is synthetic, this value is realistic for the EBS considered in RANGERS which hydraulic specifications should remain unchanged up to 50,000 years. An alteration of the EBS is expected only afterwards.

21.3.4 Conclusions on System Behavior

The numerical results of modeling case 1 offer significant insights into the hydraulic flow evolution, pressure and saturation dynamics, and water accumulation behavior expected within the shaft system over time. Modeling case 1 is a synthetic model situation that allows us to investigate the system behavior under idealized conditions.

The simulation highlights that the system undergoes progressive saturation, with key elements such as the bentonite seal and MgO seal reaching full saturation only after extended periods. The gradual development of hydrostatic pressure equilibrium throughout the shaft is achieved only after half a million of years. This long-term evolution aligns with the expectations for the safe containment of radioactive waste, where the EBS and shaft sealing system maintain functionality well beyond the 50,000-year regulatory requirement.

The accumulation of water in the infrastructure area is gradual and follows a logarithmic progression. Initially, about 100 m³ of water is computed due to the nonlinear water retention curve. At around 5,000 years, an inflection point is observed where the volume of water increases more significantly, signaling the vanishing capillary forces in the basalt gravel, allowing easier saturation. By the end of the simulation, the infrastructure area reaches full saturation,

with over 150,000 m³ of water accumulated. At the critical verification period of 50,000 years, less than 20,000 m³ of water has reached the infrastructure area, which is consistent with the hydraulic specifications of the EBS in the RANGERS project.

The following conclusions can be drawn for the case where water flows down the shaft from penetrated overlying aquifers, based on the simulation:

- the lower gravel column and the crushed salt/clay mixture will be the last components in the shaft to be saturated.
- Water accumulation in the lower gravel column will only begin after the infrastructure area has been fully saturated.
- The MgO seal will experience an initial desaturation phase lasting up to 5,000 years or more before becoming saturated much later.
- It is only after the full saturation of the shaft (i.e., the connection of hydraulic processes in the lower and upper part of the shaft) that a hydrostatic pressure from the surface to the disposal depth will be achieved.
- By the end of the 50,000-year verification period, no significant hydrostatic pressure is expected in the infrastructure area, indicating that hydrostatic load does not need to be considered in the design and integrity assessment of the drift seals.

Two important implications arise from these conclusions:

- Monitoring the water level in the lower gravel column is an effective way to demonstrate that the repository system is functioning as intended, providing a reliable indication of its long-term integrity. In other words, if water pressure is detected in the lower gravel earlier than predicted by modeling, it could indicate that the repository is not performing as expected. However, it is essential to evaluate the feasibility of implementing such a wireless monitoring strategy within the shaft, especially over depths of several hundred meters.
- The volume of the infrastructure area reservoir can be designed to prevent any fluid migration from the overburden into the repository mine beyond the infrastructure area. This ensures that long-term confinement can rely primarily on the shaft sealing system and the reservoir, extending for a significant portion of the one-million-year verification period. A detailed quantification of this implication will be addressed in modeling case 2.

In conclusion, the hydraulic evolution, pressure dynamics, and saturation processes of the shaft system show that the sealing components work as intended, progressively stabilizing over time. The hydraulic specifications of the EBS appear robust, and the design is expected to perform reliably up to the required time frame of 50,000 years, with only minor alterations expected afterward.

21.4 Numerical results for modeling case 2

The numerical model setup and parametrization are identical to those in modeling case 1 for the first 50,000 years. Refer to Table 21.-1 for detailed information about the model parameters. To simulate the system behavior under the shaft seal failure scenario after 50,000 years, the permeability values of several sealing components were increased.

For the bentonite sealing element, an average permeability of 5×10^{-16} m^2 was adopted, representing a marl clay material used here as a substitute for an insufficiently compacted binary bentonite mixture, as described in Müller-Hoeppe et al. (2012a). For the Sorel concrete sealing element, Müller-Hoeppe et al. (2012a) proposed an integral permeability of 1×10^{-15} m^2. This permeability value was achieved even under challenging location conditions in an initial experimental structure (PSB A2, a pilot flow barrier made of Sorel concrete) at the Asse site (Weise et al., 2006; Meyer et al., 2008; Kamlot et al., 2012) as reported in Müller-Hoeppe et al. (2012b). The same permeability value was applied to the Sorel concrete abutment. To increase the numerical stability and reduce the computational time, we performed the simulation by increasing the permeability of the seals by one order of magnitude instead of two.

For the crushed salt clay mixture, due to the limited data available for this novel material, we assumed the same permeability as in modeling case 1, where a conservative permeability of 1×10^{-14} m^2 was already assumed for the state pre-failure.

21.4.1 Hydraulic flow evolution

The system evolution is identical for modeling cases 1 and 2 during the first 50,000 years. Here, we focus on the hydraulic behavior after 50,000 years when the permeability of the shaft sealing structure is increased to simulate its failure. The effects of this failure are illustrated in Figure 21.-9, which shows the saturation distribution during the post-failure phase.

After the sealing failure, the infrastructure area becomes progressively saturated. By 73,500 years, the entire porous volume of the infrastructure area is almost fully saturated. This behavior contrasts with the previous modeling case, where no degradation of the sealing material was assumed, and the saturation of the infrastructure area occurred only after 300,000 to 450,000 years.

The figure further demonstrates that the lower gravel column becomes saturated only after the infrastructure area is fully saturated. Following this, the saturation of the surrounding anhydrite layer begins to increase over time. By 180,000 years, the anhydrite layer in the domain of investigation becomes fully saturated. However, to estimate the extent of saturation in the anhydrite layer over a million years, a larger model domain would be required. This highlights the impact of seal degradation on the hydraulic evolution and emphasizes the need for extended modeling to capture the long-term behavior of the system.

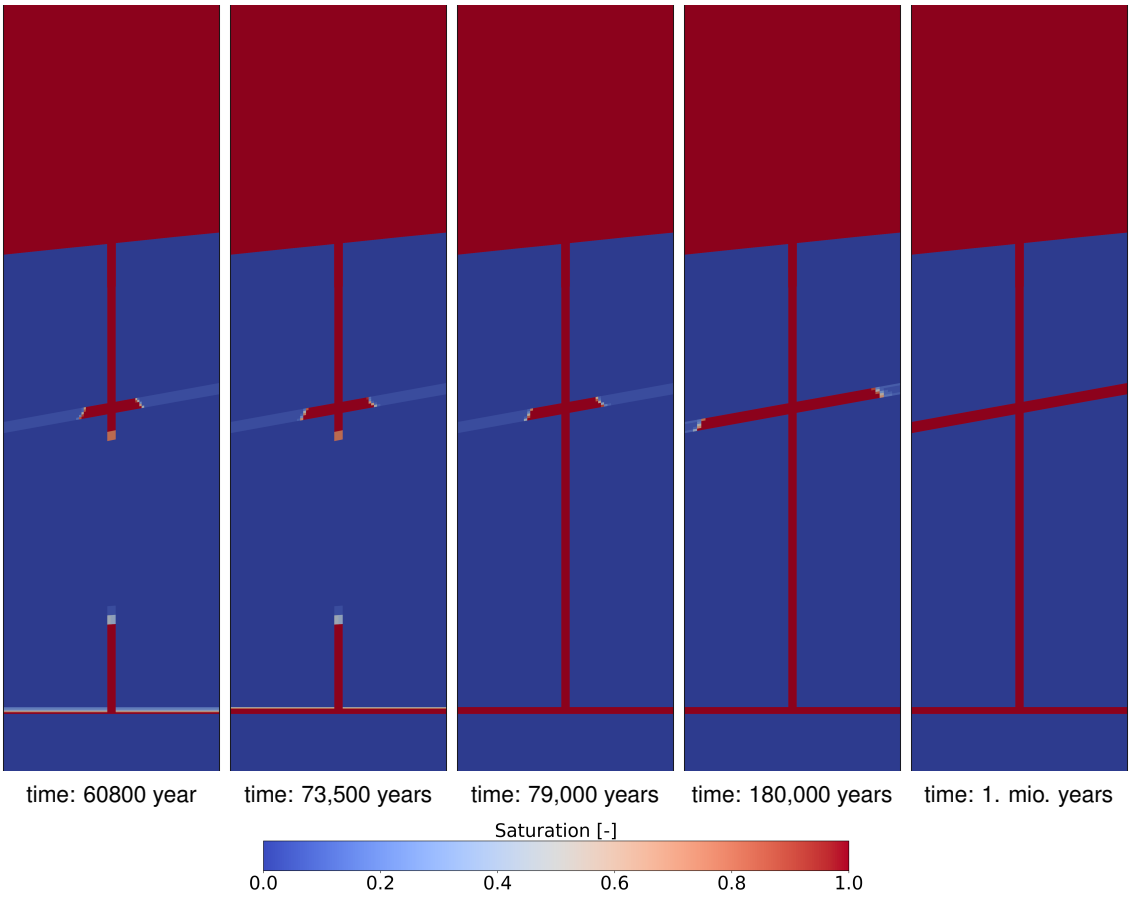

Figure 21.-9: Saturation distribution in the shaft and near field: Long-term evolution beyond 50,000 years (modeling case 2).

With the saturation of the shaft, there is a corresponding buildup of hydraulic pressure. The pore pressure distribution in the shaft is shown in Figure 21.-10. Although the shaft becomes fully saturated by 79,000 years, the hydrostatic pressure regime remains divided between the upper and lower sections. In the upper part of the shaft, hydrostatic pressure occupies the porous voids up to the bentonite seal, creating a relatively uniform pressure profile. In the lower section, pressure values of at least 3 MPa develop from the infrastructure area to the bottom of the gravel column. Within the lower gravel column, a distinct pressure gradient is observed, with pressures exceeding 3 MPa at the bottom and dropping to less than 1 MPa just below the bentonite seal. This gradient reflects the influence of the water retention properties of the materials in the lower shaft section.

The water retention properties contribute to a retardation effect that limits the pressure buildup within the shaft to moderate levels up to 100,000 years, despite the loss of the shaft's sealing function at 50,000 years. This delay in pressure equalization highlights the role of material properties in slowing hydraulic responses even in the absence of an intact seal.

Over time, however, pressure in the shaft continues to rise. By 180,000 years, the pressure within the infrastructure area reaches approximately 8 MPa, not shown in the figure. This marks the eventual establishment of a near-hydrostatic pressure regime, driven by the progressive saturation and hydraulic connectivity throughout the shaft and its surrounding re-

gions.

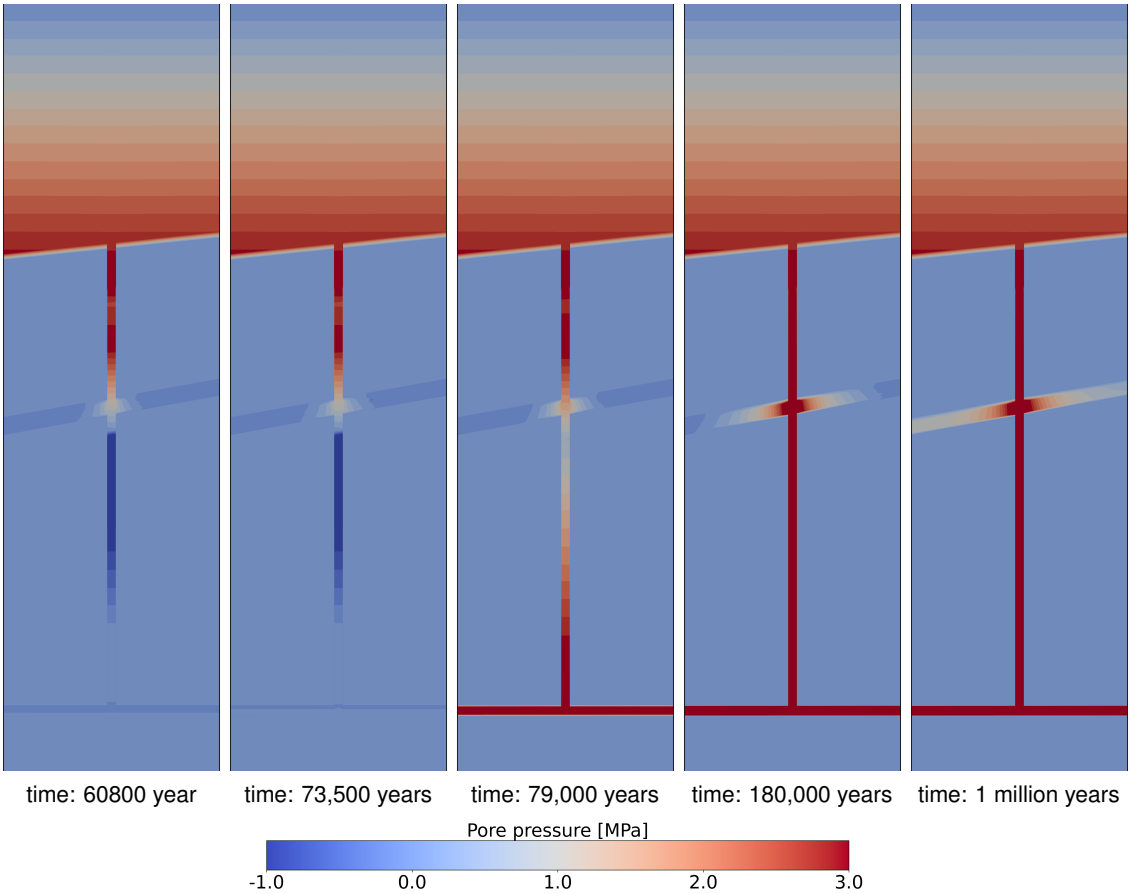

Figure 21.-10: Pore pressure distribution in the shaft and near field: Long-term evolution beyond 50,000 years (modeling case 2).

21.4.2 Pressure and saturation evolution in the shaft

A quantitative evaluation of the pressure and saturation evolution within the shaft is presented in Figure 21.-11, illustrating the profiles of saturation and pore pressure over time along the shaft.

The pressure built-up within the bitumen and saturation of the EDZ occurs relatively quickly, with full saturation achieved before 100 years. By 500 years, hydrostatic pressure is already established within this element, highlighting its rapid response to inflowing water. In contrast, the salt/clay mixture seal exhibits a much slower saturation process due to its particular water retention properties. This element remains unsaturated for an extended period, achieving saturation only after 1,000 years. Despite this, the pore pressure within the salt/clay mixture remains low throughout the simulation, underscoring its limited hydraulic connectivity. Water flowing through the salt/clay mixture infiltrates the bentonite seal, initiating its saturation. Due to the bentonite's high suction capability, its saturation progresses slowly, with full saturation of the upper portion occurring only after 1,000 years.

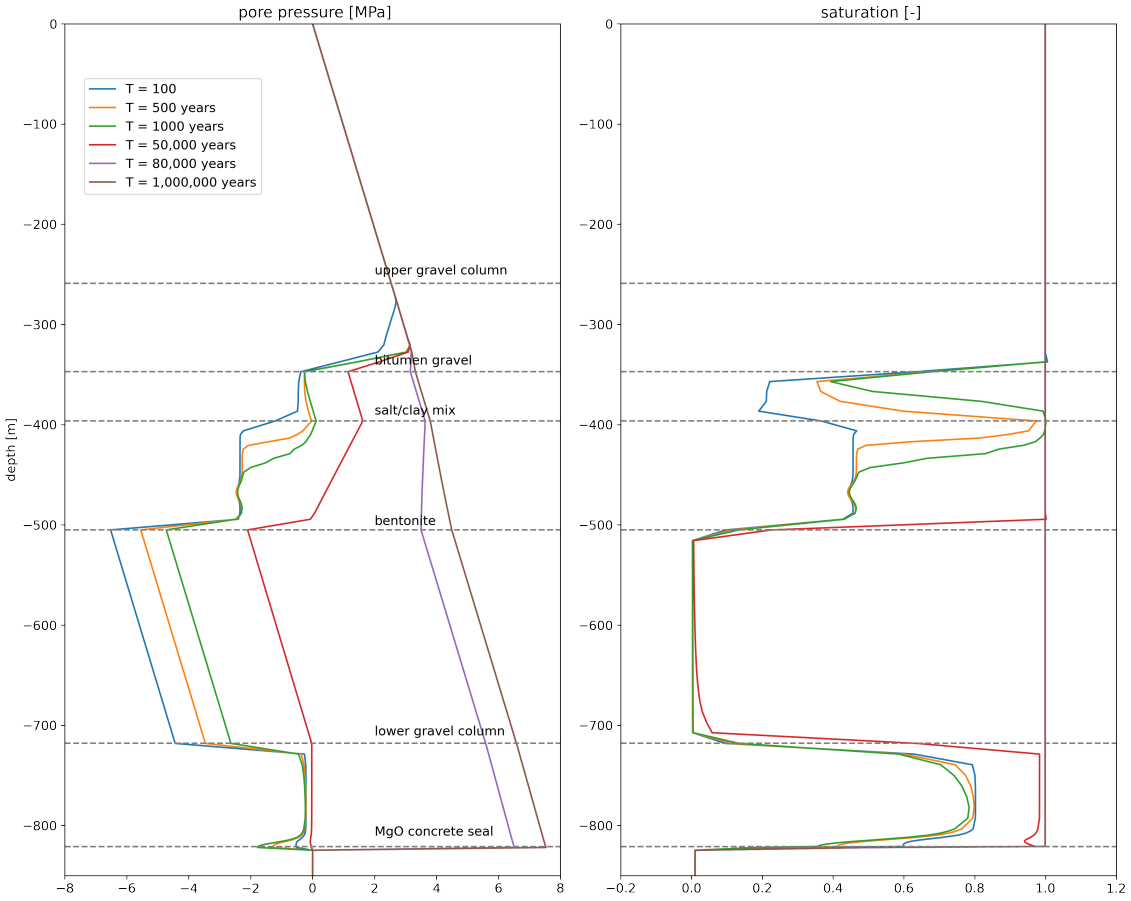

Figure 21.-11: Pore pressure and saturation profiles with depth over various time periods for modeling case 2.

By 50,000 years, the bentonite seal is fully saturated across its depth with a hydraulic gradient from about 2 MPa at the top to 0 MPa at the bottom of the seal. This indicates obviously a saturation of the bentonite from the top. At this time, the lower gravel column is still unsaturated and the MgO concrete elements are now closed to full saturation. The lower gravel column experiences suction effects – indicating the drainage of that element – over the first 50,000 years of the simulation, delaying its saturation. The situation remains almost unchanged by 75,000 years. At this time, the pore pressure has increased in the upper seals and the MgO elements are now full saturated.

By 80,000 years, positive pore pressure values in the lower gravel column, indicating saturation, are observed. The pore pressure in this column has significantly increased. There is now an uniform pressure gradient from the disposal depth to the top of the lower gravel column. The sudden change in the hydraulic regime occurring in this column is explained by the saturation of the infrastructure area leading to a pressure build-up in the lower part of the shaft. Once the infrastructure area is saturated, the lower gravel column begins its saturation process. This sequential behavior highlights the interconnected hydraulic evolution of the system and the critical role of the water retention and permeability properties of the individual sealing elements in controlling long-term water flow and pressure development within the shaft.

21.4.3 Water accumulation in the infrastructure area

Figure 21.-12 shows the volume of water accumulating in the porous space of the infrastructure area, which is backfilled with non-compacting basalt gravel. The volume of fluid accumulated grows first steadily in a double logarithmic representation. Then at around 5,000 years an inflection point is reached where the volume increase is more important. This inflection point marks the time when the capillary forces are vanishing in the basalt gravel and therefore, there is less resistance for the saturation of the porous space. At the end of the verification period of the EBS, at 50,000 years, less than 20,000 m³ of fluid have reached the infrastructure area. After this period, however, there is a drastic increase in the volume of fluid within the infrastructure area, eventually reaching the maximum capacity of the pore space in the gravel backfill. A closer look in Figure 21.-12 shows that the reservoir is full with an assumed capacity of 150,000 m³ at 77,500 years.

Figure 21.-12 indicates that the rate of fluid inflow is so high that it would be impractical to design a reservoir large enough to contain the total volume of fluid entering the infrastructure area up to the end of the verification period of 1 million years. Therefore, the reservoir should be designed to accommodate the expected fluid volume up to the end of the shaft sealing system's functional life at 50,000 years, estimated to less than 20,000 m³. As the repository is made of two shafts, one should plan reservoir volume of 40,000 m³ in the infrastructure area.

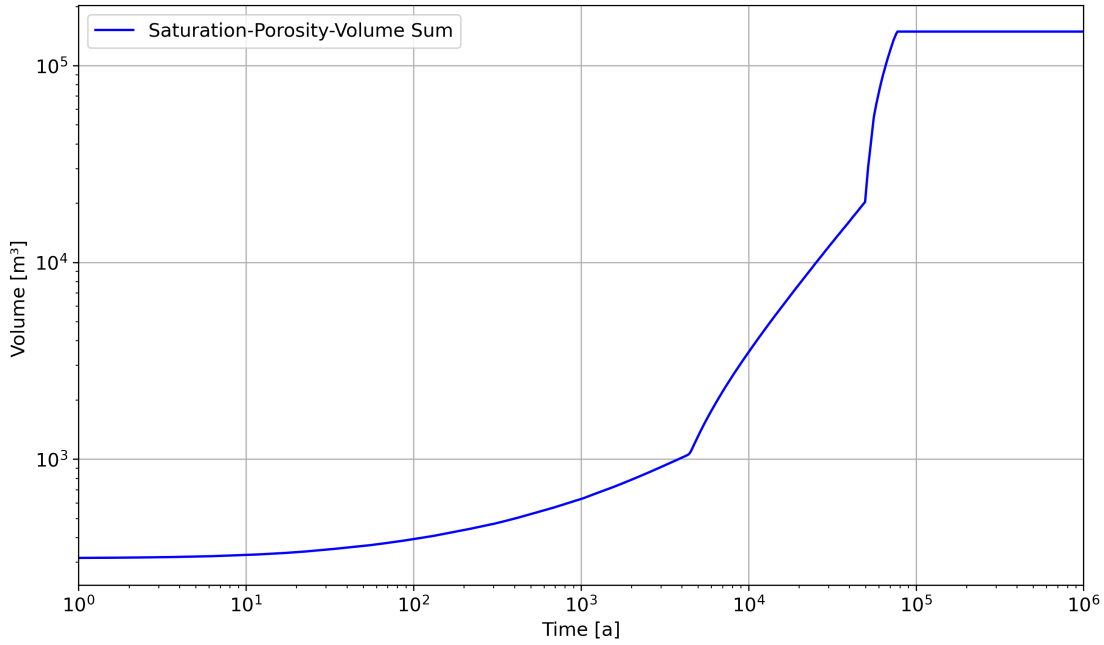

Figure 21.-12: Volume of water accumulating in infrastructure area through time for modeling case 2.

21.4.4 Conclusions on System Behavior

The numerical results from modeling case 2 provide critical insights into system behavior under a shaft seal failure scenario after 50,000 years. Initially, the hydraulic evolution in case 2 closely mirrors that of case 1, exhibiting similar patterns of water accumulation and saturation within the shaft and infrastructure area. However, following the assumed failure at 50,000 years, significant changes in system behavior are observed.

The simulations indicate that the system undergoes progressive saturation, with components such as the bentonite seal and MgO seal reaching full saturation only after extended periods. Hydrostatic pressure equilibrium throughout the shaft is achieved only after 80,000 years even when a damage is assumed at 50,000 years. Up to this time, the crushed salt seal and backfill in the repository is fully compacted and can take over the sealing function. Also, no hydraulic load is acting on the drift seals helping these structure to further improve their sealing capability through rock convergence. This long-term evolution supports the safe containment of radioactive waste, demonstrating that the EBS and shaft sealing system maintain functionality well beyond the 50,000-year regulatory requirement. After loss of functionality/initial tightness of the shaft sealing system, the infrastructure area undergoes progressive saturation, reaching full capacity within approximately 30,000 years. While the seals may be damaged, it still takes a significant amount of time for the infrastructure area to fully accommodate inflowing fluid.

The current results show that, up to 80,000 years, all fluid entering through the shafts remains confined within the repository system. However, these results may be optimistic, as the simulation assumes only a one-order-of-magnitude increase in seal permeability after failure, rather than the potentially higher degradation that could occur. Repeating the simulation with a two-order-of-magnitude increase in permeability is necessary to confirm this hypothesis.

The retardation potential of the shaft seals is highly dependent on their post-lifetime permeability, and the results suggest that fluid retardation into the repository could remain effective for up to 100,000 years. Consequently, accurate characterization of the sealing materials' permeability is crucial for optimizing the EBS's performance.

The saturation of the infrastructure area further indicates that, following seal failure, fluid inflow is substantial, and the infrastructure area cannot accommodate the total inflow over the 1-million-year verification period. As a result, it is recommended that the infrastructure reservoir be designed to contain only the expected fluid volume by the end of the shaft seal's functional life at 50,000 years, estimated at 40,000 m^3 for two shafts.

In summary, the shaft seal system effectively controls water ingress during its functional lifespan. However, after failure, the system faces challenges from significant water inflow and rising pressures. These findings highlight the importance of robust design strategies, focusing on seal permeability, water retention, and reservoir capacity, to ensure long-term functionality and containment within the repository infrastructure.

21.5 Projected system behavior and implications for modeling case 3

Based on the results from modeling case 2, we can predict the system behavior anticipated for modeling case 3, as well as for any scenario where the shaft sealing system loses its sealing function earlier than planned. As observed in case 2, once the shaft's sealing function fails, permeability increases immediately, leading to a rapid influx of water into the infrastructure area. Since the only difference between cases 2 and 3 is the timing of this assumed sealing failure, it is reasonable to expect a similar pattern at 5,000 years. Consequently, after 5,000 years, the infrastructure area would likely fill with water from the overburden within a few decades.

In this scenario, the hydrostatic pressure would increase rapidly, presenting a critical design consideration for the drift sealing system. For robustness, the MgO concrete seals installed in the drifts should be capable of withstanding the hydrostatic pressure exerted by the water column within the shaft.

21.6 Evaluation of the hydraulic resistance at the contact zone

The hydraulic properties of shaft sealing structure are determined by the behavior of three key components: the sealing material, the excavation-damaged zone, and the contact zone.

The primary sealing material (e.g., bentonite, MgO concrete, or other engineered barriers) plays a crucial role in controlling water flow and permeability. Its intrinsic hydraulic conductivity, swelling capacity (in the case of bentonite), and long-term stability under repository conditions determine how effectively it can limit fluid migration. The hydraulic assessment of the sealing material in the shaft was the focus of the previous section. Their mechanical integrity ensuring their hydraulic resistances over time was proven in chapter 20.

The excavation process inherently disturbs the surrounding rock, leading to the formation of cracks and an increase in permeability. This zone, often referred to as the excavation-damaged zone (EDZ), can act as a potential pathway for water and gas. Over time, self-healing mechanisms and convergence of the rock may mitigate these effects. We showed already in Figure 19.-14 that the EDZ is expected to recover over time due to creep and rock convergence with computed state of dilatancy well below the microfracture limit after Cristescu and Hunsche (1998). At this level no advective transport is possible in the EDZ. At this point the EDZ has similar hydraulic properties as the intact salt rock mass, i.e. impermeable.

As for the contact zone, the interface between the sealing materials and the surrounding host rock is another critical factor influencing hydraulic behavior. Issues such as poor adhesion, material shrinkage, incomplete compaction, or tensile damage may create preferential flow paths, compromising the sealing function. Ensuring a tight and well-bonded interface is therefore essential to maintaining the integrity of the seal and preventing bypass flow. To demonstrate the hydraulic resistance of the contact zone, we refer to the specific requirements for essential barriers outlined in § 5 (2) of EndlSiAnfV (2020). These requirements emphasize the need to evaluate both the fluid pressure criterion and the dilatancy criterion for the barrier and apply also at the contact zone.

To achieve this, we leverage the hydraulic evolution results for the shaft presented above, in conjunction with the stress development analysis in the near field of the shaft, as discussed in Chapter 20.. Since the thermomechanical simulations assessing the integrity of the shaft sealing structure extend up to 25,000 years, the fluid pressure and dilatancy criteria are evaluated at this specific point in time.

The fluid pressure criterion is evaluated as the ratio of pore pressure to the maximum principal stress along the depth at the contact zone of the shaft contour. For this calculation, we conservatively assume a brine density of 1.2 kg/m³. Figure 21.-13 (left) presents the pore pressure distribution along depth, extracted from hydraulic simulations and scaled by a factor of 1.2 to account for brine density. We also eliminate negative suction values by setting them to zero in regions where the shaft is still dry. Additionally, we provide the maximum principal stresses derived from the thermomechanical evolution of the repository system at 25,000 years. These components are then used to compute the fluid pressure criterion along the contact zone of the shaft, as shown in Figure 21.-13 (right).

The utilization rate of the fluid pressure criterion remains well below 1 throughout the salt formation, indicating that fluid migration is not expected at this evaluation time point. The highest

utilization rate occurs in the bitumen gravel, as this sealing component is the first to be bypassed by inflowing water from the overburden. Below this point, the utilization rate decreases rapidly to zero where no significant water accumulation has yet occurred, particularly in the lower gravel column.

These results confirm that the contact zone remains hydraulically tight against inflowing water, further demonstrating its resistance to fluid migration, as required in the safety demonstration concept.

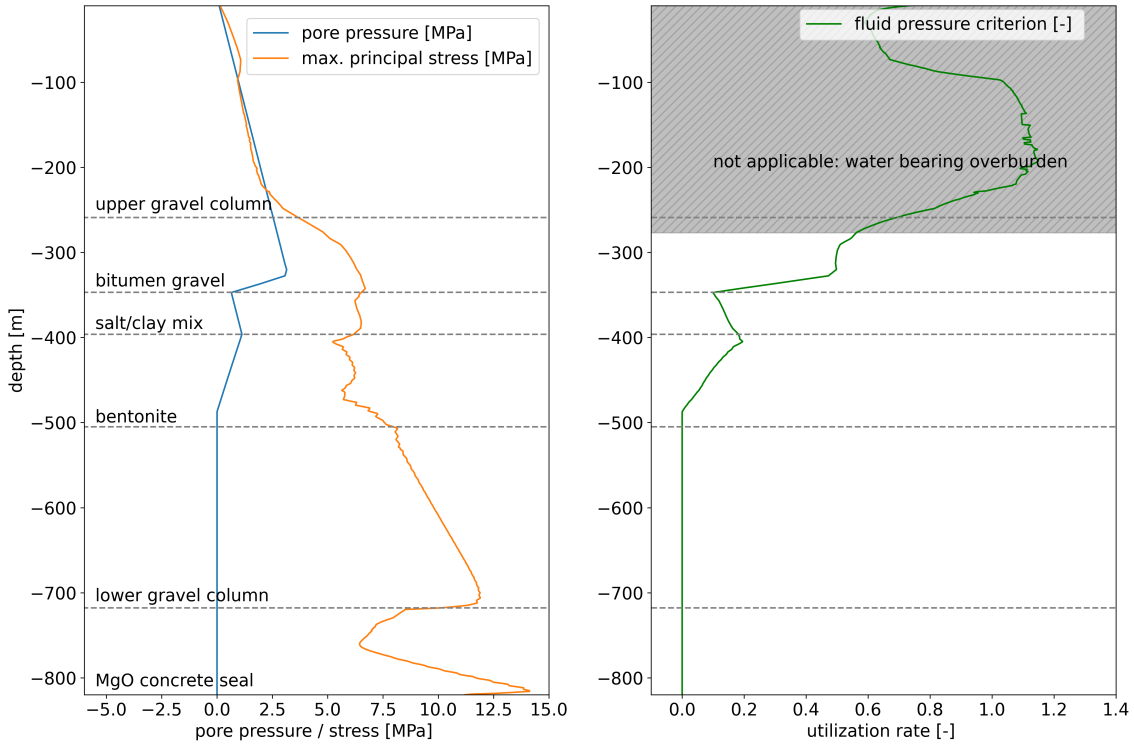

Figure 21.-13: Fluid pressure criterion along the shaft at the contact zone at time 25,000 years.

In a similar way, we evaluate the dilatancy criterion along the depth in Figure 21.-14. Figure 21.-14, left shows the component of the stress tensor extracted from the thermomechanical simulation at the contour of the shaft. From these streses, we can compute the mean stress and the octahedral stresses for the evaluation of the dilatancy criterion. Because of the acting fluid pressure at the contact zone, the dilantacy criterion is evaluated for the effetive stress following:

$$\eta = \frac{\tau}{-0.01697 \cdot (\sigma')^2 + 0.8996 \cdot \sigma'} \leq 1$$

where:

- τ = Octahedral shear stress, defined as:

$$\tau = \frac{1}{3}\sqrt{(\sigma_1 - \sigma_2)^2 + (\sigma_2 - \sigma_3)^2 + (\sigma_3 - \sigma_1)^2}$$

- σ' = Effective mean stress, given by:

$$\sigma' = \frac{1}{3}(\sigma_1 + \sigma_2 + \sigma_3 - 3p)$$

- η = Utilization rate
- p = Brine pressure

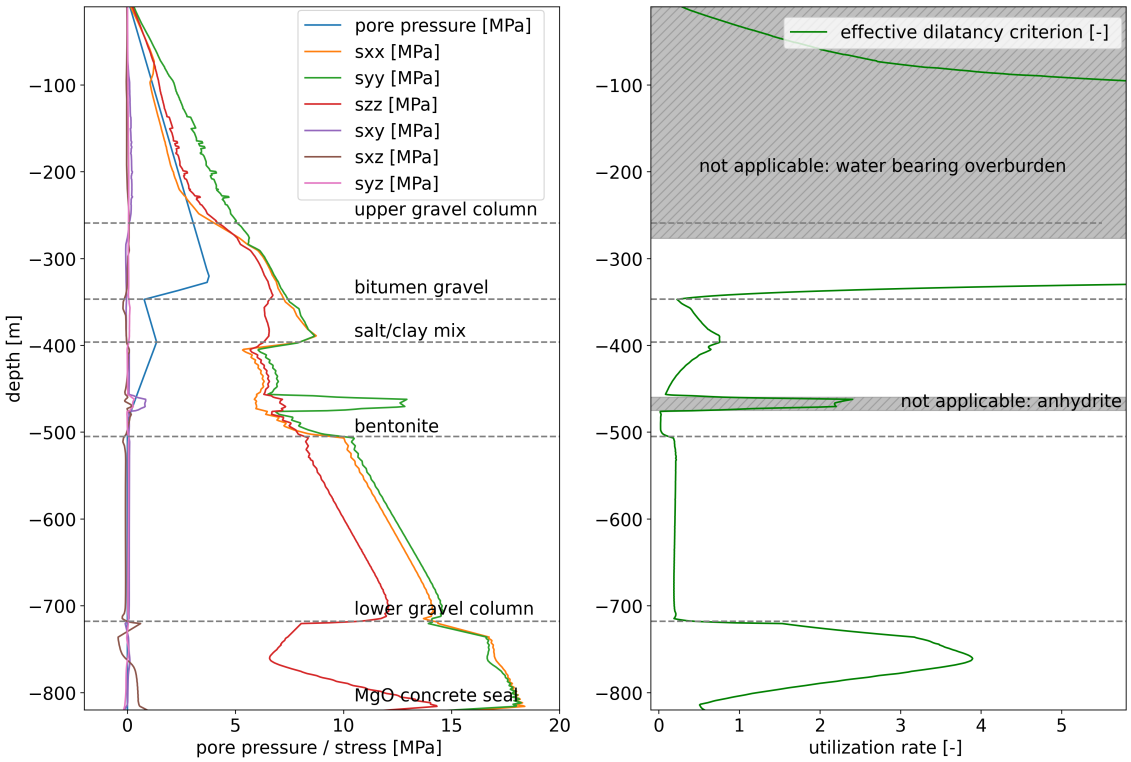

Figure 21.-14: Dilatancy criterion along the shaft at the contact zone at time 25,000 years.

This effective dilatancy criterion allows us to estimate the influence of the acting fluid on the dilatant strength at the contact zone. The results of this evaluation are presented in Figure 21.-14. At 25,000 years, the utilization rate of the effective dilatancy criterion exceeds 1 in the bitumen gravel region, indicating that this seal is already surrounded by inflowing brine. Further along the shaft, the utilization rate drops below 1 in the subsequent sealing elements but increases again at the bentonite-anhydrite interface. However, since the criterion is formulated for rock salt, it does not apply in this zone.

At the shaft base, the utilization rate once again rises above 1 due to the high shear stresses at the salt-MgO seal interface. This is attributed to the high stiffness of the MgO seal, which accommodates the thermal expansion of salt through increased stresses. Consequently, fluid percolation along the contact zone may become feasible at this stage. However, at this time, the lower part of the shaft remains dry, and the upper sealing components continue to fulfill their sealing function.

Over time, as thermal effects dissipate, the utilization rate of the dilatancy criterion is expected to decline. Further thermomechanical analyses of the shaft sealing system are required to confirm this long-term evolution.

22. Performance Assessment of the EBS

The driving forces for radionuclide transport away from a heat-generating waste repository in salt include pressurization of the gas and brine phases due to:

- thermal expansion (expansion of gas and brine volumes);
- drift closure (reduction of available pore space for gas and brine);
- addition of brine from inflow down the shafts or directly to the repository level (increase of mass of brine); and
- addition of gas from corrosion (increase of mass of gas).

The thermal-hydrological-chemical numerical models in this section are posed to investigate these potential driving processes in ways not previously possible. New capabilities have been added to PFLOTRAN that allow the consideration of fully coupled chemical changes to the salt/brine system. Coupling with the mechanical response of the system is known to be important, but is still under development. Mechanical response can either be added to PFLOTRAN or coupled with PFLOTRAN. There is an existing effort to implement a simplistic geomechanical capability in PFLOTRAN, but this capability will not allow large strains, include complex salt constitutive models, or include creep closure. Coupling PFLOTRAN with existing models that handle creep and large strains with complex constitutive models, like FLAC3D, is one possible approach.

Solute transport simulations were started but were not successfully completed. Placing a solid-phase tracer source term in the drifts resulted in essentially no transport during the longest simulations (only minor amounts of diffusion–Figure 22.-30), because the drifts were essentially air filled. Solute transport was attempted with the PFLOTRAN liquid-phase solute transport mode that allows for complete dry-out (i.e., NUCLEAR_WASTE_TRANSPORT mode). Most of the drifts were single-phase gas-filled, even as late as 2,000 years (see Section 22.3.8). During the re-saturation process, flow of brine is from the far field towards the drifts. This does not promote solute advection away from the waste. Any solute transport would happen after the waste re-saturates, and would require an assumption of rapid failure of waste packages, and rapid dissolution of the waste form. Practically, solute transport requires very long-term simulations (approaching 1,000,000 years) and adds additional degrees of freedom to the simulation, which makes them require more memory and take longer to perform.

Several thermal-hydrological-chemical numerical models of the disposal area EBS were developed in PFLOTRAN to illustrate different aspects of the relevant processes–including newly implemented features–across scales and resolutions. These model implementations have different levels of detail or realism in their representation of the waste and disposal drifts.

The models presented here include:

1. Closure of drift filled around a heated waste package with crushed salt, with the waste package explicitly represented using an unstructured mesh;

2. Closure of a drift filled with a crushed salt, using a distributed heat source on a structured mesh; and
3. Closure of heated drifts filled with crushed salt and closure of drift seals while considering the entire repository system and surrounding salt pillow host rock using an unstructured mesh.

The following sub-sections will present these different analyses, which used a recently developed version of PFLOTRAN that was modified with the following abilities:

- A thermal conductivity model that varies thermal conductivity with changes in both temperature and porosity (Section 15.1.3);
- A non-Darcy flow model that implements a threshold gradient for flow that is proportional to the permeability (Section 15.1.4);
- Reduction in porosity (i.e., drift closure) through injection of solid mass fraction;
- Implementation of equations of state for halite-saturated brine in PFLOTRAN (Section 15.1.1);
- Specification of a solid material as “soluble halite” and the the fluid phase as “saturated brine” (Section 15.1.2), allowing:
  - dissolution of solid-phase halite into brine (i.e., **porosity increase**) when:
    - fresh water is added (i.e., through condensation of vapor or injection of fresh water) or
    - brine is heated so it becomes under-saturated with halite (due to temperature-dependent solubility limits); and
  - precipitation of solid-phase halite from brine (i.e., **porosity decrease**) when:
    - water from the brine is boiled or evaporated away (i.e., through addition of heat or dry air) or
    - hot saturated brine is cooled so it becomes super-saturated with halite (due to temperature-dependent solubility limits).

For several of these new features, the RANGERS project was both the motivation for their development, and the first major use of the capability for a large-scale performance assessment type model in PFLOTRAN.

22.1 Explicit waste package in a single drift

This model includes a representation of one-quarter of a waste package through two planes of symmetry with an unstructured grid. This problem includes the effects of drift closure through injection of solid phase into the crushed salt, and shows the effect of a strong thermal gradient across the crushed salt (i.e., from the hot waste package to the EDZ).

The injection of a solid phase into a source/sink in PFLOTRAN general flow mode results in the increase of pressure (and a slight increase in temperature) in the liquid phases that occupy the pores, through conservation of mass of the liquid species and the fixed volume of the element.

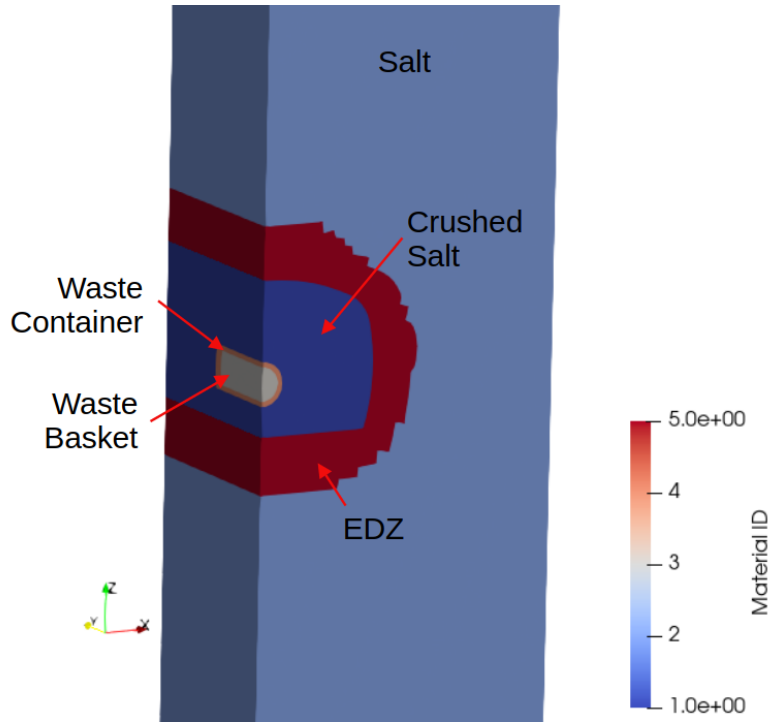

Figure 22.-1: Distribution of regions in a near field model of the disposal drift with waste package.

In hydrological-mechanical simulators (e.g., FLAC3D), an analogous process is achieved by reducing the volume of the element through mechanical compaction. The compaction process is accompanied by an increase in liquid saturation, due to the much higher compressibility of gas compared to liquid at typical pressures. In a mechanical simulator, the volume of the elements gets smaller during compaction, while in PFLOTRAN the elements only get filled with solid. This leads to an approximation, because the drift becomes smaller in reality (i.e., distances from the center of the drift to the EDZ become shorter), while in PFLOTRAN the drift is the same dimensions, even at late time.

The domain cuts a cylindrical waste package at the x = 0 and y = 0 faces (Figure 22.-1 shows the quarter symmetry), with the model domain extents of $0 \leq x \leq 7.5$ m, $0 \leq y \leq 4.81$m, and $0 \leq z \leq -900$ m. The large vertical extent of the domain came from its initial use for mechanical simulations in FLAC3D, where it is important to move the upper and lower boundary conditions far from the waste package.

The domain consists of five materials (Figure 22.-1), summarized in Table 22.-1. The linear resistivity thermal conductivity model is used for intact salt thermal conductivity [$W/(m \cdot K)$] with the parameters

$$\lambda_{\text{lin res}}(T) = 5.2/\left(1 + 0.0045T\right) \tag{19}$$

illustrated in Figure 22.-2, while the “crushed salt” model is introduced in Section 15.1.3, here using the parameters

$$\lambda_{\text{cr salt}}(T, n) = 6.1\left(1 + 0.0045T\right) \cdot \left(1 - \frac{n}{0.35}\right)^{1.14} + \frac{n}{0.35} \cdot \left(0.42 + 0.0027T\right), \tag{20}$$

and is illustrated in Figure 22.-3.

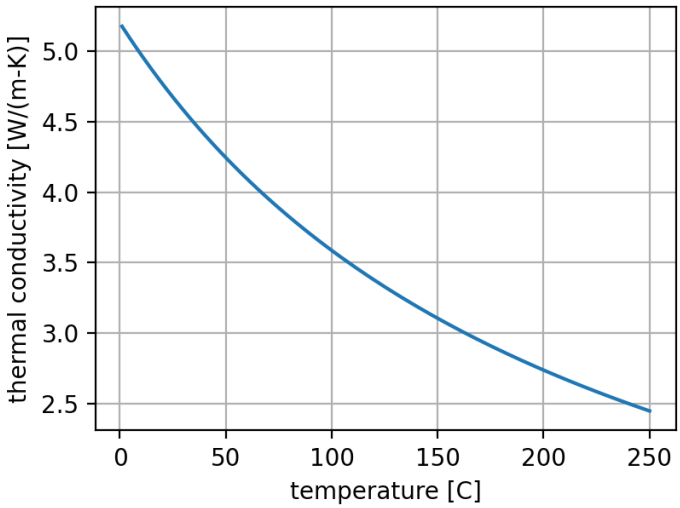

Figure 22.-2: Linear resistivity thermal conductivity model (Eq. 19) used for intact salt.

Table 22.-1: Material properties used in quarter-symmetry model of waste package and drift.

Material	Permeability (k) [m^2]	Init. Porosity (n) [$-$]	Thermal Cond. (λ) [$W/(m \cdot K)$]	Heat Cap. (ρc_p) [$MJ/(m^3 \cdot K)$]
Salt	$1.0 \cdot 10^{-20}$	0.0002	linear resistivity	3.48
Crushed Salt	$8.79 \cdot 10^{-15}$	0.35	crushed salt	1.02
Waste Basket	$1.0 \cdot 10^{-18}$	0.05	20.0	7.80
Waste Container	$1.0 \cdot 10^{-18}$	0.05	15.0	7.21
EDZ	$3.16 \cdot 10^{-16}$	0.05	crushed salt	1.79

The heat capacity (ρc_p) values listed in Table 22.-1 are for the solid phase. PFLOTRAN computes the overall heat capacity for an element as the porosity- and saturation-weighted mixture averages for all the phases present, with the density and heat capacity of brine and air coming from tabulated equations of state.

The hydrologic properties (i.e., porosity and permeability) of the Waste Basket and Waste Container materials are set to values to allow air or water to leave them during the simulation, so the waste packages do not pressurize (a process that can lead to very small time steps in the simulation); the material properties are not intended to be representative of dense, impermeable steel. The salt, crushed salt, and the EDZ materials use the same van Genuchten (vG) capillary pressure curve functions ("salt" row in Table 22.-2), while the Waste Basket and Waste Package materials use the other set of capillary pressure curve parameters ("man-made" row in same table). For salt, although impermeable, we assume a permeability low enough to limit advective transport in the framework of Darcy law assumed in PFLOTRAN. The waste package remains dry for the entire simulation because of three factors: 1) the waste package starts dry, 2) the man-made materials have essentially no capillarity to draw in water (maximum p_c = 1 Pa), and 3) the waste packages are hot.

The heat source starts after 2 years to allow time for the hydrologic parameters to stabilize before adding heat (from -2 to 0 years). The power source, which decays exponentially with time, is shown in Figure 22.-4. The porosity closure source term is applied across the crushed salt material. The rate is computed to reduce the initial porosity (35%) to a low value (2%)

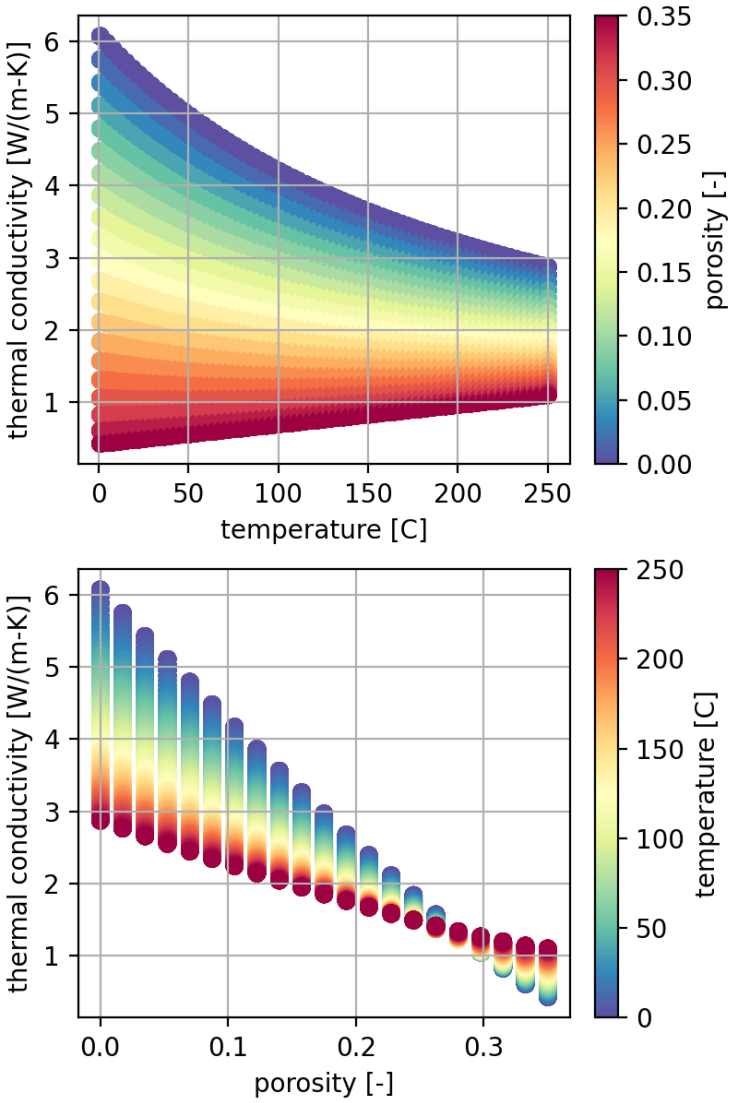

Figure 22.-3: Crushed salt thermal conductivity model (Eq. 20) used for crushed salt backfill and drift seals.

uniformly over 100 years (from 1 to 100 years).

The domain is made up of 182,940 hexahedral elements; Figure 22.-5 shows the mesh near the waste package. Moving far above and below the disposal horizon (located at approximately 650 m depth), the elements become regular “brick” elements (i.e., a structured mesh).

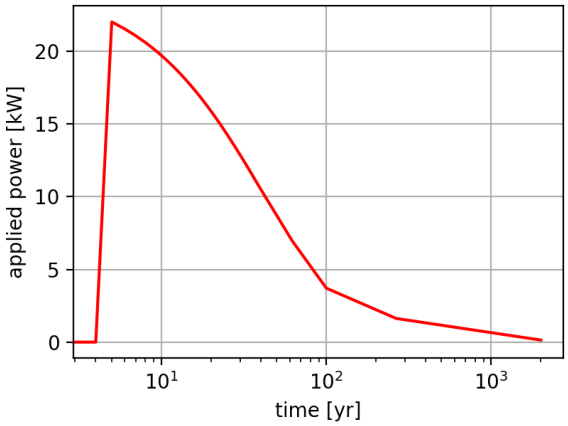

Figure 22.-4: Thermal input applied to 1/4 of waste package through time.

Table 22.-2: Capillary pressure curve function (van Genuchten) parameters used in quarter-symmetry waste package model.

Material	vG alpha [1/Pa]	vG m [−]	Liq. Res. [−]	Gas Res. [−]	Max p_c [Pa]
Salt	10^{-6}	0.6	0.02	0.01	10^9
Man-made	10^{-4}	0.5	0.001	0.001	1.0

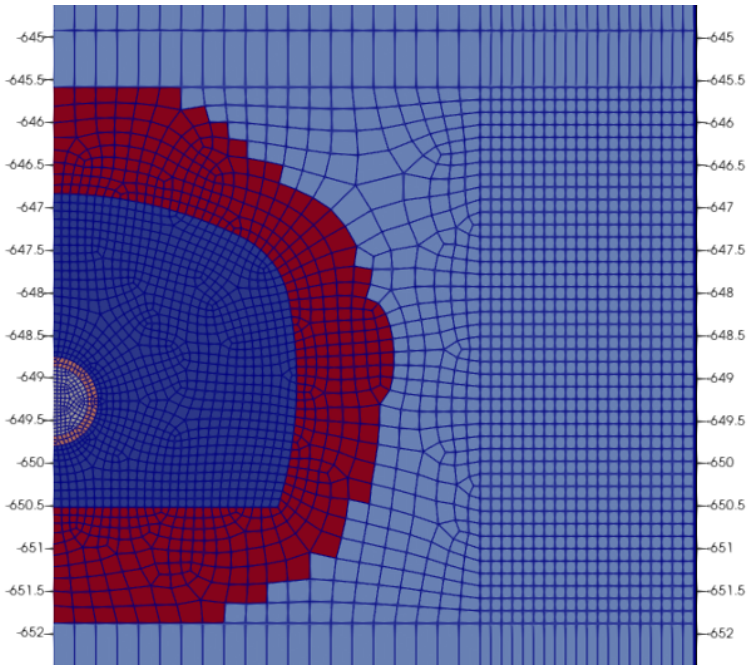

Figure 22.-5: XZ view of a section of the quarter-symmetry model at waste package with mesh shown and elements colored by material ID.

Figures 22.-6 through 22.-9 show results from the near waste-package region through time for four key variables. Temperature and porosity are changed, due to the input of thermal energy into the waste basket material and the input of solid phase in the crushed salt material. Thermal conductivity and liquid saturation then change in response to imposed changes in temperature and porosity. Between the system startup and the beginning of heating (-2 yr $\leq$ t $\leq$ 0), the liquid brine re-distributes a bit at the transition from crushed salt to EDZ and at the transition from EDZ to intact salt, due to capillarity.

Figures 22.-6 and 22.-7 show the results in the earlier part of the simulation. By 5 years, much of the crushed salt has dried out (98% air-filled initially), the porosity has reduced slightly, and the thermal conductivity has increased. By 25 years, the porosity has increased at the boundary between the crushed salt and the EDZ, where condensation is happening (dissolving salt, see red region in porosity sub-figure).

Figures 22.-8 and 22.-9 show model results for later parts of the simulation. By 50 years, the porosity that had increased due to dissolution has now reduced, and most of the crushed salt has reduced to 20% porosity or less. At 100 years, the porosity near the edge of the initial crushed salt region has reduced to nearly zero, and the liquid saturation in this area increased. This increase in saturation is because the small amount of water in these elements is now enough to saturate them with water, since the porosity has reduced. At later time (t = 200 and 400), the porosity in the crushed salt has reached its assigned lower value ($\approx$ 2%), and the saturation at the edge of the crushed salt has reduced, that was previously fully saturated. The temperature has reduced by this point (because the heat source is reduced), so the thermal conductivity is increasing, but it is nearly constant across the domain (besides the higher thermal conductivity of the metal waste package and waste basket). A small part of the dissolution (and porosity increase) and precipitation (and porosity decrease) is due to the change in halite solubility with temperature. When temperatures are rising, the brine is undersaturated, so there will be dissolution and an increase in porosity. When temperatures are decreasing, the brine is super-saturated and there will be a precipitation and a reduction in porosity.

The crushed salt near the waste package heats up rapidly beyond the boiling point, so it dries out (precipitating halite). Further away from the waste package the salt is cooler, so the steam from drying out the crushed salt condenses and dissolves salt. Also, a smaller change is associated with the brine that heats up and is now unsaturated with respect to halite, so porosity increases. In reality, natural salt deposits are heterogeneous (i.e., mostly halite, but some other minor evaporite components–some more soluble than halite, others less soluble than halite), but the current implementation in PFLOTRAN assumes the salt is uniformly pure halite.

In summary, this model illustrates how the crushed salt around the waste package dries out and can reduce porosity quickly. Complex thermal-hydrological-chemical dissolution, precipitation, and solubility-related processes happen at the edges of the boiling region during heating and cooling. Once porosity is reduced, the brine in the surrounding EDZ and intact salt can re-saturate the edge of the crushed salt, but the waste package stays dry during the first 400 years of heating. The permeability (not plotted here), varies as porosity changes through an exponent (here k = n^4); porosity reduced one order of magnitude, so permeability reduced four orders of magnitude–this significantly slows down water moving back towards the waste packages.

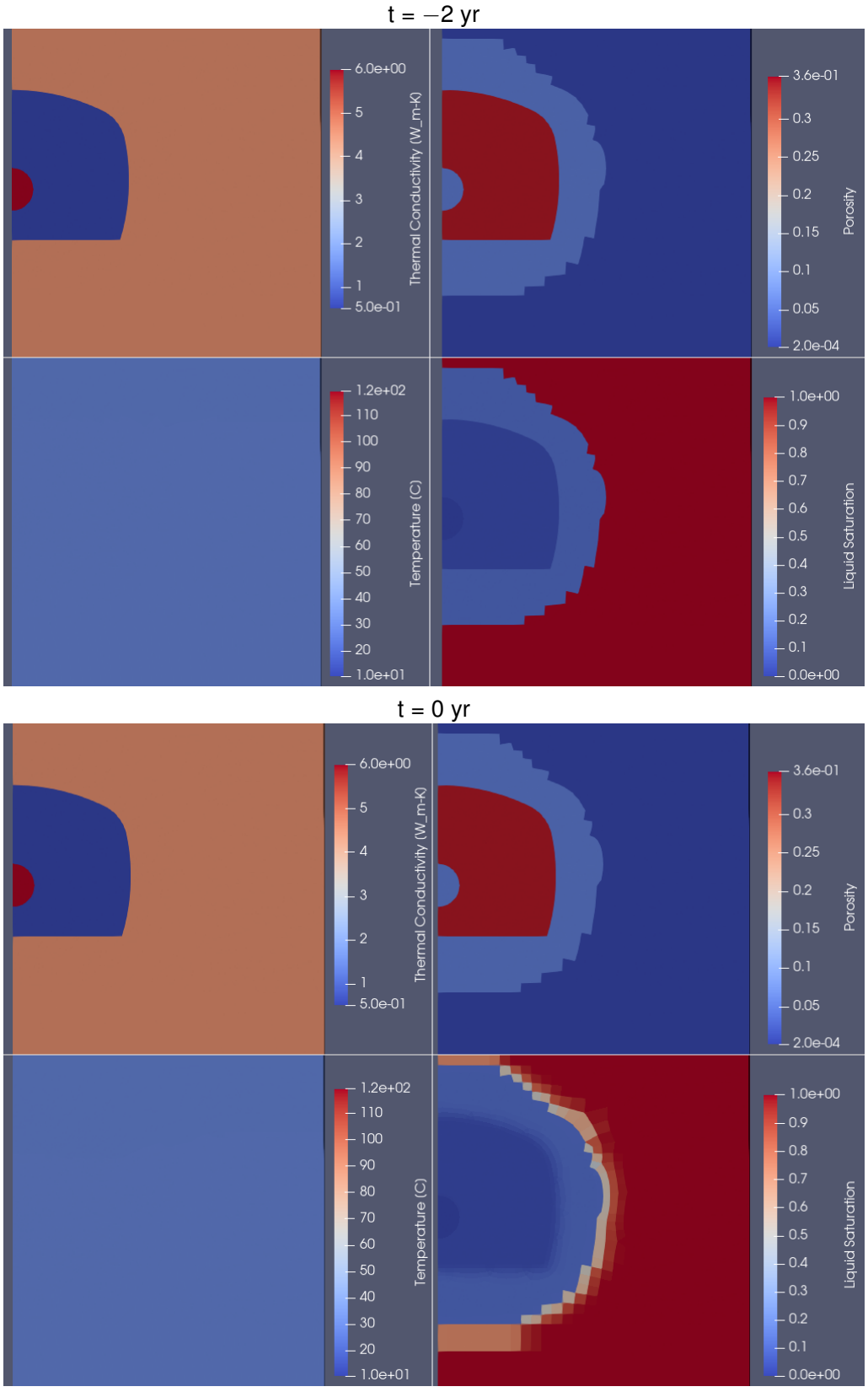

Figure 22.-6: XZ view of quarter-symmetry model showing thermal conductivity (upper-left panel), porosity (upper-right panel), temperature (lower-left panel), and liquid saturation (lower-right panel) at four times (t = $\{-2, 0\}$ yrs after heating began).

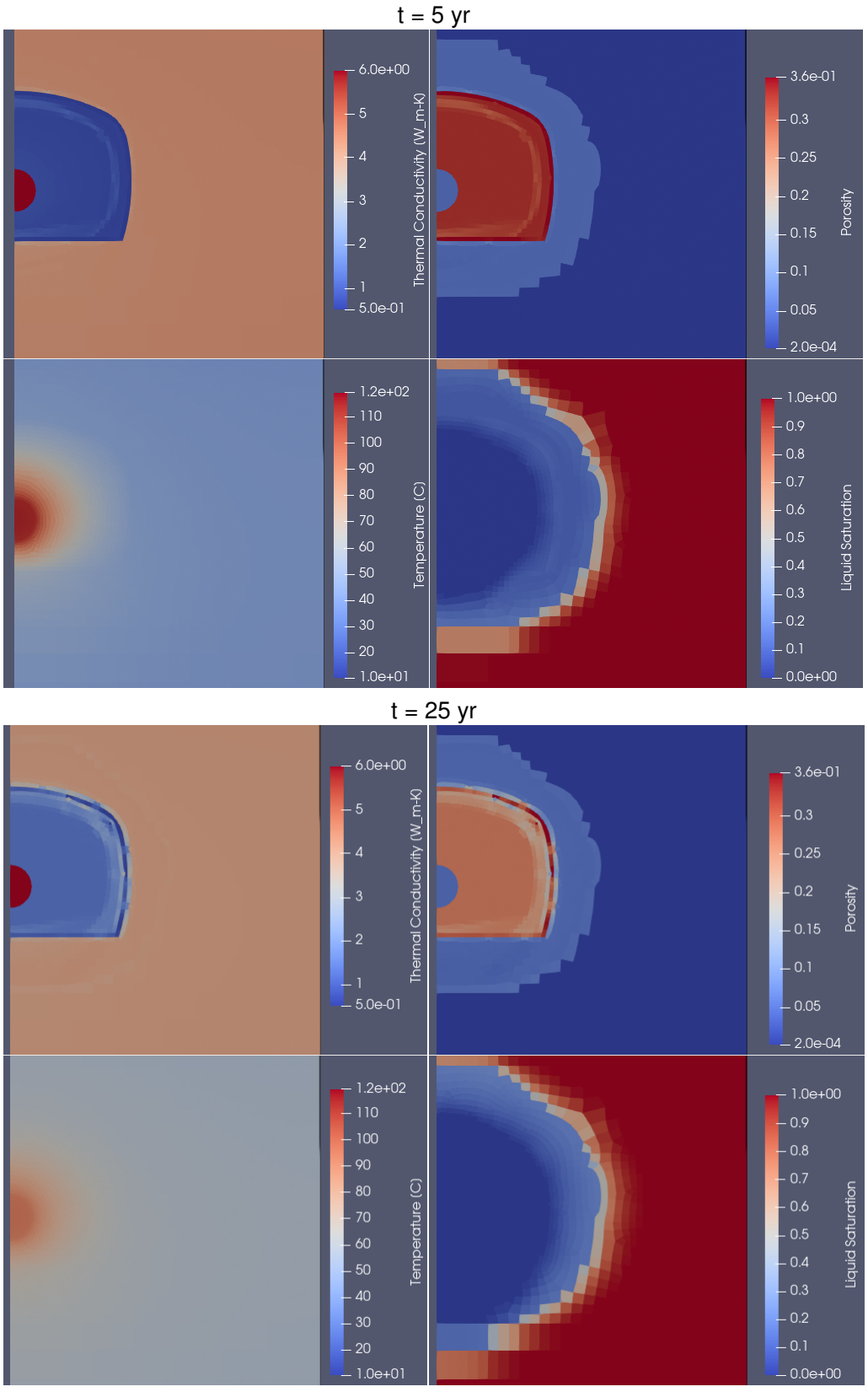

Figure 22.-7: XZ view of quarter-symmetry model showing thermal conductivity (upper-left panel), porosity (upper-right panel), temperature (lower-left panel), and liquid saturation (lower-right panel) at four times (t = $\{5, 25\}$ yrs after heating began).

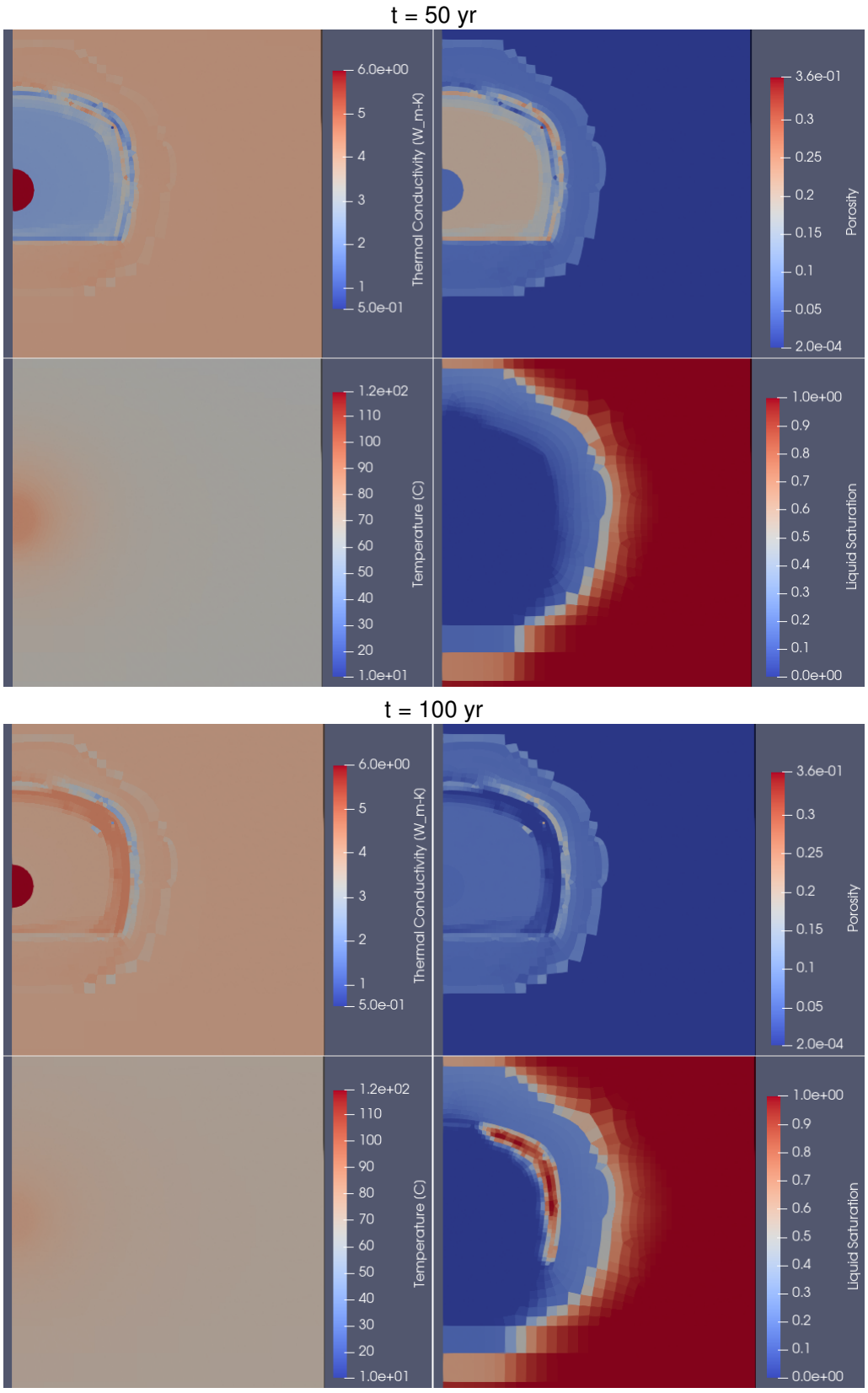

Figure 22.-8: XZ view of quarter-symmetry model showing thermal conductivity (upper-left panel), porosity (upper-right panel), temperature (lower-left panel), and liquid saturation (lower-right panel) at two times (t = $\{50, 100\}$ yrs after heating began).

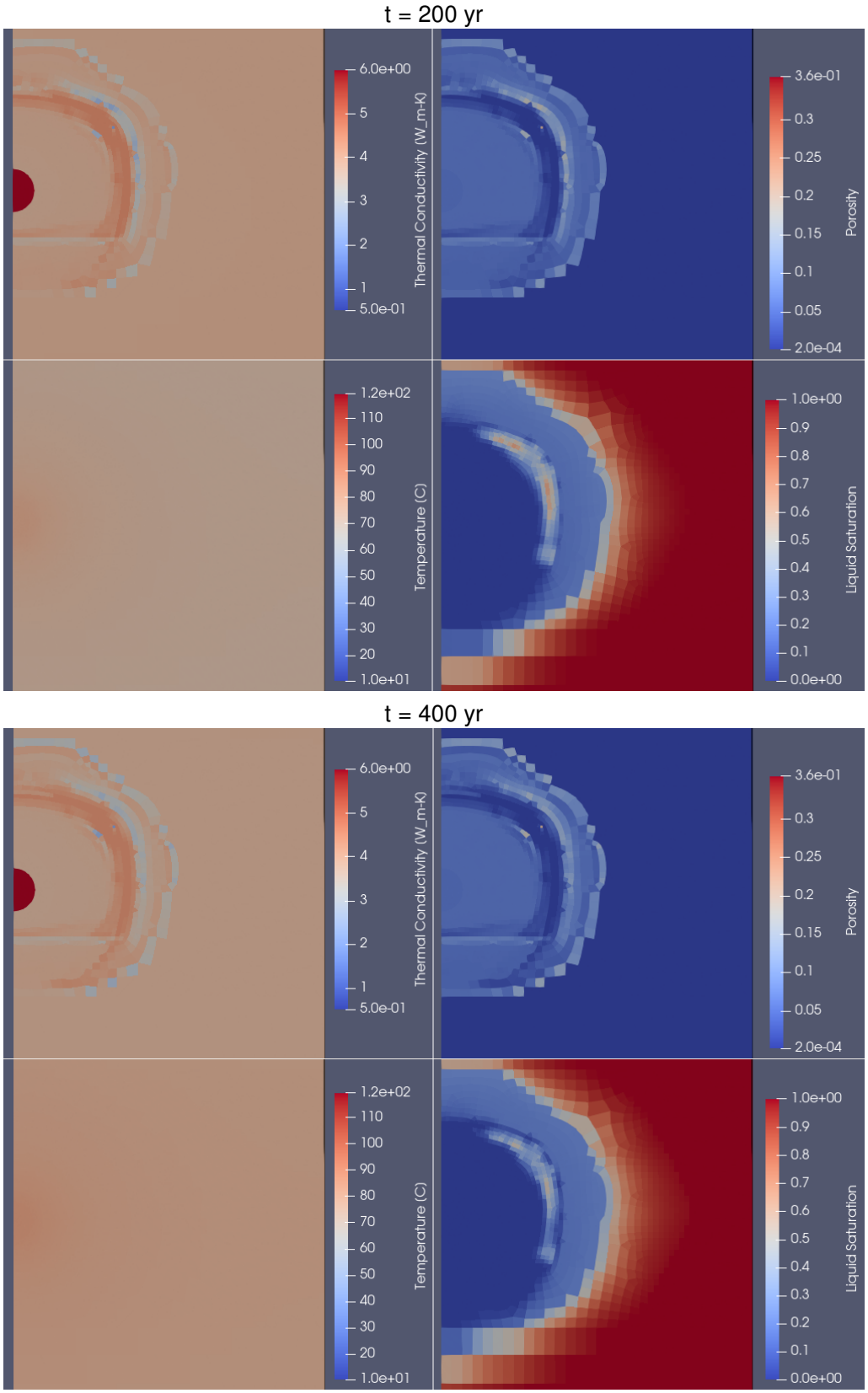

Figure 22.-9: XZ view of quarter-symmetry model showing thermal conductivity (upper-left panel), porosity (upper-right panel), temperature (lower-left panel), and liquid saturation (lower-right panel) at two times (t = $\{200, 400\}$ yrs after heating began).

22.2 Distributed heat source in a single drift

This PFLOTRAN model was created to validate/illustrate the porosity change process for a smaller structured grid 2D simulation (fewer elements) that includes the disposal drift, EDZ surrounding the drift, and intact salt, but does not include the waste package explicitly (the heat source is spread out across the disposal drift). This arrangement is similar to how the disposal drifts and waste are simulated in the large-scale model of the entire domain (Section 22.3), but the simpler structured mesh allows closer examination of the processes going on in the drift at different resolutions, and is orders of magnitude faster to run than the large models (allowing the problem to run on a single workstation) for debugging and understanding the implementation.

Figure 22.-10 shows the structured mesh used to illustrate the thermal-hydrological-chemical processes going on inside a single drift with heating and drift closure. The mesh includes 1/8 of the drift, by cutting the disposal drift in half in all three Cartesian directions. The grid extends two elements in the y-direction, with one element representing a disposal drift (187 m extent in y-direction), and an adjacent layer (0.5 m extent in y-direction) of elements representing connection to a neighboring drift (e.g., an infrastructure drift - Figure 22.-12). The neighboring drift has a single element fixed at the initial pressure and temperature, to facilitate allowing gas to escape elsewhere in the repository. The disposal drift was dimensioned to be analogous to the larger model that includes all the repository components explicitly.

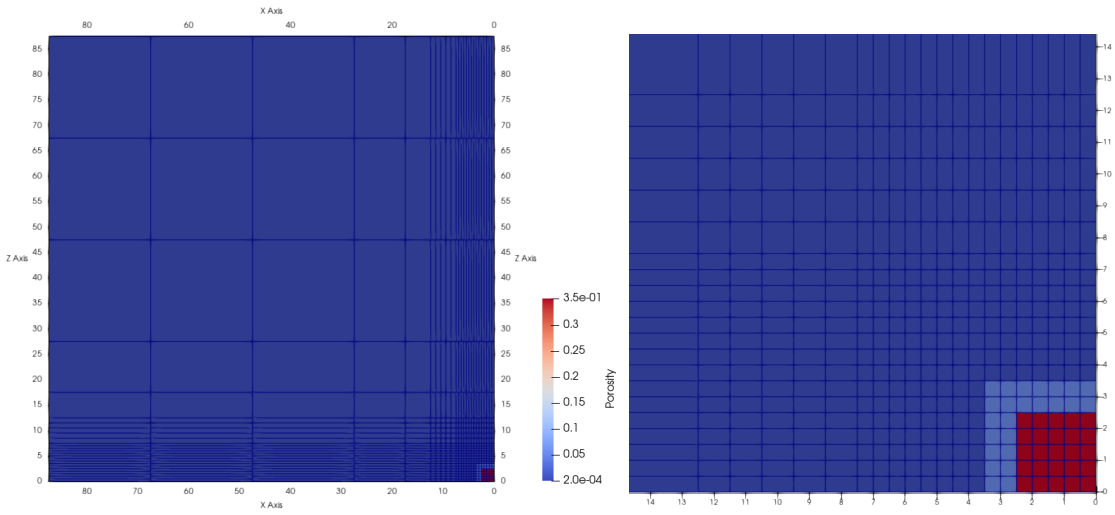

Figure 22.-10: End view (XZ) of entire domain (left) and zoom into drift portion (right) of structured mesh used to represent a 1/8 symmetry disposal drift. High initial porosity (0.35) is crushed salt; moderate initial porosity (0.05) is DRZ; low porosity (0.0002) is intact salt.

The structured 1/8-symmetry model used the salt, EDZ, and crushed salt materials from the unstructured 1/4-symmetry model of the previous section (Section 22.1). The power source applied across the crushed salt material is shown in Figure 22.-11. The power source is homogenized to account for the volume of the drift.

Figure 22.-13 shows the evolution of several variables and parameters in the system due to the specified reduction in porosity and addition of thermal energy. The porosity of the crushed salt in the drift is reduced from 35% to $\approx$ 2% over the course of 100 years, through the constant-

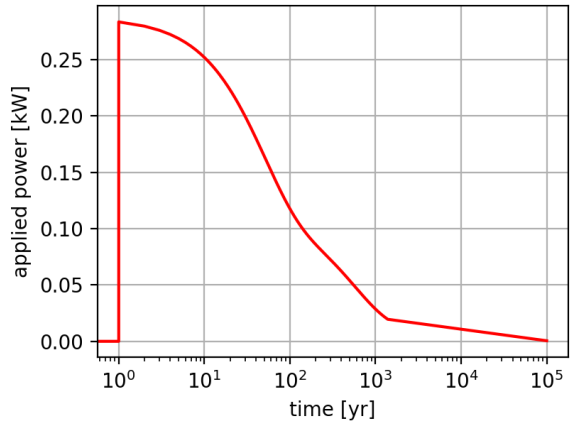

Figure 22.-11: Power applied to 1/8 of waste disposal drift through time.

rate addition of solid phase across the crushed salt material, and a related reduction (from 5% to 2% porosity) in the EDZ. At the beginning of heating, there is a small jump in porosity within the crushed salt and EDZ (red and green shaded areas) associated with the change in the solubility of halite with temperature and the condensation of vapor. The permeability of the crushed salt reduces 4 orders of magnitude due to this change in porosity due to a power-law relationship between porosity and permeability (with exponent 4). The thermal conductivity increases from 0.5 to about 5.0 $W/(m \cdot K)$ due to the constitutive law for thermal conductivity (section 15.1.3 and Figure 22.-3). Gas pressure and gas density increase significantly during the compaction (with some elements in the crushed salt approaching 10 MPa), especially near the end of the specified compaction (at 102 years). The gas pressure then quickly leaks off, by escaping into the neighboring access drift. In a coupled hydrological-mechanical simulation, the rise of gas pressure would reduce the rate of closure.

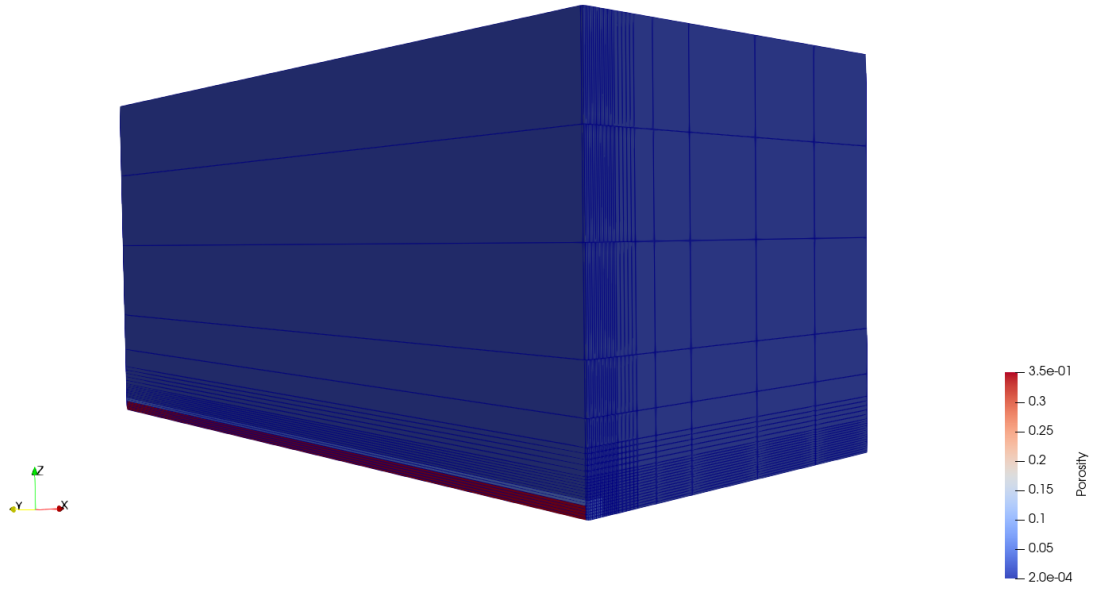

Figure 22.-12: Side view of structured mesh used to represent the near-drift region and connection to adjacent drift in 1/8 symmetry.

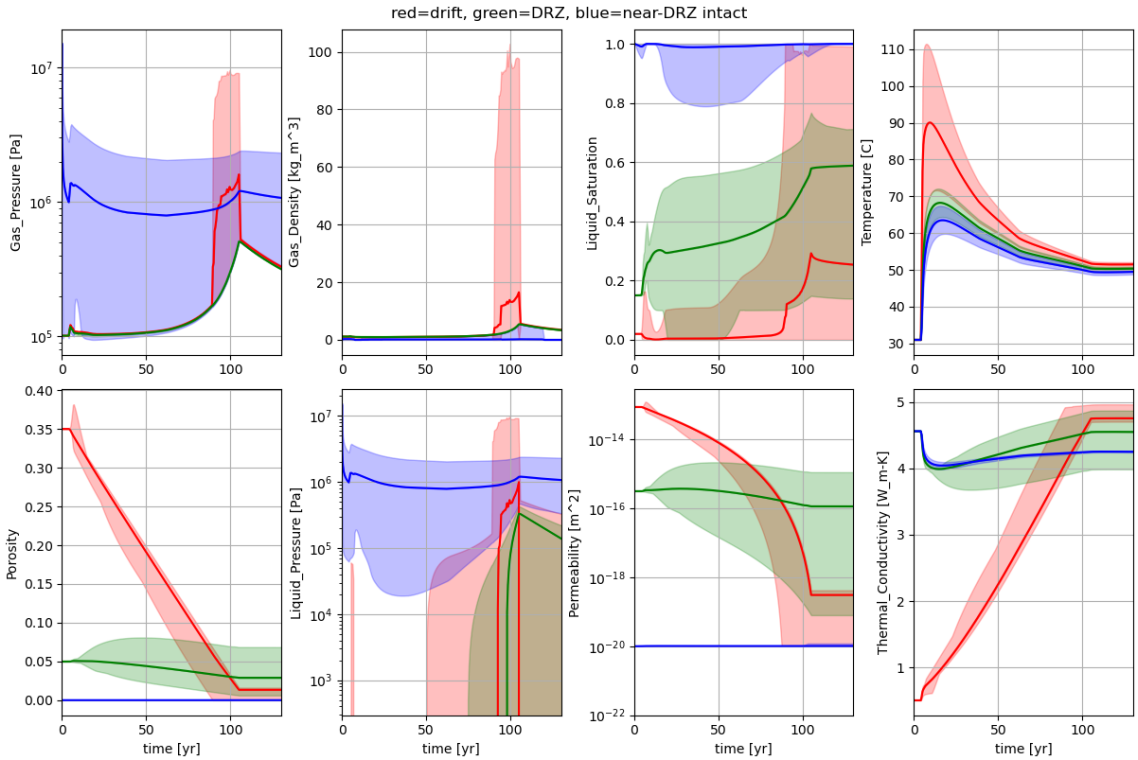

Figure 22.-13: Average (line) and bounding (min/max shading) predictions for single-drift distributed-source problem. Gas pressure, gas density, liquid saturation, temperature, porosity, liquid pressure, intrinsic permeability, and thermal conductivity are shown. Red represents the elements in the heated drift (i.e., crushed salt), green represents the EDZ, and blue represents the two elements of adjacent intact salt.

Figures 22.-14 and 22.-15 show the spatial distribution of porosity, liquid saturation, temperature, and thermal conductivity at four times. At the beginning of heating (t = 0, after 4 years of equilibration), the liquid saturation in the intact salt adjacent to the EDZ has decreased slightly. After 50 years of heating, the crushed salt (with the distributed heat source and the distributed injection of solid mass) is essentially dry, and its porosity has reduced by 1/2 (resulting in higher thermal conductivity). In these figures it is clear the corner of the drift is wetter, since it is adjacent to or nearly surrounded by the wetter EDZ. After 100 years of heating, the porosity has reached its specified low value, and the corner of the crushed salt is also at high liquid saturation (since a small amount of liquid can saturate the now nearly closed-off pore space). Like seen in the previous section with the explicit waste package (section 22.1), by approximately 200 years the higher saturation in this region has reduced. The migration of the water back towards the heat source has slowed down significantly, due to the reduced permeability in the crushed salt (Figure 22.-13).

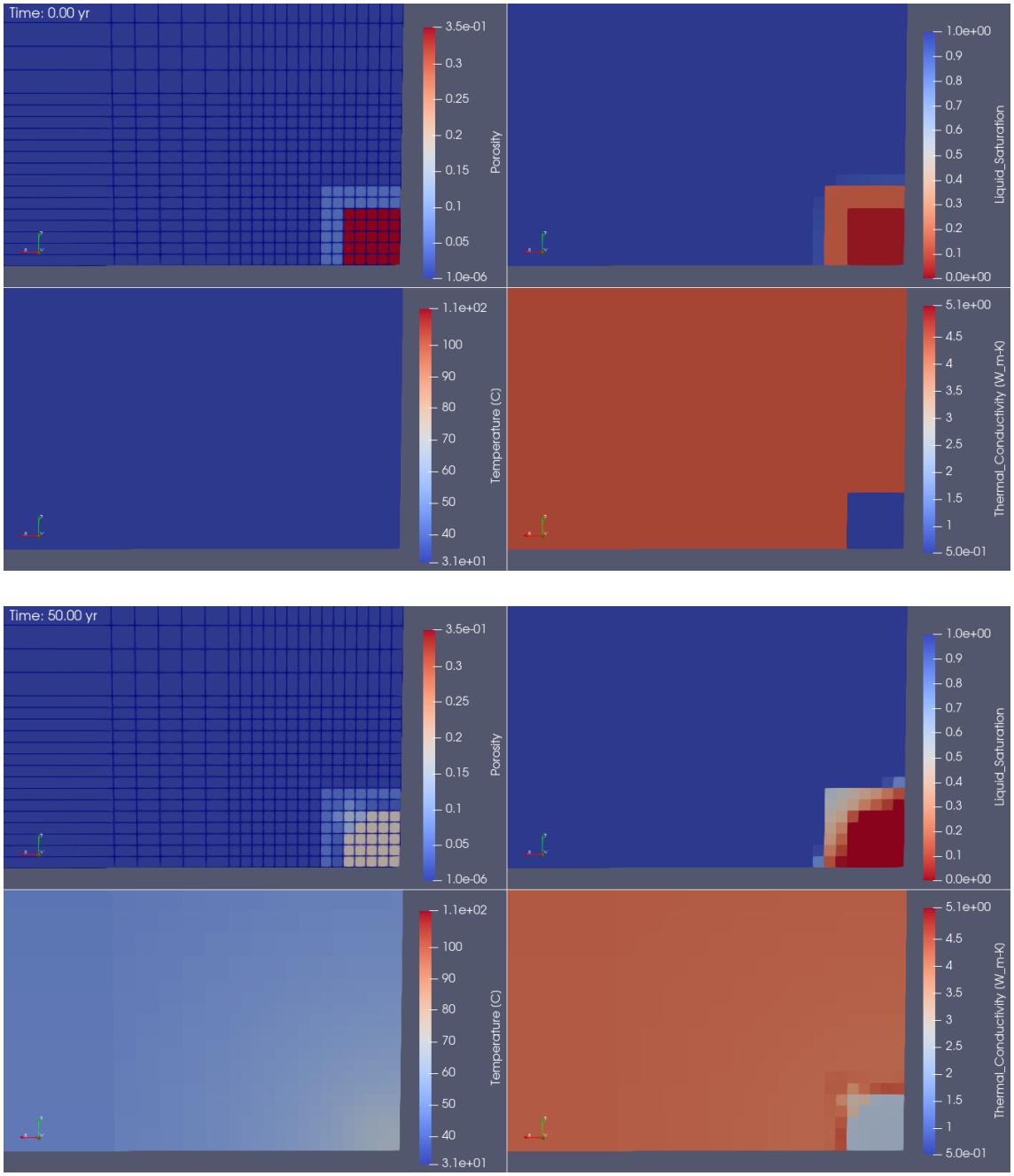

Figure 22.-14: Distribution of porosity (upper left), liquid saturation (upper right), temperature (lower left), and thermal conductivity (lower right) at two early times during heating (t = 0, 50 years).

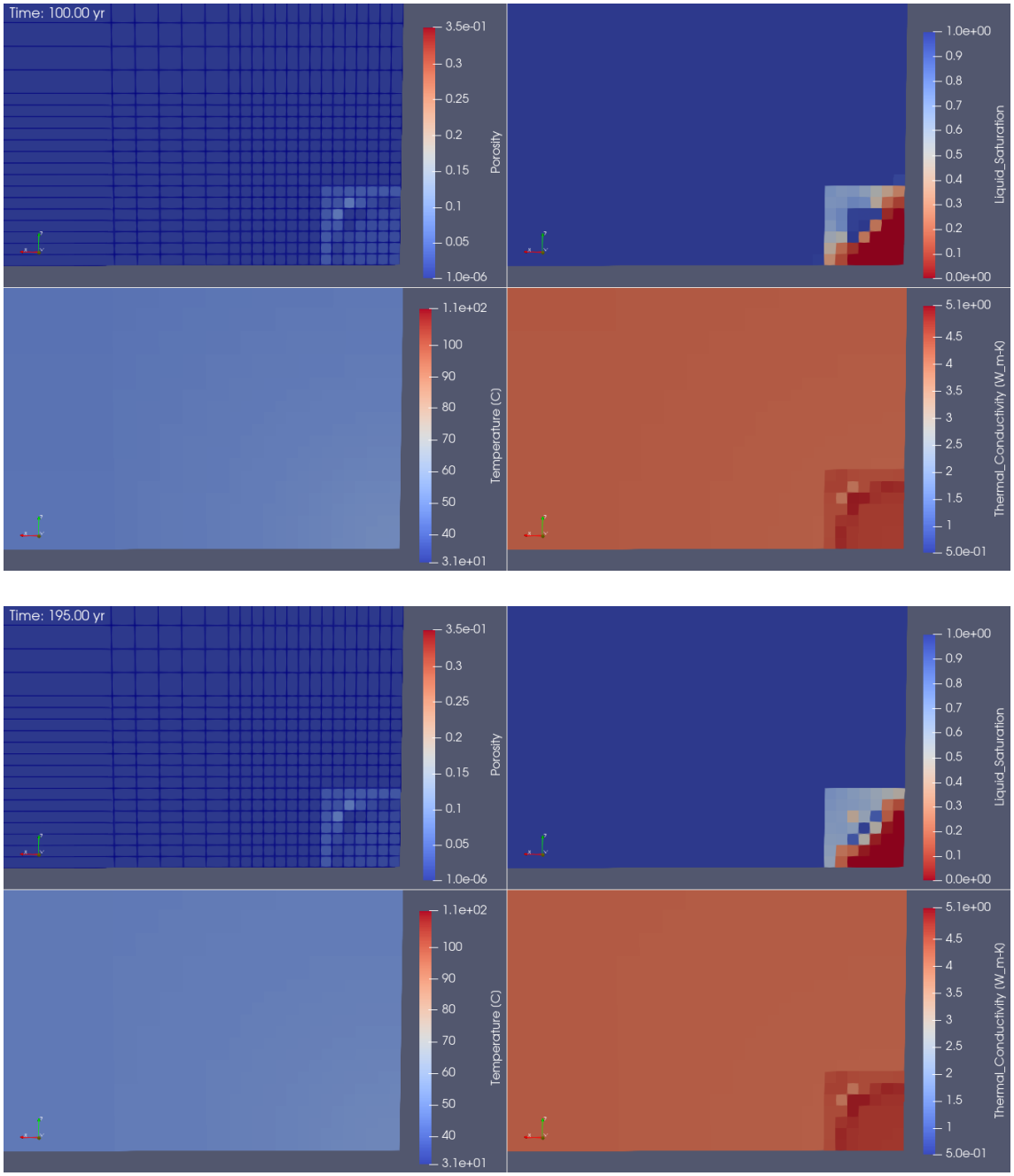

Figure 22.-15: Distribution of porosity (upper left), liquid saturation (upper right), temperature (lower left), and thermal conductivity (lower right) at two later times during heating (t = 100, 195 years).

22.2.1 Grid refinement study

One benefit of a quicker-to execute model is the ability to perform a grid refinement study. To compare to the results presented in the previous section (1,250 elements), the mesh was both coarsened (288 elements) and refined (5,000 or 20,000 elements). This section compares results, including the effects of the non-linear thermal-hydrological-chemical processes related to precipitation and dissolution of salt. The time evolution of the properties in similar regions are presented in Figures 22.-16 and 22.-17. All the meshes are only 2 elements in extent in the y direction, with the refinement occurring only in the x and z directions.

These results show similar averages (lines), but more extreme minimums and maximums (e.g., the finest mesh results in porosity of 100% at some elements in the crushed salt when heating begins). The crushed salt and EDZ have large increases in porosity at the beginning of heating, due primarily to the condensation of vapor, but also secondarily due to the increase in solubility with temperature. The temperature responses for all except the coarsest mesh are nearly identical. In the more refined meshes, the dissolution and precipitation processes can dissolve or precipitate entire elements, compared to smaller impacts on larger elements. Large changes in porosity then also have impact on the thermal conductivity and permeability, which are both coupled to the porosity value. Porosity values of 100% are not physically realistic, but are a consequence of the thermal-hydrological-chemical PFLOTRAN model with mechanical closure effects added through solid mass injection, rather than explicit inclusion of mechanical response.

The predicted peak of gas pressure at the end of the closure process is highest in the base resolution (Figure 22.-13), with the peak gas pressure predicted to be lowest in the most refined mesh. The predicted average liquid saturation is also lower in the crushed salt in the more refined models, while the liquid saturation is higher in the coarser model.

This grid resolution study shows that even a coarse representation of the drift (as used in the larger models presented in the next section), similar physical processes occur to more refined meshes–for the case where the waste package is not explicitly represented. These complex thermal-hydrological-chemical processes are effectively similar, but the simulation is much faster, allowing large-scale simulations more readily.

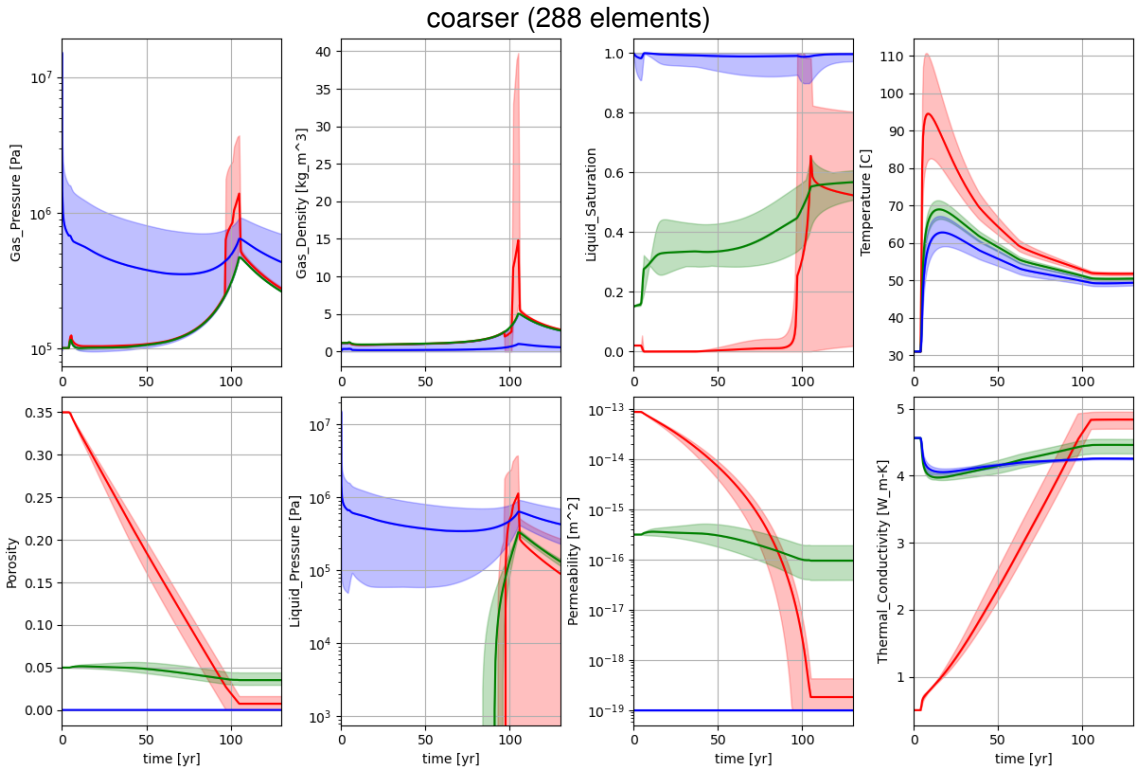

Figure 22.-16: Average (line) and bounding (min/max shading) predictions for single-drift problem with coarser mesh. Red represents the heated drift, green represents the EDZ, and blue represents adjacent intact salt.

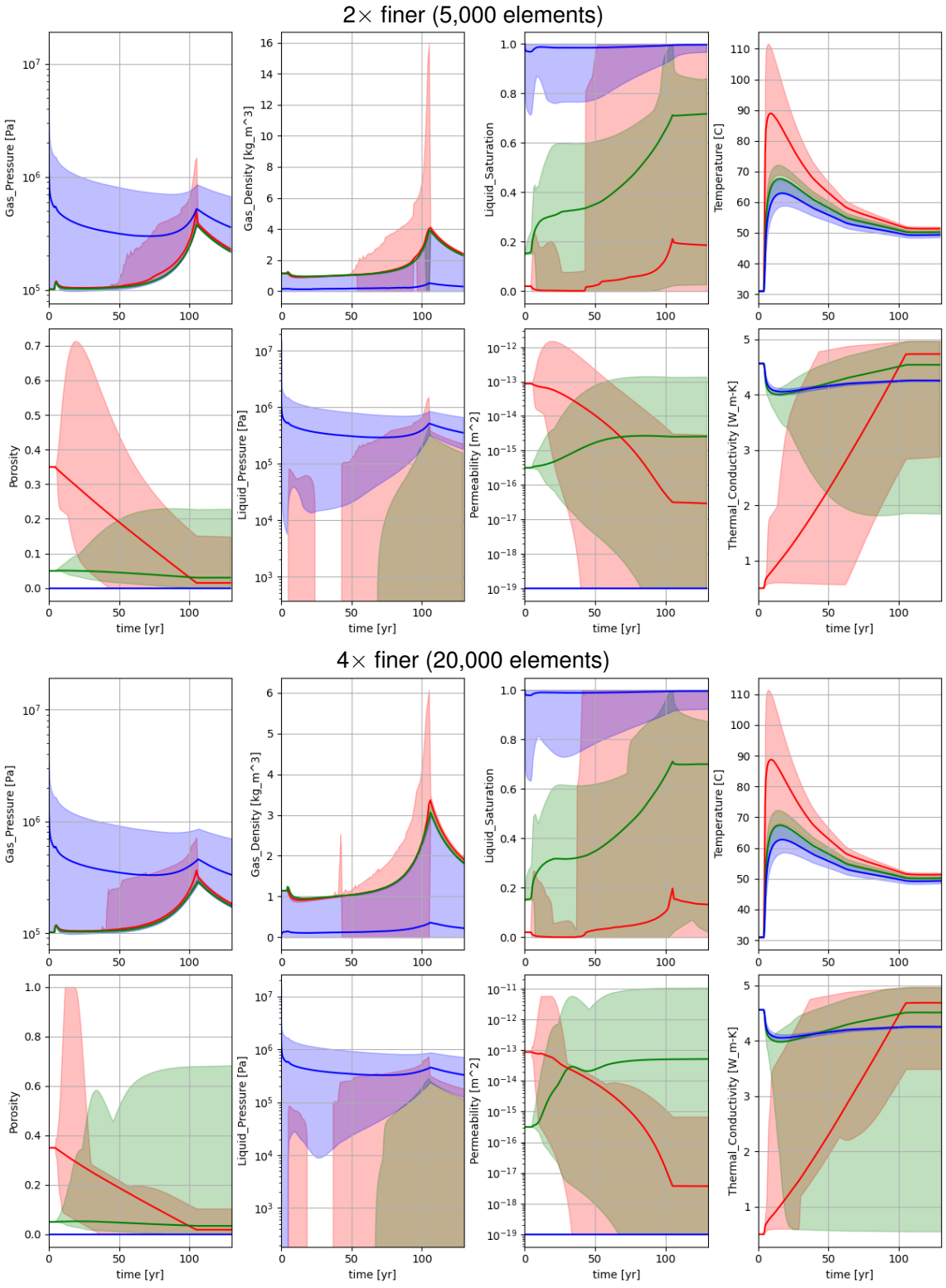

Figure 22.-17: Average (line) and bounding (min/max shading) predictions for single-drift problem with 2× finer (top) and 4× finer (bottom) mesh. Red represents the heated drift, green represents the EDZ, and blue represents adjacent intact salt.

22.3 Full repository domain with EDZ surrounding drifts

This model includes the specified variability in the regional salt pillow geology, the entire layout of the repository and shafts, and sequential emplacement of waste in disposal drifts over 30 years of operation. The heat sources are distributed across the crushed salt filled drifts (no explicit waste packages), like the previous section 22.2.

22.3.1 Computational mesh

A mesh comprised of both hexahedral and wedge elements was created using meshing tools for FLAC3D. The mesh was then converted to an implicit unstructured mesh usable by PFLOTRAN via conversion tools developed for the RANGERS project. In PFLOTRAN, an implicit unstructured mesh is specified completely by mesh coordinates and the listing of mesh points associated with each volume or area elements. PFLOTRAN then computes element volumes, face areas, and element connectivity relationships from the mesh. To improve start-up times, the implicit unstructured mesh and region definitions were converted from ASCII text files ($>$ 1.6 GB in size) to the HDF5 binary file format (305 MB). This process brought in the mesh coordinates, element definitions, and regions specifications from FLAC3D, and defined the same elements and regions in PFLOTRAN, allowing direct comparison between modeling results, with the intention of transferring information between the simulations.

A series of several meshes were created and used to test this conversion, from as few as 3.5 M elements to as many as 24 M elements. Coarser meshes often ran faster, but sometimes had convergence issues related to representing steep pressure and saturation gradients around the disposal drifts. Coarser meshes also allowed simulations to be tested and debugged on a workstation, while the larger simulations required more memory than is available on a single workstation (e.g., more than 500 GB, depending on the number of variables per element), and could only be run on an institutional cluster.

A computational mesh was settled on with 13.8 M elements that included a refined EDZ region surrounding the drifts and shafts that was not prohibitively large to simulate with PFLOTRAN using available institutional computer resources at Sandia National Laboratories. Larger meshes are possible, but they require the use of a large number of cluster nodes, leading to long waits in the cluster management queue, and they can be difficult to load and visualize results (i.e., output files are several hundreds of GB in size). The final mesh included 13,786,080 hexahedra (i.e., 8 corners per element – a 2D quadrilateral extruded perpendicularly in the third dimension) and 336 wedge (i.e., 6 corners per element – a 2D triangle extruded perpendicularly in the third dimension) elements. Using 100 computational nodes (each node has 18 processors, resulting in 1,800 processors total), the simulations presented here required at least one week of time each (simulated in 36-hour chunks, as this is the maximum wall-clock for individual jobs on the cluster). The 197 defined regions were used to specify geologic layers, repository components, shaft components, the EDZ surrounding drifts and shafts, and specify the individual disposal drifts

The domain spans $0 \leq x \leq 3918$ m, $0 \leq y \leq 5922$ m, and -3090 m $\leq z \leq 0$; the domain is a 71 km^3-rectangular prism with the repository located at a depth of approximately 816 to 820 m (with the EDZ extending above and below these depths). The mesh follows the stratigraphy of the salt pillow, but is finest vertically near the repository depth, and is coarser going away from the repository, especially below the repository (Figure 22.-18).

In map view, the mesh is much more refined around the repository elements (i.e., disposal drifts, access drifts, sealing drifts, and shafts – Figure 22.-19), representing each drift and its surrounding EDZ with several elements (Figure 22.-20). The refined area associated with the repository exists at each vertical "layer" of the model, even the top and bottom of the domain, far away vertically from the repository level. This type of mesh was the most straightforward to create, but is not the most economical in terms of the number of elements. It was decided this was a good compromise for the current application.

This "flexed hexahedral" mesh was used because it allowed direct comparison between the FLAC3D (finite difference) and PFLOTRAN (finite volume) results, but other mesh types may result in more accurate thermal-hydrological-chemical flow simulations in PFLOTRAN. The most accurate PFLOTRAN meshes require the faces between elements be perpendicular to a line connecting the centers of the elements (i.e., a Voronoi partition). This ideal convention is violated in some areas, most notably at the transitions from fine to coarse mesh (e.g., see bottom subplot of Figure 22.-20). The choice to keep the same xy-discretization at each level helped to reduce errors that would otherwise have been associated with coarsening and deforming the mesh vertically as well as horizontally. This potential loss of accuracy was seen as not too significant a source of error at this point in the development, where the illustration of new capabilities is the main goal. Future efforts may use unstructured Voronoi computational meshes (e.g., those made by VoroCrust) or uniform structured meshes (a very specific type of Voronoi mesh) to improve this (LaForce et al., 2023a,b), but would require either converting between the PFLOTRAN and FLAC3D meshes, or require creating a mesh that FLAC3D could use (i.e., a conversion from PFLOTRAN to FLAC3D).

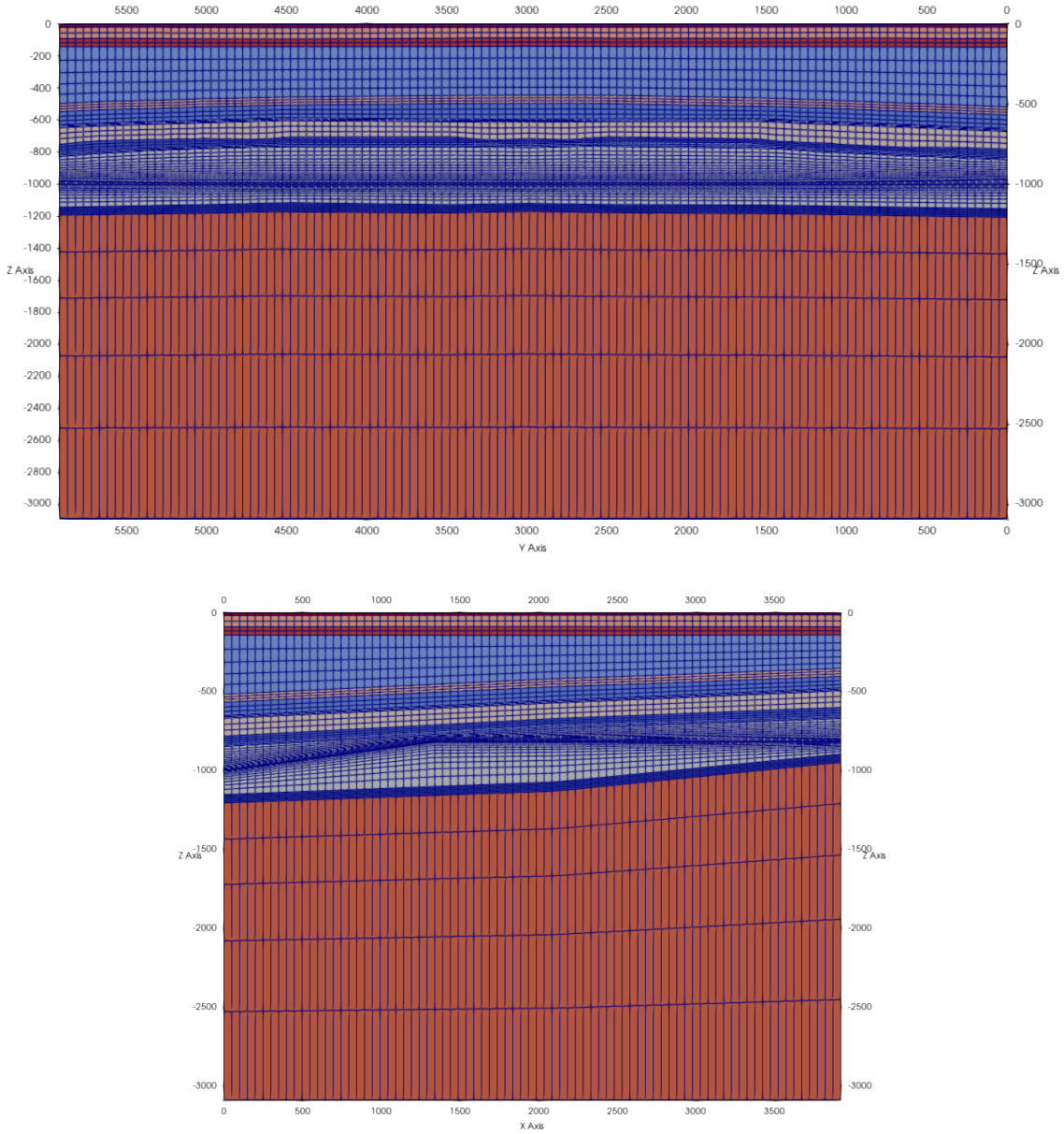

Figure 22.-18: Side views (YZ–top and XZ–bottom) of domain colored by material ID.

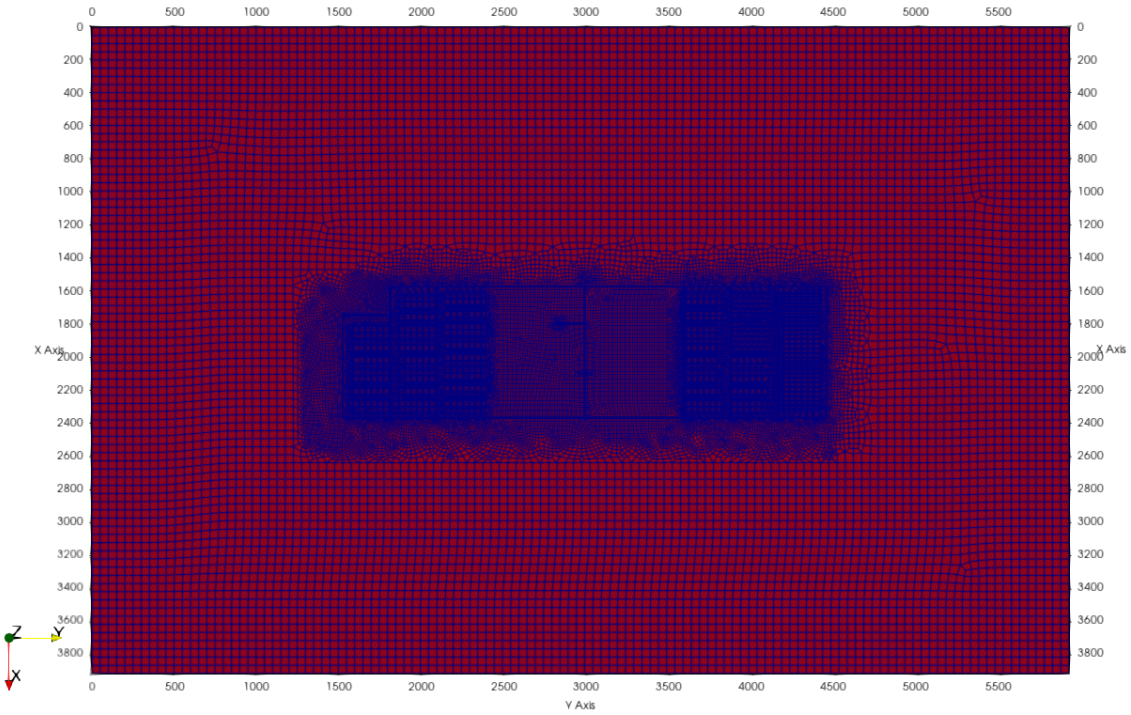

Figure 22.-19: Top view (XY) of domain colored by material ID.

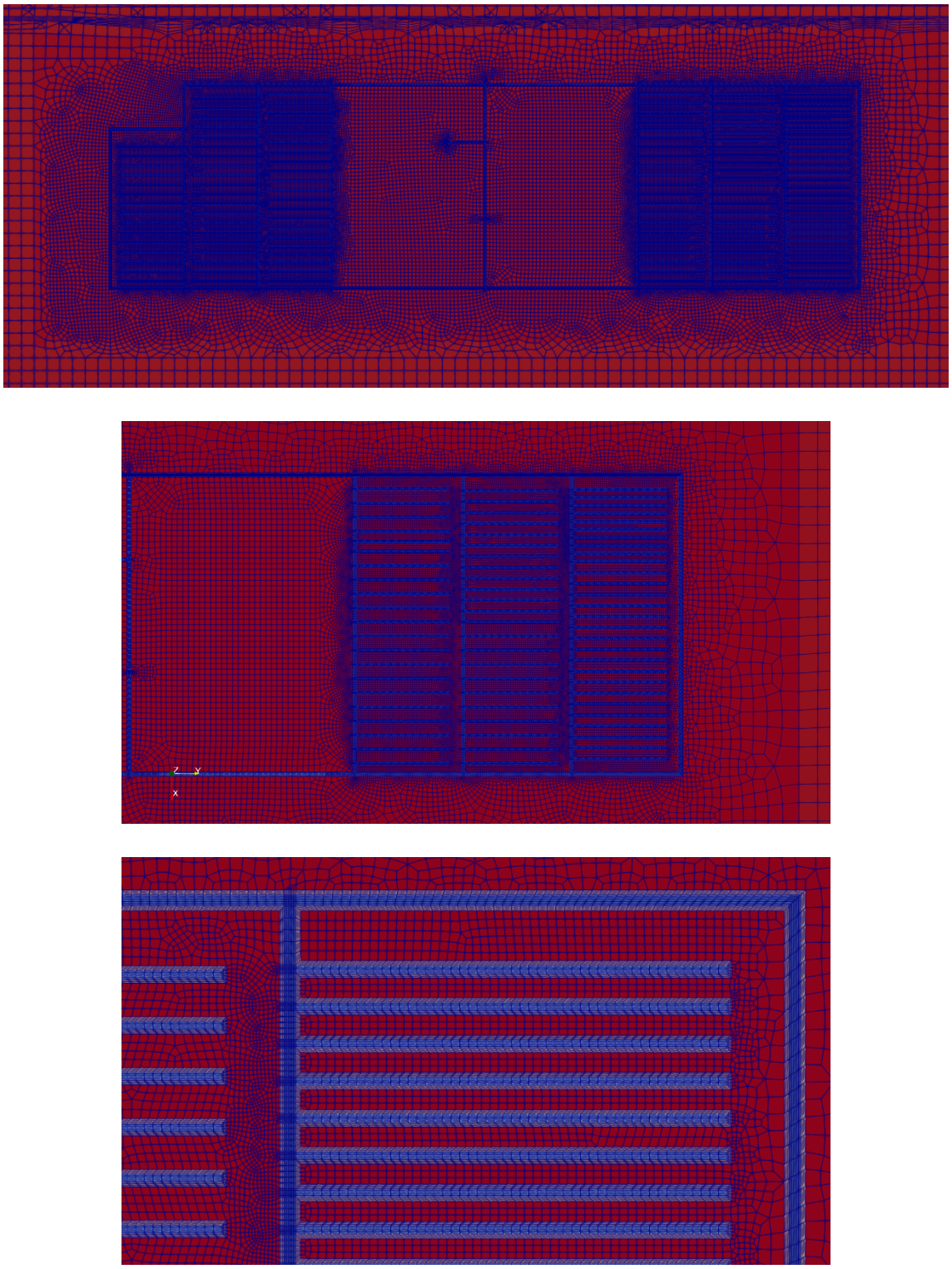

Figure 22.-20: Map views (XY) slicing through the repository elevation (z = −817 m) colored by material ID. Top view shows entire repository footprint, middle view shows half repository footprint, bottom view shows mesh refinement around disposal drifts and their EDZ.

22.3.2 Material properties

The region IDs from FLAC were modified when importing into PFLOTRAN. IDs had offsets added to them, based on the material's group identity. Geologic layers were incremented by 300 (Figure 22.-21 (top)), EDZ regions were incremented by 200, shaft materials were incremented by 100, while disposal drifts and access drifts at the repository level were left with their imported ID.

Portions of the shaft do not include an EDZ surrounding them, as is evident in the bottom two sub-panels of Figure 22.-21. The extent of the EDZ is clearer in both map (XY) and cross-section (XZ) extent in Figure 22.-22.

The main thermal and hydrologic properties were assigned to geologic units and repository-related units. Rows in the bottom section of Table 22.-3 map onto more than one material region. The disposal drifts and the seals were filled with the crushed salt material (even before the heating and drift closure were turned on during staged emplacement).

The equations of state for the halite-saturated brine liquid phase were used, as presented in section 15.1.1. This made the salinity a function of temperature, assuming the water is a saturated brine. The salinity, pressure, and temperature controls the liquid-phase density, viscosity, vapor pressure (i.e., boiling point), and enthalpy. These were implemented for a pure sodium-chloride brine system that is equilibrium with halite. In reality, there are also other accessory evaporite minerals in the system, but halite is clearly the dominant one. The brine was also assumed to be in equilibrium with halite, essentially setting the kinetic rate of halite dissolution and precipitation to be infinitely large (the dissolution rate of halite is many orders of magnitude higher than the dissolution rate for silicate rocks – (Alkattan et al., 1997)). This is not a bad simplifying assumption over long time-scale simulations, but may not be accurate over very short time scales with very large, rapid changes.

Table 22.-3: Thermal hydrological material properties assigned to geologic layers (top) and material groups (bottom). Thermal conductivity of NA2, EDZ, and crushed salt materials were assigned temperature-dependent functions (see equation numbers). Asterisk indicates initial porosity; this was changed, altering the thermal conductivity and permeability ($k = n^4$). Low permeability values were assumed for impermeable salt layers to limit advective transport using Darcy law.

Material	Therm. Cond. (λ) [$W/(m \cdot K)$]	Heat Cap. (ρc_p) [$MJ/(m^3 \cdot K)$]	Porosity (n) [$-$]	Perm. (k) [m^2]
A2C2	4.2	2.32	0.01	$1.0 \cdot 10^{-20}$
A3	4.2	2.32	0.01	$4.24 \cdot 10^{-19}$
AM3	5.0	1.96	0.01	$1.0 \cdot 10^{-20}$
BunterSS	2.6	1.90	0.15	$1.0 \cdot 10^{-18}$
K2	1.5	2.57	0.0002	$1.0 \cdot 10^{-19}$
K3	1.5	1.67	0.0002	$1.0 \cdot 10^{-22}$
NA2	(Eq. 19)	1.90	0.0002	$1.0 \cdot 10^{-20}$
NA3	5.2	1.86	0.0002	$1.0 \cdot 10^{-20}$
NA4	5.2	1.92	0.0002	$1.0 \cdot 10^{-25}$
Quat	2.3	1.90	0.25	$1.0 \cdot 10^{-15}$
Red	2.7	1.90	0.01	$1.0 \cdot 10^{-21}$
Tert	2.1	1.90	0.25	$3.2 \cdot 10^{-15}$
EDZ	(Eq. 19)	2.1	0.05	$3.2 \cdot 10^{-16}$
Gravels	3.0	2.30	0.25	$1.0 \cdot 10^{-18}$
Drifts	3.0	2.30	0.05	$1.0 \cdot 10^{-16}$
Drift Seals	3.0	2.30	0.01	$3.0 \cdot 10^{-19}$
Shafts	3.0	2.30	0.01	$1.0 \cdot 10^{-20}$
Crushed Salt	(Eq. 20)	1.02	0.35*	$8.8 \cdot 10^{-15}$

Table 22.-4: Capillary pressure curve functions assigned to materials.

Material	vG alpha [$1/Pa$]	vG m [$-$]	Liq. Res. [$-$]	Gas Res. [$-$]	Max p_c [Pa]
All other materials	10^{-5}	0.6	0.1	0.001	10^9
Crushed salt	10^{-4}	0.6	0.1	0.001	10^6

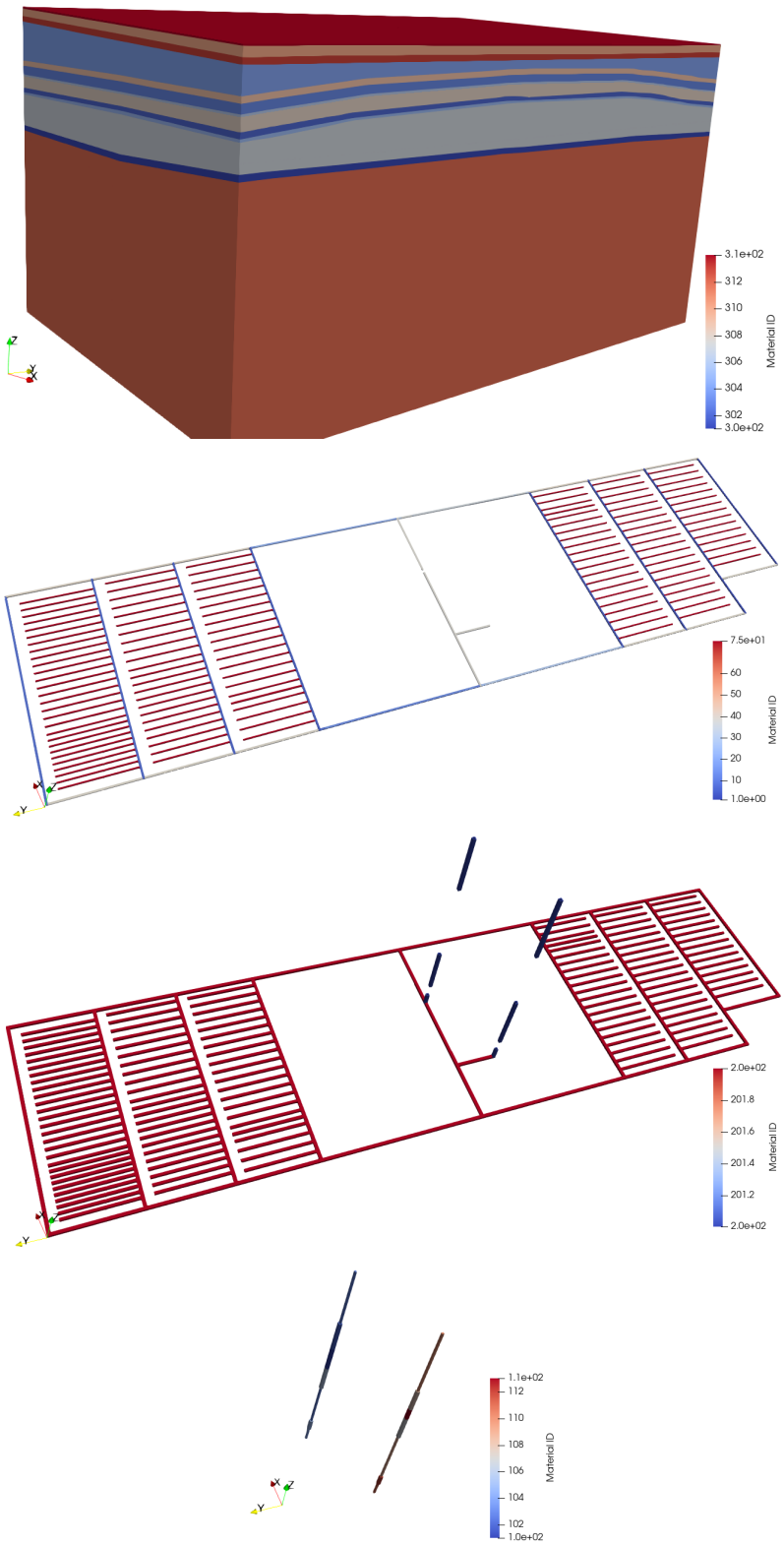

Figure 22.-21: Domain view colored by material ids for geological units on domain outer surface (top – materials 300–314). Material ids shown in oblique view (with geologic materials removed) for drifts (top middle – materials 1–75), EDZ (bottom middle – materials 201 & 202), and shafts (bottom – materials 101–113).

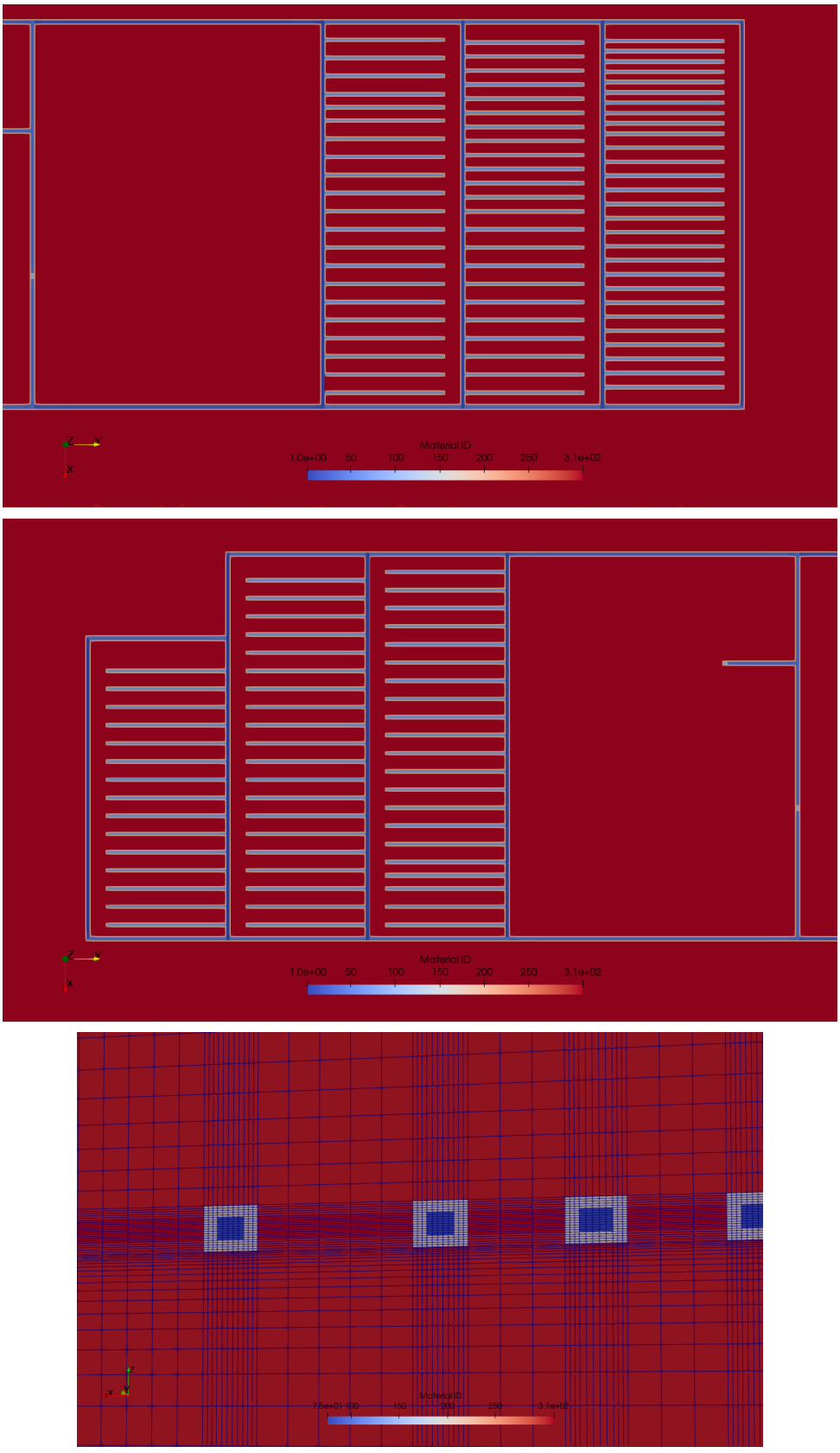

Figure 22.-22: Map view (XY) of material ids associated repository halves (top panels) and vertical cross-section (XZ) of mesh through disposal drift showing surrounding EDZ (bottom).

22.3.3 Initial and boundary conditions

The geologic layers away from the repository were given a fully liquid-saturated initial condition. Drift and shaft materials were assigned an initial liquid saturation of 2%. The EDZ was assigned an initial liquid saturation of 15%.

The liquid pressure and temperature were specified with linearly variable vertical profiles across the domain. The hydrostatic gradient liquid pressure profile had a slope of 10 MPa/km, starting from 0.102 MPa at z = 0, resulting in a liquid pressure of 31.02 MPa at z = -3091 m. This gradient was assumed also in the salt layers although salt is impermeable and dry. This assumption was necessary to model salt as porous medium in the context of Darcy simulations in PFLOTRAN. As the permeability assumed for these layers is low enough, only negligible advective transport is expected. The geothermal gradient had a slope of 30 K/km, starting from 9℃ at z = 0, resulting in a temperature of 101.8℃ at z = -3091 m. These were computed externally and specified as gridded datasets in PFLOTRAN.

22.3.4 Energy, solid, and gas sources

The energy sources were converted directly from the input files used in FLAC3D input, and were specified previously (section 16.). Heat sources were specified by a power level for all the waste packages associated with a drift through time, the timing of when the heat source started, and the physical extent of the source (specified in the region definitions). Not all disposal drifts had heat sources associated with them (e.g., some low-level waste disposal drifts had no heat-generating waste). The heat source magnitude decayed as a sum of several exponentials, which were specified out beyond the end of the simulation (Figure 22.-23).

Solid salt was injected into the crushed salt that filled the heated drifts and drift seals to account for the effect of convergence of the rock and subsequent compaction of the crushed salt. The rate of injection was computed to reduce the porosity from a high initial value (35%) to a low value (2%) 100 years after emplacement (the beginning of which was staged over 30 years).

Gas sources were injected into unheated disposal drifts at rates proportional to the surface area of the waste and an expected corrosion rate, depending on the type of waste packages emplaced. Assuming a minimum corrosion rate of 4.0×10^{-8} m/yr and a maximum corrosion rate of 1.5×10^{-5} m/yr for waste packages associated with non-zero water content, the hydrogen gas generation rate are given in Table 22.-5 are computed from the following assumed reaction for iron corrosion

$$3Fe_{(s)} + 4H_2O \leftrightarrow \left(Fe_2^{3+}\ Fe^{2+}\right) O_4 + 4H_{2(g)}. \tag{21}$$

If the water used in this chemical reaction was solely in the vapor phase, there would be no change in pressure, since 4 moles of gas would exist on both sides of the equation. Converting liquid H_2O to H_2 gas would result in an increase in pressure associated with the much larger molar volume of hydrogen, compared to liquid water.

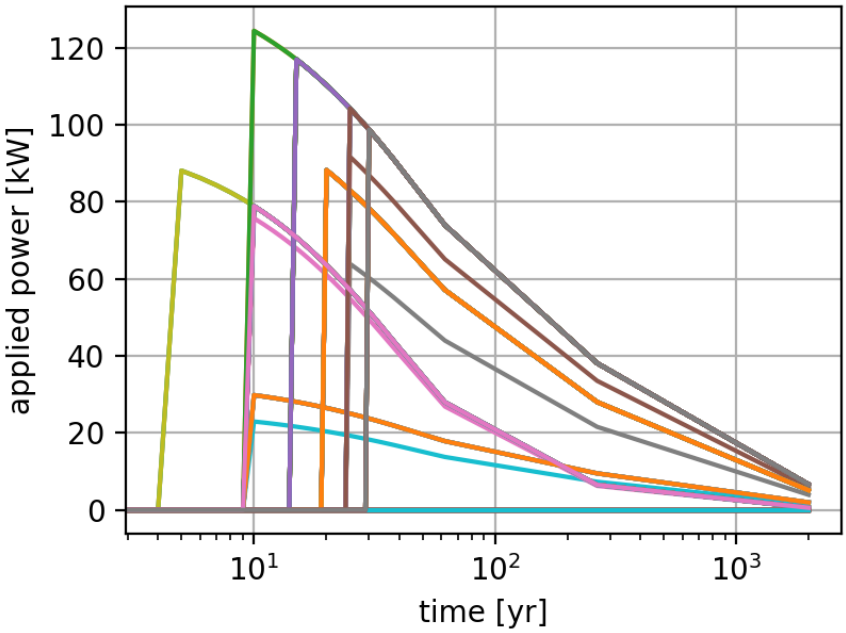

Figure 22.-23: Total power applied to individual waste disposal drifts through time, showing the staggered emplacement of waste at six different times, with several different heat load profiles (including some with no applied power).

Table 22.-5: Per waste package corrosion-related inputs used to compute gas generation rate.

Container Type	Surface Area [m^2]	Min Gas Gen. Rate [kg H_2/yr]	Max Gas Gen. Rate [kg H_2/yr]
POLLUX	30.9	4.66×10^{-4}	1.75×10^{-1}
CASTOR	44.0	6.65×10^{-4}	2.49×10^{-1}
MOSAIK	16.0	2.41×10^{-4}	9.06×10^{-2}

A set of several cases were investigated with this large mesh:

1. Base case
2. Darcy flow case
3. Higher-permeability seals case
4. Base case with porosity closure case
5. Base case with porosity closure and gas generation case

22.3.5 Case 1: Base

The base case used the material properties as presented in Tables 22.-3 and 22.-4, with non-Darcy flow (i.e., no flow until a threshold gradient is exceeded). No change in porosity was specified for this base case to represent drift closure, therefore the changes in thermal conductivity were only a function of temperature in the crushed salt, EDZ, and NA2 materials. Absolute permeability did not change, but relative permeability was still a function of phase saturation according to the capillary pressure and relative permeability model of van Genuchten (1980) and Mualem (1976), as extended by Parker et al. (1987) to two-phase.

Figure 22.-24 shows the temperature distribution in the repository at the beginning of each emplacement sequence (every 5 years until all waste is emplaced), and the peak of temperatures in the repository between 100 and 1,000 years. By 2,000 years, the repository has begun to cool down significantly.

Figure 22.-25 shows the evolution of the liquid phase flow velocity with time. These velocities are averaged over the entire rock, and do not represent actual pore velocity, which would require dividing by the porosity. After the initial 5 years of hydrologic initialization ($-5 \leq$ yrt $\leq$ 0), there is a narrow halo of non-zero flux around the repository. This only grows a bit during the heating. By 1,000 years the halo has grown significantly, partially due to the decrease in viscosity of the brine with temperature, which depressurizes a larger portion of the salt formation.

Figure 22.-26 shows the evolution of liquid saturation in the repository. The host rock is saturated or almost saturated, while the drifts remain mostly air-filled. By 1,000 years, the EDZ surrounding the drifts have desaturated, and the portion of the host rock adjacent to the EDZ (especially between heated drifts) has reduced from full saturation, but only by a small amount.

Figure 22.-28 illustrates that the biggest change in saturation is at late time, when there is a continuous gas phase through much of the disposal area, including the pillars between rooms (this area has a connected gas phase, but is still mostly brine saturated). The dark blue areas (p_{gas} = 0) in these plots are areas where there is only single-phase liquid (i.e., there is no defined gas pressure). PFLOTRAN general mode includes three different states:

1. Single-phase gas (no liquid water, only humidity in air);
2. Single-phase liquid (no air, only dissolved gas in liquid water); and

3. Two-phase flow (air with humidity and dissolved gas in liquid water).

The far-field begins in single-phase liquid state, and only once gas infiltrates these elements do they become two-phase flow elements. The drifts and EDZ begin in two-phase flow mode. The hotter drifts become single-phase gas once the liquid water boils off (Figure 22.-27).

The gas pressure in the drifts is hightest in the hottest disposal drifts, and experiences a maximum of 3.1 bar. This gas pressure is only due to the heating and expanding of the trapped gas in the repository, along with some minor increases of gas pressure due to the flow of the water phase towards the drifts, as there is no closure or gas generation to increase gas pressure.

Figure 22.-29 summarizes the evolution of gas pressure across the 6 disposal fields through time. The line is the average, while the shaded region illustrates the range of pressure observed. The maximum gas pressure is observed just before 200 years in Field 2, while the lowest gas pressure is observed in Field 6 (the first one to be emplaced). A sharp rise in gas pressure is experienced right at emplacement (except in Field 6), and by 1000 years, all the gas pressures are decreasing.

As an indicative proxy for solute transport at early time, the diffusion of dissolved gas in the brine-saturated salt is shown in Figure 22.-30. Gas dissolves into the liquid phase at EDZ and drift–starting even before waste emplacement–and diffuses into the single-phase liquid region under a dissolved gas concentration gradient. Roughly a distance of two drift diameters into the intact salt is still at the initial condition for dissolved gas after 2,000 years. A tortuosity of 1.0 is used in geologic materials, so this represents an upper-bound conservative estimate of diffusive transport of an ideal tracer.

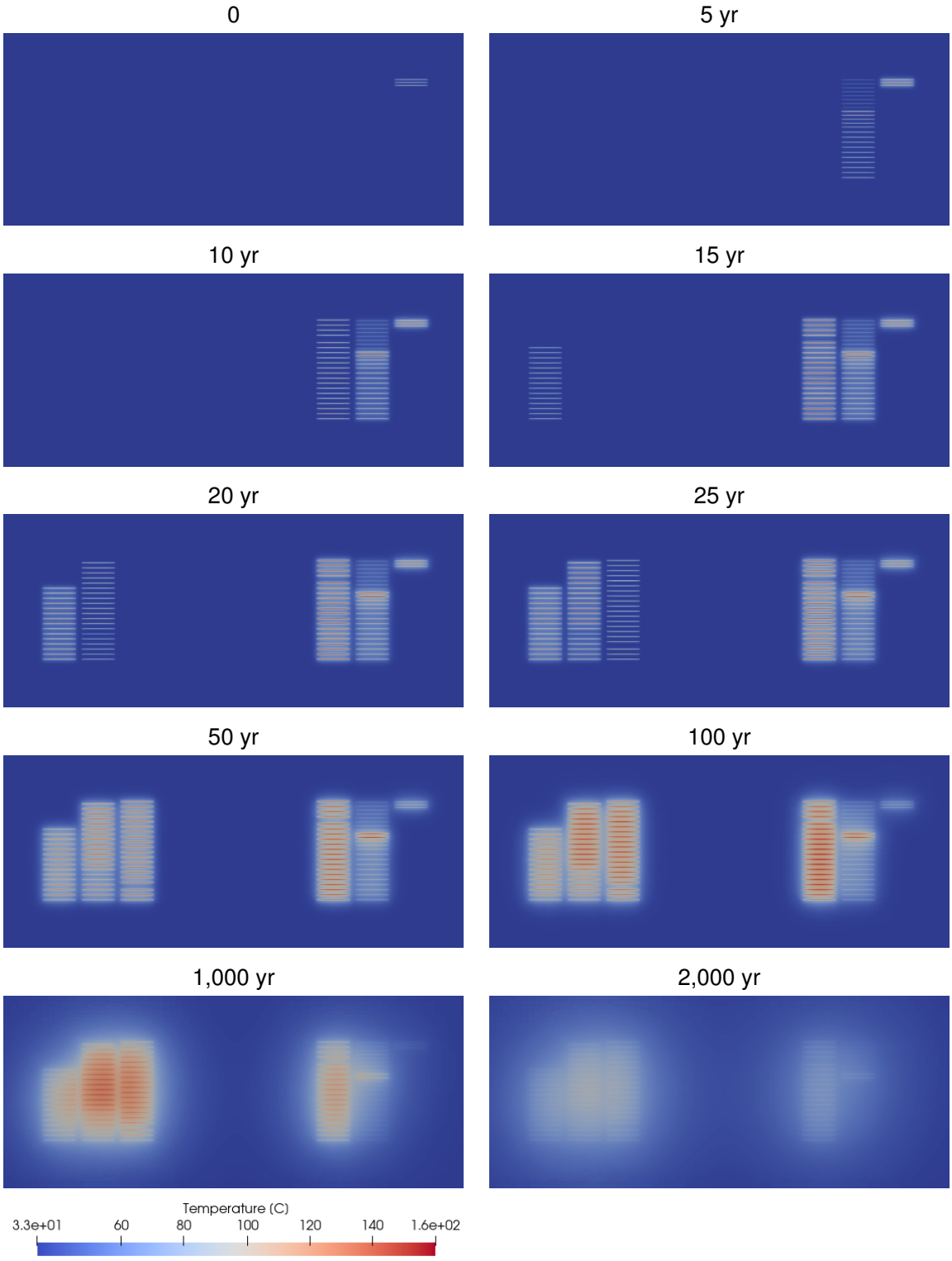

Figure 22.-24: Temperature response in and around repository (horizontal XY slice through repository at z = −817 m), showing staged emplacement of waste.

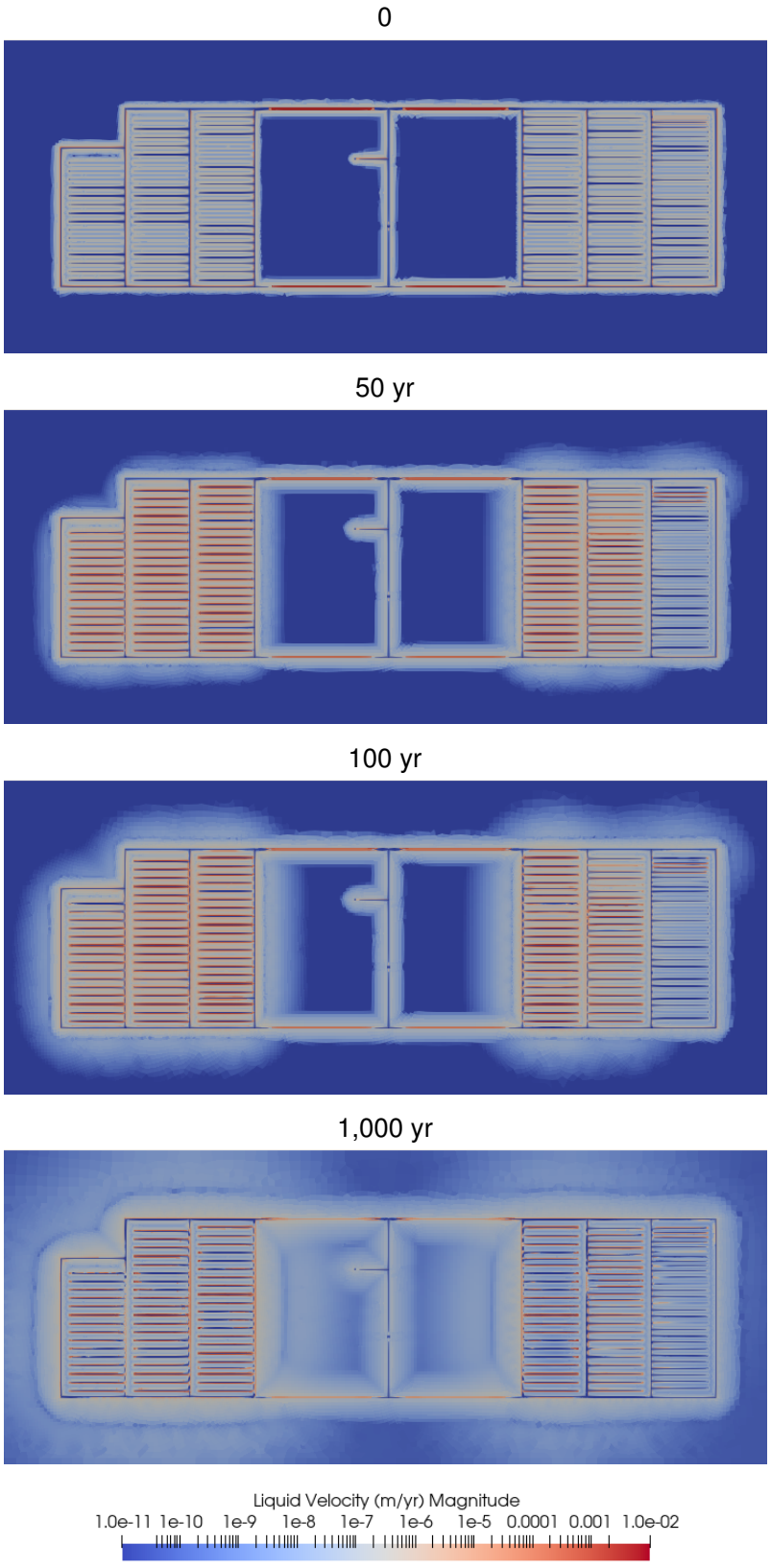

Figure 22.-25: Liquid velocity in and around repository (horizontal XY slice through repository at z = −817 m).

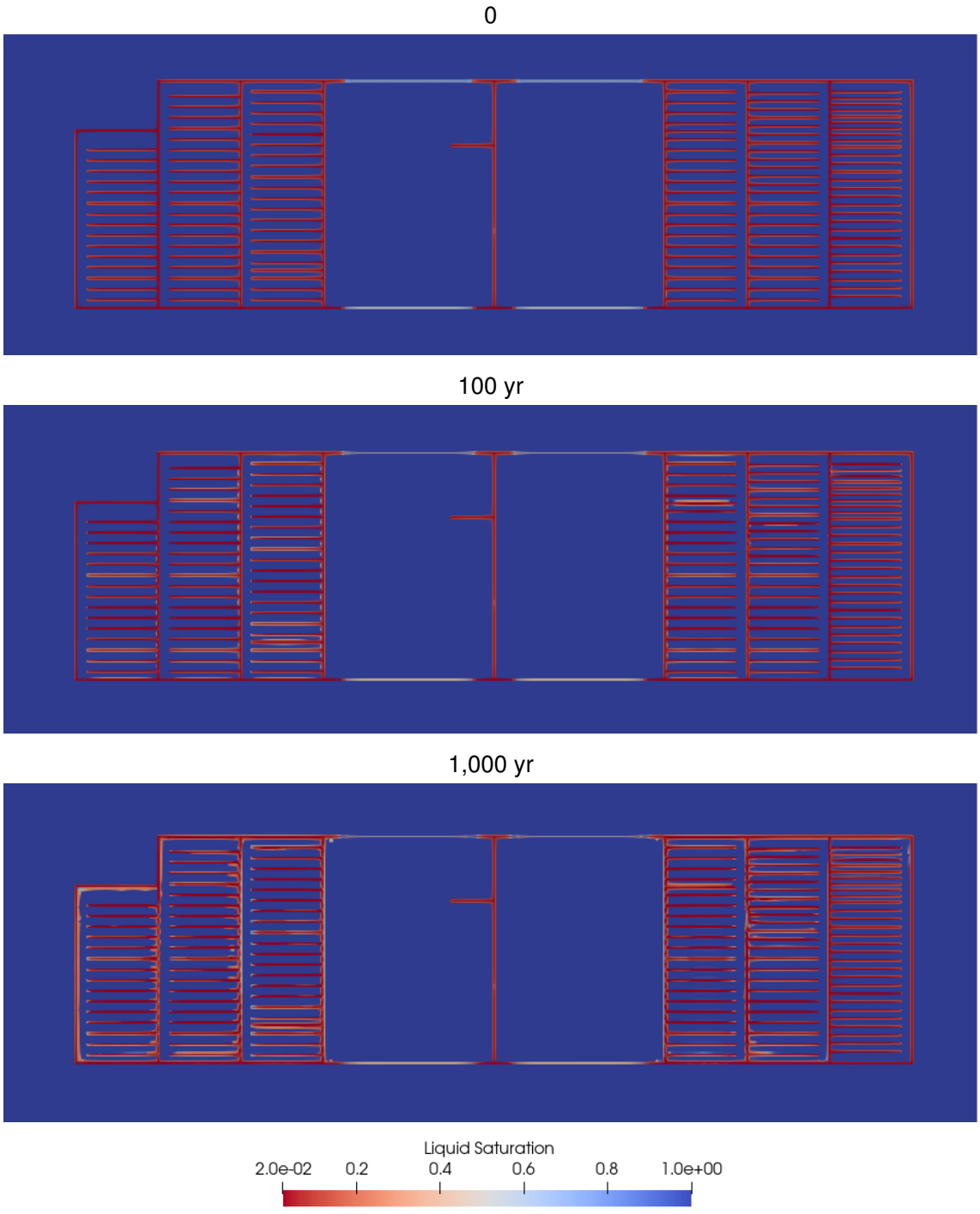

Figure 22.-26: Liquid saturation in and around repository (horizontal XY slice through repository at z = −817 m).

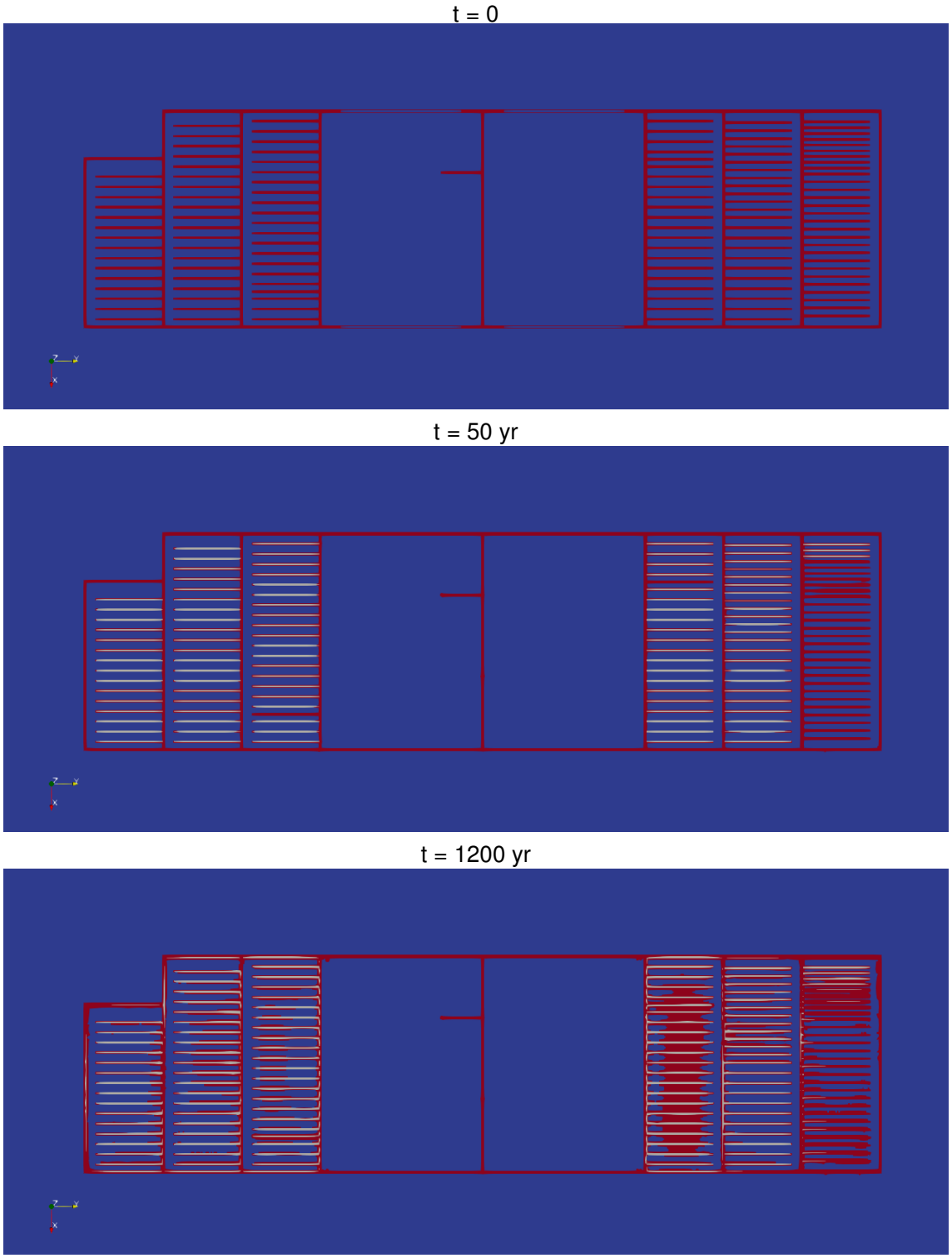

Figure 22.-27: Flow state in and around repository (horizontal XY slice through repository at z = −817 m) at three times t = $\{0, 50, 1200\}$ years; blue is single-phase liquid, white is single-phase gas, and red is two-phase.

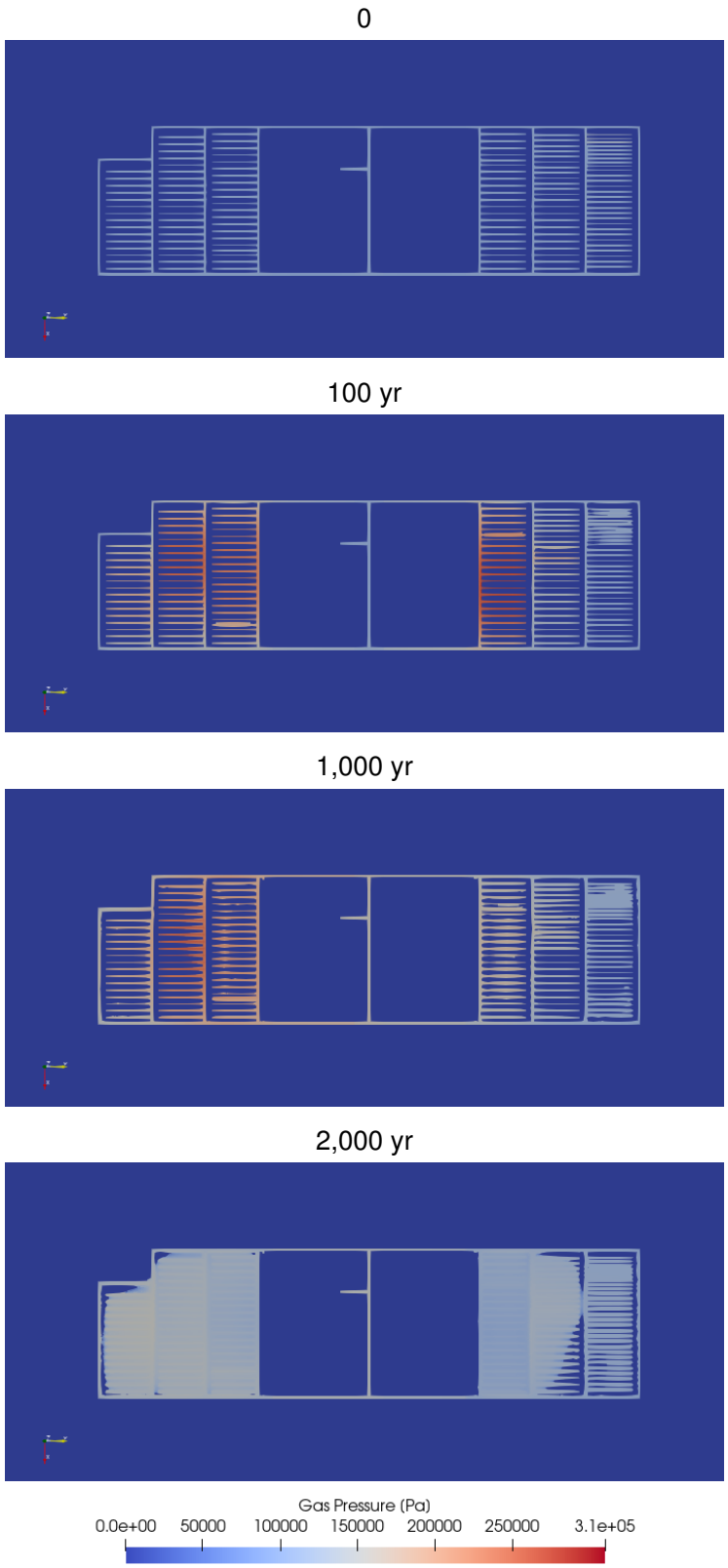

Figure 22.-28: Gas pressure in and around repository (horizontal XY slice through repository at z = −817 m).

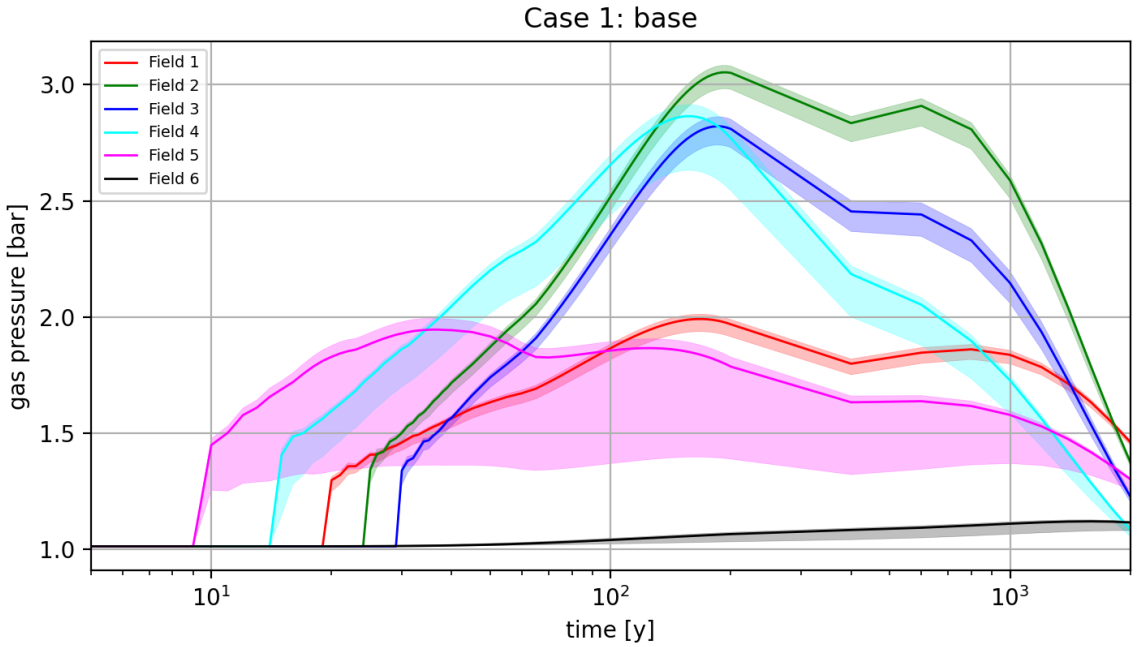

Figure 22.-29: Gas pressure in disposal drifts through time. Lines are mean gas pressure, while shaded regions denote the range observed.

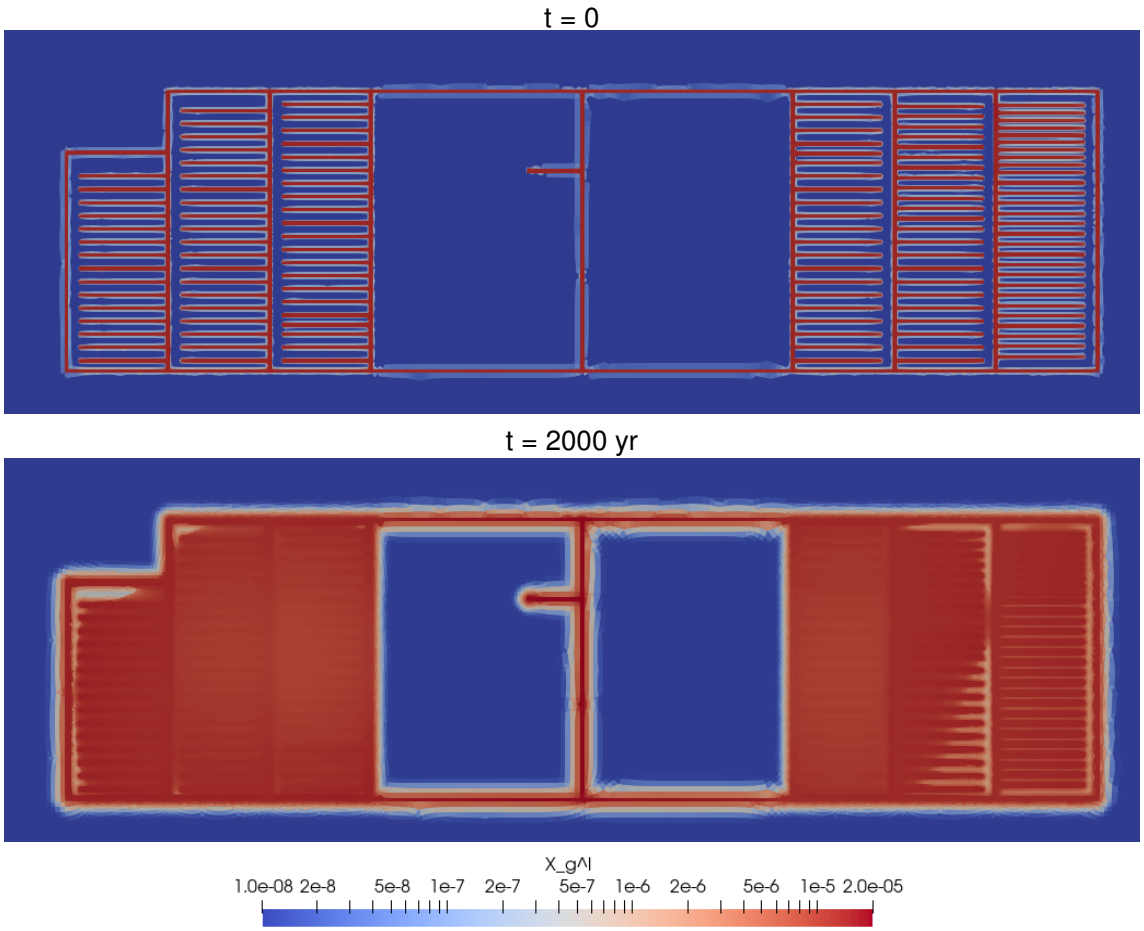

Figure 22.-30: Migration of dissolved gas away from the excavations during the extent of the simulations, showing extent of gas initially (10^{-8} is the initial condition) and after 2,000 years of diffusion (logarithmic concentration scale).

22.3.6 Case 2: Darcy flow

In this case, non-Darcy (i.e., threshold gradient – section 15.1.4) flow was disabled. The predictions in this case are what is considered “default” behavior.

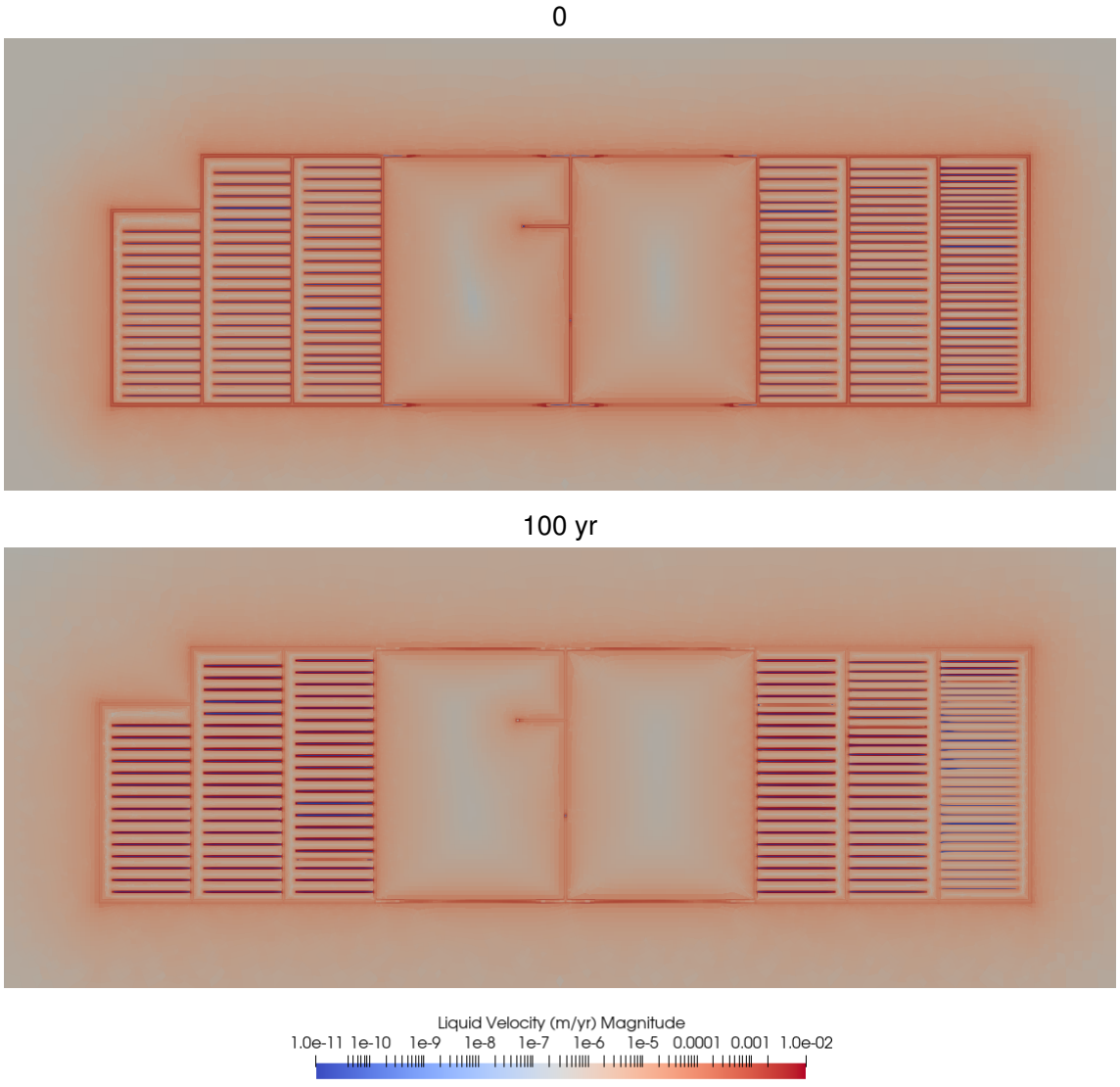

Figure 22.-31: Liquid velocity around repository (horizontal XY slice through repository at z = −817 m) for Darcy flow case.

Even at the end of the initialization period (-5 yr $\leq$ t $\leq$ 0), the flow velocity is non-zero throughout the entire domain. The permeability is very low in the formation, but the pressure gradient is also very high, so the flow is small, but non-zero. At the edge of the domain, the flux is $\approx$ 1 μm/yr for the case with Darcy flow (Figure 22.-31), while when non-Darcy flow is activated (Figure 22.-25), the flow velocity is close to zero ($< 10^{-11}$ m/yr) tens of meters outside the domain soon after excavation, and only at much later time does the increased temperature lead to higher flow velocities associated with surpassing the threshold gradient.

Through a regression Liu et al. (2012) found the threshold gradient could be expressed in terms of the intrinsic permeability, given in Eqn 18, that results in a threshold gradient of

1.6×10^4 (m head)/(m distance).

The non-Darcy flow behavior is well-documented for low-permeability rocks (Liu, 2014), where it is supported by the observation that the effect of the repository should not propagate several km through impermeable rock over short time periods. This implementation of the non-Darcy conceptual model brings together the US approach of modeling all the geologic barrier with a hydrologic model with the German approach, where flow is not calculated in the salt, because it is known to be impermeable to flow.

22.3.7 Case 3: Higher-permeability seals

This case is the base case (i.e., non-Darcy flow), but the MgO seals on the ends of the crushed salt drift seals are 100$\times$ more permeable.

The difference in gas pressure between the two scenarios is small (only visible at late time). This may be due to two factors: 1) the permeability of the EDZ surrounding the seals remained its base case value, and 2) the gas pressures were not high, so the excess gas pressure from heating was able to bleed off easily.

22.3.8 Case 4: Base case with porosity closure

This case is the base case (i.e., non-Darcy flow), with the injection of solid phase to reduce the permeability of the heated emplacement drifts and the drift seals over 100 years. Porosity is specified to change linearly from the initial value (35%) at emplacement to a low value (2%) after 100 years.

As in the simpler meshes (§ 22.2), there is a period at the beginning of heating where the water is driven off from the crushed salt. This water moves away from the heat source as vapor and condenses once the temperature drops below the boiling point, leading to local dissolution. Figure 22.-35 shows how the decrease in porosity associated with the disposal drifts is surrounded above and below by increases in porosity in the EDZ (up to 11% porosity increase). The unheated crushed salt drift seals (seen in the rear of the image) do not have this rind of increased porosity, because they are not heated and do not drive off the initial moisture in the crushed salt.

Changes in porosity and temperature drive the thermal conductivity to change (Figure 22.-36). The intact salt uses the “linear resistivity” model, that is only a function of temperature (hot salt has lower resistivity than cold salt – Figure 22.-2). The crushed salt has a more complex behavior (Figure 22.-3); decreasing porosity has the largest impact on the thermal conductivity, while increased temperature reduces the thermal conductivity at low porosity (near intact), and increased temperature increases the thermal conductivity at high porosity (near starting). The behavior at high porosity accounts for some convection and even radiation that may effectively increase the thermal conductivity, due to the large amount of air-filled space.

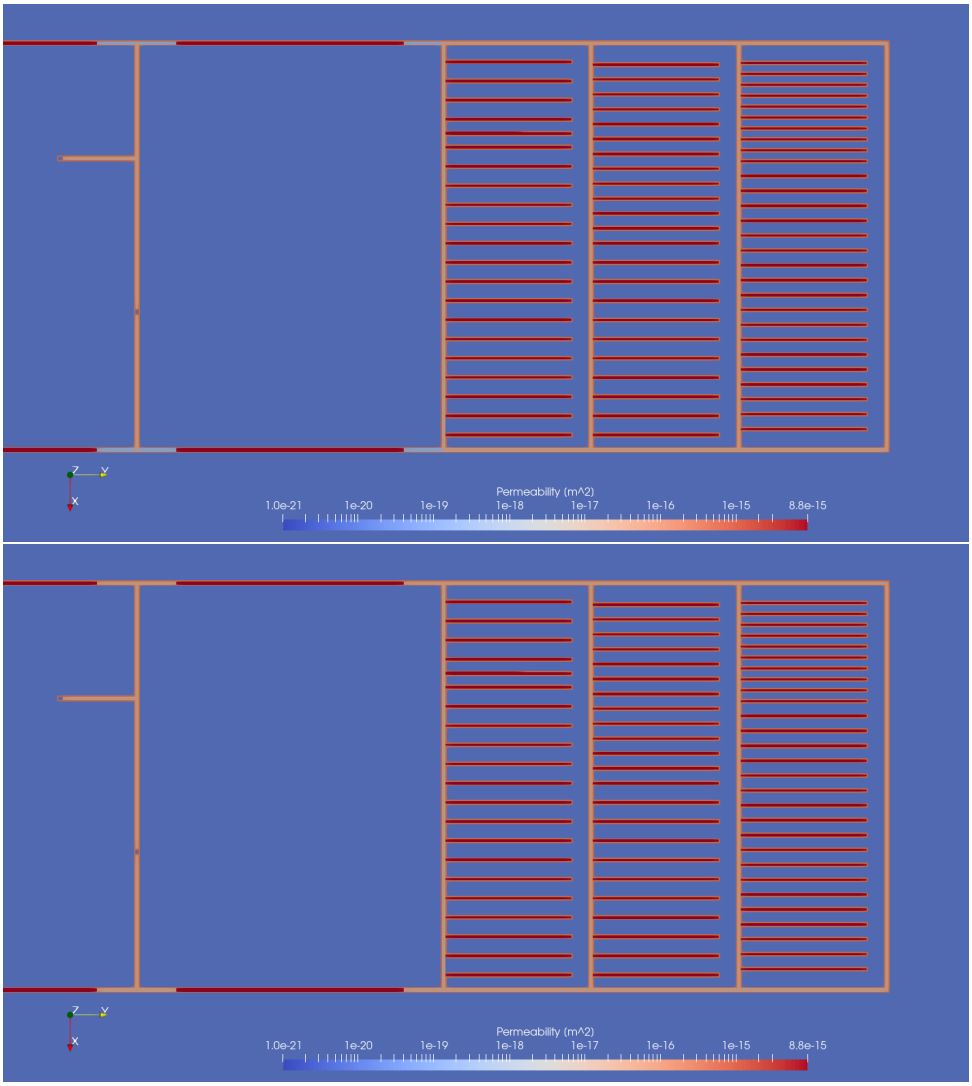

Figure 22.-32: Intrinsic permeability at repository elevation (XY plot at z = −817 m) in case 1 (top) and case 3 (bottom). Note lower permeability for MgO seals at the ends of the crushed salt seals in base case (top).

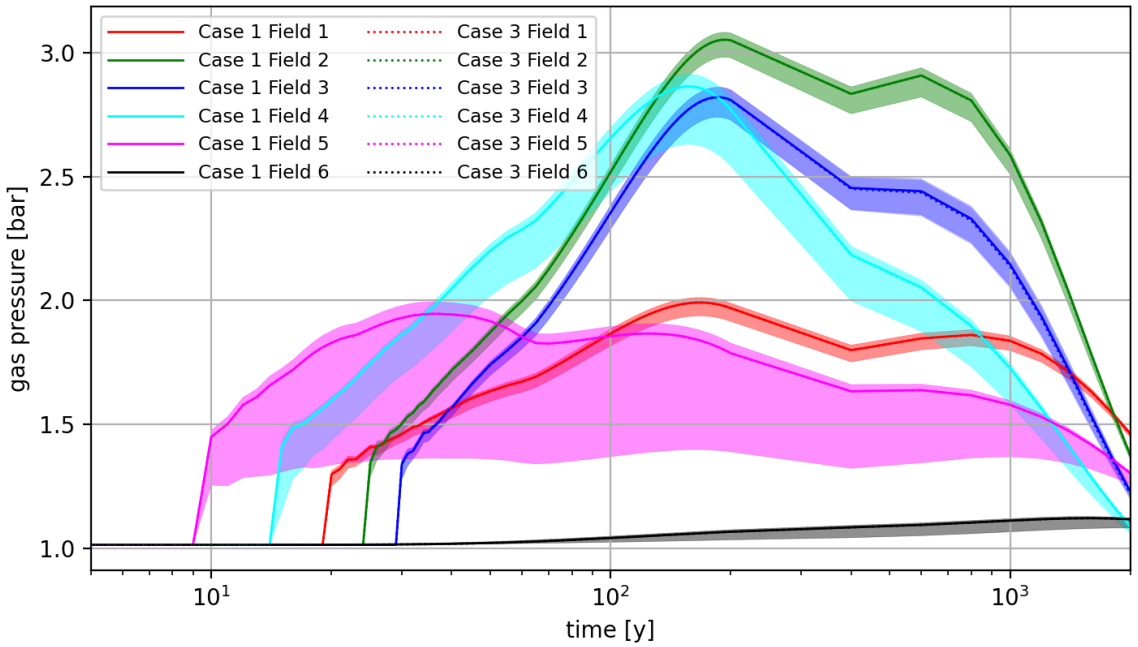

Figure 22.-33: Gas pressure in disposal drifts through time. Lines are mean gas pressure, while shaded regions denote the range observed.

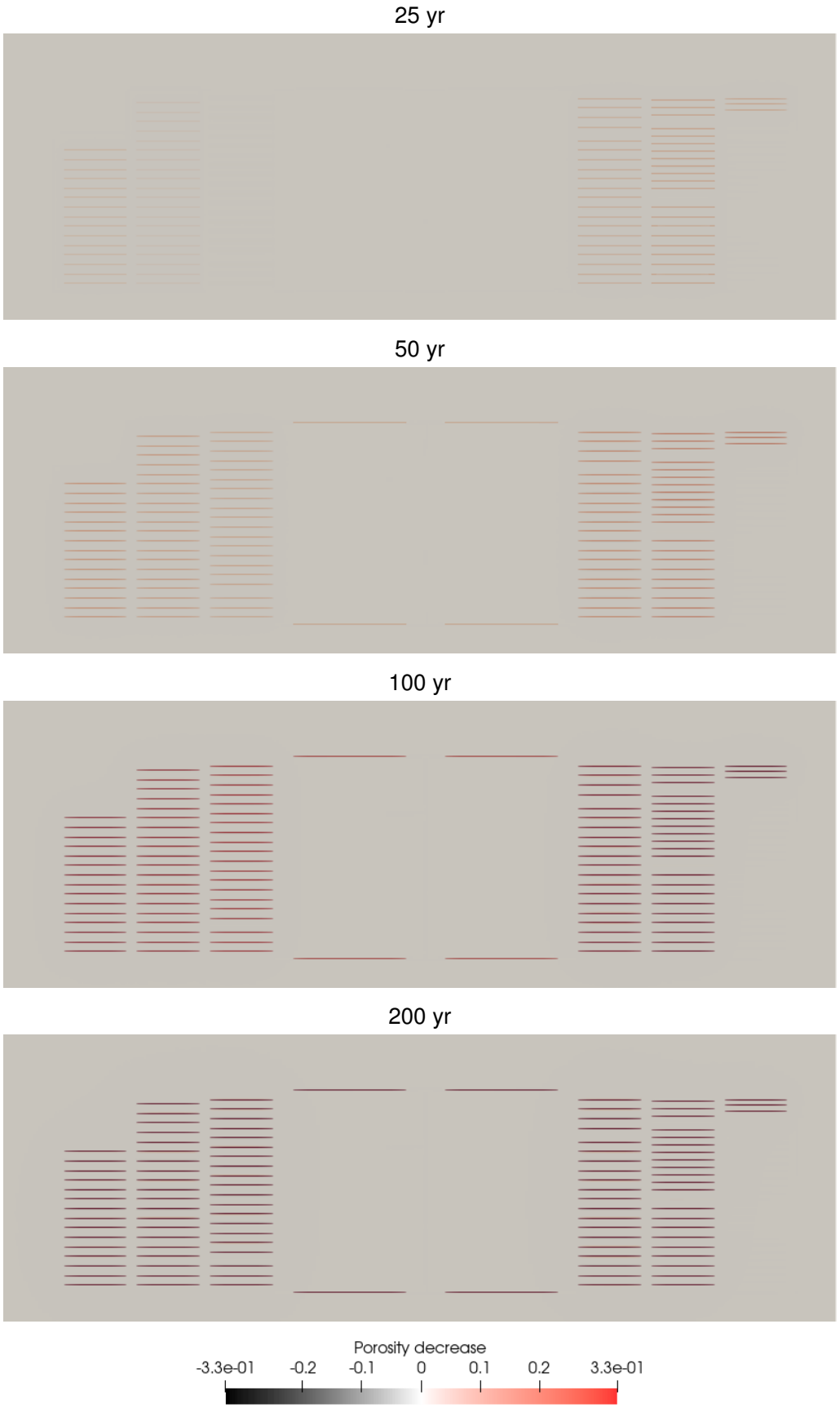

Figure 22.-34: Change in porosity (from initial value) in and around repository (horizontal XY slice through repository at z = −817 m).

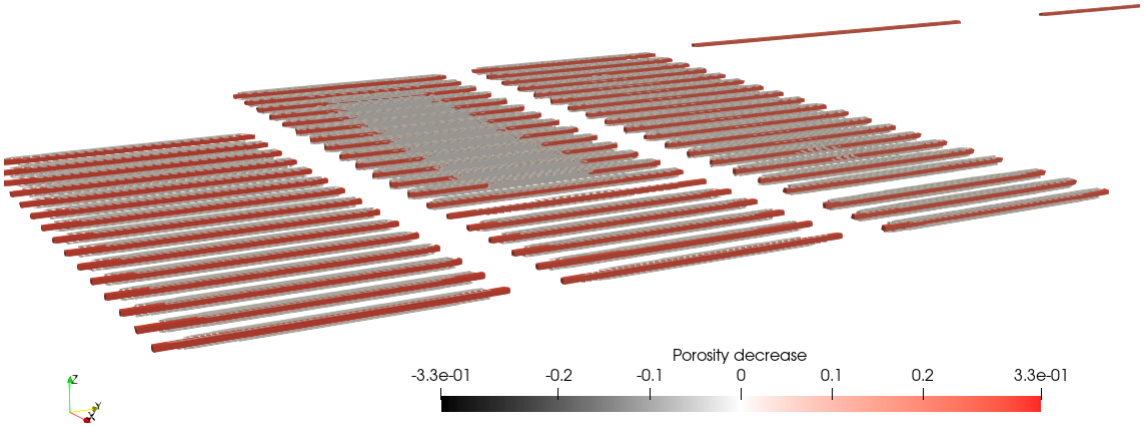

Figure 22.-35: Change in porosity from initial value shown in oblique view near disposal drifts (crushed salt seals seen in background) at 100 years. Small changes ($-0.02 \leq \delta \leq +0.02$) are set to transparent.

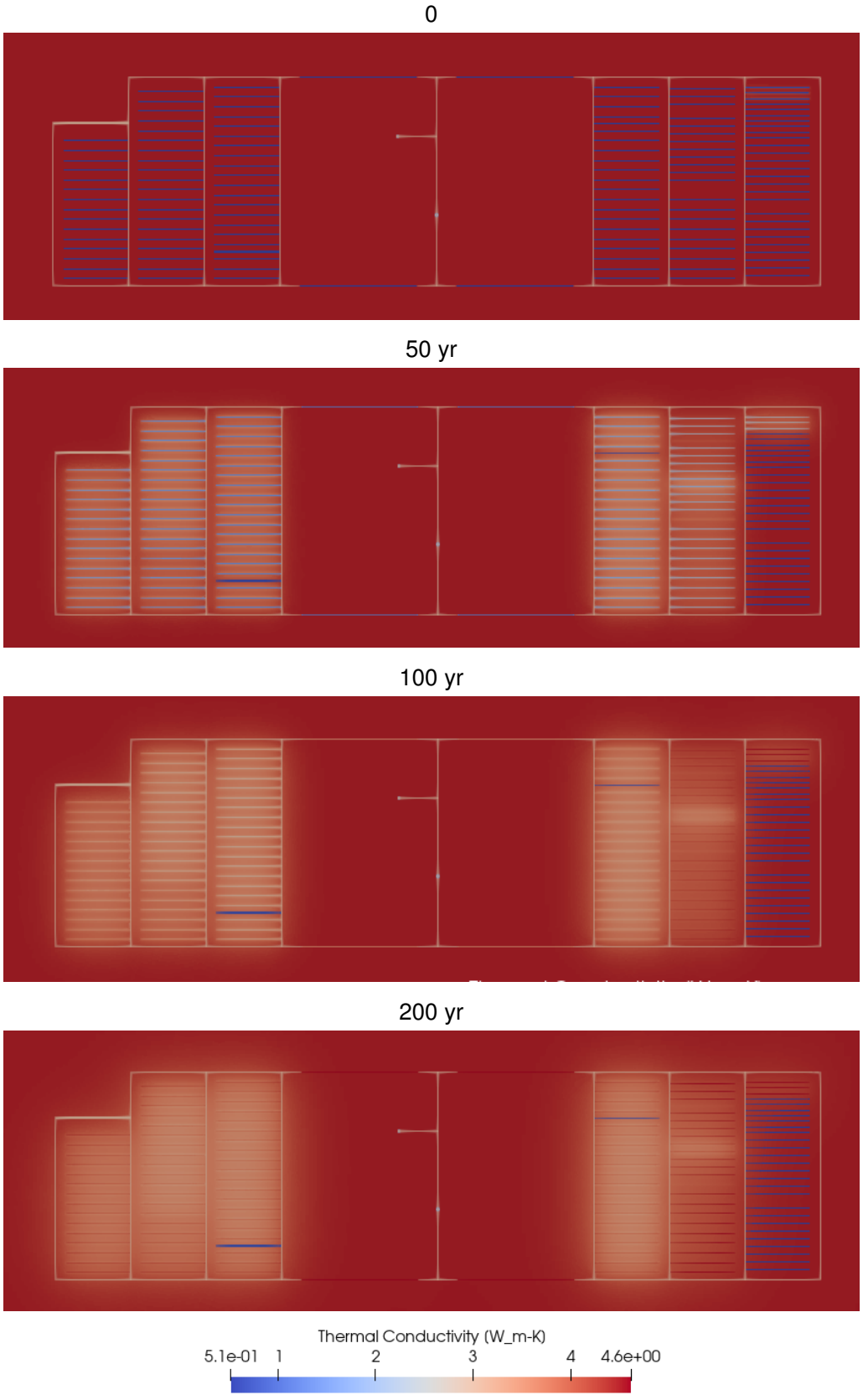

Figure 22.-36: Thermal conductivity in and around repository (horizontal XY slice through repository at z = −817 m) at several times (t = $\{0, 50, 100, 200\}$ yr).

Figure 22.-38 shows the sharp increase in gas pressure associated with the final part of porosity closure (i.e., when porosity is near its minimum), but gas pressure decays quickly after that, and then decays more after 1,000 years. The uncoupled closure of porosity, without consideration of gas pressure is not realistic – porosity closure should slow down as the gas pressure increases, pushing back somewhat on the lithostatic pressure that is driving closure.

Figure 22.-37 shows the distribution of single-phase gas, single-phase liquid, and two-phase states in the model domain is quite similar between the case with closing porosity and the base case (Figure 22.-27). One notable difference is the presence of more two-phase (red) cells near the MgO abutments at the disposal ends of the drift seals. This indicates relatively gas was flowing around the MgO abutments in response to the increase in pressure at the end of compaction, and this switched the intact salt from single-phase liquid (blue) to two-phase (red).

In this simulation, only the heated drifts and the crushed salt seals were closed by injecting solid mass of halite into the pores at the same rate. In reality, the access drifts and the EDZ should close too (albeit at a slower rate than the heated drifts). The definition of the regions (all EDZ elements were a single zone) and the current implementation in PFLOTRAN made it difficult to close the porosity of the EDZ in a physically realistic manner. The current porosity closure mechanism is specified in the input file (i.e., before the simulation begins). In future efforts, the injection of solid mass would incorporate feedback from the simulation. Closure could be a function of the temperature (faster closure under hotter conditions) and liquid pressure (high back pressure of gas or brine would reduce the closure rate). Both of these approaches would be more physically realistic and should improve some of the model convergence issues that happened during some porosity closure simulations (the model would resort to very small time steps when pressures would increase rapidly).

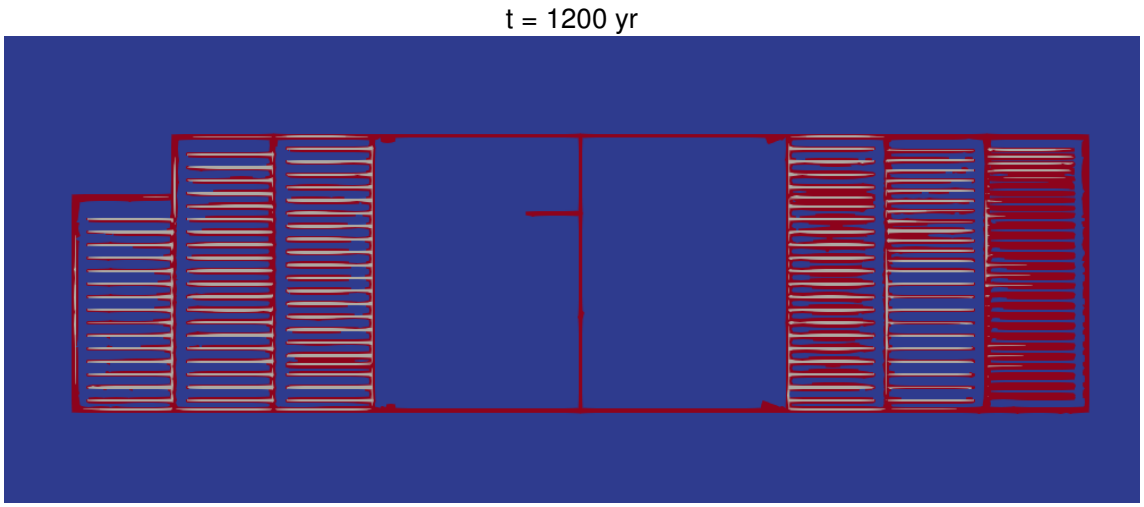

Figure 22.-37: Flow state in and around repository (horizontal XY slice through repository at z = −817 m) at t = 1200 years for porosity change case; blue is single-phase liquid, white is single-phase gas, and red is two-phase.

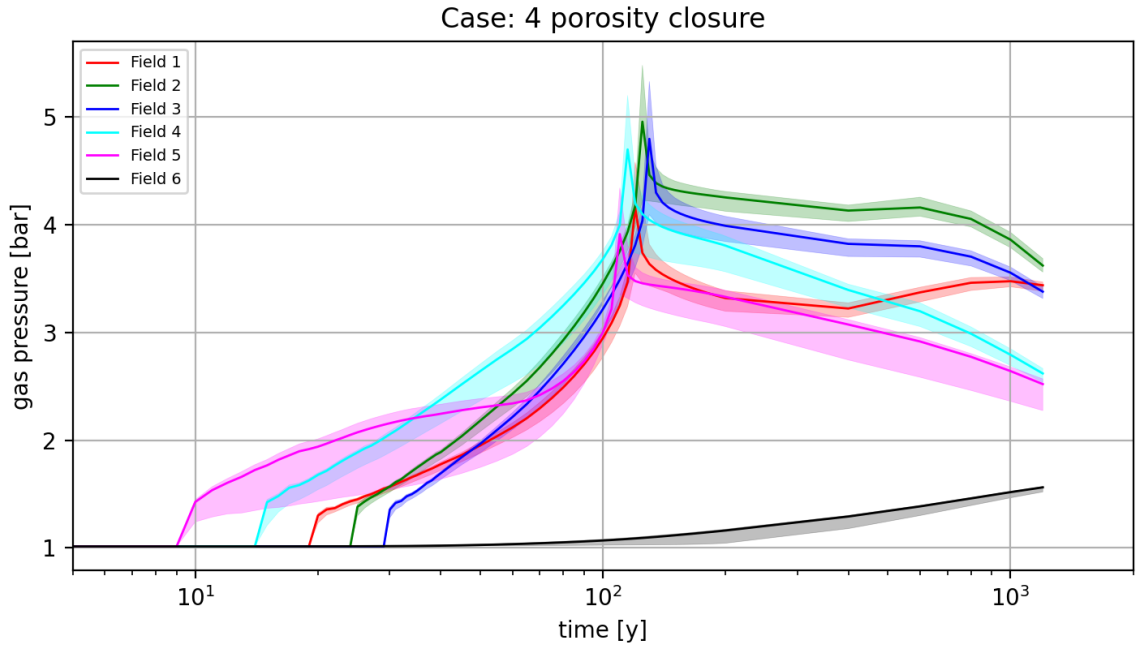

Figure 22.-38: Gas pressure in disposal drifts through time for closing porosity case. Lines are mean gas pressure, while shaded regions denote the range observed.

22.3.9 Case 5: Porosity closure case with gas generation

Gas generation is added to the unheated disposal drifts because the heated drifts are essentially dry and would not produce significant gas generation (which requires free liquid water). The effects of gas generation are minimal (the lines in Figure 22.-39 are indistinguishable), since the gas generation is assigned to single drifts in Fields 3 and 4, and most of Field 6 (clearly visible as blue in thermal conductivity plots in Figure 22.-36).

It is clear that the effects of gas generation, as specified, were insignificant compared to the effects of drift closure, which agrees with intuition. More extreme gas generation rates can be tested in future simulations, or the effects of the EDZ could be reduced, to decrease the redistribution of gas during the simulations.

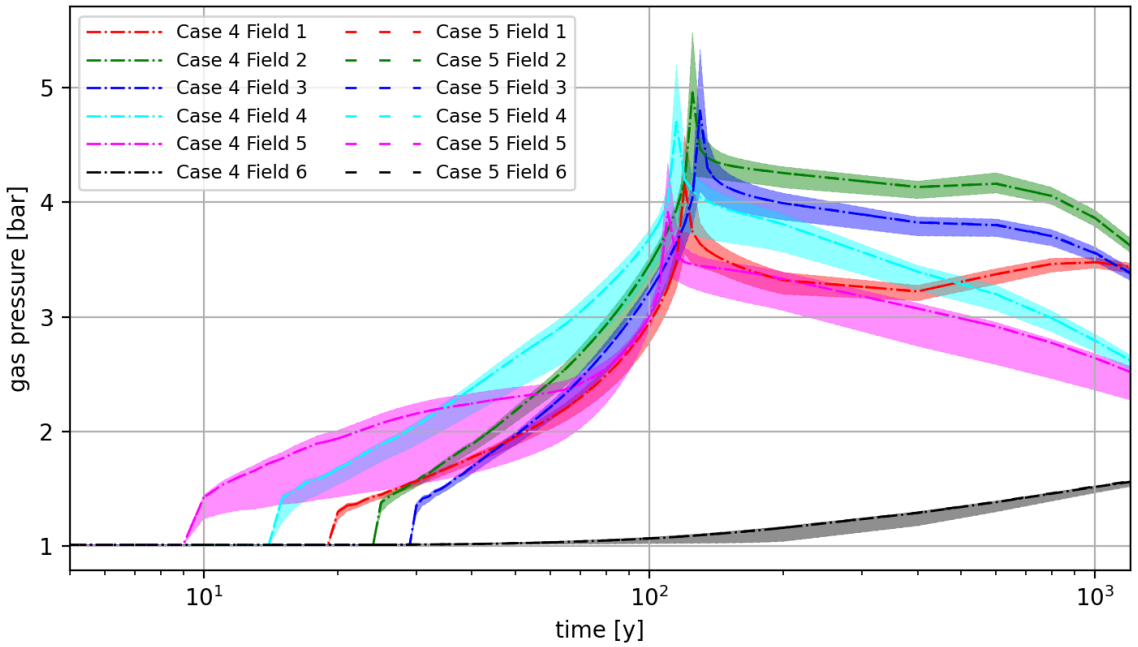

Figure 22.-39: Gas pressure in disposal drifts through time for closing porosity case and gas generation in unheated drifts. Lines are mean gas pressure, while shaded regions denote the range observed.

23. Effect of gas pressure build up on the EBS performance

The compaction of crushed salt used as backfill and long term seal in salt repositories depends primarily on the creep behavior of the salt host rock and the heat input in the repository. Due to heat, the creep behavior of the rock is accelerated as well as the compaction behaviour. However, the hydrologic and geochemical processes taking in place in the repository may affect the repository closure and thus the compaction of crushed salt. This is because the equilibrium state is a result of the concurrent processes of salt creep and fluid flow and the interaction between them (Freeze, 1996).

First analysis regarding the effect of fluid pressure in a salt repository was carried out in the scope of the WIPP Performance Assessment for disposal room closure, they were not backfilled with crushed salt (Stone et al., 1985; Stone, 1995). Due to the complexity of coupling the mechanical creep process of salt and its interaction with multiphase fluid flow, an approximate approach was followed. This approach consists of repository porosity functions that were computed in room closure simulations as function of gas generation. In these FE-simulations, the resistance to closure was provided by pressure produced by waste generated gas computed from the ideal gas law. The repository closure was driven by salt creep and waste and backfilled consolidation taken into account through different constitutive models. Stone (1995) used this approach to analyze the closure of a single perfectly sealed disposal room filled with waste and backfill under five different gas-generation rate histories. The five rate histories were generated by multiplying a defined gas generation curve by a factor f ranged from 0.0 to 1.0. At f = 0.0 no gas is generated. At f = 1.0 a total of 1600 moles per drum are generated over 2,000 years. The results of this analysis by Stone (1995) are presented in Figure 23.-1. These results suggest factors such as room porosity and gas pressure play a significant role. The simulations show that with a higher rate of gas generation ($f \geq 0.4$), pressurization of the room occurs rapidly, yet the impact on the room's closure is modest due to the minimal compression of waste, as most of the resistance is attributed to the gas pressure itself. In situations where gas pressure is high, the room may even expand, increasing the void volume and moderating room pressurization. Conversely, when the gas generation rate is lower ($f \leq 0.2$), there is a more substantial closure of the room and more pronounced compression of waste. In scenarios without gas generation (f = 0.0), the room stabilizes at a porosity of 0.22 after 2,000 years of closure. The porosity remained high due to the presence of the waste in the disposal room.

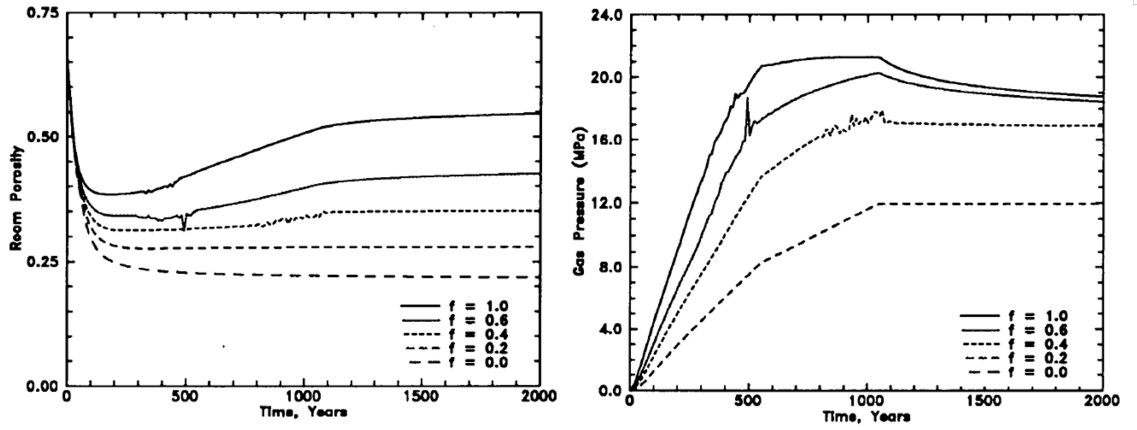

(a) Room Porosity

(b) Room Pressure

Figure 23.-1: Simulation results for the closure of a perfectly sealed disposal room under five gas-generation rate histories, differentiated by a rate multiplier f (after Stone (1995)).

The porosity-time-pressure functions were eventually included in PA calculations. Simulation results with TOUGH2 using this approach have shown the validity of this approach as long as the room pressurization in the PA simulation was similar to the obtained pressurization from mechanical analyses. It was noted that even if there is a notable deviation in the pressurization history, the approximation remains reasonable as long as the pressures in the repository are sufficiently low to prevent any substantial room expansion.

In the scope of RANGERS, the effect of gas in the considered repository system was analyzed in a similarly simplified manner. However, different assumptions were required to account for the specific characteristics of the German repository concept and the limited data available on gas production from POLLUX casks. In difference to the study by (Stone, 1995), no compaction can occur in the cask so that only the compaction of crushed salt is of interest and the porosity can decrease to zero. in the absence of gas generation curve, the compaction of the crushed salt was analyzed for fixed gas pressure in the drift. The main focus of this analysis was to estimate how much the gas can affect the closure of disposal drifts backfilled with crushed salt.

The model used for this analysis is similar to the one already described in section 18.1 to analyze the compaction behavior in a single drift located in the middle of an emplacement field where the thermal output is maximum. This model consist of a single drift embedded in the geological model in which a POLLUX cask is disposed and the drift is backfilled with crushed salt. The cask in the model comprises two components: an outer casing for shielding against radioactive radiation and a container basket holding the high-level radioactive wastes, acting as a heat source in the model. The numerical model takes account the thermal superposition and the resulting temperature increases coming from the neighboring drifts by considering thermal symmetry boundary conditions as a quarter model of a cask embedded in a partial model of the rock formation, allowing the simulation of a large disposal field. In this model, the distance from the drift axis to the model boundary in the transverse direction of the drift equals half the drift distance, and the distance from the cask's end face to the model boundary in the drift direction equals half the cask distance. In this model, we assume a different cask spacing of 20 m as the one optimized in the design of the repository (3 m). This helps us to better estimate the compaction of part of the drift that are fully backfilled with crushed

salt next to drift section where the cask is disposed. The model is depicted in Figure 23.-2. The computations was carried out thermal-mechanically with FLAC3D in the version 7 (Itasca Consulting Group, Inc., 2021). All material parameters and models used in this study can be found in Chapter 18.. The lithostatic pressure at the disposal level is around 18 MPa.

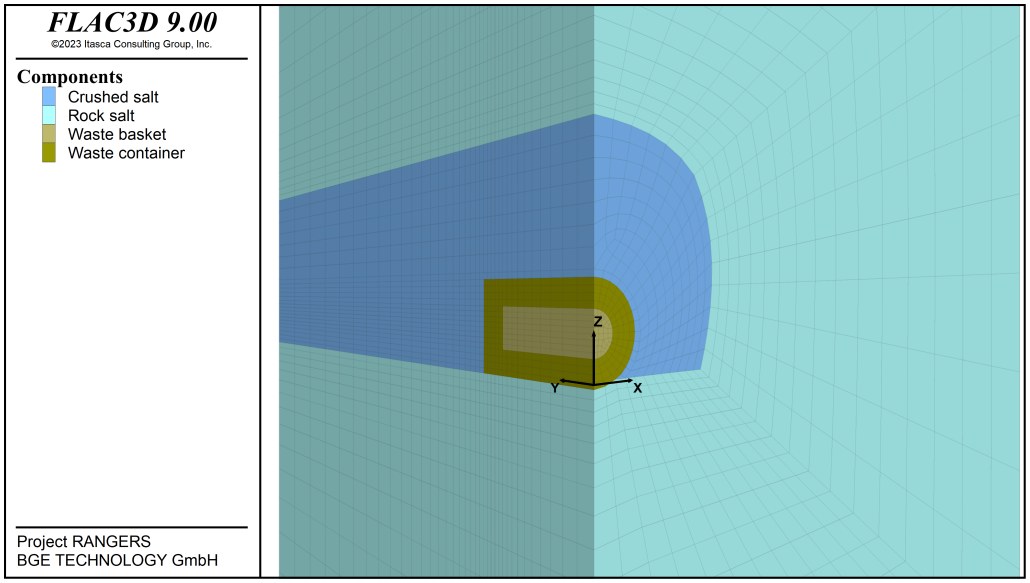

Figure 23.-2: Numerical model for the investigation the effect of gas on crushed salt compaction.

As previously noted, this study does not account for gas generation per se. Instead, it incorporates the impact of gas generation by initializing a corresponding gas pressure within the disposal drift. This approach facilitates an investigation into the compaction behavior under varying constant gas pressures, thereby enhancing our understanding of compaction dynamics across both low and high gas pressure conditions.

Initially, we juxtapose the outcomes of the thermal-hydrological-mechanical (THM) simulation, which assumes an absence of gas pressure, with those of the thermal-mechanical (TM) simulation as delineated in chapter 8. The benchmark results, as depicted in Table 23.-1, focus on a key mechanical variable: displacement. Specifically, the table illustrates the displacement magnitude distribution, calculated as the square root of the sum of the squares of the displacement components, observed at a decade post disposal and backfill operations.

A comparative analysis reveals a near-identical match between the results from both simulation types, which aligns with expectations. Such a correlation serves to affirm the accuracy of the THM simulation, lending credibility to the simulation results and methodologies employed.

Table 23.-1: Comparison of compaction analysis with THM and TM numerical framework of FLAC3D.

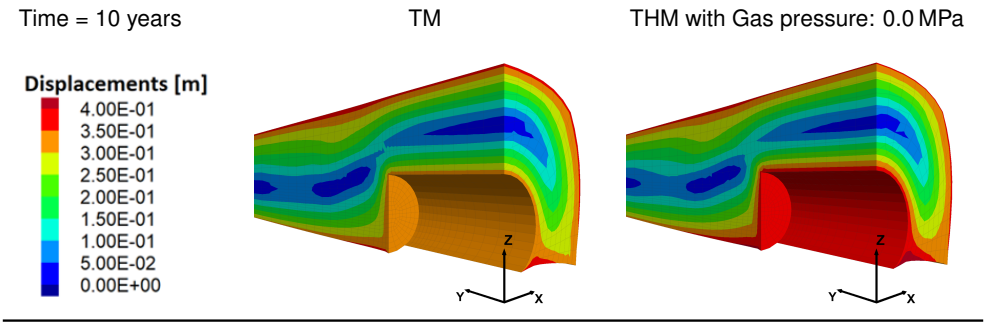

In order to analyze the compaction behaviour at low gas pressure regime, three simulations with fixed gas pressure of 0.25 MPa, 0.5 MPa and 1 MPa were performed. The results of these simulations are reported in Table 23.-2. The table showcases the porosity distribution at different times (1 year, 5 years, 10 years, 30 years, and 40 years) and at varying low gas pressures (0.25 MPa, 0.5 MPa, and 1 MPa) and illustrates how porosity and compaction evolve over time under the influence of different levels of gas pressure. As time progresses from 1 year to 40 years, the porosity in the disposal drift decreases, indicative of increasing compaction of the crushed salt backfill. Here the effect of gas pressure is clearly noticeable as higher gas pressure hinders the compaction process in this simulated environment. Nevertheless, the effect of gas pressure remains limited. By the 40-year mark, the material under all three gas pressure conditions is fully compacted and by a time of 30 years, the difference in the porosity distribution becomes negligible.

Table 23.-3 shows the analogous investigation at high gas pressure regime. In this case, three simulations were carried under gas pressure of 5 MPa, 10 MPa, and 20 MPa. The porosity distribution at different times (1 year, 20 years, 40 years, 70 years, and 100 years) carried out under the three gas pressures is shown in the table. Here, the previous observation from the simulation at low gas pressure conditions remains true with the difference that at high pressure, the compaction is this time severely hindered. For example, the porosity distribution under 5 MPa of gas pressure at 20-year mark is roughly similar to the one under 10 MPa at a time of 100 years. This means that increasing the gas pressure from 1 to 10 MPa delays the compaction process to nearly 80 years. Interestingly, no compaction is observed at gas pressure of 20 MPa. These observations are clearly evidence in Figure 23.-3 where the average porosity over time is displayed for the three gas pressure conditions here. The figure shows that the compaction is clearly retarded at 10 MPa compared to 5 MPa but the porosity remains nearly at the initial value after 100 years. This means that at high gas pressure can completely stop the compaction process or even lead to a dilation as it has been shown by Stone, 1995.

Table 23.-2: Porosity evolution under different low gas pressures acting in the disposal drift.

Gas pressure: 0.25 MPa	Gas pressure: 0.5 MPa	Gas pressure: 1 MPa
Time: 1 year		
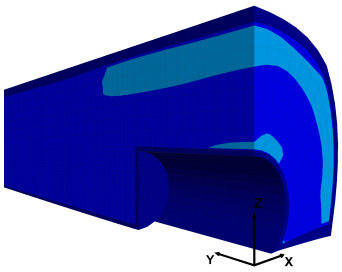	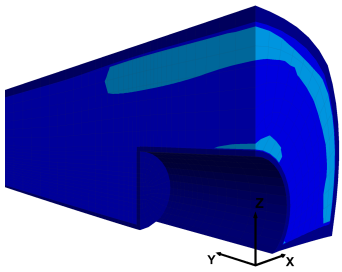	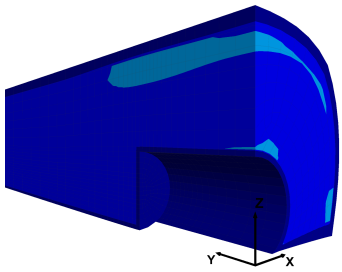
Time: 5 years		
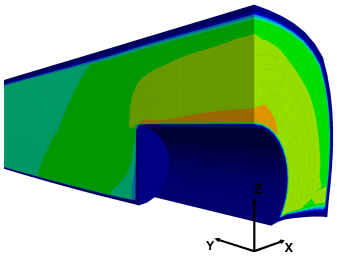	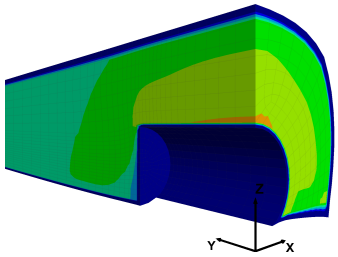	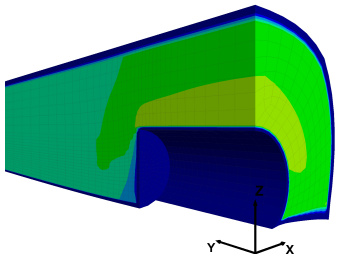
Time: 10 years		
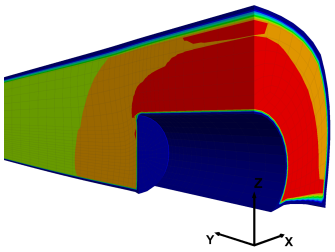	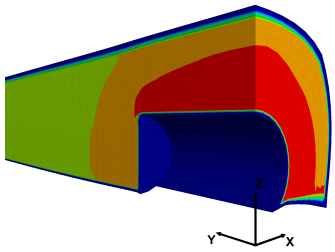	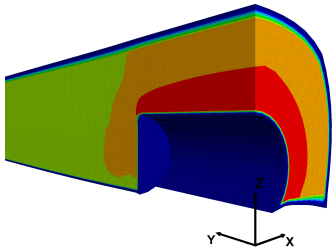
Time: 30 years		
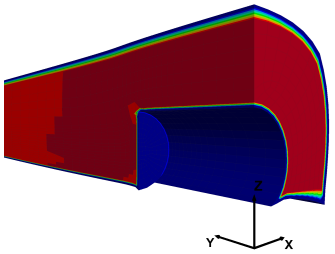	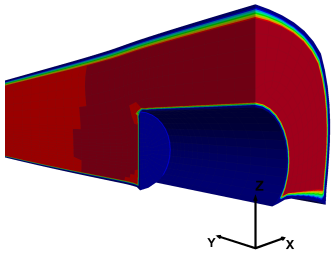	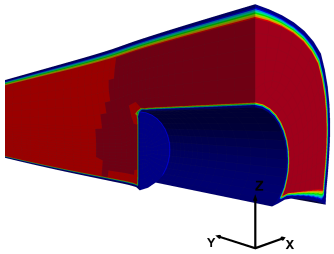
Time: 40 years		
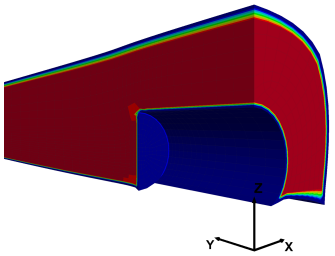	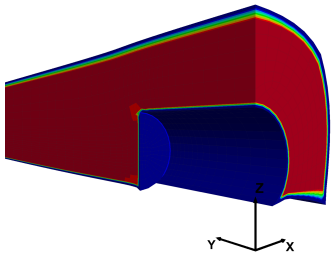	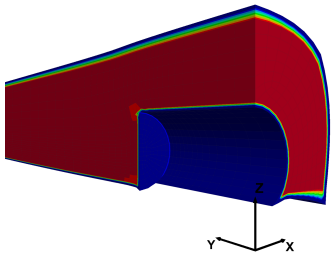

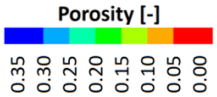

Table 23.-3: Porosity evolution under different high gas pressures acting in the disposal drift.

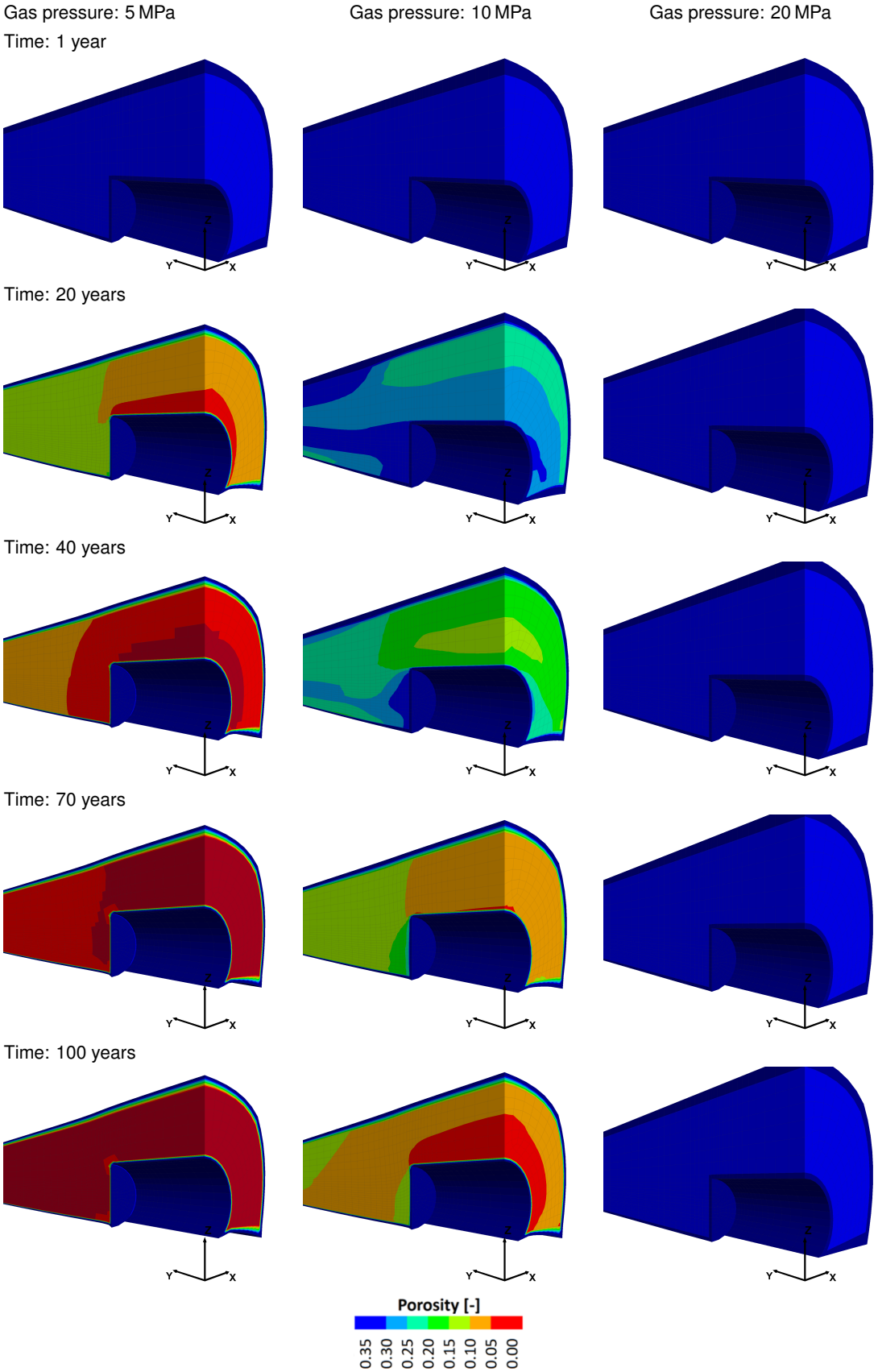

These outcomes are visualized in Figure 23.-3, which presents a comparative overview of average porosity changes over time for the different high-pressure environments. This visualization confirms that a pressure of 10 MPa -— approximately half the confining pressure —- significantly slows compaction compared to 5 MPa. Even after 100 years, porosity levels under high pressure of 20 MPa slightly above the lithostatic pressure remain close to their initial values, implying that such pressure levels can halt compaction entirely or may reverse the compaction process by dilating the backfill similar to the findings presented by Stone (1995).

From the analysis conducted within this study, several key insights have been ascertained:

- Under low gas pressure conditions, the influence of gas pressure on the compaction of crushed salt is relatively modest.
- Conversely, at elevated gas pressures, the impact on compaction is marked, with the potential to significantly postpone the compaction process by several decades, and in some cases, even centuries.
- In instances of extremely high gas pressures, there is a possibility for gas pressure to not only halt the compaction process entirely but also to induce a reversal, resulting in the dilation of the backfill.

These conclusions underscore the significance of gas pressure as a decisive factor affecting the long-term evolution and integrity of salt repositories. Incorporating the effect of gas pressure into performance assessment is therefore necessary to ensure the long term safety and effectiveness of those repositories.

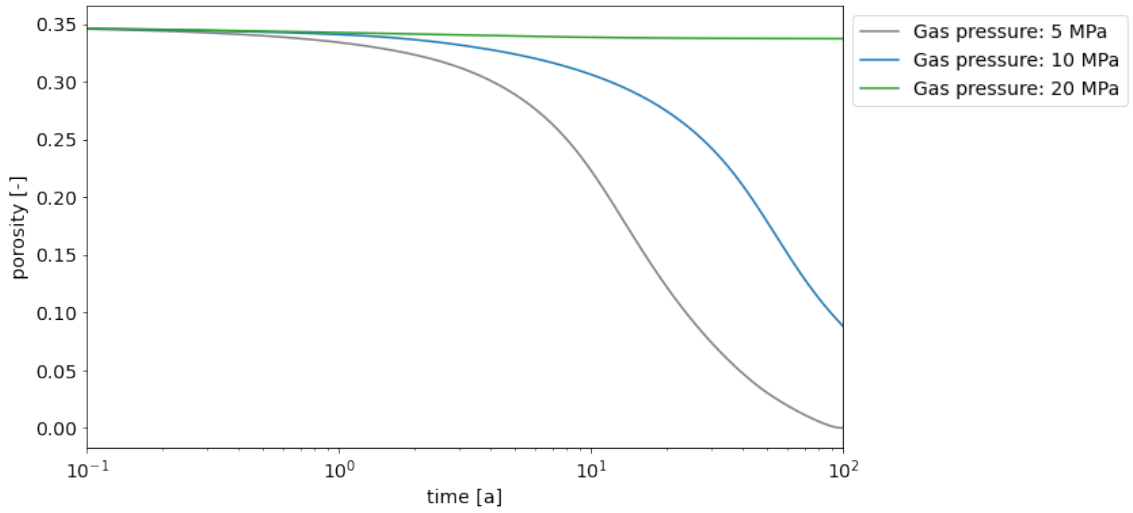

Figure 23.-3: Porosity evolution at different gas pressures in the drift.

24. Safety Evaluation of the Engineer Barrier System in Salt

In this chapter, we evaluate the results of the integrity and performance assessment of the Engineered Barrier System for a generic salt formation as designed in the project RANGERS. The developed EBS consists of two shaft sealing systems installed in the shafts of the repository complemented with four drift sealing systems installed in the two main drifts of the repository mine closing the access to the emplacement wings. These sealing system maintain the confinement of the repository until the long term seal made of crushed salt has taken its function. Therefore the analyses regarding the gain of function of the crushed salt backfill were complementary performed.

The methodology developed in this project recommends the independent analysis of the reference scenario evolutions as well as of the alternative scenarios. Whereas for the reference scenario a quantitative integrity and performance assessment is required, the study of the alternatives scenarios lies in the understanding of the system behavior in severe conditions and thus helps to better assess the robustness and optimization potential of the EBS.

For both kind of analyses, the methodology allows us to derive in a stringent manner the loads acting on the EBS based on the evaluation of the available FEPs and scenarios development known for salt repositories. From these FEPs and scenarios a modeling concept was developed from which the modeling case to be analyzed derived. The main idea coming from this modeling concept is to consider as much FEPs as possible in a single modeling case in order to account for their interaction. For those FEPs that cannot be included in the main modeling case, additional modeling cases can be defined.

For the reference scenario evolution, the mechanical integrity assessment of the shaft and drift sealing structures was conducted in this report in an indicative yet non-exhaustive manner. This was complemented with the hydraulic assessment of the shaft sealing structure. A similar assessment for the drift sealing structure derives from the application of the methodology but is still pending.

Five modeling cases could be identified as a result of the FEP analysis. The first one comprises the main processes that have a direct effect on the mechanical integrity such as the FEPs heat flow, thermal expansion/contraction, mechanical stress changes, convergence. This permanent loading conditions are further enhanced by considering the time dependency of the sealing materials from which a degradation can be expected over time. The third modeling case consists of hydraulic loading situations that will come over time. The fourth modeling case considers the effect of seismicity and gas explosion on the EBS. The last case studies the EBS behavior in the scope of the alternative scenario evolutions.

The main results deriving from the drift sealing structure integrity assessment is that the drift seals in the repository will subjected to horizontal stresses coming from the thermal expansion of the salt. This horizontal stresses will lead to the extension or elongation of the seals. Thus, tensile stresses will developed in the seals eventually leading to vertical cracks in the sealing body, orthogonal to the drift axis and preferential fluid pathway. Nevertheless, the results of the assessment for the designed seal shows that the seals will remain intact. The heat load in the emplacement fields are not high enough to induce cracks. Even for thermal impacts, simple mitigation measures can be taken to ensure that the seals remain crack free. Furthermore, based on the results, the drift seal design can be optimized by incorporating constructive joints,

creating smaller sealing segments and thereby reducing stress development within them.

The analyses for the drift sealing structure indicate the formation of a loosening zone, or Excavation Damaged Zone (EDZ), in areas close to the drift contour after excavation. This means that the dilatancy strength is exceeded in these areas, causing the rock to begin losing stability and displaying increased porosity. The dilatancy criterion is a critical factor in assessing the integrity of salt as it shows where potential microcracking and increased permeability could allow minimal but notable fluid migration. However, the EDZ and the zone with high dilatancy remains spatially limited. Over time, the regions with high dilatancy vanish as the EDZ compacts. Furthermore, no loosening zone is observed at the contour of the drift seals after the installation of the MgO seal. This is due the high stiffness of the MgO concrete helping to rapidly compact the EDZ when convergence of the rock occurs. Taking into account the self-sealing potential of the salt, it can be expected that the EDZ will quickly recover over time.

It has been also showed in the compaction analyses that the long-term seal between the drift seals will quickly gain its function. This sealing components will reach full compaction in a period of time of less than 1,000 years according to the constitutive model used for this analysis. As this model is a very simple one, a better prediction will be attended by considering the use of more advanced and calibrated models.

Also from the compaction analyses, it has been shown that the crushed salt in all of the drifts in the emplacement fields as well as in the main and cross drifts will be quickly compacted in few decades after disposal due the accelerated effect of temperature. The simulation showed that the part of the repository behind the drift sealing system will be closed at less than 100 years. This means that the sealing of the repository is achieved right after the closure of the repository.

The integrity assessment of the shaft sealing structure has shown that the sealing elements installed in the shafts will not experience any damage over time. This is for crucial importance for the MgO concrete element were cracks undermine their sealing effectiveness. The bentonite elements modeled with Cam Clay constitutive model shows some plastic strains which is inherent to high plastic materials such as bentonite and cannot be interpreted as failure.

Along the shaft, a zone surrounding the shaft with high dilatancy was observed. This zone gradually decreases over time and eventually completely vanishes due to the convergence of the rock acting towards the sealing elements.

The hydraulic integrity analyses showed for the reference scenario that only 20,000 m^3 of inflowing fluids will reach the infrastructure area through one of the shafts by the end of the lifetime of the shaft sealing system after 50,000 years. Twice this amount can be assumed for both shafts. After the assumed loss of function of the shaft seals, the capacity of the infrastructure area is expected to be reached within several thousand to several tens of thousands of years, depending on the capacity of the fluid reservoir in the infrastructure area and permeability of the sealing components following their expected degradation. Only after full saturation of the infrastructure area, do the shafts start to fill up with brine. Only at this moment, does an increase towards hydrostatic pressure happen in the shaft. This pressure subsequently acts on the surface of the drift seals. This is computed to occur after 80,000 years a reservoir capacity of 150,000 m^3.

The evaluation of the EBS in the scope of the integrated performance assessment has shown that no significant gas pressure increase is to be expected in the repository. The phenomenon behind this low gas pressure is the high temperature transforming water to steam, which migrates away from the cask through the backfill into the EDZ. Therefore the EDZ will be enriched with water, while the backfill will be dried out. During this phase, the crushed salt becomes so highly compacted that its permeability is too low to allow the solution to return to the containers after cooling. In the absence of water, no corrosion is to be expected. The few atmosphere of gas pressure that was computed in the simulation was due to the corrosion of the waste packages with negligible heat-generation.

The low gas pressure in the repository also means that no further hydraulic load is to be expected for the drift seals within the repository. This also implies that the gas transport over time within the repository and through the seals is limited. The low gas pressure in the repository is also beneficial to the crushed salt compaction in the repository. As it has been shown in the additional analyses of compaction under gas pressure in the repository, the compaction under low gas pressure is slightly retarded but it is severely hindered at high gas pressure. This finding of low gas pressure in the repository needs however further investigations and experimental evidence to be conclusive.

Due to the high computation effort required for the integrity assessment, analysis in regard to the integrity evaluation could not be carried out in the fullest extent. Nevertheless a strategy to carry out the required simulation can be derived from the modeling concept established in this report.

For the mechanical integrity of the EBS, the integrity evaluation is mostly relevant for the drift sealing system. The alternative scenario of a shaft sealing failure results in an hydraulic load acting on the drift seal near the shaft. At the end of the simulation time of the analysis of the drift sealing system, the seals are still subjected to tensile stresses. Longer simulation time is required to see at which period of time the seals will return in the compressive domain. Mitigation measures may be necessary to increase the robustness of the systems at early in the repository.

For the alternative scenario of drift seal failure, no additional load is to be expected from gas pressure build up on the lower components of the shaft sealing systems as it has been demonstrated in the scope of the performance assessment that the gas generation due to corrosion in the repository is minimal. A similar assumption was assumed in integrity assessment of the shaft seals in VSG (Müller-Hoeppe et al., 2012a).

Compared to the assessment methodology from previous projects which relied on component models such as in the VSG, the proposed approach of using repository scale models has the advantages of considering as much FEPs as possible in a single model. It is also more precise regarding the loads acting on the EBS as these loads results from the global response of the repository system upon THMC evolution. However, special effort is necessary to develop adequate meshes that combine all components of the repository system in the necessary accuracy to satisfy an integrity assessment. Also, it is to mention that for specific studies or for the investigation of specific FEPs that cannot be included in the repository scale model, local model may be necessary.

It is worthy to mention that the loads deriving from the application of the FEPs analysis was

similar to those considered in the VSG. In Müller-Hoeppe et al. (2012b), five design situations were identified based on the scenario development. These include the design situations of the reference scenario without earthquake, reference scenario with earthquake, failure of the shaft seal, failure of the drift seal, as well as the modified impact of uncertainties concerning the creepability of salt (one creep class below/above the probable range), which should be addressed within the scope of an extraordinary design situation (Müller-Hoeppe et al., 2012b).

As suggested by Müller-Hoeppe et al. (2012a), the scenario involving variations in the creepability can be excluded, as these uncertainties can be narrowed down during during the geological site assessment. Accordingly, (Müller-Hoeppe et al., 2012a) conducted a calibration based on available convergence measurements from the Gorleben site. For the generic site considered in the RANGERS project, no such data is available, and thus this design scenario is not considered.

In this regard, the potential relevant failure mechanism of the drift seals, which results from the horizontal stresses, induced by thermal expansion of the salt in the emplacement fields, was not identified in the VSG drift seal assessment. In the VSG assessment, the lithostatic stress was assumed to be present at the location of the drift seals in the component model used for this analysis. In contrast, in this project, the stresses at the drift location result additionally from the thermal-mechanical evolution of the repository.

As reported in Müller-Hoeppe et al. (2012a), in the design scenario “failure of the shaft seal”, the EDZ is subjected to high compressive stresses at the drift seal location after 1,300 years, resulting in a sufficiently high pressure that the fluid pressure criterion for the hypothetical pore pressure is met.

Similar to the VSG assessment of the shaft, the thermal-mechanical evolution of the repository system facilitates the build up compressive stresses towards the excavation-damaged zone and the contact zone. Müller-Hoeppe et al. (2012a) further explain, by comparing two simulation cases–with and without thermal impact–that thermal-mechanical effects do not fundamentally result in different critical stress states for design. Instead, these stress states occur at an earlier time, indicating that the thermal-mechanical influence from the repository essentially accelerates the process.

In the VSG assessment, the integrity criteria were evaluated by comparing the stresses acting on the sealing elements with the material and dilatancy strengths. A similar approach was applied to evaluate the state of the contact zone, where compressive stresses are present in the normal direction, and shear stresses remain well below the design limit. In this project, the evaluation was enhanced by using suitable constitutive models for each material, allowing damage assessment based on material-specific behavior. The contact zone is assessed similarly to the VSG assessment. We apply the dilatancy criterion along the shaft, which indicates rock loosening and provides a more conservative assessment compared to the strength criterion.

The seismic impacts on the Engineered Barrier System (EBS) were not analyzed in the VSG study, nor were they evaluated in this report. According to Müller-Hoeppe et al. (2012a), seismic loading conditions do not typically govern the design in cases of low additional accelerations, such as those expected during a safety-level earthquake. This is because dynamic material strengths (resistances) usually increase more than the applied stresses under seis-

mic conditions. However, an exception exists if the failure mode is associated with shear failure and is not geometrically restricted. In such cases, shear strengths may decrease due to earthquake-induced reductions in normal stress, which could potentially affect the contact zone, as shear failure in this zone is a possible failure mode. Due to the planned complete backfilling of the repository, such scenarios are unlikely to occur. Nonetheless, since shear strength utilization in the contact zone is minimal, potential failure of the contact zone is deemed unlikely. This assessment, however, requires further verification.

The use of large models for assessment poses a drawback due to the high computational effort required. Consequently, with the computational tools available, it was not feasible to perform fully coupled THM (thermal-hydrological-mechanical) simulations to accurately represent the hydraulic evolution of the repository system. Further advancements in numerical modeling for salt structures under THM conditions are therefore essential.

Uncertainties remain regarding the contact zone, as it hard to handle in the numerical models, and appropriate modeling approaches such as the use of interface elements need further development and validation. Additionally, the constitutive models for salt used in this report do not account for rock damage, a feature that is critical in the contact zone analysis in describing the evolution of the EDZ, especially in terms of its hydraulic behavior. Depending on the modeling assumptions, damage may occur in the sealing material, the contact zone, or the surrounding rock. This aspect should be addressed in future analyses and calibrated against experimental data.

25. Concluding Remarks

The RANGERS project has successfully developed and demonstrated the application of a methodology for the integrity and performance assessment of an Engineered Barrier System (EBS) for high-level waste (HLW) and spent nuclear fuel (SNF) repositories in salt formations in accordance with the regulation in force. As part of a multi-barrier containment system, the EBS and the natural salt barriers maintain confinement, ensuring safety over a defined functional period until long-term backfill compaction is achieved.

This methodology provides a workflow to evaluate EBS integrity in salt-based repositories, incorporating integrated performance assessments. It builds upon extensive experience and knowledge from research conducted in Germany and the United States on the design, construction, and evaluation of seals.

In this report, the RANGERS methodology was applied to evaluate the integrity and performance of a generic salt repository for HLW and SNF. Starting from a Features, Events, and Processes (FEP) analysis, a structured modeling concept was developed to guide the integrity assessments through numerical simulations. This approach enabled an analysis of the thermal, mechanical, and hydrological evolution within the EBS and surrounding salt rock.

For the integrity assessment of the reference scenario, the analyses carried out in this report highlights that the EBS as designed in the project RANGERS is able to sustain the thermal-mechanical loads resulting from the heat generated by the waste in the formation. Dilatant zones, which form locally around the drift and shaft walls, display spatial limitations and are expected to recover over time due to salt's natural creep and convergence properties.

The crushed salt backfill, forming the long-term seal in the drifts, is projected to reach full compaction within approximately 1,000 years, ensuring containment for extended timescales. This finding is supported by rapid compaction computed in elevated temperature zones, suggesting effective sealing of backfilled drifts within decades. Hydraulic assessment of the shaft seal reveals minimal fluid migration, with a calculated inflow volume into the infrastructure area remaining below significant levels for up to 50,000 years.

A key outcome from the performance assessment is the expectation of low gas pressures within the repository, owing to initial high temperatures driving the migration of evaporated water into the surrounding rock, reducing corrosion potential. This, in turn, minimizes gas generation and reduces the associated hydraulic load within the repository, ultimately supporting the EBS's long-term containment function.

The RANGERS findings underscore the reliability of salt formations as containment solutions for radioactive waste disposal. The methodology provides a rigorous, adaptable framework for future performance assessments. Based on this methodology, the analyses of the integrity assessment can be extended for the integrity evaluation, optimization and robustness assessment. The results obtained so far for the integrity assessment already validate the EBS's capacity to maintain its integrity and functionality under regulatory timescales, thus establishing a basis for sustainable, long-term radioactive waste management in salt repositories.

References

ACI 318-14 (2014). *Building Code Requirements for Structural Concrete (ACI 318-14) and Commentary*. American Concrete Institute (ACI), Farmington Hills, MI.

AkEnd (2002). Empfehlungen des Arbeitskreises Auswahlverfahren Endlagerstandorte.

Alkattan, M., Oelkers, E. H., Dandurand, J.-L., and Schott, J. (1997). Experimental studies of halite dissolution kinetics: The effect of saturation state and the presence of trace metals. *Chemical Geology*, 137(3-4):201–219.

Amelung, P., Jobmann, M., Lerch, C., Polster, M., and Schonebeck, M. (2005). Berechnungen zur Endlagerauslegung im Steinsalz und Tongestein - Eine vergleichende Gegenüberstellung. Präsentation auf dem Workshop "Gegenüberstellung von Endlagerkonzepten im Salz und Tonstein" - GEIST: Peine, 2005.

Baldschun, R., Binot, F., Fleig, S., and Kockel, F. (2001). Geotektonischer Atlas von Nordwest-Deutschland und dem deutschen Nordsee-Sektor. Strukturen, Strukturentwicklung, Paläogeographie. In BGR, editor, *Geologisches Jahrbuch, A 153*. Bundesanstalt für Geowissenschaften und Rohstoffe, Hannover.

Batzle, M. and Wang, Z. (1992). Seismic properties of pore fluids. *Geophysics*, 57(11):1396–1408.

BAW (2013a). Merkblatt Anwendung von Kornfiltern an Bundeswasserstraßen (MAK). Technical report, Bundesanstalt für Wasserbau (BAW), Karlsruhe.

BAW (2013b). Merkblatt Materialtransport im Boden (MMB). Technical report, Bundesanstalt für Wasserbau (BAW), Karlsruhe.

Bertrams, N., Bollingerfehr, W., Eickemeier, R., Fahland, S., Flügge, J., Frenzel, B., Hammer, J., Kindlein, J., Liu, W., Maßmann, J., Mayer, K.-M., Mönig, J., Mrugalla, G., Müller-Hoeppe, N., Reinhold, K., Rübel, A., Schubarth-Engelschall, N., Simo, E., Thiedau, J., Thiemeyer, T., Weber, J. R., and Wolf, J. (2020). RESUS - Grundlagen zur Bewertung eines Endlagersystems in flach lagernden Salzformationen.

Beuth, T., Bracke, G., Buhmann, D., Dresbach, C., Keller, S., Krone, J., Lommerzheim, A., Mönig, J., Mrugalla, G., Rübel, A., and Wolf, J. (2012). Szenarienentwicklung - Methodik und Anwendung: Bericht zum Arbeitspaket 8 ; vorläufige Sicherheitsanalyse für den Standort Gorleben.

BGE (2022a). Konzept zur Durchführung der repräsentativen vorläufigen Sicherheitsuntersuchungen gemäß Endlagersicherheitsuntersuchungsverordnung.

BGE (2022b). Methodenbeschreibung zur Durchführung der repräsentativen vorläufigen Sicherheitsuntersuchungen gemäß Endlagersicherheitsuntersuchungsverordnung.

Bilke, L., Naumov, D., Wang, W., Fischer, T., Kiszkurno, F. K., Lehmann, C., Max, J., Zill, F., Buchwald, J., Grunwald, N., Kessler, K., Aubry, L., Dörnbrack, M., Nagel, T., Ahrendt, L., Kaiser, S., and Meisel, T. (2025). Opengeosys.

BMU (2010). Safety Requirements Governing the Final Disposal of Heat-Generating Radioactive Waste as at 40 September 2010.

Bollingerfehr, W., Bertrams, N., Buhmann, D., Eickemeier, R., Fahland, S., Filbert, W., Hammer, J., Kindlein, J., Knauth, M., Liu, W., Minkley, W., Mönig, J., Popp, T., Prignitz, S., Reinhold, K., Simo, E., Thiemeyer, T., Völkner, E., and Wolf, J. (2018). Concept developments for a generic repository for heat-generating waste in bedded salt formations in Germany.

Bollingerfehr, W., Buhmann, D., Filbert, W., Keller, S., Krone, J., Lommerzheim, A., Mönig, J., Mrugalla, S., Müller-Hoeppe, N., Weber, J. R., and Wolf, J. (2013). Status of the safety concept and safety demonstration for an HLW repository in salt.- Summary report ISIBEL project, FKZ 02E107 and 02E10729.

Bollingerfehr, W., Filbert, W., Dorr, S., Herold, P., Lerch, C., Burgwinkel, P., Charlier, F., Thomasuske, B., Bracke, G., and Kilger, R. (2012). Vorläufige Sicherheitsanalyse Gorleben (VSG). AP6: Endlangerauslegung und optimierung. Technical Report GRS-281, Gesellschaft für Anlagen- und Reaktorsicherheit (GRS) gGmbH.

Bradshaw, R. L. and McClain, W. C. (1971). Project salt vault: A demonstration of the disposal of high-activity solidified wastes in underground salt mines. Technical Report ORNL-4555, Oak Ridge National Laboratory.

Bräuer, V., Jobmann, M., Langer, M., Schlüter, R., and Schatz, T. (2016). Entwicklung und Bewertung eines generischen Endlagerkonzepts für hochradioaktive Abfälle in Tongestein. *Entsorgungsbericht*, 45:345–367.

Buchwald, J., Kaiser, S., Kolditz, O., and Nagel, T. (2021). Improved predictions of thermal fluid pressurization in hydro-thermal models based on consistent incorporation of thermo-mechanical effects in anisotropic porous media. *International Journal of Heat and Mass Transfer*, 172:121127.

Buhmann, D., Mönig, J., Wolf, J., Heusermann, S., Keller, S., Weber, J. R., Bollingerfehr, W., Filbert, W., Kreienmeyer, M., Krone, J., and Tholen, M. (2008). Review and Appraisal of the Tools available for a Safety Assessment of Final Repositories for HLW (ISIBEL).

Council on Environmental Quality (1978). Council on Environmental Quality Regulations for Implementing the Procedural Provisions of the National Environmental Policy Act. `https://www.ecfr.gov/current/title-40/chapter-V/part-1500`. 40 CFR Parts 1500-1508.

Cristescu, N. and Hunsche, U. (1998). *Time Effects in Rock Mechanics*. Wiley Series in Materials, Modelling and Computation. John Wiley & Sons, Chichester.

Czaikowski, O. and Friedenberg, L. (2020). Benchmarking for Validation and Verification of THM Simulators with special Regard to Fluid Dynamic Processes in Repository Systems Project BenVaSim. Technical Report GRS - 588, GRS, Braunschweig.

Czaikowski, O., Friedenberg, L., Wieczorek, K., Müller-Hoeppe, N., Lerch, C., Eickemeier, R., Laurich, B., Liu, W., Stührenberg, D., Svensson, K., Zemke, K., Lüdeling, C., Popp, T., Bean, J., Mills, M., Reedlunn, B., Düsterloh, U., Lerche, S., and Zhao, J. (2023). KOMPASS: Compaction of Crushed Salt for the Safe Containment. Technical Report GRS-608, Gesellschaft für Anlagen- und Reaktorsicherheit (GRS).

DAfStb (2011). *Betonbau beim Umgang mit wassergefährdenden Stoffen Teil 1: Grundlagen, Bemessung und Konstruktion unbeschichteter Betonbauten*. Deutscher Ausschuss für Stahlbeton (DAfStb), Berlin.

DBE (1995). Direkte Endlagerung ausgedienter Brennelemente (DEAB) - Handhabungsversuche zur Streckenlagerung T60: Technischer Bericht.

DGGT (1997). *GDA-Empfehlungen Geotechnik der Deponien und Altlasten*. Verlag Ernst und Sohn, Berlin, 3 edition.

DIN 18196 (2011). DIN 18196: Erd- und Grundbau - Bodenklassifikation für bautechnische Zwecke.

DIN EN 1990 (2010). DIN EN 1990. Eurocode: Grundlagen der Tragwerksplanung, Deutsche Fassung, 2010.

DIN EN 1991 (2010). Eurocode 1: Actions on structures. Includes national annex NA:2010.

DIN EN 1997 (2014). DIN EN 1997-1:2014-03, Eurocode 7 - Entwurf, Berechnung und Bemessung in der Geotechnik_- Teil_1: Allgemeine Regeln; Deutsche Fassung EN_1997-1:2004_+ AC:2009_+ A1:2013.

DOE (2019). Title 40 CFR Part 191 Subparts B and C Compliance Recertification Applicaiton 2019 for the Waste Isolation Pilot Plant. Technical Report DOE/WIPP-19-3609, US Department of Energy Carlsbad Field Office.

Eberth, S. and Müller-Hoeppe, N. (2009). Übertragung des Sicherheitsnachweiskonzeptes für ein Endlager im Salz auf andere Wirtsgesteine, Forschungsprojekt ÜBERSICHT, Abschlussbericht. Technical Report TEC-30-2008-AB, DBE TECHNOLOGY GmbH, Peine.

EN ISO 9001:1994-08 (1994). Quality management systems - Requirements. International Organization for Standardization (ISO).

Endlagerkommission, D. B. (2016). *Bericht der Kommission Lagerung hoch radioaktiver Abfallstoffe*. Deutscher Bundestag, Berlin.

EndlSiAnfV (2020). Verordnung über Sicherheitsanforderungen an die Endlagerung hochradioaktiver Abfälle (Endlagersicherheitsanforderungsverordnung - EndlSiAnfV).

EndlSiUntV (2020). Verordnung über Anforderungen an die Durchführung der vorläufigen Sicherheitsuntersuchungen im Standortauswahlverfahren für die Endlagerung hochradioaktiver Abfälle Endlagersicherheitsuntersuchungsverordnung - EndlSiUntV).

Engelmann, H.-J., Lommerzheim, A., Biurrun, E., Hubert, R., and Pöhler, M. (1995). Direkte Endlagerung ausgedienter Brennelemente DEAB (02E8371), Untersuchung zur Rückholbarkeit von eingelagertem Kernmaterial in der Nachbetriebsphase eines Endlagers. Technical report, Deutsche Gesellschaft zum Bau und Betrieb von Endlagern für Abfallstoffe (DBE).

Freeze, G. (1996). Repository closure reasoned argument for fep issue dr12. Technical Report ERMS-413328, INTERA Inc.

Friedenberg, L., Bartol, J., Bean, J., Beese, S., de Bresser, H., Coulibaly, J. B., Czaikowski, O., Düsterloh, U., Eickemeier, R., Gartzke, A.-K., Hangx, S., Jantschik, K., Laurich, B., Lerch, C., Lerche, S., Liu, W., Lüdeling, C., Mills, M. M., Müller-Hoeppe, N., van Oosterhout, B., Popp, T., Rabbel, O., Rahmig, M., Reedlunn, B., Rogalski, A., Rölke, C., Saruulbayar, N., Spiers, C. J., Svensson, K., Thiedau, J., and Zemke, K. (2024). KOMPASS-II: Compaction of Crushed Salt for Safe Containment – Phase 2. Technical report, GRS, COVRA, Sandia, BGR, UU, TUC, BGE-TEC, IfG. Phase 2 of the Compaction of Crushed Salt for Safe Containment project.

Gast, S. and Riesenberg, C. (2016). AP1: Erstellung eines Informationssystems über Salzstrukturen sowie von geologischen Niveauschnittkarten. In BGR, editor, *Informationssystem Salzstrukturen: Planungsgrundlagen, Auswahlkriterie und Potenzialabschätzung für die Errichtung von Salzkavernen zur Spei-cherung von erneuerbaren Energien (Wasserstoff und Druckluft)*. Bundesanstalt für Geowissenschaften und Rohstoffe, Hannover.

Haas Jr., J. L. (1976). Physical Properties of the Coexisting Phases and Thermochemical Properties of the H_2O Component in Boiling NaCl Solutions. Technical Report Bulletin 1421-A, US Geological Survey.

Hampel, A., Günther, R.-M., Salzer, K., Minkley, W., Pudewills, A., Leuger, B., Zapf, D., Staudtmeister, K., Rokahr, R., Herchen, K., Wolters, R., Lux, K.-H., Schulze, O., Heemann, U., and Hunsche, U. (2010). Benchmarking of Geomechanical Constitutive Models for Rock Salt. In *Proceedings of the 44th U.S. Rock Mechanics Symposium*, ARMA10-287. American Rock Mechanics Association (ARMA).

Hampel, A., Günther, R.-M., Salzer, K., Minkley, W., Pudewills, A., Yildirim, S., Rokahr, R., Gährken, A., Missal, C., Stahlmann, J., Herchen, K., and Lux, K.-H. (2015). Joint project III on the comparison of constitutive models for the mechanical behavior of rock salt, I. Overview and results from model calculations of healing of rock salt. In Roberts, L., Mellegard, K., and Hansen, F., editors, *Proceedings of the 8th Conference on the Mechanical Behavior of Salt (SaltMech VIII)*. Taylor & Francis Group.

Hampel, A., Lüdeling, C., Günther, R.-M., Sun-Kurczinski, J., Wolters, R., Düsterloh, U., Lux, K.-H., Yildirim, S., Zapf, D., Wacker, S., Epkenhans, I., Stahlmann, J., and Reedlunn, B. (2022). WEIMOS: Simulations of two Virtual Demonstrators. In *Proceedings of the 10th Conference on the Mechanical Behavior of Salt (SaltMech X)*.

Herchen, K., Düsterloh, U., and Lux, K.-H. (2016). Verbundprojekt: Vergleich aktueller stoffgesetze und vorgehensweisen anhand von modellberechnungen zum thermo-mechanischen verhalten und zur verheilung von steinsalz (tv 5: Tuc). Technical report, Lehrstuhl für Deponietechnik und Geomechanik, Technische Universität Clausthal, Clausthal-Zellerfeld. Final report, BMWi-FKZ 02E10820.

Herold, P., Jobmann, M., Müller, C., and Gruner, M. (2020). Schachtverschlusskonzepte Teilbericht zum AP1 ELSA 2: Technischer Bericht.

Herold, P., Prignitz, S., Bertrams, N., Simo, E., Filbert, W., Friedrich, C., and Becker, A. (2018). Technische Konzepte für die Rückholung der Einlagerungsvariante horizontale Streckenlagerung in Salzformationen. In *Entwicklung technischer Konzepte zur Rückholung von Endlagerbehältern mit wärmeentwickelnden radioaktiven Abfällen und ausgedienten Brennelementen aus Endlagern in Salz- und Tongesteinsformationen (ERNESTA)*. BGE TECHNOLOGY GmbH, Peine.

Hess, H. H., Adkins, J. N., Heroy, W. B., Benson, W. E., Hubbert, M. K., Frye, J. C., Russell, R. J., and Theis, C. V. (2057). The disposal of radioactive waste on land. Technical Report Publication 519, National Academies of Sciences - National Research Council.

Heydorn, M., Teichmann, L., and Meyer, T. (2016). Schachtanlage Asse II Anwendungsversuch Pilotströmungsbarriere PSB A1. *bergbau*, page S.165 ff.

Hou, Z., Wolters, R., Düsterloh, U., Rokahr, R., Zapf, D., Salzer, K., Günther, R.-M., Minkley, W., Pudewills, A., Heemann, U., Schulze, O., Zetsche, F., and Hampel, A. (2007). Comparison of advanced constitutive models for the mechanical behavior of rock salt - results from

a joint research project, II. Numerical modeling of two in-situ case studies and comparison. In Lux, K.-H., Minkley, W., Wallner, M., and Hardy, H. J., editors, *Basic and Applied Salt Mechanics: Proceedings of the 6th Conference on the Mechanical Behavior of Salt (SaltMech VI)*. Taylor & Francis (Balkema).

IAEA (2008). *The Management System for the Disposal of Radioactive Waste*. IAEA Safety Guide No. GS-G-3.4. International Atomic Energy Agency (IAEA), Vienna.

International Atomic Energy Agency (IAEA) (2006). *Geological Disposal of Radioactive Waste*. International Atomic Energy Agency, Vienna, Austria.

International Atomic Energy Agency (IAEA) (2011). *Disposal of Radioactive Waste, Specific Safety Requirements*. IAEA Safety Standards Series No. SSR-5. International Atomic Energy Agency, Vienna, Austria.

Itasca Consulting Group, Inc. (2021). *FLAC3D Manual*. Minneapolis, MN. Version 9.0.

Johnson, K. S. and Gonzales, S. (1978). Salt deposits in the united states and regional geologic characteristics important for storage of radioactive waste. Technical Report Y/OWI/SUB–7414/1, Office of Waste Isolation.

Kamlot, P., Weise, D., Gärtner, G., and Teichmann, L. (2012). Drift sealing elements in the asse ii mine as a component of the emergency concept – assessment of the hydromechanical functionality. In *The Mechanical Behavior of Salt: 7th Conference (SaltMech7)*, London. Taylor & Francis.

Keller, A., Mills, M., Hagdu, T., Herold, P., Jayne, R., Kuhlman, K., Lommerzheim, A., Matteo, E., and Simo, E. (2021a). State of the Art and Sciences on Engineered Barrier Systems in Salt Formations. Technical Report BGE TEC 2021-13 / SAND2022-0204 R, BGE TECHNOLOGY GmbH, SANDIA, Peine, Albuquerque.

Keller, A., Simo, E., Herold, P., Lommerzheim, A., Matteo, E., Hadgu, T., Jayne, R., Mills, M., and Kuhlman, K. (2021b). Design Methodology Comparison for HLW/SNF Repositories in Germany and the US: proposed for poster presentation at the Waste Management Conference 2021, Phoenix.

Kerntechnische Ausschuss (KTA) (1988). Sicherheitstechnische Regel des KTA - Reaktorsicherheitsbehälter aus Stahl, Teil 1: Werkstoffe und Erzeugnisforme. Technical Report 3401.1, Kerntechnischen Ausschusses, Salzgitter.

Kindlein, J., Buhmann, D., Mönig, J., Spießl, S., and Wolf, J. (2018). Bewertung der Wirksamkeit des Radionuklideinschlusses für ein Endlager in flach lagernden Salzformationen: Ergebnisse aus dem Vorhaben KOSINA.

Klinge, H., Boehme, J., Grissemann, C., Houben, G., Ludwig, R. R., Rübel, A., Schelkes, K., Schildknecht, F., and Suckow, A. (2007). Standortbeschreibung Gorleben: Die Hydrogeologie des Deckgebirges des Salzstockes Gorleben. In BGR, editor, *Geologisches Jahrbuch, Reihe C, Band 71*. E.Schweizerbart'sche Verlagsbuchhandlung, Stuttgart.

Kock, I., Eickemeier, R., Friedling, G., Heusermann, S., Knauth, M., Minkley, W., Navarro, M., Nipp, H.-K., and Vogel, P. (2012). Integrität der geologischen Barriere: Bericht zum Arbeitspaket 9.1 Vorläufige Sicherheitsanalyse für den Standort Gorleben GRS-286.

Köhler, J., Teichmann, L., Heydorn, M., and Wolff, P. E. (2019). Application of Sorel Concrete for Barrier Construction and Cavity Stabilisation at Schachtanlage Asse II. *Mining Report Glückauf*, page 485 ff.

Kreienmeyer, M., Lerch, C., Polster, M., and Tholen, M. (2008). Überprüfung und Bewertung des Instrumentariums für eine sicherheitliche Bewertung von Endlagern für HAW ISIBEL - AP5: Nachweiskonzept zur Integrität der einschlusswirksamen technischen Barrieren.

Krull, P., Hoth, P., Bräuer, V., and Wirth, H. (2004). Endlagerung radioaktiver Abfälle in Deutschland Untersuchungswürdige Regionen mit potentiellen Wirtsgesteinsformationen: Bericht.

Kudla, W. and al., e. (2020). Synthesis Report ELSA 2 project: Final report, in preparation.

Kudla, W., Schreiter, F., Gruner, M., Jobmann, M., Bollingerfehr, W., Müller-Hoeppe, N., Herold, P., Freyer, D., Wilsnack, T., and Grafe, F. (2013). Schachtverschlüsse für Endlager für hochradioaktive Abfälle. Abschlussbericht ELSA Teil 1.

Kuhlman, K., Mills, M., Jayne, R., Matteo, E., Herrick, C., Nemer, M., Heath, J., Xiong, Y., Choens, C., Stauffer, P., Boukhalfa, H., Guiltinan, E., Rahn, T., Weaver, D., Dozier, B., Otto, S., Rutqvist, J., Wu, Y., Hu, M., Uhlemann, S., and Wang, J. (2020). FY20 Update on Brine Availability Test in Salt. Technical Report SAND2020-9034R, Sandia National Laboratories.

Kuhlman, K., Wagner, S., Kicker, D., Kirkes, R., Herrick, C., and Guerin, D. (2012). Review and evaluation of salt r&d data for disposal of nuclear waste in salt. Technical Report SAND2012-8808P, Sandia National Laboratories.

Kuhlman, K. L., Bartol, J., Carter, A., Lommerzheim, A., and Wolf, J. (2024). Scenario development for safety assessment in deep geologic disposal of high-level radioactive waste and spent nuclear fuel: A review. *Risk Analysis*.

Kuhlman, K. L., Lopez, C. M., Mills, M. M., Rimsza, J., and Sassani, D. (2018). Evaluation of Spent Nuclear Fuel Disposition in Salt (FY18). Technical Report SAND2018-11355R, Sandia National Laboratories.

Lafleur, J., Mlynarek, J., and Rollin, A. L. (1993). Filter criteria for well graded cohesionless soils. In Brauns, J., Heibaum, M., and Schuler, U., editors, *Filters in Geotechnical and Hydraulic Engineering*, pages 97–106, Rotterdam. Balkema.

LaForce, T., Basurto, E., Bigler, L., Chang, K. W., Ebeida, M., Jayne, R., Leone, R., Mariner, P., and Sharpe, J. (2023a). GDSA repository systems analysis investigations for FY 2023. Technical Report SAND2023-09454R, Sandia National Laboratories.

LaForce, T., Ebeida, M., Jordan, S., Miller, T. A., Stauffer, P. H., Park, H., Leone, R., and Hammond, G. (2023b). Voronoi Meshing to Accurately Capture Geological Structure in Subsurface Simulations. *Mathematical Geosciences*, 55(2):129–161.

Liu, H.-H. (2014). Non-Darcian flow in low-permeability media: key issues related to geological disposal of high-level nuclear waste in shale formations. *Hydrogeology Journal*, 22(7):1525.

Liu, H.-H. (2017). *Fluid flow in the subsurface*. Springer.

Liu, H.-H., Li, L., and Birkholzer, J. (2012). Unsaturated properties for non-Darcian water flow in clay. *Journal of Hydrology*, 430:173–178.

Liu, W., Völkner, E., Popp, T., and Minkley, W. (2017). Zusammenstellung der Materialparameter für THM-Modellberechnungen - Ergebnisse aus dem Vorhaben KOSINA. In BGR, editor, *Konzeptentwicklung für ein generisches Endlager für wärmeentwickelnde Abfälle in flach lagernden Salzschichten in Deutschland sowie Entwicklung und Überprüfung eines Sicherheits- und Nachweiskonzeptes (KOSINA)*. Bundesanstalt für Geowissenschaften und Rohstoffe, Hannover.

Lomenick, T. F. (1996). The siting record: an account of the program of federal agencies and events that have led to the selection of a potential site for a geologic repository for high-level radioactive waste. Technical Report ORNL/TM-12940, Oak Ridge National Laboratory.

Lommerzheim, A., Jobmann, M., Meleshyn, A., Mrugalla, S., Rübel, A., and Stark, L. (2019). Safety concept, FEP catalogue and scenario development as fundamentals of a long-term safety demonstration for high-level waste repositories in German clay formations. *Geological Society, London, Special Publications*, 482(1):313–329.

Lux, K.-H., Rutenberg, M., Feierabend, J., Czaikowski, O., Friedenberg, L., Maßmann, J., Pitz, M., Sentis, M., Graupner, B., Hansmann, J., Hotzel, S., Kock, I., Rutqvist, J., Hu, M., and Rinaldi, A. P. (2021). International Benchmarking for Verification and Validation of TH2M Simulators with Special Consideration of Fluid Dynamical Processes in Radioactive Waste Repository Systems (BenVaSim) Synthesis report. Technical report, TU Clausthal.

MacKinnon, R. J., Sevougian, S., D., and Leigh,C. D. and Hansen, F. D. (2012). Towards a Defensible Safety Case for Deep Geologic Disposal of DOE HLW and DOE SNF in Bedded Salt.

Mariner, P. E., Gardner, W. P., Hammond, G. E., Sevougian, S. D., and Stein, E. R. (2015). Application of Generic Disposal System Models. FCRD-UFD-2015-000126 / SAND2015-10037R.

Mariner, P. E., Nole, M. A., Basurto, E., Berg, T. M., Chang, K. W., Debusschere, B. J., Eckert, A. C., Ebeida, M. S., Gross, M., Hammond, G. E., Harvey, J., Jordan, S. H., Kuhlman, K. L., LaForce, T. C., Leone, R. C., McLendon III, W. C., Mills, M. M., Park, H. D., Perry, F. V., Salazar III, A., Seidl, D. T., Sevougian, S. D., Stein, E. R., and Swiler, L. P. (2020). Advances in GDSA Framework Development and Process Model Integration. Technical Report SAND2020-10787R, Sandia National Laboratories.

Mašín, D. (2013). Double structure hydromechanical coupling formalism and a model for unsaturated expansive clays. *Engineering Geology*, 165:73–88.

Matalucci, R. V. (1987). In situ testing at the waste isolation pilot plant. Technical Report SAND87-2382, Sandia National Laboratories.

Meyer, T., Müller-Hoeppe, N., v.Borstel, L., Engelhardt, J., carstensen, A., Teichmann, L., Heydorn, M., and Tresper, M. (2019). Modyfing magnesia cement for preparing geotechnical constructions and injection grout. *Proceedings of the 10th US/German Workshop "Salt Repository Research, Design, and Operation*, page 386 ff.

Meyer, T., Teichmann, L., and Heydorn, M. (2008). Geotechnische messungen an einer pilotströmungsbarriere. *Messen in der Geotechnik 2008, Mitteilung des Instituts für Grundbau und Bodenmechanik*, 87.

Mönig, J., Buhmann, D., Rübel, A., Wolf, J., Baltes, B., and Fischer-Appelt, K. (2012). Sicherheits- und Nachweiskonzept - Bericht zum Arbeitspaket 4, Vorläufige Sicherheitsanalyse für den Standort Gorleben.

Mualem, Y. (1976). A new model for predicting the hydraulic conductivity of unsaturated porous media. *Water Resources Research*, 12(3):513–522.

Müller-Hoeppe, N., Breustedt, M., Wolf, J., Czaikowski, O., and Wieczorek, K. (2012a). Integrität geotechnischer Barrieren Teil 2: Vertiefte Nachweisführung: Bericht zum Arbeitspaket 9.2; vorläufige Sicherheitsanalyse für den Standort Gorleben.

Müller-Hoeppe, N., Buhmann, D., Czaikowski, O., Engelhardt, H.-J., Herbert, H.-J., Lerch, C., Linkamp, M., Wieczorek, K., and Xie, M. (2012b). Integrität geotechnischer Barrieren Teil 1: Vorbemessung: Bericht zum Arbeitspaket 9.2; vorläufige Sicherheitsanalyse für den Standort Gorleben, keywords = Chemische Vorbemessung;Gorleben;Hydraulische Vorbemessung;Mechanische Vorbemessung;Schachtverschlüsse;Streckenverschlüsse;Vorläufige Sicherheitsanalyse Gorleben.

Müller-Hoeppe, N. and Eberth, S. (2009). ÜBERSICHT - Übertragung des Sicherheitsnachweiskonzeptes für ein Endlager im Salz auf andere Wirtsgesteine - Abschlussbericht.

Müller-Hoeppe, N. and Krone, J. (1999). Ein neuer Ansatz zur Bewertung der Wirksamkeit von Barrieren im Endlager (02 E 9087) - Final report.

Müller-Hoeppe, N., Krone, J., and Engelhardt, H.-J. (2017). Überprüfung und Bewertung des Instrumentariums für eine sicherheitliche Bewertung von Endlagern für HAW - ISIBEL / KOMTESSA: Zur Übertragung der Methode der Teilsicherheitsbeiwerte auf endlagerrelevante Zeiträume. Technical report, DBE Technology GmbH, Peine.

NEA (2016). Scenario Development Workshop Synopsis. Integration Group for the Safety Case.

Nole, M., Beskardes, G. D., Fukuyama, D., Leone, R. C., Mariner, P., Park, H. D., Paul, M., Salazar, A., Hammond, G. E., and Lictner, P. C. (2022). PFLOTRAN development FY2022. Technical Report SAND2022-10526R, Sandia National Laboratories.

Nole, M., Beskardes, G. D., Fukuyama, D., Leone, R. C., Park, H. H., Paul, M., Salazar, A., Hammond, G. E., and Lichtner, P. C. (2023). Recent Advancements in PFLOTRAN Development for the GDSA Framework. Technical Report SAND2023-07655, Sandia National Laboratories.

Nuclear Energy Agency (2004). Post-closure Safety Case for Geological Repositories, Nature and Purpose. Technical Report NEA Report No. 3679, OECD/NEA, Paris, France.

Office of Civilian Radioactive Waste Management (1988). Site Characterization Plan Deaf Smith County Site, Texas – Overview. Technical Report DOE/RW-0163, US Department of Energy.

Orzechowski, J. (2018). *Entwicklung eines methodischen Ansatzes zur langzeitsicheren Auslegung eines Streckenverschlussbauwerks für ein Endlager für wärmeentwickelnde radioaktive Abfälle im Salz - Dissertation*. PhD thesis, TU Clausthal, Clausthal-Zellerfeld.

Ottosen, N. S. (1977). A Failure Criterion for Concrete. *Journal of the Engineering Mechanics Division*.

Parker, J., Lenhard, R., and Kuppusamy, T. (1987). A parametric model for constitutive properties governing multiphase flow in porous media. *Water Resources Research*, 23(4):618–624.

Parkhurst, D. L. and Appelo, C. A. J. (2013). Description of input and examples for PHREEQC version 3—A computer program for speciation, batch-reaction, one-dimensional transport, and inverse geochemical calculations. Technical Report USGS Survey Techniques and Methods, Book 6, Chapter A43, US Geological Survey.

Pierce, W. G. and Rich, E. I. (1962). Summary of rock salt deposits in the united states as possible storage sites for radioactive waste materials. Technical Report Bulletin 1148, US Geological Survey.

Pollok, L., Hölzner, M., and Fleig, S. (2016). AP2: Erfassung des Internbaus von Salzstrukturen und geologische 3D-Modellierung. In BGR, editor, *Informationssysteme Salzstrukturen: Planungsgrundlagen, Auswahlkriterien und Potentialabschätzung für die Errichtung von Salzkavernen zur Speicherung erneuerbarer Energien (InSpEE)*. Bundesanstalt für Geowissenschaften und Rohstoffe, Hannover.

Pötzsch, S. (2021). Investigations on in-situ material behavior of matrix-stabilized crushed rock salt backfill under consideration of different filling technologies - Review of the GESAV II project. *11th US/German Workshop on Salt Repository Research, Design, and Operation*.

Pötzsch, S., Pannach, M., Freyer, D., Popp, T., Gruner, M., and Mischo, H. (2018). Entwicklung und in situ-Erprobung eines langzeitbeständigen, matrixstabilisierten Versatzmaterialsauf Steinsalz-Polyhalitbasis. *13. Projektstatusgespräch zu BMWi-geförderten FuE-Projektenzur Entsorgung radioaktiver Abfälle*.

Powers, D. W., Lambert, S. J., Shaffer, S. E., Hill, L. R., and Weart, W. D. (1978). Geological Characterization Report, Waste Isolation Pilot Plant (WIPP) site, Southeastern New Mexico – Volumes 1 & 2. Technical Report SAND78-1596, Sandia National Laboratories.

Reinhold, K., Hammer, J., and Pusch, M. (2014). Verbreitung, Zusammensetzung und geologische Lagerungsverhältnisse flach lagernder Steinsalzfolgen in Deutschland: Zwischenbericht.

Reinhold, K., Krull, P., and Kockel, F. (2008). Salzstrukturen Norddeutschlands 1 : 500 000.

Rübel, A., Buhmann, D., Kindlein, J., and Lauke, T. (2016). Performance Assessment of Sealing Systems - Conceptual and integrated modelling of plugs and seals, GRS-415.

Salzer, K., Günther, R.-M., Minkley, W., Naumann, D., Popp, T., Hampel, A., Lux, K.-H., Herchen, K., Düsterloh, U., Argüello, J., and Hansen, F. (2015). Joint project iii on the comparison of constitutive models for the mechanical behavior of rock salt, ii. extensive laboratory test program with clean salt from wipp. In Roberts, L., Mellegard, K., and Hansen, F., editors, *Proceedings of the 8th Conference on the Mechanical Behavior of Salt (SaltMech VIII)*. Taylor & Francis Group.

Sanders, I. (2020). Konzepte für die Auslegung und den Nachweis von geotechnischen Barrieren in einem Endlager für wärmeentwickelnde radioaktive Abfälle in Steinsalz - Masterarbeit.

Schulze, O., Heemann, U., Zetsche, F., Hampel, A., Pudewills, A., Günther, R.-M., Minkley, W., Salzer, K., Hou, Z., Wolters, R., Rokahr, R., and Zapf, D. (2007). Comparison of advanced constitutive models for the mechanical behavior of rock salt - results from a joint research project. I. Modeling of deformation processes and benchmark calculations. In Lux, K.-H., Minkley, W., Wallner, M., and Hardy, H. J., editors, *Basic and Applied Salt Mechanics: Proceedings of the 6th Conference on the Mechanical Behavior of Salt (SaltMech VI)*. Taylor & Francis (Balkema).

Simo, E., Herold, P., Hagdu, T., Jayne, R., Keller, A., Kuhlman, K., Lommerzheim, A., Matteo, E., and Mills, M. (2024). Methodology Report on Design and Performance Assessment of Engineered Barrier Systems in a Salt Repository for HLW/SNF. Technical Report BGE TEC 2024-XX / SAND2024-XXXX R, BGE TECHNOLOGY GmbH, SANDIA, Peine, Albuquerque.

Somerton, W. H., Keese, J. A., and Chu, S. L. (1974). Thermal behavior of unconsolidated oil sands. *Society of Petroleum Engineers Journal*, 14(5):513–521.

Sparrow, B. S. (2003). Empirical equations for the thermodynamic properties of aqueous sodium chloride. *Desalination*, 159(2):161–170.

StandAG (2023). Standortauswahlgesetz vom 5. Mai 2017 (BGBl. I S. 1074), das zuletzt durch Artikel 8 des Gesetzes vom 22. März 2023 (BGBl. 2030 I Nr. 88) geändert worden ist.

Stone, C. (1995). Creep closure behavior of waste disposal rooms in bedded salt due to gas generation produced by several alternatives of the engineered alternatives task force. Technical report, Sandia National Laboratories, Albuquerque, NM. Memorandum to B.M. Butcher (October 6, 1992) in A Summary of Methods for Approximating Salt Creep and Disposal Room Closure in Numerical Methods of Multiphase Flow, SAND94-0251.

Stone, C., Krieg, R., and Beisinger, Z. (1985). Sancho, a finite element computer program for the quasistatic, large deformation, inelastic response of two-dimensional solids. Technical Report SAND84-2618, Sandia National Laboratories, Albuquerque, NM.

Teichmann, L., Neydeck, J., Manthee, F., and Bollingerfehr, W. (2002). FuE-Vorhaben Schachtverschluss Salzdetfurth, Geotechnische Messungen, Untersuchungen zur Schottersäule Schacht 1. Technical report, DBE, Peine.

U.S. Congress (1969). National Environmental Policy Act of 1969. `https://www.epa.gov/laws-regulations/summary-national-environmental-policy-act`. 42 U.S.C. §4321 et seq.

U.S. Congress (1992). Waste Isolation Pilot Plant Land Withdrawal Act. `https://www.congress.gov/bill/102nd-congress/house-bill/2637`. Public Law 102-579, as amended by Public Law 104-201.

U.S. Congress (1996). National Defense Authorization Act for Fiscal Year 1997, Section 12. `https://www.congress.gov/bill/104th-congress/house-bill/3230`. Public Law 104-201, Section 12, Amending Public Law 102-579.

US Department of Energy (1980). Environmental impact statement waste isolation pilot plant – volumes 1 & 2. Technical Report DOE/EIS-0026, US Department-of-Energy.

U.S. Department of Energy (1996). Title 40 CFR Part 191 Compliance Certification Application for the Waste Isolation Pilot Plant. Technical Report DOE/CAO-1996-2184, U.S. Department of Energy.

U.S. Department of Energy (2008). Yucca Mountain Repository License Application: Safety Analysis Report. Technical Report DOE/RW-0573, Revision 0, U.S. Department of Energy. Accessed: September 30, 2024.

U.S. Department of Energy (DOE) (1997). Waste Isolation Pilot Plant Disposal Phase Final Environmental Impact Statement: Summary. Technical Report DOE/EIS-0026-S-2, U.S. Department of Energy.

U.S. Environmental Protection Agency (1985). Environmental Radiation Protection Standards for Management and Disposal of Spent Nuclear Fuel, High-Level and Transuranic Radioactive Wastes. `https://www.ecfr.gov/current/title-40/chapter-I/subchapter-F/part-191`. 40 CFR Part 191.

U.S. Environmental Protection Agency (2001). Public Health and Environmental Radiation Protection Standards for Yucca Mountain, Nevada. `https://www.ecfr.gov/current/title-40/chapter-I/subchapter-F/part-197`. 40 CFR Part 197.

U.S. Nuclear Regulatory Commission (1983). Disposal of High-Level Radioactive Wastes in Geologic Repositories. `https://www.ecfr.gov/current/title-10/chapter-I/part-60`. 10 CFR Part 60.

U.S. Nuclear Regulatory Commission (2001). Disposal of High-Level Radioactive Wastes in a Geologic Repository at Yucca Mountain, Nevada. `https://www.ecfr.gov/current/title-10/chapter-I/part-63`. 10 CFR Part 63.

U.S. Nuclear Regulatory Commission (2004). Risk-Informed Regulation of Nuclear Facilities. `https://www.nrc.gov/about-nrc/regulatory/risk-informed.html`. NUREG-2150.

van Genuchten, M. Th. (1980). A closed-form equation for predicting the hydraulic conductivity of unsaturated soils. *Soil Science Society of America Journal*, 44(5):892–898.

Van Sambeek, L. L., Stickney, R. G., and Wagner, R. A. (1980). Thermomechanical Assessment of In Situ Heater Tests in Dome Salt at Avery Island, Louisiana. In *The 21st U.S. Symposium on Rock Mechanics (USRMS)*. American Rock Mechanics Association.

Villar, M., Besuelle, P., Cernochova, K., Collin, F., Cuevas, J., Cuss, R., de Lesquen, C., Dizier, A., El Tabbal, G., Gens, A., Gimeno, N., Graham, C., Grgic, D., Harrington, J., Imbert, C., Kašpar, V., Kaufhold, S., Leupin, O., Levasseur, S., Mašín, D., Najser, J., Narkŭnienè, A., Ollin, M., Reijonen, H., Šachlová, v., Sayenko, S., Simo, E., Svensson, D., Svoboda, J., Tatomir, A., Vettese, G., Yliharju, J., and Zoblenko, B. (2023). D7.2 HITEC. Updated State-of-the-Art on THM behaviour of Buffer Clay Materials and Host Clay Formations. Technical Report Deliverable n° 7.2, EURAD Project, Horizon 2020. 129 pp.

Völkner, E., Kühnlenz, T., and Hammer, J. (2017a). Arbeitspaket: 2 - Entwicklung generischer geologischer Modelle für flach lagernde Salzformationen (KOSINA). In BGR, editor, *Konzeptentwicklung für ein generisches Endlager für wärmeentwickelnde Abfälle in flach lagernden Salzschichten in Deutschland sowie Entwicklung und Überprüfung eines Sicherheits- und Nachweiskonzeptes (KOSINA)*. Bundesanstalt für Geowissenschaften und Rohstoffe, Hannover.

Völkner, E., Kühnlenz, T., and Hammer, J. (2017b). KOSINA - Arbeitspaket: 2 - Entwicklung generischer geologischer Modelle für flach lagernde Salzformationen. In BGR, editor, *Konzeptentwicklung für ein generisches Endlager für wärmeentwickelnde Abfälle in flach lagernden Salzschichten in Deutschland sowie Entwicklung und Überprüfung eines Sicherheits- und Nachweiskonzeptes (KOSINA)*. Bundesanstalt für Geowissenschaften und Rohstoffe, Hannover.

von Goerne, G., Fleig, S., Rokahr, R. B., and Donadei, S. (2016). Informationssystem Salzstrukturen: Planungsgrundlagen, Auswahlkriterien und Potentialabschätzung für die Errichtung von Salzkavernen zur Speicherung von erneuerbaren Energien (Wasserstoff und Druckluft).

Wagner, K. (2005). *Beitrag zur Bewertung der Sicherheit untertägiger Verschlussbauwerke im Salinargebirge - Dissertation*. PhD thesis, TU Bergakademie Freiberg, Freiberg.

Weise, D., Kamlot, P., Brückner, D., and Naumann, D. (2006). Abschlussbericht zu laborativen voruntersuchungen an sorelbetonproben der chargen 1 bis 26. Technical Report B IfG 16/2005, Institut für Gebirgsmechanik (IfG) GmbH, Leipzig.

Wolery, T. J. (2010). EQ3/6 a software package for geochemical modeling. Technical Report LLNL-CODE-638958, Lawrence Livermore National Laboratory.

Wolf, J., Behlau, J., Beuth, T., Bracke, G., Bube, C., Buhmann, D., Dresbach, C., Hammer, J., Keller, S., Kienzler, B., Klinge, H., Krone, J., Lommerzheim, A., Metz,V., Mönig,J., Mrugalla, S., Popp, T., Rübel, A., and Weber, J. R. (2012). FEP-Katalog für die VSG.

Wolters, R., Sun-Kurczinski, J., Düsterloh, U., Lux, K., Günther, R.-M., Lüdeling, C., Hampel, A., Yildirim, S., Zapf, D., Wacker, S., Epkenhans, I., Stahlmann, J., and Reedlunn, B. (2022). *WEIMOS: Laboratory investigation and numerical simulation of damage reduction in rock salt*, pages 190–199. CRC Press.

Wunderlich, A., Jobmann, M., León Vargas, R. P., and Seidel, D. (2022). Analysen zur Integrität der technischen und geotechnischen Barrieren eines HAW Endlagers im Tongestein in Deutschland. AP-Bericht im Rahmen von ANSICHT-II: Aktualisierung der Sicherheits- und Nachweismethodik für die HAW-Endlagerung im Ton-gestein in Deutschland. Technical Report BGE TEC 2021-22, BGE TECHNOLOGY GmbH, Peine.

BGE TECHNOLOGY GmbH
Eschenstraße 55
31224 Peine – Germany
T + 49 5171 43-1520
F + 49 5171 43-1506
info@bge-technology.de
www.bge-technology.de